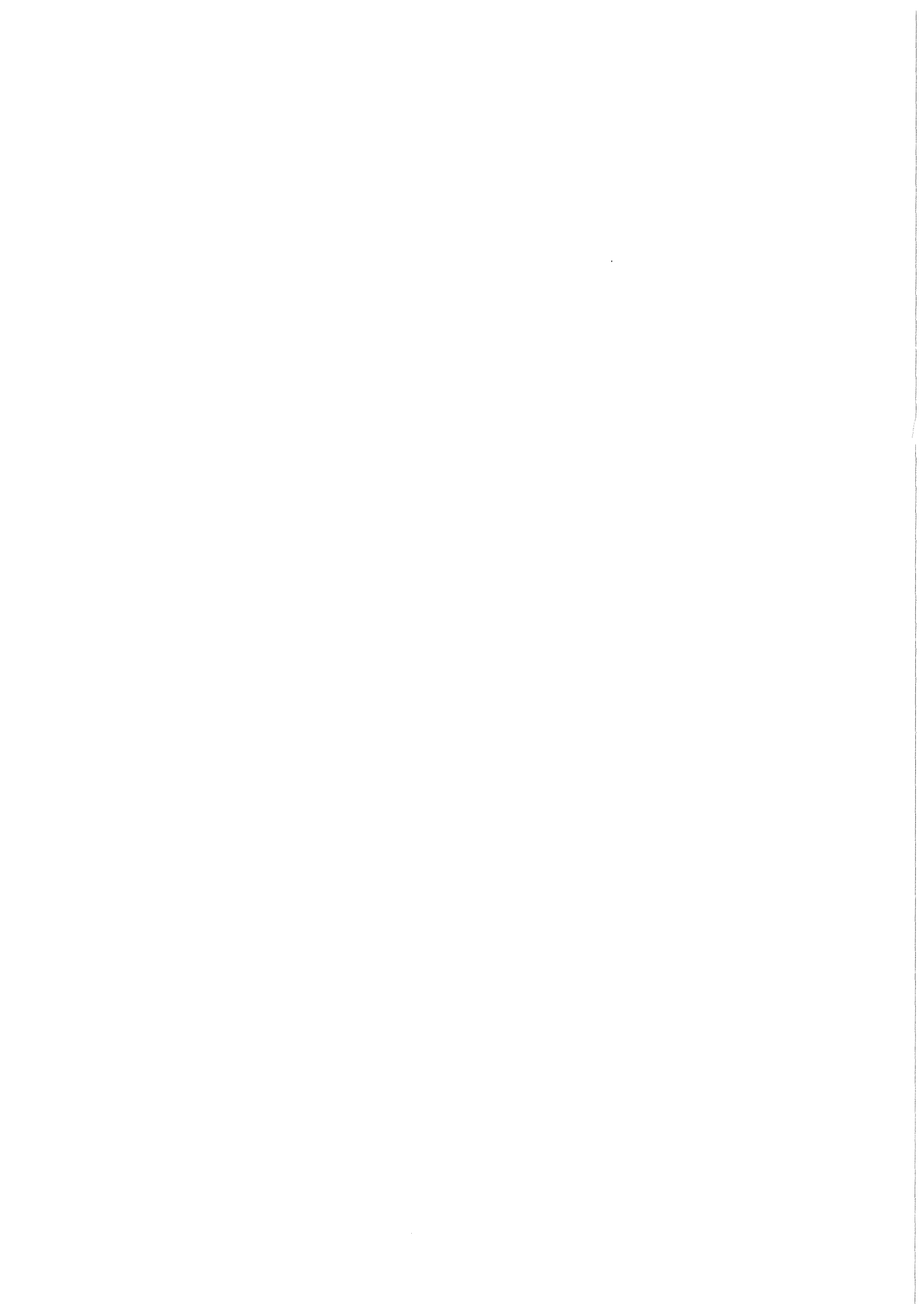


KfK 4204
Mai 1987

Atomic Ordering, Phase Stability and Superconductivity in Bulk and Filamentary A15 Type Compounds

R. Flükiger
Institut für Technische Physik

Kernforschungszentrum Karlsruhe



KERNFORSCHUNGSZENTRUM KARLSRUHE
Institut für Technische Physik

KfK 4204

ATOMIC ORDERING, PHASE STABILITY AND SUPERCONDUCTIVITY IN BULK AND
FILAMENTARY A15 TYPE COMPOUNDS *)

R. FLÜKIGER

KERNFORSCHUNGSZENTRUM KARLSRUHE, GMBH, KARLSRUHE

*) Habilitationsarbeit am Physikinstitut der Universität Genf, Schweiz.

Als Manuskript vervielfältigt
Für diesen Bericht behalten wir uns alle Rechte vor

Kernforschungszentrum Karlsruhe GmbH
Postfach 3640, 7500 Karlsruhe 1

ISSN 0303-4003

Abstract

The influence of atomic ordering effects and ordering kinetics on the superconducting and metallurgical properties of A15 type compounds are critically discussed based on own and literature data.

First, the techniques for determining the order parameter are reviewed. The dependence of T_C vs. S in various A15 type compounds as a function of the quenching temperature and of the high energy particle irradiation fluence is discussed. A model for the disordering mechanism in A15 compounds is established, based on the new concept of the virtual lattice site. It is shown that the disordering mechanism is the same in both cases, high temperature heat treatment and high energy particle irradiation. The very complete representation of ordering effects also contains the variation of other properties, e.g. γ , θ_D , ρ_0 and $B_{C2}(0)$. Furthermore, it allows to draw empirical correlations between atomic ordering and A15 phase stability.

Finally, it is shown on selected examples that the optimization of the critical current density at high fields in Nb_3Sn wires by alloying is nothing else than a consequence of the occurrence of perfect atomic ordering in binary Nb_3Sn .

ATOMARE FERNORDNUNG, STABILITÄT UND SUPRALEITUNG IN MASSIVEN UND FILAMENTAREN A15-VERBINDUNGEN

Zusammenfassung

Der Einfluß von Ordnungseffekten und der Ordnungskinetik auf die supraleitenden und metallurgischen Eigenschaften von A15 Verbindungen wird kritisch diskutiert aufgrund von eigenen und Literatur-Daten.

Es werden zunächst die Methoden zur Bestimmung der Ordnungsparameters vorgestellt. Dann wird die Abhängigkeit von T_C als Funktion von S für alle bekannten A15-Verbindungen vorgestellt, wobei S mittels Abschrecken aus hohen Temperaturen und Bestrahlung mit Hochenergie-Teilchen variiert wurde. Ein Modell für den Entordnungsmechanismus in A15-Verbindungen wird vorgeschlagen, der auf dem neuen Konzept der Existenz von metastabilen, sogenannten "virtuellen", Gitterplätzen beruht. Aufgrund dieses Modells ist der Entordnungsmechanismus in beiden Fällen, also Hochtemperaturbehandlung und Bestrahlung, derselbe (bei nicht allzu großen Bestrahlungsdosen, die T_C auf $> T_{C0}/2$ reduzieren). Es wird eine vollständige Studie der Änderung anderer physikalischer Eigenschaften mit S erstellt, wie γ , θ_D , ρ_0 , $B_{C2}(0)$. Ein empirischer Zusammenhang zwischen Ordnungsgrad und A15-Phasenstabilität wird aufgestellt.

Schließlich wird gezeigt, daß die Optimierung der kritischen Stromdichte in Nb_3Sn -Drähten bei hohen magnetischen Feldern durch Zulegierung mit ternären Elementen eine direkte Folge des Auftretens eines perfekt geordneten Zustands im binären Nb_3Sn ist.

1. INTRODUCTION	1
2. SUPERCONDUCTIVITY AND POLYMORPHISM IN INTERMETALLIC COMPOUNDS	5
3. THE BRAGG-WILLIAMS LONG-RANGE ORDER PARAMETER IN A15 TYPE COMPOUNDS	12
3.1 Definition of the Bragg-Williams Order Parameter, S	12
3.2. Experimental Determination of S	14
3.2.1. Thermal and Static Mean Square Amplitudes	14
3.2.2. Least Square Refinement Procedure	16
3.2.3. Determination of S on Irradiated Thin Films	18
3.3. Factors Influencing the Determination of S	20
3.3.1. Systematic Factors	20
- The Atomic Scattering Factor	20
- The Anomalous Dispersion Correction	24
3.3.2. The Metallurgical State of the Sample	25
- Homogenization Heat Treatments	25
- The Presence of Additional Phases	28
- Preferred Orientations	32
3.4. Indirect Determination of the Order Parameter	32
4. NONEQUILIBRIUM STATES IN QUENCHED AND IRRADIATED A15 TYPE COMPOUNDS	35
4.1. Ordering Changes Induced by Thermal Methods	36
4.1.1. Diffusion Mechanism: the "Virtual" Site	36
4.1.2. Variation of S with Quenching Temperature	42
4.1.3. Homogeneity of S in Quench-Disordered Crystals	45
4.2 Radiation Damage and Disorder	49
4.2.1. Coexisting Defect Mechanisms	52
4.2.2. Arguments in Favour of Homogeneous Atomic Disordering after Irradiation	53
a. Irradiation with High Energy Electrons and Neutrons	54
b. Comparison between Irradiated and Quenched Nb ₃ Pt	56
c. Calorimetric Observations on Irradiated A15 Compounds	57
d. The Irradiation Temperature	63
4.2.3. The Virtual Site Exchange Mechanism in Irradiated A15 Type Compounds	66
4.2.4. Disordering as Produced by Quenching and by Irradiation: A Comparison	70
4.3. Additional Radiation Induced Effects	72
4.3.1. The Lattice Expansion	73
a. The Effect of AB Overlapping	73
b. The Effect of AA Overlapping	74
c. Irradiation and the Lattice Parameter	75
d. Atomic Radii and Their Limitations	80
- The Geller Model	80
- The Pauling Model	83
- The Machlin Model (Crystal Field Model)	84
4.3.2. The Radiation Induced Lattice Expansion and the Variation of T _c	85

4.3.3. Static Displacement from Equilibrium Atomic Positions	88
4.3.4. Radiation Induced Phase Changes	91
4.3.5. The "Saturation" Region of T_c after Heavy Irradiation	93
4.3.6. Increase of T_c in Irradiated Mo_3Ge , Mo_3Si and Nb_3Ir : An Ordering Effect?	97
a. Quenching Experiments	98
b. Irradiation Experiments	101
- The System Mo_3Ge	101
- The System Mo_3Si	103
- The System Nb_3Ir	105
c. Comparison Between the Irradiation Behavior of Low and High T_c A15 Type Compounds	108
4.3.7. Recombination Effects	111
4.3.8. Radiation Damage in A15 Type Compounds: A Synopsis	113
5. THE DEGREE OF ORDERING IN A15 TYPE COMPOUNDS	116
5.1. Presentation and Discussion of the Ordering Data	118
5.1.1. Nb Based A15 Type Compounds	118
Nb_3Sn , Nb_3Ge , Nb_3Al , Nb_3Ga , Nb_3Au , Nb_3Pt , Nb_3Ir , Nb_3Os	
5.1.2. V Based A15 Type Compounds:	135
V_3Si , V_3Ga , V_3Ge , V_3Au , V_3Pt , V_3Ir , V_3Rh , V_3Pd , V_3Ni , V_3Co , V_3Ir , V_3Os , V_3Re	
.62 .38 .50 .50 .29 71	
5.1.3. Mo Based A15 Type Compounds:	148
Mo_3Si , Mo_3Pt , Mo_3Ir , Mo_3Os	
5.1.4. Cr Based A15 Type Compounds:	151
Cr_3Si , Cr_3Ga , Cr_3Pt , Cr_3Ir , Cr_3Os , Cr_3Ru , Cr_3Rh	
5.1.5. Ti Based A15 Type Compounds	153
Ti_3Au , Ti_3Pt , Ti_3Ir	
5.2. The Order Parameter in A15 Type Compounds: A Comparison	154
5.2.1. The Order Parameter at Room Temperature	154
5.2.2. The Order Parameter at High Temperature	159
6. LATTICE VIBRATIONS, PHASE STABILITY	162
6.1. Lattice Vibrations and Debye Temperatures	162
6.1.1. Vibrational Anisotropy of Atoms on 6c Sites	162
6.1.2. Mean Square Vibration Amplitudes at the 6c and 2a Sites	164
6.1.3. Isotropic Vibration Amplitudes and θ at 300 K	167

6.1.4.	The Debye Temperatures Between 0 and 300 K	174
	a. $\theta_D(T)$ at $T < 50$ K	178
	b. $\Delta\theta_D(300K \rightarrow 0)$ From Calorimetry and X Ray Diffraction	182
6.1.5.	The Effect of Composition and Ordering on the Debye Temperature	184
	a. Ordering Effects on $\theta_D(0)$	186
	b. Compositional Effects on $\theta_D(0)$	188
	c. Extrapolation of $\theta_D(0)$ for the Metastable V_3Al	190
6.1.6.	Lattice Vibrations at High Temperatures	192
6.1.7.	Thermal Expansion in A15 Type Compounds	194
	a. $\alpha(T)$ Below $T = 300$ K	195
	b. $\alpha(T)$ Above $T = 300$ K	198
6.2.	Phase Stability and Atomic Ordering	200
	6.2.1. Raynor's Stability Index	201
	6.2.2. Stability Considerations Based on Machlin's Model	204
	a. The Energy of Formation	205
	b. The Degree of Long-Range Ordering	208
6.2.	6.2.3. The Quasiharmonic Potential Approximation	209
	6.2.4. Electron Charge Transfer	211
7.	ELECTRICAL RESISTIVITY	213
7.1.	Resistivity at High Temperatures	213
7.2.	The Shunting Model	214
7.3.	Electrical Resistivity in Quenched and Irradiated Samples	218
7.4.	Electrical Resistivity at Low Temperatures	218
	7.4.1. Description of $\rho(T)$ Below 50 K	
	7.4.2. The Exponent n in $\rho(T)$ at Low Temperatures: The Experimental Situation	
7.5.	Compositional Effects on ρ	229
	7.5.1. The System V_3Si	229
	7.5.2. The System Nb_3Sn	231
	7.5.3. Comparison Between the Systems V_3Si , Nb_3Sn and Nb_3Ge	233
	7.5.4. The System Nb_3Al	234
	7.5.5. The System Nb_3Ir	234
7.6	The Effect of Atomic Ordering on ρ_0	235
8.	TECHNICAL ASPECTS OF ATOMIC ORDERING IN A15 TYPE COMPOUNDS	240
8.1.	General Remarks About Multifilamentary Wires	240
8.2.	Wire Preparation	241
	8.2.1. The Equilibrium Phase Diagrams of the Systems Nb_3Sn , Nb_3Al and V_3Ga	243
8.3.	Variation of Physical Properties with Composition in Various A15 Type Compounds	243
	8.3.1. The Superconducting Transition Temperature	243
	8.3.2. The Electronic Specific Heat	247
	8.3.3. The Electrical Resistivity	249
	8.3.4. The Upper Critical Magnetic Field	249
	8.3.5. The Upper Critical Field Slope in Nb_3Sn	255

8.4. The Case of Alloyed Nb ₃ Sn Wires	257
8.4.1. Preparation and Characterization of the Alloyed Nb ₃ Sn Wires	258
8.4.2. Atomic Ordering in Multifilamentary Nb ₃ Sn Wires	260
8.4.3. The Martensitic Phase Transformation in Alloyed Nb ₃ Sn Wires	261
8.4.4. Superconducting Transition Temperature and Electrical Resistivity in Alloyed Nb ₃ Sn Wires	265
8.4.5. Critical Current Density in Alloyed Nb ₃ Sn Wires	267
8.4.6. Upper Critical Fields in Alloyed Nb ₃ Sn Wires	269
8.4.7. Low Temperature Irradiation of Alloyed Nb ₃ Sn Wires	273
9. CONCLUSIONS	278
10. REFERENCES	291

I. INTRODUCTION

Most ordered intermetallic compounds exhibit an order-disorder phase transformation at a temperature T_M . After fast quenching of ordered compounds as Cu_3Au /1/ or CuZn /2/ from temperatures $T < T_M$, these materials can be retained at different degrees of atomic ordering, depending on temperature and cooling rate. Up to the present day, order parameters differing from perfect ordering have been detected on an appreciable number of ordered structures, one of them being the A15 phase. The particular interest in the observation of order parameter changes in A15 type compounds resides in the unique correlation between deviations from perfect ordering and the superconducting transition temperature, T_C . Such a correlation has so far not been detected in any other superconducting phase.

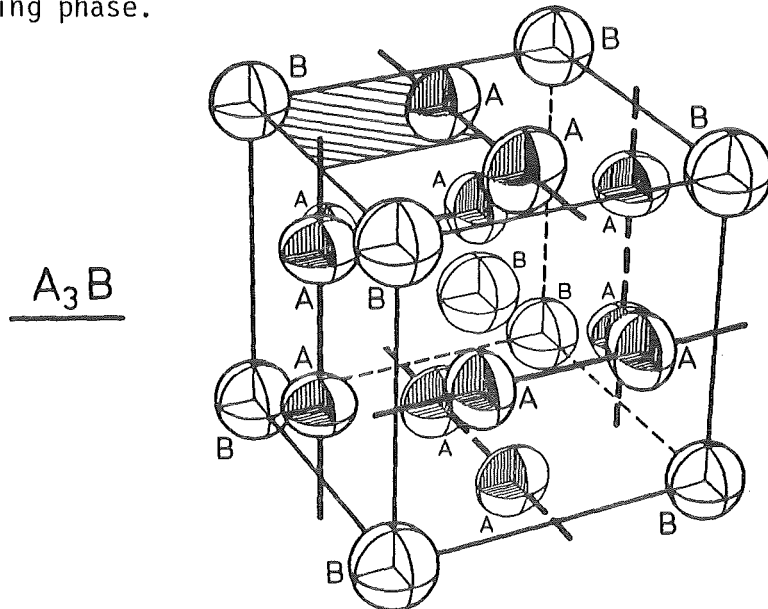


Fig. 1.1. The A15 structure.

The observation of ordering effects on the low temperature properties of A15 type compounds is nothing else than a consequence of the existence of different nonequilibrium states in the A15 superlattice, induced either by rapid quenching or by high energy irradiation. Quenching experiments have induced small, but observable changes in the degree of long-range atomic ordering of the A15 structure, reflecting the temperature dependence of the equilibrium order parameter. These small changes of the order parameter, S , have been found to affect the values of T_C /3,4/. Since the first observation of these effects by Van Reuth et al. /3/, other electronic properties at low temperature have been found to be affected by changes in S , as the electronic specific heat coefficient, γ , the

magnetic susceptibility, $\bar{\chi}$, the upper critical magnetic field, H_{c2} , the electrical resistivity in the normal state (just above T_c), ρ_0 , and others. To a certain extent, lattice properties as the Debye temperature, θ_D , have also been found to vary with S , the change being considerably smaller than for γ , at least for high T_c A15 type compounds.

The accurate determination of the absolute value of the order parameter S requires time-consuming experiments and is particularly difficult for samples having a film geometry where grain texturing occurs. For this reason, many investigations on ordering effects in A15 type compounds are restricted to the study of variations of selected low temperature properties as a function of the thermal or irradiation history, without a direct determination of the order parameter. In these cases, its value is indirectly determined starting from reference values obtained elsewhere. The first reliable order parameter determination in A15 type compounds by Van Reuth and Waterstrat /3/. After different heat treatments have furnished a first evidence for a possible correlation between superconductivity and degree of ordering in A15 type compounds. It appeared soon that the value of T_c for an A15 compound of the general formula $A_{1-\beta}B_\beta$ depends on two parameters, i.e. the chemical composition β , and the Bragg-Williams long-range order parameter, S . From a systematical work undertaken by the author /7/, it follows that this is in contrast to the behavior in bulk superconducting compounds crystallizing in other known structures, where within the superconducting phase field T_c^* depends on the chemical composition only.

The interest in studying the correlation between atomic ordering and superconductivity in A15 compounds was originally motivated by the question whether it would be possible to raise the highest known T_c values by improving the degree of atomic ordering. For this purpose, attempts were undertaken to vary the order parameter by rapid quenching or by high energy irradiation. The observation of a strong decrease of T_c in A15 compounds after neutron irradiation /8/ raised the question about the lifetime of a superconducting Nb_3Sn magnet exposed to heavy neutron irradiation in a fusion reactor. Besides this technological aspect, it is of fundamental interest to know whether the decrease of T_c in quenched and irradiated A15 type compounds is caused by the same mechanism, i.e. whether the decrease of the order parameter with increasing fluence is dominant with respect to various additional effects occurring during high energy irradiation. This question will be discussed in detail in the present work, based on a model recently proposed by the author /6/ which attributes the initial decrease of T_c (down to $T_c/T_{c0} = 0.5$) with

increasing fluence to the occurrence of nonequilibrium states of the A15 lattice /5/. The discussion will be extended to the cases of heavily irradiated A15 type superconductors, where the value of T_c is influenced by phonon softening rather than by changes of the electronic density of states.

When studying atomic ordering effects in A15 type compounds, a particular emphasis has to be given to the metallurgical state (homogeneity, compositional distribution, precise determination of composition). The preparation of homogeneous samples at compositions close to the A15 phase boundary (where T_c mostly reaches its maximum) requires an accurate knowledge of the corresponding A15 phase field. A previous review by the author /7/ will be used as a broad reference basis for additional details concerning preparation and analysis. The author has accomplished numerous works in many aspects of ordering and phase stability of A15 type compounds, the treated subjects comprising

- a) the work on the high temperature phase fields of various high T_c A15 systems,
- b) the determination of the order parameter and the vibration amplitudes by diffractometry on most A15 type compounds
- c) the study of ordering changes (induced by argon jet quenching) on the electronic properties, e.g. T_c , γ , ρ_0 , H_{c2} and others.

In recent years the activity was extended to high energy irradiation of bulk and multifilamentary A15 materials, to the study of the disordering mechanisms and of the ordering kinetics. All these data were condensed in the present work, which also contains a considerable amount of critically selected literature data in order to get a better insight into the reality of small changes of the degree of atomic ordering producing important effects on the properties of A15 materials.

The present work is organized as follows. In Section 2, a survey of the superconducting properties in ordered and disordered compounds showing polymorphism is presented. These data will later be used for comparison when studying the influence of deviations from perfect ordering. In Section 3, the Bragg-Williams long-range atomic order parameter is defined and experimental methods for the determination of absolute values (on bulk samples) and relative values (on films) are discussed.

A detailed description of various deviations from thermodynamical equilibrium as induced by rapid quenching from high temperatures or by irradiation with high energy particles is given in Section 4. A strong analogy between the disordering mechanisms in the A15 lattice during the processes of fast

quenching and irradiation is established, based on the hypothesis of occupied "virtual" sites /6/.

All ordering data on A15 type compounds available to date are critically analyzed and listed in Section 5. In Section 6, an attempt is made to establish a correlation between the degree of ordering and stability of A15 phases, the latter being represented by the vibrational behavior of the lattice. The conditions for the occurrence of phonon softening below 300 K in A15 type compounds are studied, revealing systematic differences between high γ and low γ materials. The latter are found to exhibit a strong hardening of the lattice below 100 K which has got little attention so far. As well deviations from perfect ordering as from stoichiometry are found to reinforce this "low temperature hardening" for A15 type compounds with $\gamma > 7 \text{ mJ/K}^2\text{g-at}$. In low γ compounds, the inverse behavior is observed, disordering by high energy irradiation leading to softening of the lattice. The latter is responsible for the enhancement of T_c in Mo_3Ge and Mo_3Si , the electronic density of states remaining essentially unchanged. Several stability considerations lead to a consistent picture for the instability of A15 type compounds with B elements from the Zn (or IIB) column, with a tendency of reduced stability (mainly expressed by a lower degree of long range ordering) for the neighbouring compounds with B elements from the Cu (or IB) or from the B (or IIIA) column.

In Section 7, the influence of atomic ordering and composition on the electrical resistivity ρ is studied. Own data and literature data on the variation $\rho(T)$ at low and high temperature are discussed. A particular attention has been given to the study of the temperature exponent at $T > 40 \text{ K}$, where an unexplained T^2 dependence has been repeatedly reported for high γ A15 type compounds.

In Section 8, it will be shown that the degree of ordering has also a strong influence on industrial Nb_3Sn multifilamentary wires. In particular, the improvement of the critical current density in such wires after alloying with ternary additives is a direct consequence of perfect ordering occurring in this compound. The case of V_3Ga and Nb_3Al wires is also discussed, both compounds forming with a slight deviation from perfect ordering.

In Section 9 finally, the effects of ordering and compositional changes on T_c of several A15 type compounds are presented and discussed. The discussion also includes effects on other electronic properties as the electronic specific heat γ and the upper critical magnetic field H_{c2} .

2. SUPERCONDUCTIVITY AND POLYMORPHISM IN INTERMETALLIC COMPOUNDS

Intermetallic compounds are usually characterized by their crystal structure. Within the same crystal structure, superconducting as well as nonsuperconducting compounds can be encountered, but some crystal structures are particularly favourable to the occurrence of high T_c superconductors. The most interesting ones are

- the A15 type structure ($T_c = 23$ K for Nb_3Ge /13/)
- the B1 type structure ($T_c = 18$ K for $NbN_{1-x}C_x$ /14/)
- the rhombohedral structure in molybdenum chalcogenides ($T_c = 15$ K for $PbMo_6S_8$ /15/).
- the Pu_2C_6 type structure ($T_c = 17$ K for $Y_{.7}Th_{.3}C_{1.58}$ /16/).

The nature of the correlation between superconductivity and crystal structure is complex and depends on the particular electronic density of states, phonon spectrum and electron-phonon coupling. The influence of the crystal structure on T_c is particularly evident when polymorphic transformations occur, i.e. when the number of electrons per atom, e/a , is constant for both modifications. Unfortunately, no case of a classical order-disorder transformation at equilibrium (involving site exchanges only, as for example in Cu_3Au) has been found up to the present day between two superconducting phases. The only known cases concern the transformation between incommensurable phases, as for example the A2(bcc) and the A15 phases. Several examples for the polymorphism A2 - A15 are listed in Table 2.1. In the three cases $Nb_{.76}Au_{.24}$ /17/, $V_{.76}Au_{.24}$ /18/ and $V_{.75}Ga_{.25}$ /19,20/, the transformation A2 \rightarrow A15 occurs by a congruent solid reaction, while a massive transformation is observed in the case of $Nb_{.78}Al_{.22}$ /21,35/. In the systems Nb-Au, V-Au, V-Ga and Nb-Al, both modifications are equilibrium phases, and the high temperature A2 phase can be obtained by argon jet quenching. This is in contrast to the systems "Nb₃Nb" and "W₃W", where the A15 phase is metastable and must be prepared by sputtering/22/ or by coevaporation/23/.

The values of the electronic heat coefficients, γ , for the modifications $Nb_{.76}Au_{.24}$, $V_{.76}Au_{.24}$ and $Nb_3(Nb_{.92}Ge_{.08})$, the latter being simplified to "Nb₃Nb" are listed in Table 2.1, while specific heat data for the other systems are not available to date. In the known cases, the γ values for the ordered A15 phase exceed those of the disordered one, i.e. the bcc phase, by a factor of 2. Although the change in symmetry also affects the

Compound	Structure	T _c (K)	Ref.	γ (mJ/K ² at-g)	Ref.
Nb ₃ Au ^a	A2	1.2	24	4.8	29
	A15	11	24	8.96	25
V _{0.76} Au _{0.24}	A2	<0.03	18	5.02	25,30
	A15	3.0	3,18	13.09	25
V _{0.75} Ga _{0.25}	A2	2.7	20		
	A15	15.9	26	24.22	25
Nb _{0.78} Al _{0.22} ^b	A2	1.2	27		
	A15	17.0	28		
Mo _{0.40} Tc _{0.60}	A2	12.7	29	6.8	29
	A15	13.2	29	3.3	29
Nb ^c	A2	9.2	32	7.80	34
	A15	5.2	22	4.65	22
W ^d	A2	0.012	33		
	A15	5	23		

Table 2.1. Superconductivity in ordered (A15) and disordered (A2) polymorphic modifications.

^a The stoichiometric composition Nb₃Au is not stable in the system Nb-Au. Very accurate microprobe measurements by R.M. Waterstrat yielded an effective composition Nb_{0.734}Au_{0.236} /31/.

^b In Refs. 28 and 35, it has been shown that the highest solubility of Al in the A2 phase is 22 at.%Al at 1940°C.

^c The A15 phase reported by Stewart et al./22/, referred to as "Nb₃Nb" was found for an alloy containing a slight amount of Ge, 2 at.%, the total composition being Nb₃(Nb_{0.92}Ge_{0.08}).

^d The A15 phase in this system was found to be stabilized by a small amount of oxygen, the formula being W₃(W₀O) /23/.

Debye temperature, Θ_D , the strong difference of T_C between both modifications is generally attributed to changes in the electronic density of states.

The calculated band structures for the A15 and A2 modifications are shown in Figs. 2.1 and 2.2. The main features distinguishing the two density of states curves are essentially independent on the chosen model. The density of states for V_3Au (A15) and Nb_3Au (A15) has recently been calculated by Jarlborg /36/. Comparable band calculations on 3d-5d combinations in the A2 structure are not available, but earlier calculations of Mattheiss /37/ on 5d elements shown in Fig. 2.1 can be used as an approximation, which is justified by the validity of the rigid band model in materials crystallizing in this structure type. This is in contrast to the A15 structure, where the strong localization of d electrons excludes a rigid band approximation. As expected, the Fermi energy E_F for V_3Au (A15) lies at the top of a sharp density of states peak (Fig. 2.2). The corresponding Fermi energy for V_3Au (A2) with $e/a = 4.0$ (counting 1 valence electron for Au, as proposed in Ref. 7, p.547) is situated near to the bottom of a density of states peak (Fig. 2.1) which is markedly broader than for the corresponding V_3Au (A15) phase. There are no other cases than those listed in Table 2.1 where T_C and γ of the A2 and A15 modifications can be compared. Nevertheless, the T_C values for the A2 phase in other V or Nb based systems, e.g. Nb-Sn/7/, V-Ge/38/ or Nb-Ge/38/, extrapolated to stoichiometry, lead to the same result as above: the hypothetical stoichiometric A2 modification would exhibit T_C values which are almost one order of magnitude smaller than for the A15 modification.

A completely different situation is encountered in compounds based on Mo and Cr (with 6 valence electrons). This can be seen in Fig. 2.3, where the T_C values of the A2 phase in different Mo - X systems are extrapolated to compositions where the A15 phase is stable, i.e. 25 at.% Os, 24 at.% Ir, 19.5 at.% Pt, ~ 50 at.% Re and 25 at.% Ge. In contrast to the V and Nb based systems, the polymorphism A2 \rightarrow A15 in Cr and Mo based systems has little effect on the superconducting transition temperature. In systems containing transition elements only, the T_C values of the A2 and the A15 phase are very similar. A particular behavior is observed in Mo systems containing non transition elements, as Mo-Ge or Mo-Si: these are the only known cases where another phase exhibits a higher T_C value than the A15 phase. As shown in Fig. 2.3, the T_C value for the bcc Mo-Ge solid solution reaches 2.2K at ~ 8 at.% Ge/39/, which would extrapolate to ~ 4.8 K at 25 at.% Ge, where the A15 phase exhibits only $T_C = 1.3$ K/39/.

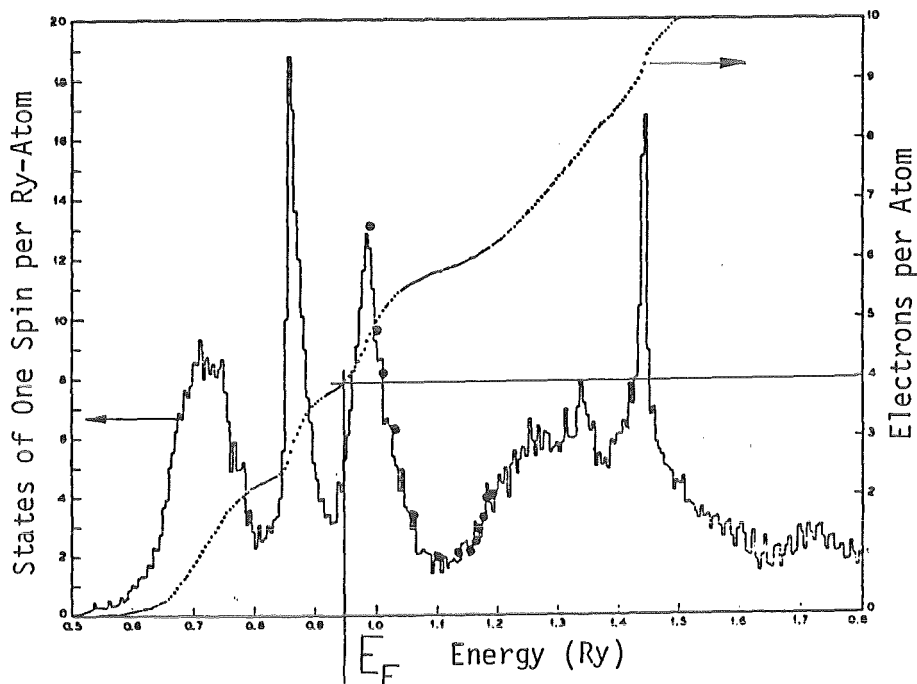


Fig. 2.1. Density of states for W after Mattheiss /36/ and experimental data for superconducting 5d compounds (●) crystallizing in the A2 (bcc) structure after Bucher /40/. The position of E_F for $V_{.75}Au_{.25}$ (bcc modification) has been obtained assuming the validity of the rigid band model and a value of $e/a = 4.0$ (see Ref. /7/).

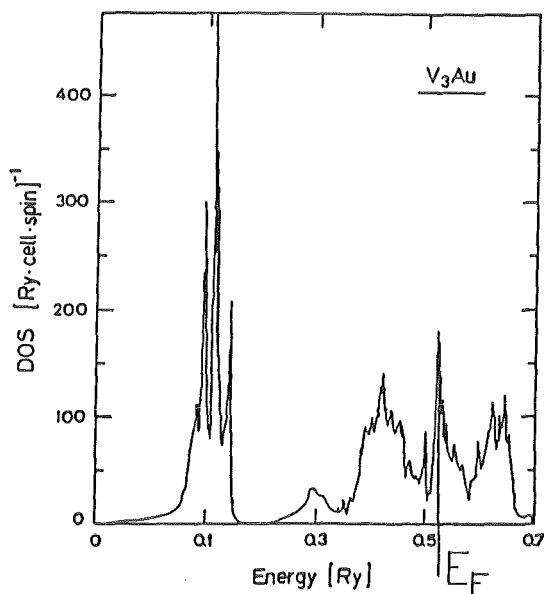


Fig. 2.2. Density of states for V_3Au (A15 modification) after Jarlborg/36/. E_F is close to the top of a sharp peak of the density of states curve.

Ghosh et al./41/ found T_c values of 3.5 K and 5.7 K in sputtered Mo - Ge samples. These authors assigned the lower value to the tetragonal Mo_5Ge_3 phase, but could not determine the origin of the higher T_c value. The question is still open, and three configurations are possible, a highly disordered A15 phase, a metastable A2 phase at 25 at.% Ge (see Fig. 2.3) or an amorphous phase. The particular problem of Mo_3Ge will be treated in Sect. 4.3.6.

Compound	Structure Type	Composition (at.% X)	T_c (K)	Ref.
Mo-Os	A2	15	8.5	7
	A15	25	13.1	7,39
	σ	29	7.3	42,49
	A3	49	6	7,43
Mo-Ir	A2	10	5.4	7
	A15	24	8.7	39,43
	A3	38	6	7
Mo-Re	A2	43	14.2	7
	(A15) ^a	(~ 50) ^a	15	44
	$\chi(\alpha-Mn)$	77	9.89	45
	A3	78	10.0	7
Mo-Tc	A2	~60	12.7	29
	A15	~60	14.7	29,47
	$\chi(\alpha-Mn)$		12	47
	A3	87	14.0	47

Table 2.2. Superconducting transition temperatures of intermetallic phases in the bulk systems Mo-X (X = Os, Ir, Re, Tc), showing that the maximum T_c values of the intermediate phases of these systems are comparable. ^aThe A15 phase in the system Mo-Re is metastable and has been obtained by sputtering /44/.

The case of Mo_3Si is better understood. As shown by Johnson et al. /42/, amorphous Mo-Si exhibits T_c values around 6K, i.e. substantially higher than the value corresponding to the ordered Mo_3Si compound crystallizing in the A15 structure: $T_c = 1.3K$ /39/.

The behavior of T_c in the A2 and A15 phases of Cr and Mo based systems can be generalized to other intermetallic phases. As shown in Table 2.2, the maximum

of T_C for the phases α -Mn, σ or A3 (hcp) is comparable to that of the neighbour phase. An exception to this behavior was reported in the system Mo-Ir, where Sadagopan et al. /48/ found an increase from $T_C = 1.2$ to 8.8K after annealing an as-cast $\text{Mo}_{.50}\text{Ir}_{.50}$ alloy at 1200°C . A careful reexamination of this system

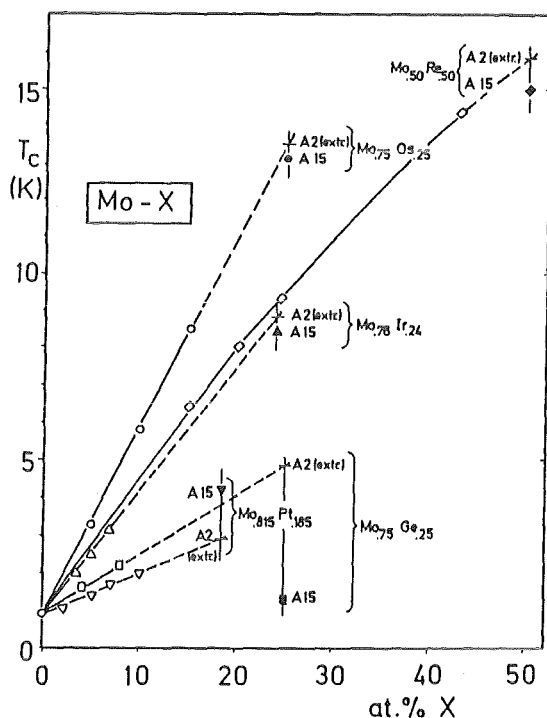


Fig. 2.3. Superconductivity in A2 solid solutions of the systems Mo-Re, Mo-Os, Mo-Ir, Mo-Pt and Mo-Ge. The T_C values of the A2 phase is stable, i.e. 50 at.% Re, 25 at.% Os, 24 at.% Ir, 18.5 at.% Pt and 25 at.% Ge. At these compositions, T_C in both phases is similar, except for Mo-Ge, where it is higher for the A 2 phase (Flükiger /7,39/).

/38/ confirmed the sudden increase of T_C after annealing below 1200°C , but only for nominal Ir contents below 50 at.%. As can be seen from the Mo-Ir phase diagram/51/, this corresponds to the two-phase region A15 + B19. It follows that the high T_C value in Ref. 48 belongs thus in reality to the A15 phase at the composition $\text{Mo}_{.76}\text{Ir}_{.24}$ /39/.

After these remarks, it is not surprising that the value of T_C in the A15 phase of all known Cr and Mo based systems varies very little with composition. From Ref. 7, where the variation of T_C with composition has been plotted for most A15 systems, the largest variation is reported for the system Mo-Pt-Re /39/, with 0.25 K/at.%Mo. This is still one order of magnitude smaller than for the corresponding V and Nb based systems.

There is thus an antagonism between the behavior of V and Nb based compounds on one hand and Cr and Mo compounds on the other hand, not only with respect to the behavior of T_C in different modifications, but also to the correlations between T_C and the electronic density of states, which is very different for both classes of materials /39/. This antagonism also extends to crystallochemical properties, for example to the difference in sign of the deviation from Vegard's law (applied to the atomic volume) /7,50/. It may be recalled that T_C for amorphous Mo alloys is ordinarily higher than in their crystallized state. Amorphous Mo alloys exhibit the highest T_C of amorphous alloys known so far ($T_C = 9K$ for Mo-Ru-Zr /52/). This is in contrast to Nb or V based alloys, for which the amorphous modification has a tendency to lower T_C values with respect to the crystallized state.

The difference between T_C in crystalline and amorphous systems is represented by the plot in Fig.2.4, which was established by Collver and Hammond /52/.

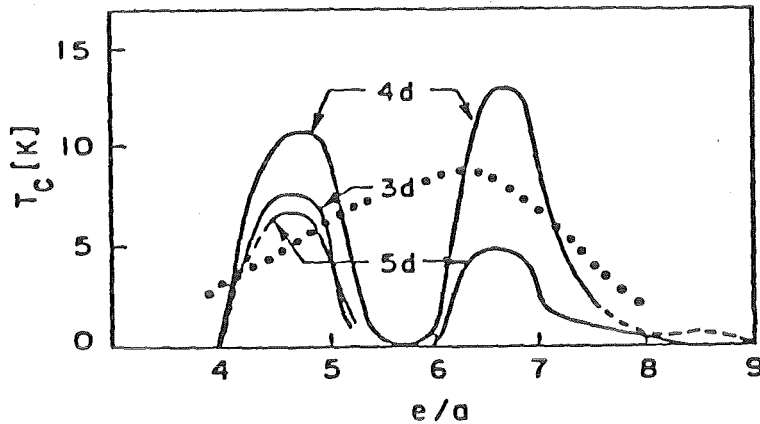


Fig. 2.4. Experimental T_C curves for elements and near neighbour alloys of the 3d, 4d and 5d transition metals. Dotted line for amorphous 4-d. Amorphous Nb ($e/a = 5$ has a lower T_C than in the cubic state, while Mo ($e/a = 6$) shows the opposite behavior (after Collver and Hammond /52/).

It will be shown in Sect. 4 that in addition to the amorphous state, there are other nonequilibrium states of the A15 lattice, produced either by quenching or by irradiation.

3. THE BRAGG-WILLIAMS LONG-RANGE ORDER PARAMETER IN A15 COMPOUNDS

Atomic ordering is a collective phenomenon and is understood as a thermodynamic equilibrium distribution of atoms over the lattice points of the crystal. The order parameter S thus depends on temperature: $S = S(T)$. Theoretically, the order parameter value of A15 compounds at low temperatures would be $S = 1$. However, a certain amount of disorder can be "frozen in" since the cooling process from the melt or from the annealing temperature, T_A , occurs in finite times. The order parameter in a given A15 type compound will thus in general be $S \leq 1$, the deviation from unity depending on the thermal history of the measured sample. Thus, all order parameter measurements performed at room temperature describe in reality a nonequilibrium state. The equilibrium order parameter can only be measured at temperatures above the diffusion limit, T_D , which will be defined later (see Table 4.1).

3.1. Definition of the Bragg-Williams Order Parameter S

The perfectly ordered A15 crystal structure A_3B is described by the space group $Pm\bar{3}n$ with A atoms in 6c sites at $(1/4, 0, 1/2)$ and B atoms in 2a sites at $(0, 0, 0)$. Partial disorder in this structure is introduced by a random site exchange between A and B atoms (Fig. 3.1).

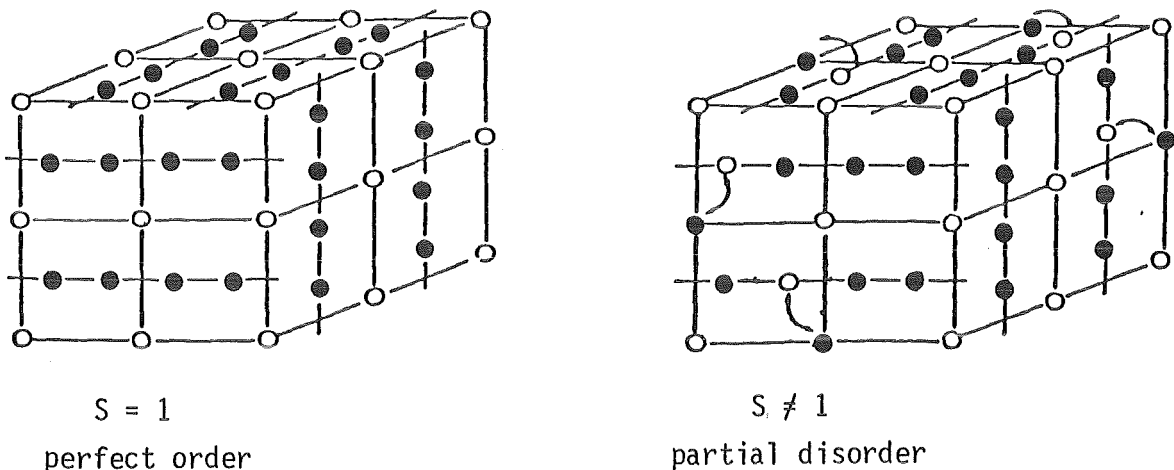


Fig. 3.1. The A15 type structure of a system A_3B with different occupation of the 6c (●) and the 2a (○) sites by the two atomic species.

The degree of atomic ordering in an A_{1-β}B_β type compound of the general formula A_{1-β}B_β can be described in different ways:

- a) the occupation factors, r_a and r_b , where r_a is defined by the fraction of 6c sites (or a sites) occupied by A atoms and r_b by the fraction of 2a sites (b sites) occupied by B atoms, or
- b) the Bragg-Williams order parameters, S_a and S_b for each lattice site, defined by

$$S_a = \frac{r_a - (1-\beta)}{1 - (1-\beta)} = \frac{r_a - (1-\beta)}{\beta} \quad \text{and} \quad S_b = \frac{r_b - \beta}{1 - \beta} \quad (3.1)$$

where r_a is the fraction of a sites occupied by A atoms and r_b the fraction of b sites occupied by B atoms. The parameters S_a and S_b , r_a and r_b are interconnected by the formulas

$$S_b = \frac{3\beta}{1-\beta} S_a \quad \text{and} \quad (3.2)$$

$$r_b = 3r_a - 3 + 4\beta \quad (r_b = 3r_a - 2 \quad \text{for } \beta = 0.25).$$

Thus, the degree of atomic ordering for a given sample at the composition β is sufficiently described by one parameter only, either S_a or S_b . It follows from Eq.(3.2), that $S_a = S_b = S$ at the stoichiometric composition $\beta = 0.25$.

The Bragg-Williams order parameter is defined in such a way that $S = 1$ for the perfectly ordered lattice and $S = 0$ for complete disordering (or random distribution). These two states correspond to $r_a = 1$ (or $r_b = 1$) and $r_a = 0.75$ ($r_b = 0.75$) at the composition β . However, neither S_a or S_b nor r_a or r_b describe the tendency of the different atom species to occupy a certain site. In

5.2.1, a "relative" occupation factor will be used, which is defined by

$$r'_a = \begin{cases} r_a \frac{0.75}{1 - \beta} & \text{for } \beta > 0.25 \\ r_a & \text{for } \beta \leq 0.25 \end{cases} \quad (3.3)$$

$$r'_b = \begin{cases} r_b \frac{0.25}{\beta} & \text{for } \beta < 0.25 \\ r_b & \text{for } \beta \geq 0.25 \end{cases}$$

The relative occupation factors, r'_a and r'_b , relate the fraction of A atoms being effectively on 6c sites to the highest possible concentration of 6c sites which can be occupied by A atoms in a compound of the composition β .

3.2 Experimental Determination of the Long-Range Order Parameter

The long-range order parameter of a crystal structure can be determined by using either by X ray or neutron diffraction. The measured intensities, I_{hkl}^m , are compared with the calculated values, I_{hkl}^c , where

$$I_{hkl}^c \sim n \cdot LP \cdot |F_{hkl}(S)|^2 \cdot \exp B_n, \quad (3.4)$$

by means of a least-square refinement procedure. In this formula, n represents the multiplicity, LP the Lorentz polarization factor, $F_{hkl}(S)$ the structure factor depending implicitly on the order parameter, and B_n is the temperature dependent term.

3.2.1 Thermal and Static Mean Square Amplitudes

The term B_n in Eq. (3.4) is generally called the temperature factor. It is connected with the mean square amplitude of the atomic oscillations around the site n , which is expressed by the coefficient $U_{ij,n}^2$. In the case of harmonic anisotropic vibrations, $U_{ij,n}^2$ is a second rank tensor, which is reduced to the scalar U_n^2 for isotropic conditions. For simplicity, the notation U_n^2 will be used here instead of $\langle U_n^2 \rangle$, the complete notation generally used in the literature. The value of the oscillation amplitude is generally called the root mean square amplitude or the r.m.s. amplitude and will be denoted here as U_n instead of $\langle U_n^2 \rangle^{1/2}$.

For isotropic vibrations, the term B_n can be written as

$$\exp B_n = \exp (-8\pi^2 U_n^2 \sin^2 \theta / \lambda^2), \quad (3.5)$$

where θ is the diffraction angle and λ the wavelength. The quantity $B_n = 8\pi^2 U_n^2$ is ordinarily called the isotropic temperature factor. It is customary in powder diffractometric investigations to define also an "overall" temperature factor, $B = 8\pi^2 U^2$, which constitutes an average over all atoms and their sites. However, the physical meaning of an overall temperature factor is very restricted when comparing to the isotropic temperature factors, B_n , or the anisotropic temperature factors, $B_{ij,n}$.

In the most general case of anisotropic harmonic oscillations, the term B_n in Eq. (3.4) can be written as

$$\begin{aligned} \exp B_n = & (-8\pi^2 [U_{11,n}^2 h^2 + U_{22,n}^2 k^2 + U_{33,n}^2 l^2 + \\ & + 2U_{12,n}^2 hk + 2U_{13,n}^2 hl + 2U_{23,n}^2 kl]) \sin^2 \theta / \lambda^2. \end{aligned} \quad (3.6)$$

The number of coefficients $U_{ij,n}^2$ is reduced for the atoms lying on particular sites. Depending on the quality of the data, the refinement is performed for isotropic or for anisotropic temperature factors. For the A15 structure, the isotropic temperature factors for the A and B atoms on the 6c and 2a sites are named B_a and B_b , respectively. If single crystal refinements are available, the anisotropic temperature factors can also be given. In this case, the anisotropic oscillations around the 6c sites are described by the anisotropic temperature factors B_{11} and B_{22} , the behavior on the 2a sites being assumed as isotropic and being characterized by B_b .

The constraints for the anisotropic vibrations on the site 6c of the A15 structure are:

$$\begin{aligned} U_{11}^2 & \text{ free} \\ U_{22}^2 & = U_{33}^2 \\ U_{12}^2 & = U_{13}^2 = U_{23}^2. \end{aligned} \quad (3.7)$$

The isotropic mean square amplitudes on the 6c sites are obtained by the average:

$$U_a^2 = \frac{1}{3} (U_{11}^2 + 2U_{22}^2) = \frac{1}{24\pi^2} (B_{11} + 2B_{22}). \quad (3.8)$$

From the values of U^2 , it is possible to calculate the Debye temperature, according to the equation

$$\theta_X = \frac{1}{U^2} \frac{3 h^2}{4 \pi^2 M} T \left\{ \phi(x) + \frac{x}{4} \right\} \quad (3.9)$$

where U^2 is the mean square vibrational amplitude, $h = 6.6262 \times 10^{-34}$ Js, $k = 1.38062 \times 10^{-23}$ JK⁻¹, M the atomic mass and $x = \theta/T$. The function $\phi(x) = 1/x \int_0^x \xi / (e^\xi - 1) d\xi$ is tabulated in Table 5.2.2B of the International Tables of Crystallography. The Debye temperature obtained by diffractometry is denoted here by θ_X in contrast to θ_D , the Debye temperature derived from calorimetric measurements, where $\theta_D(0)$ and $\theta_D(300)$ stay for the values at $T = 0$ (obtained by extrapolation) and at 300 K (see 6.1.3).

Beside the coefficients $U_{ij,n}^2$ representing the mean square thermal vibration amplitudes (dynamic displacements from the equilibrium lattice sites), other coefficients will be defined in 3.2.2 for describing static displacements, occurring after high energy irradiation provided that the irradiation temperature T_{irr} is low enough. In analogy to U_{ij}^2 , the static mean square amplitudes are denoted here by u^2 , the rms static amplitude by u (instead of the notations $\langle u^2 \rangle$ and $\langle u^2 \rangle^{1/2}$, respectively, used in the literature /54,55/). The total displacement in an irradiated crystal can be approximated by the sum of thermal and static displacements:

$$U_{tot}^2 = U^2 + u^2 \quad (3.10)$$

3.2.2 Least Square Refinement Procedure

The structure factor for a perfectly ordered, stoichiometric A15 type compound A_3B can be written as

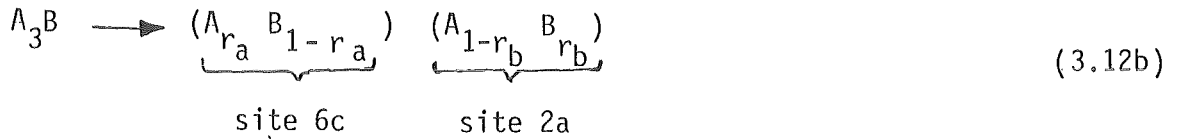
$$\left. \begin{aligned} F_{hkl} &= f_B \left| 1 + \cos 2\pi \left(\frac{h+k+l}{4} \right) \right| + \\ &+ 2f_A \left| \cos 2\pi \left(\frac{l}{2} + \frac{h}{4} \right) + \cos 2\pi \left(\frac{h}{2} + \frac{k}{4} \right) + \cos 2\pi \left(\frac{k}{2} + \frac{l}{4} \right) \right| \end{aligned} \right\} \quad (3.11)$$

In Eq. (3.11), f_A and f_B represent the scattering factors for A and B atoms lying on the 6c and 2a sites, respectively. The A15 type structure for both perfect order ($S = 1$) and partial disorder ($S \neq 1$) is schematically represented in Fig. 3.1.

If deviations from perfect order or from ideal stoichiometry are introduced, the form factors f_A and f_B for the atoms A and B have to be replaced by the effective form factors of the averages at the 6c and 2a sites, which will be called f_a and f_b , respectively. For a disordered A15 structure with ideal stoichiometry, there is:

$$\begin{aligned} f_a &= r_a f_A + (1-r_a) f_B \\ f_b &= (1-r_b) f_A + r_b f_B \end{aligned} \quad (3.12a)$$

i.e. the formula A_3B is generalized to

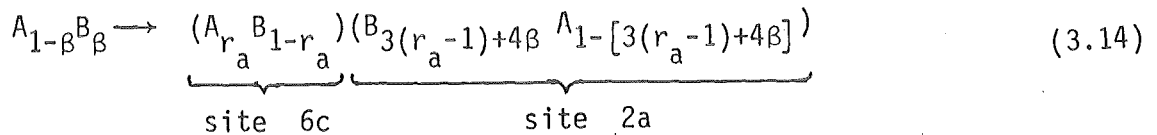


Calculated structure factors for different hkl are listed in Table 3.3.

For the general case of a disordered nonstoichiometric A15 structure, the structure formula becomes



or using (3.3):



The least-square refinement of the integrated measured intensities I_{hkl}^m can now be carried out with the occupation factor r_a the temperature factor B and an instrumental scale factor as variable parameters.

For an A15 single crystal with a very narrow compositional distribution, the chemical composition, β , can be introduced as a supplementary variable in the crystallographical refinement process. For powder samples, however, (polycrystalline samples have to be treated as powders), the number of measured peaks is much lower, the number of variables has thus to be kept as low as possible. Under these conditions, it is preferable to determine the chemical composition by another method, keeping β fixed during the refinement process. The precision in determining the chemical composition has a strong influence on the absolute value of the order parameter. The compound Nb_3Al is

a case where difficulties in determining the precise composition have led to erroneous conclusions about the absolute value of S . This case will be discussed in Section 5.

The criterion for the refinement of the structure parameters is a minimum in the conventional agreement factors R and R_w when comparing observed and calculated integrated intensities. These factors are defined by:

$$R = \frac{\sum |I_{hkl}^m - I_{hkl}^c|^2}{\sum I_{hkl}^m} \quad , \text{ and} \quad (3.15)$$

$$R_w = \frac{\sum \frac{1}{\sigma_{hkl}^2} (I_{hkl}^m - I_{hkl}^c)^2}{\sum \frac{1}{\sigma_{hkl}^2} I_{hkl}^m} \quad (3.16)$$

where $\frac{1}{\sigma_{hkl}^2}$ is the observed standard deviation.

For well-defined, homogeneous powder samples where the difference between the atomic numbers of the two constituting elements is $\Delta Z \geq 8$, this refinement method yields absolute values of S with an uncertainty of $\Delta S = \pm 0.02$. All proceeding steps in determining S described in this paragraph are equally valid for both X ray and neutron diffraction. Some characteristic differences between these two diffraction sources are discussed in detail in 3.3, where all factors influencing the experimental determination of the order parameter are discussed.

3.2.3. Determination of S on Irradiated Thin Films

If the sample is only available in a film geometry, texturing renders the refinement procedures extremely difficult: at present, the problem of determining an absolute value of S on this film samples has not been rigorously solved. For the special case where the relative change of S has to be measured on the same film, as for example after consecutive irradiations, it has been shown by Linker/54/ that a quantitative determination of the order parameter variation is possible, provided that the absolute value of the initial order parameter S_0 is known, e.g. from diffractometric measurements on bulk samples. This procedure, first applied on Nb_3Al films /55/ is valid under the assumption that the dynamic behavior of the crystal remains essentially unaffected by irradiation and will now be briefly described.

The diffraction lines are subdivided in four different groups where the structure factor, $F(hkl)$, depends on the same way on S and on the form factors f_A and f_B (see Table 3.3):

$$\begin{aligned}
 h + k + l = 2n: & \quad 1) F(hkl) = 2S(f_B - f_A) \\
 h + k + l = 2n+1: & \quad \begin{cases} 2) F(hkl) = S(f_B - f_A) + (3f_A + f_B) \\ 3) F(hkl) = S(f_B - f_A) - (3f_A + f_B) \end{cases} \\
 h + k + l = 4n: & \quad 4) F(hkl) = 2(3f_A + f_B)
 \end{aligned} \tag{3.17}$$

The data are analyzed in terms of a modified Wilson plot, where the logarithm of the intensity ratio $I(\phi t)/I_0$ is plotted against $\sin^2\theta/\lambda^2$, where I_0 and $I(\phi t)$ are the intensities of a particular line before and after irradiation, λ the wavelength and θ the scattering angle. Linker /54/ assumed that the decrease of the X ray line intensity as a consequence of statistically distributed static displacements can be described by means of a modified temperature dependent term in Eq. 3.4. Under the condition that the dynamic behavior of the solid is not influenced by static displacements, the term B_n can be written as a sum of a thermal and a radiation induced component:

$$\begin{aligned}
 B_n &= B_n(U_n^2) + B_n(u^2) \\
 &= -8\pi^2 \sin^2\theta/\lambda^2 (U_n^2 + u_n^2)
 \end{aligned} \tag{3.18}$$

Since U_n^2 is assumed to be unchanged after irradiation, only the term u_n^2 figures in the quotient $I(\phi t)/I_0$ and can be determined by a Wilson plot. For group 1 in Eq. (3.17), the superstructure group, it is

$$\begin{aligned}
 \ln|I(\phi t)/I_0| &= \\
 &= -16 \pi^2 (\sin^2\theta/\lambda^2) \cdot u^2 + 2 \ln (S_a/S_{a0}) + \ln c
 \end{aligned} \tag{3.19}$$

where u^2 is the mean square displacement amplitude (see 4.3.3) of the atoms perpendicular to the reflecting planes, S_{a0} and S_a the order parameters on the 6c sites before and after irradiation and c a constant including the volume of the material contributing to X ray scattering. The static mean square

displacement amplitude, u^2 , can be determined from the slope of a straight line by least square fits of the representation $I(\phi t)/I_0$ vs. $\sin^2\theta/\lambda^2$.

From the intersection of the straight line with the axis, one obtains the quantity $2 \cdot \ln(S_a/S_{a0}) + \ln c$, from which S_a can be determined. As pointed out by Schneider et al./55/, $\ln c$ contributes only if parts of the material are either removed by sputtering or rendered amorphous by radiation damage. Such a contribution can be detected by comparing the axial section values $2 \ln(S_a/S_{a0}) + \ln c$ for the data points of group 2 and 3 reflections, which should be approximately equal and of opposite sign if $\ln c = 0$. This test was used in Ref. 55 for detecting the possible creation of amorphous regions during irradiation.

3.3 Factors Influencing the Determination of S

The various factors influencing the determination of the order parameters can be subdivided in two main groups. A first group is formed by the systematic factors, i.e. the calculation of the X ray form factor, the neutron scattering amplitude, the anomalous dispersion correction and the choice of source and wavelength. The second group concerns the metallurgical state of the analyzed sample, which includes the presence of additional phases, homogeneity in composition, residual stresses, thermal history and/or irradiation history. A very important difficulty may arise from the presence of preferential orientations.

3.3.1 Systematic Factors

3.3.1.1 The Atomic Scattering Factor

The most important criterion for the accurate determination of the order parameter is the relative intensity of the A15 superstructure lines, represented by the terms $n \cdot S(f_B - f_A)$ in Table 3.3, where $n = 0, 1, 2 \dots$

hkl	S Contribution to F	hkl	S Contribution to F
110	$2S(f_B - f_A)$	420	$S(f_B - f_A) + (3f_A + f_B)$
200	$S(f_B - f_A) + (3f_A + f_B)$	421	$S(f_B - f_A) - (3f_A + f_B)$
210	$S(f_B - f_A) - (3f_A + f_B)$	332	$S(f_B - f_A) + (3f_A + f_B)$
211	$S(f_B - f_A) + (3f_A + f_B)$	422	$2S(f_B - f_A)$
220	$2S(f_B - f_A)$	510,431	$2S(f_B - f_A)$
310	$2S(f_B - f_A)$	520,432	$S(f_A - f_B) + (3f_A + f_B)$
222	$3S(f_B - f_A) - (3f_A + f_B)$	521	$S(f_B - f_A) + (3f_A + f_B)$
320	$S(f_A - f_B) + (3f_A + f_B)$	440	$2(3f_A + f_B)$
321	$S(f_B - f_A) + (3f_A + f_B)$	530,433	$2S(f_B - f_A)$
400	$2(3f_A + f_B)$	600,442	$S(f_B - f_A) + (3f_A + f_B)$
411,330	$2S(f_B - f_A)$	610	$S(f_B - f_A) - (3f_A + f_B)$
		611,532	$S(f_B - f_A) + (3f_A + f_B)$

Table 3.3. Contribution of the long-range order parameter, S, to the structure factor, F, for stoichiometric compounds of the A15 structure. The factors f_A and f_B represent either the X ray form factor or the elastic neutron scattering amplitude.

It is obvious that if f_B approaches f_A , the determination of the order parameter becomes more and more uncertain, the intensity of the superstructure lines tending to zero. The magnitude of $(f_B - f_A)$ will thus decide if X ray or neutron diffraction is the appropriate experimental method. The latter is more favourable to ordering studies of compounds containing appreciable quantities of vanadium, which has a particular behavior with respect to elastic neutron scattering. This is demonstrated in Fig. 3.2, which compares the X ray and the neutron diffraction patterns of $V_3Ga/20/$, for

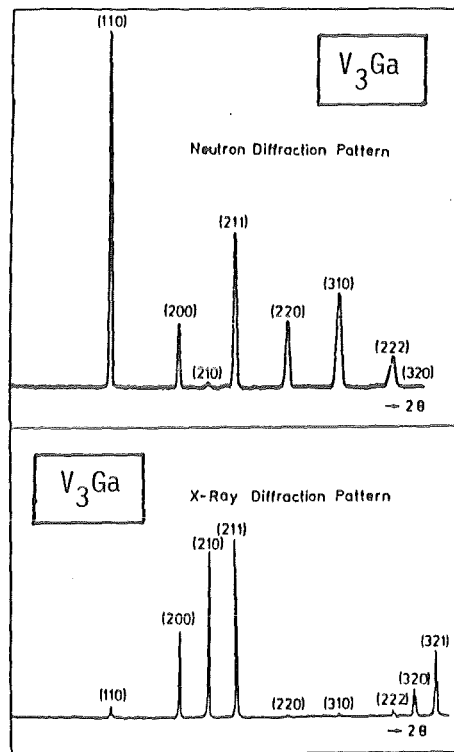


Fig. 3.2. Comparison between neutron ($\lambda = 0.2319 \text{ nm}$) and X ray (MoK_{α} , $\lambda = 0.07093 \text{ nm}$) diffraction patterns for V_3Ga (after Flükiger et al. /20/). Note: The scales of 2θ have been adjusted in order to allow direct comparison for each peak.

which the neutron scattering amplitudes are $b_V = - 0.05 \times 10^{-14} \text{ m}$ and $b_{\text{Ga}} = + 0.72 \times 10^{-14} \text{ m/56/}$. It is seen that the intensity of the superlattice lines is drastically enhanced in the neutron case. The corresponding variation of the calculated intensity ratio between a superlattice line and a fundamental line, I_{110}^C/I_{211}^C , in the system V_3Ga /20/ with $\beta = 0.25$ has been represented in Fig. 3.3. as a function of the occupation number, $r_a = 1/4(S_a + 3)$.

It follows that for V_3Ga , $\Delta S = \pm 0.03$ represents a limit for an accurate determination of S by X ray diffraction: In the following, the S value as determined by neutron diffraction/20/ will thus be quoted. Some cases are even more unfavourable than V_3Ga . As shown by Waterstrat and Dickens/57/, neutron diffraction is the only way to determine accurate values of S in the systems V_3Ni and V_3Co , where the difference in atomic number is $\Delta Z = 4$ and 5 , respectively, and therefore $(f_B - f_A)$ is small. The inverse situation is en-

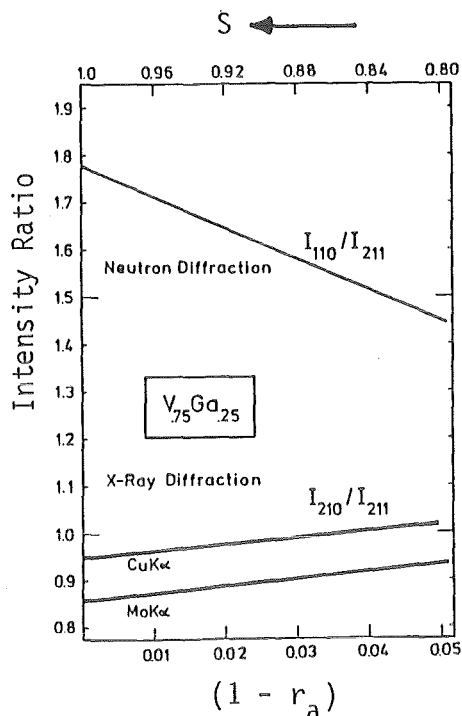


Fig. 3.3. Variation of the calculated intensity ratios between a superlattice line and a fundamental line, I_{110}^C/I_{211}^C , in V_3Ga for X ray and neutron diffraction as a function of the order parameter and of the occupation factor, $r_a = 1/4(S_a + 3)$ /Flükiger et al./20/).

countered in Nb_3Sn , where the neutron scattering amplitudes for Nb and Sn are nearly identical /56/. Here determination of the order parameter is only possible by means of X rays. However, the situation is still not ideal, since ΔZ between Nb and Sn is only 9. A recent determination of S in Nb_3Sn /12/ will be discussed in Section 5.

The most frequently used values of the atomic form factors as a function of $\sin\theta/\lambda$ are those calculated by Cromer et al./58/ on the basis of Hartree-Fock wave functions. Fukamachi/59/ calculated the isolated atom form factor of several elements using Clementi's Hartree-Fock quality atom wave functions. The calculation with both sets of values/58,59/ for V_3Ga with $\Delta Z = 8$ did, however, not show significant differences in S /20/. This problem is less pronounced for the neutron diffraction case, where the elastic scattering amplitude, b, does not depend on $\sin\theta/\lambda$.

3.3.1.2. The Anomalous Dispersion Correction

As well in the X ray as in the neutron diffraction case, the factors f are real functions if the wavelength λ of the incident beam is significantly different from the wavelength λ_K of the K absorption edge for an atom of the scattering material. If, however, $\lambda \approx \lambda_K$, there is an interaction leading to a frequency dependence of the absorption coefficient. This effect, the anomalous dispersion, can be expressed analytically by introducing an imaginary term and a small real term in the atomic scattering factor. The X ray scattering factor for an atom A becomes

$$f_A = f_{A_0} + f'_A + i f''_A \quad (3.20)$$

where f'_A and f''_A are the real and imaginary dispersion correction, calculated by Cromer/60/, to be found in the "International Tables for Crystallography", Volume IV. As first shown by Jones and Sykes/61/, it is possible to use anomalous dispersion for increasing the relative intensity of superlattice lines, thus considerably diminishing the error in the determination of S in compounds with similar atomic numbers. For this purpose, an X ray radiation with a wave length as close as possible to that of the K absorption edge of an atom of the scattering material is used. Taking $S = 1$ in Table 3.3, the intensity ratio between a superlattice and a fundamental line becomes

$$\frac{I_{110}}{I_{211}} = \frac{|F_{110}|^2}{|F_{211}|^2} = \frac{|f_B - f_A|^2}{|f_B + f_A|^2} \quad (3.21)$$

In the cases where $|f_{B_0} - f_{A_0}|$ is small, the term $|f_B - f_A|$ can be enhanced by the appropriate anomalous dispersion correction terms f' and f'' . The effect of anomalous dispersion for CuK_α and MoK_α radiation in V_3Ga is shown in Fig. 3.3. Another example is Nb_3Sn , where for $S = 1$ the choice of MoK_α radiation instead of CuK_α radiation increases the ratio I_{110}/I_{211} by a factor of 1.4 to a value of 0.039. This ratio is still low, but allows a reason-

ably accurate determination of the order parameter S in Nb_3Sn . Anomalous dispersion corrections have not to be considered in neutron diffraction experiments on A15 compounds, since the few isotopes with complex scattering factors, i.e. ^{10}B , ^{113}Cd , ^{149}Sm or ^{157}Gd do not form compounds of this structure.

3.3.2. The Metallurgical State of the Sample

3.3.2.1. Homogenization Heat Treatments

The ideal conditions for order parameter determination are given by 100% single phase samples with a very narrow composition distribution. These conditions are difficult to be achieved, but can be approximated by long homogenization heat treatments at high temperature. In order to find the appropriate homogenization and cooling conditions, a precise knowledge of the A15 phase field is necessary, in particular at high temperatures /7/. Typical homogenization conditions for obtaining single phase samples for several A15 compounds are listed in Table 3.4, together with the appropriate cooling conditions. The data in Table 3.4 result from practical experience with each compound. Most of them can be extracted from Refs. 7,26,39,62, a small part deriving from own unpublished data/38/. In Table 3.4, "single phase" A15 samples are characterized as containing less than 2 vol.% foreign phases, detected by microscopical observation. The determination of small amounts of additional phases by optical means is more reliable than by X ray diffraction, in particular if these phases are ductile, e.g. bcc Nb, V or Mo. In this case, the plastic deformation during the crushing process leads to serious line broadening, thus rendering the detection of faint lines quite difficult. Of course, this effect can in principle be eliminated by "flash-annealing" /7,79/ of the powders prior to the diffraction experiments. In practice, however, this procedure is not often used, mainly because of the risk of oxydation or reaction with the container material.

Compound	Composition β	Homogenization Heat Treatment	Argon Pressure (atm)	Cooling Mode
V ₃ Co	0.25	48 h/1500°C + 2 weeks/950°C		
V ₃ Ni	0.27	48 h/1500°C + 1 month/800°C		
V ₃ Pd	0.22	48 h/1500°C + 1 month/700°C		
V ₃ Rh	0.16 to 0.25	48 h/1600°C		
VOs	0.48 to 0.51	48 h/1800°C		Q(T>1600°C)
V ₃ Pt	0.19 to 0.32	48 h/1700°C		
V ₃ Ir	0.25 to 0.37	48 h/1700°C		
V ₃ Au	0.20 to 0.24	48 h/1400°C + 1 week/1200°C	>1	
V ₃ Si	0.22 to 0.25	>48 h/1800°C		
V ₃ Ge	0.235	48 h/1650°C	>1	
V ₃ Ga	0.22 to 0.28	48 h/1450°C + 48 h/1250°C	>1	
	$\beta < 0.22$; $\beta > 0.28$	48 h/1450°C + 100 h/1000°C	>1	R($\beta > 0.25$)
Nb ₃ Rh	0.25	>48 h/1800°C + 1 month/1200°C		
Nb ₃ Os	0.26 to 0.29	>48 h/1800°C		
Nb ₃ Ir	0.22 to 0.28	>48 h/1800°C		
Nb ₃ Pt	0.20 to 0.28	>48 h/1800°C		
Nb ₃ Au	0.20 to 0.24	>48 h/1650°C	>1	
Nb ₃ Al	0.21 to 0.23	>48 h/1900°C	>1	
Nb ₃ Ge	0.23 to 0.24	>48 h/1800°C	>1	Q($\beta > 0.24$)
	0.20 to 0.23	>48 h/1700°C	>1	Q($\beta > 0.23$)
Nb ₃ Sn	0.20 to 0.24	48 h/1800°C	1	
	$\beta > 0.24$	>48 h/1500°C + 2 weeks/1050°C	>1	
Mo ₃ Os	0.25	48 h/2000°C		
Mo ₃ Ir	0.22 to 0.24	48 h/1800°C		
Mo ₃ Pt	0.185	48 h/1600°C		R(T>1600°C)
Mo ₃ Si	0.23 to 0.25	48 h/1600°C		
Cr ₃ Ru	0.28	48 h/1450°C + 1 month/750°C	>1	
Cr ₃ Rh	0.22	48 h/1400°C + 2 weeks/1200°C	>1	
Cr ₃ Os	0.26 to 0.28	48 h/1350°C	>1	
Cr ₃ Ir	0.18 to 0.26	48 h/1500°C	>1	
Cr ₃ Pt	0.18 to 0.23	48 h/1450°C	>1	
Cr ₃ Si	0.22 to 0.28	48 h/1600°C	>1	
Ti ₃ Au	0.25	48 h/1300°C	>1	
Ti ₃ Pt	0.23 to 0.27	48 h/1200°C		
Ti ₃ Ir	0.25 to 0.27	48 h/1400°C		

Table 3.2. Homogenization heat treatments and cooling conditions required for obtaining single-phase samples of different A15 type compounds, i.e. samples containing less than 2 vol.% foreign phases. The compounds or compositions not listed here could not be produced single-phased. Argon pressure or cooling mode are only indicated when necessary (Q = argon jet quenching, R = radiation quench). (Refs. 7, 10, 18, 19, 28, 38, 39, 62, 76).

The effective concentration profile of an alloy is usually measured by electron probe analysis, by Auger spectroscopy or by secondary ion mass spectroscopy (SIMS). In superconducting compounds, the global distribution of compositions can be measured by an additional method, i.e. the observation of the calorimetrically measured superconducting transition. The width and the shape of the latter are excellent indicators for the composition distribution in the sample, provided that the variation of T_C with composition is known. This is not a serious restriction since T_C vs. β is known for all known compounds with appreciably high T_C /7/. The consequences of homogenization on the compositional profile of Mo_3O_s and Nb_3Al can be seen in Figs. 3.4 and 3.5. Figure 3.4. shows the specific heat curves of the same Mo_3O_s sample after heat treatments of 1 hour at $1770^\circ C$ and after 20 hours at $1800^\circ C$ /7,63/, respectively. The longer heat treatment at the higher temperature reduces the

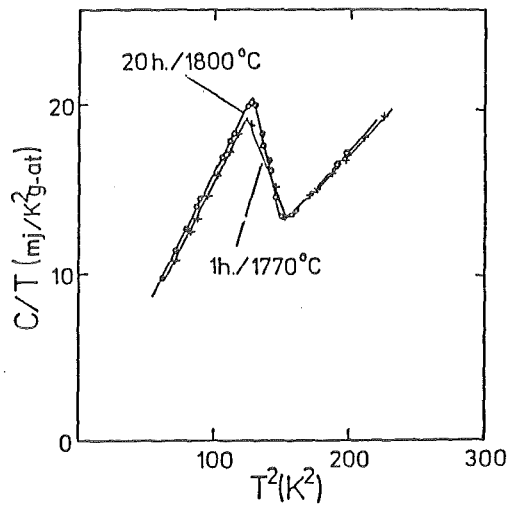


Fig. 3.4. Different states of homogenization for Mo_3O_s revealed by specific heat measurements at the superconducting transition (Flükiger /7/).

total width of the superconducting transition from 1.50 to 1.05K, the value of T_c (midpoint) being slightly increased from 11.70 to 11.85K. At the same time, the height of the specific heat jump is increased by 20%. This point is important: in virtue of the correlation between T_c and the composition β specific heat curves of inhomogeneous alloys are always characterized by broad transitions at T_c .

An even stronger effect is observed after homogenizing Nb-Al alloys, where the variation T_c vs. β is more pronounced than in Mo_3Os /28,39/. Figure 3.5. shows specific heat curves for two different samples, the first one corresponding to an effective Al content of 24 at.% /64/ and annealed 5 days at $750^\circ C$ (without homogenization heat treatment), the second one to an effective Al content of 23.1 at.% after a homogenization heat treatment of 48 hours at $1850^\circ C$ under an argon pressure of 4 atmospheres /28/. Comparison shows that the transition width is reduced from 1.5K to 0.7K after the homogenization heat treatment. At the same time, the height of the jump in specific heat at T_c of the homogenized sample is doubled in spite of its lower T_c value. The homogenization effects on the specific heat curves in Figs. 3.4 and 3.5 have also an influence on the quantitative analysis. Indeed, the size of the specific heat discontinuity is typically represented by $(C_s - C_n)/C_n$ at T_c or $\Delta C/\gamma T_c$, and is a measure of the electron-phonon coupling. It is obvious that for a broad superconducting transition the value ΔC (peak of the transition minus the normal state extrapolation at the peak temperature) will be lower than for a narrower transition.

3.3.2.2. The Presence of Additional Phases

There are many reasons for the presence of additional phases. Some A15 compounds, as Nb_3Al , Nb_3Ge , Nb_3Ga , ... have temperature-dependent phase limits, the stoichiometric composition being, if at all, only stable at high temperatures. Compositions close to stoichiometry ($\beta = 0.25$) have thus to be

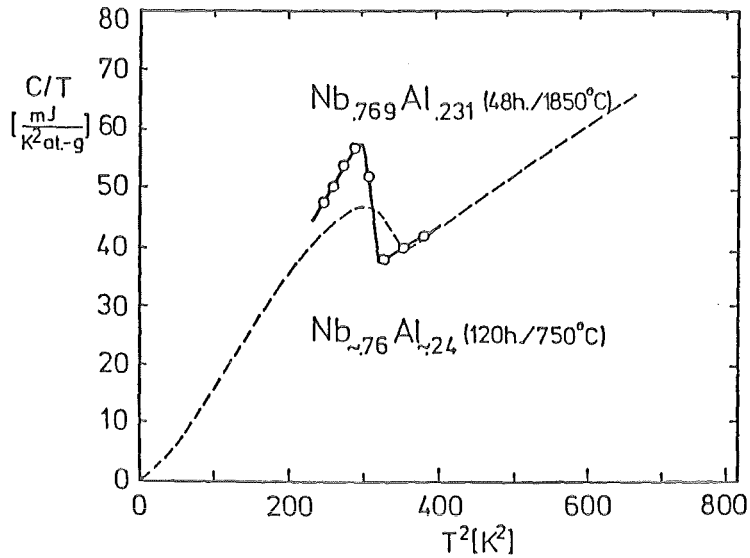


Fig. 3.5. Effect of the homogenization heat treatment on Nb_3Al revealed by specific heat measurements. The alloy with the effective composition $Nb_{0.769}Al_{0.231}$ has been homogenized 48 hours at $1850^{\circ}C$; the alloy $Nb_{0.76}Al_{0.24}$ (nominal composition $Nb_{0.75}Al_{0.25}$) was heat-treated for only 5 days at $750^{\circ}C$ and shows a wide transition (Flükiger /7/).

prepared by non-equilibrium methods, i.e. rapid quenching techniques, CVD or PVD (evaporation, sputtering). These procedures lead in some cases to the presence of small amounts of neighbouring phases, e.g. $bcc(Nb)$, $\sigma(Nb_2Al)$, $D_{8b}(Nb_5Ge_3)$ or others. Other compounds, as V_3Ga /20/ or Nb_3Ga /65/ have the tendency to pick up oxygen during the melting process. This leads to the formation of small amounts of oxygen stabilized phases, i.e. V_3GaO_x /20,66/, or Nb_3GaO_x /65/. A determination of the order parameter can in principle be performed even if additional phases are present, provided that their respective crystal structures are known. The corresponding spectra can be refined and

subtracted from A15 diffraction pattern. However, a possible lap with A15 superstructure lines would lead to seriously enhanced error limits, these lines having usually unfavourable peak/background ratios and thus a poor counting statistics. Another cause influencing the precision of the order parameter determination is the presence of unrecognized, small amounts of additional phases, which alter the background intensity of superlattice lines.

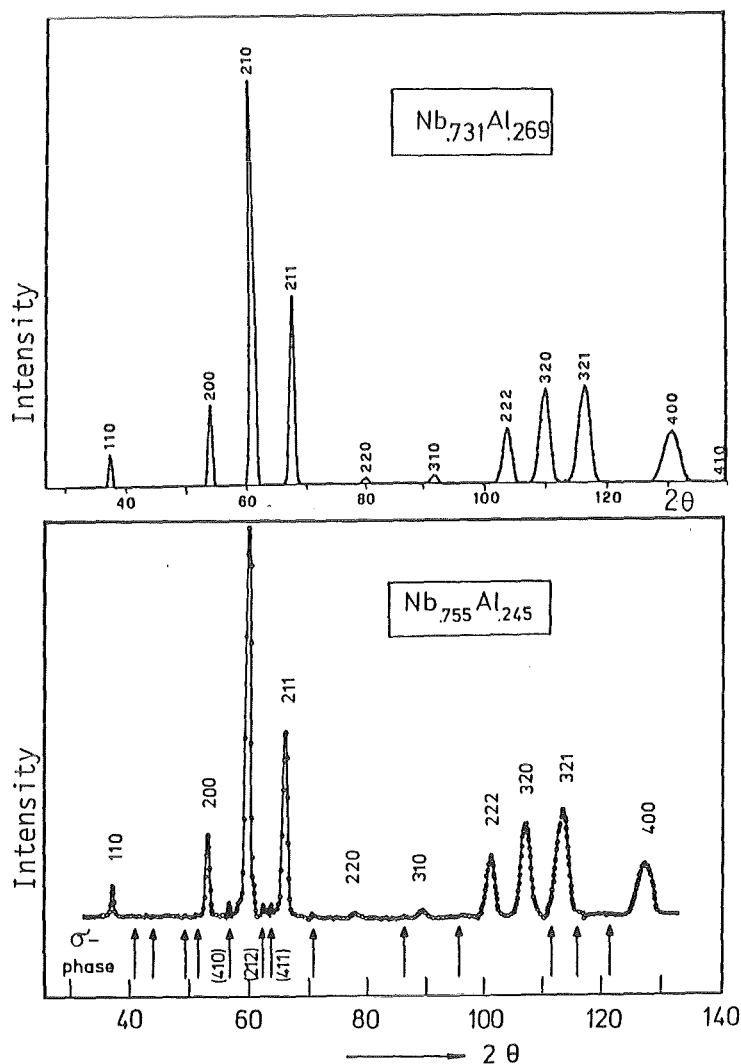


Fig. 3.6. Neutron diffraction patterns ($\lambda = 0.263$ nm) for $Nb_{1-\beta}Al_{\beta}$ compounds with effective Al contents in the A15 phase of 23.1 and 24.5 at.%, homogenized 48 hours at $1850^{\circ}C$ and radiation quenched. Due to the temperature dependent Al rich phase boundary, a small volume fraction of Nb_2Al phase (peaks indicated by arrows) is formed on cooling in the compound with the higher Al content (Flükiger et al. /28/).

An example where the order parameter of the A15 phase can be accurately determined in spite of a second phase is the system Nb_3Al . The neutron diffraction pattern of the alloy $\text{Nb}_{.769}\text{Al}_{.231}$ shown in Fig. 3.6 shows no trace of additional lines, while ~5 vol.% Nb_2Al phase can be detected in a sample of the nominal composition $\text{Nb}_{.75}\text{Al}_{.25}$ (effective Al content in the A15 phase: 24.5 at.% /28/).

In the system Nb - Ge, it is particularly difficult to obtain single phase samples of the A15 structure at compositions close to stoichiometry. This is due to a) the strongly temperature dependent Ge rich phase boundary /67/ and b) to the extremely rapid formation of Nb_5Ge_3 precipitations during the cooling process. Fig. 3.7 illustrates the difficult conditions for the order parameter determination encountered by Sweedler et al. /68,69/ on a CVD Nb_3Ge sample. The X ray pattern, taken after removing the substrate and

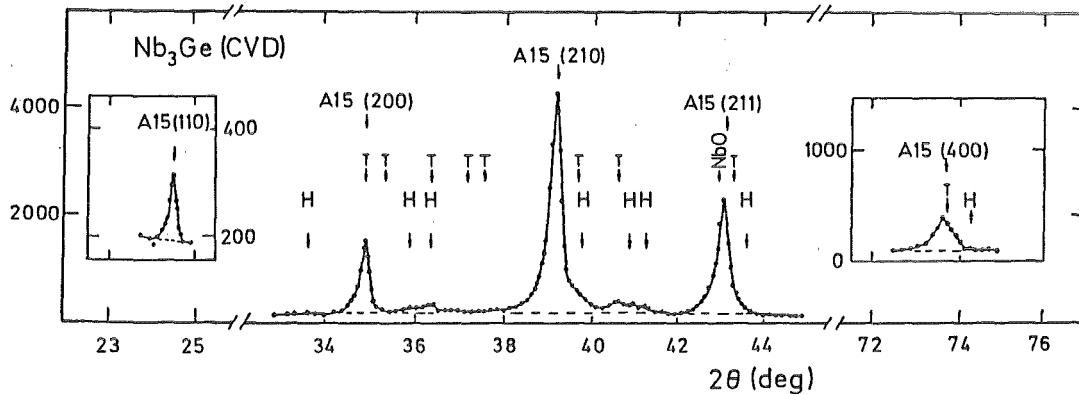


Fig. 3.7. X ray ($\text{CuK}\alpha$) diffraction pattern for Nb_3Ge as produced by CVD. The reflections are identified as A15, hexagonal (H) and tetragonal Nb_5Ge_3 (T) and NbO. (Sweedler et al. /68,69/).

crushing the deposited Nb_3Ge to powders, shows the presence of several additional phases as Nb_5Ge_3 , NbO and the oxygen stabilized modification Nb_3Ge_2 /68/. Due to the rather complex pattern it is even possible that small amounts of other unidentified phases are present, contributing to the background only. It is obvious that the determination of the order parameter from such complex

diffraction patterns will lead to large uncertainties in S . However, no better Nb_3Ge samples close to stoichiometry are available in sufficient quantity allowing order parameter determination. Another preparation technique, coevaporation, yields Nb_3Ge films with considerably improved homogeneity /73,74/, but the film geometry is not suitable for direct order parameter determinations, due to preferred orientations as shown in the following.

3.3.2.3. Preferred Orientations

It follows from several investigations /4,18,20,62/ that the difficulty of completely removing preferred orientations is a major factor limiting the accuracy of the order parameter. The occurrence of preferred orientations can be checked by establishing the intensity ratios of the reflection pairs for which the long-range order contribution to the structure factor is identical (Table 3.1): I_{200}/I_{211} , I_{420}/I_{211} , I_{332}/I_{211} ,... (I_{211} corresponds to the highest intensity). Ordinarily, these ratios can be brought closer to the calculated values by repeated crushing and repacking of the powders, the final size being of the order of $10\mu m$, smaller sizes leading to line broadening. The problem of preferred orientations is a consequence of the operations producing a flat surface, and is characteristic for X ray diffraction while it is still negligible in neutron diffraction experiments. As mentioned in 3.2.2, thin film samples prepared by CVD or PVD techniques generally show textured growth with preferred orientations obtained by homoepitaxy. It should be added that the texturing can also lead to large errors in the determination of second phase contents in thin film samples. All these reasons explain why the determination of order parameters in thin films has so far only been possible by the indirect method of Linker et al. /54,55/, which still requires the knowledge of S_0 as determined by a complete refinement on a sample having random grain orientations.

3.4. Indirect Determination of the Order Parameter, S

The diffraction experiments described in the preceding section are a direct way to determine absolute values of the atomic order parameter in A15 compounds. If a change in the degree of ordering is caused by fast neutron irradiation, the order parameter $S(\phi t)$ corresponding to the irradiation dose ϕt can in principle be obtained indirectly by using the Aronin formula /71/

$$S(\phi t) = S_0 \exp(-k\phi t), \quad (3.22)$$

where k depends on the type of projectile and its energy and S_0 is the order

parameter prior to irradiation, which has to be determined by diffraction methods.

Equation (3.22) was derived for fast neutron irradiation of the ordered compounds Cu_3Au and Ni_3Mn , using simple theoretical considerations /71/. The parameter k in Eq. (3.22) is related to random replacements due to irradiation and is independent of the degree of ordering. It can be calculated by making some assumptions on the average number of displaced atoms, the threshold energy for atomic displacement and the kinetic energy of the primary knock-on-atom, by using the models developed by Kinchin and Pease/72/ and Dienes and Vineyard/129/, which were later modified by Sigmund/116/ and Norgett et al./147/. For fast neutron irradiated Nb_3Sn , Brown et al./151/ calculated the value $k = 1.9 \times 10^{-24} \text{ m}^2$. Experimental values for k in several neutron irradiated A15 systems are shown in Table 3.3. This table contains only such systems where S_0 as well as S were measured by diffractometric means. It is seen that there is a considerable scatter in the k values, arising from uncertainties in the determination of the correct dose ϕt of S and S_0 .

System	k ($\times 10^{-24} \text{ m}^2$)	Reference
Nb_3Al	1,8	53
Nb_3Ge	1,84	70
Nb_3Pt	3,54	76
V_3Si	0.7 ± 0.1	78

Table 3.3. Aronin constant k for different neutron irradiated A15 type compounds ($E > 1 \text{ MeV}$).

Once the value of the parameter k is known, Eq. (3.22) gives in principle the possibility to determine the long-range order parameter, $S(\phi t)$, in a solid submitted to a dose ϕt provided that the value of S_0 has previously been determined by diffraction.

Using the correlation between T_c and S , it is tempting to measure T_c only and to deduce the value of S_0 from the literature. This procedure is currently used, but contains implicitly the assumption that a value of T_c corresponds unambiguously to one value of the order parameter. The validity of this assump-

tion has, however, to be verified in each case, since T_c in A15 compounds is not only a function of S , but also of the chemical composition β . Equation 3.22 offers the possibility of estimating order parameter changes in highly textured thin film samples (3.2.3). Thin films are suitable for irradiation studies with charged high energy particles, e.g. protons, ^4He , ^{14}N , ^{16}O , ^{32}S , ..., which penetrate only thicknesses of $\leq 5\mu\text{m}$, but do not activate the sample. Further advantages of the thin film geometry are: i) possibility to study metastable compounds as Nb_3Ge or $\text{Mo}_{.50}\text{Re}_{.50}$, which cannot be prepared in the bulk state, ii) accurate determination of ρ_0 , the electrical resistivity just above T_c , and iii) analysis by means of X ray diffractometry and electron microprobe without any further preparation steps. There is, however, a difficulty which may arise when irradiating thin films with heavy particles, due to local heating causing an inhomogeneous recovery and thus a gradient in T_c . The measured value of T_c would in such cases not be representative for the whole sample unless measured calorimetrically.

4. NONEQUILIBRIUM STATES IN A15 TYPE COMPOUNDS

The possibility to obtain different degrees of atomic ordering in a compound is a consequence of the fact that at room temperature, thermodynamic equilibrium cannot be reached in finite times. Strictly speaking, the study of ordering effects on the superconducting properties in A15 compounds corresponds in reality to an investigation of the consequences of deviations from equilibrium. For an A15 type compound, deviations from equilibrium can be obtained either by a) quench disordering, including quenching and annealing processes, b) irradiation with high energy ($E \geq 1\text{MeV}$) electrons, neutrons or ions, or c) by a combination of both.

In the quench disordered case, the situation is relatively simple, the only known deviation from equilibrium being a homogeneous change in The Bragg-Williams order parameter. Unfortunately, the effect of quench disordering is limited to order parameter changes $\Delta S \leq 0.10$, even after quenching at the highest rates (between $\geq 10^3$ and $\sim 10^6$ °C/s). This is due to a generally fast reordering in A15 type compounds during the quenching process (see Sect. 7). Nevertheless, this relatively small reduction of the long-range order parameter is sufficient to cause substantial changes of the superconducting properties.

The interest in irradiation experiments with high energy particles thus also resides in their ability to further decrease the superconducting transition temperature, down to very low T_c values. However, a multitude of effects are present in irradiated A15 compounds, leading to different types of defects (see 4.2.). There is evidence that some of these defects are inhomogeneously distributed over the crystal volume, which has raised a controversy about the real cause of the observed strong decrease of the superconducting properties in irradiated compounds. The difficulty in determining the dominant cause resides in the fact that all these defects occur simultaneously.

4.1. Ordering Changes Induced by Thermal Methods

4.1.1. Vacancy Diffusion: The "Virtual" Site

In the tightly packed A15 structure, each atom is closely surrounded by its neighbours (see Fig. 4.1). The atoms would need to be considerably compressed before any two could squeeze past one another and interchange positions as required for ordering changes. Among different possible diffusion mechanisms, vacancy diffusion is the most probable one.

The vacancy diffusion mechanism is based on the fact that at thermal equilibrium each solid at a temperature above zero contains a certain number of vacant lattice sites. An atom will now jump into a neighbouring vacancy, thus creating a new vacant site. Atoms and vacancies undergo a series of position exchanges, in order that a very small number of vacant lattice sites is sufficient to induce a substantial diffusion. Most of the studies dealing with diffusion have been undertaken on bcc or fcc structures. In the A15 structure, however, the situation is much more complex, due essentially to the fact that the 6c and the 2a sites are not equivalent from the point of view of electronic bonding. Indeed, interactions between atoms on the 6c and on the 2a sites are characterized by metallic bonding, while the intrachain bonding between two A nearest neighbours is of the covalent type, as was shown by Staudenmann /91,95/, who established electron density maps of V_3Si . This covalent bond is correlated with the very short AA distances on the chains of A15 type compounds, which are noticeably shorter than the sum of the atomic radii of the A element (different sets of atomic radii will be discussed in 4.3.1d. It is obvious that such a configuration leads to highly non-spherical shapes for the A atoms. The region of covalent bonding between two A atoms on 6c sites will be called "overlapping region" in the following. As

shown by Staudenmann /91,95/, this region corresponds to a high electron density in V_3Si .

The question arises whether this overlapping (or covalent bonding) between two neighbouring A atoms on the chain sites still resides if one of them is next to a 6c vacancy. Welch et al. /5,80/ have recently shown by means of pair potential calculation that such an individual vacancy of an A atom on a 6c site is unstable. They found that the state of lower energy corresponds to a configuration where one of the two A atoms adjacent to the single 6c vacancy is shifted towards a new site which is equidistant from the next two A neighbours (see Fig. 4.1). This particular type of vacancy, called "split va-

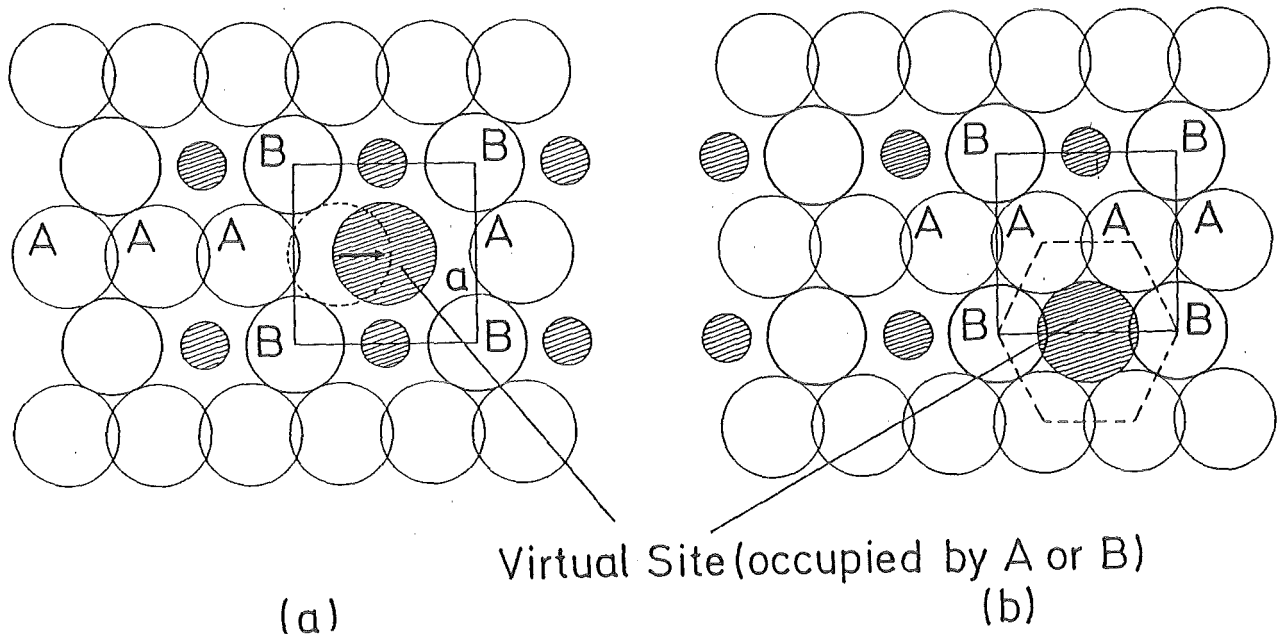


Fig. 4.1. Occupation of the "virtual" site in the A15 structure after irradiation or during exposure to high temperatures, a) in a chain parallel to the plane, b) in a chain perpendicular to the plane. The small circles indicate the regions of d electron localization (covalent bonding), drawn for simplicity as overlapping regions between two neighbouring chain atoms of spherical shape. Note the hexagonal environment of an occupied "virtual" site (Flükiger /6,81/).

cancy" by Welch et al. /5,80/ (it could also be called "negative crowdion" following the nomenclature of Seeger /109/) is correlated to the occupation of a nonequilibrium or "virtual" lattice site /6,81/. This site is located at the region of overlapping between two neighbouring A atoms on a chain.

The main result of the calculation of Welch et al. /80/ is that vacancies on the 2a site (thus Sn vacancies in Nb₃Sn) are thermodynamically unstable. They can be decomposed by the mechanism



where V_{Sn} is a 2a vacancy, V_{Nb} a 6c vacancy and Nb_{Sn} a Nb atom on 2a sites (representing an antisite defect). The energy of a Nb₃Sn lattice as a Nb atom originally adjacent to a Sn vacancy (V_{Sn}) jumps into the vacancy to yield a V_{Nb} split-vacancy and a Nb_{Sn} antisite defect is plotted in Fig. 4.2, thus showing that the Sn vacancy V_{Sn} is metastable.

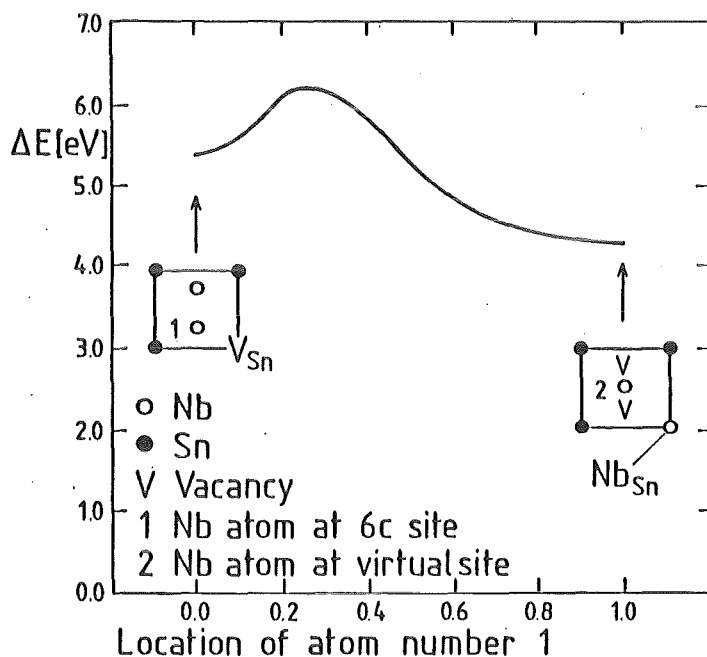


Fig. 4.2. Energy of the relaxed Nb₃Sn lattice as a Nb atom close to a Sn vacancy (V), denoted as I in the figure, jumps into this vacancy, thus causing the neighbour Nb atom to move into the virtual site I' (After Welch et al. /80/).

Two possibilities of site exchange by vacancy diffusion in A15 type compounds are illustrated in Fig. 4.3. In this figure, the atomic radii of the A and B atom have been chosen as the Pauling radii (see 4.3.1) of Nb and Al, respectively, in order to give a more realistic picture. As will be discussed later, this does not imply the hypothesis of spherical atoms in the A15

structure, but was chosen for simplicity. The diffusion mechanism (4.1), $V_{Sn} \longrightarrow V_{Nb} + Nb_{Sn}$, as described in Fig. 4.2 is represented in Fig. 4.3a. In Fig. 4.3b the complementary mechanism $V_{Nb} \longrightarrow V_{Sn} + Sn_{Nb}$ is shown. This complementary mechanism is necessary, the number of antisite defects Nb_{Sn} and Sn_{Nb} being correlated: $Nb_{Sn} = Sn_{Nb}$. As mentioned above, the vacancy V_{Sn} is, however, unstable, thus leading to the mechanism of Fig. 4.3a, and so on.

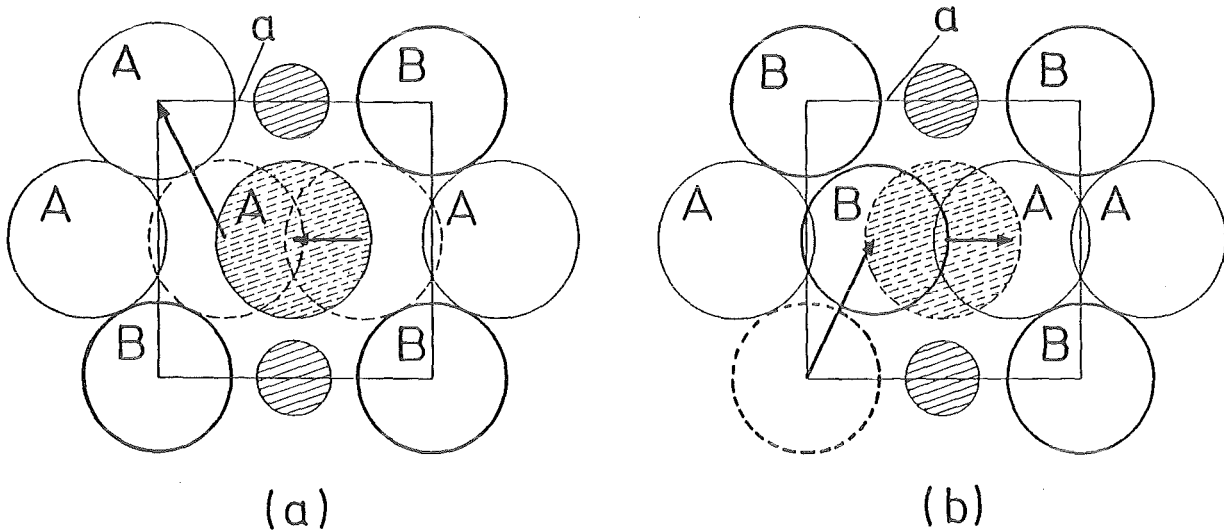


Fig. 4.3. $A \leftrightarrow B$ exchanges by vacancy diffusion in A15 type compounds.

- a) jump of an A atom into a V_{Sn} vacancy, followed by the occupation of the vacant "virtual" site by the neighbour A atom,
 - b) jump of a B atom into an equilibrium 6c site (two-step processes).
- Small circles: overlapping region between two A atoms or region of covalent bonding (Flükiger /6,81/).

It thus appears that the vacancy diffusion mechanism in the A15 type structure comprises at least two steps, in contrast to the one-step mechanism acting in simple bcc or fcc structures. As follows from Ref. 80, the mobility of 6c vacancies is quite high, and that not only the above mentioned split-vacancies are theoretically possible, but also split-n vacancies, i.e. not only one atom is on a virtual site, but an array n ($n = 1, \dots, 5$ have been calculated). However, for the present considerations only the situation with the single virtual site will be retained.

It would lead too far to discuss here in detail the calculations of Welch et al. /80/. The result of their calculation, leading to the above mentioned split-vacancy (or "virtual" site) will later (in 4.2.3) be used as a basis for

a new mechanism of homogeneous disordering in irradiated A15 tape compounds (Flükiger, /6,81/). A close look to the boundary conditions may thus be of interest. The structure and energetics of point defects in the A15 type compound Nb_3Sn were studied by Welch et al. /5,80/ by means of the pair potential $\phi(r)$,

$$\phi(r) = A_R \exp(-b_R r) - A_A \exp(-b_A r) \quad (4.1)$$

where $\phi(r)$ is the energy of interaction of two atoms separated by a distance r , the subscripts R and A referring to the repulsive and attractive part of the potential, respectively. The potentials in Eq. (4.1) were used for separations of less than 0.35 nm (just beyond the second Nb - Nb neighbour separation) and were smoothly truncated to zero at 0.45 nm (just below the third Nb - Nb neighbour separation) with the potential function

$$\begin{aligned} \phi(r) &= -a_1(0.45 - r)^2 - a_2(0.45 - r)^3 & (0.35 \leq r \leq 0.45 \text{ nm}) \\ \phi(r) &= 0 & (r \geq 0.45 \text{ nm}). \end{aligned} \quad (4.2)$$

The parameters a_1 and a_2 were chosen to match the potential value given in Eq.

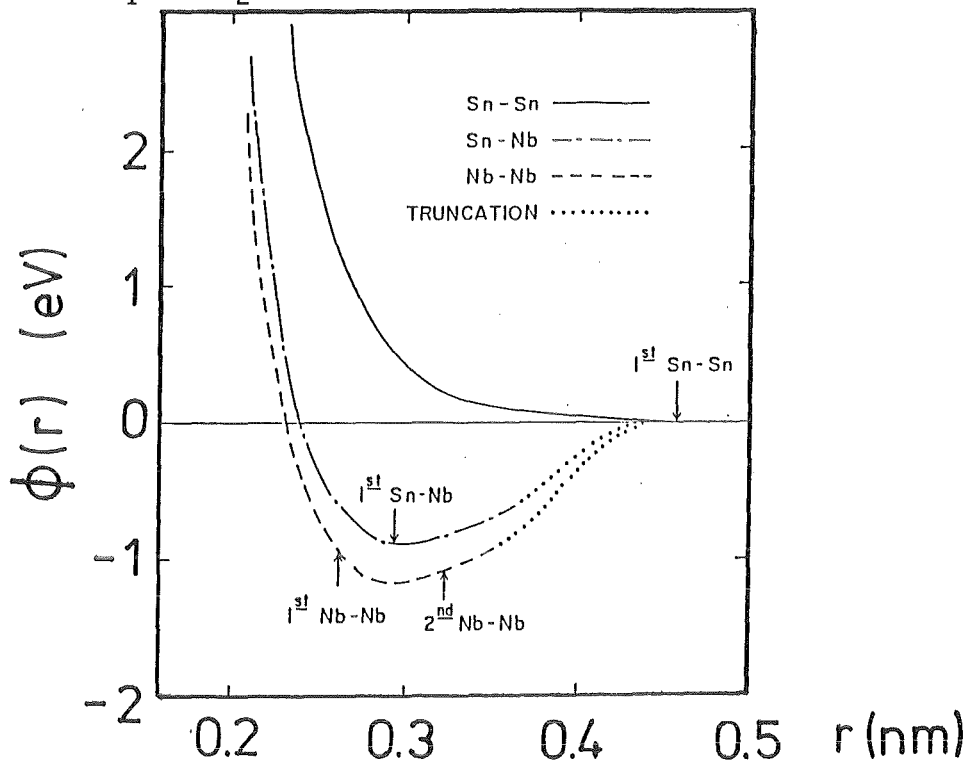


Fig. 4.4. Nb-Nb and Nb-Sn potentials given by Eq. (4.1) for separations less than 0.35 nm and by Eq. (4.2) for greater separations. The Sn-Sn potential is given by Eq. (4.1) for all separations (Welch et al./80/).

(4.1) and its slope at the separation distance $r = 0.35$ nm. The potential calculated for a Nb_3Sn phase field extending to the Nb rich side according to Charlesworth et al. /174/ and Devantay et al. /86/ is reproduced in Fig. 4.4 /80/.

The vacancy diffusion mechanism is governed by the diffusion coefficient $D = D_0 \exp(-E/kT)$, where E is the sum of the energies of formation and migration for vacancies. The activation energy E is related to the binding energy of the atoms, which is reflected by the proportionality between E and the melting temperature T_M : $E/T_M = \text{const.}$ An enhanced number of vacancies is expected at dislocations, grain boundaries and surfaces of the crystal, where the regular lattice structure breaks down, thus favourizing vacancy diffusion processes. Compared to ordinary volume diffusion, surface and grain boundary diffusion is characterized by smaller values of both D_0 and E . The small atomic packing density with the enhanced number of vacancies at grain boundaries reduces the activation energy E and thereby accelerates the diffusion process. The fact that surface diffusion is not isotropic but favors only certain directions leads to a smaller D_0 compared to volume diffusion. As the temperature is lowered, the smaller activation energy for grain boundary diffusion leads to an increased ratio of $D_{\text{gr.b.}}/D_{\text{vol.}}$. This means that surface diffusion mechanisms are relatively important at lower temperatures, while volume diffusion is dominant at high temperature. In A15 compounds, surface mechanisms may somewhat influence the diffusion kinetics at the lowest temperatures where ordering takes place, i.e. between 500 and 800 °C depending on the compound (see temperature T_D in Table 4.1). Indeed, as cast V_3Pt powders of 40 μm size were found to reach the highest T_C value ($T_C = 3.7$ K /82/ after a shorter annealing time than for a bulk 30 g sample (both at 800 °C) /38/. A similar effect was also observed in Nb_3Pt /38/.

From other compounds, it is known that the number of vacancies necessary to site exchange by vacancy diffusion is very small. In V_3Si single crystals /87/, Nb_3Al polycrystals /28/ and $\text{Cr}_{.72}\text{Os}_{.28}$ polycrystals /6/, the number of vacancies determined experimentally is always below the accuracy limit, e.g. $\leq 0.2\%$. Argon jet quenching experiments at 1900°C on $\text{Nb}_{.74}\text{Ir}_{.26}$ failed in producing vacancy concentrations above this limit /7/. The only case where a substantial number of vacancies was reported on bulk samples is Nb_3Sn , where Courtney et al. /85/ found up to 4% Sn vacancies after prolonged annealing at 1800°C. Recent experiments on levitation melted Nb_3Sn alloys by Devantay et al. /86/ did, however, not confirm any vacancy concentration within the experi-

mental error limits. The reproduction of these experiments by the author /38/ revealed indeed the presence of voids, a consequence of the extremely high annealing temperature which caused serious evaporation losses. It

can thus be said that the number of vacancies in unirradiated A15 type compounds at 300K is generally below 2×10^{-3} , the experimental error limit. This is in agreement with other dense structures, for which vacancy concentrations of the same order of magnitude have been reported. The only case where a measurable amount of vacancies could be produced in A15 crystals was reported by Cox and Tarvin /78/, who found that the density of a V_3Si single crystal after a fast neutron irradiation dose of $22,2 \times 10^{18} \text{ n/cm}^2$ decreased by $\sim 0.3\%$.

4.1.2. Variation of the Order Parameter with Quenching Temperature

Various statistical mechanical treatments of the dependence of the equilibrium order parameter on the temperature were performed for cubic AB and AB_3 compounds /2,88,89,90/. In all models there is a decrease of the order parameter with increasing temperature, until a temperature T_F is reached above which there is complete disorder. In these models, T_F characterizes an order-disorder transition, which may be of first or second order. Since no order-disorder transition was observed so far in A15 type compounds, a qualitative comparison will be made replacing T_F by the temperature T_F^0 , defined as the formation temperature of the A15 phase at the composition β , which is known for most A15 compounds (Ref. 7, see also Table 4.1).

The variation of S as a function of temperature for different A15 compounds is reproduced in Fig. 4.5. The order parameter values in this figure were determined at room temperature after argon jet quenching from the temperature T and are not identical with the equilibrium order parameter values, $S_E(T)$ which would have to be measured directly at the temperature T (see (see also 5.5.2). This is important to know, since T_C is obviously correlated with the quenched-in degree of ordering, S , rather than with $S_E(T)$.

In analogy to the classical order-disorder transformations, the order parameter, S , has been drawn as a function of the ratio T/T_F^0 (Fig. 4.5), where

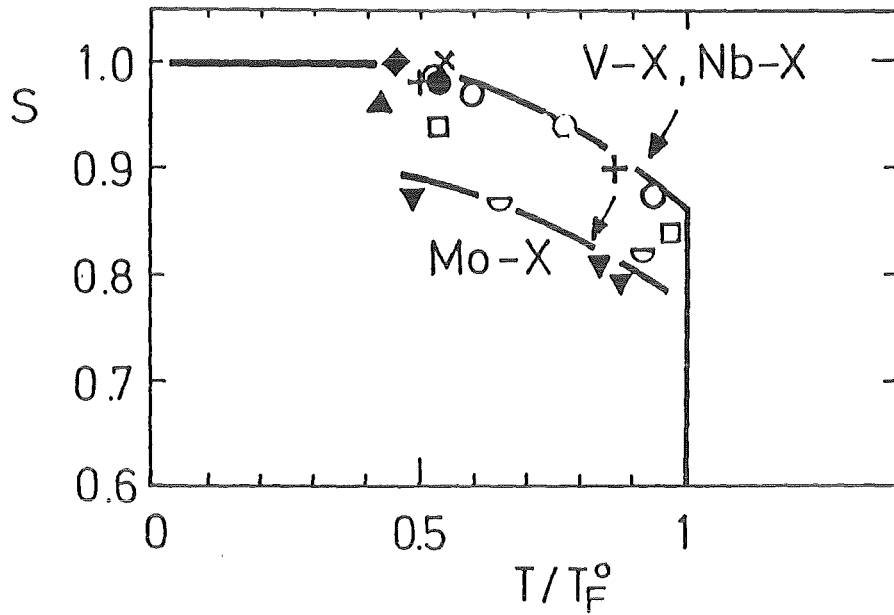


Fig. 4.5. Measured room temperature order parameter, S , for different A15 type compounds as retained by argon jet quenching from the temperature T . T_F^0 was chosen as the formation temperature of the A15 phase at the appropriate composition. The curves were drawn as a guide for the eye.

+ : V_3Pt /62,82/, ● : V_3Ga /20/, □ : $V_{.76}Au_{.24}$ /18,62/, ○ : Nb_3Pt /62, 112/, ▲ : $Nb_{.769}Al_{.231}$ /28/, ◆ : V_3Si /38/, ▼ : Mo_3Os /39/, ◐ : $Mo_{.76}Ir_{.24}$ /39/.

The arrows indicate that the S values are too high, due to partial reordering during the quenching process.

T_F^0 is now the formation temperature of the A15 phase at the composition β . In Fig. 4.5, the temperature T_D represents the estimated lower diffusion limit i.e. the lowest annealing temperature at which changes of T_C can be observed. This definition is reasonable, T_C being far more sensitive to small changes of S than any quantity determined by diffraction measurements.

By definition, T_C remains thus unchanged at temperatures below T_D , even after prolonged heat treatments of several weeks. At T_D , there is thus $S = S_E(T)$, while for $T > T_D$, S is always larger than $S_E(T)$. Recent direct measurements of $S_E(T)$ by Flükiger and Isernhagen /162/ (see Sect. 5.2.2) on Nb_3Sn , Nb_3Ir and Nb_3Pt show that the difference $\Delta S = S - S_E(T)$ up to temperatures around $1000^\circ C$ is of the order of the measuring error, $\Delta S = 0.02$. The results will be discussed in 5.2.2. Considerably larger differences of ΔS are expected

at higher temperatures, but the experimental difficulties were not yet resolved, in order that no ordering data at $T > 1050$ °C are available so far. The difference ΔS is due to a partial reordering during the quenching process which cannot be avoided at the relatively low cooling rates of 5×10^3 °C/s obtained by argon jet quenching (see also Sect. 8). It is possible that a certain degree of re-ordering can never be avoided, even at the highest attainable quenching rates.

The diffusion limit temperature, T_D , for several A15 type compounds is listed in Table 4.1. The same table also contains the formation

A15 Type Compound	Formation Type	Formation Temp. T_F^0 (K)	Solidus Temp. T_S (K)	Diffusion Limit T_D (K)	T_D/T_F^0	Ref.
Nb ₃ Pt	peritectic	2180	2180	1023	0.47	82,92
Nb ₃ Al	peritectic	2233	2233	923	0.42	21,28,35,83
Nb ₃ Ga	peritectic	2023	2023	923	0.46	26,65,93,96
V _{.76} Au _{.24}	congruent from bcc sol. solution	1517	1783	813	0.53	4,18
V ₃ Ga	congruent from bcc sol. solution	1568	1843	837	0.53	20,84,94
V ₃ Pt	peritectic	2037	2037	1013	0.50	82,94
Mo ₃ Os	peritectoidic	2483	2680	1193	0.48	39
Mo _{.76} Ir _{.24}	peritectic	2242	2383	1173	0.52	39
Cr _{.72} Os _{.28}	peritectoidic	1813	2173	953	0.53	39

Table 4.1. Phase formation temperature, T_F^0 , solidus temperature T_S and diffusion limit temperature, T_D , for several A15 type compounds. The ratio T_D/T_F^0 is comprised within the limits $0.42 \leq T_D/T_F^0 \leq 0.53$ (T_D and T_F^0 are taken in degrees Kelvin).

temperatures, T_F^0 , of the corresponding A15 phases at the composition β , as well as the solidus temperatures, T_S , for this composition. It is seen that the ratio T_D/T_F^0 between the diffusion limit and the formation temperature is contained within the limits $0.42 \leq T_D/T_F^0 \leq 0.53$, i.e. the limit for thermally induced site exchanges is close to 50% of the A15 formation temperature. Although the analogy with order-disorder transformations should not be pushed too far, it is interesting that for a series of intermetallic compounds, similar values, e.g. $T_0/T_F \sim 0.5$, are found, where T_0 is the order-disorder transformation temperature and T_F the formation temperature of the disordered (high temperature) phase.

4.1.3. Homogeneity of S in Quench Disordered Crystals

The long-range order parameter is defined as a statistical average over the whole crystal. Local deviations from the average value of S cannot be detected by diffraction measurements, since the line width is not a function of S. The measurement of the superconducting properties is in this case the only way to determine the distribution of the order parameter through the crystal, in virtue of the unequivocal correlation between T_C and S. The width of the superconducting transition as determined by resistive or inductive measurements reflects the distribution of S in the measured sample, but may be subjected to shielding effects, which tend to mask the low T_C tail due to the lower order parameters (the various possibilities for shielding lower T_C values have been described in Ref. 7, p. 539).

The most sensitive method to determine a distribution of T_C values over the crystal volume consists in studying the superconducting transition by calorimetry. For this purpose, it is necessary to start with a sample which must be homogeneous with respect to two criteria, composition and atomic ordering. Several examples will now be presented, showing that the distribution of S in quench disordered A15 type compounds is homogeneous.

As representative for Mo - X compounds, the specific heat measurements for Mo_3Os are represented in Fig. 4.6. The two curves were measured for the same Mo_3Os sample, after homogenization at $1800^\circ C$ and after an additional ordering heat treatment of 6 days at $1050^\circ C$, with the corresponding order parameter values of $S = 0.81$ and 0.87 /39/. It can be seen that T_C changed by $0.51K$, but that the transition width was not affected by the different heat treatments.

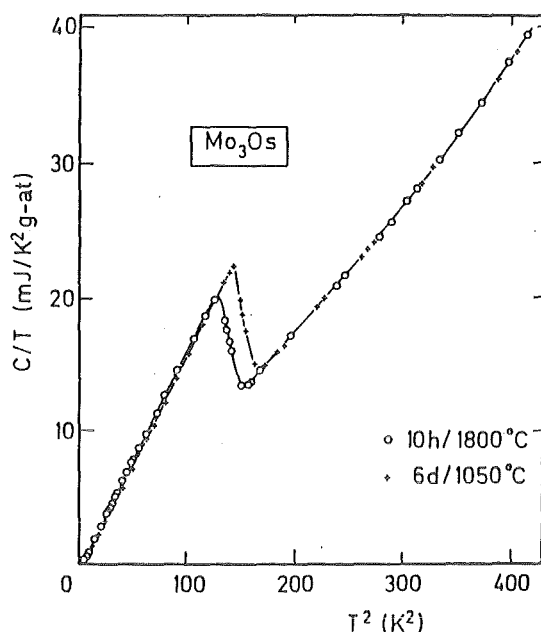


Fig. 4.6. Specific heat of Mo_3Os after a heat treatment of 10 hours at 1800°C and after an additional anneal of 6 days at 1050°C . The transition width, $\Delta T_c = 0.51\text{K}$, is almost unchanged by the corresponding order parameter change from $S = 0.81$ to $S = 0.87$ (Flükiger et al./39,63/).

The relative invariance of the superconducting transition width after different ordering heat treatments has also been verified for Cr - X compounds /63/. Specific heat measurements on the compound $\text{Cr}_{.72}\text{Os}_{.28}$ after homogenization at 1350°C and after an additional heat treatment of 30 days at 780°C are shown in Fig. 4.7. The corresponding order parameters (measured on the same sam

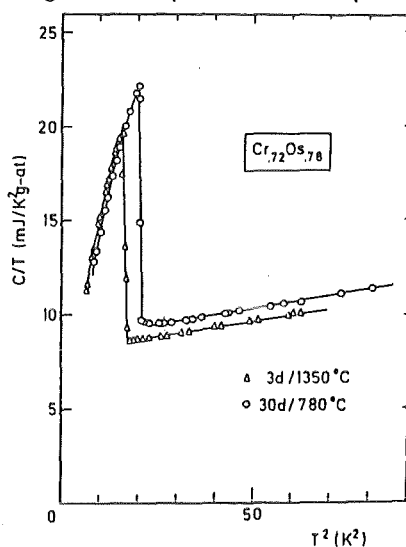


Fig. 4.7. Specific heat of $\text{Cr}_{.72}\text{Os}_{.28}$ after homogenization at 1350°C (3 days) and after an additional heat treatment of 30 days at 780°C , showing an unchanged transition width, $\Delta T_c = 0.16\text{K}$ (Flükiger and Paoli /63/).

ple after the respective heat treatments) were $S_a = 0.70 \pm 0.05$ and $S_a = 0.78 \pm 0.05/39,62/$, respectively.

A similar behavior was observed in the system V_3Au (effective composition $V_{.76}Au_{.24}$ /18/, where the calorimetric superconducting width was measured after several heat treatments, corresponding to different degrees of ordering, reaching from $S_a = 0.84$ to $S_a = 0.94$ /18,98/, as illustrated in Fig. 4.8.

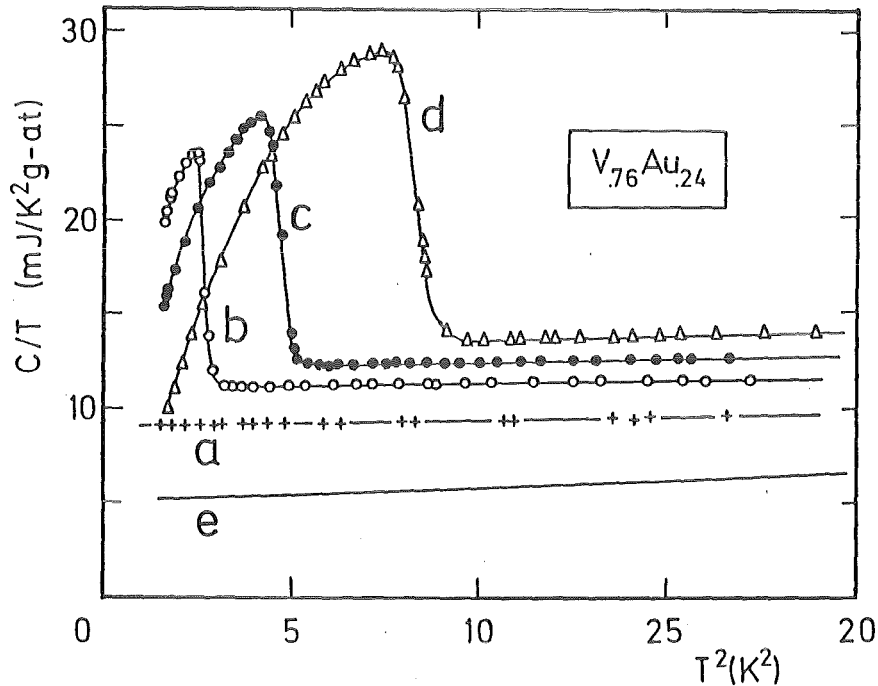


Fig. 4.8. Specific heat of the compound $V_{.76}Au_{.24}$ after different heat treatments. A15 phase: a) $1150^{\circ}C$, followed by quenching in water, b) $800^{\circ}C$, c) $700^{\circ}C$, d) $560^{\circ}C$ (slow cooling after b), c) and d)). A2 phase: e) $1300^{\circ}C$, followed by argon jet quenching. (Spitzli /122/, Junod et al. /30,98/).

In the three systems Mo_3Os , $Cr_{.72}Os_{.28}$ and $V_{.76}Au_{.24}$ mentioned above, cooling after heat treatments occurred slowly, the highest cooling rate occurring in curve d) in Fig. 4.8 (cooling rate after quenching into ice water: $\sim 100^{\circ}C/s$). It is interesting to study the homogeneity of S in after cooling at higher quenching rates from temperatures sufficiently high to induce an appreciable order parameter change. Such a case is illustrated in Fig. 4.9, representing the specific heat curves of V_3Ga after a heat treatment at the same temperature, $1250^{\circ}C$, but cooled at different rates. Both measurements were effectuated on the same sample, the first one after slow cooling ($\sim 15^{\circ}C/s$), the second one after argon jet quenching ($>10^3^{\circ}C/s$). In order to improve the

efficiency of quenching in retaining a lower degree of ordering, the sample with a mass of 10 g was cut into slices of ≤ 1 mm thickness, which were individually argon jet quenched from 1250°C (the quenching device has been described in Ref. 7). As demonstrated by Fig. 4.9, the distribution of the order parameter is even narrower after the quenching procedure. The rounding off of the superconducting transition at the lower T_c limit reflects a slight local inhomoge-

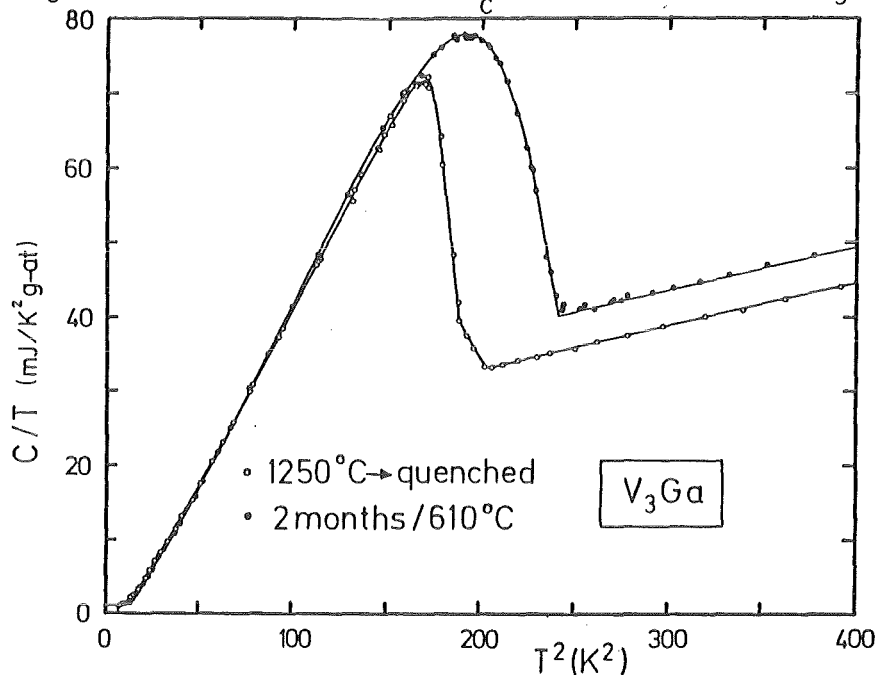


Fig. 4.9. Specific heat of V_3Ga after homogenization at 1250°C, but cooling at different rates, 15°C/s and $>10^3$ °C/s, leading to order parameters of $S = 0.98$ and $S = 0.95$, respectively (Flükiger et al. /20/, Junod et al. /97/).

neity. The values of S corresponding to the different heat treatments are $S = 0.98$ and $S = 0.95$, respectively /20/.

It can be concluded from the data in Figs. 4.5 to 4.9 that the order parameter distribution in A15 type compounds is quite narrow. From the corresponding calorimetric superconducting widths, the gradient of S across these samples can be estimated to be $\delta S < 0.02$.

4.2. Radiation Damage and Disorder

The decrease of T_c in different A15 type compounds as a function of the irradiation dose, ϕt , for neutrons with $E \leq 1$ MeV at irradiation temperatures $T_{irr} \leq 150^\circ\text{C}$ is represented in Fig. 4.10, according to Sweedler et al. /69/. It is seen that the variation of T_c with ϕt is similar

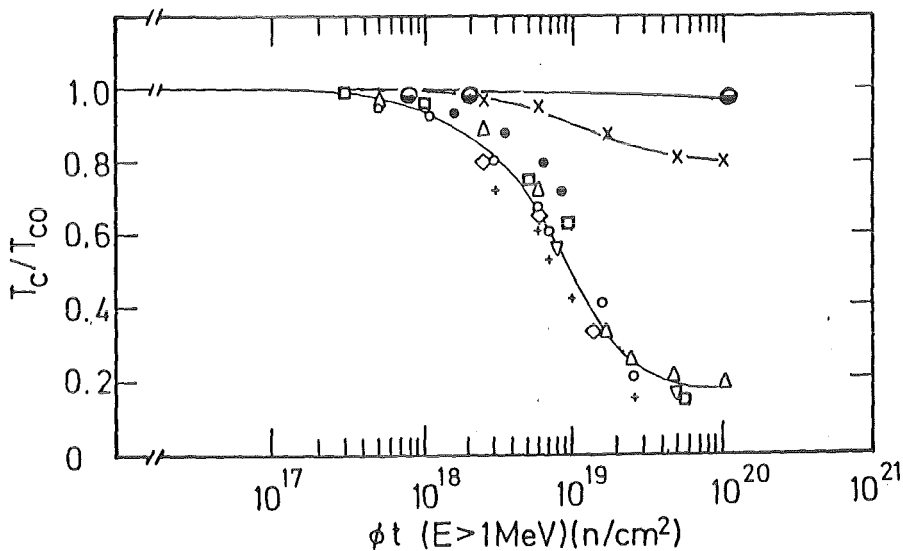


Fig. 4.10a. T_c as a function of neutron dose ($E \leq 1$ MeV, $T_{irr} \leq 150^\circ\text{C}$).
 + : V_3Si , o : Nb_3Ge , Δ : Nb_3Al , \diamond : Nb_3Pt , ∇ : Nb_3Ga , x : Mo_3Os
 (all data from Sweedler et al. /69/), o : V_3Ga (Francavilla et al. /134/), \bullet : $\text{Mo}_{.40}\text{Tc}_{.60}$ (Giorgi et al. /293/).

for most analyzed compounds except for the atypical compound Mo_3Os , which shows a much slower decrease of T_c . In their review article, Sweedler et al. /69/ concluded that the decrease of T_c in the low dose regime, say, below 10^{19} neutrons/cm² (where $T_c/T_{c0} \simeq 0.5$) is mainly caused by a decrease of the long-range order parameter, S .

The data in Fig. 4.10a were obtained after irradiation with $E > 1$ MeV neutrons at $T_{irr} = 150^\circ\text{C}$ /69/. A comparison with data obtained after low temperature irradiation and measured without warming up to room temperature would be interesting. Such data are not available for neutron irradiation, but for irradiation of Nb_3Sn films with 20 MeV ^{32}S ions /136,152/, showing a

very similar behavior of T_c vs, ϕt as in Fig. 4.10a. In a very recent work, Flükiger et al. /156/ have studied the variation of T_c , J_c and B_{c2} of binary and alloyed Nb_3Sn multifilamentary wires after irradiation at $T_{irr} = 4.2$ K with 14.8 MeV neutrons allowing, however, warming up to 300 K prior to the low temperature measurements (The experimental conditions will be described in Sect. 11.3). The variation of T_c for both types of wires is shown in Fig. 4.10b and agrees quite well with the behavior shown for bulk Nb_3Sn in Fig. 4.10a. It may be advanced (in particular comparing with the data in Refs. 136) that warming up to room temperature has little effect on T_c , thus meaning that recovery effects up to 300 K would not affect the degree of ordering (the correlation between atomic ordering and T_c will be discussed just below). Other defects may, however, recover in this temperature range: The behavior of both, J_c and B_{c2} on the same Nb_3Sn wires as in Fig. 4.10b /156/ is affected by the simultaneous change in ρ_0 and is thus more complex, as will be discussed in Sect. 11.3.

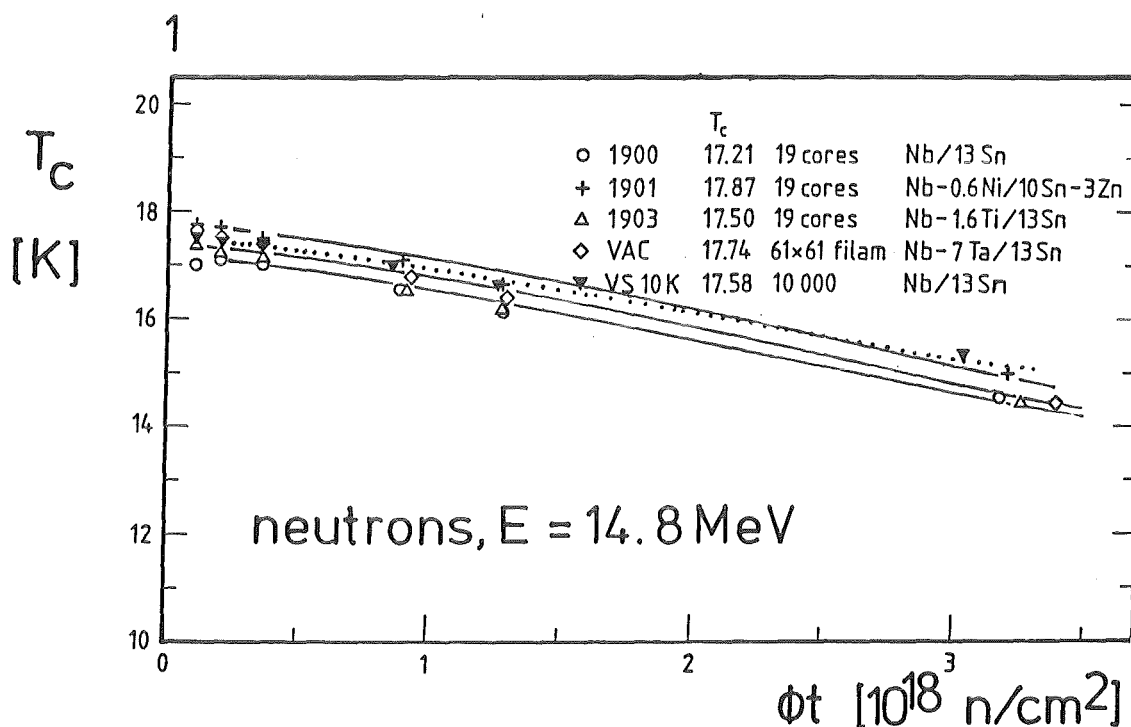


Fig. 4.10b. T_c as a function of dose for binary and alloyed Nb_3Sn multifilamentary wires after irradiation with 14.8 MeV neutrons at $T_{irr} = 4.2$ K (Flükiger et al. /156/).

The arguments of Sweedler et al. /69/ can be considered as strongly supporting the hypothesis of a correlation between order parameter and T_c in irradiated A15 type compounds, but they do not furnish a definitive proof

for its validity. In particular, Sweedler et al./69/ gave no indication for a possible mechanism leading to a homogeneous decrease of the order parameter throughout the sample volume. As pointed out by Pande/103/, the weakening of A15 superstructure lines after irradiation (which was interpreted by Sweedler et al./69/ as a decrease of S) could also arise from an increasing volume fraction of disordered A15 phase (e.g. in the depleted zones), concentrated in regions of ~ 5 nm diameter. Since the observation of such "disordered" zones by TEM was limited to ≤ 2 nm in the experiments of Pande/103/, the question whether disordering in irradiated A15 type compounds is homogeneous or inhomogeneous remained thus still controversial.

At this point, it is necessary to give a precise description of the phenomenon. It has indeed to be distinguished between

- a) the presence of inhomogeneities in the sample after irradiation, observed as well by transmission electron microscopy /103,104/ as by small angle neutron scattering (Nikulin et al. /121/), and
- b) the causes for the decrease of T_c with dose, which were attributed either to an inhomogeneous state after irradiation (thus being correlated to the inhomogeneities mentioned in a)) or by a homogeneous change of a material property, e.g. the long-range order parameter, which would be superposed to the observed inhomogeneities.

A mechanism able to explain the occurrence of $A \leftrightarrow B$ site exchanges in irradiated A15 type compounds and giving a qualitative picture of the observed lattice expansion and static deviations in this class of compounds was recently proposed by the author /6,81/. It is the scope of this paragraph to give a definitive and irrevocable proof for ordering effects as the main cause for the initial decrease of T_c in the low dose regime. For this purpose, the above mentioned mechanism as well as an extensive use of comparisons between data on irradiated and quench disordered A15 type compounds will serve as major arguments. For experimental details concerning the irradiation experiments it will be referred to the literature /55,69,102/, the points of main interest being here atomistic considerations and crystallochemical aspects of the various processes occurring as a consequence of irradiation of A15 type compounds with high energy particles.

4.2.1. Coexisting Defect Mechanisms

From the wealth of published data, it follows that the decrease of T_C in irradiated A15 type compounds has in the past been attributed to three concurrent defect mechanisms:

a) Homogeneous Disordering: The "defects" are here lattice sites occupied by the wrong atoms (in analogy to the quenched state), also called "antisite defects".

A decrease of S in irradiated A15 compounds was first observed by Sweedler and Cox/53/ for Nb_3Al . It was later confirmed by Moehlecke et al./99/ on Nb_3Pt and Cox and Tarvin/78/ on V_3Si . Recently, Schneider et al./55/ have reported a decrease of S in Nb_3Al after irradiation with 700 keV N^{2+} ions. In all cases, the diffraction analysis was carried out following the principles and methods described in 3.2. Of course, the attribution of the change in superlattice line intensities to ordering changes implies the assumption of homogeneous disordering over the sample volume after irradiation. The decrease in T_C is explained by changes of the electronic density of states at the Fermi energy (see Section 8).

b) Inhomogeneous defects: the defects are represented by the depleted zones (or disordered microregions, following the nomenclature of Pande/103,104/) of ~ 4 nm diameter, generally observed in solids after high energy irradiation. The main difference between the inhomogeneous defect mechanism /103,104/ and the antisite defect mechanism/53/ can be represented as follows. In the inhomogeneous case, the matrix enclosing the depleted zones is assumed to be essentially unaffected by the radiation, while the antisite defect (or disordering) mechanism is assumed to be homogeneous over the whole volume. The inhomogeneous defect mechanism explains an overall degradation of the superconducting properties by the proximity effect /104,105/ between the ordered, high T_C matrix and the disordered low T_C microregions of a size comparable to the coherence length, $\xi_0 \approx 5$ nm.

c) Static Displacement of the Atoms from their Equilibrium Positions: this kind of defect was first observed by Meyer/106/ and Testardi et al./107/ on V_3Si single crystals by means of the channeling technique.

The existence of the defect types a, b and c is based on sound experimental data. It is also ascertained that all three types of defects occur simultaneously during irradiation. In the past, each of these defects has been independently made responsible for the decrease in T_c , without taking into account the effects of the other two ones. As will be shown in this section, all three types of defects participate in one way or another in altering the superconducting properties of irradiated A15 type compounds. Depending on the total irradiation dose, each one of these defect types will be dominant over the concurrents.

4.2.2. Arguments in Favor of a Homogeneous Atomic Disordering After Irradiation

The attribution of the initial decrease of T_c in irradiated A15 type compounds to one of the three (possibly interdependent) simultaneous mechanisms can be compared to a system of equations with too many unknown parameters: only additional informations about these parameters will lead to a solution of the problem. Such informations could be furnished by irradiation experiments with different projectiles and energies on A15 materials with thicknesses varying in the range between 50 and 500 nm: the depth of the displacements is indeed different for light and heavy particles, as follows from the channeling measurements of Meyer and Seeber/106/. However, such experiments have so far not been reported.

In order to demonstrate the dominant effect of homogeneous antisite defects in decreasing T_c of irradiated "typical" A15 type compounds, several arguments will now be presented and discussed in detail:

- a) the comparison between the effects caused by irradiation with high energy electrons and other projectiles (neutrons, ions),

- b) the comparison of the variation of T_c vs. S for A15 type compounds after irradiation and after fast quenching from high temperatures (S is measured by diffraction methods),
- c) the observation of the increase of the calorimetric superconducting transition width, ΔT_c , after irradiation at different doses, and
- d) the effects of varying the irradiation temperature, T_{irr} , on T_c .

It is interesting that none of these arguments alone is sufficient to identify without any doubt the cause of the initial decrease of T_c at low doses after irradiation: only the combination of these complementary arguments furnishes an irrevocable proof for the decrease of the order parameter as the responsible effect for the decrease of T_c after low irradiation doses.

a) Irradiation with High Energy Electrons and Neutrons

According to Seeger/109/, the complex situation in an irradiated crystal can be described as follows. The high energy particle transfers a kinetic energy, E_T , to an atom of the target, the primary knock-on atom. At sufficiently high values of E_T , this atom will be removed from its equilibrium lattice site: a Frenkel defect is formed. Due to inelastic collisions with electrons, the energy of the primary knock-on atom towards the end of its path falls to values of the order of E_d , the displacement energy (~ 25 eV), and almost every collided atom is displaced/110/. As a result of this displacement cascade, regions with high concentrations of vacancies are formed, the so-called "depleted zones", which are surrounded by a zone enriched with interstitial atoms. In A15 type compounds, the existence of depleted zones has first been reported by Pande/103/, who called them "disordered microregions". In reality, the structure of this region can be either amorphous, of the A15 type (but strongly or completely disordered, $S = 0$), or of another structure type, as for example bcc (A2 type) in Nb_3Al /55/ or in Nb_3Si /108/. The currently used term "depleted zone" seems thus to be more appropriated and will be adopted in the present work.

In contrast to irradiation with fast neutrons or high energy ions, electrons with energies of the order of ~ 1 MeV do not produce the displacement

cascade described above. This is essentially due to the low electron mass, as pointed out by Schulson/100/. 1 MeV electrons create isolated Frenkel pairs, resulting in a homogeneous distribution of defects. This is in contrast to fast neutron or high energy ion irradiation, where at the end of the process, the vacancies and interstitials forming initially a Frenkel pair (produced by primary collisions) are separated by several atomic distances, which leads to a collective inhomogeneous defect, the depleted zones.

Ghosh et al./111/ have irradiated Nb₃Sn films with 2 MeV He ions and with 2 MeV electrons, respectively, while Rullier-Albenque et al./101/ have irradiated Nb₃Ge films (with T_{co} = 19.5K) with 1 MeV neutrons and 2,5 MeV electrons, respectively. Both investigations lead to the same conclusion, i.e. a strong decrease of T_c is observed, regardless of the nature of the projectile. In particular, Rullier-Albenque et al./101/ found that the ratio ΔT_c/Δρ (where Δρ is the increase of the residual resistivity after irradiation) for Nb₃Ge does not differ between fast neutron and high electron irradiation. The results of Rullier-Albenque et al./101/ are shown in Fig. 4.11.

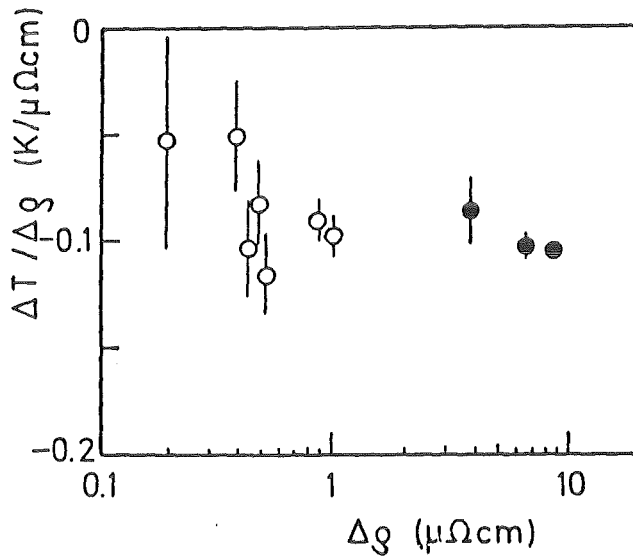


Fig. 4.11. Variation of the ratio $\Delta T_c/\Delta\rho$ with $\Delta\rho$ in Nb₃Ge irradiated at T_{irr} = 20 K by fast neutrons (E > 1 MeV), (●), and by 2.5 MeV electrons, (o). After Rullier - Albenque et al. /101/.

Although these experiments do not give any evidence that the order parameter is equivalent in both cases, they lead to an important conclusion: the possibility of lowering T_c by proximity effects between the matrix (assumed to retain the initial degree of ordering /103/) and the depleted zones (with much lower T_c values) is now very improbable.

b) Comparison between Irradiated and Quench Disordered Nb₃Pt

Quench induced disordering constitutes a particularly simple case, where the only possible defects are the antisite defects (a few percent) and quenched-in vacancies ($\leq 0.2\%$ at 300K). Based on the determination of S in neutron irradiated Nb₃Al, Sweedler and Cox/53/ first assigned the initial decrease of T_c after irradiation to antisite defects. This was later justified by a comparison in the Nb₃Pt system, where the order parameters on irradiated and on quenched samples were experimentally determined by diffraction. As shown in Fig. 4.12, the variation of T_c with S for Nb₃Pt after neutron irradiation (Moehlecke et al./76/) are in good agreement with the corresponding data after fast quenching (Flükiger/62,112,142/).

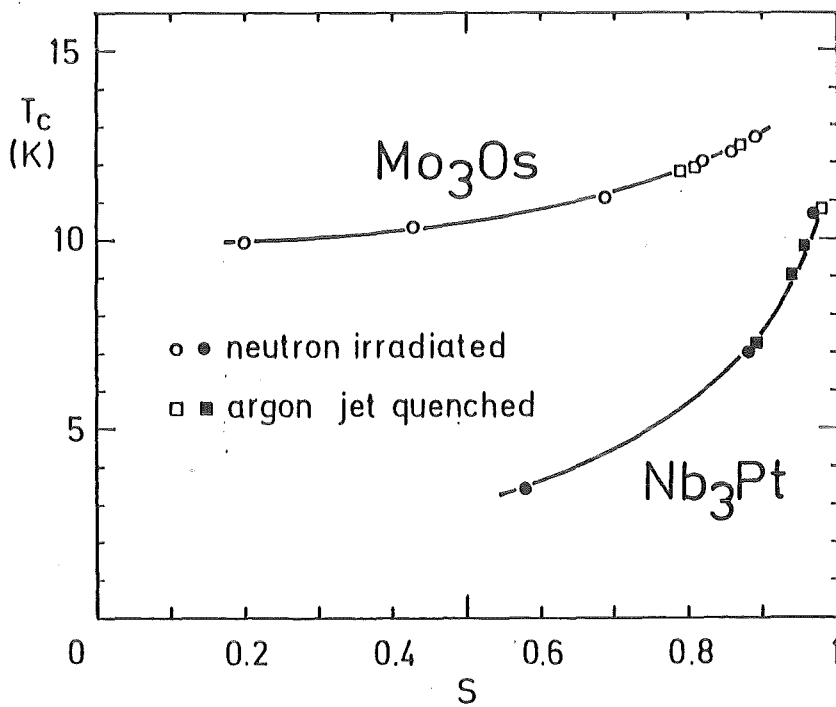


Fig. 4.12, Superconducting transition temperature, T_c, vs. long-range order parameter (determined by diffraction) for the compounds Mo₃O_s and Nb₃Pt in the neutron irradiated and in the quenched state.

○: Sweedler et al./77/, □: Flükiger et al./39/, ●: Moehlecke et al./76/, ■: Flükiger/62,112,142/.

In the review paper of Sweedler et al./69/, the comparison of T_c vs. S between irradiated and quench disordered Nb₃Pt represented in Fig. 4.12 consti-

tutes the major (and only) argument in favour of the dominance of homogeneous atomic disordering over inhomogeneous defects. However, even the excellent agreement between the S values of irradiated and quenched Nb_3Pt in Fig. 4.12 cannot furnish a definitive answer to this problem, and this for two reasons: i) this comparison has so far only been effectuated for the system Nb_3Pt , ii) the decrease of the superlattice line intensities after irradiation could be only apparent, being in reality due to the superposition of two different phases, i.e. the fully ordered A15 phase (the matrix) and the disordered A15 phase in the depleted zones (the presence of depleted zones in neutron irradiated Nb_3Pt has later been reported by Pande/113/, but no indication about the depleted volume fraction was furnished). There are no sufficient data for neutralizing the important objection ii). However, the highest volume fraction of depleted zones reported so far in an A15 type compound is ~6% in Nb_3Sn /105/, which would be too low for producing the observed decrease of the superlattice line intensities by 50%. In addition, a marked decrease of the superlattice line intensities on neutron irradiated V_3Si has been reported/78/, a compound where no depleted zone could be observed by transmission electron microscopy at 300K/113/. It is important to mention, however, that in Ref. 113, the compound V_3Si was irradiated at temperatures lying between room temperature and 150°C, in order that partial recovery could have reduced the size of the depleted zones to values below the detection limit, i.e. ~2 nm (the effects of varying T_{irr} will be discussed in paragraph 4.2.2.d).

c) Calorimetric Observations on Irradiated A15 Type Compounds

Calorimetry is a powerful method for detecting superconducting phases exhibiting different T_c values in multiphase systems. In analogy to the measurements on quenched samples in 4.1.3, specific heat measurements on irradiated samples are thus expected to furnish precious informations about their metallurgical state, in particular the composition profile and the distribution of the order parameter, S . Such measurements have been reported for:

- V_3Si , by Viswanathan et al. /115,117/,
- Nb_3Sn , by Karkin et al. /160/,
- Nb_3Al , by Cort et al. /114/,
- Mo_3Ge , by Ghosh and Caton /153/, and
- Mo_3Si , by Mirmelshteyn et al. /158/.

All these irradiations were performed with ≥ 1 MeV neutrons at temperatures $T_{irr} = 150$ °C /114,117,153/ and 70 °C /158,160/.

The present discussion will be centered on the first three compounds with $T_c \geq 17$ K, while Mo_3Ge and Mo_3Si will be treated in 4.3.6. Besides individual differences in the respective change of the electronic density of states in V_3Si , Nb_3Sn and Nb_3Al (which will be discussed in Section 8), these systems exhibit a common feature: The width of the calorimetric superconducting transition increases somewhat with neutron dose, particularly for Nb_3Sn (see Fig. 4.15). When comparing the transition width after irradiation, one aspect must be taken into account: The size of the sample.

The Size of the Irradiated Sample.

Viswanathan et al. /117/ pointed out that V_3Si single crystals exceeding a certain size corresponding to a mass of ~ 1 g exhibited additional heating during irradiation, leading in one case even to a visible darkening of the surface, i.e. to estimated temperatures T_{irr} of 300°C and above. This is due to increasing difficulties in transferring the nuclear heat to the sample environment (in this case, Ar gas) with increasing volume to surface ratio. In the present case, only the masses of V_3Si and Nb_3Al were below 1 g, in contrast to Nb_3Sn , where a mass of 11 g was indicated by Karkin et al. /160/. The discussion of the latter will thus be carried out separately.

For illustration, the specific heat curves for V_3Si /117/ and Nb_3Al /114/ are reproduced in Figs. 4.13 and 4.14, respectively, after irradiation at different neutron doses. Following conclusions can be drawn:

- 1) After irradiation there is no trace of the original superconducting transitions at T_{c0} . This implies that the size of the depleted zones is in each case smaller than that of the coherence length, ξ_0 , which is of the order of 3 to 5 nm for these three compounds.
- 2) In spite of the observed slight broadening at high doses, the superconducting transition widths in Figs. 4.13 and 4.14 still remain narrow. For Nb_3Al , the width ΔT_c increases from 0.8K in the unirradiated state to 1.3K after $1.3 \times 10^{19} \text{ n/cm}^2$, where the ratio T_c/T_{c0} is equal to 0.51 /114/. For V_3Si , an increase of ΔT_c from 0.5 to 1.2K was observed after $2.22 \times 10^{19} \text{ n/cm}^2$, where $T_c/T_{c0} = 0.4$ /117/. Keeping in mind that for high T_c A15 type compounds a change of 1% in S causes a change in T_c of nearly 1K (see Section 8), it follows that there is still a high degree of homogeneity in the long-range order parameter, the total gradient across the sample being $\delta S \leq 0.02$. This necessarily implies that radiation induced site exchanges occur over large distances from the primary colli-

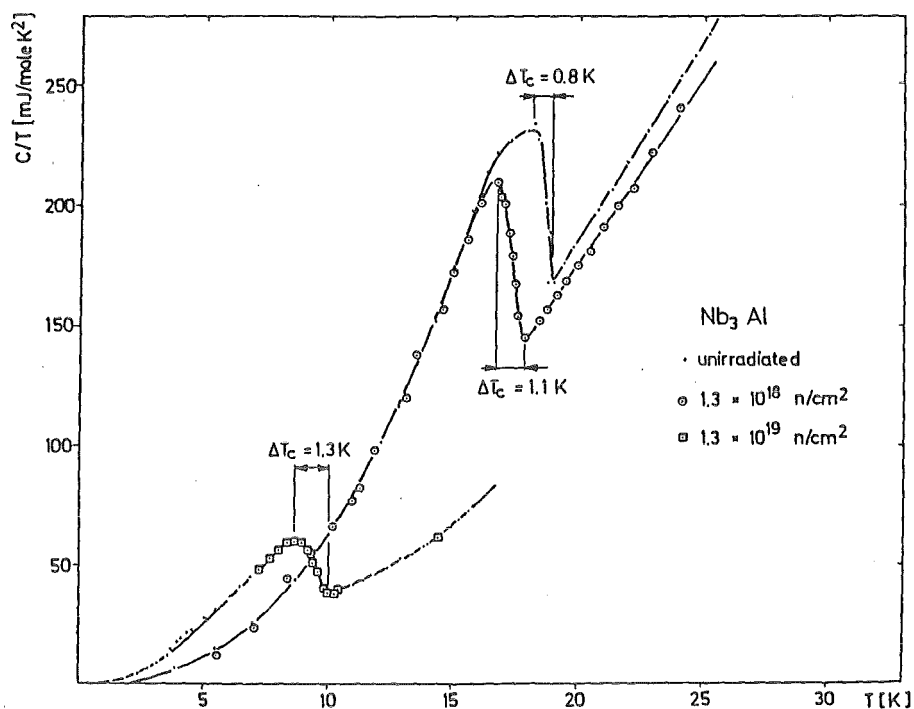


Fig. 4.13. Specific heat of Nb₃Al in the unirradiated state and after irradiation at doses of $1.3 \times 10^{18} \text{ n/cm}^2$ and $1.3 \times 10^{19} \text{ n/cm}^2$, respectively. The linear representation C/T vs. T has been chosen in order to visualize the moderate increase in ΔT_c with dose (after original data of Cort et al./114/).

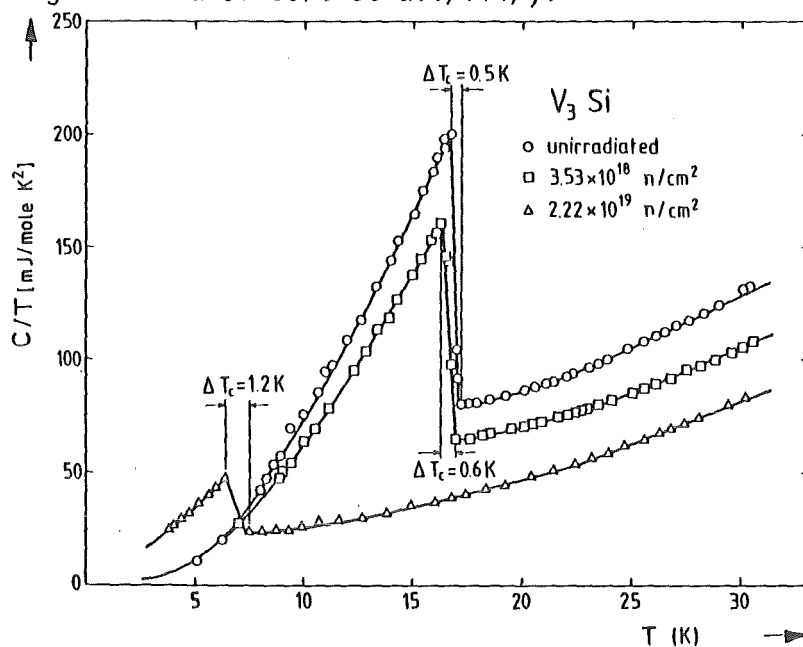


Fig. 4.14. Specific heat of V₃Si in the unirradiated state and after irradiation doses of $3.52 \times 10^{18} \text{ n/cm}^2$ and $2.22 \times 10^{19} \text{ n/cm}^2$, respectively. The linear representation of C/T vs. T was chosen in order to visualize the moderate increase in ΔT_c with dose (after original data of Viswanathan et al./117/).

sion event.

3) In spite of a small mass (< 1 g) the Nb₃Al and V₃Si samples still show nuclear heat recovery effects. At the given neutron doses, their T_c values are indeed considerably higher than those corresponding to the behavior T_c vs. ϕt for small samples shown in Fig. 4.10. From the values listed in Table 4.2, the increase of T_c due to nuclear heat recovery at ϕt = 1 × 10¹⁹ n/cm² can be estimated to ~2 K for V₃Si and Nb₃Al. The increase for the larger Nb₃Sn sample /160/ is more important: ΔT_c = + 3.5 K.

Compound	Dose n/cm ²	T _c (cal.) [K]	ΔT _c [K]	γ [mJ/at-gK ²]	Θ _D [K]	Ref.	T _c (Fig. 4.10a) [K]
Nb ₃ Al	0	18.7	0.6	9.0	272	114	18.7
	1.3×10 ¹⁸	17.5	1.0	8.5	276		17.0
	1.3×10 ¹⁹	9.6	1.2	4.25	325		7.5
	2.6×10 ¹⁹	7	376		5.1
V ₃ Si	0	17.0	0.5	16.2	407	117	17.0
	0.25×10 ¹⁸	16.85	0.6	16.3	397		16.8
	1.65×10 ¹⁸	16.95	0.5	14.7	411		15.5
	3.53×10 ¹⁸	16.75	0.6	13.3	436		13.7
	2.22×10 ¹⁹	6.8	1.2	5.3	454		4.4
Nb ₃ Sn	0	18.0	0.7	12.8	227	179	-
Nb ₃ Sn	0	17.9	0.6	12-14 ^{a)}	268 ^{a)}	160	17.9
	1.0×10 ¹⁹	12.0	2.1	8-10 ^{a)}	287 ^{a)}		8.7

Table 4.2. Transition temperature and width, electronic specific heat coefficient and Debye temperature for Nb₃Al /114/, V₃Si /117/ and Nb₃Sn /160/ before and after neutron irradiation. For comparison, the specific heat data of Junod /179/ on unirradiated Nb₃Sn have been added. The T_c values from Fig. 4.10 are reference values, measured on small samples by Sweedler et al./69/.

^{a)} The γ and Θ_D values from Karkin et al. /160/ can only be estimated, since the specific heat measurements were not performed to temperatures low enough for applying the entropy condition.

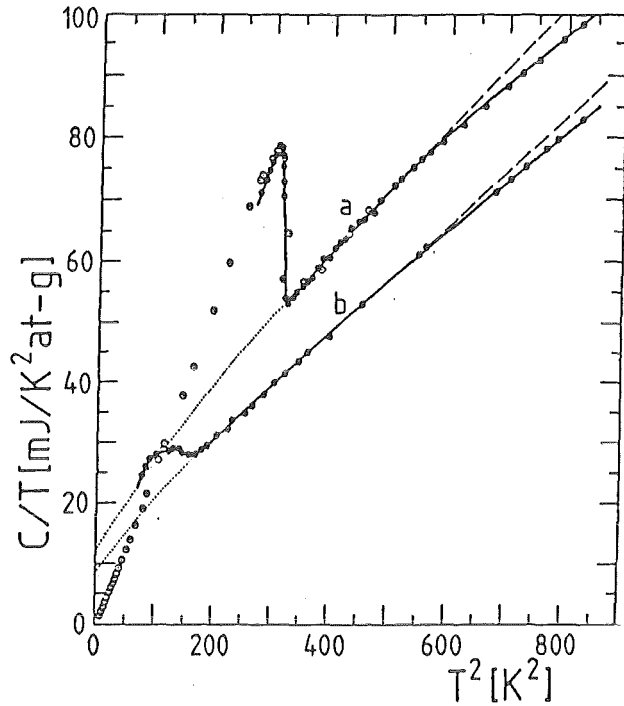


Fig. 4.15. Specific heat of Nb₃Sn, a) in the unirradiated state and b) after a dose of 1.0×10^{19} n/cm² according to Karkin et al. /160/, (●). Since these authors did not perform the measurements at temperatures low enough to allow a precise determination of γ (and of $\theta_D(0)$), data of Junod et al. /179/ for unirradiated Nb₃Sn have been superposed for comparison, (○).

The specific heat curves for the 11 g Nb₃Sn sample analyzed by Karkin et al. /160/ before and after neutron irradiation to a dose of 1.0×10^{19} n/cm² are represented in Fig. 4.15. The preceding discussion suggests that the observed increase of the transition width in Nb₃Sn and to a smaller extent also for Nb₃Al and V₃Si is mainly due to nuclear heat recovery effects. As shown in the following paragraph, the simple fact to increase the temperature T_{irr} from < 150 °C (but still above room temperature) to 240 °C was found to have a strong effect on T_c of V₃Si /119/ (see Fig. 4.16).

- 4) From Table 4.2, it can be seen that the electronic specific heat coefficient γ , of the systems Nb₃Al, V₃Si and Nb₃Sn decreases strongly with increasing neutron dose. In all three systems, a decrease of T_{c0} to $T_{c0}/2$ leads to a decrease from γ_0 , the value prior to irradiation, to $\sim \gamma_0/2$. In the case of Nb₃Sn, this conclusion can only be drawn approximately, since Karkin et

al. /160/ measured the specific heat only down to temperatures slightly below T_c (see Fig. 4.15), in order that a precise evaluation of γ (and of θ_D) is not possible. Their γ values given in Table 4.2 are not correct, being only based on the fit with the third power term, but without using the necessary entropy condition. A comparison with a measurement of Junod /191/ on an un-irradiated Nb_3Sn sample (see Fig. 4.15) shows, however, that the quality of both the sample and the measurement were comparable in Refs. 160 and 191, in order that similar values of γ_0 can be expected. Knowing that the error in γ is considerably smaller when extrapolating the data for an irradiated sample with $T_c = 12$ K (compared to the unirradiated sample with $T_c = 17.9$ K), it can be safely concluded that the variation of the electronic specific heat coefficient of Nb_3Sn with irradiation is very similar to that of Nb_3Al and V_3Si . The variation of the electronic density of states as a function of the degree of ordering will be discussed in Sect. 8.

- 5) The Debye temperature, θ_D , shows a marked increase with irradiation dose in the three systems Nb_3Al , V_3Si and Nb_3Sn , as follows from the values listed in Table 4.2. The value of θ_D for Nb_3Al increases from 272 K in the un-irradiated state to 325 K at 1.3×10^{19} n/cm², where $T_c = 9.6$ K, while a change from 407 K to 454 K is observed in V_3Si after 2.22×10^{19} n/cm² ($T_c = 6.8$ K). For Nb_3Sn the same uncertainty as for the γ values also subsists for θ_D . Under the same assumptions as above, a change of θ_D from 227 ± 20 K to 287 ± 20 K can be considered as reasonable after a dose of 1.0×10^{19} n/cm² ($T_c = 12$ K). In all the considered three compounds, a comparable decrease of T_c to values around $T_{c0}/2$ thus causes an increase of θ_D by ~ 50 K.

For V_3Si , the stiffening of the A15 lattice after irradiation has also been observed by the measurement of the elastic constants by Guha et al. /87/ and by inelastic scattering measurements by Cox and Tarvin /78/. The decrease of the order parameter by quenching also leads to a stiffening of the lattice, as shown by small, but significant increases of θ_D in several A15 type compounds /98/.

d) The Irradiation Temperature

The existence of depleted zones is obviously restricted to low temperatures where neither interstitials nor vacancies show any mobility. An increase of the irradiation temperature, T_{irr} , is expected to favourize self-annealing effects. This was demonstrated by Meier-Hirmer and Küpfer/119/, who irradiated V_3Si single crystals with fast neutrons up to $T_{irr} = 700^\circ C$. As shown in Fig. 4.16, the decrease of T_c with increasing dose is substantially reduced for $T_{irr} = 240^\circ C$ /119/ when compared with data taken at $T_{irr} \leq 150^\circ C$ by

Sweedler et al./69/. The "saturation" of T_c at different levels after heavy irradiation doses with different T_{irr} values has its reasons in recombination effects, which will be discussed in 4.3.7.

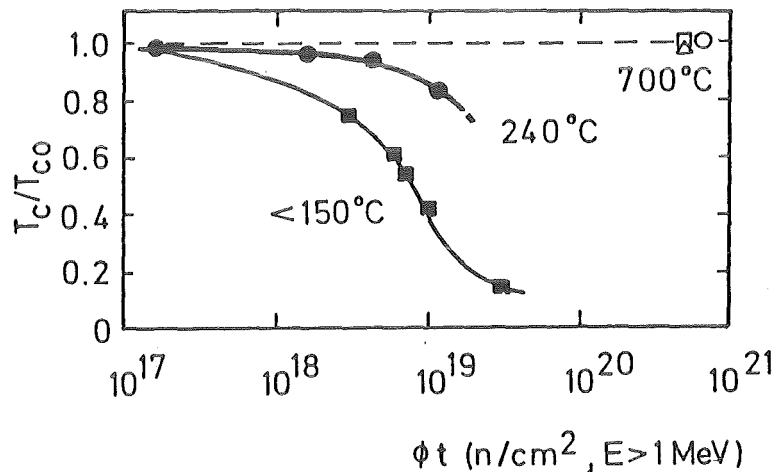


Fig. 4.16. T_c as a function of fast neutron irradiation dose for V_3Si .

■: $T_{irr} \leq 150^\circ C$ (Sweedler et al./69/), ●: $T_{irr} = 240^\circ C$
 ◇: $T_{irr} = 610^\circ C$, □△○: $T_{irr} = 700^\circ C$ (Meier-Hirmer and Küpfer/119/).

The data in Fig. 4.16 can be interpreted as follows: the activation of vacancies at $T_{irr} > 150^\circ C$ has the effect of an annealing which not only increases the average order parameter of the crystal, but leads in addition to the break-down and elimination of the depleted zones. The effect of T_{irr} on size and concentration of the depleted zones has so far not been investigated directly. However, an indirect conclusion is possible on the basis of recovery experiments by Meier-Hirmer and Küpfer/119/ on the same neutron irradiated V_3Si single crystal as shown in Fig. 4.16 (see Section 7). Their data on the recovery of T_c after 2 hours isochronal annealing at different temperatures, T_A , show the existence of two distinctly different recovery stages. The first recovery stage at $T_A \sim 400^\circ C$ is only present for $T_{irr} \geq 150^\circ C$, while the second stage at $T_A \sim 600^\circ C$ is seen at $T_{irr} = 150^\circ C$ as well as for $T_{irr} = 240^\circ C$. Meier-Hirmer and Küpfer /119/ interpreted the first stage as being due to the mobility

of the radiation induced vacancies, i.e. the split vacancies with the corresponding occupied "virtual" sites, the second being correlated to the diffusion of thermal vacancies.

The data in Fig. 4.16 are very suggestive, but would alone not provide sufficient evidence for the exclusion of the inhomogeneous mechanism /103,104,105/ as the cause for the decrease of T_c at low irradiation doses. It is easily seen that not only the radiation induced vacancies, but in principle also the depleted zones could be annealed out at $T_{irr} = 240$ °C. On the other hand, Pande /113/ could not detect any depleted zones at 300 K in neutron irradiated V_3Si (dose: 1.3×10^{19} n/cm², $T_{irr} \leq 150$ °C) by means of transmission electron microscopy. Due to experimental resolution limits, this means either that only depleted zones with sizes considerably below 2 nm (the resolution limit) were present or that they had already been annealed out at this irradiation temperature.

The second possibility has to be favored, since the reordering and diffusion kinetics in V_3Si is generally very rapid compared to that of other A15 type compounds. In order to lower T_c of V_3Si samples by quenching methods, cooling rates well above 10^4 °C/s had to be applied by Pannetier et al./120/ (see also Sect. 7).

In combination with the arguments a) and b) discussed earlier in this section, the present considerations about the effects of T_{irr} on T_c strongly contribute in attributing the responsibility for the decrease of T_c in the low dose regime to a homogeneous lowering of the order parameter. An interesting result was obtained by Meier-Hirmer and K pfer /119/, who reported an increase of T_c up to 17.0 K, i.e. 0.51 K above the initial value, on a V_3Si single crystal after neutron irradiation at $T_{irr} = 700$ °C. The crystal at the initial state was tetragonal at low temperatures while the state after irradiation was cubic, as shown by low temperature diffraction and specific heat measurements. This would mean that the vacancies activated during the irradiation at 700 °C stabilize the cubic phase (which is otherwise unstable for 25 at.% Si under equilibrium conditions), while the crystal is still perfectly ordered. An important consequence can be drawn from this result: activated vacancies as produced by high T_{irr} could contribute in increasing T_c of various A15 type compounds, e.g. transforming, stoichiometric Nb_3Sn or the systems Nb_3Al and

V_3Ga where the atomic order parameter is substantially different from $S = 1$, i.e. $S_a = 0.95$ for Nb_3Al /28/ and $S = 0.95$ to 0.98 for V_3Ga /20/. In the case of Nb_3Al , there is experimental evidence for an increase of T_c after neutron irradiation at $T_{irr} = 500$ °C /167/.

The effects of T_{irr} on T_c presented in this paragraph permit to understand the discrepancies on the decrease of T_c reported in the literature for similar doses. At the same time, they confirm the effects due to the large sample size for specific heat measurements as described in 4.2.2c. These effects are particularly important for high doses. For example, Cort et al./114/ found in Nb_3Al a T_c value of 7.1 K after a neutron dose of 2.6×10^{19} n/cm², while the value measured by Sweedler et al./69/ on small samples is ~ 4 K. Cox and Tarvin /78/ found that their V_3Si single crystal was superconducting at 7.5 K after a neutron dose of 2.22×10^{19} n/cm², while a value of $T_c = 3.4$ K would have been expected /69/, as follows from Fig. 4.10.

It has been shown above that an increase of T_{irr} above room temperature has strong effects on T_c . The question arises whether irradiation at low temperatures, say below 30 K, would lead to other results than for $T_{irr} = 300$ K. Numerous irradiations have been carried out so far on A15 type compounds at low temperatures, with neutrons or ions as radiation source. Although a really systematical work is still missing, the known data do not show relevant differences on T_c when compared to irradiations at $T_{irr} \leq 150$ °C, thus indicating that little recovery occurs in this temperature range.

Another superconducting property, however, the critical current density of A15 based superconducting wires, J_c , could be more affected by the change of T_{irr} from low temperature to ≤ 150 °C. As an example, very recent measurements on J_c as well as on T_c on binary and ternary Nb_3Sn wires after neutron irradiation at $T_{irr} = 4.2$ K ($E = 14$ MeV) have been reproduced in Fig. 10b. An important point when irradiating at low temperature is whether the change of the superconducting properties has been measured "in situ" or after warming up at room temperature after irradiation. In situ measurements have so far only been carried out after heavy ion irradiation. A facility allowing in situ measurements of T_c and J_c after low temperature neutron irradiation just completed at the Oak Ridge National Laboratory will be used by the author and his coworkers for answering the open questions about the effects of T_{irr} .

4.2.3. The Virtual Site Exchange Mechanism in Irradiated A15 Type Compounds

In spite of the fact that the observations in 4.2.2. strongly support a homogeneous decrease of the long-range order parameter over the whole sample volume in irradiated A15 type compounds, a very important question arises: How is it possible that a homogeneous decrease of S implying site exchanges over several lattice spacings can occur during irradiations at temperatures $T \leq 150^\circ\text{C}$, where little thermal diffusion takes place?

Under these conditions, disordering in irradiated A15 type compounds can be caused either by a) local cascade replacements or b) focused replacement collision sequences, a superposition of both being even more probable.

a) Local Cascade Replacements

Interaction between high energy incident particles and the lattice atoms produces a cascade, i.e. the atoms are displaced to produce Frenkel defects in a three-dimensional zone, the depleted zone (see 4.2.2.a). Simultaneously, an even larger number of atoms change their mutual positions (i.e. they are replaced), thus producing locally a decrease of the degree of ordering. In principle, it could be argued that the atomic replacements produced in the cascade would be sufficient to produce disorder in the whole A15 lattice.

However, this argument cannot be generalized, since electron irradiation of A15 type compounds causes the same effect on the superconducting transition temperature, T_c , and the electrical resistivity $|101|$, but produces only isolated Frenkel defects rather than depleted zones (or cascades). Thus, an additional mechanism must be effective in causing a homogeneous decrease of the order parameter. Such a mechanism, requiring atomic transport over several interatomic distances (the condition for a collective phenomenon) is constituted by the focused replacement collision sequences.

b) Focused Replacement Collision Sequences

The so-called focusing replacement collision sequences, introduced by Seeger/109/, represent the transport of matter and energy in irradiated crystals along dense crystallographical directions. Regardless of the crystal structure, an interstitial atom produced by irradiation processes is transported several interatomic distances away from its associated Frenkel vacancy along these "focalizing" crystallographical directions.

Focused replacement collision sequences can occur at the external boundaries of depleted zones with sizes of 4 to 5 nm for neutron irradiation [103] and

up to 15 nm for irradiation with ^{32}S ions/165/. At these boundaries, highly disordered regions are adjacent to the matrix, and a sufficient (but still small number of virtual sites is thus occupied, a necessary condition for the occurrence of focused replacement collision sequences (it may be recalled that this number is still very small, $< 0.1\%$). As irradiation further proceeds, the number of occupied virtual sites will increase, thus leading to an increase of site exchange processes. At the same time, thermal reordering will occur, as follows from the recombination theory of Liou and Wilkes /177/, discussed in 4.3.7.

It can be immediately seen that in the unirradiated state the replacement collision sequences in A15 type compounds occurring in the $\langle 100 \rangle$ and $\langle 111 \rangle$ directions, i.e. along the chains and the diagonal of the cube, are not effective in producing $A \leftrightarrow B$ site exchanges. The only focusing direction where collision sequences could in principle produce $A \leftrightarrow B$ site exchanges is the $\langle 102 \rangle$ direction. However, the atomic sequence in the $\langle 102 \rangle$ direction is oABAoABAo, the space between two ABA sequences coinciding with the region of overlap of two A atoms on the chain being perpendicular to the $\{100\}$ plane. It can be easily shown that this configuration excludes extended site exchanges. Indeed, the potential encountered by A or B atoms on their way along the $\langle 102 \rangle$ direction, calculated using a Born-Mayer interatomic potential /125/ (see Fig. 4.17) shows that $V_{A \rightarrow B}$ and $V_{B \rightarrow A}$ are of the same order of magnitude, ~ 10 eV,

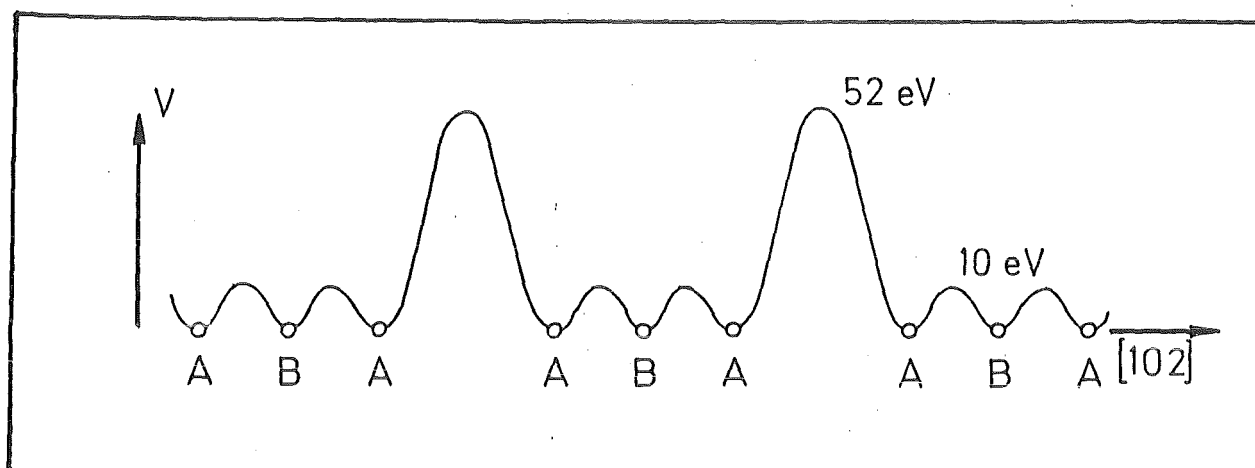


Fig. 4.17. Potential encountered by the A and B atoms on their way along the focusing $\langle 102 \rangle$ direction in the unirradiated state. Since only equilibrium lattice sites are occupied, replacing sequences $A \leftrightarrow A$ are highly improbable /81/.

while $V_{A \rightarrow A}$ reaches 52 eV.

The situation in irradiated crystals is, however, quite different from that encountered prior to irradiation. With the occupation of the virtual sites (a very small number of occupied nonequilibrium sites represented in Figs. 4.1. and 4.3 is sufficient), the potential $V_{A \rightarrow A}$ is considerably lowered. The new sequence of atoms in the focalsing $\langle 102 \rangle$ direction around the occupied virtual site is now oABAAABAOABAo or oBABABAOABAo, depending on the occupation of the virtual site by an A or a B atom, respectively (see Fig. 4.18).

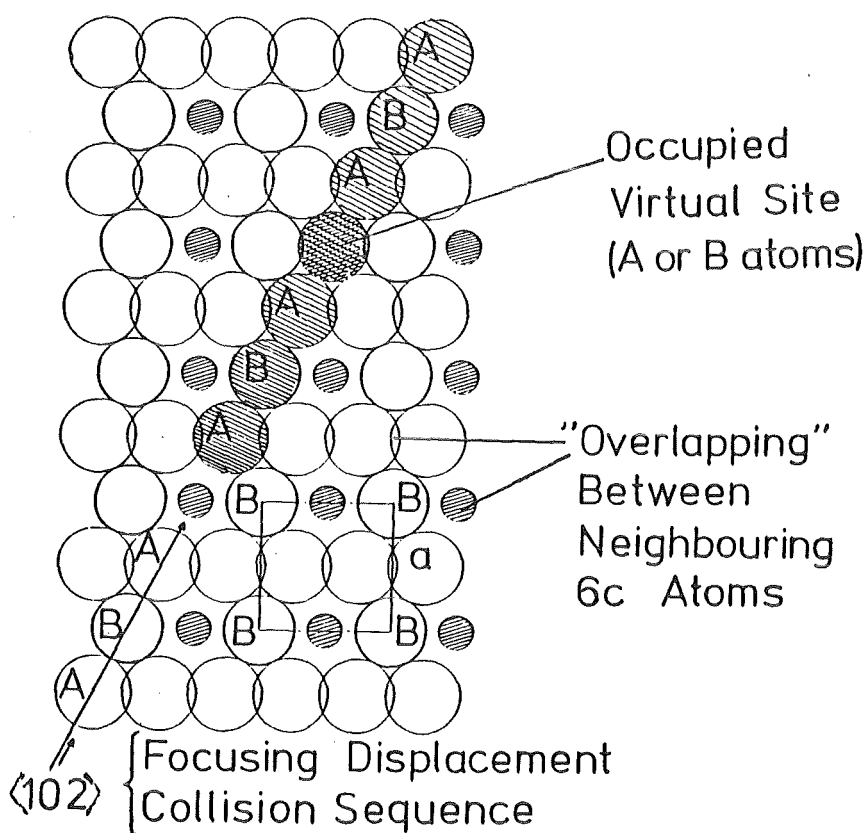


Fig. 4.18. Representation of the $\{100\}$ plane of the A15 lattice (the radii are scaled for Nb_3Al). The small circles correspond to the overlapping region between two A atoms belonging to the chains perpendicular to the $\{100\}$ plane. The occupation of the virtual site by an A or a B atom leads to the sequences oABAAABAO or oBABABAO, respectively instead of oABAOABAo as in the unirradiated case, thus enabling $A \leftrightarrow B$ site exchanges in the $\langle 102 \rangle$ direction. a is the lattice parameter. (Flükiger /6,81/).

As mentioned above, a very small amount of vacancies (or occupied virtual sites) is sufficient for the occurrence of the present mechanism. It should be recalled that for example, density measurements have revealed $\sim 0.3\%$ of lattice vacancies in neutron irradiated V_3Si after a dose of 22.2×10^{18} n/cm², corresponding to a decrease of T_C to a value less than one half of the initial T_C value. Due to the very large number of replacement collisions over the whole crystal volume, the virtual sites will be many times occupied and abandoned again, alternatively by A or B atoms, respectively. The latter constitute a "bridge" between neighbouring ABA sequences, thus allowing $A \leftrightarrow B$ exchanges over several interatomic distances. This is a necessary condition for a homogeneous decrease of the degree of ordering over the whole crystal after irradiation at low temperatures.

A very important conclusion can be drawn from a consideration of the close neighbourhood of an occupied "virtual" lattice site. Its nearest neighbours, 6 A and 2 B atoms, are in close contact with the interstitial, which is either an A or a B atom. In the {100} plane, this leads to the hexagonal arrangement shown in Fig. 4.1.b. The close neighbourhood of the virtual interstice, reproduced in Fig. 4.19, shows some particularities of this nonequilibrium arrangement. If the interstitial atom is of the A type, the occupation of the virtual site leads to 4 additional AA contacts, with AA distances of $5/16a = 0.559 a$, thus 6% more than the AA distances in the chains, $a/2$. In addition, there are 2 AB contacts with interatomic distances of $a/2$ compared to $9/16a$ in the unirradiated A15 lattice, i.e. 6% shorter.

This situation could be compared to that occurring in quench disordered A15 type compounds, where the AB distances are the same, i.e. $a/2$. The case of a B element occupying the virtual site with 4 AB and 2 BB close contacts is more interesting. The AB distances are now $5/16a$, i.e. they are still the same as in the unirradiated A15 structure, but the BB distances are now 36% shorter ($a/2$ with respect to $3a/2$). This would mean that in each case, BB distances shorter than the sum of two B radii would be encountered. Such an "overlapping" between B elements is only possible in the nonequilibrium situation caused by low temperature irradiations or in a dynamic situation during site exchanges at high temperature. It is particularly interesting to consider the case of nontransition B elements, where such close BB contacts are expected to cause strong electrostatic repulsive forces. The occurrence of such BBB sequences (see Fig. 4.19) furnishes the key for understanding

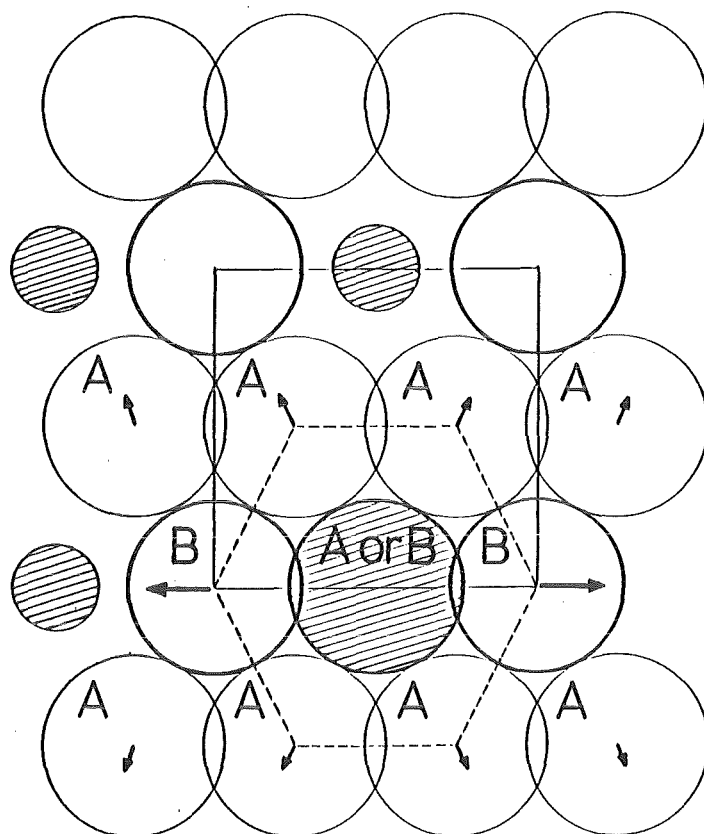


Fig. 4.19. The hexagonal arrangement around the virtual site. Note the BBB sequence if this site is occupied by a B atom.

the causes of the lattice expansion and the static displacements observed in irradiated A15 type compounds (see 4.3.1.).

From these remarks, it can be recognized that the diffusion in the A15 structure is not a simple vacancy diffusion as suggested by Sweedler et al. /69/ nor it corresponds to a so-called interstitialcy diffusion mechanism, where the atom can diffuse from a normal site to an interstitial site. In the case of the A15 structure, the situation is complicated by the fact that a jump into the virtual site (which is an interstitial site) requires simultaneously a rearrangement of the other atoms.

4.2.4. Disordering as Produced by Quenching and by Irradiation: A Comparison

Based on the virtual site exchange mechanism /6,81/, it is now possible to compare the process of disordering in A15 type compounds submitted to apparently very different processes, as quenching from high temperatures or irradiation at high or low temperatures, defined by $T_{irr} \gg 150^{\circ}\text{C}$ and $T_{irr} < 150^{\circ}\text{C}$, respectively. It is immediately seen from Fig. 4.1 a and b that these processes are essentially based on the same mechanism: The occupation of virtual sites.

At high temperature, the occupation of the virtual site is dynamic, having the character of an intermediate state in the course of two-step or multi-step processes connected with the particular diffusion mechanism in A15 type compounds. The time of occupation of a virtual site is expected to be very short, depending on temperature and varying from compound to compound. In order to retain a significant amount of occupied virtual sites, the total cooling time during the quenching process should be shorter than the occupation time. From quenching experiments on V_3Si , where a lowering of T_c is only observed at cooling rates well above 10^5 °C/s [120], the occupation time can be estimated to $\ll 10^{-3}$ s, the probability of retaining occupied virtual sites being thus very low.

Quenching experiments thus retain a certain lattice disorder, but no virtual site occupancy, in contrast to irradiation. In this case, those virtual sites which were occupied at the moment when the sample is taken out of the incident beam remain occupied as long as the sample temperature is kept sufficiently low, e.g. below room temperature.

The main difference between quenching and irradiation resides in the formation process of the vacancies. In quenched crystals, the occurrence of vacancies is a consequence of the anharmonic thermal vibrations of the atoms around their equilibrium lattice site at a given temperature. In irradiated crystals, the formation of vacancies occurs by means of primary collision events. There is also a difference in the mechanism of disordering: In the thermal case, disordering is the consequence of random site exchange, the driving force being a function of temperature, while site exchange due to high energy irradiation occurs along focusing directions, the driving energy being due to the incident particle. As discussed above, however, both cases lead to a homogeneously distributed degree of ordering throughout the whole crystal. Both processes, irradiation and quenching, lead to a nonequilibrium state of the crystal, the major difference being the occurrence of virtual sites and of static displacements (see 4.3.4) after irradiation. The number of radiation induced vacancies is considerably higher than the equilibrium number of vacancies at high temperature, which may be explained by simultaneous occurrence of virtual sites and of static displacements. This fact is also responsible for another associate effect, the observed lattice expansion after irradiation (see next paragraph). A comparison between the mechanisms of disordering after quenching and irradiation, respectively, is given in Table 4.3.

Origin of disordering	Site exchange mechanism	Type of vacancy	Cause of diffusion	Static Displacement	Depleted zones
Quenching from high temperatures	Diffusion	Vacancy at equilibrium sites + split vacancy	Temperature	No	No
Low temperature irradiations ($T_{irr} < 150^{\circ}\text{C}$)	<102> focused replacement collision sequences	split vacancy	Energy of incident particle	Yes ^{a)}	Yes ^{a)}
High temperature irradiations ($T_{irr} \gg 150^{\circ}\text{C}$)	<102> focused replacement collision sequences + diffusion by activated vacancies	Vacancy at equilibrium sites + split vacancy	Temperature + energy of incident particle	No ^{b)}	No ^{b)}

Table 4.3. Comparison between mechanisms of disordering in A15 type compounds submitted to quenching from high temperatures (T_D is the diffusion limit as defined in Table 4.1) and to high energy particle irradiation at high ($T_{irr} \gg 150^{\circ}\text{C}$) and at low ($T_{irr} < 150^{\circ}\text{C}$) temperature.

a) Depending on the mass and energy of the incident particle,

b) Annealed out if T_{irr} is high enough.

4.3. Additional Radiation Induced Effects

4.3.1. The Lattice Expansion in Irradiated A15 Type Compounds

Based on the "virtual" site exchange mechanism /6,81/ leading to AB or BB overlapping, the variation of the lattice parameter in irradiated A15 type compounds can be interpreted as reflecting the electrostatic repulsion between overlapping atoms. In this picture, the repulsion would be smallest between two transition elements, intermediate between a transition and a nontransition element and maximum between nontransition elements. Before to discuss

the effects of irradiation on the lattice parameter, it is useful to consider the repulsion effects in the unirradiated state.

a. The Effect of AB Overlapping

It is possible to estimate the effect of AB overlapping on the lattice parameter by studying the variation of the latter as a function of composition in A15 systems where the phase field extends to both sides of stoichiometry. This is the case for four systems, where the A15 phase is stable within following composition ranges: Nb_3Pt , $0.20 \leq \beta \leq 0.30$ /92/, Nb_3Ir , $0.22 \leq \beta \leq 0.28$ /127/, V_3Pt , $0.19 \leq \beta \leq 0.325$ /62,128/ and V_3Ga , $0.18 \leq \beta \leq 0.32$ /19,20/. At compositions exceeding $\beta = 0.25$, the number of B atoms exceeds that of available 2a sites, and the quantity $(\beta - 0.25)$ of B atoms will thus be located on 6c sites, giving rise to AB overlapping. The repulsive effect of the presence of B atoms on the chain sites can be visualized

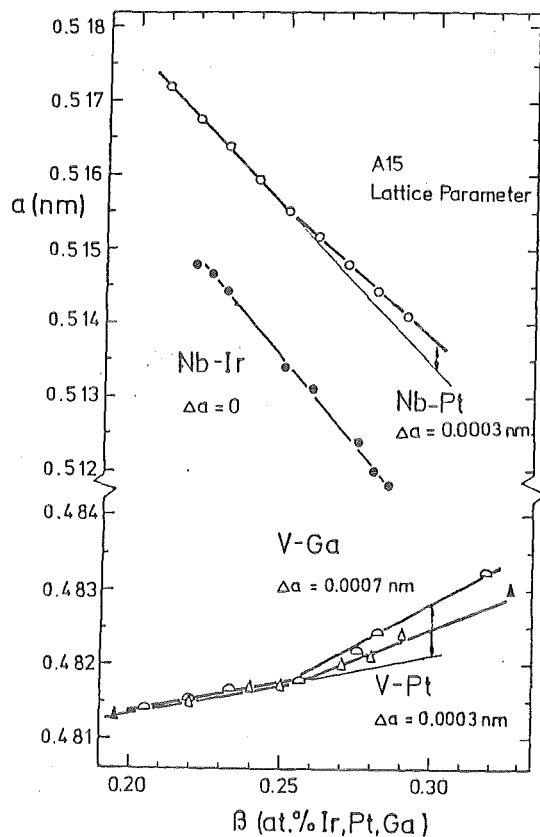


Fig. 4.20. Lattice parameter as a function of composition in the system Nb-Pt (o, Ref. 76), Nb-Ir (●, Ref. 127), V-Pt (▲, Ref. 128; △, Ref. 62) and V-Ga (◻, Ref. 19,20). For comparison, Δa has been indicated for the composition $\beta = 0.30$ and is defined as the difference between the measured lattice parameter and the value obtained by extrapolating the portion below 0.25 (Flükiger /81/).

by the different slopes $da/d\beta$ at both sides of the stoichiometric composition. It can be seen from Fig. 4.21 that a lattice expansion at compositions $\beta = 0.25$ is observed in the systems Nb_3Pt , V_3Pt and V_3Ga . In the system Nb_3Ir , no lattice expansion can be detected within the limits of accuracy.

At $\beta = 0.30$, which corresponds to 6.7% of 6c sites occupied by B atoms (or to Bragg-Williams order parameters $S_a = 0.78$ and $S_b = 1$), the measured value of a is larger than the extrapolated value from the data at $\beta < 0.25$, the positive difference (corresponding to an expansion) being $\Delta a = 0.0003$ nm for Nb_3Pt /76/, ≤ 0.0001 nm for Nb_3Ir /62,127/, 0.0003 nm for V_3Pt /62,128/ and 0.0007 nm for V_3Ga /19/. The lattice expansion $\Delta a = \Delta a(\beta)$ for V_3Ga exceeds that for the Pt based systems by more than a factor of two. This can be interpreted as the effect of stronger repulsion due to the presence of the nontransition element Ga on the 6c sites. Indeed, there are now interactions between a nontransition and a transition element (represented by V_{6c} and Ga_{6c}) and between two nontransition elements (Ga_{6c} and Ga_{2a}), the distances $V_{6c} - Ga_{6c}$ (0.2409 nm) and $Ga_{6c} - Ga_{2a}$ (0.2693 nm) being both shorter than the sum of the corresponding Pauling/139/ or Geller/140/ radii, discussed in the next paragraph.

b. The Effect of AA Overlapping

There is an additional case where a variation of the lattice parameter can be interpreted as being caused by electrostatic repulsion effects. This case, described in detail in Ref. 7, is the existence of a "bulk" limit for the lattice parameter, a , in the series $Nb_{1-\beta} B_\beta$ crystallizing in the A15 type structure, where B is nontransition element (see Fig. 4.21). The "bulk" limit is the lowest lattice parameter which can be obtained on samples prepared by melting, and is situated around $a = 0.5170$ nm. A further reduction of this value, e.g. a reduction of nearest neighbour distance between Nb atoms on the 6c sites can only be obtained by nonequilibrium procedures. In Nb_3Ga and Nb_3Ge , the values $a = 0.5163$ and 0.5150 nm, corresponding to compositions $\beta = 0.25$ /26,65,93/ and 0.23 /67,131/, respectively, have been measured after splat cooling. By means of co-evaporation or sputtering, even lower lattice parameters were obtained in the system Nb_3Ge , i.e. $a = 0.5140$ nm/73,74/. The lowest lattice parameter in the system Nb_3Si , $a = 0.509$ nm, has been obtained after explosive compression /130/, which transformed the Ti_3P phase into the A15 phase. The same compound was synthesized by sputtering/132/ or splat cooling/133/, however, with considerable deviations from stoichiometry. The lattice parameters of the Nb_3Si samples prepared by these techniques are $a = 0.5134$ nm/132/ and $0.5\dots$ nm/133/, respectively.

As follows from Fig. 4.21, the corresponding "bulk" limit of a for Nb_3B compounds with a transition B element, e.g. Os or Ir is situated at $a = 0.5117$ nm, which is considerably lower than for nontransition B elements. This fact illustrates the stronger repulsion between A and B atoms in the A15 structure if B is a nontransition element (the shortest AB distance for Nb_3Ge is 0.2827 nm, compared to the shortest AA distance, $a/2 = 0.257$ nm).

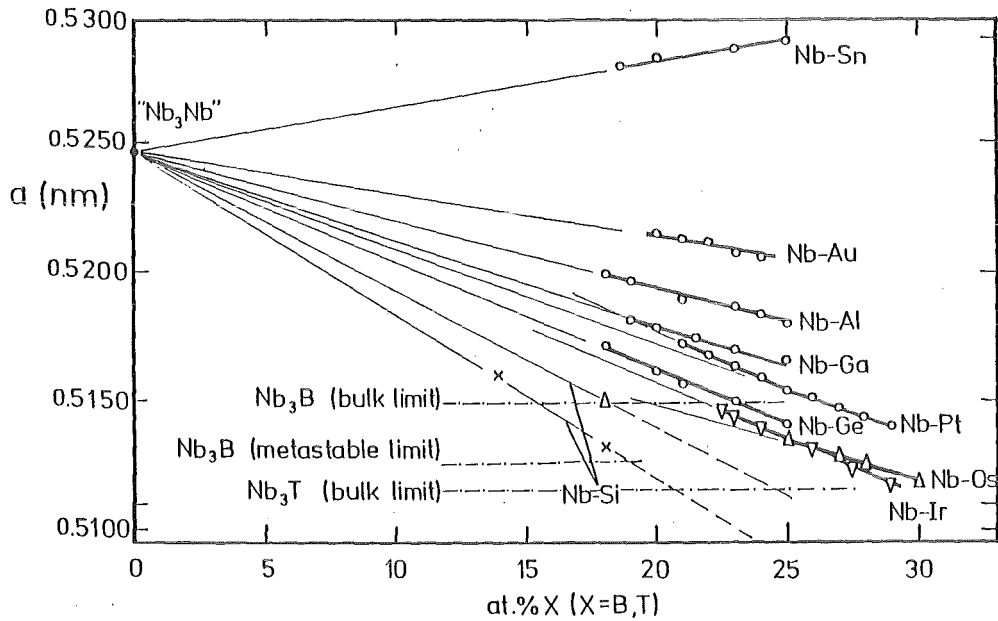


Fig. 4.21. Lattice parameter of $Nb_{1-\beta}X_\beta$ compounds as a function of the X content. For $X = B$ (nontransition element), the extrapolation to $\beta = 0$ meets the value $a_0 = 0.5246$ nm for $"Nb_3Nb"$. For $X = T$ ($T =$ transition element), a extrapolates to values $a < a_0$. This representation illustrates the stronger repulsion between Nb atoms in the case of localized d electrons. The lattice parameter of $"Nb_3Si"$ is extrapolated to values around $a = 0.509$ nm (Flükiger /7/).

c. Irradiation and the Lattice Parameter

Characteristic differences between transition and nontransition B elements can also be found when analyzing the known data on the lattice expansion in A15 type compounds after irradiation with various high energy particles. The observed increase of the lattice parameter, Δa , in several A15 type compounds is represented in Fig. 4.22 for neutron irradiation and in Figs. 4.23 a and 4.23 b for H and ^{32}S ion irradiation, respectively. In spite of the small number of reported data, it can be concluded that Δa is considerably smaller if B is a transition element, e.g. Os, Ir or Pt.

The increase of the lattice parameter, Δa , after neutron irradiation (in particular the initial expansion at low doses) is indeed considerably stronger for Nb_3Ge , Nb_3Sn , Nb_3Al and V_3Si than for the compounds Nb_3Pt and Mo_3Os , where B is a transition element, as shown in Fig. 4.22 and 4.23, where all reported data on the lattice expansion of A15 type compounds after irradiation with high energy particles are summarized.

An interesting comparison between the lattice expansion in irradiated A15 type compounds with transition and nontransition B elements is made in Fig.

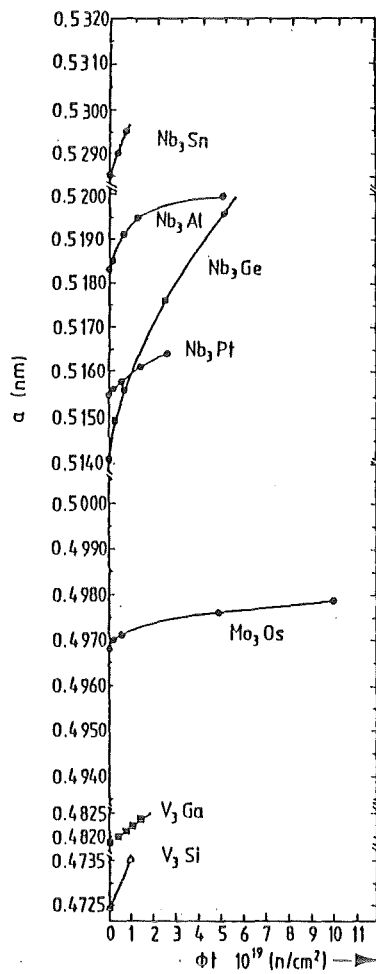


Fig. 4.22. Lattice parameters of various A15 type compounds as a function of the neutron irradiation dose ($E \geq 1 \text{ MeV}$). Data for Nb_3Sn , Nb_3Al , Nb_3Pt , Nb_3Ge , Mo_3Os : Sweedler et al./69/, for V_3Si : Cox and Tarvin/78/, for V_3Ga : Francavilla et al. /134/.

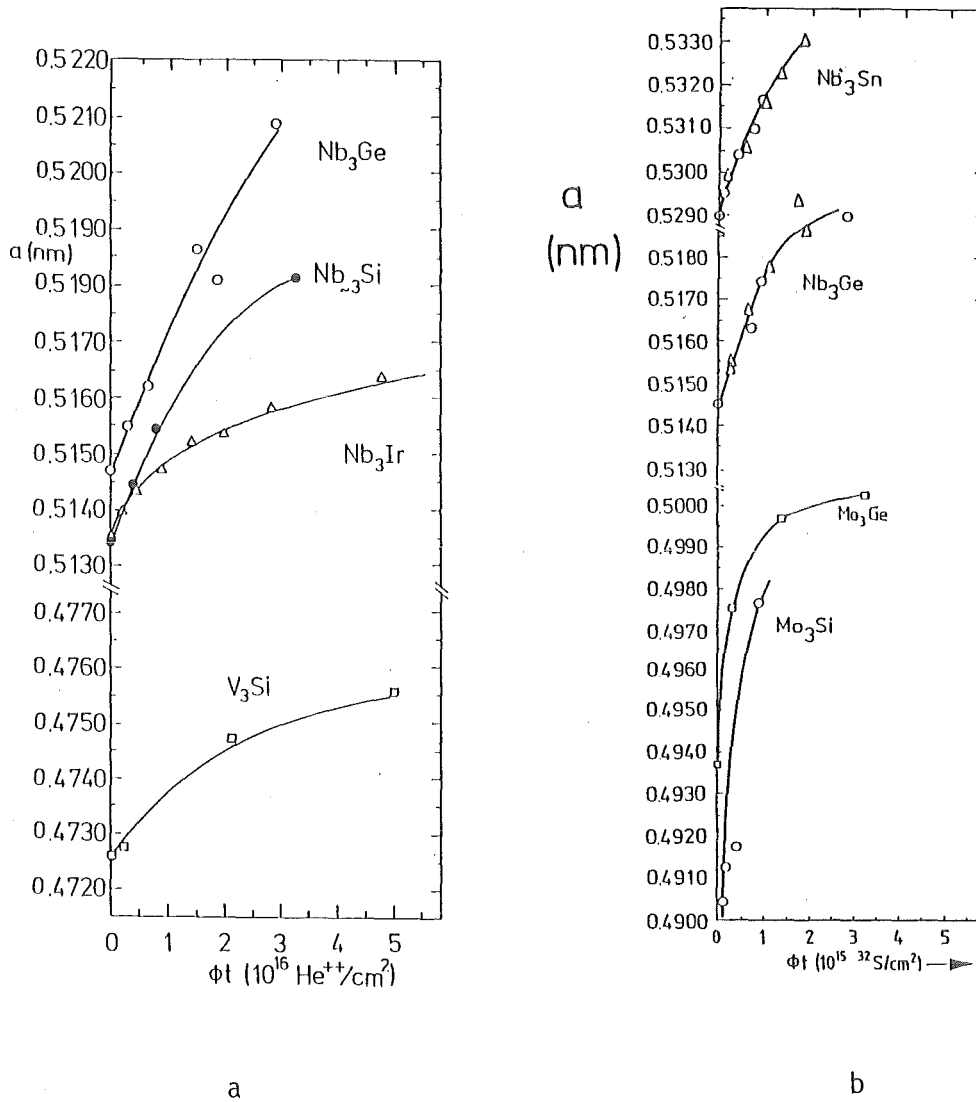


Fig. 4.23. Lattice parameters of various types of A15 type compounds as a function of irradiation dose. a) ^4He ions ($E \geq 0.3$ MeV). Data for V_3Si : Meyer and Seeber/106/, for Nb_3Al : Schneider et al./55/, for Nb_3Ir : Schneider and Linker/135/, b) ^{32}S ions ($E \geq 25$ MeV). Data for Nb_3Sn and Nb_3Ge : o P. Müller /181/, Δ Nölscher and Saemann-Ischenko /136/, for Mo_3Si : Lehmann and Saemann-Ischenko /137/, for Mo_3Ge : Lehmann et al. /138/.

4.23 a, where the values of Δa for Nb_3Ir are plotted together with those of Nb_3Si and Nb_3Ge after He ion irradiation. After a proton dose of $3 \times 10^{17} \text{ H}^+/\text{cm}^2$, the increase of the lattice parameter in Nb_3Si and Nb_3Ge is 0.0047 and 0.0059 nm, respectively, i.e. more than twice as large as the corresponding value for Nb_3Ir , $\Delta a = 0.0021 \text{ nm}/55/$. The large lattice expansion in Mo_3Ge and Mo_3Si , $\Delta a = 0.0072 \text{ nm}$ or $\Delta a/a = 1.3\%$ reported by Lehmann and Saemann-Ischenko /137/ and Lehmann et al./138/ after irradiation with ^{32}S ions is also in sharp contrast to the value $\Delta a/a = 0.18\%$ reported for neutron irradiated Mo_3Os by Sweedler et al./69/.

From Figs. 4.22 and 4.23, it can further be seen that the magnitude of the lattice expansion is very similar for all the radiation sources, the maximum values of the lattice parameter in the region where T_c saturates being, however, slightly smaller for neutron irradiations. The case of Nb_3Al shows the most apparent difference between neutron and N^{++} irradiations.

At low doses, the compound Nb_3Al shows the same initial lattice expansion as the other A15 type compounds with nontransition B elements (see Fig. 4.22). At high doses (in the saturation region of T_c), Schneider et al./55/ reported a maximum value of $\Delta a = 0.0032$ nm (at $10^{15} N^{2+}/cm^2$), i.e. nearly twice as the "saturation" value of the lattice expansion in Nb_3Al after neutron irradiation, $\Delta a = 0.0017$ nm (at $4.7 \times 10^{19} n/cm^2$) as reported by Sweedler et al./69/ and Moehlecke/183/.

For the present work, the behavior at high doses is of secondary interest, since the behavior of T_c is dictated by a superposition of several effects, leading finally to the "saturation" of T_c . Nevertheless, it is interesting that at high doses, the damage caused by different projectiles at different irradiation temperatures leads to specific differences in the values of Δa and T_c even to a radiation-induced phase transformation in N^{++} irradiated Nb_3Al , as found by Schneider et al./55/.

The question arises about the possible reasons for the individual changes of $\Delta a/a$ in each A15 type compound. A correlation between $\Delta a/a$ and the atomic radius ratio, r_A/r_B , has been proposed by Sweedler and Cox/53/. However, it will be shown in the following paragraph that the dominant factor influencing Δa is the nature of the B element, the ratio r_A/r_B being of secondary importance only. This ratio is only relevant when comparing the behavior of Δa among compounds with non-transition B elements. All known data have been summarized in Table 4.4. These results confirm the hypothesis of an enhanced electrostatic repulsion between AB neighbours but particularly between BB neighbours around an occupied "virtual" site if B is a nontransition element. A detailed comparison will be made in the next paragraph where different sets of atomic radii are discussed.

System	a (nm)	$\Delta a/a$ (%)				r_A^G/r_B^G	r_A^P/r_B^P	Ref.
		y=1	y=2	y=3	($y \cdot 10^{15}$ $^{32}\text{S}/\text{cm}^2$)			
Nb ₃ Ge	0.5140	0.61	0.87	1.05	1.119	1.111	149	
Nb ₃ Sn	0.5289	0.51	0.73	(0.91)	1.041	0.950	136	
Mo ₃ Ge	0.4937	1.11		1.32	1.044	1.066	138	
Mo ₃ Si	0.4900	1.16			1.068	1.112	137	

System	a (nm)	$\Delta a/a$ (%)				r_A^G/r_B^G	r_A^P/r_B^P	Ref.
		y=0.5	y=1	y=3	y=5 ($y \cdot 10^{16}$ He/cm ²)			
Nb ₃ Ge	0.5147	0.23	0.42	1.20	1.119	1.111	149	
Nb _{~3} Si	0.5134	0.27	0.47	0.93	1.144	1.158	123	
Nb ₃ Ir	0.5133	0.20	0.25		1.110	1.077	135	
V ₃ Si	0.4727	0.13	0.21		0.992	1.057	148	

System	a (nm)	$\Delta a/a$ (%)			r_A^G/r_B^G	r_A^P/r_B^P	Ref.
		y=1	y=3	y=5 ($y \cdot 10^{19}$ n/cm ²)			
Nb ₃ Ge	0.5140	0.38	0.76	1.07	1.119	1.111	69
Nb ₃ Sn	0.5289	0.25			1.041	0.950	69
Nb ₃ Al	0.5183	0.19	0.27	0.31	1.094	1.047	69
Nb ₃ Pt	0.5155	0.08	0.17		1.094	1.051	69
Mo ₃ Os	0.4968	0.10	0.12	0.18	1.037	1.036	69
V ₃ Ga	0.4818	0.10			0.956	0.965	134
V ₃ Si	0.4725	0.21			0.992	1.057	78

Table 4.4. Lattice parameter changes in several A15 type compounds after irradiation with neutrons ($E \geq 1$ MeV), He ions ($E = 300$ keV) and ^{32}S ions ($E \geq 20$ MeV). For comparison, the ratios between the Pauling/139/ and the Geller/140/ radii of the A and B atoms have been added. For Nb and Mo based compounds, the values of $\Delta a/a$ are considerably smaller if B = Os, Ir, Os, i.e. if B is a transition element.

d. Atomic Radii and their Limitations in Disordered A15 Type Compounds

There have been different attempts to calculate the lattice parameter of the A15 structure for various compounds by assuming spherical shapes for the A and B constituents. Different sets of atomic radii have been proposed, which differ more or less from the more general definition of Goldschmidt radii, defined for a coordination number 12. Two sets of atomic radii have been most used, the Pauling/139/ and the Geller radii/140/. Before to compare them, it should be recalled that no set of radii will ever be able to predict the correct lattice parameters of A15 type compounds, since the AA interatomic distance between 6c atoms is always smaller than the interatomic distance in the elementary form. This means that nonspherical atomic shapes should be introduced, a problem of great complexity. Nevertheless, both models /139,140/ have been able to predict the A15 lattice parameters of stoichiometric A15 type compounds within a precision of 1%. However, their application to nonstoichiometric compounds or to disordered compounds reveals the limits of both models.

The Geller Model

On the basis of neutron irradiation studies on Nb₃Al and Nb₃Pt, Sweedler and Cox/53/ and later Moehlecke et al./99/ attributed the observed lattice expansion to site exchanges of the atoms A and B having different radii. This explanation is based on geometrical arguments due to Geller/140/, who proposed a simple model for calculating the lattice parameter, based on atomic contacts between spherical A and B atoms. He found the formula

$$a = \frac{4}{\sqrt{5}} (r_A^G + r_B^G) \quad (4.3)$$

where r_A^G and r_B^G are the corresponding Geller radii, listed in Table 4. for several elements. However, it can be easily shown that the agreement between the above mentioned data on Nb₃Al with Eq. (4.3) found by Sweedler et al./53/ is accidental and is due to the fact that Al has a considerably smaller atomic radius than Nb (see Table 4.4). For this purpose, the lattice parameter for a stoichiometric A15 type compound A₃B is calculated, using average radii for the respective occupation of the sites 6c and 2a:

$$\begin{aligned} r_A(S) &= r_a r_A + (1 - r_a) r_B \\ r_B(S) &= r_b r_B + (1 - r_b) r_A \end{aligned} \quad (4.4)$$

where r_a and r_b are the occupation probabilities for atoms A and B on the sites 6c and 2a, respectively.

Compound	r_B (nm) Goldschmidt radius	r_B^G (nm) Geller radius/140/	r_B^P (nm) Pauling radius/139/	a_0 (nm)
Nb ₃ Pt	0.139	0.138	0.1388	0.5155
Nb ₃ Ge	0.137	0.136	0.1314	0.5140
Nb ₃ Ga	0.141	0.137	0.1381	0.5167
Nb ₃ Al	0.143	0.138	0.1393	0.5180
Nb ₃ Sn	0.162	0.145	0.1536	0.5290
V ₃ Ga	0.141	0.137	0.1381	0.4816
V ₃ Si	0.132	0.132	0.1260	0.4724
Nb	0.146	0.151	0.1459	
V	0.134	0.131	0.1332	
Mo	0.139	0.141	0.1401	

Table 4.5. Different sets of atomic radii for A and B elements in some high T_c A15 type compounds. The different radii are defined in the text.

If the radii $r_A(S)$ and $r_B(S)$ are introduced in Eq. (4.4), the increase Δa between the lattice parameter of the unirradiated crystal (which for simplicity will be supposed to be perfectly ordered, i.e. $S = 1$) and that of the irradiated crystal with the order parameter S will be

$$\Delta a = a(S) - a(S = 1) = \frac{8}{\sqrt{5}} (1 - r_a) (r_A^G - r_B^G), \quad (4.5)$$

which leads to the conditions

$$\Delta a > 0 \text{ for } r_A^G > r_B^G \quad (4.6)$$

and $\Delta a < 0$ for $r_A^G < r_B^G$.

The validity of Eq. (4.5) is, however, contradicted by the absence of observed lattice parameter changes in quenched disordered A15 type compounds. Indeed in quenched Nb₃Al/28/ Nb₃Ga/26/, V₃Ga/20/, V₃Au/18/ and Nb₃Pt/62,142/ with a change in S up to 0.08 and a T_c reduction of ~4K, the author and his coworkers

could not detect any changes in the lattice parameter within the experimental error, ± 0.0001 nm. The largest depression in T_c , ~ 4 K, was observed after argon jet quenching in the system $Nb_3Pt/62,142/$, after the treatments described as follows. Arc melted Nb_3Pt was homogenized at $1800^\circ C$ for 24 hours and then annealed 30 days at $900^\circ C$, thereafter it was characterized by $T_c = 11.1K$ and $S = 0.98$ (for the absolute value of S in Nb_3Pt (see Sect. 5)). The same Nb_3Pt sample was then argon jet quenched from $1900^\circ C$, after which the values $T_c = 7$ K and $S = 0.88 \pm 0.03$ were measured, while the lattice parameter remained unchanged within the experimental accuracy of ± 0.0001 nm. It is now interesting that in neutron irradiated Nb_3Pt with $T_c = 7K$ and $S = 0.88$ after the dose of $5.8 \times 10^{18} n/cm^2$, an increase of the lattice parameter from $a = 0.51545$ nm to $a = 0.51575$ nm was observed/76/. This variation is still smaller than the value expected using Eq. (4.4), i.e. $a = 0.51625$ nm.

From the small variations of $\Delta a = \Delta a(\beta)$ in Fig. 4.20, it can be understood why no lattice parameter changes have been observed so far in quench disordered A15 type compounds. Indeed, the variations of the order parameter after quenching are limited to $S \leq 0.10 /142/$ (or $S_a \leq 0.10 /142/$), while the values of Δa have been taken up to $\Delta \beta = 0.05$, i.e. $\Delta S_b = 0.22$. For V_3Ga , a change $\Delta S = 0.02$ has been observed, which would correspond to a variation $\Delta a = 0.00007$ nm. The corresponding change for Nb_3Pt is $\Delta S = 0.06$, which would lead to the expansion $\Delta a = 0.00008$ nm. In both cases, V_3Ga and Nb_3Pt , the value of Δa is just below the accuracy of lattice parameter determinations, ± 0.0001 nm. (It is of course possible to measure the lattice parameter with a higher accuracy, but the necessary sophisticated procedures have not been used in the works mentioned above).

From these remarks, it follows that the Geller model/140/ is inappropriate in describing the variation of the lattice parameter in A15 type compounds as a function of either the atomic order parameter or stoichiometry:

- i) Eq. (4.5) would predict a contraction of the lattice for A15 systems with $r_A^G < r_B^G$, as for example V_3Ga . However, measurements of Francavilla et al./134/ have shown that a lattice expansion is observed in neutron irradiated V_3Ga , similarly as in all other A15 type compounds measured so far (see Fig. 4.23 a).
- ii) The Geller model/140/ also fails in describing the effects of stoichiometry on the lattice parameter changes. For example, the lattice parameter in the system $Nb_{1-\beta}Sn_\beta$ as a function of the Sn content should be minimum at the stoichiometric composition, $\beta = 0.25$, if the Geller radius for Sn, 0.144 nm, were correct. In reality, the lattice parameter is maximum at $\beta = 0.25$,

$a = 0.5289$ nm, as shown in Fig. 4.21. Similarly, stoichiometric V_3Si should exhibit a maximum of a , while in reality a minimum is observed: $a = 0.4724$ nm for $\beta = 0.25$ and $a = 0.4736$ nm for $\beta = 0.20/141/$.

iii) The positive change of the slope $da/d\beta$ at $\beta \geq 0.25$ in Fig. 4.20 for V_3Pt and Nb_3Pt can also be found by applying the Geller model/140/, while no change is predicted by the Pauling model /139/. However, the agreement with the Geller model is again accidental, since a) the calculated change of $da/d\beta$ would be much larger than the measured value and b) in the case of V_3Ga , a contraction instead of the observed expansion would be expected.

The Pauling Model

Pauling/139/ has proposed a formula for calculating the A15 lattice parameter which takes into account the relative proportions of A and B atoms,

$$a = \frac{4}{\sqrt{5}} (3/2 r_A^P + r_B^P) \quad (4.7)$$

where r_A^P and r_B^P are the corresponding Pauling radii (also listed in Table 4.5).

As reported earlier by the author /81/, there are several arguments in favour of the Pauling model, in spite of the unsatisfactory situation of approximating 6c atoms by spheres:

- a) It describes correctly the trend of the lattice parameter with composition, $a = a(\beta)$, represented in Figs. 4.20 and 4.21,
- b) It gives correctly the invariance of the lattice parameter against order parameter changes. The same procedure as in Eq. (4.4) yields indeed $\Delta a(S) \equiv 0$, independently of the size of the respective radii, thus agreeing with the results for quenched A15 type compounds,
- c) The Pauling radii are in general very similar to the Goldschmidt radii, as can be verified from the column $\Delta(r^P - r^{Gold})$ in Table 4.5. The difference is below 0.0010 nm for transition metals, the discrepancy observed for the elements Ru, Co, Ni, Ti and Ta mainly arising from the fact that r^P in these cases was calculated using lattice parameters of nonstoichiometric compounds/140/. The main conclusion which can be drawn from this comparison is the negative difference $\Delta(r^P - r^{Gold})$ for the nontransition elements Al, Ga, Si, Ge, Sn and As, which is comprised between 0.0030 and 0.0080 nm (see Table 4). A possible way to interpret this result consists in assuming that these nontransition elements are under considerable compression in the A15 structure. This would lead to the picture the A15 structure composed by or-

thogonal chains with strong attractive forces between AA neighbours, exerting a compression on B atoms on the 2a sites. This compression would be strongest for nontransition elements.

More recently, Lam and Cohen/143/ have shown that the calculation of A15 lattice parameters for stoichiometric as well as for nonstoichiometric compounds can be performed by using either atomic radii or volumes. For an A15 type compound of the general formula $A_{1-\beta}B_\beta$, they derived the formula

$$a = 8^{1/3} ((1 - \beta)V_A + \beta V_B)^{1/3} \quad (4.8)$$

where β is the atomic content of the atom B and V_A and V_B are the effective volumes, obtained by refinement with the known a values. From the effective volumes, a new set of radii, R , was found, which is very similar to that originally proposed by Pauling/139/ and will not be introduced here. It is interesting that by expanding Eq. (4.7) and using the approximation $\Delta V/V = 3\Delta R/R$, Lam and Cohen/143/ essentially reproduced the Pauling formula (Eq. (4.7)).

As a conclusion, there is no simple correlation between the lattice expansion in irradiated A15 type compounds and the atomic radius ratio, r_A^P/r_B^P of the constituents. The value of Δa is primarily influenced by the nature (the electronic configuration) of the B element, which in turn influences the repulsion between B atoms in the complex around the "virtual" site (see the hexagonal arrangement in Figs. 4.18 and 4.19). The ratio r_A^P/r_B^P has a small influence on Δa only for B elements with similar electronic configuration, e.g. nontransition elements. The lattice expansion is smallest for transition B elements as Os, Ir and Pt.

The Machlin Model (Crystal Field Modified Model)

A main objection towards the Pauling model is obviously the spherical approximation. Machlin and Whang/294/ have developed a model, the "Crystal Field Modified Model", which for simplicity will be called the Machlin model in the following. The denomination "Crystal Field" arises from the fact that instead of a spherical electron density distribution associated with point site symmetry the calculation is effectuated with that of an oblate spheroid taking into account the D_{2d} point symmetry of an atom on a chain site in the A15

structure (The tetragonal crystal field arises from the D_{2d} point symmetry) /294/. The crystal field induced electron transfer between orthogonal d states results in a change in screening such that the screening of the outermost sp shell of electrons by the inner d electrons is no longer spherically symmetric. A main feature of Machlin's model is the introduction of an ionicity correction the results thus depending on the choice of a suitable electronegativity scale. The electronegativity correction was introduced as an empirical correction, in order to eliminate the systematic deviations of the calculated lattice parameter values with respect to the observed ones. The correction consists in modifying the electronegativity of the component situated at particular sites of a given structure. For the A15 structure, the electronegativity of the atom occupying the chain sites (6c) was taken to 0.68 of its normal value. Machlin and Whang /294/ mention that no other adjustable parameter were needed for calculating the lattice parameters. As a main result, the Machlin model allows to calculate the lattice parameter of A15 type compounds within a r.m.s. deviation of 0.4 % (approximately 0.0020 nm) with respect to the observed values.

It is clear that such a way to calculate the A15 lattice parameters taking into account the crystal symmetry, thus calculating with oblate spheroids is physically more meaningful than using spherical atomic shapes. On the other hand, it requires more complex calculations and a rather empirical electronegativity correction. As will be shown in 6.2.2, the Machlin model can be used for calculating the energies of formation in selected (cubic) phases, e.g. A1, $L1_2$, A2 and A15. In addition, it gives the approximate order parameter in a series of A15 type compounds.

4.3.2. The Radiation Induced Lattice Expansion and the Variation of T_c

Since the lattice expansion and the decrease of the atomic order parameter occur simultaneously in irradiated A15 type compounds, it is difficult to decide whether the lattice expansion has an influence on T_c or not. This question can be answered by comparing with the data of quench disordered compounds, where important changes of T_c were measured without any observable variation of the lattice parameter /142/. After having demonstrated that homogeneous changes of the order parameter occur during irradiation (see 4.2.2.), the variation of T_c vs. S for Nb_3Pt in Fig. 4.12 suggests that the variation of the lattice parameter has, if at all, a small influence on the observed variation of T_c . Of course, this conclusion would be more stringent if the direct comparison of

T_C vs. S could have been effectuated for a compound with a nontransition B element, which is unfortunately not possible, the variation of S in V_3Ga or Nb_3Al after quenching being too small.

By comparing the variation of T_C and of the lattice parameter after irradiation with different particles, it can be seen that these two quantities are not directly correlated. Fig. 4.24 shows the variation T_C vs. a for Nb_3Sn after irradiation with neutrons ($E > 1$ MeV, $T_{irr} = 150$ °C, Ref. 69), 4He ions (1.9 MeV, $T_{irr} = 300$ K, Ref. 144) and ^{32}S ions ($E = 20$ MeV, $T_{irr} \leq 30$ K, Ref. 136). The data in Refs. 136, 144 have been obtained on thin Nb_3Sn films, where the stresses arising from the differential thermal contraction between superconductor and substrate have to be corrected. A correction formalism developed by Haase/160/ has been used in these cases. It is seen from Fig. 4.24 that the same value of T_C can correspond to different lattice parameter values, $\Delta T_C/\Delta a$ ranging from 30.1 to 51.8 K/nm, depending on the projectile and on T_{irr} . The case of Nb_3Al is

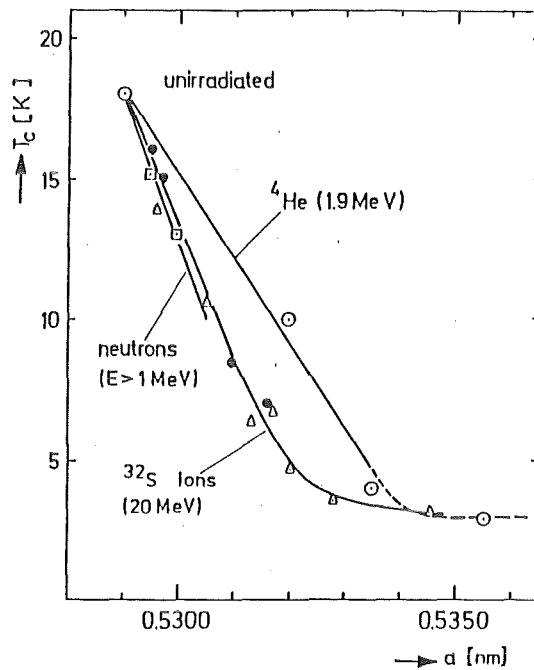


Fig. 4.24. T_C of Nb_3Sn as a function of the lattice parameter after irradiation with neutrons ($E > 1$ MeV, $T_{irr} = 150$ °C, Sweedler et al./69/), 4He ions ($E = 1.9$ MeV, $T = 300$ K, Burbanks et al./144/) and ^{32}S ions ($E = 20$ MeV, $T = 20$ K, Nölscher and Saemann-Ischenko /136/).

illustrated in Fig. 4.25, showing the decrease of T_C as a function of the lattice parameter variation, Δa , for three types of projectile, i.e. > 1 MeV neutrons/69/, 300 keV protons and 700 keV He ions/55/, the corresponding ratios $\Delta T_C/\Delta a$ being -77, -85 and -60 K/nm, respectively. In both cases; Nb_3Al and Nb_3Sn , it is thus seen that very different values of T_C are observed at the same lattice parameter value.

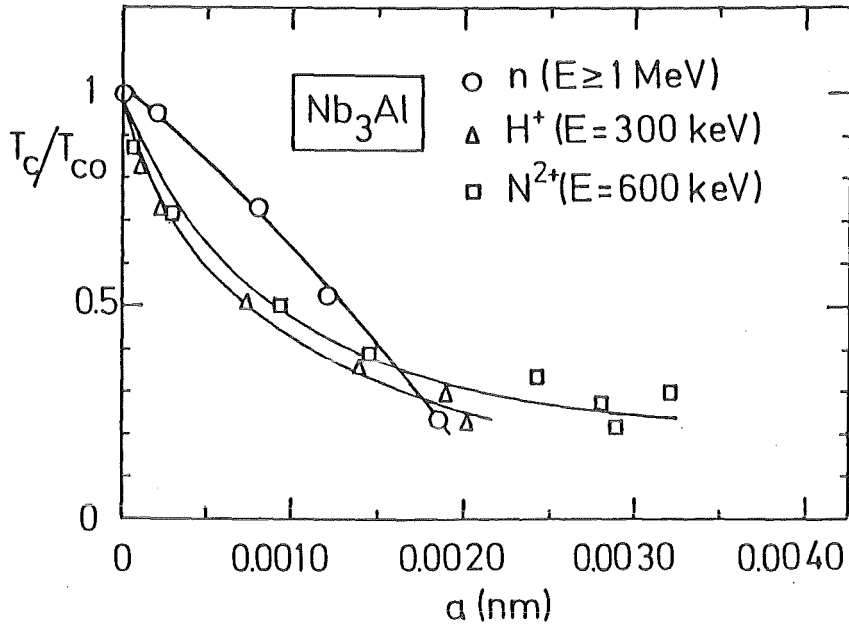


Fig. 4.25. T_c/T_{c0} of Nb_3Al as a function of the lattice parameter change after irradiation with fast neutrons ($E \geq 1$ MeV, Sweedler and Cox/53/) N^{2+} ions (700 keV) and protons (300 keV, Schneider et al./55/). T_c/T_{c0} was chosen because of different values of T_{c0} in Refs. 53 and 55.

Compound	T_{c0} (K)	a_0 (nm)	source	Energy (MeV)	$\Delta T_c/\Delta a$ (K/nm)	Ref.
Nb_3Ge	20.2	0.5141	n	≥ 1	-54.5	Sweedler /69/
	20.3	0.5140	^{32}S	20	-46.3	
Nb_3Sn	18.0	0.5290	n	≥ 1	-51.8	Sweedler et al./69/
	18.0	0.5289	^{32}S	20	-50.0	Nölscher et al. /136/
	18.0	0.5290	4He	1.9	-30.1	Burbanks et al./144/
Nb_3Al	18.6	0.5183	n	≥ 1	-77.0	Sweedler /53/
	15.6	0.5191	H^+	0.3	-85.0	Schneider /55/
	15.6	0.5191	N^{2+}	0.7	-60.0	Schneider /55/
V_3Si	17.0	0.4725	n	≥ 1	(-95.0)	Cox /78/
Nb_3Pt	10.6	0.5155	n	≥ 1	-120.0	Moehlecke /76/
V_3Ga	14.6	0.4818	n	≥ 1	-64.1	FrancaVilla /134/

Table 4.6. Lattice expansion and T_c changes in different A15 type compounds after irradiation with high energy particles.

The available data for the ratio $\Delta T_C / \Delta a$ as determined for different A15 type compounds after irradiation with various high energy particles are summarized in Table 4.6. Although the number of investigations on this subject is rather small, it follows from Table 4.6 that irradiation with heavier particles leads to smaller values of $\Delta T_C / \Delta a$. This means that the lattice parameter correlates with the total amount of damage, in particular the amount of static displacements, rather than with T_C .

When searching for an estimation of the lattice expansion on T_C after irradiation, it is tempting to compare these effects with those caused by hydrostatic compression. However, no direct comparison is possible, as shown for V_3Ge , where the hydrostatic compression causes an increase of T_C from 6 to 12 K, as shown by Testardi /219/, in contrast to Nb_3Sn , Nb_3Al and other A15 type compounds. After irradiation, T_C of all these compounds invariably was found to decrease. For a detailed comparison, the individual electronic structure for each one of these compounds should thus be known.

4.3.3. Static Displacement from Equilibrium Atomic Positions

Static displacements with average rms amplitudes (defined in 3.2.1) up to 0.01 nm were first detected by channeling studies on He irradiated V_3Si by Meyer and Seeber/106/ and by Testardi et al./107/. Prior to these observations, a weakening of the X ray line intensities at higher 2θ angles had been observed by Testardi et al./145/ and Poate et al./146/ on irradiated Nb_3Ge and Nb_3Sn . This weakening could neither be accounted for by a lowering of the long-range order parameter nor by a particular choice of the temperature factor. It was found to be related to static displacements of the chain atoms from their ideal lattice sites, in addition to the normal thermal displacements.

It would exceed the task of the present work to discuss the complex technique of channeling effect measurements for detecting the static r.m.s. amplitudes u (defined in 3.2.1), it will thus be referred to the description of Meyer and coworkers in a series of publications /148,150/. Later on, the same authors have shown a way to determine the quantity u by means of X ray diffraction measurements (Pflüger and Meyer /149/, Linker /54/ and Schneider et al. /55/), described in 3.2.2.

After their first detection, the static displacements were invoked as being the main responsible for the initial decrease of T_C after high energy irradiation /106,107,144/. This hypothesis was influenced by the fact that i) irradiation at higher doses leads to larger static displacements and that ii) the occurrence of focused replacement collision sequences in the A15 structure (and thus the homogeneous decrease of the order parameter) were at that time considered as being highly improbable /100,103,104/. The virtual site exchange mechanism /81/ described in 4.2.3, in combination to the arguments given in 4.2.2. shows convincingly that the effect of static displacements on T_C at low doses, $\phi t \leq 10^{19}$ n/cm², is of secondary importance with respect to the simultaneous decrease of the order parameter after irradiation.

A similar comparison as for the case of lattice expansion (see 4.3.2) can now be made between irradiated and quenched A15 type compounds. Indeed, even after fast quenching, no static displacements could be detected by means of X ray diffraction by the authors and coworkers in the system Nb₃Pt/112, 142/, V₃Au/18/, V₃Ga/20/, Nb₃Al/28/ and Mo₃Os/39/. From a comparison of all known static displacement data, it can be seen that the amplitude of static displacements depends on the nature of the irradiation source. After irradiating V₃Si with Kr and He ions, respectively, Meyer and Linker/148/ found increased static rms amplitudes, u , for the heavier ion. After irradiation doses reducing the T_C value from $T_{C0} = 17$ K to 4 K, these authors /148/ determined u values of 0.008 and 0.005 nm for Kr and He ions, respectively. Later on, Schneider et al./55/ determined the static rms amplitudes on Nb₃Al films after N²⁺ and H⁺ irradiation, using the X ray diffraction method developed by Linker /54/ (see Fig. 4.26). For proton irradiations, these

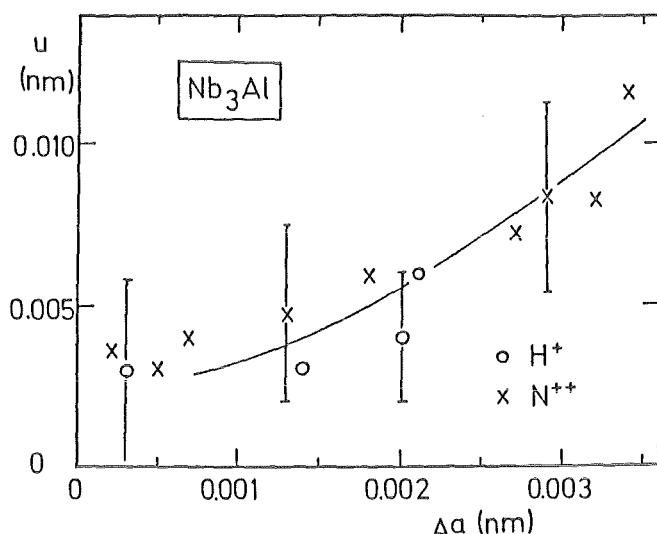


Fig. 4.26. Static rms amplitude, u , in Nb₃Al after irradiation with 300 keV protons and 700 keV nitrogen ions (After Schneider et al. /55/).

authors/55/ found that displacements substantially different from zero were encountered after high doses only. Their value, $u = 0.004 \pm 0.003$ nm, agrees with the very small displacement values which can be estimated from the neutron irradiation data of Sweedler and Cox/53/ on Nb_3Al and by Cox and Tarvin/78/ on neutron irradiated V_3Si . In the case of N^{2+} irradiation, the static rms amplitude reported in Ref. 55 after high doses reached 0.01 nm, which is of the same order of magnitude as in He irradiated V_3Si /106,107/.

Recently, Nölscher and Saemann-Ischenko /136/ also determined the variation for u of Nb_3Sn after irradiation with 20 MeV sulfur ions and found a maximum value of 0.008 nm at a dose characterized by $T_c = 3.2$ K.

Since the same value of T_c correspond to very different values of u (Fig. 4.26), it can be followed that static displacements are certainly not the dominant factor causing the initial decrease of T_c in high T_c A15 type compounds.

It is certainly not a coincidence that the variation of u with ϕt and the relationship between light and heavy ion irradiation shows such strong similarities with the behavior of the lattice expansion, Δa . The occurrence of static displacements from the equilibrium atomic positions observed in several A15 type compounds after irradiation could also be related to the proposed virtual site exchange mechanism/81/. From Fig. 4.19, it can be deduced that an occupied virtual site must cause a perturbation of the potential in the surrounding complex hexagonal configuration, which not only leads to an increase of the lattice parameter, but also to displacements of this group of atoms from their equilibrium lattice positions. It thus appears that both quantities, u and Δa , are coupled. The comparison between irradiation of the same compound with light and heavy ions/55,148/ (see Figs. 4.25 and 4.26) shows that for the heavier ions, both quantities, u as well as Δa , are enhanced. However, if these data seem to confirm a certain tendency, they suffer from an inherent lack of precision in the measurement of the static displacements, because the measurements on irradiated films are not appropriate for determining anisotropies in the displacement amplitudes. Structural refinements on single crystals, irradiated with different high energy particles, should be undertaken for more clarity. Indeed, the anisotropy of both, the thermal and the static displacement amplitudes should be known in order to establish a detailed correlation with the corresponding superconducting properties.

4.3.4. Radiation Induced Phase Changes

Radiation induced transformations from the A15 phase into the cubic A2 or into the amorphous phase have been repeatedly reported. When a highly ordered intermetallic compound, e.g. an A15 type compound, is in thermal equilibrium with the adjacent phase of the phase diagram, disordering of this compound can modify the stability conditions with respect to the adjacent phases. In an ordered compound, the equilibrium order parameter (called S_E in 4.1.2) corresponds to the atomic arrangement with the lowest free energy. By irradiation, the A15 phase may be brought into a state where the free energy is higher than the equilibrium value, due to the strong decrease of the order parameter, as shown theoretically for the case of Cu_3Au by Liou and Wilkes/177/. Therefore, a new free energy balance between adjacent phases can be established, as shown schematically in Fig. 4.27, where the ordered compound β_0 represents the A15 phase and one of the adjacent phases the cubic A2 phase. The large increase of the free energy with increasing disordering under irradiation shifts the free energy curve of the A15 phase above the common tangent for the two adjacent phases. At the composition β , there will thus be a two-phase region (A2 + γ in the chosen example) instead of the original A15 phase. Of course, a similar mechanism can be imagined replacing one of the adjacent phases by the amorphous phase.

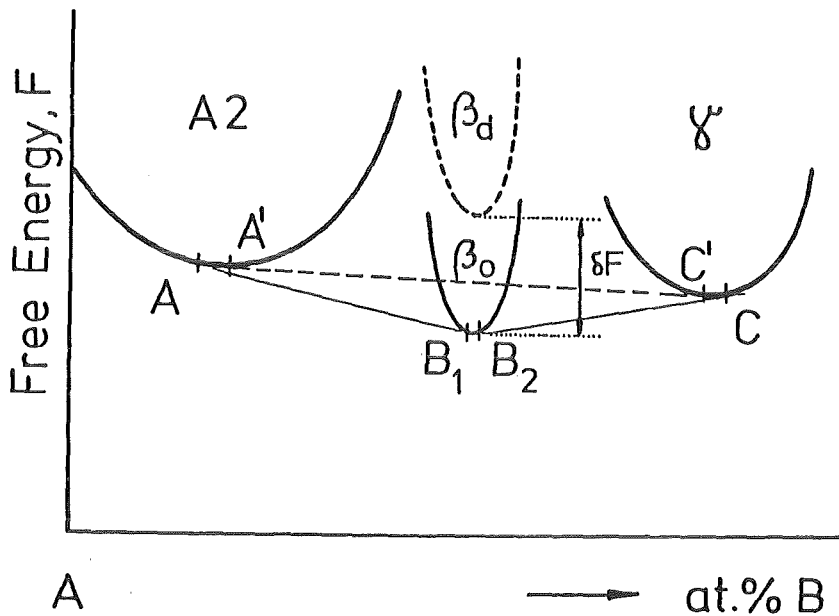


Fig. 4.27. Schematical representation of the increase of the free energy of the A15 phase by δF as it disorders from S_1 to S_2 ($S_1 > S_2$) under irradiation. The tangent line between the A2 and the γ phase indicates the new equilibrium

The first case of amorphous phase formation after heavy irradiation in A15 phases has been reported by Sweedler et al. /69,70/. Schneider et al. /55/ have produced the A2 phase in Nb_3Al after irradiation with N^{2+} ions, while Ruzicka et al. /108/ observed the formation of both, A2 and amorphous phase, in Kr^+ irradiated $Nb_{\nu 3}Si$. Recently, Meyer et al. /155/ observed the presence of both modifications, A2 and amorphous phase, in Nb_3Ir after irradiation with Kr^+ ions. It is not known at present why such similar systems exhibit such a different transformation behavior. One reason could be correlated to the individual differences in the kinetics of recovery and recombination, which in turn could arise from the electronegativities of the components. A possibility which has also to be considered is the temperature during the irradiation, T_{irr} , which may change from one experiment to another. Since recovery have been observed even at room temperature, this could lead to possibly erroneous interpretations if the sample is warmed up between two subsequent experiments after low temperature irradiation.

At present, it is not clear what is the factor causing the breakdown of the A15 structure. A priori, different isolated factors could be invoked. The structure could become unstable in the following cases:

- a) the mean static displacements exceed a certain value, $u = 0.0115$ nm being the largest value reported so far /55,106,150/
- b) the lattice expansion exceeds certain limits, the largest reported value being $\Delta a = 0.0065$ nm for Nb_3Ge /69/ and Mo_3Ge /138/ and $\Delta a = 0.0053$ nm for Nb_3Sn /154/,
- c) the degree of atomic ordering is too low. After neutron irradiation, the A15 structure was found to be maintained at order parameters as low as $S_a = 0.4$ for Nb_3Al /53/ and Nb_3Ge /69,70/, while after irradiation with N^{2+} and H^+ ions, the lowest reported order parameter for Nb_3Al was $S \cong 0.2$ /55/. It is still open whether the completely disordered state, characterized by $S = 0$, must be reached by the crystal before to undergo a radiation induced phase transformation.
- d) the number of radiation induced vacancies is too important. So far, the only reported value, $\sim 0.3\%$, was reported on a V_3Si single crystal after neutron irradiation to $S = 0.90$ /78/.

In reality, however, these factors are certainly tightly coupled, thus resulting in a weakening of the covalent bond between chain atoms. The formation of vacancies may be considered as the primary effect, causing or favorizing as well disordering as lattice expansion or static displacements. It could even be

advanced that the A15 structure with a high degree of disorder is stabilized by the presence of static displacements introducing additional bonding between the atoms on the 2a and the 6c sites, but also between the different chains.

As discussed in 4.3.1, atomic disordering alone (as induced by rapid quenching procedures) does not lead to essential changes of the interatomic distances. This is in contrast to the observed lattice expansion after irradiation reaching up to 1.3% /55,69,136,137,138,144/, simultaneously to static displacements involving statistical deviations from the equilibrium atomic positions reaching as high as 2% of the lattice parameter. It can thus be advanced that the instability of the A15 phase after low temperature high energy irradiation occurs when the static displacements and/or the lattice expansion exceed a certain value. This value is expected to vary from compound to compound, but an upper limit of 1.5 to 2 % of the original value of a at 300 K seems to be a reasonable condition for radiation induced instability in A15 type compounds. It will be seen later that this condition also holds at very high temperature for another type of instability: Melting. Indeed, Isernhagen and Flükiger /162/ have shown that at the melting points of a series of A15 type compounds, the thermal rms amplitude reaches ~ 2 % of the lattice parameter value at 300 K (see also 5.4.2). In spite of the fact that in this case, dynamic and static deviations are comparable, it is interesting to note that the lattice parameters, too, show an expansion of ~ 2 % with respect to the unirradiated room temperature value, as well at the melting point as after irradiation. In a general sense, it could thus be said that low temperature irradiation and high temperature treatments on A15 type compounds have analogous consequences on the lattice expansion and the deviations of the atoms from their equilibrium positions, the latter being, however, static in the low temperature case.

4.3.5. The "Saturation" Region of T_c at High Doses

Regardless to the nature of the irradiation source, fast particle irradiation of A15 type compounds at high doses leads to a region where T_c shows a saturation behavior. For Nb_3Al , this region is reached at $\phi t \approx 3 \times 10^{19} \text{ n/cm}^2$ (neutrons with $E \geq 1\text{MeV}$), at $\phi t \approx 1 \times 10^{15} \text{ sulfur ions/cm}^2$ (^{32}S with $E \geq 25\text{MeV}$) or at $\phi t \approx 6 \times 10^{16} \text{ nitrogen ions/cm}^2$ (^{14}N with $E \geq 770\text{keV}$). If the saturation would be caused by ordering effects, the curve T_c vs. (ϕt) (see Fig. 4.10) should reach the saturation value, $T_c(\text{sat.})$, by a gradual change. There are several investigations where this region has been carefully studied and which permit to decide if there is a sudden change in slope or not. Obviously, only data for low temperature irradiations, followed by T_c measurements without intermediate

warming up to room temperature can be used for this comparison. The saturation region at high doses has been investigated in the systems Nb_3Ge and Nb_3Sn /74,102,136,146,152,155,157/. As an example, the behavior of Nb_3Sn /157/ after irradiation with different particles has been reproduced in Fig. 4.28. It is seen that after low temperature irradiation with oxygen ions, the saturation value of T_C is attained after a sudden change in slope. T_C exhibits a minimum of 3.5 K after a dose of $2 \times 10^{16} O^{2+}/cm^2$, a further increase of the dose leading to the saturation value, $T_C = 4.1$ K. After recovery anneals at temperatures up to $410^\circ C$, T_C decreases again, down to 3.42 K (right side of Fig. 4.28).

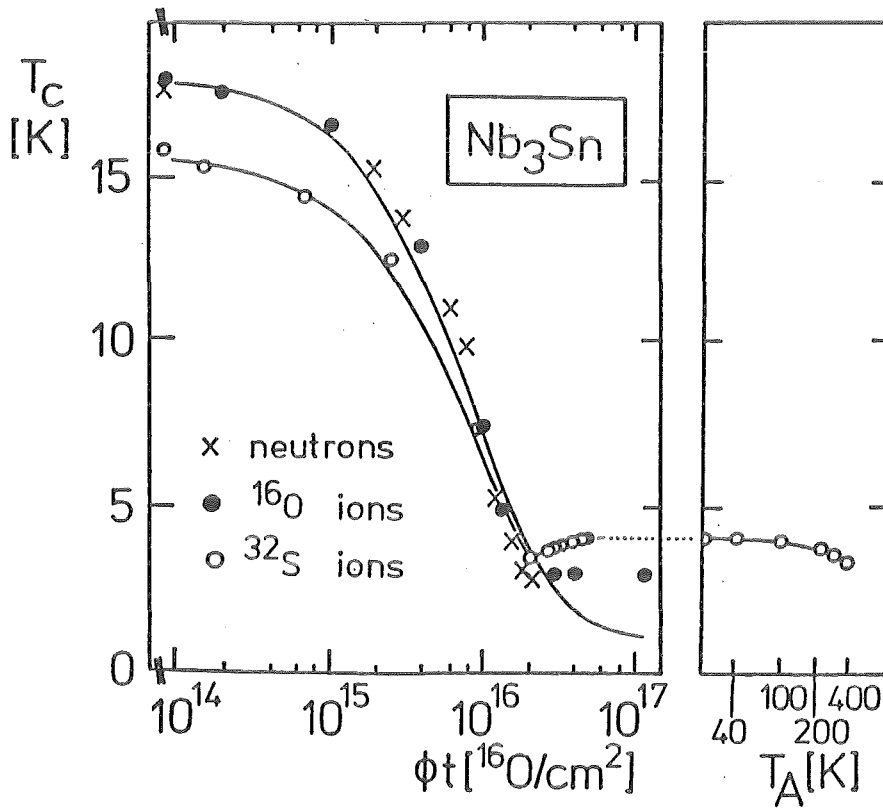


Fig. 4.28. T_C of Nb_3Sn after irradiation with oxygen ions at $T_{irr} = 30$ K/157/, by He ions at $T_{irr} = 300$ K/146/ and by fast neutrons at $T_{irr} = 150^\circ C$ /69/. The doses have been normalized by a factor $k(N) = 3,1 \times 10^{-4}$ $k(He) = 0.195$ for better comparison/157/.

A comparison with the irradiation data at higher T_{irr} by Poate et al./146/ and Karkin et al./159/ shows that the observed slight increase of T_C at the highest doses is strongly influenced by the irradiation temperature, T_{irr} . Such a minimum of T_C after high dose irradiation at low temperatures has also been observed by Krämer et al. /74/ on Nb_3Ge and by Haase and Ruzicka /123/ on $Nb_{\sim 3}Si$. The behavior in Fig. 4.28 clearly indicates the occurrence of another mechanism influencing the variation of T_C at high doses and low T_{irr} , in addition to the decrease of the long-range order parameter. What kind of "disorder" is now present?

In all cases known so far, a small but significant increase of the superconducting transition width, ΔT_c , has been observed with increasing dose. The maximum of ΔT_c , approximately 1.5 K, was observed at doses where the initial value of T_c was decreased to $T_c/T_{c0} \simeq 0.4$ /117,136,157/. For illustration, the ratio $\Delta T_c/T_c$ deriving from specific heat measurements of Viswanathan et al. /117/ on neutron irradiated V_3Si is reproduced in Fig. 4.29 as a function of T_c . It is seen that down to $T_c \simeq 8$ K, the increase of ΔT_c is moderate (which had been discussed in 4.2.2 b). Below this T_c value, a marked maximum of $\Delta T_c/T_c$ occurs, followed by a quite rapid decrease to very small values at the saturation dose. It is obvious that this effect cannot be explained by any homogeneous model. The observations of Pande /103,104,105/(depleted zones (or "disordered microregions") of 2 to 5 nm size) are here helpful in trying to find an explanation. Indeed, with the increasing volume fraction of depleted zones at high doses, the sample becomes more and more inhomogeneous. After having excluded these

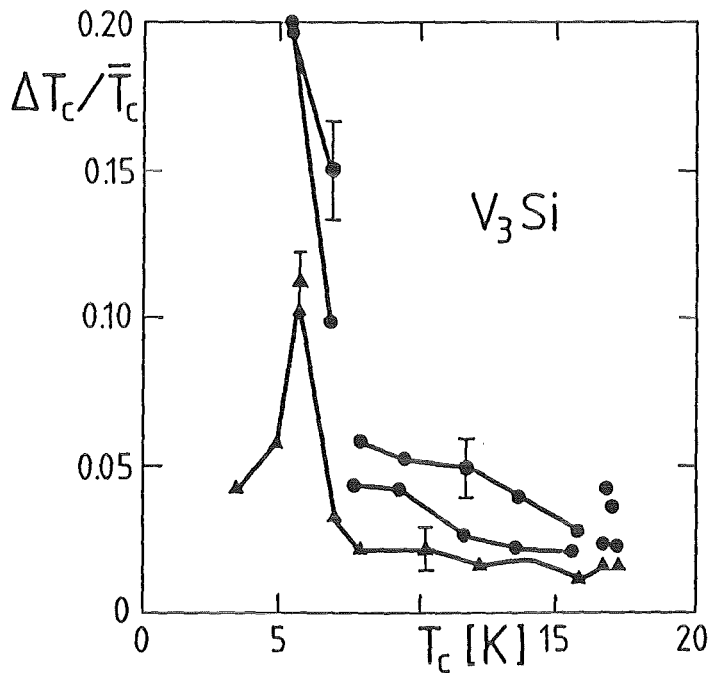


Fig. 4.29. Change of the relative superconducting transition width, $\Delta T_c/T_c$, as a function of T_c for an irradiated V_3Si single crystal, from heat capacity measurements /117/. \blacktriangle : heat capacity measurements, \bullet : resistivity measurements.

inhomogeneities as a reason for the decrease of T_c after high energy irradiation (4.2.2), the existence of two modifications, i.e. the partly disordered matrix and the completely disordered depleted zones can be used as a basis for understanding the increase of ΔT_c .

The present model assumes, similarly to Pande /103/, that the matrix and the depleted zones have strongly different T_C values. The observed small size of the latter, 2 to 5 nm /103/, certainly leads to proximity effects. However, due to the very small volume fraction of depleted zones /113/, these proximity effects leading to a decrease of T_C are only effective in a very small region of the crystal, letting the matrix unaffected. The conclusion is very simple: proximity effects in irradiated A15 type compounds cause a broadening of the superconducting transition width, ΔT_C , towards lower values, the overall T_C value being little affected. The sharp decrease of ΔT_C at higher doses is attributed to the steady decrease of the interspace between depleted zones below a critical value, thus leading to "percolation" between depleted zones.

On the basis of this two-phase model (the two phases being the A15 and the amorphous phase) it is possible to understand the observed minimum of T_C after high dose irradiation at low temperatures, according to Haase and Ruzicka /123/. This simple qualitative model is visualized in Fig. 4.30, where the data of Krämer et al. /74/ on 20 MeV ^{32}S irradiated Nb_3Ge ($T_{C0} = 21.92 \text{ K}$) is plotted. It is seen that T_C would continue to decrease with higher doses if disordering would be the only acting mechanism. The slight increase would thus be due to the presence

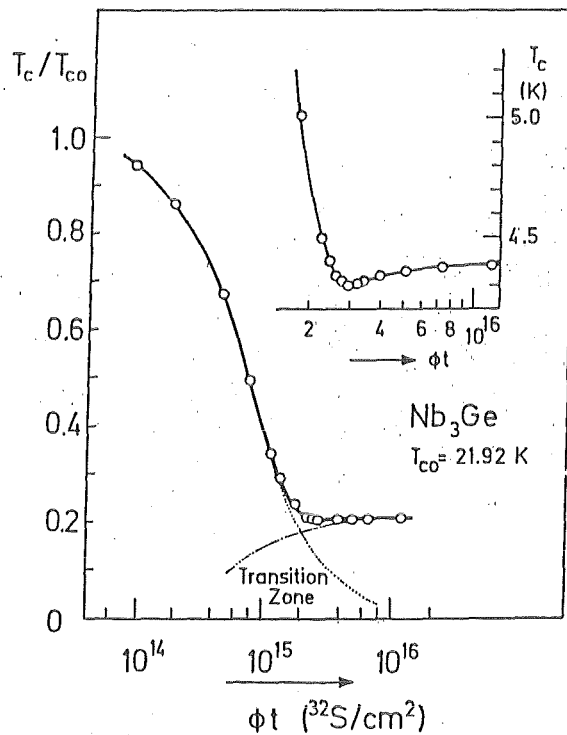


Fig. 4.30. The minimum of T_C in Nb_3Ge after high dose ^{32}S irradiation at low temperature (Krämer et al. /74/) and its explanation by a two-phase mechanism. (The dotted curves are qualitative, the increase of T_C of the amorphous phase arising from proximity effects).

of amorphous phase, which reaches its maximum at $T_c = 4.38$ K, the transition zone being characterized by proximity effects.

4.3.6. Increase of T_c in irradiated Mo_3Ge , Mo_3Si and Nb_3Si : A Phononic Effect

The three low T_c systems Mo_3Ge , Mo_3Si and Nb_3Ir crystallize in the A15 structure and are superconducting at 1.3, 1.3 and 1.7 K, respectively. Their electronic density of states values are among the lowest reported so far for A15 type compounds. It is not surprising that the variation of T_c with composition in these systems is quite slow (Flükiger et al. /39,62/). With $dT_c/d\beta = -0.13$, -0.13 and $+0.43$ K, respectively, the effect of composition on T_c is almost one order of magnitude smaller than for "typical" /39/ A15 type compounds. From various points of view, the behavior of some physical properties on Mo_3Ge , Mo_3Si and Nb_3Ir is opposed to that encountered in the former class of materials. For example, the stoichiometric composition does not correspond to a maximum, but to a minimum of T_c . The main interest, however, arises from the fact that high energy irradiation leads to a substantial increase of T_c in all three systems in contrast to the generally reported decrease illustrated in Fig. 4.10.

The question arises about the mechanism causing the increase of T_c in these low T_c materials after irradiation. In the past, it has been advanced that atomic disordering would be the cause of this behavior, with the argument that the Fermi energy, situated in a valley between two peaks would be shifted by any change of the system towards higher densities of states. This was apparently corroborated by many measurements of ρ_0 and of the initial slope of the upper critical magnetic field, $dH_{c2}/dT|_{T=T_c}$, from which the electronic density of states was indirectly determined by calculation. This procedure had been successfully applied before on high T_c A15 type compounds, and there was no reason why it should not apply to low T_c A15 type compounds. Direct measurements of the electronic specific heat coefficient, however, have led to a completely opposed picture. Ghosh and Caton /153/ and Mirmelshteyn et al. /158/ found for Mo_3Ge and Mo_3Si , respectively, that the electronic density of states after neutron irradiation remained essentially unchanged, although T_c was raised by a factor ranging between 3 and 4. These authors /153,158/ found that the Debye temperature in both systems considerably decreased after irradiation, the lattice softening thus being the real cause of the enhancement of T_c . This is obviously

in sharp contrast to the behavior found in high T_c A15 type compounds. At this point, it should be recalled that the observed lattice hardening observed in the latter after high energy irradiation has to be considered as an exception.

The aim of this paragraph is to present a new picture of the superconducting behavior of low T_c A15 type materials. For this purpose, all known investigations on these materials, including own data obtained by quenching procedures, will be critically discussed. First of all, it is important to analyze whether the increase of T_c is really a property of the A15 phase, since additional phases are known to be formed after irradiation, e.g. the amorphous phase in Mo_3Si /137/ and Nb_3Ir /155/ and the bcc (or A2) phase in Nb_3Ir /155/. It is further of fundamental interest to analyze this question by comparing disordering effects induced by both, fast quenching from high temperatures and high energy irradiation. In order to facilitate the discussion, all calorimetric data known so far on the three systems of interest are summarized in Table 4.7. This is also necessary since the data for Mo_3Si and Mo_3Ge obtained by Flükiger and Paoli /63/ were not published before. The corresponding variation of T_c after irradiation is shown in Fig. 4.31 (Mo_3Ge , Mo_3Si) and 4.32 (Nb_3Ir).

a) Quenching Experiments

In analogy to the high T_c systems discussed in 4.1, a comparison with the data on quenched samples will first be made. As shown in Table 4.7, the samples annealed at higher temperatures followed by radiation quenching show always a slightly smaller T_c value. For example, Nb_3Ir exhibits $T_c = 1.45$ K and $T_c = 1.58$ K after anneals at 1700 and 1500°C, respectively. The corresponding T_c values for $\text{Mo}_{.762}\text{Si}_{.238}$ after annealing at 1600 and 1400°C, followed by radiation quenching are 1.57 and 1.63 K, respectively. Although the order parameter corresponding to both heat treatments was not measured, it can be safely concluded from thermodynamics arguments that the higher quenching temperature yields a slightly lower degree of ordering (see also Fig. 4.5). This behavior of T_c with annealing temperature has been confirmed by numerous quenching experiments, as well by irradiation as by quenching procedures (see Sect. 8 and Refs. 20,39,62). The decrease of T_c and γ with lower degrees of long-range ordering induced by quenching and annealing has been observed in all A15 type compounds studied so far by the author and coworkers, i.e. in more than

40 systems, regardless whether the electronic density of states was very high (e.g. V_3Ga), intermediate (e.g. Nb_3Pt , V_3Pt ,...) or very low, as the presently discussed systems Mo_3Ge , Mo_3Si and Nb_3Ir . This effect seems to be inherently coupled to the particularities of the A15 electronic structure, while the position of the Fermi energy relative to a peak of the electronic density of states curve influences merely the rate of variation of T_c and $N(E_F)$ with S .

Compound	Annealing	a (nm)	T_c (K)	γ (m J/at-g·K ²)	Θ_D (K)	Ref.
$Nb_{.72}Ir_{.28}$	360 h/900°C	0.5120	2.85	2.63 ± 0.03	362 ± 10	62,208
$Nb_{.75}Ir_{.25}$	4 h/1700°C	0.5135	1,45	-	-	62
$Nb_{.75}Ir_{.25}$	24 h/1500°C	0.5135	1.58	-	-	62
$Nb_{.75}Ir_{.25}$	as cast	0.5135	1,63	2.13 ± 0.01	409 ± 8	25, 62
$Nb_{.775}Ir_{.225}$	24 h/1650	0.5147	0.30	$1,81 \pm 0.01$	374 ± 10	62,208
$Mo_{.75}Si_{.25}$	3 h/1600°C	0.4893	1.33	-	-	62
$Mo_{.762}Si_{.238}$	3 h/1400°C	0.4900	1.63	1.78 ± 0.01	538 ± 25	63
$Mo_{.762}Si_{.238}$	3 h/1600°C	0.4900	1.57	1.76 ± 0.01	510 ± 20	63
$Mo_{.75}Si_{.25}$	100 h/1100°C	0.485	1.56	$2.44^a)$	560	158
$Mo_{.75}Si_{.25}$	100 h/1100°C + $1.0 \times 10^{20} n/cm^2$	0.489	6.00	2.53^a	330	158
$Mo_{.75}Ge_{.25}$	3 h/1600°C	0.4933	1.48	1.85 ± 0.02	510 ± 20	63
$Mo_{.765}Ge_{.235}$	3 h/1600°C	0.4937	1.68	1.92 ± 0.03	476 ± 30	63
$Mo_{.751}Ge_{.249}$	16 h/1600°C		1.45	1.22	392	153
$Mo_{.751}Ge_{.249}$	16 h/1600°C + $2.2 \times 10^{19} n/cm^2$		4.25	1.35	322	153

Table 4.7. Superconducting transition temperature, electronic specific heat and Debye temperatures of the A15 type systems Nb-Ir, Mo-Si and Nb-Ir at different compositions. The samples $Mo_{.75}Si_{.25}$ /158/ and $Mo_{.751}Ge_{.249}$ /153/ were irradiated at $T_{irr} = 70$ and $\leq 150^\circ C$, respectively. ^{a)} These values are given in mJ/K²mole, but should probably be indicated in mJ/K²at-g.

There is also a more general argument which tends to exclude the possibility of an increase of T_C after irradiation as a consequence of decreasing order parameter in Mo_3Ge : in all A15 type compounds known so far (including Mo and Cr based systems with transition B elements), the variation of T_C with composition or with ordering is comparable (see Sect. 8). For example, T_C in Mo_3Ir (after slow cooling from 1800 °C) varies from 8.35 to 8.12 K between 22 and 24 at.% Ir/39,62/, thus corresponding to a rate of - 0.12 K/at.%. In the same compound, T_C decreases with S at a rate of 0.05 K per 1%/39/. For Mo_3Ge , where only the variation of T_C with composition is known, T_C varies at a rate of - 0.13 K/at.% between 23 and 25 at.% Ge/39/. Thus, a comparably small variation of T_C as a function of S would be expected, rather than the increase by >5 K observed after irradiation (see Fig. 4.31) leading to the extremely high value $dT_C/dS = - 22.2$ K per 1% order parameter change, given in Table 4.8. In this table, all known values about the variation of T_C with composition and order parameter in low T_C A15 type compounds are summarized for comparison.

Compound	$dT_C/d\beta$ [K/at. %]	Reference	dT_C/dS [K]	Reference
Mo_3Ge	- 0.13	Flükiger et al. /39/	- 22.2	Lehmann et al. /138/
Mo_3Si	- 0.13	"	- 20	Lehmann et al. /137/
Mo_3Si	- 0.13	"	- 10	Mirmelshteyn et al. /58/
Mo_3Ir	- 0.12	"	+ 0.05	Flükiger et al. /39/
Nb_3Ir	+ 0.43	Flükiger et al. /62/	$\left\{ \begin{array}{l} + 2 \pm 0.5 \\ - 1.8 \end{array} \right.$	Schneider et al. /155/ "
Cr_3Ir	- 0.09	Blaugher et al. /75/		
	- 0.09	Flükiger et al. /223/		
V_3Ir	+ 0.14	Blaugher et al. /75/		

Table 4.8. Variation of T_C with composition and order parameter in low T_C A15 type compounds. Ordering changes were induced by fast quenching /39,62,75,223/, neutron irradiation at $T_{irr} = 70^\circ C$ /158/, low temperature 20 MeV ^{32}S irradiation /137,138/ and room temperature 300 keV H^+ irradiation /155/.

b) Irradiation Experiments

The system Mo₃Ge.

The variation of T_c with dose for Mo₃Ge /138/ and Mo₃Si /137/ after irradiation with 20 MeV ³²S ions is represented in Fig. 4.31, where the above mentioned increase of T_c is illustrated. At high doses, both systems show a significant difference, a saturation being observed for Mo₃Si /137/, while a strong peak was reported for Mo₃Ge /138/. The reasons for this behavior will now be analyzed.

It is remarkable that independently on the radiation source, i.e. either He ions /111,164/, ³²S ions /138/ or neutrons /153/, no amorphous phase could ever be detected in the Mo₃Ge system. The absence of amorphous phase was deduced from diffractometric measurements /138,163,164/ and is confirmed by the behavior of the electric resistivity at temperatures below 300 K, which always showed a positive $d\rho/dT$ slope, even after heavy irradiation /111,137/. As will be seen below, this is in contrast to the behavior of $\rho(T)$ observed in Mo₃Si /137/.

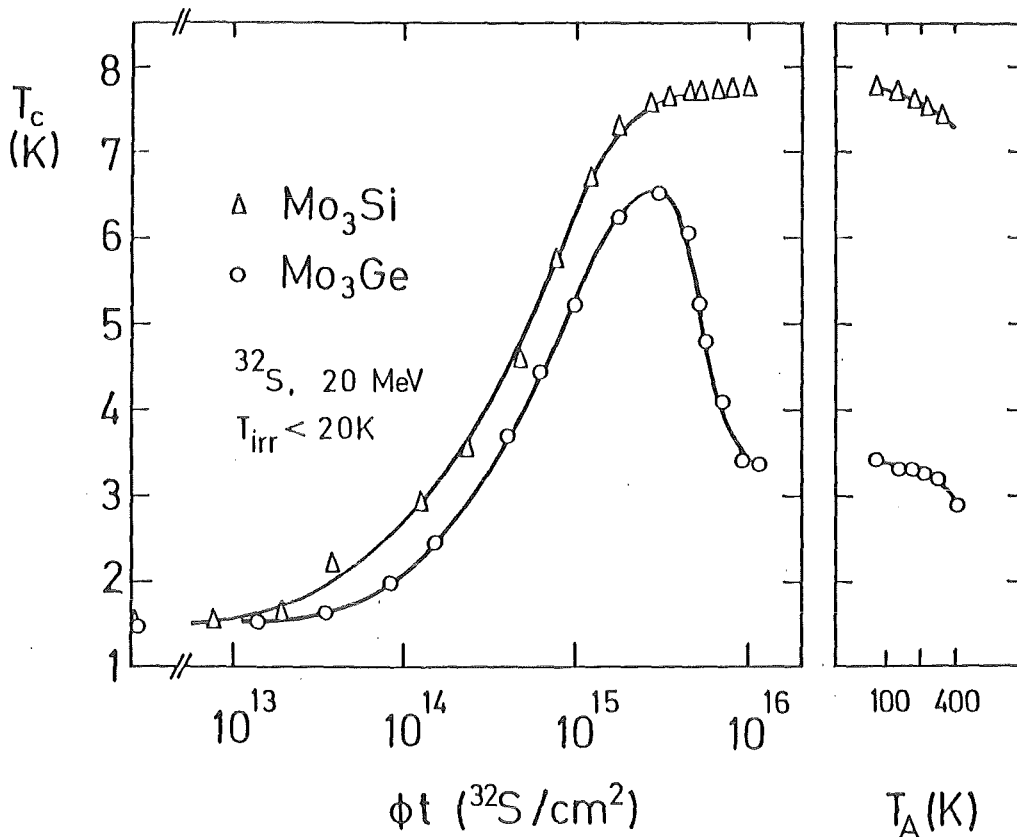


Fig. 4.31. Variation of T_c in Mo₃Ge/138/ and Mo₃Si/137/ films after low temperature irradiation with ³²S ions ($E = 20$ MeV), as a function of the irradiation dose. At the right side, the recovery behavior of T_c up to 410 K is shown. T_A is the annealing temperature.

After heavy irradiation, Lehmann et al. /138/ observed a decrease of the lattice parameter of the bcc Mo rich solid solution initially present in the sample as secondary phase, from $a = 0.3145$ nm to $a = 0.3140$ nm after a dose of $1.4 \times 10^{15} \text{ }^{32}\text{S/cm}^2$, where T_C nearly corresponds to $T_C(\text{max})$ i.e. 6.9 K. According to Fig. 2.3, the A2 phase with the metastable composition $\text{Mo}_{.75}\text{Ge}_{.25}$ could cause an increase of T_C , but certainly not as high as 6.9 K! An effect of amorphous elementary Mo, produced by dissociation, can be excluded: Gurvitch et al./164/ did not find any T_C enhancement after implanting Ge in Mo films.

The increase of T_C in irradiated Mo_3Ge , identified above as a property of the A15 phase, is a bulk effect as follows from specific heat measurements of Ghosh and Caton/153/. These authors analyzed the effect of neutron irradiation on both the A15 phase Mo_3Ge and the tetragonal neighbour phase Mo_5Ge_3 by calorimetry. They found that in both phases, the electronic density of states after irradiation was essentially unchanged, in contrast to the Debye temperature, which decreases considerably. For Mo_3Ge a decrease of θ_D from 392 to 322 K and for the tetragonal Mo_5Ge_3 , a decrease from 377 to 320 K was observed after neutron irradiation /153/. This result is particularly important for the present discussion. Since lattice softening, accompanied by an enhancement of T_C (from < 1.6 to 3.3 K for Mo_5Ge_3 /153/) after irradiation seems to be little dependent on the crystal structure, it is really questionable whether this change can be explained by ordering effects only.

Thus, the A2 phase cannot cause the increase of T_C in irradiated Mo_3Ge but is very probably responsible for the sharp decrease of T_C at doses $\Phi t \geq 1.4 \times 10^{15} \text{ }^{32}\text{S/cm}^2$ represented in Fig. 4.31. Indeed, the most obvious explanation for the sharp decrease of T_C would consist of assuming that only the A2 phase would be present in this highly damaged state. This is at least partly confirmed by the observation/138,163/ that the strongest A15 peaks (the only ones being present besides the A2 peaks) had only 5 % of their initial intensity. It can be assumed that the presence or absence of such a small amount of A15 phase in a sample is influenced by small inhomogeneities. The lowest T_C values at high doses, $T_C = 3.5$ K/138/, fit very well with the extrapolated values for metastable A2 Mo_3Ge in Fig. 2.3. From all the arguments discussed above, i.e. comparison between irradiation and quenching data, changes of T_C with ordering and composition, calorimetric analysis, crystallographical observations and resistivity measurements, it follows that the increase of T_C in irradiated Mo_3Ge is a property of the damaged A15 phase, but has no unique character limited to

this phase only. Irradiation of Mo_3Ge with 20 MeV ^{32}S ions /138/ produced an increase of the lattice parameter from 0.4937 to 0.5002 nm, the strongest observed so far in A15 type compounds (see Fig. 4.23 b). The strong decrease of line intensities reflects particularly high static displacements. It may thus be advanced that here the static displacements, possibly in combination with the lattice expansion are responsible for the enhancement of T_c rather than ordering effects. In contrast to high T_c A15 superconductors, the electronic density of states is not a relevant parameter for describing the changes in T_c of this class of materials. In some respect, the situation in Mo_3Ge may be compared to that encountered in heavily irradiated Nb_3Sn , where T_c was also found to increase (see Fig. 4.28).

The system Mo_3Si .

After having shown that the enhancement of T_c in irradiated Mo_3Ge is due to the damaged A15 phase, a similar explanation can be advanced for Mo_3Si . The main difference between these two irradiated systems is the appearance of the amorphous phase in Mo_3Si . The saturation value for Mo_3Si after heavy irradiation, $T_c = 7.8 \text{ K}$ /137/, corresponds to that obtained for amorphous films obtained by coevaporation at 77 K by Johnson et al. /175/. It can thus safely be concluded that the increase of T_c in both, Mo_3Ge and Mo_3Si is a property of the damaged A15 phase, the different behavior of T_c at high doses shown in Fig. 4.31 being due to a different T_c of the corresponding radiation induced phases.

A detailed calorimetric investigation was performed on neutron irradiated Mo_3Si by Mirmelshteyn et al. /158/ ($T_{\text{irr}} = 70^\circ\text{C}$). An arc melted Mo_3Si sample was homogenized 100 hours at 1100°C , irradiated at a dose of $1 \times 10^{20} \text{ n/cm}^2$ and submitted to successive isochronal anneals ($t = 20$ minutes) in the range between 300 and 700°C . The data prior to and after the irradiation are listed in Table 4.7. This direct determination of γ can be considered as the key work in the field, the systematical choice of 9 different recovery anneals covering the whole range of T_c from 6.0 K (just after irradiation) to 1.56 K after recovering at 700°C . The latter value is the same one as that of the original sample after homogenizing. After each recovery anneal, the specific heat and the order parameter were determined, thus giving a clear picture of the process.

It is interesting that no small-angle scattering effects could be detected in Mo_3Si /158/, in contrast to Nb_3Sn (It may be recalled that the presence of such effects in Nb_3Sn , observed by Karkin et al. /159/ was a major argument supporting the inhomogeneous damage hypothesis /103/). Mirmelshteyn et al. /158/ observed after neutron irradiation a mainly amorphous sample, in agreement with Lehmann et al. /137/. In this case, the difference in T_{irr} between 70 °C /158/ and 30K /137/ thus seems to have little effect on the radiation induced phase. The retransformation from the amorphous to the crystalline state was observed at ~ 450 °C. It is remarkable that the A15 phase was present at all observed states and that it was even possible to determine the order parameter just after irradiation, i.e. where the A15 phase is only present in ~ 5 % of the sample. The order parameter was originally $S = 0.86$, which is considerably smaller than the value $S = 0.99$ reported in 5.3.1. At present, the reasons for this difference cannot be understood. In spite of some criticism about the absolute value of γ and the measurement of the specific heat at temperatures $T > 4.2$ K only, the data of Mirmelshteyn et al. /158/ lead to following conclusions:

- a) Neutron irradiation up to 1×10^{20} n/cm^2 causes a considerable softening of the phonon spectrum: A decrease of θ_{D} from 560 to 330 K is observed.
- b) The electronic density of states is not affected by irradiation nor by the transition from amorphous to crystalline state.
- c) The factor $N(E_{\text{F}}) \langle J^2 \rangle$ in the MacMillan equation also remains unaffected, being situated at the value ~ 700 eV nm^{-2} (or 7 eV \AA^{-2}).

The above results illustrate the danger of deducing γ from measurements of ρ_0 and of the initial slope of the upper critical field, $dH_{\text{c2}}/dT|_{T=T_{\text{C}}}$, simply assuming the validity of the equation

$$\gamma \sim \frac{1}{\rho_0} dH_{\text{c2}}/dT|_{T=T_{\text{C}}} \quad (\text{dirty limit}) \quad (4.9)$$

without taking into account the changes of the phonon spectrum. As will be shown in Sect. 8, the approximation (4.9) gives certainly the right tendency if the phonon spectrum does not change dramatically or if electronic density effects are dominant, as it is the case for irradiated high T_{C} A15 type compounds.

In the present case, however, it has led to an incorrect conclusion, as shown in Fig. 4.32.

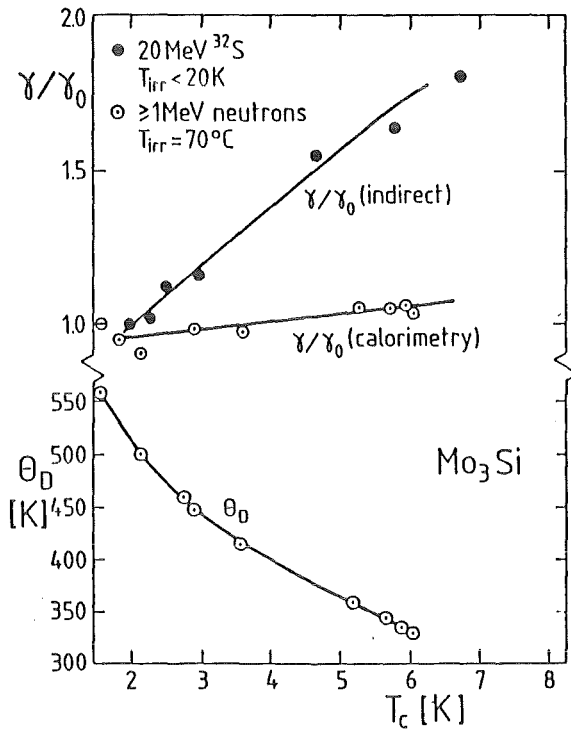


Fig. 4.32. Variation of γ and θ_D with T_c in irradiated Mo_3Si , from data of Mirmelshteyn et al. /158/ ($T_{\text{irr}} = 70^\circ\text{C}$, calorimetry) and Lehmann et al. /137/ ($T_{\text{irr}} < 20\text{K}$, thin films). This figure illustrates how the indirect determination of γ from the values of dH_{c2}/dT and ρ_0 (see Eq. (4.9)) may be erroneous in the case of low T_c A15 type compounds.

The system Nb_3Ir .

In a recent room temperature irradiation work on Nb_3Ir , Schneider and Linker /135/ observed a very interesting behavior of T_c at low doses of H^+ and He^{++} ions, respectively (both with an energy of 300 keV). The irradiation with He ions leads to increased T_c values, the tendency being the same as in previously reported Kr^+ irradiations at 77 K on the same compound/155/. After proton irradiation, however, a new behavior was observed, T_c showing an initial decrease at low doses, from 1.74 to 1.39 K, the minimum occurring after the dose $\phi t = 3 \times 10^{16} \text{H}^+/\text{cm}^2$ /135/, as shown in Fig. 4.33. At this dose, the order parameter was determined to $S = 0.95$ by X ray diffractometry, using the method of Linker/54/ for thin films. With higher proton doses, T_c was found to increase up to a saturation value of 2.59 K, at which the static rms amplitude, u , reaches 0.007 nm. In the light of the quenching experiments mentioned above, the initial decrease of T_c must be attributed to the decrease of the long-range order parameter.

It is interesting that the initial decrease of T_c in Nb_3Ir was observed after proton irradiation only. A comparison with the Kr^+ and He^+ irradiations/155/

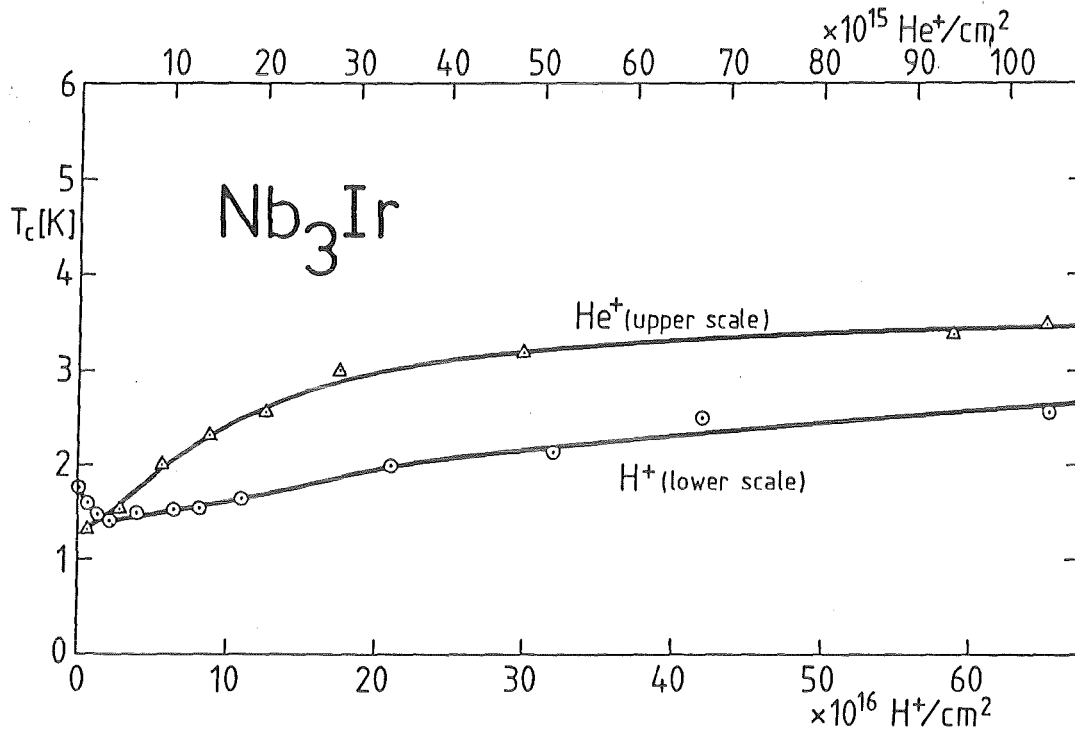


Fig. 4.33. Variation of T_c in Nb_3Ir films after low temperature irradiation with H and He ions (both with $E = 300$ keV), as a function of the deposited energy. Note the minimum of T_c for the proton irradiation and the different level of T_c saturation. The value for amorphous Nb_3Ir , produced by Kr^+ irradiation/155/ is shown for comparison. (This figure has been established based on the data of Schneider and Linker /135/).

shows that the latter lead to considerably higher static rms amplitudes, the highest measured values being $u = 0.007, 0.0085$ and 0.01 nm, respectively. The minimum of T_c is observed at a very low static displacement of 0.003 nm.

From Fig. 4.34, it can be seen how the highest values of u and Δa as well as the lowest values of S after irradiation depend on the projectile: as stated earlier (see Figs. 4.24 and 4.25), the heavier particles cause the larger damage. The variation of Δa as well as of u scales over the whole dose range for both, H^+ and He^+ irradiation. This observation fits well with the virtual site exchange mechanism/81/, where the increase of a and the static displacements in irradiated A15 type compounds depend mainly on the chemical nature of the elements A and B.

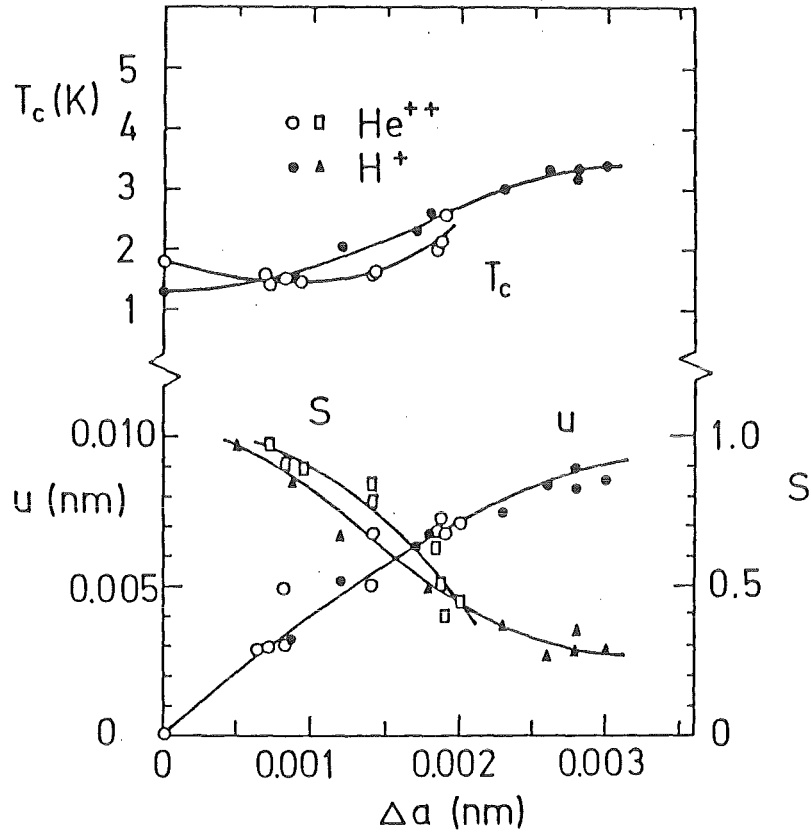


Fig. 4.34. Variation of T_c , S and the static rms amplitude, u , in Nb_3Ir films as a function of the lattice parameter expansion after low temperature irradiation with He and H ions (both with $E = 300$ keV). At $\Delta a = 0.0008$ nm, T_c of proton irradiated Nb_3Ir undergoes a minimum (After Schneider and Linker /135/).

The variation of T_c in irradiated Nb_3Ir can thus be understood as a superposition of two opposite changes, i.e. an initial decrease of T_c with decreasing order parameter and at high doses an increase of T_c with higher static displacements, possibly connected with lattice softening. The increase of T_c can now be compared to that observed after heavy irradiation on Nb_3Sn /157/ (see also Fig. 4.28) or on Nb_3Ge (Krämer et al. /134/), shown in Fig.4.30. Thus, a common feature has been found between high T_c and low T_c A15 type compounds submitted to heavy irradiation doses: The increase of T_c observed in both cases could be attributed to the occurrence of static displacements, possibly combined with lattice softening.

c) Comparison between the Irradiation Behavior of Low and High T_c A15 Compounds

The discussion of irradiation data on the low T_c systems Mo_3Ge , Mo_3Si and Nb_3Ir reveals that many physical properties exhibit just the opposite behavior with respect to high T_c A15 type materials. It is beyond any doubt that it is the superconducting transition temperature of the damaged A15 phase which increases with irradiation of the three discussed low T_c A15 type compounds, in sharp contrast to the behavior shown by Fig. 4.10. It is remarkable that the property showing the strongest variation is the Debye temperature (see Fig. 4.32), in contrast to the high T_c A15 type compounds, where it is the electronic density of states. The opposite behavior of different physical properties in high T_c and in low T_c A15 type materials is shown by the comparison in Table 4.9.












Physical Property	High T_c A15 Compound	Low T_c A15 Compound
T_c		
γ		-
θ_D		
λ		
a		
u		

Table 4.9. Opposite behavior of various physical properties in high and low T_c A15 type compounds after irradiation.

It is certain that the respective change of phonon spectrum and electronic density of states is responsible for the different effects on T_c after irradiation of these two classes of materials. A question arises: Why do the lattice vibrational modes react in such a different way when going from one class to the other?

For a discussion about the reasons for the different lattice response to irradiation in the case of high or low T_c A15 type compounds, it is useful to recall that the former class of materials exhibits a lattice softening when cooling from 300 K to 4.2 K. In some cases, e.g. V_3Si or Nb_3Sn , this softening even leads to a low temperature lattice instability, leading to the

martensitic cubic-tetragonal transformation. Other systems, e.g. Nb_3Ge , Nb_3Al , V_3Ga and others are still stable at low temperature but exhibit a lattice softening when cooling from room temperature to low temperatures. It is on the other hand known that the compound Cr_3Si (normal even at 0.015K) not only does not show any lattice softening, but exhibits even an increase of θ_D by 100 K: $\theta_D(300K) = 530$ K and $\theta_D(0) = 640$ K /229/. The same behavior is encountered in Mo_3Si , where $\theta_D(300K) = 470$ K and $\theta_D(0) = 560$ K were reported /158/. In both cases, the calorimetrically measured value of $\theta_D(T)$ show an increase by ≥ 100 K below 60 K, thus reflecting a phonon hardening, in contrast to the phonon softening encountered in high T_C materials.

In high T_C A15 type compounds, irradiation thus leads to a gradual canceling of the low temperature phonon softening, the correlated decrease of T_C being mainly due to the simultaneous decrease of the electronic density of states. This is the point of departure for the understanding of the radiation behavior of the low T_C superconductors considered in this paragraph: It is the lattice hardening at low temperature which is now gradually reduced by irradiation, thus leading to the observed increase of T_C . In contrast to the high T_C A15 type compounds, however, the electronic density of states has practically no influence on the enhancement of T_C , which is now entirely due to the lowered phonon frequency $\langle\omega\rangle^2$. The behavior of A15 type compounds after irradiation will thus be different, depending on the initial electronic density of states and the variation of $\theta_D(T)$ between 300 K and low temperature:

- a) High T_C materials. High electronic density of states, phonon softening
 V_3Si , Nb_3Sn , Nb_3Al , Nb_3Ge ,.....
 —→ Strong decrease of T_C with increasing dose, as for most compounds in Fig. 4.10a. $N(0)$ is dominant.
- b) Low T_C materials: Low electronic density of states, phonon hardening
 Mo_3Si , Mo_3Ge , Nb_3Ir ,.....
 —→ Considerable increase of T_C with increasing dose, as for Mo_3Ge and Mo_3Si in Fig. 4.31 and Nb_3Ir in Fig. 4.33. $\langle\omega\rangle^2$ is dominant.
- c) Intermediate T_C materials: Intermediate electronic density of states, phonon hardening
 Mo_3Os , $Mo_{.76}Ir_{.24}$, $Mo_{.50}Re_{.50}$,.....
 —→ Moderate decrease of T_C with increasing dose, as for Mo_3Os in Fig. 4.10a and Mo-Re in Ref. 239.
 Combined effect of $N(0)$ and $\langle\omega\rangle^2$.

It is suggested that the picture developed for irradiated low T_c A15 type materials may be applied to heavily irradiated high T_c materials, as Nb_3Sn in Fig. 4.28 and Nb_3Ge in Fig. 4.30. In fact, both highly disordered compounds exhibit T_c values below 4 K, corresponding certainly to low values of the electronic density of states. Above the state of high disorder ($S < 0.40$) characterized by the minimum of T_c in Figs. 4.28 and 4.30, it can be imagined that further irradiation leads again to phonon softening, thus leading to the observed slight increase of T_c in Nb_3Sn /157/ and Nb_3Ge /34/ after irradiation at the highest doses. Like for the low T_c A15 type materials, the electronic density of states is expected to be of little importance, the small increase in T_c being due to slightly lowered $\langle \omega \rangle^2$ at low temperatures.

The changes of the phonon spectrum during disordering are connected with the change in character of the interatomic forces acting in a compound. At this point, it may be interesting to compare the pair potential between the two systems Nb_3Sn /224/ and Mo_3Si /225/, which have been carried out under the same conditions and using the same Heine-Abarenkov-Animalu model pseudopotential (see Fig. 4.35). The difference between the pair potential for Nb_3Sn of Figs. 4.4 and 4.35 arise from different boundary conditions and will thus be neglected for instance.

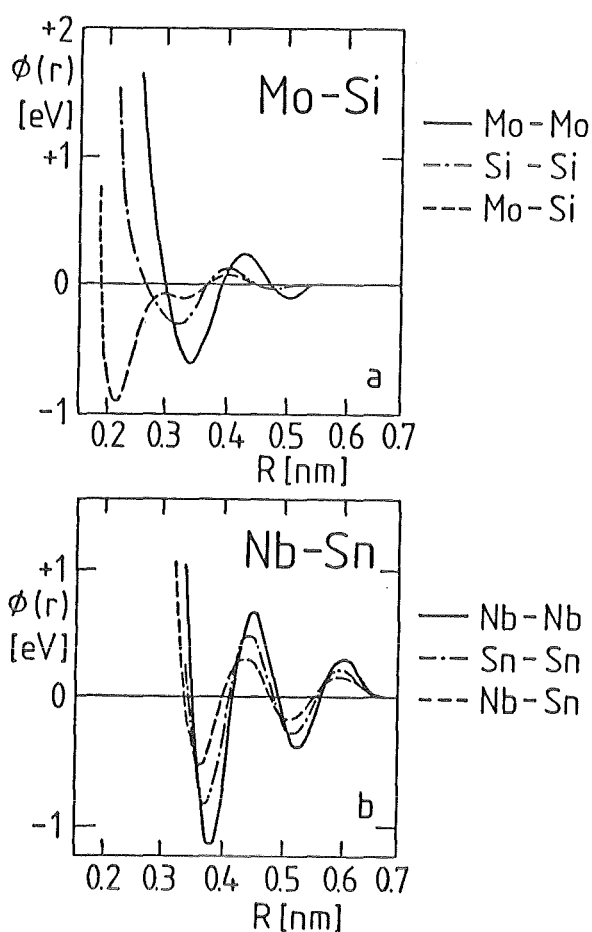


Fig. 4.35. Pair potentials in the systems Nb_3Sn /224/ and Mo_3Si /225/, calculated using the same pseudopotential approximation. Note the difference between the potentials for Mo-Si and Nb-Sn.

A comparison between the potentials in Fig. 4.35 shows that the main difference is encountered for the potentials between different elements, i.e. Mo-Si and Nb-Sn. It is expected that simultaneous static displacements and atomic disordering would particularly affect these interactions, but there is no further proof for this hypothesis. It is possible that the difference between the Mo-Si and Nb-Sn pair potentials is at the basis of the antagonism between Cr, Mo and V, Nb based A15 type compounds repeatedly mentioned in the present work.

4.3.7. Recombination Effects

When analyzing the irradiation data presented in this section, a question arises: Why is the level of saturation for various properties, as T_c , a , S or u in irradiated A15 type compounds different for each particle? In particular, the saturation behavior of the order parameter is of interest, since even prolonged irradiation does not produce complete disorder, the minimum values of S_{sat} lying in the range between 0.20 and 0.40 as stated in 4.3.5.

Recently, Zee and Wilkes/178/ have established a model describing the decrease of the long-range order parameter in Cu_3Au after irradiation, in particular also the saturation behavior at high doses. In their model, the variation of the order parameter in an irradiated compound is described by the differential equation

$$\frac{dS}{dt} = \left(\frac{dS}{dt}\right)_{irr} + \left(\frac{dS}{dt}\right)_{therm} \quad (4.10)$$

The first term represents the disordering rate due to irradiation,

$$\left(\frac{dS}{dt}\right) = -\epsilon k S, \quad (4.11)$$

which is nothing else than the Aronin equation, Eq.(3.22). The second term represents the radiation induced thermal ordering, a consequence of the enhanced vacancy concentration (in the case of Cu_3Au , the vacancies are single in contrast to the present A15 structure, where the split-vacancy structure is more complex).

The second term in Eq. (4.10) implies that the point defects have reacted their steady-state concentration, taking into account for the irradiation temperature, T_{irr} . It is quite complex:

$$\begin{aligned}
 \left[\frac{dS_a}{dt} \right]_{\text{therm}} &= \frac{v_v}{2} c_v \frac{Z_b}{X_b} (Z_a + Z_b - 2) \\
 &\times \exp(-E_m^0 / K_B T) \\
 &\times (X_A X_B \{1 - S_a\}^2 - \exp\left(\frac{-V_0 S_a}{K_B T}\right) \\
 &\times \{S_a + X_A X_B (1 - S_a)^2\})
 \end{aligned} \tag{4.12}$$

(The symbols are explained in Table 4.10).

It would lead too far to treat in detail all considerations of the theory of Zee and Wilkes /178/, based on a first model of Liou and Wilkes /177/. Schneider and Linker /135/ have performed the calculation for He⁺ and H⁺ irradiated Nb₃Ir. The result of S_a as a function of the irradiation time is shown in Fig. 4.36. The level of the steady-state, S_{sat}, depends on the projectile and its energy, but is also strongly influenced by the irradiation temperature. The material properties enter with the vacancy ordering motion energy, which is of the order of 0.84 eV for Cu₃Au and is estimated to the same value for Nb₃Ir /135/. It is interesting to give a list of the other parameters used for this calculation /135,224,225/: this is done in Table 4.10.

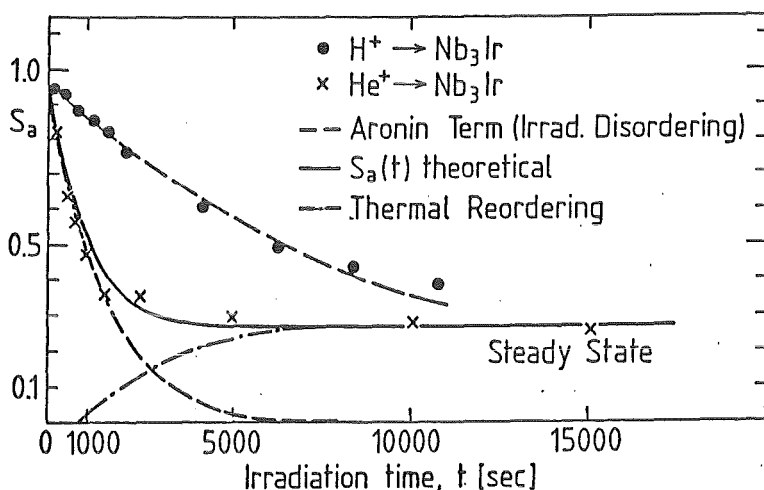


Fig. 4.36. Long-range order parameter in irradiated Nb₃Ir as function of the irradiation time, determined by Schneider and Linker /135/.

Boltzmann constant	$K_B = 8.62 \cdot 10^{-5} \text{ eV/K}$
Number of 6c sites next to a 2a site	$Z_a = 12$
Number of 2a sites next to a 6c site	$Z_b = 4$
Fraction of A atoms	$X_A = 0.75$
Fraction of B atoms	$X_B = 0.25$
Vibrational frequency	$\nu_v = 1 \cdot 10^{13} \text{ Hz}$
Irradiation temperature	$T_{irr} = 300 \text{ K}$
Vacancy concentration at equilibrium	$C_{ve} = 2 \cdot \exp(-E_{fv}/K_B T)$
Vacancy formation energy	$E_{fv} = 1 \text{ eV}$
Recombination coefficient	$\alpha/D_i = 1 \cdot 10^{17} \text{ cm}^{-2}$
Dislocation bias for vacancies	$Z_v = 1$
Diffusion constant for vacancies	$D_v = D_{ov} \exp(-E_m^v/K_B T)$
Vacancy preexponential diffusion coefficient	$D_{ov} = 0.82 \text{ cm}^{-2} \text{ s}^{-1}$
Vacancy motion energy	$E_m^v = 0.79 \text{ eV}$
Vacancy ordering motion energy	$E_m^o = 0.84 \text{ eV}$
Ordering energy	$V_o = 0.35 \text{ eV}$

Table 4.10. Parameters used for fitting the Nb₃Ir data /135/.

4.3.8. Radiation Damage in A15 Type Compounds: A Synopsis

Although irradiations on A15 type compounds have been carried out since more than 20 years, some questions are still open due to the lack of simultaneous relevant experiments, in particular specific heat, lattice parameter, thermal and static rms amplitudes and others on one and the same sample. The attention has too much been concentrated on the decrease of T_C only, while a combination of these properties would have been needed for a further understanding. A very important missing point is the lack of neutron irradiations at low T_{irr} , followed by in situ low temperature measurements. As shown by the author and coworkers /156/, this point is of particular technical importance (see Sect. 11.3).

In spite of the sometimes rather incomplete sets of data, the present analysis has led to a good overall understanding of the irradiation phenomena in high and low T_C A15 type compounds. It has been shown that the complexity of the effects

produced by high energy particle irradiation cannot be described by a simple effect alone: there is no "universal" defect. The fact that the behavior of T_C vs. ϕt almost coincides for several "typical" A15 type compounds (see Fig. 4.10a) indicates that the Fermi energy lies in a region where the density of states of these compounds varies strongly as function of E . After having shown that the initial decrease of T_C is correlated to a decrease in the degree of atomic ordering, it is clear that the similarity of T_C vs. ϕt between "typical" A15 type compounds simply reflects a similar variation of T_C vs. S for this class of materials.

The different types of deviations from the perfectly ordered state observed in irradiated A15 type compounds have been schematically represented in Fig. 4.37. Each one of these non-equilibrium states of the matter has an effect on the superconducting properties of the analyzed compound, depending on the radiation dose, the energy of the irradiating particle and the irradiation temperature, T_{irr} , but also on the compound itself (high or low T_C A15 type compound). At very low doses, the first low temperature physical property to be affected is the electrical resistivity, ρ_0 , which will be discussed in Sect. 8 and in Sect. 11.3 together with the data on Nb_3Sn multifilamentary wires. At low doses the lowering of T_C in high T_C A15 type compounds is without any doubt dominantly influenced by the decrease of the order parameter, as a consequence of a decrease of the electronic density of states and lattice hardening. In low T_C A15 type compounds, the primary effect seems to be the marked lattice softening, while the electronic density of states remains essentially unchanged. At intermediate doses, where T_C approaches the saturation value, proximity effects between regions with decreased order parameter and depleted zones or disordered zones become important and lead to a maximum of the superconducting transition width, ΔT_C . After heavy irradiation finally, various effects are encountered, as the presence of amorphous phase or of radiation induced phases.

After having shown the occurrence of a series of additional effects at high irradiation doses, it is obvious that the description of the decrease of T_C after irradiation in high T_C as a function of atomic disordering is only valid for doses sufficiently far away from the beginning of these effects. This dose is reached when T_C/T_{C0} as a function of fluence starts to curve upwards. From Fig. 4.10a, this level can be set at doses where T_C/T_{C0} falls below $T_C/T_{C0} \approx 0.4$.

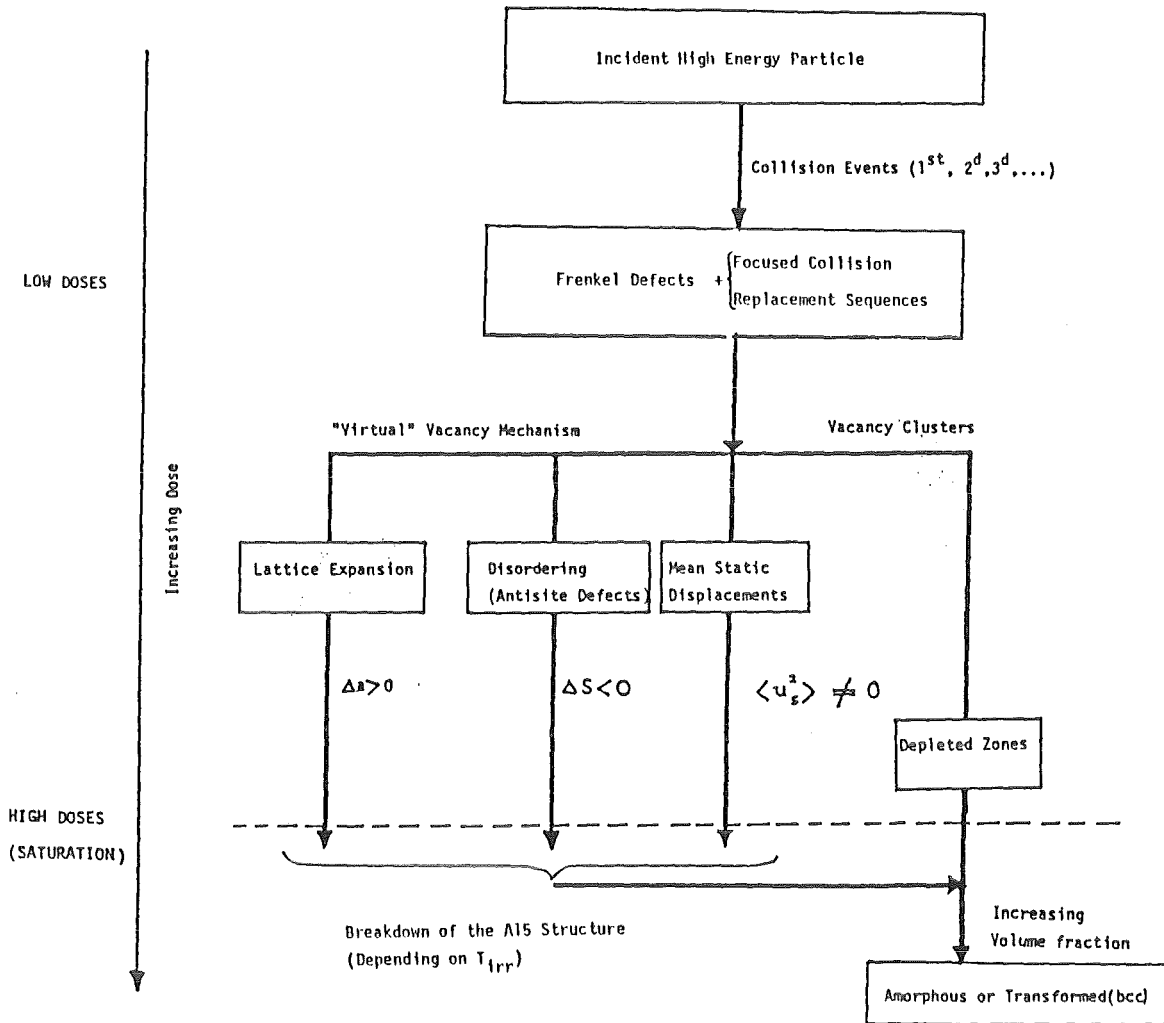


Fig. 4.37. Sequence of possible radiation induced effects in A15 type compounds. Depending on T_{irr} and the energy of the incident particle, a different steady-state can be reached after heavy irradiation.

5. THE DEGREE OF ORDERING IN A15 TYPE COMPOUNDS

In analogy to the system Cu_3Au , A15 type compounds can under certain conditions undergo small deviations from the perfectly ordered state. The achievement of perfect order in a compound is intimately connected to the kinetics of site exchanges in the temperature range between the formation temperature of the A15 phase, T_F , and the diffusion limit, T_D (see Fig. 4.5). In a certain number of A15 type compounds the state of perfect order can be reached, while in others, a certain amount of disorder cannot be eliminated, even after prolonged anneals at intermediate temperatures just above T_D (T_D lies between 560 and 900°C, as follows from Table 4.1). The factors governing the ordering kinetics in A15 type compounds have so far not been studied in detail: Several arguments, as the ratio between the atomic radii of the constituents or the difference in electronegativity have been introduced, but without any theoretical justification. This problem will be discussed at the end of this Section.

All ordering data on A15 type compounds based on least square refinement procedures performed either on X ray or neutron diffraction measurements will be critically reviewed in the following. The order parameter (either S , S_a or S_b depending on the effective composition of a compound), as well as mean square vibration amplitude U^2 and the lowest R factor (as defined by Eq. 3.15) are separately listed for each system.

Most data have been obtained by powder diffractometry, thus inherently yielding larger error margins than those based on single crystal refinements. Nevertheless, the reproducibility of the measured intensities as well as the comparison with the single crystal data show that the order parameter values as obtained on powder diffractometry can be considered as representative under the condition that the number of analyzed peaks is sufficiently high, thus reducing statistical errors. This obviously corresponds to measurements up to values of $\sin\theta/\lambda$ as high as possible. Most diffraction measurements on powdered A15 type compounds, however, have only been performed up to values of $\sin\theta/\lambda$ lying between 0.5 and $0.7 \times (10^{-10} \text{ m})^{-1}$. This allows to maintain the uncertainty of the order parameter below 2%, in more unfavourable cases below 3%. Unfortunately, this limited angle range leads to much larger errors in the mean square vibration amplitudes,

up to 20%, as can be seen from a comparison of the data in the following tables of this Section. In particular, it is virtually impossible to make a significant distinction between isotropic and anisotropic thermal vibrations based on refinements of powder diffraction data. In these cases, U_a^2 and U_b^2 were determined by using the method described in 3.2.1.

The lack of precision in the determination of the vibration amplitudes, in particular those on the 2a and on the 6c sites is the most serious criticism to the diffraction work accomplished so far on A15 type compounds. As will be shown in Sect. 6, however, the knowledge of the vibration amplitudes U^2 or U_a^2 and U_b^2 is very useful for the description of this class of compounds. It must be mentioned that the earliest order parameter determinations on A15 type compounds by Van Reuth and Waterstrat /4/ and by Flükiger /4,18,62/ were performed without to take into account the vibration amplitudes, which were held at $U^2 = 0$ or at $U^2 = 0.0063 \times 10^{-20} \text{ m}^2$ ($B = 0.5$). This illustrates the low importance which was originally given to this property, with the result that additional errors were introduced in the determination of S . Complete refinements were only effected in the works published after 1975. In the cases where earlier raw data were still available, a complete refinement was performed by the author in order to include the results in the present work.

Since most refinement data reported here have been performed on powder samples, some uncertainties still subsist in particularly difficult cases, e.g. Nb_3Ge or Nb_3Sn . Where available, data on electrical resistivity at low temperature, ρ_0 , are of considerable help for determining how close to perfect ordering is the compound in reality (See Sect. 7). Recently, values well below $\rho_0 = 1 \times 10^{-8} \Omega\text{m}$ ($\text{RRR} = 80$) were measured by Flükiger et al. /220/ on V_3Si single crystals which were prepared by recrystallization. For a stoichiometric, perfectly ordered A15 type compound, $\rho_0 \approx 1 \times 10^{-8} \Omega\text{m}$ can thus safely be assumed. This condition is confirmed by measurements of Caton and Viswanathan /217/, Orlando et al. /186/, Testardi /219/ and Williamson and Milewits /218/ on V_3Si and Arko et al. /185/ on Nb_3Sn single crystals, yielding $\rho_0 \leq 4 \times 10^{-8} \Omega\text{m}$ in each case. The variation of ρ_0 with S has so far only been measured in one A15 type compound, Nb_3Pt , by Flükiger et al. /142/ on argon jet quenched samples. The result is represented in Fig. 8.5.

5.1 Presentation and Discussion of the Ordering Data

5.1.1 Nb Based A15 Type Compounds

a) Nb₃Sn (Single Crystal)

A single crystal, grown by Hanak et al. /168/ by means of the CVD technique was characterized by measurements of the specific heat (Vieland and Wicklund /169/), of the electrical resistivity (Woodard and Cody) /170/ and of the Debye-Waller factor, $M = B \sin^2 \theta / \lambda^2$ (Vieland /171/). On the same sample, Keller and Hanak /172/ measured the elastic moduli and Mailfert et al. /173/ the low temperature lattice parameter variation at the cubic-tetragonal phase transition. The reported data are $T_c = 18$ K, $\gamma = 13.1$ mJ/K²at-g /169/, $\rho_{T \geq T_c} = \rho_0 = 10^{-8}$ Ω m /170/, $a = 0.5290$ nm, while the composition was stoichiometric, $\beta = 0.25$.

Unfortunately, Vieland /171/ did not refine the long range order parameter for his Nb₃Sn single crystal. His measurements up to the (14,1,0) line corresponding to $\sin \theta / \lambda = 1.326 \times 10^{-1} \text{ nm}^{-1}$ (MoK α radiation) yielded, however, a high precision in the temperature factor, B, which was determined for both, the Nb atoms on the 6c sites (B_a) and the Sn atoms on the 2a sites (B_b). He did not differentiate between the thermal vibrations along and perpendicular to the chain directions, and performed the refinement with fixed values ($\beta = 0.25$ and $S = 1$, the results being summarized in Table 5.1.

A single crystal refinement on Nb₃Sn by Kodess et al. /180/ with fixed order parameter at $S = 1$ yielded the isotropic temperature factors $B_a = 0.445$ and $B_b = 0.486$ for Nb and Sn respectively, i.e. slightly different values with respect to those of Vieland /171/, but show the same tendency of $B_a < B_b$ (or $U_a^2 < U_b^2$) (see Table 5.1). The same data of Kodess et al. /180/, refined for anisotropic temperature factors for Nb, yielded a smaller R factor (0.035 instead of 0.045) and the values $U_{11}^2 = 0.0042 \times 10^{-20} \text{ m}^2$, $U_{22}^2 = 0.0062 \times 10^{-20} \text{ m}^2$ and $U_b^2 = 0.0052 \times 10^{-20} \text{ m}^2$ (or $B_{11} = 0.33 \times 10^{-20} \text{ m}^2$, $B_{22} = 0.491 \times 10^{-20} \text{ m}^2$ and $B_b = 0.483 \times 10^{-20} \text{ m}^2$), i.e. $(B_{22} - B_{11})/B_{22} = 0.328$. Kodess et al. /180/ also report the result of a refinement for $\sin \theta / \lambda > 0.65 \times 10^{10} \text{ m}^{-1}$, yielding a smaller R factor, $R = 0.013$ and showing a similar anisotropy: $U_{11}^2 = 0.0052 \times 10^{-20} \text{ m}^2$ and $U_{22}^2 = 0.0074 \times 10^{-20} \text{ m}^2$, i.e. U_{22}^2 is 28.9 % larger than U_{11}^2 .

There is thus a high anisotropy in the thermal vibrations of Nb atoms in the compound Nb_3Sn . This illustrates the covalent character of the Nb-Nb interaction, earlier shown for V-V interactions in V_3Si by Staudenmann /91, 95, 181/. Since the measurements of Vieland /171/ and Kodess et al. /180/ were both performed at room temperature, it can be said that at temperatures close to the Debye temperature, the vibration of the Nb atoms is mainly governed by their tetragonal environment (point symmetry $4\bar{2}m$).

b) Nb_3Sn (Polycrystals)

In spite of a considerable interest in knowing the degree of ordering of the high T_c compound Nb_3Sn , the first reliable determinations of S by powder diffractometry in this compound have been performed only recently by the author and coworkers /9/. This is due to two reasons: i) the small difference between the form factors f_{Nb} and f_{Sn} , a consequence of the proximity of Nb and Sn in the periodic system ($\Delta Z = 9$) leads to low intensities of the X ray superlattice lines 110, 220, 310, ..., thus increasing the uncertainty ΔS . Neutron diffraction cannot be used at all, since the neutron scattering factors for Nb and Sn are identical /56/, ii) it is very difficult to obtain a homogeneous Nb_3Sn sample, due to the particular shape of the Sn rich A15 phase boundary, the formation temperature falling indeed very rapidly from $2230^\circ C$ to $931^\circ C$ in the narrow composition range between ~ 22 and 25 at.% Sn /174/.

The availability of a Nb_3Sn sample with a very narrow compositional distribution was the necessary condition for a determination of S in Nb_3Sn , where $f_B - f_A = 9$ is rather unfavourable. Thus, the Nb_3Sn sample on which the order parameter was measured /9/ was a piece of the same sample on which Junod et al. /179/ previously measured the specific heat. The calorimetric superconducting transition width is very narrow, $\Delta T_c \leq 0.7$ K, corresponding to a compositional variation throughout the sample of 0.3 at.% Sn (see Fig. 5.1).

The Sn content of this sample was determined from the variation of T_c vs. β as well as from a vs. β both being established by Devantay et al. /86/. From the values $a = 0,5288(7)$ nm and $\bar{T}_c = 17.8$ K (\bar{T}_c is the average value of the calorimetric transition), an effective Sn content of 24.5 ± 0.2 at.% Sn was found. The specific heat value was $\mathcal{C} = 13.2$ mJ/K² at-g, which is very close to the value determined by Vieland and Wicklund /169/ on their Nb_3Sn single crystal.

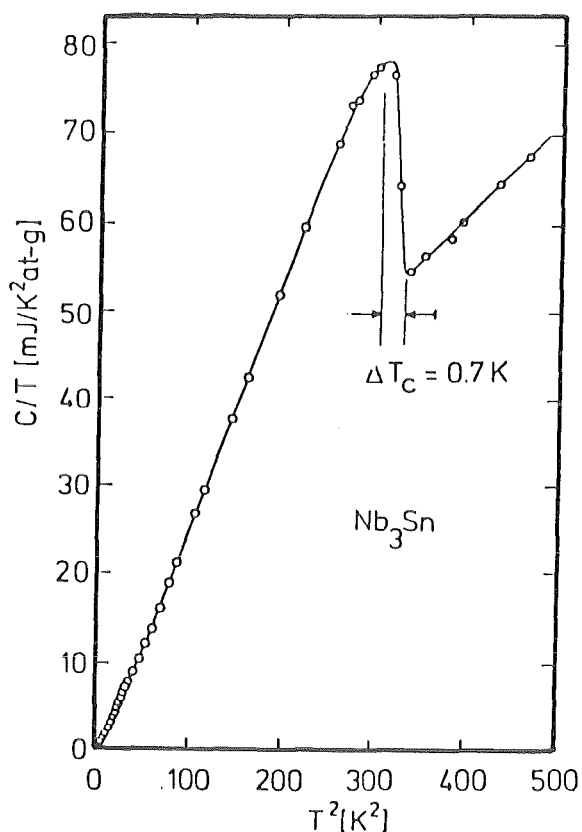


Fig. 5.1. The calorimetric superconducting transition in the Nb_3Sn sample used for the order parameter determination by Flükiger et al. /9/, measured by Junod et al. /179/. The superconducting transition width is ≤ 0.7 K, corresponding to a compositional variation of ≤ 0.3 at.% Sn.

The Nb_3Sn sample was further characterized by low temperature X ray diffractometry using a quartz monochromator for suppressing the $\text{CuK}\alpha$ radiation, revealing the presence of 45% tetragonal and 55% cubic phase at 10 K /9,215/ (See also (11.1)). The observed mixture of cubic + tetragonal (denoted as T_1 in Ref. 9), determined earlier to ~ 24.5 at.% Sn /86/, lies within the composition range exhibited by this sample. The information about the low temperature structure of the analyzed Nb_3Sn sample will be important for the discussion in Section 10 about the influence of the martensitic transformation on the electronic properties of this compound. Indeed, Junod et al. /179/ assumed in their paper that the present sample would completely transform to the tetragonal phase at low temperature, which raised a controversy about the question whether the cubic or the tetragonal phase would exhibit the higher electronic density of states /184/. This will be discussed in Section 11.

The results of the various refinements, listed in Table 5.1 show that with an uncertainty of $\Delta S = \pm 0.02$, Nb_3Sn is in reality perfectly ordered. The low error margin was obtained by repeated measurement and averaging of the

System	Preparation	Irradiation	a (nm)	β	T_c (K)	Beam	$\sin\theta/\lambda$ (10^{-10} m^{-1})	Order Parameter	U^2 ($\times 10^{-20} \text{ m}^2$)	R	Ref.
Nb ₃ Sn	CVD, Single Cryst.	-	0.52889	0.25	18.0	MoK $_{\alpha}$	1.3	(S = 1) ^a	$U_a^2 = 0.0048$ $U_b^2 = 0.0056$	-	171
Nb ₃ Sn	CVD, Single Cryst.	-	0.5294	0.25	18.2	MoK $_{\alpha}$	1.2	(S = 1) ^a	$U_a^2 = 0.0056$ $U_b^2 = 0.0062$	0.045	180
		-	0.5294	0.25	18.2	MoK $_{\alpha}$	1.2	(S = 1) ^a	$U_{11}^2 = 0.0042$ $U_{22}^2 = 0.0062$ $U_b^2 = 0.0061$	0.013	180
Nb ₃ Sn	Sintered 7h/1550°C	-	0.5288	0.245	17.8	CuK $_{\alpha}$	0.6	$S_a = 1.0$	$U^2 = 0.0054$	0.09	9
									$U_a^2 = 0.0049$ $U_b^2 = 0.0059$	0.060	162
Nb ₃ Sn	Arc Melted	Fission Fragn.	0.5350	0.25	-	CuK $_{\alpha}$	$\frac{I_{211}}{I_{210}}$	(S = 0) ^b	-	-	154
Nb ₃ Sn	Films	unirrad.	0.5288	0.25	17.85	CuK $_{\alpha}$	0.63	(S=0.98) ^c	-	-	136
		^{32}S ions ^d	0.5298		13.85			S = 0.84			
			0.5307		10.54			S = 0.74			
			0.5318		6.80			S = 0.64			
			0.5322		4.89			S = 0.57			
			0.5329		3.62			S = 0.42			
			0.5345		3.25			S = 0.20			

Table 5.1. Structural parameters from least square refinements for Nb₃Sn, as prepared by various methods: CVD = chemical vapor deposition, sintering and arc melting. The data of samples irradiated with ^{32}S ions (E = 20 MeV) are also added.

^a) The refinement was carried out with fixed order parameter, S = 1,

^b) The order parameter is only estimated, based on the I_{211} and the I_{210} intensities, ^c) For the unirradiated sample, $S_0 = 0.98$ was assumed in Ref. 136, ^d) The individual dose was not precised in Ref.

136. R is the reliability factor.

measured intensities. The overall temperature factor, $B = 0.43 \times 10^{-20} \text{ m}^2$, is in good agreement with the data of Vöeland /171/ and Kodess /180/. As will be shown later in Sect.7, there are additional arguments for the occurrence of perfect ordering in Nb₃Sn, in particular the low value of the electrical resistivity, $\rho_0 < 4 \times 10^{-8} \Omega\text{m}$ /185/, following the argumentations of Devantay et al. /86/. The occurrence of the martensitic phase transition at low

temperature in V_3Si and Nb_3Sn could also be considered as an argument for perfect ordering (Section 10), but this correlation cannot be invoked as a proof, the number of transforming A15 type systems being too low.

It is interesting that T_c in Nb_3Sn is only little influenced by fast quenching procedures /38,131/, which could have the following reasons: i) The order parameter does not vary up to the highest quenching temperatures where the stoichiometric composition is included in the A15 phase field /86,174/, i.e. 1500 °C, or ii) the reordering kinetics is extraordinarily fast, and lower degrees of ordering than $S = 1$ cannot be retained by conventional quenching techniques. Recent order parameter determinations up to 900 °C /162/ only indicate that no measurable change of S can be detected up to this temperature (see 5.2.2). Nevertheless, the second hypothesis has to be retained for thermodynamical reasons.

The occurrence of perfect ordering in Nb_3Sn was also observed after the formation of the A15 phase by diffusion reaction starting from the Cu bronze, as in Nb_3Sn multifilamentary wires. As recently shown, the order parameter in the Nb_3Sn filaments after etching away the bronze matrix was found to be very high, too: $S_a = 1$, with an uncertainty $\Delta S = \pm 0.03$ /9/.

An order parameter $S = 0$ indicating complete disorder has been reported by Skvortsov et al. /154/ after irradiating Nb_3Sn with fission fragments. This value was, however, obtained on the basis of the ratio I_{211}/I_{210} only, and the error may thus be considerable. This would be the only case reported so far where a completely disordered A15 phase was observed. Obviously, this structure is very far from an ideal fundamental structure, with a lattice parameter of $a = 0.5350$ nm /154/ and mean static displacements of the order $u^2 = 0.02$ nm², as estimated by a comparison with the data of Burbank et al. /144/. In Table 5.1, recent measurements of Nölscher and Saemann-Ischenko /136/ on Nb_3Sn films after irradiation with 20 MeV ^{32}S ions were included, where the starting value of the order parameter was assumed as $S_0 = 0.98$.

c) Nb_3Ge (Single Crystal)

As follows from the Nb-Ge phase diagram of Jorda et al. /67/, the stoichiometric composition is not comprised in the equilibrium A15 phase field. It is, however, possible to form small single crystals (0.1 mm³) at compositions $\beta \leq 0.20$, as shown by Rasmussen and Hazell /166/, who used floating zone melting. These authors found almost perfect ordering of the Nb atoms on the 6c sites. Depending on the composition chosen for the

refinement, ($\beta = 0.1875$ or $\beta = 0.20$, they found $S_a = 1.0$ or $S_a = 0.965$, respectively. From a comparison of their lattice parameter, $a = 0.51698$ nm /166/ with the correlation $a = a(\beta)$ given by Jorda et al. /67/, a value of $\beta = 0.19$ can be deduced, so that the order parameters $S_a = 1$ and $S_b = 0.76$ (with an estimated uncertainty $\Delta S = \pm 0.02$) can be considered as reliable (see Table 5.2).

From the single crystal refinement of Rasmussen and Hazell /166/ (Table 5.2) it follows that the smallest vibration amplitude for Nb atoms occurs in chain direction. The r.m.s. vibration amplitude in chain direction is 20 % smaller than those perpendicular to them. This result is not surprising, since it reflects the "overlapping" between neighbouring A atoms on 6c sites discussed in Sect. 4, thus giving a quantitative picture for the deviation from sphericity in A15 type compounds. A comparison between the measured anisotropies in different A15 type compounds will be made in 6.1.1.

Stoichiometric Nb_3Ge would be expected to show even a more pronounced thermal anisotropy than $Nb_{0.81}Ge_{0.19}$, due to the smaller lattice parameter ($a = 0.5140$ nm), compared with $a = 0.5169$ nm and the correlated stronger intrachain repulsive forces. However, no single crystals are available above $\beta = 0.19$, and the poor quality ("poor" from the point of view of the crystallographer) of the polycrystalline samples produced by nonequilibrium methods does not allow at present to verify this hypothesis.

d) Nb_3Ge (Polycrystals)

All reported order parameter determinations in Nb_3Ge polycrystals have been carried out at the Brookhaven National Laboratory /68,69,70/, on samples prepared by chemical vapour deposition /182/. The results are summarized in Table 5.2. The achievement of Nb_3Ge samples with Ge contents exceeding 20 at.% by CVD allows to study the variation of T_c or of the lattice parameter at the vicinity of the stoichiometric composition. However, secondary phases cannot be avoided, their amount oscillating between

System	Preparation	Irradiation	a (nm)	β	T_c (K)	Beam	$\sin\theta/\lambda$ ($10^{-10}m$) ⁻¹	Order Parameter	U^2 ($\times 10^{-20} m^2$)	R	Ref.
Nb ₃ Ge	ZM, Single Crystal	-	0.51693	0.19	-	AgK _{α}	1.6	$S_a = 1.00$	$U_{11}^2 = 0.0040$ $U_{22}^2 = 0.0063$ $U_b^2 = 0.0057$	0.034	166
Nb ₃ Ge	CVD, Polycrystal 1350°C	-	0.5179	0.17	5.8	CuK _{α}	0.45	$S_a = 0.99$	$U^2 = 0.0114$	0.049	68,70
Nb ₃ Ge	CVD, Polycrystal	-	0.5412	0.24	19.4	CuK _{α}	0.47	$S_a = 0.86$	$U^2 = 0.0101$	0.066	68,70
Nb ₃ Ge	CVD, Polycrystal	-	0.5143	0.24	20.2	CuK _{α}	0.47	$S_a = 0.92$	$U^2 = 0.0038$	-	70,182
Nb ₃ Ge	CVD, Polycrystal	-	0.51415	0.24	20.9	CuK _{α}	0.47	$S_a = 0.83$	$U^2 = 0.0089$	0.043	70,182
		0.75×10^{19} n/cm ²	0.5152		14.2			$S_a = 0.75$	$U^2 = 0.0089$	-	
		2.1×10^{19} n/cm ²	0.5158		9.1			$S_a = 0.65$	$U^2 = 0.0025$	-	
		3.4×10^{19} n/cm ²	0.5174		4.4			$S_a = 0.46$	$U^2 = 0.0140$	-	
Nb ₃ Ge	CVD, Polycrystal	5×10^{19} n/cm ² + 750°C	0.5148	0.23	15	CuK _{α}	0.47	$S_a = 0.91$	$U^2 = 0.0051$	-	70

Table 5.2 Structural parameters from least-square refinements for Nb₃Ge as prepared by different methods. CVD = chemical vapor deposition, ZM = zone melting. The data for neutron irradiated samples /68,69,70/ are also shown.

18 and 40 wt.% in the samples analyzed in Refs. 68-70,182 and 183 (see Fig. 3.7). As pointed out in 3.3, the refinement of such multiphase samples is not only very difficult, but leads to systematical uncertainties. Cox et al. /70/ have nevertheless carried out a very careful study in order to take into account the additional phases, which in addition have diffraction lines overlapping with most of the A15 reflexes (see Fig. 3.7). These authors refined the parameters for each additional phase separately, i.e. for the tetragonal Nb₅Ge₃ phase, the hexagonal Nb₅Ge₃ phase (this phase is not an equilibrium phase of the binary Nb-Ge phase diagram /67/, it only appears in CVD samples) and NbO. The result from a subtraction of all these line spectra from the measured one was assumed to be the A15 line spectrum, which was then used for the refinement procedure.

This procedure is in principle correct, but is nevertheless subject to criticism: i) Since even in single-phased samples preferred orientations cannot be accounted for, this will also be true for each one of the various additional phases present in the CVD Nb₃Ge samples. However, the line intensities of all additional phases were assumed /70, 182/ to correspond to the case of no preferential orientations. It may be mentioned that in order parameter determinations, where the line intensities vary by a few percent only, even a very small amount of preferential orientations can affect the final result. Further, a systematical enhancement of a peak intensity compared to others is very frequent in powder diffractometry, as a result of the necessity to dispose the powders in planar geometry, ii) order parameter measurements are seriously influenced by the background intensity, which in turn may depend on the presence of small amounts of additional phases, as described in 3.3. It thus cannot be completely excluded that small amounts (<2%) of bcc Nb, NbH or other phases are present, contributing to the background intensity, but without to appear as isolated peaks.

For these reasons, the ordering data on Nb₃Ge polycrystals listed in Table 5.2 have an indicative character only, in spite of the sophisticated analysis performed by Cox et al. /70/, thus indicating the actual experimental limitations. These limitations appear when comparing the values of S_a on unirradiated Nb₃Ge samples, reaching from $S_a = 0,83$ to $S_a = 0,92$ (Table 5.2), revealing an uncertainty up to $\Delta S = 0.09$. An even larger uncertainty is observed for the temperature factor B, which varies between 0.3 and $0.8 \times 10^{-20} \text{ m}^2$ (or 0.0038 and $0.0101 \times 10^{-20} \text{ m}^2$ for U^2). This observation is of particular importance since the uncertainty in B (or U^2) is a good indicator for the quality of the refinement. This can be easily seen when carrying out the refinement for a given A15 type compound setting different values of U^2 and S, respectively. In this case, the reliability factor, R, will vary much slower if U^2 is varied.

These critical remarks show that there is an experimental limitation to the accuracy of order parameters in Nb₃Ge as produced by CVD. Complementary observations on physical properties, as for example the electrical resistivity, ρ_0 , give fortunately additional informations about the degree of ordering in Nb₃Ge. It was indeed shown by Kihlström et al. /73/ on coevaporated Nb₃Ge films that ρ_0 in Nb₃Ge films with $T_c = 20 \text{ K}$ and $a = 0.51 \text{ nm}$ can be as low as $30 \times 10^{-8} \Omega\text{m}$. This low value of ρ_0 has been confirmed by Schauer et al. /216/ on a coevaporated Nb₃Ge sample with $T_c = 21.9 \text{ K}$.

By analogy with the system Nb_3Pt , where ρ_0 increases from 20 to $86 \times 10^{-8} \Omega\text{m}$ /142/ when S decreases from $S = 0.98$ to $S = 0.88$ (Fig. 6.5), it follows that the order parameter of Nb_3Ge with $\rho_0 = 30 \times 10^{-8} \Omega\text{m}$ should certainly be considerably closer to perfect ordering than suggested by the data of Cox et al. /70/.

Due to the twofold dependence of ρ_0 as a function of S and β (the dependence ρ_0 vs. β has been established by Devantay et al. /86/ and Orlando et al. /186/ for Nb_3Sn and by Kihlström et al. /73/ on Nb_3Ge), it follows that the low value of $\rho_0 = 30 \times 10^{-8} \Omega\text{m}$ could correspond to either i) a Ge content lying around 24 at.% Ge, when assuming perfect ordering or ii) to an order parameter lying between $S = 0.96$ and $S = 0.98$, if the composition is assumed to be perfectly stoichiometric. It is thus probable that the mentioned resistivity value corresponds to a completely ordered, but slightly nonstoichiometric alloy. An additional argument for the occurrence of perfect ordering in Nb_3Ge is furnished by the comparison of the general behavior of S when varying the B element in Nb_3B compounds, represented in Figs. 5.2 and 5.3. The arguments in favour of perfect ordering in Nb_3Ge are summarized in 7.5.

Table 5.2 also contains the ordering data on neutron irradiated Nb_3Ge samples. Due to the seriously enhanced background accompanying the presence of amorphous volume fractions, the accuracy of the S determination becomes even worse than in the unirradiated state, but the trend is certainly correct. The correlation between T_c and S will be discussed in Sect. 9.

e) Nb_3Al (Polycrystals)

The A15 phase field in the system Nb - Al established by Jorda et al. /35/ is characterized by strongly temperature dependent phase boundaries, in a similar way to the system Nb - Ge. The Al rich A15 phase limit varies from 21 at.% Al at 1000°C /28, 35/ to 25 at.% Al at 1940°C . As shown by Flükiger et al. /28/, it is possible to retain the stoichiometric composition (or at least a composition within 0.5 at.% from stoichiometry) by argon jet quenching from 1940°C , while cooling by radiation quenching (i.e. with 50°C/s cooling rate) only allows to retain single phase samples up to 24 at.%. Several order parameter determinations have been carried out on Nb_3Al alloys, by Sweedler and Cox /53/, Moehlecke et al. /99, 183/, Flükiger et al. /28/ and finally, by Isernhagen und Flükiger /162/. The results of the crystallographic refinements are summarized in Table 5.3.

In all these cases /28,53,99,183,191/, the Nb - Al samples have been obtained by arc melting under moderate argon pressure, followed by ordering or homogenization heat treatments. As pointed out in Ref. /28/, there is an excellent agreement between the values for the line intensities for all the mentioned works. However, there is an apparent disagreement between the order parameter values in Refs. 53, 99 and 183 and those in Ref. 28, the latter being considerably higher. The author and coworkers /28/ have demonstrated that the origin of this difference, $\Delta S \leq 0.06$, resides in different assumptions about the effective composition in the relative refinement procedures. Indeed, Sweedler and Cox /53/ have originally performed their refinement on the basis of the composition ($\beta = 0.26$ which led to a value $S_a = 0.88$). Later, Moehlecke et al. /99, 183/ refined the same Nb₃Al data as in Ref. 53, but assuming ($\beta = 0.25$ and found the value $S_a = 0.92$). However, the stoichiometric composition in Nb₃Al is stable at the highest temperatures only, i.e. 1940°C /28, 35/ and must be retained by severe argon jet quenching /28/, after which it exhibits the lattice parameter $a = 0.5180$ nm, i.e. somewhat smaller than the value $a = 0.5183$ nm for the sample of Sweedler and Cox /53/, which thus has a composition $\beta = 0.24$. Using this composition and refining again the data of Sweedler and Cox, the value $S_a = 0.96$ was found /28/, which is essentially the same as that given by Flükiger et al. /28/, i.e. showing a good agreement. A comparison between the data at the compositions $\beta = 0.23$ ($S_a = 1.0$ /70/) and $\beta = 0.231$ ($S_a = 0.97$ /28/) with the values at $\beta = 0.24$ ($S_a = 0.96$ /53/) and $\beta = 0.245$ ($S_a = 0.95$ /28/) shows that the order parameter of Nb₃Al decreases when approaching the stoichiometric composition. A possible correlation with the A15 phase stability will be discussed in Sect. 6.

Table 5.3 also contains the ordering data of Schneider et al. /55/ on coevaporated Nb₃Al films after irradiation with 300 keV H⁺ ions. The initial conditions of these films were $T_{co} = 15.6$ K and $a = 0.5191$ nm, thus corresponding to an estimated composition ($\beta = 0.22$). In their paper, Schneider et al. /55/ determined the order parameters by using the procedure of Linker /54/ for samples with film geometry, assuming a value $S_{ao} = 0.90$ for the unirradiated sample. Referring to Ref. 28, the order parameters in Table 5.2 have been corrected to an initial order parameter of $S_{ao} = 0.97$.

Belovol et al. /167/ performed order parameter determinations on 3 Nb₃Al samples with the compositions $\beta = 0.223$, 0.247 and 0.263. Their results are reproduced in Table 5.3 and show a large scattering in S_a . This scattering is not surprising, since their Nb₃Al samples have been prepared by melting, followed by rapid cooling in the mold, but without any homogenization heat treatment (see Table 3.2).

System	Preparation	Irradiation	a (nm)	β	T_c (K)	Beam	$\sin\theta/\lambda$ (10^{-10} m^{-1})	Order Parameter	U^2 ($\times 10^{-20} \text{ m}^2$)	R	Ref.
Nb ₃ Al	AM 750°C,R	-	0.5183	0.24 ^a	18.6	n	0.54	$S_a = 0.96^a$	$U_a^2 = 0.0073$ $U_b^2 = 0.0070$	0.020	53,99
		0.58 $\times 10^{19}$ n/cm ²	0.5191	-	13.6	-	-	$S_a = 0.86^a$	$U_a^2 = 0.0060$ $U_b^2 = 0.0050$	0.06	
		1.2 $\times 10^{19}$ n/cm ²	0.5195	-	9.6	-	-	$S_a = 0.80^a$	$U^2 = 0.0060$	0.024	
		1.9 $\times 10^{19}$ n/cm ²	-	-	-	-	-	$S_a = 0.70^a$	-	-	
		5.0 $\times 10^{19}$ n/cm ²	0.5202	-	-	-	-	$S_a = 0.41^a$	-	-	
Nb ₃ Al	AM 750°C,R	-	0.5187	0.23	18.6 ^b	n	0.54	$S_a = 1.00$	$U^2 = 0.0050$	0.084	70
Nb ₃ Al	AM 1900°C,R	-	0.51857	0.231	17.8	n	0.47	$S_a = 0.97$	$U^2 = 0.0084$	0.007	28
Nb ₃ Al	AM 1850°C,Q	-	0.51837	0.236	17.0	n	0.47	$S_a = 0.96$	$U^2 = 0.0079$	0.010	28
Nb ₃ Al	AM 1900°C,R	-	0.51814	0.245	18.0	n	0.47	$S_a = 0.95$	$U^2 = 0.0068$	0.010	28
		-	-	-	-	CuK _{α}	0.63	$S_a = 0.93$	$U_a^2 = 0.0064$ $U_b^2 = 0.0070$	-	162
Nb ₃ Al	CE	-	0.5191	0.22 ^c	15.6	CuK _{α}	0.66	$(S_a=0.97)^d$	-	-	55
		-	0.5194	-	12.8	-	-	$(S_a=0.90)^d$	-	-	
		H ⁺ /cm ²	0.5197	-	10.9	-	-	$(S_a=0.88)^d$	-	-	
		H ⁺ /cm ²	0.5211	-	5.9	-	-	$(S_a=0.79)^d$	-	-	
Nb ₃ Al	MC	-	0.5186	0.223	16.75	CuK _{α}	0.60	$S_a=0.93\pm 0.13$	^{e)}	-	167
		-	0.5184	0.247	18.50	-	-	$S_a=0.83\pm 0.09$	^{e)}	-	167
		-	0.5181	0.263	18.40	-	-	$S_a=0.96\pm 0.09$	^{e)}	-	167
Nb ₃ Al	AM	-	0.51842	0.24	-	MoK _{α}	1.38	not given	$U_a^2 = 0.0044$ $U_b^2 = 0.0072$	-	242

Table 5.3. Structural data from least-square refinements for Nb₃Al, prepared by various methods: AM = arc melting, CE = coevaporation, MC = melting, followed by rapid cooling in the mold. R = radiation quenching, Q = argon jet quenching.

^{a)} These order parameters have been refined using the corrected composition $\beta = 0.24$ (see text), ^{b)} Too high T_c value, probably affected by shielding effects, ^{c)} Composition estimated from the lattice parameter, ^{d)} S values obtained by the procedure of Linker /54/ for film geometry, corrected for $S_{a0} = 0.97$ /28/, ^{e)} no indications about the value of U^2 .

In addition, no indications were given about the refinement procedure and the vibration amplitudes, in order that these data will not be retained for the discussion in the following Section.

The vibration amplitudes U_a^2 and U_b^2 in Nb_3Al were determined both by refinement procedures /53,99/ and by the study on selected lines /162,242/ described in 3.2.1. The result show a considerable uncertainty, U_a^2 varying from 0.0044 to $0.0073 \times 10^{-20} \text{ m}^2$ and U_b^2 from 0.0068 to $0.0070 \times 10^{-20} \text{ m}^2$. The uncertainty for the isotropic vibration amplitude U^2 is somewhat smaller, ranging from 0.0050 to $0.0071 \times 10^{-20} \text{ m}^2$. Nevertheless, it can be said that the vibration amplitudes in Nb_3Al are larger than those measured on other A15 type compounds (See 6.1.3).

f) Nb_3Ga

A sample of the composition $Nb_{.81}Ga_{.19}$, characterized by $T_c = 9.0 \text{ K}$ and by $a = 0.5181 \text{ nm}$ was found to be completely ordered after 48 hours at 1700°C , followed by slow cooling /38/, the order parameter being determined to $S_a = 1$ with an uncertainty of ± 0.03 . The specific heat measurement on the same sample yielded $\gamma = 9 \text{ mJ/K}^2\text{at-g}$ /195/. The occurrence of perfect ordering at Nb rich compositions ($\beta = 0.19$) in Nb_3Ga suggests a similar tendency to that reported above for the compounds Nb_3Ge and Nb_3Al . Unfortunately, it was impossible to obtain single phase A15 samples with $\beta = 0.20$, in order that the question of a possible decrease of the order parameter toward stoichiometry cannot be studied in the system Nb_3Ga . By analyzing selected lines (see 3.2.1), Försterling /242/ found the vibration amplitudes $U_a^{2'} = 0.0046$ and $U_b^2 = 0.0043 \times 10^{-20} \text{ m}^2$ (see Table 5.4). However, these data need a further confirmation since the sample was insufficiently characterized, neither the lattice parameter (thus the effective composition) nor the metallurgical state being precised.

g) Nb_3Au

Order parameter data in Nb_3Au have been reported by Van Reuth and Waterstrat /4/, Flükiger /62/, Muller et al. /194/ and more recently, by Wire et al. /192/. In this system, the A15 phase forms by a congruent reaction from the solid bcc phase /196/, but the stoichiometric composition is not comprised in the A15 phase field /7, 142/. The Au rich phase limits at 1000°C and 1530°C are situated at 23 and 24 at.% Au, respectively, the Nb rich limit at 1200°C lying at 20 at.% Au /7, 31, 62/.

In their original paper, Van Reuth and Waterstrat /4/ assumed a composition $\beta = 0.25$, the Nb - Au phase diagram /196/ being not yet established at that time. Ulterior refinements were performed on the basis of the composition $\beta = 0.236$ /31, 62/ and $\beta = 0.242$ (Wire et al. /192/), respectively. All known data are listed in Table 5.4, which also includes recent data of Isernhagen and Flükiger /162/. The earlier order parameter determination based on the composition $\beta = 0.25$ /4,62/ has been corrected, assuming the more realistic value of $\beta = 0.236$ (based on microprobe analysis data from R.M. Waterstrat /31/), which leads to an increase $\Delta S = 0.09$. (Again, the earlier refinements of Van Reuth and Waterstrat /4/ and Flükiger /18,

System	Preparation	a (nm)	β	T_c (K)	Beam	$\sin\theta/\lambda$ (10^{-10}m^{-1})	Order Parameter	U^2 ($\times 10^{-20}\text{m}^2$)	R	Ref.
Nb ₃ Ga	AM 1700°C,R	0.5156	0.19	9.0	CuK _{α}	0.54	$S_a = 1$	$(U^2=0.0063)^c$	-	38
Nb ₃ Ga	AM	d)	d)	d)	MoK _{α}	1.38	not given	$U^2 = 0.0046$ $U^2_b = 0.0043$	-	242
Nb ₃ Au	AM as cast	0.5203	0.236 ^a	9.73	CuK _{α}	0.59	$S_a = 0.84^a$ b)	-	-	4
Nb ₃ Au	AM 800°C,R	0.52024	0.236 ^a	-	CuK _{α}	0.59	$S_a = 0.95^a$ b)	-	0.034	4
Nb ₃ Au	AM 800°C,R	0.5203	0.236 ^a	11.2	CuK _{α}	0.54	$S_a = 0.96^a$	$(U^2=0.0063)^c$	0.064	62
Nb ₃ Au	AM 1500°C,Q	0.5203	0.236 ^a	8.4	CuK _{α}	0.54	$S_a = 0.85^a$	$(U^2=0.0063)^c$	0.080	62
Nb ₃ Au	AM 1150°C,R	0.5205	0.242	10.56	CuK _{α}	0.54	$S_a = 0.96$	$U^2 = 0.0051$	0.076	192
Nb ₃ Au	AM as cast	0.5203	0.236 ^a	9.8	CuK _{α}	0.54	$S_a = 0.92$	$U^2 = 0.0043$	0.017	162

Table 5.4. Structural data from least-square refinements on Nb₃Ga and Nb₃Au:

AM = arc melted, R = radiation quenched, Q = argon jet quenched.

^a) The composition has been corrected to $\beta = 0.236$ /31/, leading to a slight change of S_a with respect to Refs. 3, 4 and 62, ^b) $U^2 = 0$ was fixed during the refinement, ^c) $U^2 = 0.0063 \times 10^{-20}\text{m}^2$ ($B = 0.5 \times 10^{-20}\text{m}^2$) fixed during the refinement, ^d) No indications given.

62/ were effectuated with a fixed temperature factor, $B = 0$ and $B = 0.5$ (or $U^2 = 0$ and $0.0063 \times 10^{-20} \text{ m}^2$, respectively). As shown by the comparison in Table 5.4 this does not seriously affect the value of the order parameter, S , the difference between the atomic numbers of Nb and Au being high, $\Delta Z = 38$. From Table 5.4 it follows that Nb_3Au exhibits appreciably high order parameters, but that a considerable change ΔS can be induced by quenching methods, the lowest order parameter being $S_a = 0.85$ (/62/, corrected value). The observed total order parameter variation of $\Delta S = 0.12$ is rather large for A15 type compounds after quench and anneal processes only, but is comparable to the change in V_3Au , $\Delta S = 0.10$ (See 5.1.2). The presence of additional phases and compositional inhomogeneities in Nb_3Au may lead to large errors, of the order of $\Delta S \approx 0.05$.

h) Nb_3Pt

The degree of ordering in the system Nb_3Pt has been repeatedly investigated. A particular feature of this system is the large variation of T_c as a function of the heat treatment, ranging from 7.1 to 11.1 K corresponding to changes in the order parameter from $S = 0.88$ /62, 76, 142/ to $S = 0.98$ /62, 142, 176/. This system is ideal for order parameter investigations, single phase samples being easily obtained over the whole phase field, i.e. from 19 to 28 at.% Pt at 1800°C according to the phase diagram of Waterstrat and Manuszewski /92/.

The ordering data are listed in Table 5.5. All diffraction measurements were performed with CuK_α radiation, with one exception, where neutron radiation was used /176/. In the latter case, an order parameter $S = 1$ was originally reported by Flükiger et al. /142, 176/, i.e. slightly higher than the corresponding value found by X ray diffraction on the same sample $S = 0.98$ (see Table 5.5). Subsequent analysis has shown that the X ray value has to be preferred, due to the higher number of analyzed peaks ($\sin\theta/\lambda = 0.62$ instead of $0.43 \times 10^{-1} \text{ nm}^{-1} \text{ m}^{-1}$) and to the large difference between f_A and f_B , ΔZ being equal to 37. A further indication for a small, but significant deviation from perfect ordering is given by the electrical resistivity value, which is $\rho_0 = 20.1 \times 10^{-8} \Omega\text{m}$ for the same sample as analyzed in Ref. 142, while Caton and Viswanathan /216/ reported a value $\rho_0 = 23.3 \times 10^{-8} \Omega\text{m}$.

The overall vibration amplitude in unirradiated Nb_3Pt varies between $U^2 = 0.0038 \times 10^{-20} \text{ m}^2$ /76/ and $0.0051 \times 10^{-20} \text{ m}^2$ /38/ and is thus considerably smaller than that reported for Nb_3Sn , Nb_3Ge and Nb_3Al (see Tables 5.1 to 5.3). The original data of Van Reuth and Waterstrat /4/ have been refined again, but now allowing for variable B factor. However, the result, $U^2 =$

System	Preparation	Irradiation	a (nm)	β	T_c (K)	Beam	$\sin\theta/\lambda$ (10^{-10} m^{-1})	Order Parameter	U^2 ($\times 10^{-20} \text{ m}^2$)	R	Ref.
Nb ₃ Pt	AM 1600°C,R	-	0.51524	0.25	8.2	CuK α	0.57	S = 0.93	^a	¹ 0.008	4
								S = 0.94	($U^2=0.0009$) ^b	0.09	162
Nb ₃ Pt	AM 1900°C,Q	-	0.5155	0.25	7.2	CuK α	0.54	S = 0.88	($U^2=0.0063$) ^c		62,112
Nb ₃ Pt	AM as cast	-	0.5155	0.25	9.2	CuK α	0.54	S = 0.94	($U^2=0.0063$) ^c		62,112
Nb ₃ Pt	AM 1400°C,Q	-	0.5155	0.25	8.4	CuK α	0.54	S = 0.92	$U^2 = 0.0051$	0.070	38
Nb ₃ Pt	AM 1050°C,R	-	0.5155	0.25	9.8	CuK α	0.54	S = 0.96	($U^2=0.0063$) ^c		62,112
Nb ₃ Pt	AM 900°C,R	-	0.5155	0.25	10.5	CuK α	0.54	S = 0.98	($U^2=0.0063$) ^c		62,112
Nb ₃ Pt	AM 850°C,R	-	0.5155	0.25	11.1	n	0.43	S = 1.0 ^d	$U^2 = 0.0070$ ^d	0.103	176
						CuK α	0.54	S = 0.98	$U^2 = 0.0041$	0.032	38
Nb ₃ Pt	AM 900°C,R	-	0.51545	0.251	10.7	CuK α	0.54	S = 0.95	$U^2 = 0.0038$	0.056	76
			0.58×10^{19} n/cm ²	0.51575	7.0			S = 0.88	$U^2 = 0.0038$	0.071	76
			1.44×10^{19} n/cm ²	0.5161	3.5			S = 0.59	$U^2 = 0.0076$	0.114	76
Nb ₃ Pt	AM 900°C,R	-	0.51405	0.291	5.1	CuK α	0.54	$S_a = 0.79$	$U^2 = 0.0051$	0.075	76
	AM 1800°C,R	-	0.51725	0.21	4.8	CuK α	0.54	$S_a = 0.92$	$U^2 = 0.0063$	0.043	76
	AM 900°C,R	-	0.51725	0.21	6.2	CuK α	0.54	$S_a = 1.00$	$U^2 = 0.0051$	0.057	76
Nb ₃ Pt	AM 1800°C,R	-	0.51539	0.258	10.9	CuK α	0.60	$S_a = 0.95$	$U_a^2 = 0.0038$ $U_b^2 = 0.0073$	-	162

Table 5.5. Structural data from least-square refinements on Nb₃Pt at different compositions. AM = arc melted, Q = argon jet quenched, R = radiation quenched. ^a) the temp. factor in Ref. 4 was fixed at $U^2 = 0$, ^b) Recalculated using the same data as in Ref. 4, but with variable U^2 , ^c) refined with fixed $U^2 = 0.0063 \times 10^{-20} \text{ m}^2$ ($B = 0.5 \times 10^{-20} \text{ m}^2$), ^d) the value $S = 1$ /176/ has an uncertainty of $\Delta S = 0.04$, while for all other measurements, $\Delta S = 0.02$.

$0.0009 \times 10^{-20} \text{ m}^2$, is unreasonably low. Since the new refinement of the intensities of Van Reuth and Waterstrat /4/ yields in some cases values of U^2 close to zero (in particular for the V_3B compounds), it must be concluded that some systematic error of their intensity measurements at high angles occurred. Fortunately, this had practically no effect on the value of S , due to the large value of ΔZ (see values in Table 5.5). Isernhagen and Flükiger /162/ have determined the vibration amplitudes U_a^2 and U_b^2 on a Nb_3Pt sample with $\beta = 0.258$, using the selected line method described in 3.2.1. It was found that the value for $U_a^2 = 0.0038 \times 10^{-10} \text{ m}^2$ is markedly lower than for the compounds with $B = Sn, Al$ and Ge discussed in the preceding paragraph. The low value for the isotropic vibration amplitude in Nb_3Pt is thus primarily due to the small amplitude of the Nb atoms.

As mentioned earlier, the case of Nb_3Pt is particularly interesting since the only comparison between the change of T_c with the order parameter for both quenched and irradiated A15 type compounds has been made on this compound (see Fig. 4.12), using the data from Refs. 76, 112 and 142.

i) Nb_3Ir

Although this system exhibits quite low T_c values between < 0.1 and 3.2 K in the range between 22 and 28 at. % Ir /62/ it is very interesting as a representant of "atypical" A15 type compounds based on two transition elements. The difference between the reported ordering data arises from the quality of the refinement procedure. Van Reuth and Waterstrat /4/ and Flükiger /62/ performed the least-square refinement with fixed $B = 0$ and obtained $S = 0.95$ and 0.93 , respectively. Later, Isernhagen and Flükiger /162/ found that a least-square refinement on the data of Van Reuth and Waterstrat /4/ with B and S as variables yields $S = 1.00$ with an uncertainty of ± 0.02 . This value is considerably higher than the original value, $S = 0.95$ /4/, but also higher than the value of Flükiger, $S = 0.93$ /62/, which is due to preferential orientations. Additional evidence for high S values in Nb_3Ir is furnished by the low ρ_0 value, $14 \times 10^{-8} \Omega m$ (See Sect. 8). Recently, a new Nb_3Ir sample was measured and refined /162/, confirming the high degree of ordering in this compound ($S = 1$, see Table 5.6). The isotropic vibration amplitude U^2 was determined to $0.0030 \times 10^{-10} \text{ m}^2$, i.e. nearly half the value found for Nb_3Sn , Nb_3Ge and Nb_3Al . The values of U_a^2 and U_b^2 were determined to 0.0032 and $0.0024 \times 10^{-20} \text{ m}^2$, respectively. The vibration amplitude of the Nb atoms is even smaller than that reported above for Nb_3Pt . However, the precision of these measurements is not high enough to decide whether $U_a^2 > U_b^2$ corresponds to

System	Preparation	Irradiation ($\times 10^{16} \text{H}^+/\text{cm}^2$)	a (nm)	β	T_c (K)	Beam	$\sin\theta/\lambda$ (10nm^{-1})	Order Parameter	U^2 ($\times 10^{-2} \text{nm}^2$)	R	Ref.
Nb ₃ Ir	AM 2000°C,R		0.51333	0.25	1.7	CuK _α	0.60	S = 0.95 ^{a)}	0.0011 ^{b)}	0.001	4
								S = 1.00 ^{c)}		0.044	38, 162
Nb ₃ Ir	AM 1900°C,R		0.5134	0.25	1.7	CuK _α	0.60	S = 0.93 ^{a)}		0.071	62
Nb ₃ Ir	AM 1600°C,R		0.51345	0.25	1.7	CuK _α	0.60	S = 1.00 ^{b)}	U ² = 0.0030 ^{b)}	0.011	162
								S = 1.00		U ² _a = 0.0032 ^{d)}	-
Nb ₃ Ir	Films	-	0.5132	0.25	1.75	CuK _α	0.65	S ₀ = 1.00 ^{c)}	-	-	135
		2.2	0.5136		1.40			S = 0.97 ^{c)}	-	-	135
		6.5	0.5139		1.45			S = 0.89 ^{c)}	-	-	135
		10.9	0.5144		1.65			S = 0.79 ^{c)}	-	-	135
		32.8	0.5149		2.2			S = 0.51 ^{c)}	-	-	135
		43.8	0.5150		2.5			S = 0.45 ^{c)}	-	-	135
		65	0.5149		2.6			S = 0.40 ^{c)}	-	-	135
Nb ₃ O _s	AM 1800°C,R		0.51358	0.25	0.95	CuK _α	0.60	S = 0.90 ^{a)}	U ² = 0.0033 ^{b)}	0.009	4
								S = 1.00 ^{b)}		0.069	162

Table 5.6. Structural data from least-square refinements on Nb₃Ir and Nb₃O_s.

AM = arc melted, R = radiation quenched.

a) Refined with fixed $U^2 = 0$, b) Data of Ref. 4, refined with variable U^2 , c) film data, refined assuming $S_0 = 1.00$, d) determined using the selected line method described in 3.2.1.

reality. Due to the small difference between both quantities, the uncertainty of the selected line method is sufficiently high to allow the inverse situation, i.e. $U_a^2 < U_b^2$. Nevertheless, the average value U^2 still remains low compared to the other A15 type compounds. A comparison of the vibration amplitudes will be made in 6.1.2 and 6.1.3.

k) Nb₃O_s

The only determination of the order parameter of Nb₃O_s arises from Van Reuth and Waterstrat /4/, who assumed $B = 0$ and obtained $\hat{S} = 0.90$. A complete refinement using the data of these authors, recently performed by Isernhagen and Flükiger /62/ yielded $S = 1.0$ and $B = 0.26$ (or $U^2 = 0.0033 \times 10^{-20} \text{m}^2$, see Table

5.6). Like in Nb₃Ir, it is remarkable that the value of B is quite low (see discussion in Section 5.3). The very high degree of ordering in Nb₃Os is confirmed by the very low value of the electrical resistivity, $\rho_0 = 15 \times 10^{-8} \Omega \text{m} / 38, 206/$, again in analogy with Nb₃Ir (See Sect. 7).

5.1.2 V Based A15 Type Compounds

a) V₃Si (Single Crystal)

Extensive diffraction work on V₃Si single crystals has been performed by Staudenmann /95/ and Cox and Tarvin /78/, who used X ray and neutron diffraction, respectively. The least square refinements are listed in Table 5.7 and indicate a very high degree of ordering in V₃Si. In particular, the results of Staudenmann /95/ (MoK α radiation up to $\sin^2 \theta / \lambda^2 = 1.4 \times (10^{-10} \text{m})^{-1}$) indicate perfect ordering (to within 1% uncertainty). The results of Cox and Tarvin /78/ are in agreement to those of Staudenmann /95/, their order parameter showing a small deviation from perfect ordering: $S = 0.97$ /78/. Cox and Tarvin /78/ indicate that this small difference is not significant, due to the important extinction effects encountered when effectuating neutron diffraction of a V₃Si of a size of $5 \times 6.5 \times 7 = 227.5 \text{ mm}^3$ volume /78/, leading to an uncertainty in S of about 0.03 /78/. This higher error margin appears obvious when considering the complexity of the extinction correction which had to be used. Following Becker and Coppens /187/, a correction of the form

$$F_{\text{calc}}^2 = F_k^2 y^S \quad (5.1)$$

was used, where F_{calc} and F_k are the calculated extinguished and theoretical structure factors per unit cell, respectively, and y_s is the secondary extinction coefficient, given by

$$y_s = f(\theta, X) \quad (5.2)$$

where

$$X = \frac{r^* \lambda^2 \bar{T}^2}{V^2}, \quad (5.3)$$

where λ is the wavelength, V the unit cell volume and \bar{T} the absorption-modified path length through the crystal. The secondary extinction coefficient, y_s , is the result of complex assumptions about the occurrence of small domains in the crystal (approximated by spheres with radius r), in which primary extinction can be ignored. Assuming a Gaussian mosaic distribution, it is

$$r_G = \frac{r^*}{\left(1 + \frac{g}{8} (r \cdot \sin 2\theta / \lambda g)\right)^{1/2}}, \quad (5.4)$$

where g is the mosaic spread parameter. Finally, the dependence of y_s upon was taken into account by the expression

$$y_s = \left[1 + cX + \frac{A(\theta) X^2}{(1 + B(\theta) X)} \right]^{-1/2} \quad (5.5)$$

In this case, extinction poses a particular problem because of the correlation with the main parameters of interest, i.e. the order parameter and the temperature factor. As mentioned above, both investigations /78, 95/ yield qualitatively the same results, but the quantitative results of the investigation of Staudenmann /95/ have to be considered as being more significant, essentially because of the (size dependent) complex extinction correction which had to be introduced by Cox and Tarvin /78/ in their neutron diffraction work.

Due to the extinction effects, the neutron diffraction data give only satisfactory answer for the refinement with an isotropic temperature factor. The value $U^2 = 0.0048 \times 10^{-20} \text{ m}^2$ at 300 K is somewhat smaller than for the X ray data. The refinement for anisotropic temperature factors yields $U_V > U_{\text{Si}}$ which is physically unrealistic, the V atoms on the 6c sites being much more overlapped than the Si atoms.

In the light of the discussions in Section 4, it is interesting to mention the neutron diffraction data of Cox and Tarvin /78/ on neutron irradiation V_3Si single crystals, also listed in Table 5.6. These results suggest a decrease of the order parameter by $\Delta S = 0.07$ compared to the initial value, S_0 , after a dose of 22.2×10^{18} n/cm², characterized by a decrease in T_c from 17.3 K to 7.5 K. A comparison with the data of Sweedler et al. /69/ (see Fig. 4.10a) shows that the value of $T_c = 7.5$ K after the dose 22.2×10^{18} n/cm² is about two times higher than reported earlier. The discrepancy is certainly due to an increase of the temperature T_{irr} during the irradiation, due to the large size of the V_3Si single crystal. This case has been discussed in 4.2.4d.

The results of Staudenmann /95/ do not only reveal perfect ordering in V_3Si , but also a small, but significant anisotropy of the mean square amplitude. At 300 K, $U_{11}^2 = 0.0053 \times 10^{-20}$ m², i.e. 7 % smaller than $U_{22}^2 = 0.0057 \times 10^{-20}$ m² (Table 5.7). At 13.5 K, the difference between U_a^2 and U_b^2 is accentuated, the mean vibration amplitude of the V atoms being now 23% smaller than that for the Si atoms /95/. This shows a similar tendency as for the Nb based compounds Nb_3Sn /180/ and Nb_3Ge /166/: as expected, the thermal vibrations of A atoms on 6c sites are smaller than those for B atoms on 2a sites. This is confirmed by the results of Kodess et al. /180/ on two V_3Si single crystals with $T_c = 16.8$ and 15.4 K, corresponding to estimated compositions $\beta = 0.25$ and $\beta = 0.24$, respectively. These results are also listed in Table 5.7. The behavior of the anisotropic temperature factor given by Kodess et al. /180/ suggests an enhancement of the anisotropic character towards stoichiometry.

A determination of the order parameter by means of X ray diffractometry on a small V_3Si polycrystal after irradiation down to a T_c value of 7 K /78/ also showed a considerable decrease of the degree of ordering ($S = 0.84$ in Table 5.7). The case of V_3Si has been analyzed very carefully because of the importance of this system for the classification of all other A15 type compounds. This importance is characterized by the quantity of additional measurements which were undertaken on the same V_3Si single crystal used for the neutron diffraction experiments of Cox and Tarvin /78/, e.g. specific heat /117/ (see also Fig. 4.14), electrical resistivity, magnetic susceptibility /87/ and sound velocity /87/, before and after the neutron irradiation. Both V_3Si single crystals measured by Cox and Tarvin /78/ were found

System	Preparation	Irradiation	a (nm)	β	T_c (K)	Beam	$\sin\theta/\lambda$ (10^{-10}m^{-1})	Order Parameter	U^2 ($\times 10^{-20}\text{m}^2$)	R	Ref.						
V_3Si	ZM, Single Crystal	-	0.4724	0.25	17.0	MoK_α	1.4	(S=1) ^a	300K: $U_{11}^2=0.00452$ $U_{22}^2=0.00571$ $U_b^2=0.0057$	0.014	95						
								(S=1) ^a	13 K: $U_a^2=0.0017$ $U_b^2=0.0022$	0.024	95						
V_3Si	CVD, Single Cryst.	-	0.4724	0.25	16.8	MoK_α	1.2	(S=1) ^a	300K: $U_a^2=0.0057$ $U_b^2=0.0072$	0.013	180						
V_3Si	CVD, Single Cryst.	-	0.472	0.24 ^b	15.4	MoK_α	1.2	(S _a =1) ^a	300K: $U_{11}^2=0.0054$ $U_{22}^2=0.0066$	0.013	180						
V_3Si	ZM, Single Crystal	-	0.47255	0.25	17.3	$n:\lambda=0.235$	0.77	$S \geq 0.97$	300K: $U_a^2=0.0060$ $U_b^2=0.0048$	0.024	78						
								$S \geq 0.97$	30K: $U_a^2=0.0030$ $U_b^2=0.0021$	0.024	78						
								3.5×10^{18}	-	0.25	17.0	$n:\lambda=0.235$	0.77	$S \geq 0.96$	300K: $U^2=0.0048$	0.035	78
								2.2×10^{19} n/cm^2	0.47355	0.25	7.5	$n:\lambda=0.071$	0.77	$S = 0.90$	300K: $U^2=0.0052$ 160K: $U^2=0.0039$ 4.6K: $U^2=0.0032$	0.049	78
V_3Si	AM, Polycrystal	^{c)}	-	0.25	7.0	CuK_α	-	$S = 0.84$	-	-	198						
V_3Si	Crushed s. Crystal	-	0.4725	0.253	16.8	MoK_α	1.38	not given	300K: $U_a^2=0.0058^d$ $U_b^2=0.0070^d$ 20K: $U_a^2=0.0027^d$ $U_b^2=0.0062^d$ 600K: $U^2=0.0100^d$	-	274						

Table 5.7 Structural parameters from least-square refinement of intensity data from V_3Si single crystals at different temperatures and after different irradiation doses: ZM = zone melted, CVD = chemical vapor deposition, AM = arc melted. ^{a)} refined with fixed S=1, ^{b)} composition corrected to ($\beta=0.24$, based on the T_c and the a value, ^{c)} dose not precised in Ref. 198, irradiation state given by value of T_c , ^{d)} Determined using selected lines.

to transform into the tetragonal phase at low temperature prior to irradiation. The effect of neutron irradiation was to suppress the martensitic phase transformation.

From the above remarks it can thus be concluded that V_3Si is really perfectly ordered: $S = 1$. A strong argument confirming this result is the value of the electrical resistivity just above T_c , ρ_0 , which reaches the lowest values published so far on A15 type compounds: $\rho_0 \leq 10^{-8} \Omega m$ (see Sect. 7).

b) V_3Ga

From the point of view of the electronic properties at low temperature, the system V_3Ga can be compared to V_3Si . Both have appreciably high T_c values and exhibit the highest \mathcal{G} values among the known superconductors, $17 \text{ mJ/K}^2 \text{at-g}$ for V_3Si /64/ and $24 \text{ mJ/K}^2 \text{at-g}$ for V_3Ga /97/. The magnetic susceptibility χ in both compounds shows a strong temperature dependent behavior, reflecting the sharp structure of the density of states at the Fermi level.

The metallurgy of both systems shows, however, much less similarities. The A15 phase in the system V-Si is formed by a congruent reaction from the melt at 1900°C /141,201/, while V_3Ga is formed from the solid at 1300°C /20/. The total width of the A15 phase field is also very different, from 18 to 32 at.% Ga in the case of V_3Ga /20/ and from 20 to 25.5at.% Si in the case of V_3Si /64,141/. V_3Ga is one of the few systems where the A15 phase forms at both sides of stoichiometry, the others being Nb_3Pt /92/, V_3Pt /128/, Nb_3Ir /62/ and Ti_3Pt /207/, while in V_3Si the stoichiometric composition is very close to the phase boundary. The ordering behavior in V_3Ga is different from that observed in V_3Si , as shown in the following.

The order parameter in V_3Ga has been investigated by Koch /203/, Das et al. /19/ and Flükiger et al. /20/, all on arc melted samples. Koch /203/ and Das et al. /19/ used X ray diffractometry, while both X ray and neutron diffractometry were used by Flükiger et al. /20/, thus allowing an interesting comparison. The results of least-square refinements are represented in Table 5.8. As mentioned in 3.3.1, the error margin for the neutron diffraction experiments is very small, $\Delta S = \pm 0.01$ compared to $\Delta S = \pm 0.03$ for X ray diffraction experiments /20/, due to the particularly favourable difference between the neutron scattering factors for V and Ga. For this reason, the neutron results on V_3Ga have to be considered as the most reliable ones and will be referred to in the following.

The high volatility of Ga at high temperatures and the solid bcc \rightarrow A15 transformation renders the formation of homogeneous V_3Ga samples much more difficult than in the case of V_3Si . The compound V_3Si cannot only

be melted without appreciable losses, it can easily be obtained single-phased by subsequent homogenization heat treatments. It is interesting that large V_3Si single crystals with sizes up to 5mm can be obtained by recrystallization at temperatures $\sim 50^\circ C$ below the meltin point (Flükiger et al. /38, 220/. For the order parameter investigation in V_3Ga /20/, a sample was chosen out of 10 different ones with compositions deviating only slightly from stoichiometry, the criterion being the highest T_c value (see variation T_c vs. β for V_3Ga in Sect. 9). This sample was homogenized at $1450^\circ C$ (in the bcc phase field), followed by prolonged anneals at $1250^\circ C$ for retransforming into the A15 phase. The homogeneity of the samples can be verified by the calorimetric superconducting transition width (see Fig. 4.9). The lower formation temperature of the A15 phase in the system V-Ga with respect to V-Si may be correlated to slower ordering kinetics for V_3Ga .

It can thus be concluded that perfect ordering is reached in V_3Si (Table 5.7), while the Bragg-Williams order parameter in V_3Ga never exceeds $S = 0.98$, even after very long heat treatments /18, 20/. It follows that the perfectly ordered state in V_3Ga cannot be formed at equilibrium. Another difference between V_3Si and V_3Ga is that in the latter, different states of ordering can be retained by classical quench and anneal procedures comprising quenching by either argon jet (or water) or cooling by radiation (frequently called radiation quench). A comparison between different quenching methods with respect to their effect on T_c will be made in Sect. 8. In contrast to V_3Ga , laser quenching procedures with very high cooling rates are needed for inducing measurable T_c changes in V_3Si /120/.

The isotropic vibration amplitude in V_3Ga measured by Flükiger et al. /20/ varies between $0.0046 \times 10^{-20} m^2$ for the neutron and $0.0057 \times 10^{-20} m^2$ for the X ray diffraction experiments. Försterling /242/ found the values $U_a^2 = 0.0059 \times 10^{-20} m^2$ and $U_b^2 = 0.0041 \times 10^{-20} m^2$, the average $U^2 = 1/4(U_a^2 + U_b^2) = 0.0054 \times 10^{-20} m^2$ being in good agreement with these values. However, the large ratio $U_a^2/U_b^2 = 1.49$ in Ref. 242 seems somewhat doubtful when compared the ratios found in other A15 type compounds (see Table 6.2). This illustrates the limits of determining the atomic vibration amplitudes by using selected lines: This method is only successful if i) no preferential orientations are present and ii) a sufficient number of lines is analyzed. In particular, the value U_b^2 determined from a mixed term containing both f_A and f_B is subject to large errors, which easily reach 20 % and more, compared to 10 to 15 % for U_a^2 .

System	Preparation	a (nm)	β	T_c (K)	Beam	$\sin\theta/\lambda$ $(10^{-10}\text{m})^{-1}$	Order Parameter	U^2 $(\times 10^{-20}\text{m}^2)$	R	Ref.
V_3Ga	AM 1250°C,R	0.4817	0.25	14.9	MoK $_{\alpha}$	0.76	S = 0.97	$U^2 = 0.0057$	0.032	20
		0.4817	0.25	14.9	n	0.55	S = 0.98	$U^2 = 0.0046$	0.013	20
V_3Ga	AM 1250°C,Q	0.4817	0.25	13.8	MoK $_{\alpha}$	0.76	S = 0.92	$U^2 = 0.0057$	0.041	20
		0.4817	0.25	13.8	n	0.55	S = 0.95	$U^2 = 0.0042$	0.014	20
V_3Ga	AM	0.48202	0.25	c)	CuK $_{\alpha}$	0.64	c)	$U^2_a = 0.0059$ $U^2_b = 0.0041$	-	242
V_3Ge	AM 1300°C,R	0.4781	0.24	6.1	CuK $_{\alpha}$	0.60	$S_a = 1.0$	$U^2 = 0.0063^a$	0.062	38
V_3Ge	CVD,Single Crystal	0.4782	c)	6.0	MoK $_{\alpha}$	1.2	$(S_a=1)^b$	$U^2_{11} = 0.0058$ $U^2_{22} = 0.0068$	0.013	180

Table 5.8 Structural parameters from least-squares refinement of intensity data from V_3Ga and V_3Ge polycrystals. The heat treatments HT1 and HT2 for V_3Ga stay for the same homogenization heat treatment at 1250°C, cooling occurring at the rates of 1.5°C/s and 10°C/s, respectively.

a) the refinement was performed with fixed $U^2 = 0.0063 \times 10^{-20} \text{ m}^2$ (or $B = 0.5 \times 10^{-20} \text{ m}^2$), b) refined with fixed $S_a = 1$.
c) no indication given, d) Determined using selected lines.

c) $V_{.76}Ge_{.24}$

V_3Ge has an extremely narrow phase field, centered at $\beta = 0.24 \pm 0.005$ /62/, i.e. the stoichiometric composition is not comprised. No order parameter determination on the system V_3Ge has been published so far, Unpublished results /38/ on a sample of the effective composition $\beta = 0.24$, later used for Raman spectroscopy by Schickanz et al. /178/ are reported in Table 5.8. The least square refinement (with B fixed at 0.5) yielded $S = 1.0$, i.e. the system $V_{.76}Ge_{.24}$ can be considered as perfectly ordered. The order kinetics of V_3Ge thus shows similarities with that of V_3Si : It has so far not been possible to alter the value of T_c

(and thus the degree of long-range ordering) by using conventional heat treatment procedures as argon jet quenching or prolonged annealing in the temperature range between 600 and 1000 °C.

By means of X ray diffractometry (MoK α) Kodess /180/ determined the vibration amplitudes U_{11}^2 and U_{22}^2 on a V₃Ge single crystal. The least-square refinement, however, was effectuated with a fixed value of the order parameter, $S = 1$. A comparison of own V₃Ge data in Table 5.8 shows very similar values of both, the order parameter and the vibration amplitudes, in order that $S = 1$ can be safely concluded. The ratio $U_{11}^2/U_{22}^2 = 0.853$ reflects the anisotropy in the vibrational behavior, the smaller amplitude being measured in chain direction, in analogy to V₃Si, as will be discussed in 6.1.1.

d) $\frac{V}{3}Au$

It is not a coincidence that the correlation between atomic ordering and superconductivity was discovered on the compound V₃Au (Van Reuth et al. /3,4/). This system not only exhibits the highest relative change in T_c (from 0.3 to 3.2 K /3,4,18,62/) but can in addition easily be obtained at different degrees of ordering, ranging from $S_a = 0.84$ to $S_a = 0.94$, as reported by Flükiger et al. /18,62/. The difference $\Delta S = 0.10$ produced by classical quench and anneal procedures is quite exceptional for A15 type compounds where lower changes of the order parameter, around $\Delta S = 0.02$ or 0.03 are common. Due to the favourable difference between the atomic X ray scattering factors of V and Au, the system V₃Au appears thus as a very suitable model system for studying as well the variation of S as its consequence on T_c . The ordering data on V₃Au are summarized in Table 5.9.

The value of the order parameter in V₃Au reported by Van Reuth et al. /3/ and by Flükiger et al. /18/ showed a considerable discrepancy. As pointed out by the authors and coworkers, this discrepancy is only apparent and is merely due to a computational error in determining the intensity 110 by Van Reuth et al. /3/, leading to order parameters being 4 % to high. The erroneous outprint of the line intensities in Ref. 4 can be verified by comparing the 110 intensities of the systems V₃Ir, V₃Pt and V₃Au (Ref. 4, Table V): The normalized intensity I_{110}/I_{211} of the latter should be 0.700 instead of 0.625, this difference being well beyond the measuring error. It is interesting that all the other line intensities by Van Reuth et al. /3,4/ in more than 20 different A15 type compounds agree well with those of the author and coworkers /18,62,162/. It has to be mentioned that the

System	Preparation	a (nm)	β	T_c (K)	Beam	$\sin\theta/\lambda$ $(10^{-10}\text{m})^{-1}$	Order Parameter	Ref.
$V_3\text{Au}$	AM, as cast	0.48807	0.24 ^c	0.87	CuK_α	0.63	$S_a = 0.92^{a,b}$	4,193
	1h/800°C, R			1.85			$S_a = 0.87^{a,b}$	4,193
	1h/800°C + 5d/1000°C, R			1.79			$S_a = 0.93^{a,b}$	193,202
	1000°C, Q			0.89			$S_a = 0.87^{a,b}$	193,202
	1000°C, Q + 1h/600°C, R			0.90			$S_a = 0.87^{a,b}$	193,202
	1000°C, Q + 1h/800°C, R			1.55			$S_a = 0.87^{a,b}$	193,202
$V_3\text{Au}$	AM, 90d/560°C	0.4881	0.24	3.2	CuK_α	0.56	$S_a = 0.94^b$	18,62
	6h/1400°C, R			1.15			$S_a = 0.88^b$	18,62
	1200°C, Q			0.40			$S_a = 0.84^b$	18,62
$V_3\text{Au}$	AM, 30d/560°C	0.4878	0.225	2.03	CuK_α	0.56	$S_a = 0.90^b$	18

Table 5.9. Structural parameters from least-square refinements of intensity data of $V_3\text{Au}$. ^a) Refinement performed with $U^2 = 0$,
^b) The values of S_a from Refs. 4 and 193 have been corrected by subtracting $\Delta S = 0.05$ (see remark in the text),
^c) The composition has been corrected to the maximum solubility limit of Au in the A15 phase, $\beta = 0.24$ /18,62/. Q = Argon jet quenched.

order parameter in $V_3\text{Au}$ has to be expressed by S_a rather than by S , the highest Au content at equilibrium being 24 at. %. Both the mentioned corrections have been taken into account in Table 5.9 by subtracting $\Delta S = 0.05$ from the original values of S for $V_3\text{Au}$ reported in Refs. 3 and 4. In the same table are data on 21.5 and 22.5 at. % Au, respectively, for which the values $S_a = 0.92 \pm 0.04$ were found /62/. It is seen that within the limits of accuracy (of the order of $\Delta S_a = \pm 0.02$ in this system) the approach of stoichiometry does not lead to a decrease of the order parameter as for example in the system Nb_3Al discussed in 5.1.1e (In the system Nb_3Ge , where the data of Sweedler et al. /69,70/, Newkirk et al. /182/ and Rasmussen and Hazel /166/ also suggest a decrease of S_a for $\beta \rightarrow 0.25$, the situation is highly uncertain. This is due to the considerably larger measuring error caused by the additional phases, as shown in Sect. 3.

e) V_3Pt

The system V_3Pt exhibits a very broad phase field, extending from 19 to 32 at.% according to Waterstrat and Manuszewski /128/. The variation of T_c as a function of β exhibits a sharp maximum at the stoichiometric composition, $T_c = 3.7 K$ /82/. Order parameter determinations have been effectuated for the compositions $\beta = 0.20$ /195/, $\beta = 0.25$ /4, 6, 62/ and $\beta = 0.30$ /195/ after various heat treatments. The results, represented in Table 5.10 show that the order parameter in V_3Pt after classical quench and annealing procedures varies from 0.90 to 0.98, which is very similar to Nb_3Pt , where S varies from 0.89 to 0.98 (see Fig. 4.12 and Table 5.5).

In two cases, at the compositions $\beta = 0.20$ and $\beta = 0.30$, the order parameter was also measured for nonstoichiometric compounds /202/. At $\beta = 0.20$, the value of S_a after a heat treatment at $1400^\circ C$, followed by radiation quenching is very high, $S_a = 0.97$. This is not surprising, since in the A15 systems investigated to date the value of S_a for compositions $\beta < 0.25$ is always higher or equal to the order parameter at stoichiometry: $S_a = 0.75$ and $S_b = 0.97$, i.e. from the available V atoms, 99.2% are on the 6c site. This reflects the high tendency of V_3Pt to form at a high degree of ordering. A comparison between V_3Pt and V_3Au shows (in analogy to Nb_3Pt and V_3Au) that the optimum heat treatment for reaching the maximum value of T_c (or S_{max}) is considerably higher for the Pt based than for the Au based compounds. This optimum ordering temperature is correlated to the diffusion limit, T_D (see Table 4.1).

Like for Nb_3Au , the earlier refinements of V_3Pt /4,62/ have been performed for fixed values $U^2 = 0$. Where the intensity data were still available, the refinements have been carried out for the present work, allowing the temperature factor to vary. The results are also included in Table 5.10.

f) $V_3Ir, V_3Rh, V_3Pd, V_3Ni, V_3Co$

These atypical /39/ A15 type compounds all exhibit relatively low T_c values, their atomic order parameters have thus not been investigated

System	Preparation	a (nm)	β	T_c (K)	Beam	$\sin\theta/\lambda$ $(10^{-10}\text{m})^{-1}$	Order Parameter	Ref.
V ₃ Pt	AM, as cast 1h/800°C, R	0.48166	0.25	2.53	CuK _{α}	0.63	S = 0.95	4,193
				2.86	CuK _{α}	0.63	S = 0.98	4,193
V ₃ Pt	AM, 1500°C, Q 7d/1050°C, R 21d/900°C, R	0.4817	0.25	2.7	CuK _{α}	0.57	S = 0.90	62,94
				3.2			S = 0.96	62,94
				3.55			S = 0.98	62,94
V ₃ Pt	AM, 24h/1400°C, R	0.4812	0.20	0.30	CuK _{α}	0.63	S _a = 0.97	202
V ₃ Pt	AM, 24h/1400°C, R	0.4825	0.30	0.35	CuK _{α}	0.63	S _a = 0.75 S _b = 0.97	202

Table 5.10. Structural parameters from least-square refinement of intensity data for V₃Pt. All refinements have been performed with fixed $U^2 = 0$.

very intensively. Nevertheless, at least one order parameter determination has been performed for each compound by Waterstrat and Van Reuth /202/, Van Reuth and Waterstrat /4/, Waterstrat and Dickens /57/, Flükiger /38,62,94/ and Isernhagen and Flükiger /162/. These results are summarized in Table 5.11.

The reported S values for stoichiometric V₃Ir after similar heat treatments vary between $S = 0.94 \pm 0.02$ /4,62,202/ and $S = 0.98 \pm 0.02$ /38, 162/. Like for Nb₃Ir, the temperature factor of V₃Ir, $B = 0.14 \pm 0.05$ ($U^2 = 0.0018 \times 10^{-20} \text{ m}^2$) at 300 K, is considerably smaller than for the V based A15 type compounds containing a nontransition element. For comparison, in V₃Si and V₃Ga, the values $B = 0.41 \pm 0.05$ ($U^2 = 0.0052 \times 10^{-20} \text{ m}^2$) /78/ and $B = 0.45 \pm 0.05$ ($U^2 = 0.0057 \times 10^{-20} \text{ m}^2$) /20/, respectively, were reported for T = 300 K.

The other compounds also exhibit rather high order parameters, $S = 0.96 \pm 0.02$ for V₃Rh /4/, $S = 1.00 (+) 0.03$ for V_{0.775}Ni_{0.225} /57/ and $S = 0.90 \pm 0.05$ for V₃Co /57/, the only exception being V₃Pd, where $S = 0.69 \pm 0.05$ was reported /4/. This excessively low value is certainly correlated to the low formation temperature of V₃Pd, 900°C /4/: the slow diffusion at these temperatures (the sample in Ref. 4 has been annealed 1 month at 800°C) does probably not allow to reach the equilibrium order parameter in reasonable times.

System	Preparation	a (nm)	β	T_c (K)	Beam	$\sin\theta/\lambda$ (10^{-10}m) ⁻¹	Order Parameter	U^2 ($\times 10^{-20}\text{m}^2$)	R	Ref.
V ₃ Ir	AM, 2h/1500°C, R	0.4788	0.25	< 0.2	CuK α	0.54	S = 0.94	a)	0.036	62
	48h/1700°C, R			< 0.2			S = 0.98	$U^2 = 0.0025$	0.0042	38, 162
V ₃ Ir	AM, 40min./1800°C, R	0.47876	0.25	< 0.015	CuK α	0.63	S = 0.94	a)	0.004	4, 202
V ₃ Ir	AM, 40min./1800°C, R	-	0.38	1.71	CuK α	0.63	S _a = 0.50 S _b = 0.91	a)	-	202
V ₃ Rh	AM, 72h/1200°C + 14d/1100°C, R	0.47852	0.25	< 0.015	CuK α	0.63	S = 0.96	a)	0.0199	4
V ₃ Pd	AM, 30d/800°C, R	0.48254	0.225	0.082	CuK α	0.63	S _a = 0.69	a)	0.0007	4, 202
V ₃ Ni	AM, 6h/1250°C + 30d/850°C, Q	0.4710	0.25	0.30	n	0.50	S = 1.00	$U^2 = 0.0038$	0.09	57
V ₃ Co	AM, 3h/1350°C, R	0.4676	0.25	< 0.015	n	0.50	S = 0.90	$U^2 = 0.0038$	0.03	57
"V ₃ Os"	AM, 1year/620°C	0.4807	0.52	5.04	CuK α	0.63	S _a = 0.30 S _b = 0.96	a)	-	202
"V ₃ Re"	AM, 1600°C, Q	0.48783	0.71	8.4	CuK α		(S _a = 0.14) ^b (S _b = 1) ^b	a)	-	209

Table 5.11. Structural parameters from least-square refinements of intensity data on V₃Ir, V₃Rh, V₃Pd, V₃Ni and V₃Co and on the nonstoichiometric A15 type compounds V₅₀Os₅₀ and V₂₉Re₇₁. ^a) Refinement performed with fixed $U^2 = 0$, ^b) S_a and S_b are only estimated (no least-square refinement).

g) V₆₂Ir₃₈, V₅₀Os₅₀ and V₂₉Re₇₁

Some of the atypical A15 type compounds are stable at strongly nonstoichiometric compositions, one phase limit (the limit poor in V) being close to 6.5 electrons per atom. In spite of their crystal structure, these compounds can be considered as "electron compounds" /7/. For two of these compounds, V₃Ir and V₃Rh, the V rich limit of the homogeneity range is the stoichiometric composition,

the other phase limit being at $\beta = 0.38$ /202/, thus corresponding to $e/a = 6.62$. In the two other systems, the A15 phase field is centered at the equiatomic composition for $V_{.50}Os_{.50}$ ($e/a = 6.5$) or even beyond, as in $V_{.29}Re_{.71}$ ($e/a = 6.42$). The order parameters have been measured in the three compounds $V_{.62}Ir_{.38}$, $V_{.50}Os_{.50}$ and $V_{.29}Re_{.71}$ only and are summarized in Table 5.11.

For the compound $V_{.62}Ir_{.38}$, Waterstrat and Van Reuth /202/ found the parameters $S_a = 0.50 \pm 0.02$ and $S_b = 0.91 \pm 0.02$. The very low value of S_a of course indicates a low concentration of V atoms on the 6c sites. It would, however, be erroneous to conclude that the compound $V_{.62}Ir_{.38}$ has a tendency toward higher disordering. Indeed, it can be easily verified using Eq. (3.1) that 98% of all available V atoms are on the 6c sites. For nonstoichiometric compounds with ($\beta > 0.25$), it is useful to define this quantity as the "relative" occupation number, $r'_a = 0.98$ obtained from the ordinary occupation number, $r_a = 0.81$, by multiplying with $0.75/(1-\beta)$ (see Eq. 3.4). Since for the stoichiometric compound $V_{.75}Ir_{.25}$ the occupation number r_a is equal to 0.985, i.e. 98.5% of the V atoms are on the 6c sites, it follows that the tendency to undergo the highest possible degree of ordering in the A15 phase of the system V - Ir does essentially not depend on the composition.

In both compounds $V_{.50}Os_{.50}$ and $V_{.29}Re_{.71}$, the A15 phase decomposes eutectoidically and must be retained by a reasonably rapid quenching ($> 10^0$ C/s) from $\geq 1600^0$ C. Nevertheless, from the measurements of Waterstrat and Van Reuth /195/ a very high relative order parameter is found for $V_{.50}Os_{.50}$: $r'_a = 0.99$, i.e. 99% of the V atoms present in the lattice are on the 6c sites. The chain integrity is, of course, largely affected, as follows from the values $S_a = 0.30$ and $S_b = 0.96$, corresponding to 63.4% V on the 6c sites only.

In the system $V_{.29}Re_{.71}$, only qualitative diffraction measurements have been performed. However, Giorgi et al. /209/ were able to observe the (110) line, which can be interpreted as an indication for the occupancy of 2a sites by Re atoms only. Indeed, would all V atoms go on the 2a sites, the intensity of the (110) line would drop to zero. It was thus concluded that the V atoms would essentially occupy the 6c sites, i.e. the compound is as ordered as possible, taking into account the V deficiency ($S_a \cong 0.14$, $S_b \cong 1.0$).

It is remarkable that all three highly nonstoichiometric compounds discussed here have a common tendency to undergo the highest possible degree of ordering, as represented by $r'_a \approx 1$. The low values of S_a result from the deficiency in V for compositions $\beta > 0.25$, characteristic for electron compounds with $e/a \approx 6.5$.

In particular, there is no apparent evidence for a correlation between the absolute value of the order parameter and any peculiarity of the band structure. In agreement with Van Reuth and Waterstrat /4/, it can be concluded that the Bragg-Williams order parameter decreases when the B element approaches the Mn column in the periodic system. However, this statement has to be reformulated: the Bragg-Williams order parameter decreases mainly because the composition β rich phase limit in the systems V-Pt, V-Tr, V-Os and V-Re follows the line along $e/a = 6.5$ /7/, thus largely exceeding the stoichiometric value, $\beta = 0.25$. The tendency to form as ordered as possible is in reality unchanged, even for B = Ir, Os and Re (see 5.2).

5.1.3. Mo Based A15 Type Compounds

The reported ordering data on Mo based A15 type compounds have been reproduced in Table 5.12. It is seen that the antagonism between A15 type compounds based on V and Nb on one hand and on Mo and Cr on the other also persists for the degree of ordering of these compounds.

a) Mo₃Si

On a stoichiometric sample with $T_c = 1.24$ cooled by radiation quenching from 1400°C , an order parameter of $S = 0.98 \pm 0.03$ was formed /38/. Recently, Mirmelshteyn et al. /158/ reported the order parameter $S = 0.86$ for Mo₃Si. However, since the sample was not single-phased (95% A15 phase) and no indications about the refinement conditions were given, this result has to be treated with caution. No other ordering data have so far been reported on Mo based A15 type compounds containing nontransition B elements. Several attempts undertaken on Mo₃Ge by the author /38/ failed, due to the presence of small amounts of bcc and tetragonal phase which could not be avoided,

even after prolonged heat treatments at 1600°C, thus causing large errors in the determination of the order parameter.

b) $\text{Mo}_{.815}\text{Pt}_{.185}$

As found by Flükiger et al. /50/, the A15 phase in the system Mo-Pt forms peritectoidically at 1780°C and decomposes eutectoidically at 1280°C. The A15 phase field was found to be extremely narrow (less than 1 at.% wide and centered at the composition 18.5 ± 0.5 at.% Pt. Like in the other decomposing eutectoidically A15 system $\text{V}_{.50}\text{Os}_{.50}$ and $\text{V}_{.79}\text{Re}_{.21}$ discussed in 5.1.2g, the A15 phase has to be retained by reasonably fast cooling. As a consequence of the slower diffusion encountered in Mo based compounds, however, the cooling rate necessary to retain the high temperature A15 phase $\text{Mo}_{.815}\text{Pt}_{.185}$ is lower: "radiation quenching" (or cooling by radiation by switching off the furnace power) at a rate of $\sim 15^\circ \text{C/s}$ is sufficient. The reported order parameters are $S_a = 0.94 \pm 0.03$ /50, 62/ and $S_a = 0.98 \pm 0.05$ /4/, i.e. the compound exhibits a rather high degree of ordering. The difference between the data of Van Reuth and Waterstrat /4/ measured a sample with $\beta = 0.20$ which necessarily must contain a certain amount of secondary phases, e.g. the hexagonal DO_{19} phase /50/.

c) Mo_3Ir

The A15 phase field in the system Mo-Ir is comprised within the limits $22 \leq \text{at.\% Ir} \leq 24$, following Michalek et al. /210/ and Flükiger et al. /39/, i.e. the stoichiometric composition is not stable at equilibrium. As shown in Table 5.12, the order parameter in $\text{Mo}_{.76}\text{Ir}_{.24}$ ranges between $S_a = 0.82 \pm 0.03$ /39/ (after radiation quenching from 1800°C) and $S_a = 0.87 \pm 0.03$ /39, 62/ after prolonged annealing at 1000°C, corresponding to $T_c = 8.40 \text{ K}$ /39, 62/. Van Reuth and Waterstrat /4/ found a similar value, $S_a = 0.87 \pm 0.05$ (the recalculation with variable temperature factor yielded $S_a = 0.88$ /162/ after radiation quenching from 1800°C. It results that $\text{Mo}_{.76}\text{Ir}_{.24}$ is considerably less ordered than V_3Ir or Nb_3Ir . Attempts to optimize T_c by series of prolonged heat treatments at different temperatures from 1800°C to 900°C led to a maximum value of $T_c = 8.46 \text{ K}$ /39/. It thus appears that the order parameter $S_a = 0.88$ is very close to the highest value which can be reached in the system $\text{Mo}_{.76}\text{Ir}_{.24}$.

System	Preparation	Irradiation	a (nm)	β	T_c (K)	Beam	$\sin\theta/\lambda$ ($10^{-10}m$) ⁻¹	Order Parameter	U^2 ($\times 10^{-20} m^2$)	R	Ref.	
Mo ₃ Si	AM, 2h/1400°C, R	-	0.4893	0.25	1.24	CuK _{α}	0.54	S = 0.99	U ² = 0.0034	-	38	
Mo ₃ Pt	AM, 70h/1600°C, Q	-	0.4989	0.185	4.62	CuK _{α}	0.54	S _a = 0.94	a)	-	50, 62	
								S _a = 0.97	U ² = 0.0040	0.022	38	
Mo ₃ Pt	AM, 24h/1600°C, Q	-	0.49878	0.20	4.56	CuK _{α}	0.60	S _a = 0.98	a)	0.011	4, 193	
								S _a = 0.98	U ² = 0.0037	0.026	38	
Mo ₃ Ir	AM, 12h/1800°C, R	-	0.4970	0.24	8.12	CuK _{α}	0.54	S _a = 0.82	a)	0.026	39, 62	
								S _a = 0.85	U ² = 0.0032	0.014	38	
Mo ₃ Ir	AM, 100h/1000°C, R	-	0.4970	0.24	8.40	CuK _{α}	0.54	S _a = 0.87	a)	-	39, 62	
Mo ₃ Ir	AM, 48h/2000°C, R	-	0.49682	0.24 ^b	8.11	CuK _{α}	0.60	S _a = 0.87	a)	0.017	4, 193	
Mo ₃ Os	AM, 100h/1900°C, R	-	0.4969	0.25	11.72	CuK _{α}	0.54	S = 0.79	a)	-	39, 62	
	60h/1800°C, R	11.81			S = 0.81			a)	-	39, 62		
	14d/1000°C, R	-			12.70			S = 0.87	a)	-	39, 62	
						CuK _{α}	0.54	S = 0.88	U ² = 0.0026	0.013	38	
Mo ₃ Os	AM, 48h/1800	-	0.49689	0.25	11.68	CuK _{α}	0.60	S = 0.81	a)	0.006	4, 193	
Mo ₃ Os	AM, 15h/1850°C + 25h/1450°C + 10h/1000°C	-	0.4968	0.25	12.77	-	-	S ₀ = 0.89 ^c	-	-	-	77
					2.5X10 ¹⁸ n/cm ²	12.37	S = 0.86 ^c	-	-	77		
					5.8X10 ¹⁸ n/cm ²	12.20	S = 0.82 ^c	-	-	77		
					4.9X10 ¹⁹ n/cm ²	10.47	S = 0.44 ^c	-	-	77		
					1.03X10 ²⁰ n/cm ²	10.29	S = 0.20 ^c	-	-	77		

Table 5.12: Structural parameters from least-square refinements of intensity data on Mo_{0.815}Pt_{0.185}, Mo_{0.76}Ir_{0.24} and Mo₃Os. a) the temperature factor was fixed at U² = 0 for refinement, b) the data of Ref. 4 were corrected for the composition $\beta = 0.24$ /39, 62/, c) the order parameters in Refs. 69, 77 were determined by using the Aronin formula, starting with the value S = 0.89 reported by Flükiger et al. /39, 62/.

d) Mo₃Os

The A15 phase field in the system Mo-Os is very narrow and is centered at 25 ± 0.5 at.% Mo /39, 211/. Due to the rather high value of T_c in this compound (up to 13.1 K) and to the considerable variation $\Delta T_c \approx 2$ K after

different irradiation or quench and annealing procedures, the degree of ordering in Mo_3Os and the consequences of its variation on T_C have been intensively studied /4, 39, 62, 77/. According to Table 5.12, the order parameter in Mo_3Os varies between 0.79 ± 0.03 and 0.88 ± 0.03 , the latter value corresponding a sample with $T_C = 12.7$ K /39/. For improved annealing conditions, T_C values up to 13.1 K have been measured /38/, which indicates that the highest attainable order parameter in Mo_3Os could be of the order of 0.89 or 0.90. Like for $\text{Mo}_{.76}\text{Ir}_{.24}$, a considerable deviation from the perfectly ordered state is thus encountered in Mo_3Os .

As mentioned in 4.2.2 (see Fig. 4.12), Sweedler et al. /77/ have determined the variation of S and T_C of Mo_3Os after high energy neutron irradiation. As starting value, these authors assumed the value $S_0 = 0.89$ resulting from the data in Ref. 39. The decrease of the order parameter was then calculated by using the Aronin formula (Eq. 3.22). As mentioned earlier, the comparison between the curves T_C vs. S (see Fig. 4.12) has furnished an additional evidence for the hypothesis that the decrease of the long-range order parameter is mainly responsible for the decrease of T_C in irradiated A15 type compounds.

5.1.4 Cr Based A15 Type Compounds

The ordering data of the Cr based A15 type compounds show a marked analogy with those based on Mo. From the data summarized in Table 5.13, it follows that for transition B elements, a substantial deviation from perfect ordering is always present in both, Cr and Mo A15 type compounds.

a) Cr_3Si , Cr_3Ga

Both Cr compounds containing nontransition elements are non-superconducting down to 0.015 K. The interest in the system Cr_3Si resides in the comparison with the high T_C superconductor V_3Si . From a least-square refinement on a Cr_3Si single crystal, Staudenmann /199/ concluded that the order parameter S must exceed the value 0.98. Both systems, V_3Si and Cr_3Si , are thus almost perfectly ordered. Both are found to form congruently from the melt. The difference between them resides in the electronic density of states and in the phonon softening at low temperatures. The degree of ordering of the compound Cr_3Ga has been analyzed by neutron diffraction by

System	Preparation	a (nm)	β	T_c (K)	Beam	$\sin\theta/\lambda$ (10^{-10}m) ⁻¹	Order Parameter	U^2 ($\times 10^{-20}\text{m}^2$)	R	Ref.
Cr ₃ Si	CVD, Single Crystal	0.4550	0.25	< 0.15	MoK _{α}	1.2	(S = 1) ^a	$U_{11}^2 = 0.0042$ $U_{22}^2 = 0.0048$	0.013	180
Cr ₃ Si	RC, Single Crystal	0.4556	0.25	< 0.015	MoK _{α}	1.4	(S = 1) ^b	$U_{11}^2 = 0.0033$ $U_{22}^2 = 0.0037$ $U_b^2 = 0.0039$	0.006	95
Cr ₃ Si	AM, Polycrystal	0.45574	0.25	^c)	MoK _{α}	1.38	^c)	$U_{11}^2 = 0.0025^d$ $U_b^2 = 0.0027^d$		242
Cr ₃ Ga	AM, Polycrystal	0.4653	0.25	< 0.15	n	0.64	S = 0.92	$U^2 = 0.0063$	0.054	212
Cr ₃ Pt	AM, 9h/1300°C, R	0.46997	0.21	< 0.015	CuK _{α}	0.66	$S_a = 0.90^a$)		0.006	4,193
Cr ₃ Ir	AM, as cast	0.46810	0.25	0.168	CuK _{α}	0.66	$S = 0.89^a$)		0.004	4,193
Cr ₃ Os	AM, 24h/1400°C, R	0.46842	0.28	3.86	CuK _{α}	0.66	$S_a = 0.64^a$) $S_b = 0.75$		0.021	4,193
Cr ₃ Os	AM, 6h/1350°C, R	0.4682	0.275	3.83	CuK _{α}	0.57	$S_a = 0.55^a$) $S_b = 0.63$		0.030	39,62
	AM, 10d/900°C, R			4.10			$S_a = 0.70^a$) $S_b = 0.80$		0.028	39,62
	AM, 4weeks/680°C, R			4.68			$S_a = 0.78^a$) $S_b = 0.89$		0.041	39,62
Cr ₃ Ru	AM, 6weeks/800°C, R	0.46768	0.28	3.43	CuK _{α}	0.66	$S_a = 0.55^a$) $S_b = 0.64$		0.008	4,193
Cr ₃ Rh	AM, 3days/1200°C, R	0.46731	0.25	0.072	CuK _{α}	0.66	$S = 0.83^a$)		0.025	4,193

Table 5.13: Structural parameters from least-square refinement of intensity data on Cr based A15 compounds.

- a) the refinement was performed with fixed $U^2 = 0$,
 b) the refinement was performed with fixed $S = 1$,
 c) no indication given, d) determined using selected lines.

Girgis and Fischer /212/, which found a rather high order parameter, $S = 0.98$.

b) Cr_{0.79}Pt_{0.21}

As follows from the phase diagram of Waterstrat and Manuszewski /92/, the A15 phase in the system Cr-Pt ranges from 18 to 22 at.%. For the composition $\beta = 0.21$, these authors reported the order parameter $S_a = 0.90 \pm 0.05$ /4/.

c) Cr₃Ir

For the stoichiometric compound Cr₃Ir, Van Reuth and Waterstrat /4/ reported the order parameter $S = 0.02$. This result can be compared to that of Mo_{.76}Ir_{.24} (see Table 5.13).

d) Cr_{.72}Os_{.28}

In spite of the Cr deficiency (see Ref. 62 for the A15 phase field), this compound exhibits the highest T_c value of all Cr based A15 type compounds, 4.68 K /39/. Its order parameter has been measured by Van Reuth and Waterstrat /4/ and by Flükiger /38, 39, 62/. From the data in Table 5.13, it follows that the order parameter S_a ranges from 0.64 ± 0.04 to 0.78 ± 0.02 .

e) Cr_{.72}Ru_{.28}

The compound Cr_{.72}Ru exhibits a similar T_c value to that of Cr_{.72}Os_{.28} ($T_c = 3.43$). However, the necessity to form the A15 phase at temperatures below 800°C due to the low formation temperature, probably leads to limited diffusion and is reflected by the low value of the order parameter, $S_a = 0.55$. This case can be compared to V₃Pd, where S is also considerably lower with respect to other V based A15 type compounds /4/.

f) Cr₃Rh

The order parameter for this compound has been determined to $S = 0.83$ /4/. It is not known if heat treatments below 1200°C would lead to higher values of S .

5.1.5. Ti Based A15 Type Compounds

The only order parameter determination in Ti₃B compounds has been performed by Van Reuth and Waterstrat /4/. Their results, summarized in Table 5.14, shows a very high degree of ordering for all three compounds. The large difference between the S values for two Ti₃Ir in cast conditions, $S = 0.91 \pm 0.02$ and $S = 1.00$ (uncertainty: 0.02) is not understood. It is not excluded that this uncertainty is due to slight inhomogeneities in the as cast samples, in particular to a change in composition. Indeed, Junod et al. /207/ have shown that Ti₃Ir is stable within the range $0.25 \leq \beta \leq 0.27$.

System	Preparation	a (nm)	β	T_c (K)	Beam	$\sin\theta/\lambda$ $(10^{-10}\text{m})^{-1}$	Order Parameter	Ref.
Ti ₃ Au	As cast	0.50974	0.25	0.015	CuK _{α}	0.61	S = 0.97	4,6
Ti ₃ Pt	As cast	0.50327	0.25	0.486	CuK _{α}	0.61	S = 0.99	4,6
Ti ₃ Ir	As cast	0.50087	0.25	4.18	CuK _{α}	0.61	S = 0.91	4,6
Ti ₃ Ir	As cast	0.50082	0.25	4.63	CuK _{α}	0.61	S = 1.00	4,6

Table 5.14: Structural parameters from least-square refinements of intensity data on Ti based A15 type compounds.

5.2 The Order Parameter in A15 Type Compounds: A Comparison

The data in Tables 5.1 to 5.14 give a good picture of the degree of ordering in A15 type compounds. The main points of interest are a) the highest attainable order parameter in each compound and b) the variation of the order parameter as a consequence of quench and annealing procedures. These processes lead to nonequilibrium configurations lying quite close to the thermodynamical equilibrium, in contrast to irradiation processes, which cause large deviations from equilibrium, e.g. very low order parameter values and will therefore not be considered in this paragraph.

5.2.1 The Order Parameter at 300 K

The known ordering data have been represented in Fig. 5.2, 5.3 and 5.4, showing the V and Nb and the Cr and Mo based A15 type compounds, respectively. In these figures, the value of S_a and of r_a' , the relative occupation factor defined in Eqs. (3.4) and (3.5), and their variations after different heat treatments are plotted as a function of the B element, more precisely of its column in the periodic system (or the valence electron number). This kind of representation, introduced in Ref. 7, is useful for comparing different physical and metallurgical properties between A15 type compounds

and will also be used later in this work. It will be noted that the following discussion does not include the Ti_3B and the Zr_3B compounds, which do not exhibit the "Instability Region" observed in Cr, Mo, V and Nb based A15 type compounds. However, there are not enough data (see Table 5.14) to carry out a serious discussion on these two types of compounds.

From the variables S_a or r'_a it is possible to deduce the average chain length: the average number of A atoms lying between two B atoms on the 6c sites is equal to $(1-r_a)/r_a$, where r_a is here the occupation factor. Fig. 5.2 shows that for V and Nb based A15 type compounds there are two regions where S deviates considerably from perfect ordering, for the transition elements $B = Os, Re$ and for the nontransition elements $B = Au, Al, Ga$ (Following Ref. 7, Au is considered as behaving like a nontransition element in A15 type compounds). These regions correspond to the limits of the series of stable A15 type compounds, thus suggesting a connection between the degree of atomic ordering and the phase stability in A15 type compounds. Such a correlation will be discussed in Sect. 6.

From Fig. 5.2, it follows in particular for V based A15 type compounds that B elements closer to the Mn columns lead to a decrease of S_a , thus suggesting a tendency towards lower degrees of ordering. However, this tendency is only apparent, as will be explained in the following. For this consideration, it is necessary to recall that r_a represents the probability of encountering an A atom on the 6c sites, rather than the tendency to exhibit a

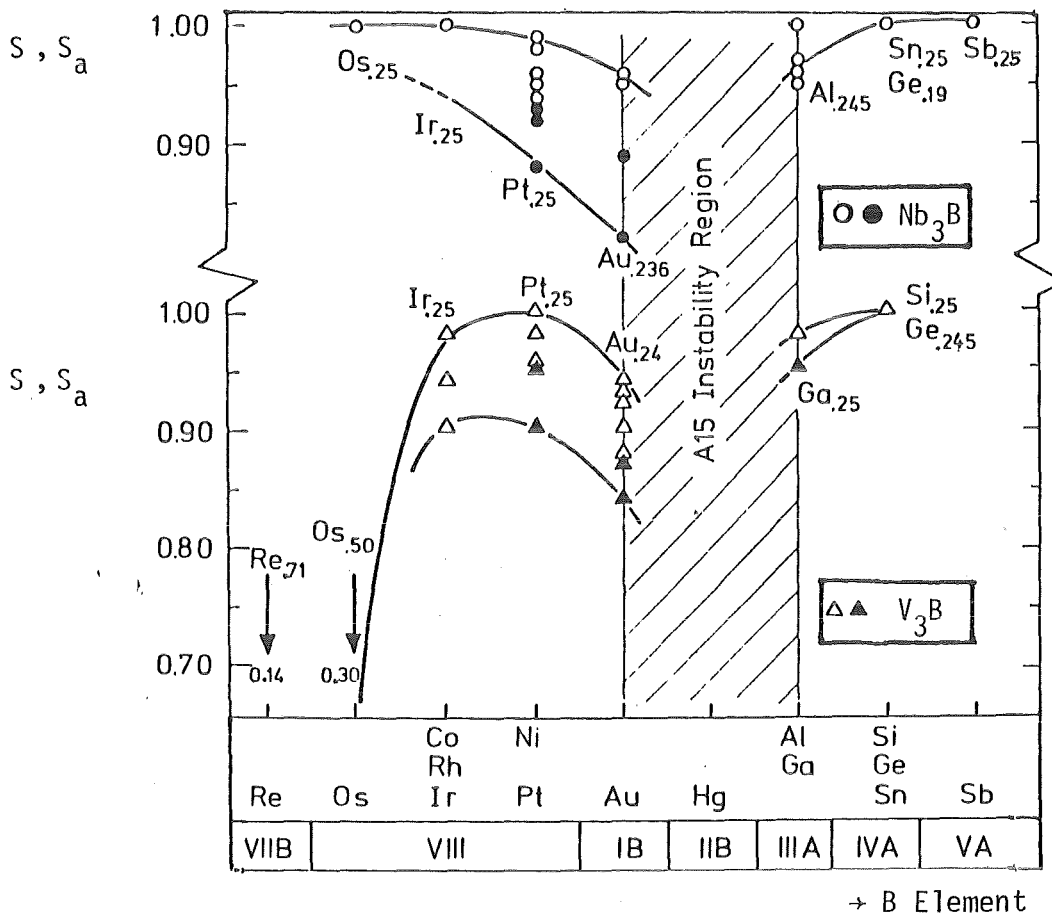


Fig. 5.2. Atomic order parameters, S or S_a , in Nb_3B and V_3B compounds. For the stoichiometric compounds, $S = S_a$. The full symbols represent data on argon jet quenched samples.

high degree of ordering (for example, for Nb atoms to occupy 6c sites). Such a tendency is better represented by the quantity r'_a relating the occupation factor to its highest possible value at a composition β (see Eqs. (3,4) and (3.5)):

$$r'_a = r_a \frac{0.75}{(1 - \beta)} \tag{5.6}$$

This "relative" occupation factor, r'_a , is only defined for $\beta > 0.25$ and simplifies to $r'_a = r_a$ for $\beta = 0.25$. From Fig. 5.3, where the variation of r'_a with the B element is plotted, it is seen that the tendency toward high ordering is present, even for B elements

approaching the Mn column ($r'_a \approx 1$ for B = Os, Re), while a certain amount of disordering subsists for B = Au, Al and Ga. Two conclusions can be drawn:

- a) the compounds where r'_a deviates substantially from 1 are those situated on both sides of the A15 instability region (B = Au, Al, Ga). For these compounds, substantial variations of the order parameter can be obtained by quench and anneal procedures: $\Delta r'_a = 0.04$ for $V_{.76}Au_{.24}$, $\Delta r'_a = 0.02$ for $V_{.24}Ga_{.76}$, which have to be compared to $\Delta r'_a = 0.0025$ for B = Ir, Os, Re, Si. Both the V and Nb based compounds with B = Pt exhibit quite high degrees of ordering, but show a large change ΔS_a , while their neighbours with B = Au show an even larger value of ΔS_a , but exhibit stronger deviations from perfect ordering.

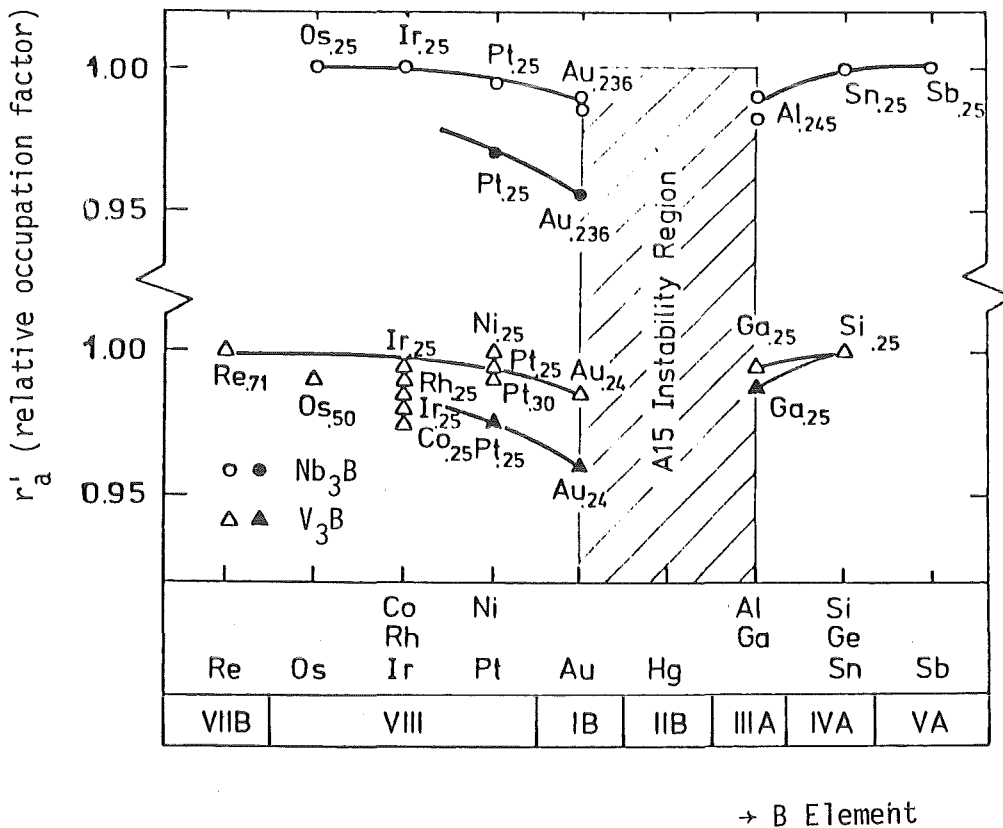


Fig. 5.3. Relative occupation factor, r'_a (as defined by Eq. 5.6), in Nb_3B and V_3B compounds, showing a marked decrease at both sides of the instability region. The full symbols represent data on argon jet quenched samples.

The variation of r'_a for Cr and Mo based A15 type compounds is shown in Fig. 5.4. In spite of the very incomplete data sets, a very high degree of ordering is observed for nontransition B elements. For transition B elements, the degree of ordering of Cr and Mo based compounds is somewhat lower than for those based on V and Nb, regardless on the B element. A comparison with Fig. 5.3 shows that the variation of S_a when the B element approaches the Mn column is much smaller than for the corresponding V_3B and Nb_3B compounds.

b) From the data in Tables 5.1 to 5.14, it appears that the substitution of the A element in the sequence $Ti \rightarrow V \rightarrow Cr$ leads to lower order parameters. At present, the reasons for this behavior are not understood. A suggestion made by Waterstrat and Van Reuth /202/ correlates the decrease of S in this sequence to increasing orbital overlapping in consecutive electronic bands. However, this hypothesis is based on the linear model, which certainly does not apply to Mo and Cr based A15 type compounds. Searching for other reasons, it should be recalled that the degree of atomic ordering as well as the equilibrium composition in A15 type compounds are high temperature properties and are frozen below T_D (see Table 4. 1). Above these

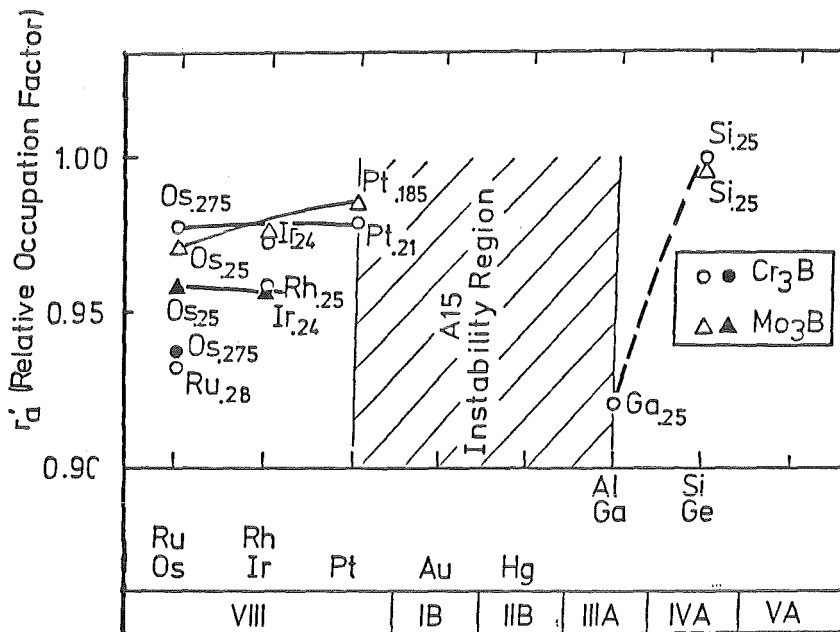


Fig. 5.4. Relative occupation factor r'_a as defined by Eq. (5.6) in Cr_3B and Mo_3B compounds. The full symbols stay for data on argon jet quenched samples.

temperatures, the number of thermal vacancies becomes sufficiently high for allowing $A \leftrightarrow B$ site exchanges. The ability of a system to undergo a certain amount of disorder this depends on the probability of two-step or multiple-step processes (see Fig. 4.3) following the occupation of a "virtual" site, i.e. on the potential differences between neighbouring configurations. In V and Nb based A15 type compounds these potential differences would be smallest for $B = Pt, Au, Al$ and Ga .

An interesting question is why so few A15 type compounds exhibit perfect ordering, e.g. V_3Si and Nb_3Sn . A recent "in situ" investigation of the order parameter by Isernhagen and Flükiger /162/ has shown that the order parameter of several Nb based A15 type compounds (Nb_3Sn, Nb_3Ir, Nb_3Pt and Nb_3Al) up to $\sim 900^\circ C$ did not vary within the error limits. This indicates that at least in these cases the ordering process is relatively slow within 100 or 200 degrees K above T_D , where $S \simeq S_E$. The reasons for the higher ordering in V_3Si and Nb_3Sn thus derive from the behavior at higher temperatures, close to T_F^0 .

5.2.2 The Order Parameter at High Temperature

The results of order parameter determinations at 300 K of A15 type compounds after quenching from different temperatures have been presented in 4.1.2. The known data have been summarized in Table 4.1. It was then expected that there would certainly be a difference between S_Q , the order parameter after quenching from a temperature T and the corresponding value of the equilibrium order parameter, S_E , measured directly at the same temperature T (The notation S_Q for the order parameter on quenched samples will only be used in the present paragraph, where the distinction between the different definitions is relevant). Obviously, there is $S_Q \geq S_E$, but it would be interesting to know for each compound the temperature up to which S_Q is a good approximation of S_E : $S_Q \simeq S_E$. The difference between S_Q and S_E at higher temperatures would then directly give an information about the ordering kinetics.

Unfortunately, no data of $S_E(T)$ have been published so far, but recent results obtained at the Institute of Technical Physics allow to give a first picture. Flükiger and Isernhagen /162/ have recently determined the "in situ" order parameters of the systems Nb_3Sn , Nb_3Pt , Nb_3Ir and Nb_3Al up to $1000^\circ C$ by X ray powder diffractometry. The measurements were performed on well homogenized, single phase samples which were crushed to powders of $20 \mu m$ size. After careful determination of the order parameter at room temperature, the powders were mounted in a ceramic sample holder particularly designed for use up to $1400^\circ C$. Partial sintering of the powders, disposed in a hole of $8 \times 8 \times 0.5 \text{ mm}^2$ provided sufficient geometrical stability, thus allowing precise angle and intensity measurements, a necessary condition for the determination of the lattice parameter and S at high temperature.

In this first work, evaporation and oxydation at high temperatures were found to be a major problem, which is hardly surprising when taking into account the large surface of the powder particles. In order to lower the time of exposition at high temperature, Flükiger and Isernhagen /162/ used a position sensitive detector, consisting of a graphite coated quartz wire in a high pressure chamber filled with argon and methane (or xenon and methane). This detector type allowed a considerable reduction of the measuring time, by a factor of 5 to 10. The highest temperature which could be achieved without excessive evaporation was $950^\circ C$ for Nb_3Sn and Nb_3Al , while the limits for Nb_3Pt are certainly above $1300^\circ C$.

The results are shown in Fig. 5.5, where the normalized in situ order parameter, S'_E/S_{\max} (S_{\max} is the order parameter prior to the heating cycle) is plotted as a function of temperature (T_F^0 is the A15 formation temperature). It is important to note that although the order parameter measurements occurred in situ, the results do not exactly represent the equilibrium order parameter $S_E(T)$. The reason resides in the fact that the exposure times at a given temperature T prior to the order parameter measurement /162/ were limited to

approximately 1 day, in order to minimize oxydation or evaporation at the surface of the powders. It may thus be that the values given in Fig. 5.5 are slightly larger than the equilibrium order parameter: $S'_E(T) \geq S_E(T)$. At higher temperatures, it is expected that $S'_E(T)$ tends towards $S_E(T)$.

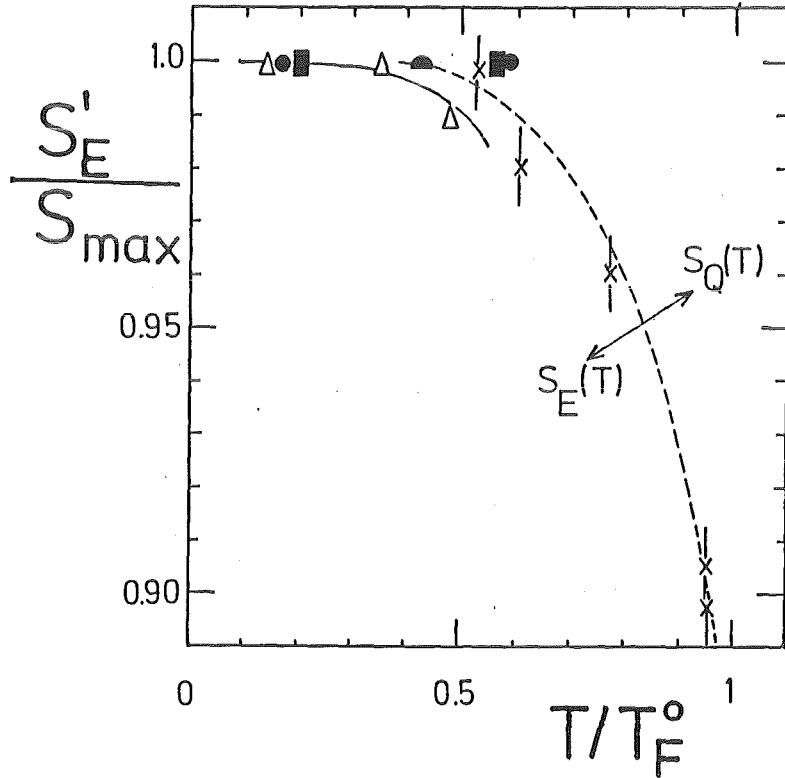


Fig. 5.5. Normalized in situ order parameter, S'_E/S_{max} as a function of temperature for different Nb based A15 type compounds. S_{max} is the order parameter prior to the heating cycle, T_F^0 is the A15 formation temperature. For comparison, the curve $S_Q(T)$ obtained on quenched Nb_3Pt samples (see Fig. 4.5) has been reproduced, \bullet : $Nb_{0.742}Pt_{0.258}$, Δ : $Nb_{0.748}Ir_{0.252}$, \bullet : $Nb_{0.754}Al_{0.246}$, \blacksquare : $Nb_{0.755}Sn_{0.245}$ (all measured in situ), \times : $Nb_{0.75}Pt_{0.25}$ (Quenched at different temperatures).

Obviously the above results suffer from the limitation in temperature (only 1050 °C. could be reached when the measurements were performed /162/), but some interesting conclusions can nevertheless be drawn:

- The order parameter changes up to $T/T_F^0 \sim 0.6$ are small and are of the order of the measuring error. For Nb_3Ir a decrease by 0.01 was observed at $T/T_F^0 = 0.48$
- Up to $T/T_F^0 = 0.5$, there is practically $S'_E(T) \simeq S_E(T) \simeq S_Q(T)$. In the particular

case of Nb₃Sn (and possibly of V₃Si, too), this indicates that if there is a difference in the ordering kinetics which leads to perfect ordering in this compound compared to others, it must act at much higher temperature than reached in the present experiments, probably even just below T_F^0 .

c) The curve $S_Q(T)$ vs T/T_F^0 for quenched Nb₃Pt in Fig. 5.5 shows without any doubt that the values of S_Q close to $T/T_F^0 = 1$ must be too high, due to partial reordering during argon jet quenching. In Sect. 7, it will be shown for V₃Ga that other quenching techniques lead to considerably higher quenching rates /227/, reducing the actually observed partial reordering on cooling. There is thus a need for order parameter measurements in A15 type compounds at temperatures approaching the formation temperature, T_F^0 , i.e. $\geq 1800^\circ\text{C}$. However, the difficulties would be considerably higher than those encountered in the present investigation up to 1050°C /162/.

6. LATTICE VIBRATIONS AND PHASE STABILITY

The scope of this Section will be to study whether an empirical correlation can be established between lattice vibrations and stability in A15 type compounds. Results on pair potential calculations will be used as a supplementary argument in favour of such a correlation.

6.1. Lattice Vibrations in A15 Type Compounds

6.1.1. Vibrational Anisotropy of the Atoms at the 6c Sites

Most data on vibration amplitudes discussed in this Section were obtained by means of powder diffractometry. It does not make a doubt that a much better picture could be given if the anisotropic vibration amplitudes would have been determined by single crystal refinements. The latter would give more informations about the phase stability and thus possibly on the degree of atomic ordering than the isotropic ones.

In general, no thermal diffusion scattering (TDS) corrections have been applied in the A15 diffraction data. It is expected that TDS corrections would affect the values of U^2 rather than those on the order parameter, since lines at higher angles 2θ have more weight on U^2 and the TDS cor-

rection factor α (see Sect. 3) increases with 2θ . To give an idea of the magnitude of α , its value for BaF_2 at the 511 line is 1.7 % and increases to 3.7 % for the 711 line. The situation is different when determining S , the most intense superstructure lines (where the structure factor depends on $2S(f_B - f_A)$ [see Table 3.3]), e.g. 110, 220, 310, 411, 422, ..., being situated at lower angles where the correction α is very small. As mentioned in Section 3, the precision in determining S is stronger coupled to the difference between the scattering factors $f_B - f_A$ than to small changes in U^2 , provided this difference is large enough.

So far, anisotropic vibration amplitudes have only been reported for single crystals of the compounds $\text{Cr}_3\text{Si}/180/$, $\text{V}_3\text{Ge}/180/$, $\text{V}_3\text{Si}/95,180/$, $\text{Nb}_{.80}\text{Ge}_{.20}/166/$ and $\text{Nb}_3\text{Sn}/171,180/$. In the system $\text{Nb}_3\text{Al}/53,99/$, powder data were used for deducing the ratio U_{11}/U_{22} between the r.m.s. amplitudes parallel and perpendicular to the chains. For simplicity, the r.m.s. amplitudes are denoted as U rather than $\langle U^2 \rangle^{1/2}$ (see definition in Sect. 3.2.1). From the known data, summarized in Table 6.1, it follows that the ratio U_{11}/U_{22} is always smaller than 1, thus reflecting the "overlapping" between A neighbours on 6c sites.

Compound	U_{11} ($\times 10^{-20} \text{m}^2$)	U_{22} ($\times 10^{-20} \text{m}^2$)	U_{11}/U_{22}	Ref.
$\text{Nb}_{.75}\text{Al}_{.245}^{\text{a}}$	0.0063	0.0079	0.80	53, 99
$\text{Nb}_{.81}\text{Ge}_{.19}$	0.0063	0.0079	0.80	166
$\text{Nb}_{.75}\text{Sn}_{.25}$	0.0064	0.0078	0.82	180
V_3Si	0.0067	0.0076	0.88	95
V_3Si	0.0073	0.0081	0.90	180
V_3Ge	0.0076	0.0082	0.93	180
Cr_3Si	0.0058	0.0062	0.94	95
Cr_3Si	0.0064	0.0078	0.82	180

Table 6.1. Anisotropic r.m.s vibration amplitudes at 300 K for various A15 type compounds. ^a) Polycrystalline sample.

The smallest ratios U_{11}/U_{22} (stands for $(U_{11}^2/U_{22}^2)^{1/2}$) between the r.m.s. vibration amplitudes of chain atoms are observed for the compounds $Nb_{.81}Ge_{.19}/166/$ and $Nb_{.755}Al_{.245}/53,99/$, thus indicating the strongest repulsion forces. As mentioned in 5.1.1c, stoichiometric Nb_3Ge would be expected to exhibit an even stronger anisotropy, due to the considerably smaller lattice parameter of 0.5140 nm instead of 0.5169 nm as measured for the composition $\beta = 0.19$. This suggests that the vibrational anisotropy could be a measure of the A15 phase stability. The question arises how large would be the ratio U_{11}/U_{22} for the metastable compounds Nb_3Si or V_3Al .

When considering the effects influencing phase stability, the question of dimerization arises (dimerization is an additional shift of the A atoms in chain direction). This effect has so far only been observed in Nb_3Sn single crystals by Axe and Shirane/273/, but could not be detected in V_3Si . Taking into account that this effect is very small, it may be justified to attribute only a small influence of dimerization on the A15 phase stability.

When considering a possible correlation between the vibrational anisotropy of the chain atoms and the A15 phase stability it must be taken into account that all refinements reported in this work have been performed at temperatures $T \leq 300$ K. High temperature refinements would be necessary to follow the development of U_{11}/U_{22} and to confirm the very plausible hypothesis of a correlation between vibrational behavior and A15 phase stability. An additional indication for such a correlation will be given in the next paragraphs, where the variation of the Debye temperatures and of the interatomic forces will be discussed.

6.1.2. Mean Square Vibration Amplitudes at the 6c and 2a Sites

Once the compound A_3B is formed, a change of the mean square vibration amplitude of U_a^2 and U_b^2 of the A and B atoms at the 6c and the 2a sites with respect to their elementary state is expected. A comparison is made in Table 6.2, where all known data are listed (in some cases, U_a^2 was obtained by the average $U_a^2 = (2U_{11}^2 + U_{22}^2)/3$).

The ratio of the mean square vibration amplitudes U_a^2 and U_b^2 in the A15 lattice is expected to be correlated to the mass ratio of the atoms A and B.

	Elementary State		A ₃ B Compound			
	U _A ²	U _B ²	U _a ²	U _b ²	(U _b ² /U _a ²) ^{1/2}	Ref
Nb ₃ Sn	0.0062	0.0092	0.0047	0.0053	1.062	171
			0.0049	0.0061	1.116	180
			0.0049	0.0059	1.204	162
Nb ₃ Al	0.0062	0.0088	0.0044	0.0072	1.280	242
			0.0062	0.0070	1.063	162
Nb ₃ Ga	0.0062	0.0061	0.0046	0.0043	0.967	242
Nb ₃ Ge	0.0062		0.0048	0.0057	1.080	166
V ₃ Si	0.0059	0.0036	0.0059	0.0070	1.089	171
			0.0049	0.0057	1.079	95
			0.0057	0.0072	1.124	180
V ₃ Ga	0.0059	0.0061	0.0059	0.0041	0.834	242
Cr ₃ Si	0.0021	0.0036	0.0034	0.0039	1.071	95
			0.0025	0.0027	1.039	242
Nb ₃ Ir	0.0062		0.0032	0.0024	0.866	162
Nb ₃ Pt	0.0062		0.0038	0.0050	1.147	162

Table. 6.2. Mean square vibration amplitudes U_a^2 and U_b^2 of the atoms on the 6c and 2a sites of A₃B A15 type compounds and the corresponding values U_A^2 and U_B^2 for the A and B atoms in their elementary state. The data are taken from Tables 5.1 to 5.13.

A simple model of two atomic species on an infinite linear chain yields the conditions:

$$\begin{aligned}
 U_a^2 &= U_b^2 && \text{(acoustic branch)} \\
 (U_b^2/U_a^2)^{1/2} &= m_A/m_B && \text{(optic branch)}
 \end{aligned}
 \tag{6.1}$$

As illustrated in Fig. 6.1, the measured values are situated close to the acoustic branch. This tendency towards lower frequencies can be explained by the dependence of U^2 on the term $\{\exp(hw/kT) - 1\}^{-1}$, which emphasizes the contributions from the low frequency spectrum.

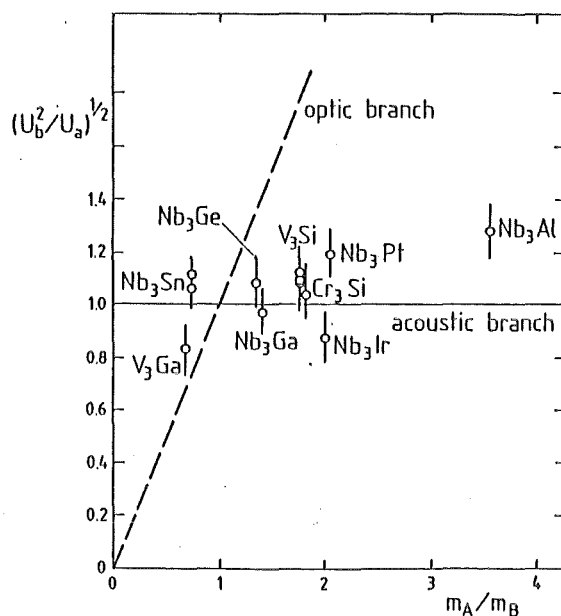


Fig. 6.1. Ratio of the r.m.s. vibration amplitudes of the A and B atoms on the 6c and 2a sites as a function of the mass ratio, m_A/m_B . Data from Table 6.2.

It follows from Table 6.2 that U_a^2 for both V and Nb varies very little with the nontransition B elements B = Sn, Al, Ga and Ge. In the case of V based compounds, U_a^2 is even equal to the value U^2 for elementary V in the bcc lattice, $U_a^2 = 0.0059 \times 10^{-20} \text{ m}^2$. In Nb based compounds, a markedly lower value of U_a^2 is encountered with respect to the elementary Nb: $U_a^2 = 0.0044$ to $0.0049 \times 10^{-20} \text{ m}^2$, compared to $U_{\text{Nb}}^2 = 0.0062 \times 10^{-20} \text{ m}^2$. It appears that U_a^2 for Nb decreases for transition B elements, to $U_a^2 = 0.0038$ and $0.0032 \times 10^{-20} \text{ m}^2$ for Nb_3Pt and Nb_3Ir , respectively. /162/. This reflects the decrease of the overall vibration amplitude in these two compounds found by Isernhagen and Flükiger /162/. On the other hand, the values U_b^2 for the different B elements on the 2a sites do not show any clear correlation to their elementary values U_A^2 .

Within the error limits, $\Delta|U_a^2/U_b^2|^{1/2} \approx 0.1$, most ratios in Table 6.2 exceed 1, reflecting a larger r.m.s. vibration amplitude for the atoms. Obviously, the occurrence of $U_b^2 > U_a^2$ is strongly influenced by the smaller values of U_{11}^2 in the chain direction, which constitute 2/3 of the overall value U^2 . In both cases where the amplitude ratio is smaller than 1, V_3Ga and Nb_3Ir , the deviation could be attributed to the measuring error. It is interesting to ask whether

the metastable compounds Nb_3Si and V_3Al would exhibit particular values of the vibration amplitudes. Figure 6.1 would suggest that the ratios $(U_b^2/U_a^2)^{1/2}$ for these two compounds would fall very close to those of Nb_3Al and V_3Si , respectively. As mentioned in 6.1.1, the difference between these two metastable compounds and the other ones must thus reside in the vibrational anisotropy U_{11}^2/U_{22}^2 . However, there is at present no mean to predict this ratio.

It is obvious that the small deviation from perfect ordering generally observed in A15 type compounds will have practically no influence on the values of U_a^2 and U_b^2 discussed in this paragraph. The question of a possible correlation between these two quantities is thus of secondary importance only.

6.1.3. Isotropic Vibration Amplitudes at 300 K and the Debye Temperatures

As mentioned in the preceding paragraphs, the informations about the mean square vibration amplitudes are not as complete as those about the order parameters. In addition, the errors in determining U^2 are higher, reaching sometimes up to 20 % of the absolute value (particularly for powder diffraction investigations). Nevertheless, an attempt will now be made to summarize and to interpret the known data. For this purpose, all known U^2 data on A15 type compounds have been listed in the Tables 6.3 and 6.4. The anisotropic vibrations having been treated in 6.1.1, the present considerations will be restricted to isotropic vibrations only. In the case where U_{11}^2 , U_{22}^2 , U_a^2 or U_b^2 are given, the "isotropic" values of U^2 have been obtained by the average $U^2 = (3U_a^2 + U_b^2)/4$ or by $U^2 = \{1/3(2U_{11}^2 + U_{22}^2) + U_b^2\}/4$. The corresponding average Debye temperature, $\theta_X(300K)$, was calculated from the U^2 values, using Eq. (3.9). For several compounds, it is possible to compare the values of $\theta_X(300K)$ with $\theta_D(300K)$, the Debye temperature at 300 K determined by Knapp et al. /222/ by means of calorimetry. It is obvious that the Debye temperature derived from different measuring techniques may exhibit systematic differences, the observed physical property (diffraction, electronic specific heat, elastic constants,...) being more or less sensitive to different portions of the phonon spectrum. Nevertheless, the agreement between $\theta_X(300K)$ and $\theta_D(300K)$ is satisfactory, as follows from Tables 6.3 and 6.4 showing always differences below 50 K for the systems V_3Si , V_3Ga , Nb_3Sn , Nb_3Al , Mo_3Si , which may also partly be due to measuring errors. This result suggests that the effect of the TDS correction (which has been taken into account in any of the diffraction works on A15 type compounds performed so far) would be situated within the present error limits for $\theta_X(300K)$, i.e. ordinarily ± 20 K, in some cases ± 30 K, or $\Delta U^2/U^2 = 5$ to 7 %. It has to be noted that $\theta_D(300K)$ as measured by sound velocity data /219/ is systematically higher than the calorimetric values.

Compound	$\theta_D(0)$ [K]	$\theta_D(300K)$ [K]	U^2 [$\times 10^{-20} m^2$]	$\theta_X(300K)$ [K]	$\Delta\theta_D(300K \rightarrow 0)$ [K]														
V_3Si	297 /30/	470 /229/ 498 /222/ 530 ^d /219/	0.0048 /78/ 0.0051 /95/ 0.0057 /78/ 0.0060 /180/ 0.0061 /274/	450 \pm 20 430 \pm 20 422 \pm 20 412 \pm 20 408 \pm 20	+ 173 + 201 [+ 237] (+ 153) (+ 133) (+ 125) (+ 115) (+ 111)														
						V_3Ga	292 /97/	390 /222/	0.0054 /242/ 0.0057 /20/	390 \pm 20 380 \pm 20	+ 98 (+ 98) (+ 88)								
												V_3Ge $\beta^3 = 0.24$	415 /122/ 392 /229/	471 ^c /256/ 478 ^d /219/	0.0061 ^b /180/ 0.0063 /38/	363 \pm 20 372 \pm 20	[+ 56] (- 48) (- 20)		
																		V_3Sn $\beta^3 = 0.19$	347 /122/
												V_3Sb V_3As V_3Au V_3Pt V_3Ir V_3Rh V_3Co V_3Ni	398 /122/ 530 /62/ 337 /97/ 413 /30/ 443 /30/ 485 /122/ 560 /122/ —	—	—	—	—		
0.0025 /38/	480 \pm 20	(- 90)																	
			$V_{.50}Os_{.50}$ $V_{.78}Pd_{.22}$ $V_{.29}Re_{.71}$	385 /122/ 400 /122/ /195/	—	—	—												
								Nb_3Sn $\beta^3 = 0.245$ $\beta = 0.25$	227 /179/ 208 /229/	370 ^d /219/ 290 /222/	0.0050 /17/ 0.0052 /9,162/ 0.0058 /180/							295 \pm 20 290 \pm 20 275 \pm 20	[+ 162] + 63 + 82 (+ 68) (+ 63) (+ 48)
			Nb_3Ga $\beta^3 = 0.24$	280 /214/	—	0.0045 /242/	340 \pm 20	(+ 60)											
									Nb_3Al $\beta^3 = 0.25$ $\beta = 0.24$	324 /248/ 283 /114/	335 /222/	0.0050 /70/ 0.0050 /70/ 0.0064 /162/ 0.0068 /28/ 0.0072 /53,99/	341 \pm 20 341 \pm 20 304 \pm 20 294 \pm 20 286 \pm 20	+ 52 (+ 56) (+ 21) (+ 11) (+ 3)					
Nb_3Sb	345 /30/	330 /222/	—	—	- 15														
						Nb_3Au $\beta^3 = 0.236$	253 /30	—	0.0043 /162/ 0.0051 /192/	296 \pm 20 270 \pm 20	(+ 43) (+ 17)								
Nb_3Pt	340 /25/	—	0.0038 /76/ 0.0041 /38/ 0.0047 /162/ 0.0051 /38,76/	316 \pm 20 305 \pm 20 284 \pm 20 273 \pm 20	(- 24) (- 35) (- 56) (- 67)														
						Nb_3Rh	398 /208/	—	—	—	—								
Nb_3Ir	378 /30/	—	0.0030 /162/	359 \pm 20	(- 19)														
Nb_3Os	378 /208/	—	0.0033 /162/	343 \pm 20	(- 35)														

Table 6.3. Debye temperatures for V and Nb based A15 type compounds. $\theta_D(0)$ and $\theta_D(300K)$ are determined by calorimetry, while the values $\theta_X(300K)$ are obtained from U^2 (Tables 5.1 to 5.11) using Eq. (3.9). ^a) The composition is given as $\beta = 0.25$, but the average Ge content is well below this value. ^b) Calculated assuming $U_b^2 \approx 1/3(2U_{11}^2 + U_{22}^2)$, ^c) Ultrasonic attenuation, by Rosen et al. /256/, ^d) Sound velocity measurements by Testardi /219/. The difference $\Delta\theta(300K \rightarrow 0)$ is taken from calorimetric data (no brackets), using sound velocity data [square brackets] or using $\theta_X(300K)$ values (round brackets).

Compound	$\theta_D(0)$ [K]	$\theta_D(300K)$ [K]	U^2 [$\times 10^{-20} m^2$]	$\theta_X(300K)$ [K]	$\Delta\theta_D(300\rightarrow 0)$ [K]
Mo ₃ Si	520 /63/ 560 /158/	470 /158/	0.0034 /38/	415 ± 20	- 50 - 90 (- 105)
Mo ₃ Al Mo ₃ Ge	500 /63/ 510 /63/				
Mo ₃ Pt β ≅ 0.185	405 /63/		0.0033 /38/	335 ± 20	(- 70)
Mo ₃ Ir β ≅ 0.24	460 /63/		0.0032 /38/	340 ± 20	(- 120)
Mo ₃ Os	430 /63/		0.0028 /38/	370 ± 20	(- 60)
Cr ₃ Si	640 /229/ 670 /223/	530 /229/	0.0028 /242/ 0.0035 /95/	607 ± 20 540 ± 20	- 110 - 140 (- 63) (- 170)
Cr ₃ Ge	670 /223/ 470 /229/	410 /229/			- 60
Cr ₃ Ga Cr ₃ Pt β ≅ 0.21 Cr ₃ Ir Cr ₃ Os β ≅ 0.275 Cr ₃ Rh Cr ₃ Ru β ≅ 0.28	584 /223/ 402 /223/ 402 /223/ 449 /223/ 442 /223/ 460 /223/ 418 /223/		0.0063 /212/		
Ti ₃ Sb Ti ₃ Au Ti ₃ Pt Ti ₃ Ir Ti ₃ Hg	282 /207/ 385 /207/ 376 /207/ 210 /25/ 330 /207/				
Zr ₃ Pb Zr ₃ Sn β ≅ 0.20 Zr ₃ Au	255 /207/ 292 /207/ 310 /207/				

Table 6.4. Debye temperatures for Cr, Mo, Ti and Zr based A15 type compounds. $\theta_D(0)$ and $\theta_D(300K)$ are determined by calorimetry, while the values of $\theta_X(300K)$ are obtained from U^2 (see Tables 5.12, 5.13 and 5.14) using Eq. (3.9). The difference $\Delta\theta_D(300\rightarrow 0)$ is taken from calorimetry (no brackets) or using the $\theta_X(300K)$ values (round brackets).

The Tables 6.3 and 6.4 also contain the Debye temperatures $\theta_D(0)$ as determined by low temperature calorimetry on all known A15 type compounds. The choice of data in Tables 6.3 and 6.4 was restricted to samples being as close as possible to stoichiometry or having the highest degree of ordering, taking care to include at least one representative for each compound. The effect of varying

either the atomic composition or the degree of ordering on the value of θ_D will be discussed in the next paragraph, where an attempt will be made to estimate whether and in which cases $\theta_D(0)$ can be used as an approximation for $\theta_D(300K)$ in order to be used for stability considerations, the latter being only known for a small number of systems.

The variation of U^2 at 300 K as well as of $\theta_\chi(300K)$ for various A15 type compounds has been reproduced in Fig. 6.2. When discussing the variation of U^2 and $\theta_\chi(300K)$ for A_3B series with fixed A and varying B element, the question arises how these quantities are connected with those of the B constituents in

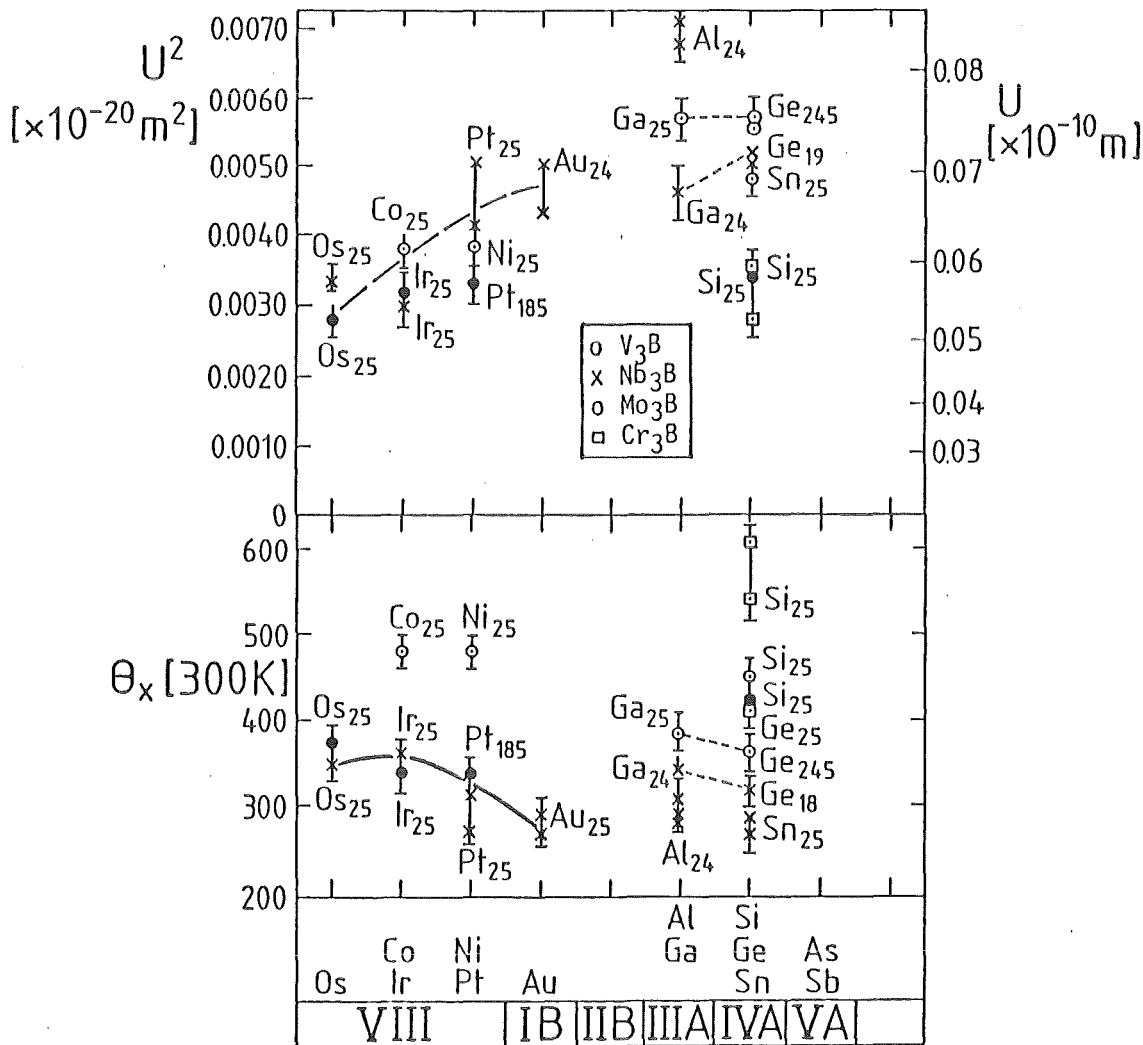


Fig. 6.2. Isotropic mean square vibration amplitudes at 300 K, U^2 , and corresponding Debye temperatures $\theta_\chi(300K)$ calculated by means of Eq. (3.9), using the data listed in Tables 5.1 to 5.14.

their elementary state. In the literature, there is no information about such correlations, the whole subject of the atomic vibrations in compounds having been somewhat neglected in the past. Based on the values in Tables 5.1 to 5.14 arising from own and from literature values, a first attempt will thus be undertaken to search for possible relationships, which also may give additional information on the A15 phase stability. Following the general philosophy of the present work, the attention will not be concentrated on one or few compounds, but will be extended to the totality of known A15 type systems. For this purpose, the U^2 and θ_D values (the latter at temperature ranges as close as possible to 300K) of a series of elements has been extracted from the International Tables of Crystallography, Vol.III, Sect. 3.3 and has been condensed in Fig. 6.3.

It is immediately seen from Fig. 6.3 that with increasing electron number U^2 exhibits significant changes starting with the IB elements, i.e. Cu, Ag and Au, followed by a very strong raise for the IIB elements Zn and Cd. A further increase in Z leads to a minimum of U^2 for the IVA elements C, Si, Ge and Sn. Besides the mentioned sharp change of U^2 for IIB and IIIA elements, the most important feature in Fig. 6.3 is the nearly parallel variation of U^2 for elements of the same period. However, an inversion of the vibrational behavior is observed between transition and nontransition elements. For transition elements, U^2 increases in the sequence 5d+4d+3d, while for nontransition elements, U^2 is smallest for the lightest elements (B and C) and increases successively when going to the elements of the 3., 4., 5. and 6. period. Of course, the variation of θ_D is opposite to that of U^2 , but the inversion is not longer present. The lightest elements in a column always exhibit the highest θ_D values, which is particularly apparent for the elements C and B, followed by Si and Al.

It is now interesting to compare the variation of U^2 and θ_D in the figures 6.2 and 6.3 in order to see how the vibrational properties of the B elements influence those of A_3B compounds crystallizing in the A15 structure. The importance of the B element on the vibrational behavior of A15 type compounds is larger than that of the A element. The reason can be easily seen from Fig. 6.3: as well U^2 as θ_D for the A elements Ti, Zr, Cr, Mo, V and Nb vary within narrow limits in contrast to the variation in B elements which is considerably larger. The following conclusions can now be drawn:

- 1) In A15 type A_3B series, the values of U^2 as well as those of θ_χ (the latter also staying for θ_D) are strongly influenced by the B element. The gradual varia-

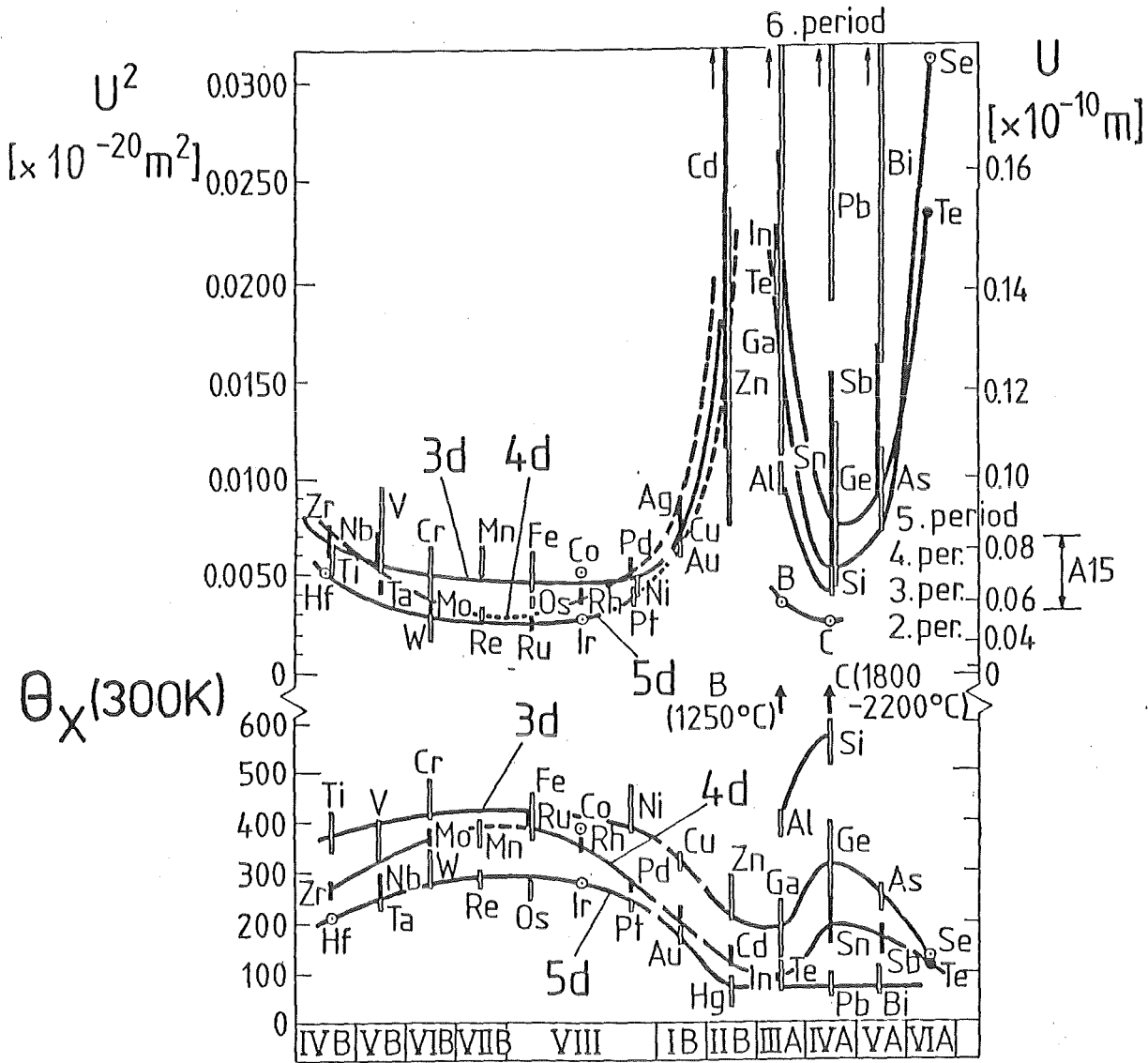


Fig. 6.3. Isotropic vibration amplitudes U^2 and Debye temperatures $\theta_{\chi}(300\text{K})$ for various elements from the 2. to the 6. period of the periodic system, from Int. Tables of Cryst., Vol.III, Sect. 3.3. The r.m.s. vibration amplitudes are given at the right scale, where the total range of U in A15 type systems is also indicated for comparison..

tion of the vibrational properties of the B element can still be observed after its inclusion in A_3B series with the A15 type structure, in spite of the low content of 25 at.% only. This is mainly observed for $B = Si$, where U^2 is smallest as well in the element as in the compound. In particular, the vibration amplitudes for transition B elements in the A15 structure are smaller than for non-transition B elements, as in the elementary case (with the exception of V_3Si , see Fig. 6.2). Typical U^2 values for V_3Si are close to $0.0030 \times 10^{-20} \text{ m}^2$, corresponding to r.m.s. amplitudes $U = 0.0547 \times 10^{-10} \text{ m}$, which have to be compared with $U = 0.0707 \times 10^{-10} \text{ m}$ for compounds with nontransition B elements (all values at $T = 300 \text{ K}$).

A similar variation to that of U^2 in Fig. 6.2 can also be plotted for the lattice parameter, thus constituting an additional indication for the regular changes of properties of the A15 structure in A_3B series. Here, the point of importance for the present discussion is the smallest possible value of a in a given compound, previously discussed in 4.3.1 (see Fig. 4.21). This value corresponds to a minimum distance between neighbour A atoms and was found to be smaller for transition B elements than for nontransition elements under equilibrium conditions. The smaller distance between Nb atoms in Nb_3Ir or Nb_3Os is not expected to lead to the large vibration anisotropy observed for example in Nb_3Ge , due to the d character of Ir and Os.

2) It is remarkable that the "Instability Region" in Fig. 6.2 would correspond to the highest U^2 values, probably lying above $0.0060 \times 10^{-20} \text{ m}^2$. At the same time, $\theta_X(300K)$ reaches minimum values at the borders of this region, i.e. $\sim 250 \text{ K}$ for $Nb_{.764}Au_{.236}$ and $Nb_{.76}Au_{.24}$. Both observations suggest that the existence of the "Instability Region" could be correlated with a particular vibrational behavior, characterized by excessively large r.m.s. vibration amplitudes $U > 0.8 \times 10^{-10} \text{ m}$, or by very low Debye temperatures $\theta_D < 250 \text{ K}$, at least for A_3B series with $A = Cr, Mo, V, Nb$ and possibly Ta . It is tempting to attribute the existence of the "Instability Region" to particularly high vibration amplitudes of the B elements in their elementary state, since only B atoms with $U^2 < 0.0150 \times 10^{-20} \text{ m}^2$ are found to form A15 phases without applying high pressures or thin film techniques. However, this criterion is certainly not sufficient to decide about stability of all A15 systems, since both the Ti_3B and Zr_3B series do not exhibit any instability for $B = Hg, Pb$ or Tl . At this point, it should be recalled that phase stability is primarily dictated by electronic requirements, which finally lead to the observed vibration amplitudes and that so far no simple electronic criteria can be given for the sta-

bility of a given compound. It will be seen later (see Fig. 6.21) that the electronic transfer in Ti_3B and Zr_3B is different than in the other A15 type compounds studied here. As shown later in Table 6.8, there are A15 phases covering the whole range of electron per atom values between $e/a = 3.25$ and $e/a = 6.8$, without any "forbidden" zone. In the case of Ti_3B and Zr_3B series, the particular electronic configuration may stabilize the phase at lower vibration frequencies than in other A15 type compounds. Indeed, as well Ti_3Ir as Ti_3Sb and Zr_3Pb exhibit very low Debye temperatures $\theta_D(0)$ when compared with other A15 type compounds, $\theta_D < 280$ K. (see Table 6.4). Unfortunately, no Debye temperatures at 300 K are known for these compounds, which would complete the picture.

3) It is remarkable that the results on powder diffractometric measurements lead to significant conclusions about the vibrational behavior in A15 type compounds, the estimated error in $\theta_X(300K)$ being of the order of ± 20 K, in some cases ± 30 K. It is important to recall that satisfactory data from powder diffractometric measurements require very careful measurements (if possible taking several runs for each sample and averaging) on well characterized samples. It is obvious that the informations will be restricted to the isotropic vibration amplitudes and to the Debye temperature. For the very important measurements of the anisotropical vibrational behavior in A15 type compounds, single crystal refinements are required.

6.1.4. The Debye Temperatures between 0 and 300 K

In the preceding paragraph, the attention was merely given to A15 phase stability, the discussion of the vibrational behavior was thus limited to 300 K. Between 300 K and 0 K, however, strong variations of the Debye temperature have been reported, which finally affect the superconducting properties. There are far more data on θ_D at low temperatures than at 300 K, allowing a more complete discussion. Nevertheless, it should be recalled that $\theta_D(T)$ is an average quantity, thus more informations about different phonon modes would be required. There is also a gap of knowledge for anisotropic properties of the crystal, U_{11}^2 and U_{22}^2 below 300 K being only known for V_3Si /95/.

The variation of θ_D between 0 and 300 K does not show the same behavior for all A15 type compounds, as follows from calorimetric data of Knapp et al. /222/. These authors found that the Debye temperatures in the systems Nb_3Sn , Nb_3Al , V_3Si , V_3Ga are higher at 300 K than at 0 K. This anomalous behavior, also called phonon softening, is correlated to a decrease of the elastic constants

and of the sound velocity as shown in the review of Testardi /219/. The shear modulus of Nb_3Sn and V_3Si vanishes at the low temperature transition from the cubic into the tetragonal phase, observed in these two compounds only. The corresponding values of θ_D are tabulated in Table 6.3 and show that V_3Si exhibit the largest variation, $\Delta\theta_D \cong 180$ K from 300 to 0 K, followed by Nb_3Sn with $\Delta\theta \cong 70$ K (It has to be noted that the value of $\theta_D(0)$ in V_3Si is particularly difficult to determine since $\gamma = \gamma(T)$, as described by Junod /30/ who found $\theta_D(0) = 297$ K). The difference $\Delta\theta$ for V_3Ga and Nb_3Al in Fig. 6.4 is smaller, 35 and <20 K, respectively. For the low T_c compound Nb_3Sb , Knapp et al. /222/ found the inverse behavior, i.e. $\theta_D(0) > \theta_D(300 \text{ K})$. Nb_3Sb thus exhibiting the behavior generally observed in other materials, where a gradual softening of the lattice is observed for increasing temperatures. In 4.3.6b, another low T_c A15 type compound, Mo_3Si , had also been reported to exhibit a lattice hardening at lower temperature, Mirmelshteyn et al. /158/ reporting $\theta_D(0) = 560$ K and $\theta_D(300 \text{ K}) = 470$ K, respectively. No attempt has been done so far to give a description about the general behavior of $\theta_D(T)$ in A15 type compounds. In the following, it will be shown that there are several rules governing this behavior. For this purpose data from Junod et al. /25,30,248,276/, Flükiger et al. /62,63,223/, Surikov et al. /229/, Knapp et al. /222/, Mirmelshteyn et al. /158/, Rosen et al. /256/, Stewart et al. /279/ and Testardi et al. /219/ will be presented and compared. In particular, it will be tried to determine the influence of composition and atomic ordering on $\theta_D(T)$.

The starting point of the present consideration will again be the system Mo_3Si , where the whole behavior of $\theta_D(T)$ from 0 to 300 K is known /158/. The $\theta_D(T)$ vs. T curves of Mo_3Si are represented in Fig. 6.4, together with those of several other A15 type compounds where the $\theta_D(T)$ measurement over an extended temperature range between 0 and 300 K are available.

The family of curves for Mo_3Si was obtained after neutron irradiation at $\phi t = 1 \times 10^{20} \text{ n/cm}^2$ (curve I), followed by recovery heat treatments at different temperatures, 450°C (II), 650°C (III) and 700°C (IV), the last one being almost identical to the unirradiated state. The corresponding variation of T_c is plotted in Fig. 4.32. It is remarkable that the excessive lattice hardening below 50 K is absent after irradiation where $T_c = 6$ K, but gradually reappears with recovery. It is seen that the variation of $\theta_D(T)$ in Mo_3Si is quite complex, consisting of two distinct regions with opposite behavior. The following discussion will be centered on these two $\theta_D(T)$

regions, one staying for phonon softening (from 300 K to < 100 K), the second one representing a lattice hardening, encountered at temperatures well below 100 K.

As shown in Fig. 6.4, a decrease of T from 300 K to lower temperatures in Mo₃Si first causes a similar anomalous decrease of θ_D as observed in high T_C compounds. The value of θ_D decreases from 470 K at 300 K to 414 K at 50 K, followed by a strong increase to 560 K at 0 K. A similar behavior was also observed for Cr₃Si (normal down to 0.015 K) by Flükiger et al. /223/.

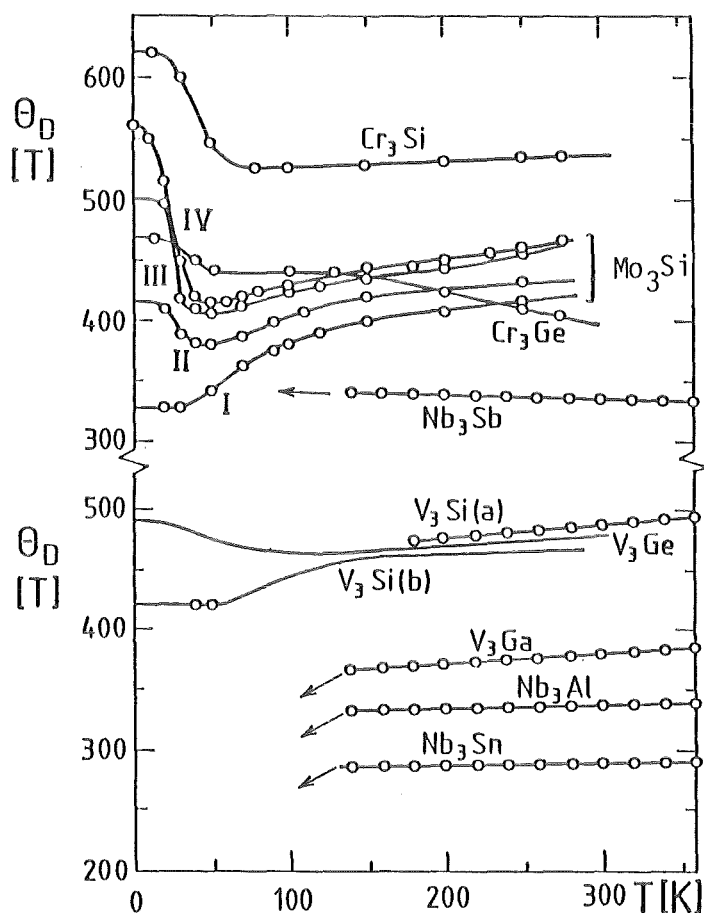


Fig. 6.4. Variation of the Debye temperature of various A15 type compounds below 300 K: Cr₃Si, Cr₃Ge and V₃Si(b) by Surikov et al. /229/, V₃Si(a), Nb₃Al, Nb₃Sb, V₃Ga and Nb₃Sn(a) by Knapp et al. /222/, Mo₃Si by Mirmelshteyn et al. /158/, V₃Ge by Rosen et al. /256/ and Nb₃Sn by Junod /30/. All data were derived from specific heat measurements except for V₃Ge, where $\theta_D(T)$ was determined from elastic constants. The meaning of Mo₃Si I, II, III and IV is explained in the text.

between 670 and 720 K on different samples, while Surikov et al. /229/ found $\theta_D = 620$ K at 300 K. Obviously, the comparison between two different calorimetric measurements on two different samples has to be considered with some caution, but the relative difference between the Debye temperatures at 0 and 300 K is large enough (120 K) to exceed the individual errors in Refs. 223 and 229.

The variation of θ_D for several A15 type compounds is reproduced in Fig. 6.4. Most data have been obtained by specific heat measurements except for V_3Ge , which was determined from the variation of the elastic constants /256/. The system V_3Ge was measured by Rosen et al. /256/ who reported an initial decrease of θ_D from 471 K at room temperature to 467 K at 150 K, followed by an increase to 486 K for $T \rightarrow 0$. These values are higher than those measured by specific heat (see Table 6.3) but certainly give the correct tendency. In contrast to Nb_3Sn and V_3Si /219/, the shear modulus of V_3Ge , $1/2 (C_{11} - C_{12})$ was not found to vanish at low temperature. Only a decrease of 5.5 % from 300 K to 75 K was observed, followed by a rapid increase at lower temperatures, up to 486 K.

The observed decrease of θ_D with decreasing temperature thus reflects the phonon-mode softening characteristic of high T_c A15 type compounds, i.e. V_3Si , Nb_3Sn , V_3Ga and Nb_3Al /237/. Temperature dependent softening is correlated to the sharp structure of the d band electronic density of states in the vicinity of the Fermi energy. This causes electronic properties such as the magnetic susceptibility to be temperature dependent, thus producing temperature dependent electronic screening of the phonon mode frequencies. The observed softening effect is not pronounced for the Nb_3Al and V_3Sn samples measured by Knapp et al. /222/ (see Table 6.3). This is attributed to inhomogeneities and to deviations from stoichiometry, as can be followed by a comparison with the specific heat data of Junod et al. /248/. These authors reported the value $\gamma = 11.4 \text{ mJ/K}^2\text{at-g}$ for a carefully homogenized, stoichiometric Nb_3Al sample, i.e. substantially higher than the value $\gamma = 7.62 \text{ mJ/K}^2\text{at-g}$ reported by Knapp et al. /222/. The latter value would rather correspond to an average Al content of 23.5 at.% than to the stoichiometric composition. The compound V_3Sn is known to be stable at the composition $\beta = 0.19$ only /62/. In both cases, Nb_3Sb and V_3Sn , phonon softening seems to be sufficiently strong to mask the usual dilatation effect.

The compounds in Fig. 6.4 are the only ones where the variation of the Debye temperature has been reported up to 300 K. Additional informations about the variation of $\theta_D(T)$ can ordinarily be obtained up to 40 K from specific heat measurements. In the following, a global comparison will be made between the $\theta_X(300K)$ values reported in the present work (Tables 6.3 and 6.4) and the $\theta_D(0)$ values derived from specific heat data.

a) Debye temperatures below 50 K. As shown in Fig. 6.4, both behavior types can occur in A15 type compounds, as well softening as hardening of the lattice when going from 300 K to lower temperatures. A complement to these data is furnished by the variation of $\theta_D(T)$ in the systems based on Nb and Ti (Fig. 6.5, from Junod /25,30,248/), on Nb and V with B = Ir, Pt and Au (Fig. 6.6, from Junod /30/) and on Mo (Fig. 6.7, from Stewart and Giorgi /279/ and Flükiger et al. /63/). In all these cases, strong deviations from the Debye model are observed, starting well below T_C . The deviations from the Debye model are different from compound to compound, but certain trends can be recognized from the analysis of the known data.

The two Nb_3Al curves in Fig. 6.5, corresponding to the states after

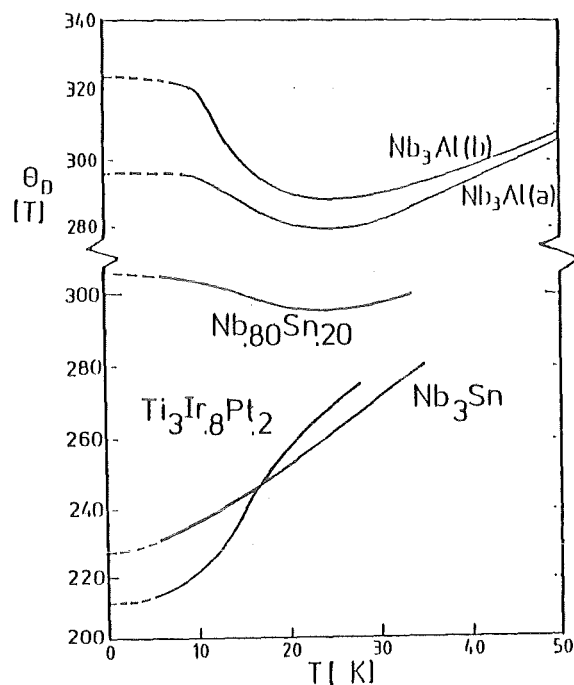


Fig. 6.5. Variation of the Debye temperature of various A15 type compounds as determined from calorimetry: Nb_3Sn and $Nb_{.80}Sn_{.20}$ by Junod /30/, Nb_3Al (a) and (b) by Junod et al. /248/ and $Ti_{.75}Ir_{.20}Pt_{.05}$ by Junod /25/. Nb_3Al (a) was quenched from 1940 °C, Nb_3Al (b) was subsequently annealed 56 days at 750 °C.

quenching (a) and after subsequent ordering (b) show a very interesting effect. It is seen that $\theta_D(T)$ is affected by the state of ordering, but mainly in the lower part of the phonon spectrum. According to Junod et al. /248/, $\theta_D(T)$ above T_C of Nb_3Al differ by less than 10 K between the curves (a) and (b). An interesting comparison can be made between Nb_3Sn samples with different compositions, also shown in Fig. 6.5. On two samples with $\beta = 0.20$ and 0.25 , Junod /30/ found that lattice softening at low temperature is almost absent in the non-stoichiometric one, while $\theta_D(T)$ converges above 40 K.

The curves for the stoichiometric Nb_3Sn sample in Fig. 6.5 can be compared with that for the pseudobinary system $Ti_{.75}Ir_{.20}Pt_{.05}$, which exhibits the lowest $\theta_D(0)$ value reported so far in A15 type compounds, 209 K/276/. This low Debye temperature and the similarity of $\theta_D(T)$ with Nb_3Sn suggested that some low temperature instability could occur. However, no phase transition could be found in $Ti_{.75}Ir_{.20}Pt_{.05}$ by means of low temperature X ray diffraction. It can be argued that the the electronic density of states in this compound is too low

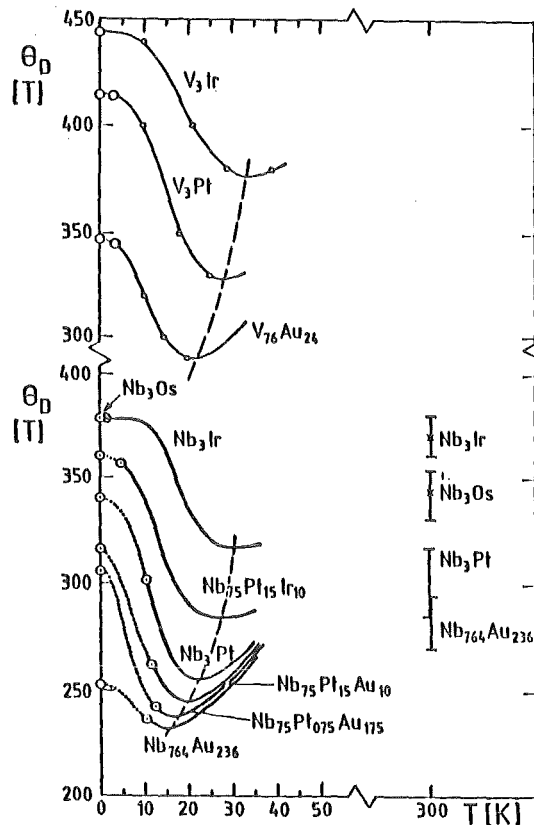


Fig. 6.6. Variation of the Debye temperature of various Nb and V based A15 type compounds with B = Ir, Pt and Au (After data from Junod /30/). For comparison, the values $\theta_D(300K)$ determined by X ray diffraction listed in Table 6.3 are also indicated.

($\gamma = 8.93 \text{ mJ/K}^2 \text{ at-g } /276/$) for inducing a lattice instability. Indeed, it appears that the occurrence of only one extreme value, either $N(E_F)$ or $\theta_D(0)$, is not sufficient for causing the cubic-tetragonal phase transition. It should be recalled that $V_3\text{Ga}$ with the highest γ value among A15 type compounds does not transform, which is attributed to a small, but significant deviation from perfect ordering /20/. Does this mean that $\text{Ti}_{.75}\text{Ir}_{.20}\text{Pt}_{.05}$ could also exhibit a deviation from perfect order on the 6c sites (or from perfect stoichiometry), without which the value of $\theta_D(0)$ would even be smaller than 200 K ? This interesting question would justify a complete reinvestigation of the vibrational and ordering properties in Ti_3B compounds, as well in the binary as in the pseudobinary state.

The Debye temperature of V and Nb based A15 type compounds with B = Ir, Pt and Au below 35 K has been determined by means of calorimetry by Junod/30/. His graphs on $\bar{\alpha} = 1/T^2(C/T - \gamma)$ have been replotted in Fig. 6.6. All compounds show the same complex behavior of $\theta_D(T)$, consisting of two branches, one indicating lattice softening from 300 K to $T \lesssim 35$ K, characteristic for high $N(E_F)$ A15 type compounds, the second one showing a considerable increase of $\theta_D(T)$ at the lowest temperatures, absent in high $N(E_F)$ compounds. It is advanced here that this lattice hardening at the lowest temperatures has a considerable influence on the superconducting properties of A15 type compounds.

When going from one B element to the next in Fig. 6.6 a gradual change of the behavior of $\theta_D(T)$ is apparent is observed. The minimum is shifted from 15 to 20 K for B = Au to 25 to 30 K for B = Pt and finally to 30 to 35 K for B = Ir. It is remarkable that in both series $V_3\text{B}$ and Nb_3B the compounds with B = Pt show the highest low temperature hardening, $\Delta\theta_D = 77$ K for $V_3\text{Pt}$ and 85 K for Nb_3Pt , the values of $\theta_D(0)$ lying well above the values $\theta_D(300\text{K})$. Note that for the compounds with B = Au the value of $\theta_D(0)$ lies below the room temperature value, like for Nb_3Sn , $V_3\text{Si}$ and $V_3\text{Ga}$. Unfortunately, the corresponding value for $V_{.76}\text{Au}_{.24}$ is not known. The question arises whether the low temperature lattice hardening would still be present in stoichiometric, perfect ordered $V_3\text{Au}$ and Nb_3Au , in contrast to Nb_3Pt and Nb_3Ir which show this effect but are already stoichiometric and perfectly ordered (Nb_3Ir) or very close to perfect ordering ($S = 0.98$ for Nb_3Pt). This question will be treated in detail at the end of this paragraph when discussing the effect of composition and atomic ordering on $\theta_D(0)$, leading to the answer that both compounds would probably behave as Nb_3Sn and the other high $N(E_F)$ compounds (see Fig. 6.4). In this case, the question of the low temperature phase stability in $V_3\text{Au}$ and Nb_3Au would be raised, $\theta_D(0)$ falling below 250 K and the electronic density of states being sufficiently high in both compounds.

The strongest deviations from the Debye model are observed for A15 type compounds based on Cr and Mo. As illustrated in Fig. 6.4, Cr₃Si shows a strong low temperature hardening with $\Delta\theta_D$ (65K-0K) = 90 K, while Mo₃Si exhibits $\theta_D = 155$ K. The variation of $\theta_D(T)$ for other Mo based compounds is reproduced in Fig. 6.7, where data on Mo₃Os, Mo_{0.75}Os_{0.20}Ir_{0.05}, Mo_{0.78}Ir_{0.22} (Flükiger et al. /63/) Mo_{0.40}Tc_{0.60} (Stewart and Giorgi /279/) and Cr_{0.72}Os_{0.28} (Flükiger et al. /63, 223/) are shown. It appears that going from B = Tc to Ir leads to higher values of $\theta_D(0)$ (350, 400 and 418 K, respectively) and of $\Delta\theta_D$ (> 80, 120 and 150 K, respectively). In the case of Mo₃Os, two different anneals at 1800°C and at 1050°C caused an increase of T_C by 0.6 K (from 11.85 to 12.45 K) but no change on the $\theta_D(T)$ curve (See also Fig. 4.6 showing no change of the C/T curve above T_C for two different heat treatments). The curve for Mo_{0.80}Pt_{0.20} (with a slight content of second phase) has not been measured at temperatures high enough for being compared with the other systems, but the general trend is the same.

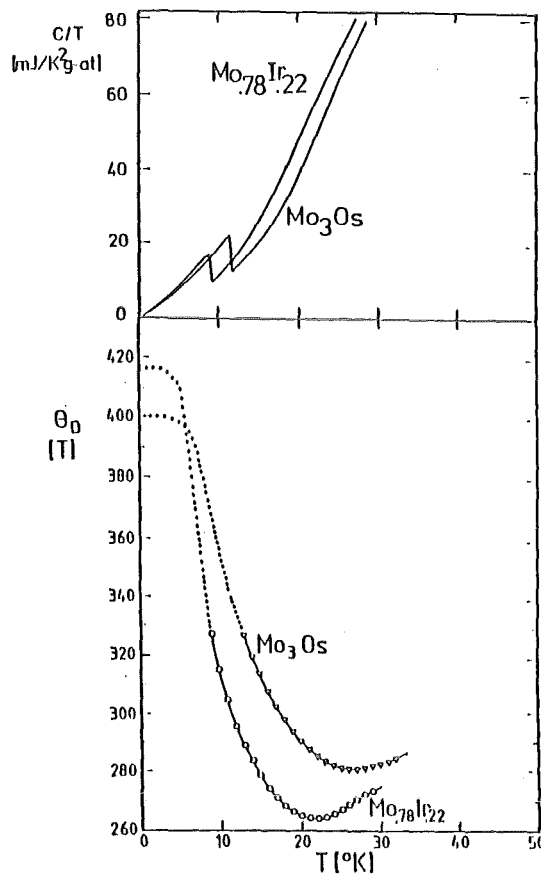


Fig. 6.7 Variation of the Debye temperatures for various Mo based A15 type compounds: Mo₃Os (10 h/1800°C), Mo_{0.75}Os_{0.20}Ir_{0.05} (6 1/2 h/1800°C), Mo_{0.78}Ir_{0.22} (7 h/1800°C) Mo_{0.80}Pt_{0.20} (3 h/1500°C) and Cr_{0.72}Os_{0.28} (Flükiger et al. /63/) and Mo_{0.40}Tc_{0.60} (Stewart and Giorgi /279/). The corresponding C/T curves of Mo₃Os and Mo_{0.78}Ir_{0.22} shown in the upper figure show the excess specific heat leading to the peculiar behavior of $\theta_D(T)$ /63/.

A comparison between Figs. 6.4, 6.5, 6.6 and 6.7 shows that the behavior of $\theta_D(T)$ for Mo_3B and Cr_3B A15 type compounds is the same regardless if B is a transition or a nontransition element. This is in contrast to V and Nb based systems and is just a further illustration of the antagonism between these two classes of compounds.

b) $\Delta\theta_D(300K \rightarrow 0)$ From Calorimetry and X Ray Diffractometry. As mentioned above, the value of $\theta_D(0)$ is of primary interest in most specific heat works, the variation of the Debye temperature being rarely discussed. A way to get an approximate idea of the change of $\theta_D(T)$ between 300 and 0 K consists in comparing the values $\theta_X(300K)$ derived from diffractometric measurements listed in Tables 6.3 and 6.4 and the values $\theta_D(0)$ obtained by calorimetry. This procedure is justified by the good agreement between the values $\theta_X(300K)$ and $\theta_D(300K)$ mentioned earlier in this work. The difference $\Delta\theta_D(300K \rightarrow 0) = \theta_X(300K) - \theta_D(0)$ is plotted in Fig. 6.8, which allows some very interesting conclusions about the vibrational behavior of A15 type compounds below 300 K.

These conclusions are still valid in spite of the complex behavior of $\theta_D(T)$ showing a minimum lying below both values, $\theta_D(0)$ and $\theta_D(300 K)$:

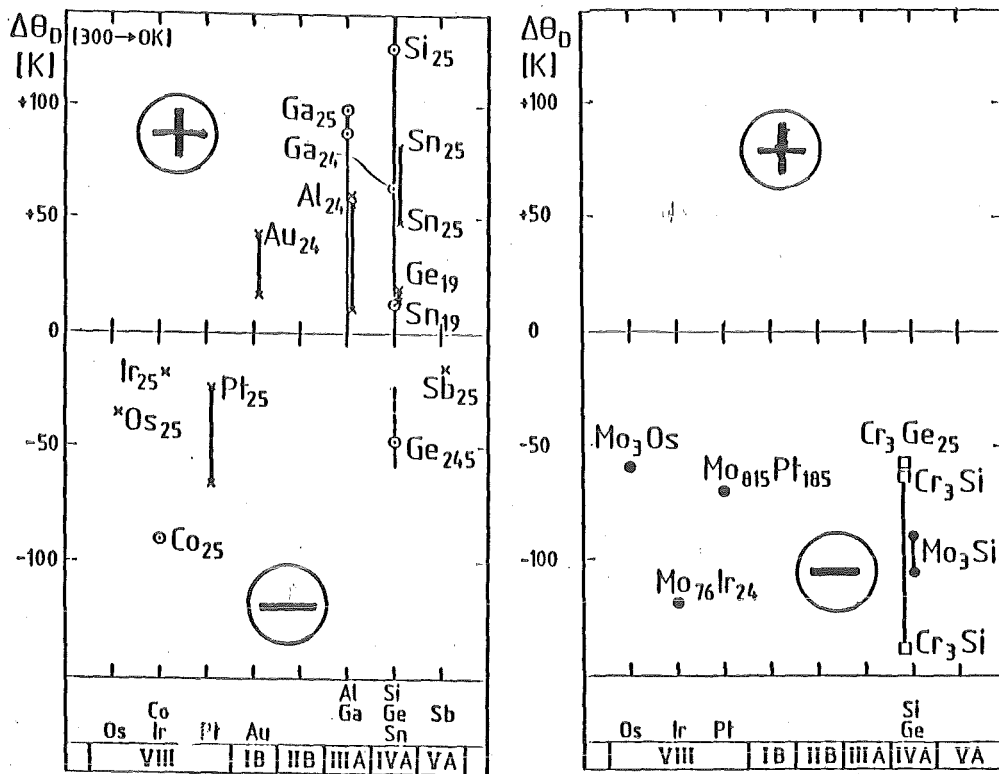


Fig. 6.8. Variation of the Debye temperature between 300 and 0 K (expressed by $\Delta\theta_D(300K \rightarrow 0)$) for various A15 type systems. The values at 300K were determined by diffractometry, those at 0 K were extrapolated from calorimetric data (see Tables 6.3 and 6.4). (a) : Nb and V based systems, show positive $\Delta\theta_D$ for $\gamma > 8 \text{ mJ/K}^2 \text{ at-g}$ and negative $\Delta\theta_D$ for $\gamma < 8 \text{ mJ/K}^2 \text{ at-g}$, (b) : Mo and Cr based systems, exhibit negative $\Delta\theta_D$ values only.

- The A15 type compounds based on V and Nb with $\gamma > 8 \text{ mJ/K}^2\text{at-g}$ all show a positive difference $\Delta\theta_D(300\rightarrow 0\text{K})$, reflecting phonon softening. This difference reaches up to 180 K for V_3Si and decreases in the sequence $\text{V}_3\text{Si} \rightarrow \text{Nb}_3\text{Sn} \rightarrow \text{V}_3\text{Ga} \rightarrow \text{Nb}_{.76}\text{Ga}_{.24} \rightarrow \text{Nb}_{.76}\text{Al}_{.24} \rightarrow \text{Nb}_{.736}\text{Au}_{.234} \rightarrow \text{Nb}_{.82}\text{Ge}_{.18} \rightarrow \text{V}_{.81}\text{Sn}_{.19}$. This behavior was known for V_3Si and Nb_3Sn after having been observed by elastic measurements /219/, calorimetry /222,229/ and neutron scattering /237/. It is reported here for the first time for the compounds $\text{Nb}_{.76}\text{Ga}_{.24}$, $\text{Nb}_{.76}\text{Al}_{.24}$ and $\text{Nb}_{.764}\text{Au}_{.236}$ and for Cr and Mo based A15 type compounds. The relatively small, but positive variation for the systems $\text{Nb}_{.81}\text{Ge}_{.19}$ and $\text{V}_{.81}\text{Sn}_{.19}$ is not surprising, due to the strong deviation from stoichiometry which enhances $\theta_D(0)$ (see next paragraph). The small value of $\Delta\theta_D$ for $\text{V}_{.81}\text{Sn}_{.19}$ confirms the calorimetric data of Knapp et al. /222/. It is expected that $\Delta\theta_D$ would be larger in the three Nb based systems with B = Ga, Al and Au if their composition would be closer to stoichiometry. Figure 6.8 shows very clearly that the high T_c and high γ compounds based on V and Nb are the only ones where phonon softening has so far been observed, thus illustrating the strong connection with the high electronic density of states.
- The negative difference $\Delta\theta_D$ for both $\text{V}_{.755}\text{Ge}_{.245}$ and $\text{V}_{.75}\text{Sb}_{.25}$ confirms the data of Rosen et al. /256/ and Knapp et al. /222/ (see Fig. 6.4). The large negative value for $\text{V}_{.755}\text{Ge}_{.245}$ may partly be due to the uncertainty in determining $\theta_X(300\text{K})$. Indeed, the own refinement (see Table 5.8) was performed with fixed U^2 , while Kodess /242/ reported only the values U_{11}^2 and U_{22}^2 , but not U^2 . In Table 6.3, θ_X was calculated assuming that U_b^2 would be equal to the average $1/3(2U_{11}^2 + U_{22}^2)$. From Fig. 6.1, however, it can be estimated that U_b^2 should be smaller than the average over the vibration amplitudes on the 6c sites. This would raise the value of $\theta_X(300\text{K})$ and thus reduce the difference $\Delta\theta_D(300\text{K}\rightarrow 0)$, which would nevertheless remain negative.
- All V and Nb based A15 type compounds with transition B elements show negative values of $\Delta\theta_D$, the fluctuation for Nb_3Pt reflecting the uncertainty in determining U^2 for this compound.
- All Cr and Mo based A15 type compounds show a strongly negative difference $\Delta\theta_D$, regardless if B is a transition or a nontransition element, thus reflecting phonon hardening at low temperature, i.e. the behavior common to "normal" compounds. These results confirm the observations of Surikov et al. /229/ on Cr_3Ge and Cr_3Si , Mirmelshteyn et al. /158/ on Mo_3Si and Flükiger et al. /63/

on Mo_3Os and $\text{Mo}_{.78}\text{Ir}_{.22}$ (the latter only up to 35 K) by means of calorimetric measurements (see Figs. 6.4 and 6.7).

The analysis of Fig. 6.8 allows to make a simple distinction between A15 type compounds with different vibrational behavior at low temperatures (except Ti_3B and Zr_3B for which no $\theta_D(300\text{K})$ values are available):

Softening: $\Delta\theta_D(300 \rightarrow 0\text{K}) > 0$: All Nb and V based compounds with nontransition B elements and $\gamma > 8 \text{ mJ/K}^2\text{at-g}$ (probably also Ti_3Ir) and

Hardening: $\Delta\theta_D(300 \rightarrow 0\text{K}) < 0$: All Nb and V based compounds with transition B elements ($\gamma < 8 \text{ mJ/K}^2\text{at-g}$),
All Cr and Mo based compounds with transition or nontransition B elements (independent on γ , which lies below 8.5 and 5.5 $\text{mJ/K}^2\text{at-g}$, respectively)

The cases of Nb_3Pt and V_3Ge in Fig. 6.8 are particularly interesting. Both compounds are known to undergo considerable enhancements of T_c , by $\sim 2 \text{ K /82/}$ and $\sim 4 \text{ K /62/}$, respectively. Originally, this increase was attributed uniquely to compositional effects, but a more detailed comparison shows that this explanation alone cannot take into account for the strong initial change of T_c reported in these pseudobinary compounds. In the light of Fig. 6.8, a new qualitative explanation can be proposed for the strong initial increase of T_c in the pseudobinary systems $\text{V}_3(\text{Ge}_{1-x}\text{Al}_x)$ and $\text{V}_3(\text{Ge}_{1-x}\text{Ga}_x)$ (both plotted in Ref. 7) after substitution of Ge by the elements Al and Ga. It appears that this initial enhancement could also be the consequence of a transition of $\Delta\theta_D$ from negative to positive values with substitution, reflecting a reduction of the low temperature hardening observed in V_3Ge /256/, Fig. 6.8/.

6.1.5. Effect of Composition and Ordering on the Debye Temperature

The values of the Debye temperature at 300 K plotted in Fig. 6.2 have been correlated with the vibrational behavior of the B constituents in A_3B series and are in some way connected with the high temperature stability of A15 type compounds. Due to the strong changes of $\theta_D(T)$ between 300 K and $T \rightarrow 0$, it is clear that $\theta_D(0)$ does not have the same meaning for stability considerations. Nevertheless, it is interesting to establish the plot $\theta_D(0)$ vs. electron number in analogy to Fig. 6.2, the number of measured values of $\theta_D(0)$ being con-

siderably higher and the precision being better than for $\theta_D(300K)$. This is realized in Fig. 6.9.

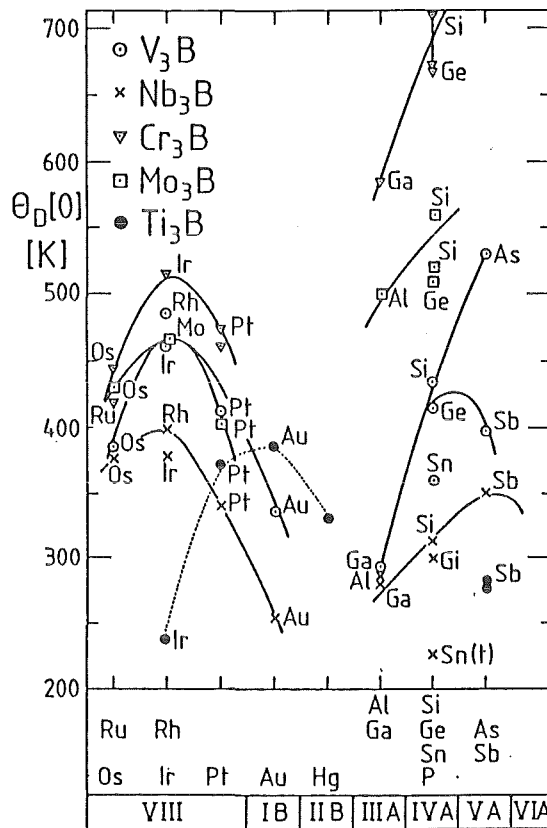


Fig. 6.9. Debye temperatures $\theta_D(0)$ derived from low temperature specific heat measurements for various A15 type compounds. The references are listed in Tables 6.3 and 6.4. The value for the metastable V_3Al , $\theta_D(0) = 280 \pm 20$ K, has been extrapolated from $V_3B_{1-x}Al_x$ series (see Fig. 6.10), while the value for metastable Nb_3Si , 310 ± 40 K, was measured by Stewart et al. /277/ on explosively compressed samples.

Compared to the Debye temperatures at 300 K, the variations of $\theta_D(0)$ are much more structured, the difference between the highest and lowest values being considerably increased. As an example, the difference between Nb_3Au and Nb_3Ir at 300 K is close to 70 K, compared to 125 K for $\Delta\theta_D$ at 0 K. The decrease of the Debye temperature at both sides of the "Instability Region" is much more pronounced than at 300 K, as illustrated by the systems V_3Ga and V_3Ge , where $\theta_D(0)$ is now close to 300 K. The $\theta_D(0)$ values for Ti_3B series are also included in Fig. 6.9, showing the fundamentally different behavior to A_3B series with $A = Cr, Mo,$

V and Nb. As mentioned above, there is no "Instability Region" for Ti based A15 type compounds. At B = Ir, where a maximum of $\theta_D(0)$ is observed in all other series, Ti_3Ir exhibits a minimum, which is even the smallest Debye temperature reported so far in A15 type compounds. The stability of the compound Ti_3Hg is correlated to a relatively high Debye temperature, $\theta_D(0) = 330$ K /207/, while values well below 250 K would be expected for the corresponding hypothetical compounds Nb_3Hg or V_3Hg .

The effect of varying the A atom on the Debye temperature of the corresponding A15 type compound can be clearly deduced from Fig. 6.9, when comparing the $\theta_D(0)$ values for compounds with the same B element. It follows that the Debye temperatures decrease in the sequence $Cr \rightarrow Mo \rightarrow V \rightarrow Nb$ for both, transition and nontransition B elements. The difference is particularly high for B = Si, where $\Delta\theta_D$ between Cr_3Si and Nb_3Si /277/ is equal to 400 K. For transition B elements, the effect of changing the A element is considerably smaller, the difference between Cr_3Ir and Nb_3Ir being only 71 K.

After having discussed the variation of $\theta_D(0)$ for various A15 type compounds, the question arises how this quantity may vary in a given compound, but for different compositions and at different degrees of atomic ordering. The effect of disordering by quenching or irradiation procedures, already treated for selected compounds in Sect. 4, is summarized in Table 6.5. It is seen that for small ordering changes the effects on $\theta_D(0)$ are quite small, a comparison thus requiring quite precise values. The error in $\theta_D(0)$ as determined by calorimetry can be estimated to below 10 K at the present day /248,278/.

a) Ordering Effects on $\theta_D(0)$

A very important remark concerning the effect of atomic ordering on $\theta_D(T)$ was made when discussing different states of Nb_3Al (see Fig. 6.5). Indeed, the difference in $\theta_D(T)$ between quenched and reannealed Nb_3Al samples mainly resides at the lowest temperatures, $\Delta\theta_D(T)$ vanishing at $T > 40$ K /248/. This means that the vibrational behavior in Nb_3Al above this temperature is nearly unaffected by a change of the order parameter of $\sim 1\%$ (from $S_a = 0.95 \pm 0.02$ to 0.94 ± 0.02 , as estimated from the change in T_c from Refs. 28 and 53). This is obviously not longer the case for larger changes of the order parameter, as shown for Mo_3Si in Fig. 6.4.

Compound	Treatment [hours/°C]	T _c [K]	γ [mJ/K ² at-g]	θ _D (0) [K]	S (or S _a)	$\frac{\Delta\theta_D(0)}{\Delta S}$ [K/7S]	Ref.
V _{0.76} Au _{0.24}	Arc Melted 200/600	2.87	9.03	342	0.86	2	276
		0.8	13.1	332	0.93		276
V _{0.75} Ga _{0.25}	1250, Q Q+ 300/610	13.5	19.9	310	0.98	6	97
		15.1	24.0	297	0.96		97
V _{0.75} Si _{0.25}	Arc Melted 2.22x10 ¹⁸ n/cm ²	17.03	<T _m 13.2 >T _m 14.7	29.7	1.0	15	276
		6.8	5.3	454	(0.90) ^b		276
							117
Nb _{0.75} Sn	1500°C/Sint.	17.97	12.2	232	1.0 ^c	4	276
		17.93	14.3	232	1.0 ^c		276
	Sintered 1x10 ¹⁹ n/cm ²	17.9	12-14 ^a	268 ^a	1.0 ^c		160
		12.0	8-10 ^a	287 ^a	(0.88)		160
Nb ₃ Al (β ~ 0.24)	120/750 1.3x10 ¹⁹ n/cm ² 2.6x10 ¹⁹ n/cm ²	18.7	9.0	272	0.96 ^d	6	114
		9.6	4.25	325	(0.84) ^d		114
		7.0	-	376	(0.79) ^d		114
Nb ₃ Al (β ~ 0.25)	1040, Q Q+1344/750	16.84	9.41	328	(0.94) ^e	16	248
		18.45	11.24	296	(0.96) ^e		248
Nb ₃ Pt	48/1450, Q 200/800	8.81	5.74	-376	(0.92) ^f	5	276
		10.03	6.17	-348	(0.98) ^f		276
Nb _{0.75} Pt _{0.15} Au _{0.10}	48/1450 200/750	11.45	7.48	316	-	-	276
		12.88	8.38	320	-	-	276
Nb _{0.75} Pt _{0.075} /Au _{0.175}	48/1450 200/750	11.52	8.40	305	-	-	276
		12.85	10.14	290	-	-	266
Mo ₃ Os	10/1800 144/1050	11.85	5.20	430	0.81	2	63
		12.45	5.21	420	0.87		63
Mo _{0.76} Ir _{0.24}	12/1800 120/1180	8.12	5.48	469	0.82	3	63
		8.40	5.34	452	0.87		63
Mo _{0.751} Ge _{0.249}	16/1600 2.2x10 ¹⁹ n/cm ²	1.45	1.22	392	(1.0)	-5	153
		4.25	1.35	322	(0.85)		153
Mo _{0.775} Si _{0.25}	1x10 ²⁰ n/cm ² + 350 °C + 450 °C + 550 °C + 650 °C 100/1100	6.00	2.53	330	(0.35)	-5	158
		5.66	2.55	342	(0.35)		
		3.58	2.40	420	(0.62)		
		2.90	2.38	444	(0.71)		
		2.13	2.14	500	(0.75)		
		1.56	2.44	560	(0.80)		

Table 6.5. Variation of T_c, γ and θ_D(0) in various Al5 type compounds at different states of ordering, induced either by quenching or by high energy irradiation. Q = Argon jet quenched. ^a) Values estimated from specific heat data above T_c, ^b) S from Ref. 78. ^c) S from Ref.9, ^d) S from Ref. 53, corrected following Ref. 28, ^e) Estimated from the T_c vs. S_a dependence in Ref. 53, ^f) For the values of S see Fig 4.12.

In order to get an idea how θ_D(0) varies with the degree of atomic ordering, the order parameter values S (or S_a for nonstoichiometric samples) have also been included in Table 6.5. However, the order parameters have not in all cases been determined on the same samples on which the calorimetric measurements were performed. The missing S (or S_a) values were thus estimated from other in-

vestigations, using the T_C values as a reference. This was the case for V_3Si ($S \approx 0.90$ for $T_C = 6.8$ K /78/), Nb_3Sn ($S \approx 0.85$ for $T_C = 12.0$ K /239/), $Nb_{.76}Al_{.24}$ ($S_a \approx 0.96$ for $T_C = 18.7$ K, $S_a \approx 0.84$ for $T_C = 9.6$ K and $S_a \approx 0.79$ for $T_C = 7.0$, as derived from the data of Sweedler et al. /53/ after the correction indicated in Ref. 28), Mo_3Ge ($S \approx 1$ for $T_C = 1.45$ K and $S \approx 0.85$ for $T_C = 4.25$ K /239/). The original order parameter for Mo_3Si /158/ are somewhat lower than own values (see Table 5.12), but the relative change is more important than the absolute values for the present considerations.

The data in Table 6.5 have been used for determining $\Delta\theta_D(0)/\Delta S$, the effect of the change of S by 1 % on $\theta_D(0)$. When discussing this ratio, it has to be taken into account that the relative error may be considerable, the small differences $\Delta\theta_D(0)$ and ΔS being in some cases of the order of the error, e.g. in the systems $V_{.76}Au_{.24}$, V_3Ga , $Nb_{.75}Al_{.25}$, Mo_3Os and $Mo_{.76}Ir_{.24}$. Nevertheless, it can be concluded that

- in V and Nb based systems, $\theta_D(0)$ increases by 4 to 6 K when S decreases by 1 %, and
- in the systems Mo_3Si and Mo_3Ge , $\theta_D(0)$ decreases by 5 K when S decreases by 1 %.

b) Compositional Effects on $\theta_D(0)$. The variation of $\theta_D(0)$ with atomic composition can be estimated from the data listed in Table 6.6. In analogy to the ordering effects, composition is expected to act in a complex manner on the vibrational characteristics of each compound. Nevertheless, a general trend can be recognized:

- For all known A15 type compounds, a minimum of $\theta_D(0)$ is always observed at the stoichiometric composition, leading to positive values of $\Delta\theta_D(0)/\beta$ for $\beta \leq 0.25$ and to negative values at $\beta > 0.25$. (The only exception, Mo-Ge, contained more than 10 % additional phase, Mo_5Ge_3 , which could have influenced the result).
- The individual change of $\Delta\theta_D(0)/\beta$ is, however, very different from compound to compound. In particular, no correlation with the relative atomic mass can be recognized. Within the uncertainties due to measuring errors the high T_C , V and Nb based A15 type compounds are found to exhibit ratios between +8 and +18. The excessively high value of the ratio $\Delta\theta_D(0)/\beta$ for V_3Si and

Compound	T_c [K]	γ_2 [mJ/K ² at-g]	$\theta_D(0)$ [K]	$\Delta\theta_D(0)/\beta$ [K/at. %]	Ref.
Nb _{0.75} Sn _{0.25}	18.0	12.8	232	+33	276
Nb _{0.78} Sn _{0.22}	6.27	4.85	331		
Nb _{0.80} Sn _{0.20}	8.0	6.0	305		

Nb _{0.75} Ge _{0.25}	21.8	7.6	302	+18 [∇]	227
Nb _{0.75} Ge _{0.25}	6.25	3.82	360		
Nb _{0.80} Ge _{0.20}					

Nb _{0.75} Ga _{0.25}	19.8	11.5	280	+15 [∇]	227
Nb _{0.81} Ga _{0.19}	9.9	5.34	341		

Nb _{0.75} Pt _{0.25}	8.9	5.55	339	+4	276
Nb _{0.80} Pt _{0.20}	3.2	3.57	358		

Nb _{0.775} Ir _{0.225}	0.3	1.81	374	-0	62
Nb _{0.75} Ir _{0.25}	1.6	2.05	377		
Nb _{0.72} Ir _{0.28}	2.85	2.63	362		

Nb _{0.75} Os _{0.25}	0.96	2.34	378	-1	122
Nb _{0.725} Os _{0.275}	0.3	2.04	374		

V _{0.75} Si _{0.25}	16.9	12.7	297	+48 ^a	276
V _{0.76} Si _{0.24}	15.1	13.9	345		
V _{0.80} Si _{0.20}	9.4	9.0	475		

V _{0.78} Ga _{0.22}	9.8	13.3	326	+10	30, 64
V _{0.65} Ga _{0.25}	15.0	24.22	297		
V _{0.73} Ga _{0.27}	12.6	16.9	310		
V _{0.68} Ga _{0.32}	4.2	6.7	363		

V _{0.778} Pt _{0.222}	0.98	5.15	475	+24	122
V _{0.75} Pt _{0.25}	2.88	7.19	403		
V _{0.72} Pt _{0.28}	1.50	6.32	471		

V _{0.75} Ir _{0.25}	<0.0115	1.97	445	-5	276
V _{0.69} Ir _{0.31}	0.91	3.67	414		
V _{0.63} Ir _{0.37}	1.71	4.34	395		

Mo _{0.734} Ge _{0.266}	1.48	1.85	510	-12	63
Mo _{0.762} Ge _{0.238}	1.68	1.92	476		

Mo _{0.76} Ir _{0.24}	8.12	5.34	452	+8	63
Mo _{0.78} Ir _{0.22}	8.4	5.70	467		

Cr _{0.75} Ir _{0.25}	0.17	8.67	449	+8	223
Cr _{0.835} Ir _{0.165}	0.77	6.72	515		

Cr _{0.79} Pt _{0.21}	<0.015	8.57	402	+28	223
Cr _{0.815} Pt _{0.185}	<1.20	7.64	473		

Cr _{0.75} Si _{0.25}	<0.015	2.57	670	+9	223
Cr _{0.75} Si _{0.25}	<0.015	2.75	720		
Cr _{0.821} Si _{0.179}	<1.20	2.81	740		

Table 6.6. Variation of T_c , γ and $\theta_D(0)$ in various A15 type compounds at different compositions. [∇]In spite of the indicated nominal composition, the compounds Nb_{0.75}Ge_{0.25} and Nb_{0.75}Ga_{0.25} in Ref. 227 are in reality nonstoichiometric, their average Ge or Ga content lying between 23 and 24 at. %.

Nb_3Sn may be connected to the peculiar properties of these compounds. It is remarkable that the Nb based compounds with transition B elements as well as V_3Ir exhibit smaller ratios, lying below 5 K/at. %. The high ratio for the V-Pt system may be due to uncertainties of $\theta_D(T)$ for the stoichiometric sample for which Spitzli et al. /122/ previously reported a markedly higher $\theta_D(0)$ value, 411 K.

c) Extrapolation of $\theta_D(0)$ for Metastable Stoichiometric Nb_3Au and V_3Au .

It is possible to estimate the value of $\theta_D(0)$ for the metastable perfectly ordered and stoichiometric modification of the systems Nb_3Au and V_3Au . Nb_3Au and V_3Au are nonstoichiometric, with $\beta = 0.236$ /7.31/ and 0.24 /18/, respectively. In addition, both show deviations from perfect ordering, with $S_a = 0.96$ /62, 162, 192/ and $S_a = 0.94$ /18/, respectively (see Tables 5.4 and 5.9). When approaching stoichiometry, the rates indicated in Table 6.6 for V_3Ga , Nb_3Ge or Nb_3Ga suggest a decrease of $\theta_D(T)$ in Nb_3Au and V_3Au by ~ 16 and 10 K, respectively. An additional decrease of $\theta_D(0)$ by ~ 20 and ~ 30 K, respectively, would be expected when reaching perfect ordering, thus resulting in hypothetical $\theta_D(0)$ values of ~ 215 K for Nb_3Au and ~ 290 K for V_3Au . The higher $\theta_D(0)$ value for V_3Au with respect to Nb_3Au follows the general tendency shown in Fig. 6.9, where V based A15 type compounds exhibits higher $\theta_D(0)$ values than those based on Nb. A look into Fig. 6.6 shows that such low $\theta_D(0)$ values would lead to the vanishing of the low temperature hardening: like for V_3Ga , V_3Si and Nb_3Sn , phonon softening only would be expected to occur in Nb_3Au and V_3Au . This estimation confirms the statement /7/ that Au has to be considered as a nontransition element in the A15 structure.

V_3Al . Another interesting case is the metastable compound V_3Al , which can only be prepared by nonequilibrium methods, e.g. sputtering, coevaporation (Hart-sough and Hammond /280/, /281/). The pseudobinary series $V_3B_{1-x}Al_x$ with $B = As, Au, Ga, Ge, Sb, Si, Sn$ have been prepared by several authors in order to extrapolate the superconducting properties of this compound (62, 280, 282 - 285). The question of interest is here whether the metastability of V_3Al is connected with a particularly low value of $\theta_D(0)$. Flükiger /62/ and Spitzli and Flükiger /195/ have undertaken a specific heat study on a series of pseudobinary $V_3B_{1-x}Al_x$ alloys and have extrapolated the following values for metastable V_3Al : $a = 0.4840 \pm 0.0005$ nm, $T_c = 17 \pm 1$ K, $\gamma = 17 \pm 1$ mJ/K² at-g and $\theta_D(0) = 280 \pm 20$ K. The extrapolation of $\theta_D(0)$ for $V_3B_{1-x}Al_x$ is shown in Fig. 6.10.

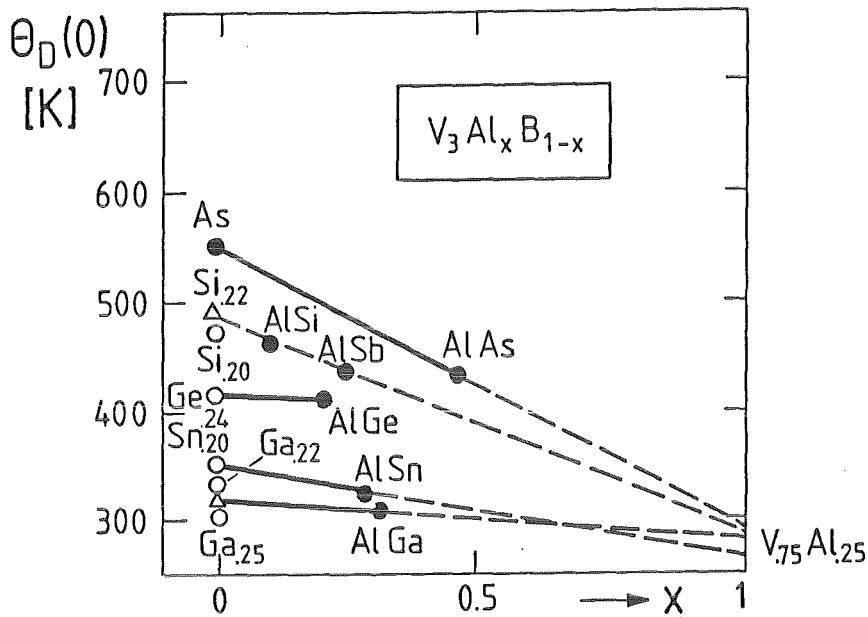


Fig. 6.10. Extrapolation of $\theta_D(0)$ for metastable V_3Al , from $V_3B_{1-x}Al_x$ series yielding $\theta_D(0) = 280 \pm 20$ K (Flükiger /62/, Spitzli and Flükiger /195/)

There is some doubt whether these values really correspond to stoichiometric V_3Al : in the original work, Flükiger /62/ had concluded that they would correspond to the composition $\beta = 0.23$. Meanwhile, it appears that his picture has to be corrected towards $\beta \geq 0.24$. Nevertheless, it results that stoichiometric V_3Al would exhibit the lowest $\theta_D(0)$ value (and probably also $\theta_D(300\text{ K})$ value) among all V based A15 type compounds known so far. It is interesting to compare the metastable V_3Al with the metastable compound Nb_3Si , which has been produced by explosive compression, starting from the stable tetragonal Ti_3P structure /286/. The reported value of $\theta_D(0)$ for Nb_3Si is 310 K /277/, which is quite low but still higher than that of Nb_3Al or Nb_3Sn (see Fig. 6.9). In contrast to Nb_3Si , where the radius ratio r_A/r_B is too large, leading to an excessive overlapping of the Nb atoms on the chains, the instability of V_3Al is rather due to the particular vibrational behavior. Unfortunately, no U^2 values of any of the $V_3B_{1-x}Al_x$ alloys has been measured. It would have been interesting to know whether U^2 really increases at the solubility limit.

6.1.6. Lattice Vibrations at High Temperatures

All the vibrational data discussed so far were determined at $T \leq 300$ K. It would be interesting to know whether the differences in U^2 observed at 300 K between Nb_3Sn and Nb_3Ir still subsist at high temperature. The only known experimental determination of the isotropic vibrational amplitudes of A15 type compounds at higher temperatures has recently been performed by Flükiger and Isernhagen /162/ on the compounds Nb_3Sn , Nb_3Al , Nb_3Pt and Nb_3Ir . The results of U_{Nb}^2 of Nb_3Sn as a function of temperature are represented in Fig. 6.11. The term U_{Sn}^2 could unfortunately not be determined from the present powder diffraction data with a sufficient precision.

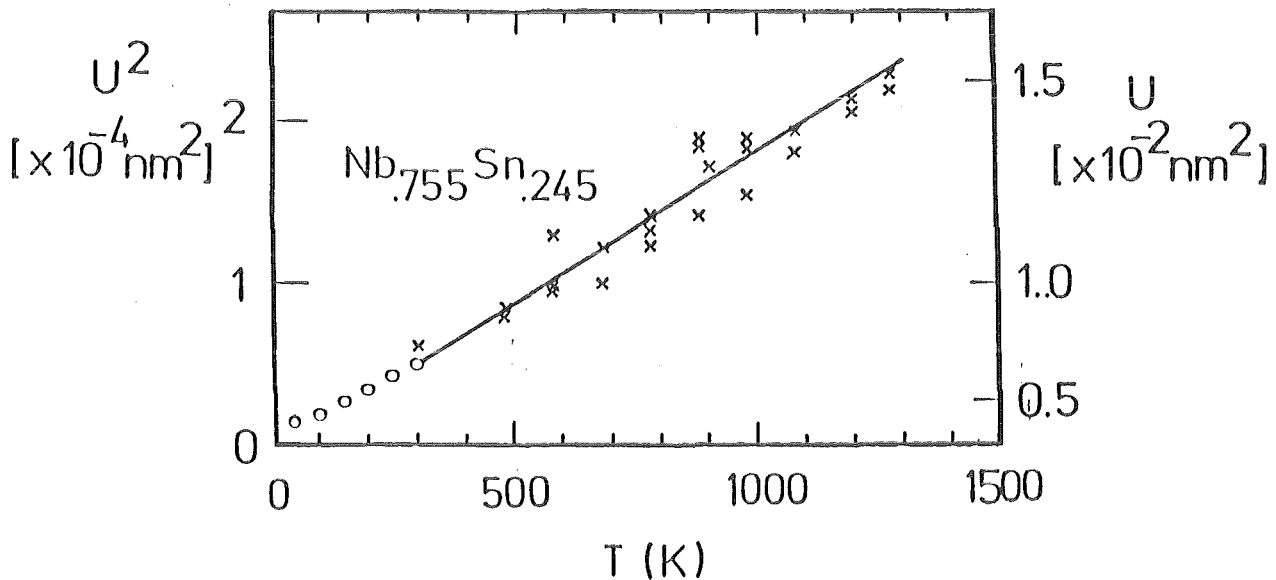


Fig. 6.11. Vibrational amplitudes U_{Nb}^2 for $Nb_{.755}Sn_{.245}$.
 o: low temperature data from Vieland /171/,
 x: powder diffractometry (Flükiger and Isernhagen /162/).

There is no diffraction line where the structure factor depends exclusively on the B atom. In spite of the considerable scattering of the data, an almost linear variation of U_{Nb}^2 with T can be found above 300 K after least-square procedures. It is seen that the above data fit very well with the data of Vieland /171/, obtained on a Nb_3Sn single crystal.

For comparison, the temperature dependence of isotropic vibrational amplitudes for the systems Nb_3Sn , Nb_3Al , Nb_3Pt and Nb_3Ir has been reproduced in Fig. 6.12 /162/. In the case of Nb_3Al two samples with the compositions $\beta = 0.21$ and 0.245 were measured, but no significant differences arising from the different Al contents could be detected. The U_{Nb}^2 values for Nb_3Sn and

Nb_3Al are almost identical over the whole temperature range $300 \leq T \leq 1200$ K, both curves being very close to that of elementary Nb. The values of U_{Nb}^2 for Nb_3Pt and for Nb_3Ir are substantially lower. At 1200 K, U_{Nb}^2 of Nb_3Pt is 12.6 %, the corresponding value of Nb_3Ir even 33 % smaller than that of Nb_3Sn and Nb_3Al . This result shows that the differences between the lattice properties of A15 compounds containing transition or nontransition B elements persist up to very high temperatures, probably up to the melting point.

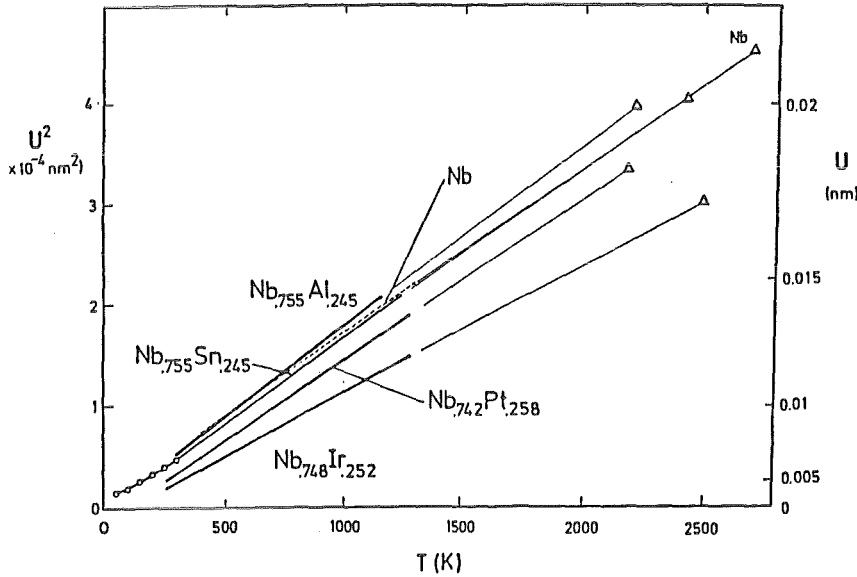


Fig. 6.12. Isotropic vibrational amplitudes, U_{Nb}^2 , for various Nb based A15 type compounds and for elementary Nb up to 1300 K. The values of U_{Nb}^2 at the respective melting points (triangles) are obtained by linear extrapolation (after Flükiger and Isernhagen /162/).

For all examples represented in Fig. 6.12, the r.m.s. amplitude at the melting point, U_M , is of the same order of magnitude, i.e. between $U_M = 0.017$ and 0.0215 nm (Lindemann's law). However, individual differences between the compounds are observed, U_M ranging from 0.0214 nm for Nb_3Al to 0.0176 nm for Nb_3Ir . Thus, the vibrational behavior at the melting point as obtained from extrapolating the r.m.s. amplitudes in Fig. 6.12 can be summarized as follows: U_{Nb} in Nb_3X compounds containing nontransition B elements, e.g. Sn or Al, behaves essentially like in elementary Nb, while it is markedly decreased by the presence of transition B elements as Pt and in particular, Nb_3Ir . The melting instability thus occurs at r.m.s. vibration amplitudes of ~ 0.02 nm. It is interesting that the static displacement amplitudes after irradiation of A15 type compounds reach approximately the same value of u , above which radiation induced phase transformation would occur.

6.1.7. Thermal Expansion in A15 Type Compounds

Although the thermal expansion in A15 type compounds is not expected to be correlated with the degree of ordering, this property will be included in the present discussion, in view of a more complete characterization of this class of compounds. The thermal expansion is the direct consequence of the anharmonicity of the lattice potential. If V_k is the potential energy of the k -th atom in the force field of its neighbouring atoms, V_k can be developed assuming small displacements v from the state of equilibrium.

$$V_k(v) = V_0 + \alpha_1 v^2 - \beta_1 v^3 - \gamma_1 v^4 - \dots \quad (6.2)$$

where the term $-\beta_1 v^3$ represents the asymmetry of the mutual repulsion of the atoms and the term $-\gamma_1 v^4$ represents the general "softening" of the vibration at large amplitudes. The average displacement can be calculated using the Boltzmann distribution function weighing the possible values of v according to their thermodynamic probability. For small displacements (low anharmonic energy) one finds

$$\bar{v} = \frac{3}{4} \frac{\beta_1}{\alpha_1^2} k_B T = \frac{3}{4} \frac{\beta_1}{\alpha_1^2} \bar{E} \quad (6.3)$$

thus giving a constant value for the temperature coefficient of thermal expansion:

$$\frac{d\bar{v}}{dT} = \frac{3}{4} \frac{\beta_1}{\alpha_1^2} k_B = \frac{3}{4} \frac{\beta_1}{\alpha_1^2} \frac{d\bar{E}}{dT} \quad (6.4)$$

Thus, the thermal expansion is smaller for larger harmonic bonding α_1 and for smaller anharmonicity β_1 of the lattice potential. The temperature independence of $d\bar{v}/dT$ and thus of the linear term of the thermal expansion α , arises from the classical assumption $k_B T = \bar{E}$ being the mean energy of the oscillator. Substituting for \bar{E} the energy of a harmonic oscillator in quantum mechanics yields

$$\bar{v} = \frac{3}{4} \frac{\beta_1}{\alpha_1^2} q \frac{\bar{h}\omega q}{\exp(\bar{h}\omega q/k_B T) - 1} \quad (6.5)$$

which meets the condition $\alpha(T) \rightarrow 0$ for $T \rightarrow 0$, which takes into account the observed behavior.

The linear thermal expansion coefficient is defined as

$$\alpha(T) = \frac{1}{a(T)} \left(\frac{da(T)}{dT} \right)_p, \quad (6.6)$$

where a is the lattice parameter.

a) $\alpha(T)$ below 300 K.

The measurements show that at $T < 300$ K α is strongly dependent on temperature. However, different types of behavior are reported for A15 type compounds. Cr_3Si /274/ shows a monotonous decrease of $\alpha(T)$ towards $T \rightarrow 0$ while negative values of α have been reported for V_3Si by Smith et al. /287/, Testardi /219/, Testardi and Bateman /288/ and Försterling and Hegenbarth /274/, V_3Ge by Testardi /219/ und V_3Ga and Nb_3Al by Herold et al. /243/. Fig. 6.13a shows that a minimum of $\alpha(T)$ between 20 and 25 K has been observed in the compounds V_3Si and V_3Ga . For the temperature region between $T = 40$ K and 300 K, Testardi /219/ has found an exponential variation $\alpha(T) \sim \ln T$, which possibly also holds for V_3Ga .

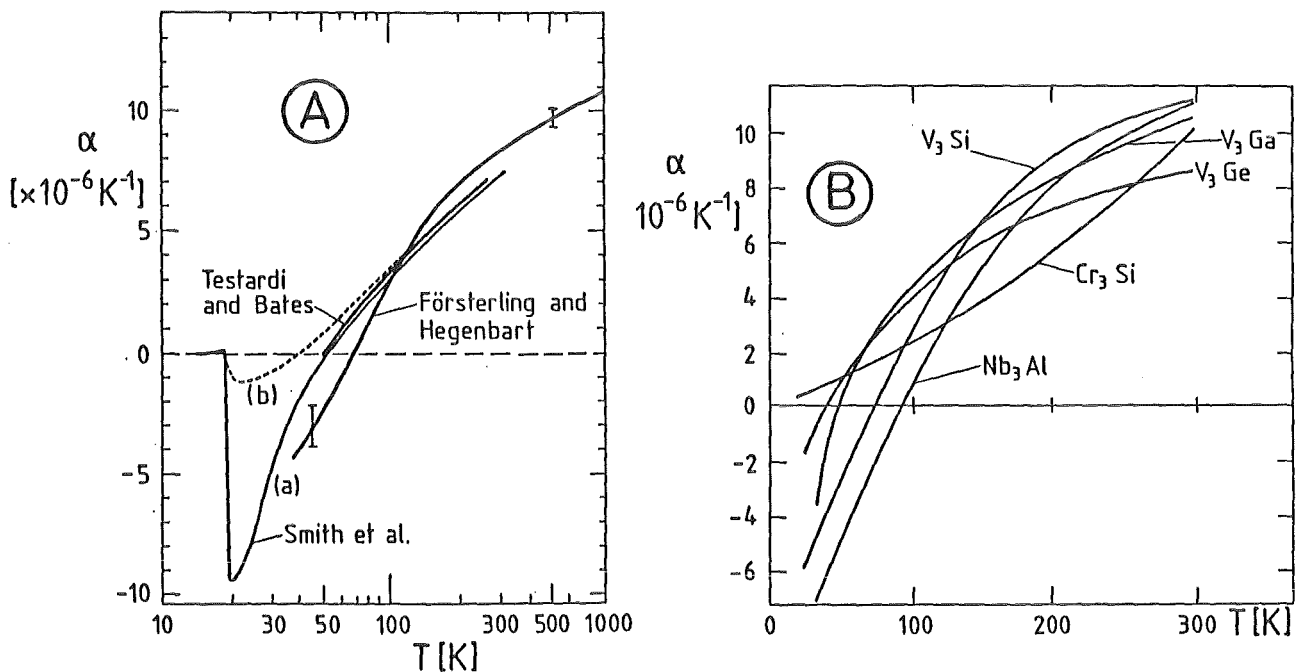


Fig. 6.13. Linear thermal expansion coefficient for various A15 type compounds.
 A) V_3Si (Smith et al. /287/, where (a) stays for $\beta = 0.25$ and (b) for $\beta = 0.227$ (Testardi and Bateman /288/, Försterling and Hegenbarth /274/, note the logarithmic abscissa).
 B) V_3Ge (Testardi /219/), Nb_3Al , V_3Ga , Cr_3Si (Herold et al. /243/).

The question has been raised whether negative $\alpha(T)$ values are an additional feature of the structural instability of high T_c A15 type compounds. Obviously, the occurrence of negative α and a minimum of α in V_3Si would confirm this hypothesis. The cases of V_3Ga , V_3Ge and Nb_3Al , however, are more difficult to answer. In analogy to V_3Si , the minimum of α at 20 K for V_3Ga could mean that this compound is very close to the low temperature instability, which does not occur because of the slight deviation from perfect ordering detected in this compound /20/. The occurrence of negative α values in V_3Ge and Nb_3Al could reflect the particular interaction between A and B elements in the A15 structure, the electronic density of states being high enough, $> 7 \text{ mJ/K}^2\text{at-g}$ for V_3Ge and Nb_3Al . Even in these cases, a negative value of α only occurs for an undisturbed lattice, characterized by perfect ordering and stoichiometry or for lattices approaching these conditions quite closely. This statement is confirmed by the experimental observation that in V_3Si , V_3Ga and Nb_3Al negative α values are not longer observed after the following perturbations:

- i) deviation from stoichiometry, ii) substitution of the A or B atom and
- iii) application of plastic strain.

These perturbations tend to render the lattice stiffer. The absence of negative $\alpha(T)$ values in strained Nb_3Al produced by deforming Nb_3Al cores was reported by Herold et al. /243/ and is represented in Fig. 6.14. These authors found that the temperature dependence of the thermal expansion coefficient is strongly influenced by the state of strain (or of distortion) of the measured sample.

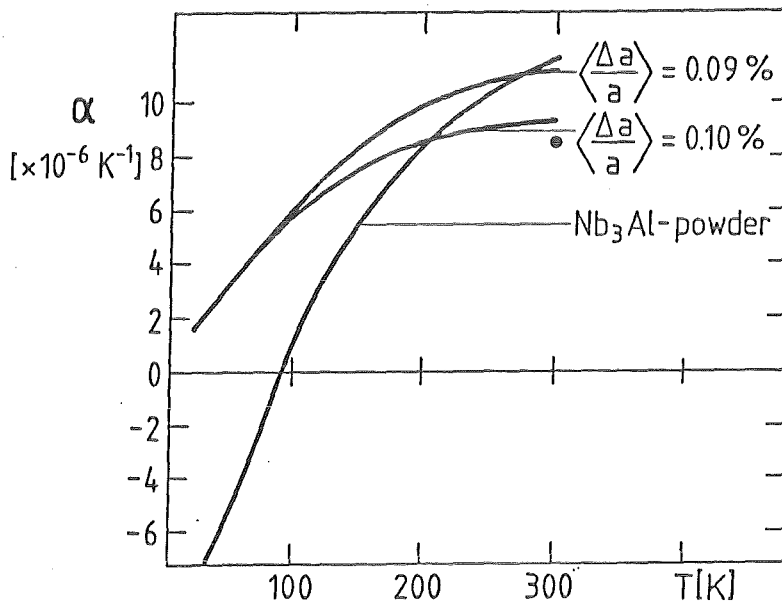


Fig. 6.14. Comparison between the temperature dependence of the thermal expansion coefficients of powdered Nb_3Al and that of Nb_3Al core wires with different lattice distortions $\Delta a/a$ (Herold et al. /243/).

● : $Nb_{.754}Al_{.246}$ (Flükiger and Isernhagen, see Table 6.7).

Fig. 6.14 shows the thermal expansion coefficients of powdered Nb_3Al and of core wires produced from this material. With increasing lattice distortions $\Delta a/a$ the temperature dependence of the thermal expansion coefficient becomes smaller and a negative sign does not appear. The lattice of the Nb_3Al gets stiffer regarding to its thermal expansion. The stiffer state of the lattice should be noticeable in other elastic properties, but measurements of such properties of these samples are not available.

Such a strained state in an A15 type compound can obviously be caused either by deviations from perfect ordering, from stoichiometry or by substituting of A or B elements. It was shown by Smith et al. /287/ that negative values in V_3Si only occur on samples showing small deviations from stoichiometry. The effect of substituting Ge in Nb_3Al combined to deviation from stoichiometry was reported by Herold et al. /243/. At 300 K, α was found to decrease from $11.52 \times 10^{-6} K^{-1}$ for Nb_3Al to $7.16 \times 10^{-6} K^{-1}$ for the nominal alloy $Nb_3Al_{0.5}Ge_{0.5}$ (see Fig. 6.15). A similar decrease of α was observed by substituting Cr for V in V_3Si : α decreased from $11.86 \times 10^{-6} K^{-1}$ to $7.01 \times 10^{-6} K^{-1}$ for $V_{.675}Cr_{.075}Si_{.25}$ /243/.

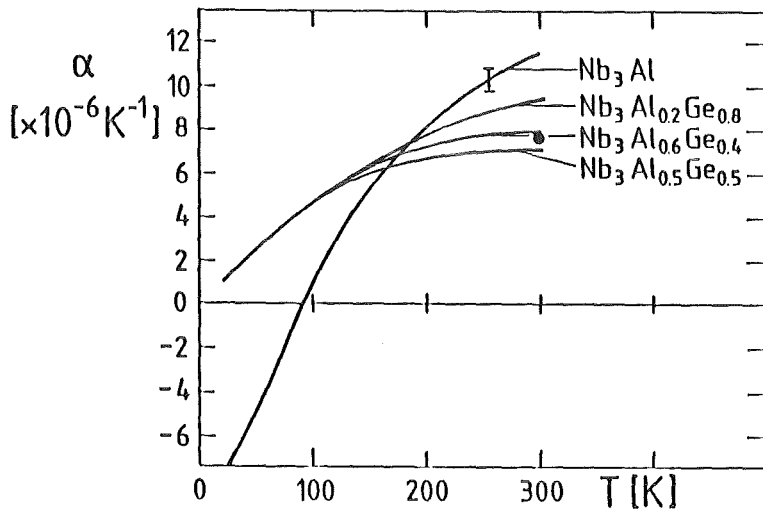


Fig. 6.15. Linear thermal expansion coefficient α for Nb_3Al and $Nb_3Al_{1-x}Ge_x$ alloys (Herold et al. /243/). ●: $Nb_{.75}Ge_{.25}$ (Flükiger and Isernhagen /162/, see Table 6.7).

Assuming that a change of the electron charge distribution takes place through the substitution of foreign atoms and through deviations from the stoichiometric composition, then follows under consideration of the results of Staudenmann /95/ that the anomalous temperature dependence of the thermal expansion coefficients of the high-temperature superconductors is also of an

electronic origin. Therefore, the investigations carried out yield that in addition to other physical properties, e.g. elastic constants (Debye temperature) and magnetic susceptibility also the thermal expansion coefficient of the A15 compounds with high T_C and $N(E_F)$ exhibits an anomalous temperature dependence below 100 K. A direct correlation between negative $\alpha(T)$ values and the occurrence of the low temperature phase transformation could not be confirmed.

b) $\alpha(T)$ above 300 K

The thermal expansion coefficient of a solid can be considered as a measure of the ease with which the amplitude of the thermal vibrations is increased with increasing temperature (Eq. 6.6). A low coefficient α is therefore indicative of strong interatomic forces. A comparison between interatomic forces in A15 type compounds is of interest when considering phase stability.

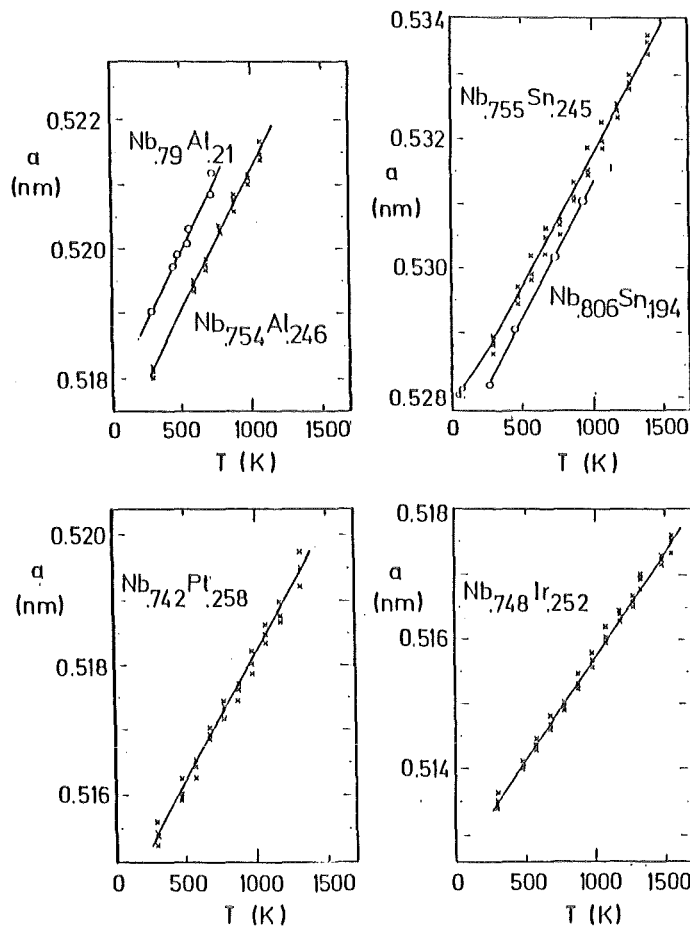


Fig. 6.16. Lattice expansion for the compounds $Nb_{.754}Al_{.246}$, $Nb_{.79}Al_{.21}$, $Nb_{.755}Sn_{.245}$, $Nb_{.806}Sn_{.194}$, $Nb_{.742}Pt_{.258}$ and $Nb_{.748}Ir_{.252}$ (After Flükiger and Isernhagen /162/).

Recent lattice parameter measurements in the systems Nb_3Sn , Nb_3Al , Nb_3Pt , Nb_3Ge and Nb_3Ir by Flükiger and Isernhagen /162/, calibrated against the lattice parameter of Si, are represented in Fig. 6.16. From these data, the value of the linear thermal expansion coefficient α can be determined (see Table 6.7).

In Nb_3Sn , the thermal expansion coefficient was measured for different compositions. The results are indicated in Table 6.7 and show little variation with composition, α values of 7.69 ± 0.11 and $7.81 \pm 0.15 \times 10^{-6} K^{-1}$ being measured for $\beta = 0.245$ and 0.194 .

Systems	α ($10^{-6} K^{-1}$)	T_F^0 (K)	$\frac{dU_{Nb}^2}{dT}$ ($\times 10^{-25} m^2 K^{-1}$)	$\alpha \frac{dU_{Nb}^2}{dT}$ ($\times 10^{-20} m^2$)
$Nb_{.755}Sn_{.245}$	7.69 ± 0.11	2100 ^{a)}	1.74	2.26
$Nb_{.806}Sn_{.194}$	7.81 ± 0.15	2403		
$Nb_{.755}Al_{.245}$	8.61 ± 0.13	2233	1.69	1.96
$Nb_{.79}Al_{.21}$	8.20 ± 0.39	2333	1.80	2.20
$Nb_{.75}Ge_{.25}$ ^{b)}	7.77 ± 0.54	2138		
$Nb_{.742}Pt_{.258}$	7.75 ± 0.19	2180	1.62	2.09
$Nb_{.748}Ir_{.252}$	6.29 ± 0.07	2403	1.33	2.11
Nb	7.03 ^{c)}	2741	1.67	2.28

Table 6.7. Linear thermal coefficient expansion coefficient, α , for various A15 type compounds in the temperature region $300 \leq T \leq 1200$ K and ratio between the derivative dU_{Nb}^2/dT and α . a) The formation temperature of Nb_3Sn at $\beta = 0.245$ is 2100 ± 100 K. b) The measurements were performed on a CVD sample supplied by G. Stewart. c) Values by Conway et al. /290/.

In Nb₃Al, α values of 8.20 ± 0.39 and 8.61 ± 0.13 were measured at compositions β = 0.21 and 0.245, respectively.

A close relationship between the variation of the lattice parameter and of the vibrational amplitude U_{Nb}^2 was found by Flükiger and Isernhagen /162/. As seen in Table 6.7, the ratio $(dU_{\text{Nb}}^2/dT)/\alpha$ is practically constant for all investigated A15 type compounds and is close to the value of Niobium. The situation at high temperature is thus much simpler than at low temperatures, where negative value of α can occur: the change of the lattice parameter is directly proportional to that of the isotropic vibration amplitude U_{Nb}^2 for the Nb atoms:

$$\frac{1}{a} \frac{da}{dT} \sim \frac{dU_{\text{Nb}}^2}{dT} \quad \text{at } T > 300 \text{ K.} \quad (6.7)$$

When comparing the values of α with literature values, a satisfactory agreement is found for Nb₃Sn, where Touloukian et al. /289/, reported $7.2 \times 10^{-6} \text{K}^{-1}$ at 300 K and for Nb₃Ge, where Hull and Newkirk /292/ reported $6.98 \times 10^{-6} \text{K}^{-1}$ at 300 K. There is, nevertheless, a considerable scatter between the values given by different authors. For example, Försterling and Hagenbarth /274/ reported for Nb₃Al α = 11.5 K at 300 K, which is 33 % higher than that in Table 6.7. Reddy and Suryanarayana /292/ reported for Nb₃O_s at 400 K α = $3.6 \times 10^{-6} \text{K}^{-1}$, which is much lower than that of the similar compound Nb₃Ir in Table 6.7. For V₃Si a considerable difference is observed between the value α = $9.3 \times 10^{-6} \text{K}^{-1}$ at 333 K /293/ and α = $7.5 \times 10^{-6} \text{K}^{-1}$ at 303 K /274/. These differences may arise from the different strain states of the powders and from possible contamination by oxygen during the long warming up and measuring times at high temperatures. It is important to note that own results in Table 6.7 have been obtained with a Si reference. Different temperature cycles were performed, showing reproducibility of the results, except for Nb₃Al, which shows a tendency to oxyde /9/.

6.2 Phase Stability and Atomic Ordering

The stable A15 phases cover the entire range of e/a = electron per atom values from 4.0 to 6.8. In particular, the "Instability Region" mentioned in the preceding sections does not correspond to particular e/a values, as shown in Table 6.8.

		B atom								
		VIIB	VIII		IB	IIB	IIIA	IVA	VA	
A atoms	IVB (Ti,Zr)			5.25	5.25-5.4	3.25	3.5	3.75	4.0	4.25
	VB (V,Nb,Ta)	6.5	5.9-6.5	6.25-6.5	6.0-6.5	4.0-4.2		4.4-4.6	4.75	5.0
	VIB (Cr,Mo)		6.5	6.5-6.75	6.5-6.8			5.25	5.5	

Table 6.8. Stable A15 phases A₃B and corresponding e/a values.

6.2.1 The Stability Index of Raynor

In 6.1, a correlation between the degree of ordering and the stability of A15 type compounds was suggested. A way of describing the stability of an inter-metallic phase P_{1-x}^Q_x was proposed by Raynor /213/, who introduced a stability index I_S, defined by

$$I_S = 10^4 \frac{T_F^0}{100 T_p + (T_q - T_p) x'} \quad (6.8)$$

where Q is the higher melting component and T_p and T_q are the melting points of the components in degrees K. T_F⁰ is the formation temperature of the phase of interest and x its mean composition in at. % of the element Q. This is equivalent of expressing the temperature of maximum stability of the phase as a percentage of the characteristic temperature at the composition x above the linear interpolation between the melting points of the components. The factor 10⁴ was introduced in order to obtain values around 100. A compound with I_S > 100 can be considered as being very stable, while a decrease of I_S corresponds to a less stable compound. The variation of I_S for A15 type compounds has been represented

in Fig. 6.17. It follows immediately that the stability is considerably higher for nontransition B elements ($92 \leq I_S \leq 110$) than for transition B elements ($73 \leq I_S \leq 95$).

It is remarkable that just the two compounds where the occurrence of perfect ordering has been experimentally confirmed, i.e. Nb_3Sn and V_3Si , exhibit the highest stability indexes, $I_S > 105$. Other A15 type compounds with very high degrees of ordering, e.g. V_3Ge ($S \approx 1$, see Table 5.8), Cr_3Si ($S \approx 1$, see Table 5.13), Nb_3Ge ($S_a \approx 1$, see remarks in 5.1.1c and Table 5.2), Nb_3Al ($S_a = 0.97$, see Table 5.3), Nb_3Pt ($S = 0.98$, see Table 5.5) and Nb_3Ir ($S = 1$, see Table 5.6) all show I_S values between 95 and 100. The compounds V_3Au and Nb_3Au exhibiting higher deviations from perfect ordering ($S_a = 0.94$ and 0.96 , respectively, see Tables 5.4 and 5.9) in addition to a deviation from stoichiometry are characterized by lower values of I_S , ~ 80 . It is obvious that such a simple correlation can only indicate a tendency and is unable to explain all details, e.g. the difference between Nb_3Al and Nb_3Ge . The general tendency is demonstrated when comparing the variation of I_S (Fig. 6.17) with that of the order parameter, S_a or r'_a (Figs. 5.2 and 5.3).

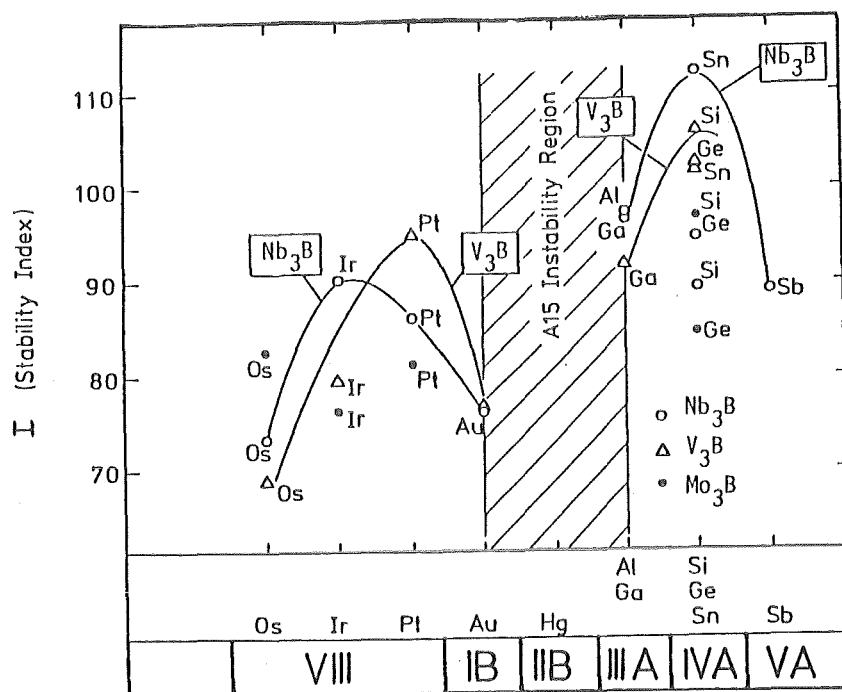


Fig. 6.17. Raynor's stability index, I_S , defined by Eq. (6.8), for some Nb_3B , V_3B , Mo_3B and Cr_3B compounds. For each class of compounds the most stable ones undergo the highest order parameters: Nb_3Sn , V_3Si , V_3Ge , Mo_3Si , Cr_3Si , Note the similarity with Fig. 5.2, where the analogous dependence of S_a is represented.

The stability index as defined by Eq. (6.8) is certainly oversimplified and should contain details like electronegativity and charge transfer /200/ in addition to considerations about the tendency to form at nonstoichiometric compositions. It appears indeed that only very few A15 type compounds are stoichiometric and exhibit perfect atomic ordering: the other ones are stabilized either by a decrease of the order parameter by a deviation from stoichiometry ($\beta > 0.25$ for $B = \text{Re, Os}$), $\beta < 0.25$ for $B = \text{Sb, Ge}$ or both ($B = \text{Au, Al, Ga}$). It should be recalled that considerations about the stability of a given phase are always high temperature considerations in the vicinity of T_F^0 . Nevertheless, they also influence the low temperature properties, i.e. the cubic-tetragonal phase transformation observed in Nb_3Sn or V_3Si . The necessary conditions for the lattice instability in these two compounds, e.g. perfect ordering and stoichiometry, have both their origin in the equilibrium conditions at high temperatures, close to T_F^0 , the A15 formation temperature. As already mentioned, a thermally induced change of the degree of ordering on V and Nb based A15 type compounds mainly occurs for $B = \text{Pt and Au}$ at one side and $B = \text{Al and Ga}$ at the other side of the instability region. The reason why such an instability region exists in V and Nb based as well as in Cr and Mo based A15 type compounds but not for Ti and Zr based compounds (Ti_3Hg , Zr_3Hg are stable) is actually not known.

A question often raised in the past is whether there is a correlation between phase instability and the occurrence of high T_c values. There is actually no general explicit theory correlating these properties, but it can be excluded that the simultaneous occurrence of low temperature instability and high T_c is fortuitous.

For the particular case of A15 type compounds, attempts have been made to establish such a correlation using the model of Labbé and Friedel /259/ which qualitatively describes the particular band structure of Nb_3Sn and V_3Si . In this picture, i.t. lattice instability is understood as a crystal Jahn-Teller effect /259/. A second approach for explaining the lattice instabilities in A15 type compounds is based on the Peierls gap instability (Gor'kov /260/ and Bhatt /261/). Both approaches described here are based on oversimplified assumptions and are thus certainly questionable, but they furnish a strong indication for the influence of the electronic structure on the low temperature lattice instability.

6.2.2. Stability Considerations Based on Machlin's Model

Machlin and Whang /294/ have attempted to calculate the relative stability of a number of binary compounds of the A_3B composition crystallizing in the cubic structures A1, $L1_2$, A2 and A15.

The main results of Machlin's model can be summarized as follows:

- 1) Calculation of the lattice parameter of A15 type compounds within a r.m.s. deviation of 0.4 % with respect to the observed values,
- 2) Calculation of the energies of formation in the 4 above mentioned cubic phases A1, $L1_2$, A2 and A15,
- 3) Calculation of the approximate order parameter in a series of A15 type compounds,
- 4) Verification of the nearly zero value for $(C_{11} - C_{12})/2$ as observed for Nb_3Sn and V_3Si .

As described in 4.3.1d, the "Crystal Field Modified Model" of Machlin assumes oblate spheroids instead of spheres for the electron density distribution associated with the D_{2d} point site symmetry. The physical concept in Machlin's model /294/ is that the repulsive parameter in transition elements arises from the outer sp shell. The repulsive pair potentials taken into account in this model are illustrated in Fig. 6.18, the pairs being $\overline{AA_1}$ (nearest neighbours on a chain), $\overline{AA_2}$ (nearest neighbours on two orthogonal chains) and \overline{AB} (chain atom and nearest B atom) located at the corner and center of the unit cell. (The chain atoms are treated as oblate spheroids). The lattice energy, E , obtained by summing over the interatomic potentials, is found to be a function of two variables: the lattice parameter a and the crystal field parameter $\Delta S_A v'$ (takes into account the screening of nuclear charge for electrons in $||sp$ orbital of A atoms, or more precisely, the excess total screen in $||d$ type orbital over that in $\perp d$ type orbital). By minimizing the lattice energy with respect to both a and $(\Delta S_A v')$, the equilibrium values of the cohesive energy, the lattice parameter and $\Delta S_A v'$ are determined. Besides, the ability of this model to calculate accurate lattice parameter values (< 0.44 % deviation from measured values, see 4.3.1d), two aspects are of interest for the present work, i.e. the

ability to calculate:

- i) the energies of formation for various A15 type compounds and
- ii) the order parameter values in these compounds. These properties will be discussed in the following.

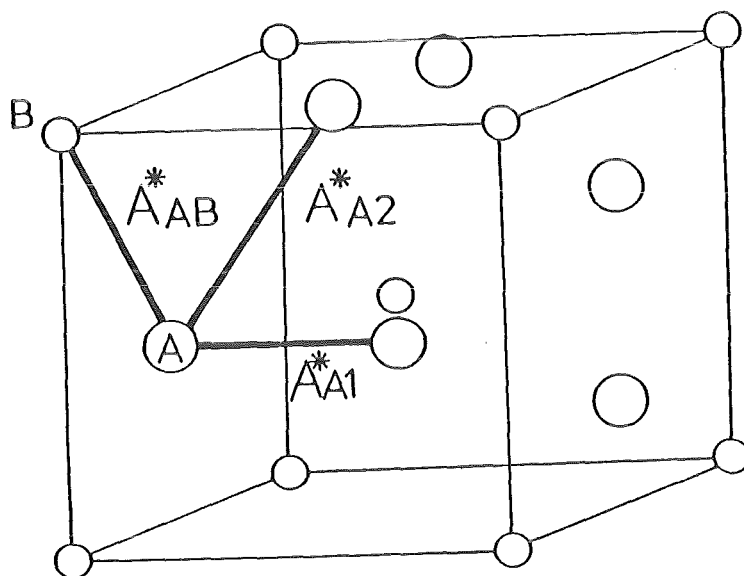


Fig. 6.18. Bonds between atomic pairs $\overline{AA_1}$ (nearest A neighbours), $\overline{AA_2}$ (nearest A neighbours in two orthogonal chains) and \overline{AB} , used in Machlin's model /294/, giving the repulsive potential parameters

$$A_{A_1}^*, A_{A_2}^* \text{ and } A_{AB}^*.$$

a) The Energy of Formation.

The crystal field modified pair potential model /294/ has been able to correctly predict the most stable structure for binary A_3B compounds out of a group of the four cubic structures A1, L12, A2 and A15. The energies of formation are summarized in Table 6.9 for those systems where the A15 structure is the most stable one (largest negative numbers).

Compound	A1	A2	L12	A15
Nb ₃ Pt	-12.86	-10.39	- 3.85	-39.97
V ₃ Pt	1.30	1.53	2.49	- 5.95
Nb ₃ Al	4.84	6.31	1.22	-29.90
Ti ₃ Au	-31.28	-25.01	-30.52	-42.09
Zr ₃ Au	-19.97	-12.49	- 4.94	-81.75
V ₃ Co	1.91	1.66	5.17	-21.20
Nb ₃ Ir	-15.73	-12.88	- 5.20	-43.20
Ti ₃ Ir	-27.63	-20.43	-14.85	-38.00
V ₃ Ir	1.01	0.42	1.45	6.96
Nb ₃ Os	- 8.97	- 5.82	0.03	-34.00
Nb ₃ Rh	-13.55	-11.10	- 4.38	-29.37
V ₃ Ni	5.03	4.76	6.89	-19.09
V ₃ Pd	0.50	0.16	3.79	-14.06
Ti ₃ Pt	-23.53	-16.72	-12.65	-34.15
Ta ₃ Sn	-27.88	-25.50	-18.02	-46.45
V ₃ Rh	- 1.38	- 1.13	2.05	-11.82
V ₃ Sn	-30.71	-30.92	-31.72	-36.54
Nb ₃ Sn	-27.38	-25.58	-18.62	-44.25
Mo ₃ Os	1.07	3.44	- 0.17	-13.14
Mo ₃ Ir	0.31	2.30	0.54	-17.72
Mo ₃ Pt	1.30	1.89	0.65	-17.72
Mo ₃ Si	- 0.46	- 0.17	- 9.97	-47.39
Nb ₃ Ga	-22.46	23.55	25.33	-15.50
V ₃ Ga	19.53	18.60	20.89	- 0.99
V ₃ Ge	- 9.680	-10.16	- 5.89	-27.11
Ta ₃ Au	- 4.94	- 2.66	0.23	-24.05
V ₃ Si	7.52	7.37	5.78	-21.58
V ₃ Au	12.65	12.07	16.38	- 7.50
Nb ₃ Au	- 9.36	- 7.58	- 5.82	-29.20
Ti ₃ Hg	-16.91	-11.84	- 4.08	-32.95
Nb ₃ In	10.41	11.54	16.05	-14.16
Nb ₃ Pb	-33.02	-31.49	-23.19	-53.15
V ₃ Pb	-12.32	-13.14	-12.30	-28.05
V ₃ Al	- 5.99	-12.78	-11.88	-28.70

Table 6.9. Structural component of energy of formation (kJ/g-at.) for A₃B phases exhibiting stable A15 structure (largest negative number).

Table 6.9 gives the correct data for A15 phase stability in most cases except for V₃Al, where the A2 phase is known to be more stable. In other cases, as Nb₃Pb or V₃Pb the results of Machlin et al. /294/ suggest a high stability of the A15 phase, which is in contrast to reality, where these phases can only be formed in the metastable state. Nevertheless, the crystal field model may

be considered as a satisfactory approach. An interesting correlation occurs when comparing the different energies of formation. The latter are represented in Fig. 6.19 in the B element representation and show a very similar variation to that observed for the order parameter (Fig. 5.2), (the Debye temperatures (Fig. 6.9)) and the stability index (Fig. 6.17). Indeed, the most stable A15 phases based on V, Nb, Cr and Mo are those with B = Ir for transition B elements and with B = Sn, Ge, Si(Pb) for nontransition B elements. Again, the systems Ti_3B and Zr_3B show a different behavior.

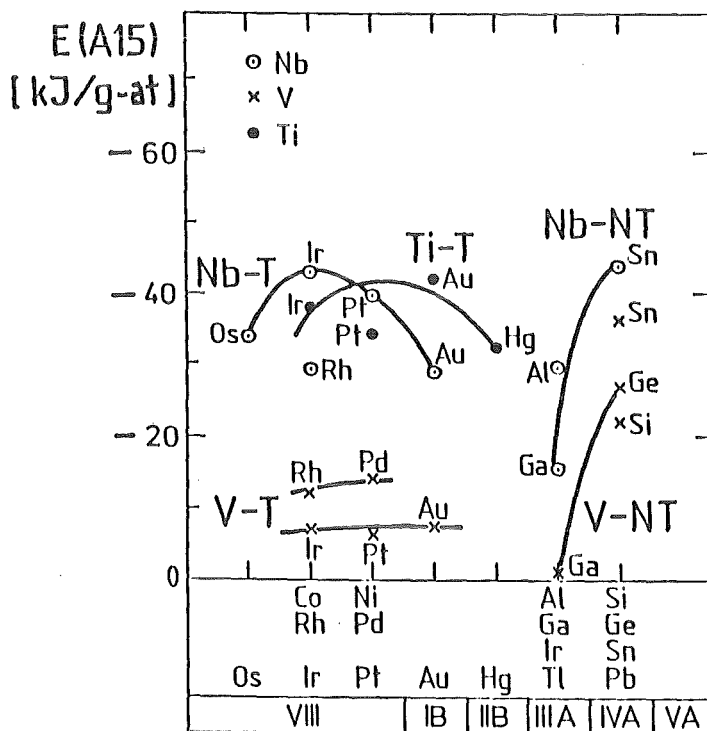


Fig. 6.19. Energy of formation for various A15 type compounds as calculated by Machlin /294/.

An interesting further result of Machlin's calculation concerns pseudobinary phases: If two binary A15 phases are not stable, neither will any region of the A15 pseudobinary be stable, i.e. the energy of formation of the A15 pseudobinary relative to the terminal A15 binary phases is never negative. In other words, this means that A15 phases never occur as true ternary phases.

b) The Degree of Long-Range Atomic Ordering.

As mentioned above, the crystal field model of Machlin /293/ also allows to calculate the long-range order parameter, S . The best way to represent the calculated values /294/ consists in plotting the calculated value of S vs. the reduced temperature T/T_F^0 , where T_F^0 is the formation temperature of the corresponding A15 type compound. In analogy to Fig. 4.5 and 5, this has been done in Fig. 6.20, which leads to the following conclusions:

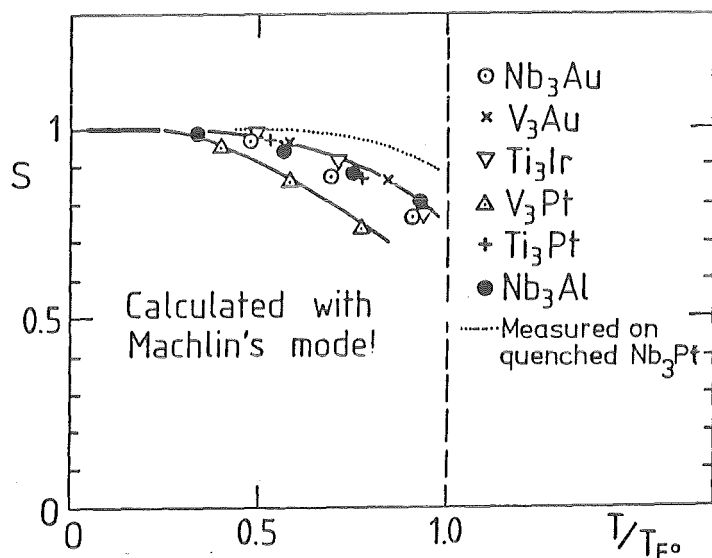


Fig. 6.20. Order parameter S vs. T/T_F^0 for several A15 type compounds as calculated by Machlin and Whang /294/ (T_F^0 is the formation temperature of the corresponding A15 type compound). For comparison, the variation S/S_{max} on quenched Nb_3Pt has been added (see Fig. 5.5).

- i) The difference between the calculated S value and that measured on quenched A15 type compounds is contained within certain narrow limits, estimated to $\Delta S \leq 0.10$ (without V_3Si , $V_{.755}Ge_{.245}$ and Nb_3Sn , for which no indication can be given, due to the impossibility to induce an observable change in S by quenching methods), and
- ii) even at the highest temperatures, ($T/T_F^0 \rightarrow 1$), S resides at values > 0.5 , thus excluding the possibility of an order-disorder phase transformation.

6.2.3. The Quasiharmonic Potential Approximation

In order to get a comparison of the interatomic forces in A15 type compounds a temperature dependent potential $V[r(T)]$ has to be defined. The vibration energy of the atoms increases linearly with T , since $E = kT$. The enhancement of the energy at $T > \theta_D$ is reflected by i) a linear increase of the vibration amplitude with T , $U^2 \sim T$, as represented in Fig. 6.12 and ii) by a linear increase of the interatomic distance with temperature, $a \sim T$, as illustrated in Fig. 6.16. An interatomic potential will now be determined from the vibration amplitudes U^2 and the linear thermal expansion coefficient α , taking the following assumptions:

- harmonic vibrations of the atoms around the equilibrium site
(the condition for this approximation, $U \ll a/2$, is well fulfilled with $U/a \sim 0.06$ for $Nb_{.755}Sn_{.245}$ at 1300 K (see Fig. 6.12))
- constant frequency ν at $T > \theta_D$
- linear increase of the interatomic space (the equilibrium position r_0 shifts linearly with T)
- independent vibration for each atom
- the potential is spherical in a first approximation: $V(r) = V_0 + 1/2 c(r-r_0)^2$.

In order to take into account the linear thermal expansion of the crystal, an anharmonic term is added to the harmonic potential, giving rise to

$$V(r) = V_0 + 1/2 C(r-r_0)^2 - 1/6 D(r-r_0)^3 \quad (6.9)$$

the quasiharmonic potential /275/, which has essentially the same form as the pair potential of Welch /80/. In the present case the displacement $(r-r_0)$ is given by the r.m.s. vibration amplitude U :

$$r(T) - r_0 = \pm U(T) . \quad (6.10)$$

Since the equilibrium positions vary themselves with T , it can be written

$$r(T) = r_0(T_0) = r_0(T_0) \alpha \Delta T \pm U(T), \quad (6.11)$$

where $T_0 = 300$ K. For the average vibration energy, it is $E = kT = 2 V(r)$, in order that

$$E = kT = V_0 + C(r-r_0)^2 - 1/3 D(r-r_0)^3. \quad (6.12)$$

The constants in Eq. (6.12) are calculated as follows. From the experimentally determined values of U^2 and α , the displacement $r-r_0 = (r-r_0)(T)$ can be determined, C and B being obtained by a least square fitting procedure. The results for a series of Nb_3B compounds and for elementary Nb are represented in Table 6.10, separately for the Nb and the B component /238/:

$Nb_{1-\beta}X_\beta$	β	C_{Nb}	C_B	D_{Nb}	D_B
		$\times 10^{-8}$ [N/nm]		$\times 10^{-6}$ [N/nm ²]	
$Nb_{1-\beta}Pt_\beta I$	0,258	9,38	10,78	4,57	6,41
$Nb_{1-\beta}Al_\beta II$	0,246	8,75	7,92	4,07	3,83
$Nb_{1-\beta}Al_\beta$	0,210	8,25	9,20	3,59	4,81
$Nb_{1-\beta}Sn_\beta$	0,245	8,75	12,78	4,33	9,06
Nb		9,12		4,55	

Table 6.10. Constants C_{Nb} , C_B , D_{Nb} and D_B in the quasiharmonic potential equation determined by least square procedures following Isernhagen /238/.

From Table 6.10, it follows that C as well as D are higher for Nb_3Sn and Nb_3Pt than for Nb_3Al . Attributing to these constants the meaning of a generalized force, it can be followed that the interatomic forces for Nb_3Sn and Nb_3Pt are higher than for Nb_3Al . This fits well in the present picture of a more unstable Nb_3Al at the border of the "Instability Region".

6.2.4. Electron Charge Transfer

When discussing about phase stability and superconductivity, it is indispensable to introduce the notions of electronegativity and of charge transfer. Miedema /200, 262, 263/ introduced an empirical approach for describing alloys, using two parameters ϕ^* , the electronegativity and n_{WS} , the density of electrons at the limit of the Wigner-Seitz cell (being empirically connected to the bulk modulus). The charge transfer was introduced by Weinkauff and Zittartz /264/ who tried to describe the superconducting properties of the metals by the local character of each of the constituents. According to Wenger et al. /265/, superconductivity and stability of an intermetallic compound are also due to the electrons transferred from one site to another.

Bongi et al. /266/ have calculated the electron transfer, Δn , between the chain atoms and those on the cubic sites using the empirical expression

$$n_{\text{alloy}} = \frac{1}{6} (n^A - \beta \Delta n_{WS} Z^B) \quad (6.13)$$

where n_{alloy} is the number of valency electrons of the A atom on the 6c site, n^A is the total number of electrons due to the A atoms in the unit cell, β is a constant which fixes the n_{alloy} value for one compound (determined to $\beta = 0.212$ by Staudenmann /267/ after adjustment for A15 compounds on the values of Miedema /200, 262, 263/, $\Delta n_{WS} = n_{WS}^B - n_{WS}^A$ is the difference between the corresponding electron densities of the atoms A and B at the limit of the Wigner-Seitz cell and Z^B is the valency of the B atoms in the A15 lattice. Bongi et al. /266/ established a correlation between the electron transfer and the superconducting properties of A15 type compound. For transition B elements, they found $n_{WS} > 0$, i.e. an electron transfer from the atom A to the atom B, while for nontransition elements, $\Delta n_{WS} < 0$. In other words, Si in V_3Si would act as "donor", while Ir in V_3Ir would act as "acceptor". The situation can best be visualized by representing n as a function of the valency of the B element (see Fig. 6.21), where $n = N_{\text{alloy}}^A - n^A$ (n^A is the number of electrons of one before alloying). The charge transfer in V_3Si has been calculated by Mattheiss and Hamann /286/ who obtained that each Si atom transfers 1.1 electrons to three V atoms, which is reasonably close to the value in Fig. 6.21.

The analysis of Fig. 6.21 suggests a possible correlation between charge transfer and phase stability: The instability region in V_3B , Nb_3B , Mo_3B and

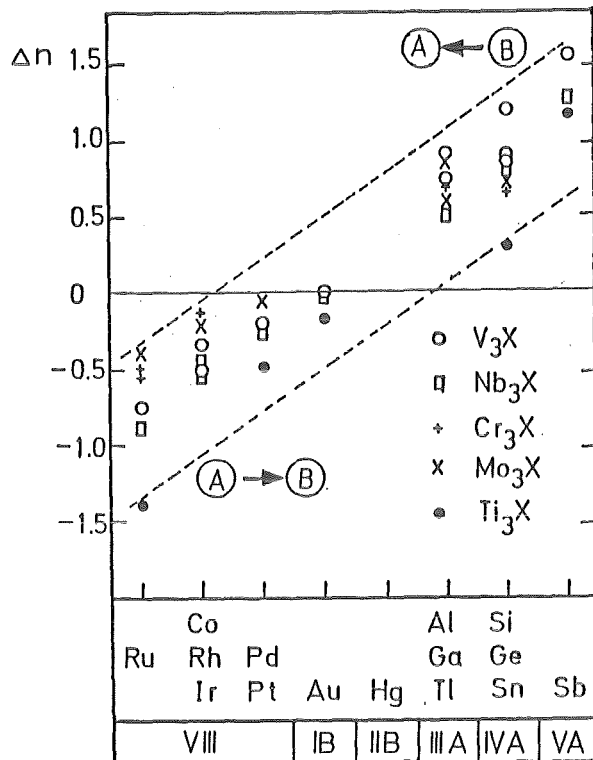


Fig. 6.21. Electron transfer in A15 type compounds calculated with the empirical equation (6.13) for n_{alloy}^A (after Bongi et al. /266/ and Staudenmann /267/).

Cr_3B compounds would correspond to $\Delta n = 0$ or to small positive values of Δn . However, this suggestive picture does not hold for Ti_3B and Zr_3B compounds, where Ti_3Hg , Ti_3Tl and Zr_3Hg exist in the region of $\Delta n \simeq 0$. As remarked by Staudenmann /267/, the value of Δn for Ti_3Ir is too high and some modifications of this simple model would be necessary. However, prior to follow the very suggesting conclusions of Fig. 6.21 about stability, more independent arguments and calculations are needed.

From the point of view of ordering, it would be interesting to know whether there is a correlation between Δn and the ability to undergo different values of the order parameter. In Nb_3B and V_3B compounds, the strongest ordering changes are encountered for Nb_3Pt , Nb_3Au , V_3Pt and V_3Au , where $\Delta n \simeq 0$. In Mo_3B and Cr_3B compounds, the strongest changes ΔS are observed for $\text{B} = \text{Os}$ and Ir , where Δn attains its largest negative values, thus showing the usual contrast with respect to Nb_3X and V_3X compounds. As a conclusion, this may reflect that a correlation exists between electron transfer, phase stability and atomic ordering in A15 type compounds.

7. ELECTRICAL RESISTIVITY AND ATOMIC ORDERING

In the preceding paragraph, the order parameters of various A15 type compounds after different treatments have been discussed. In the cases where the error ΔS exceeds certain limits, a complementary physical property reflecting the degree of atomic ordering has been introduced, the electrical resistivity just above T_C , usually denoted as ρ_0 . This is obviously only meaningful if a general correlation between ρ_0 and the degree of ordering can be established for different A15 type compounds, in a similar way as for the Cu_3Au system /257/. In the present paragraph, an attempt will be made to establish an empirical correlation $S = S(\rho_0)$ for the class of compounds with the A15 structure. For accomplishing this task, it must be taken into account that the value of ρ_0 for a given A15 type compound not only depends on the degree of atomic ordering, but also on the composition, β . The separation of both effects requires a very careful analysis of the metallurgical state and the thermal history of the sample on which ρ_0 was measured. Most of the ρ_0 data on thermally disordered A15 type compounds are taken from own data /38, 142, 220, 221/. In the following, a comparison will be made between resistivity data on thermally disordered and irradiated A15 type compounds. A particular attention will be given to the question whether ρ_0 in the irradiated case can be considered or not as an indication for the degree of ordering in the sample. An important point when comparing the ρ_0 values of various compounds resides in the particular temperature dependence, $\rho = \rho(T)$, observed in this type of compounds. At high temperatures a saturation of $\rho(T)$ is observed at values $\rho_{\text{sat}} \simeq 140$ to $160 \times 10^{-8} \Omega\text{m}$ while at low temperatures ($T < 50$ K), a variation $\rho \sim T^n$ with $2 \leq n \leq 5$ has been reported. A careful analysis of all these aspects furnishes interesting new informations about the properties of A15 type compounds and will therefore precede the considerations about the dependence of S on ρ_0 .

7.1. $\rho(T)$ at High Temperatures

Woodard and Cody /170/ observed in Nb_3Sn a saturation of $\rho(T)$ at high temperature, instead of the linear dependence predicted by the classical Bloch-Grüneisen theory. A direct estimation of ρ_{sat} can only be done for the few compounds where $\rho(T)$ has been measured up to really high temperatures, i.e. up to 800 K and above. The variation of $\rho(T)$ for the systems Nb_3Sn /170/, V_3Si /235/ and Nb_3Ir /221/ has been represented in Fig. 7.1 for comparison. The similarity

between the resistivity data for these three compounds with very different electronic density of states demonstrates that the saturation effect is not correlated to the individual electronic structure. This phenomenon does not seem to be correlated to the crystal structure either, since it has also been observed on intermetallic compounds crystallizing either in the cubic phase /232/, Laves phase /255/ or Chevrel phase /256/, all of them having a property in common: High resistivity, ρ_0 , when comparing with pure metals.

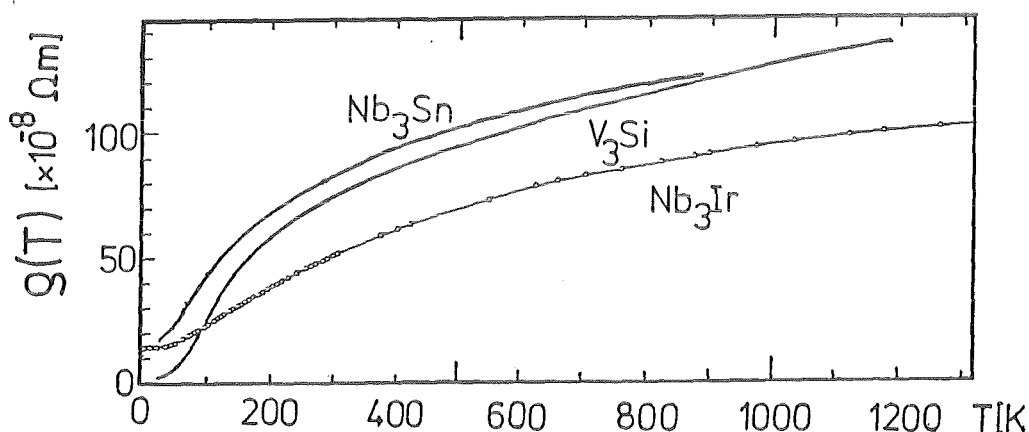


Fig. 7.1. Electrical resistivity $\rho = \rho(T)$ for the systems Nb_3Sn (Woodward and Cody /170/) V_3Si (Marchenko et al. /235/) and Nb_3Ir (Flükiger /221/) up to 1200 K, showing saturation values ρ_{sat} between ~ 100 and $\sim 140 \times 10^{-8} \Omega m$, respectively.

7.2 The Shunting Model

Meanwhile, such a saturation effect was not only reported for high T_c superconductors, e.g. Nb_3Sn /170/, V_3Si /218, 235/, V_3Ga /142/, Nb_3Ge / /, Nb_3Al /217, 220/, Mo_3Os /142/ but also for low T_c superconductors crystallizing in the A15 structure, e.g. Nb_3Sb /241/, Nb_3Ir /38, 206/, Nb_3Os /38, 206/, Mo_3Si /239/, Mo_3Ge /206, 239/ and $Ti_{.73}Pt_{.27}$ /207/.

The electrical resistivity for a series of A15 type compounds in the temperature range between T_c and 300 K has been reproduced in Fig. 7.2 for illustration. It can be seen that the saturation effects start well below room temperature, which is reflected by the inflection point varying between the limits

$40 \leq T_i \leq 250$ K, depending on the compound. The temperature of the inflection point, T_i , is not a definite physical property of the material, but rather represents the intermediate region between two different regimes of $\rho(T)$, i.e. the low temperature behavior ($T < 50$ K) and the saturation behavior at high temperatures ($T \gg 300$ K).

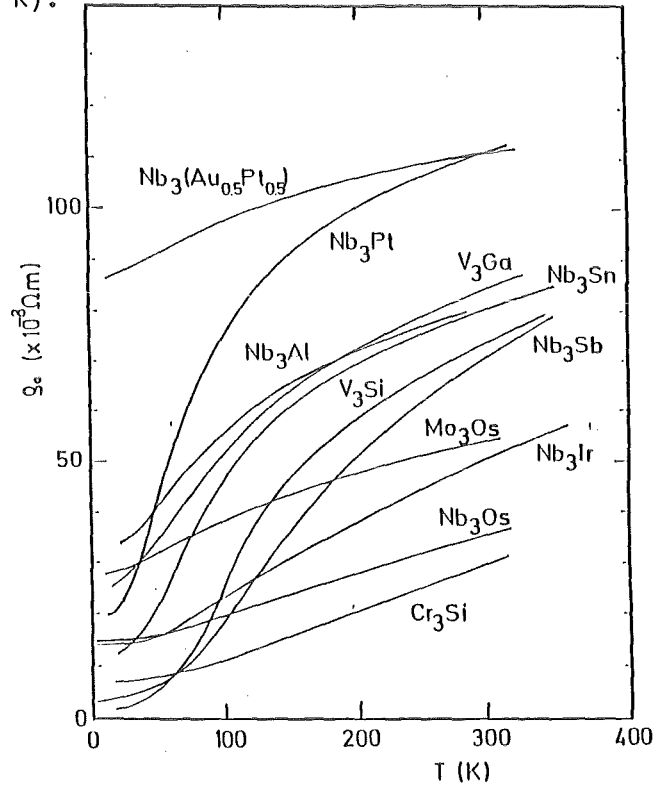


Fig. 7.2. Electrical resistivity as a function of temperature for various A15 type compounds, illustrating the saturation behavior at higher temperatures. Nb_3Sn : Woodard and Cody /170/, V_3Si : Caton and Viswanathan /217/, Cr_3Si : Devantay /206/, Mo_3Os , Nb_3Pt , V_3Ga and $\text{Nb}_3\text{Au}_{.50}\text{Pt}_{.50}$: Flükiger et al. /142/, Nb_3Al , Nb_3Ir and Nb_3Os : Flükiger et al. /220/.

The value of ρ_0 reflects as well the degree of ordering as the effective composition, as will be discussed in this paragraph. The fact that the ρ values at 300 K show considerable differences is of secondary importance only: at high temperatures, all compounds saturate at very similar value, ρ_{sat} . As can be followed from Fig. 7.1, the difference between the values of ρ_{sat} is expected to be smallest close to the melting point. From Fig. 7.2, no particular tendency can be recognized for the approach of $\rho(T)$ toward the saturation value. There is no explanation for the excessively strong increase of $\rho(T)$ for Nb_3Pt compared to the other A15 type compounds. It is interesting that the corresponding V based A15 compound with Pt, V_3Pt (not shown in Fig. 7.2) does not show this anomalous behavior.

Among different explanations for the observed saturation of the electrical resistivity at high temperatures, the most probable one assumes that this phenomenon occurs when the electronic mean free path is of the order of the interatomic spacings (Mott limit). In the empirical parallel resistor or shunting model of Wiesmann et al. /236/, there is

$$\frac{1}{\rho} = \frac{1}{\rho_{\text{sat}}} + \frac{1}{\rho_{\text{ideal}}} \quad (7.1)$$

where the ideal resistivity, ρ_{ideal} , is "in parallel" with the saturation resistivity, ρ_{sat} .

This model is independent on the crystal structure and fits very well with the reported resistivity data on A15 type materials /217,230,246,249,251,252/. An additional confirmation for the limitation of the electronic mean free path to interatomic distances at temperatures as low as 300 K is furnished by the data in Fig. 7.3. For argon quenched Nb_3Pt samples, the value of ρ_{sat} (which is very close to ρ_{300}) is indeed very little affected by the disordering process.

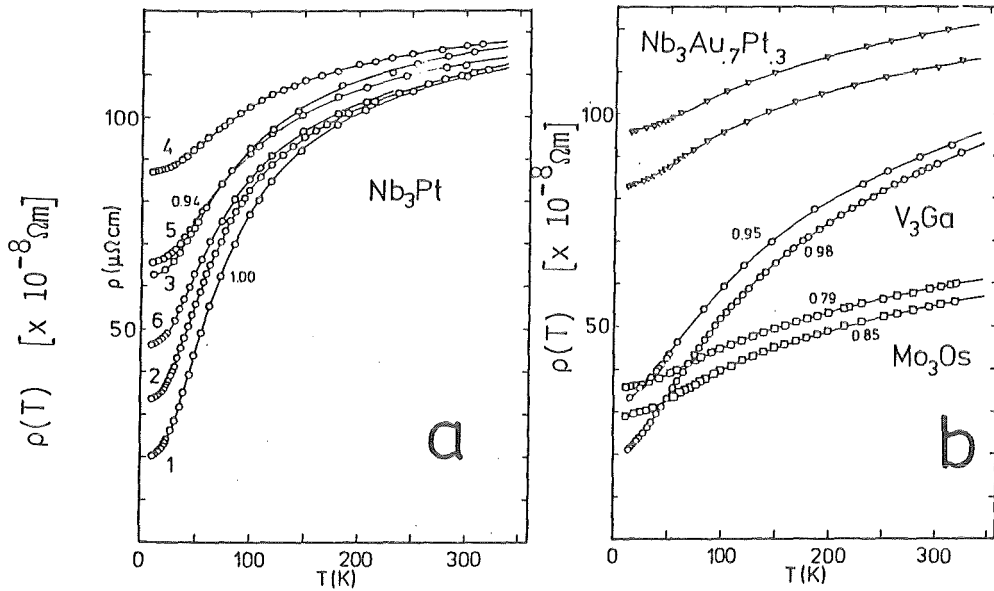


Fig. 7.3. Electrical resistivity for the same A15 phase sample after different heat treatments.

- a) Nb_3Pt . 1: 5 weeks at 900°C + 7 weeks at 750°C , 2: 3 weeks at 900°C , 3: 10 hours at 1250°C and argon jet quenched, 4: 30 min. at 1800°C and argon jet quenched, 5: same treatment as 4 + 48 hours at 1250°C , 6: same treatment as 4 + 24 hours at 1000°C (Flükiger et al./142/).
- b) Mo_3Os , V_3Ga , $\text{Nb}_3\text{Au}_{.7}\text{Pt}_{.3}$ /142/.

According to Allen /247/, $\rho_{ideal}(T)$ can be derived from the basic variational solution of the Bloch-Boltzmann equation

$$\begin{aligned} \rho_{ideal}(T) &= \rho_0 + \{(n/m)_{eff} \cdot e^2 \cdot \tau_{ph}(T)\}^{-1} \\ &= \rho_0 + \{(n/m)_{eff} \cdot e^2\}^{-1} \cdot 2\pi/\hbar \cdot k_B \cdot \lambda_{tr}(T) \cdot T \end{aligned} \quad (7.2)$$

This equation involves two coupling constants, $(n/m)_{eff} = N(0) \langle v_x^2 \rangle$, where $N(0)$ is the electronic density of states at the Fermi level and $\langle v_x^2 \rangle$ is the electronic velocity at the Fermi surface and λ_{tr} , the electron phonon coupling parameter for transport processes. At $T = 0$ and for $T > 0_D$, Eq. (7.2) can be simplified to

$$\rho_{ideal}(T) = \rho_0 + \rho_1 \cdot T \quad (7.3)$$

Theoretical estimations by Allen /247/ assuming $\lambda_{tr} \sim \lambda$, where λ is the electron-phonon interaction parameter and calculating $(n/m)_{eff}$ from band theory have shown that if the Boltzmann theory would work, the electron mean free path at 300 K would be of the order of 0.3 to 0.4 nm for Nb_3Ge and Nb_3Al .

From the values in Fig. 7.3., the term ρ_{ideal} can now be calculated for V_3Ga using the shunting model (Eq. 7.1) and assuming a saturation value $\rho_{sat} = 120 \times 10^{-8} \Omega m$. The results are represented in Fig. 7.4 and show that the

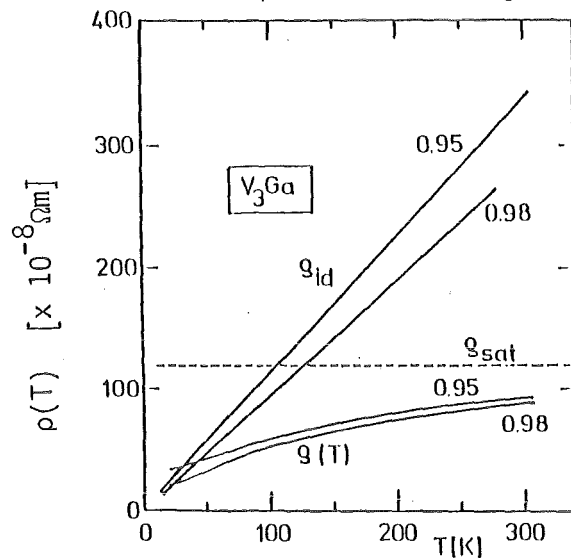


Fig. 7.4. Decomposition of $\rho(T)$ for V_3Ga at different degrees of ordering characterized by $S = 0.98$ and 0.95 (see Fig. 7.3) following the shunting model with $\rho_{max} = 120 \times 10^{-8} \Omega m$, based on the data of Flükiger et al. /142/.

slope of $\rho_1(T)$ decreases with disordering. It can thus be concluded that the Matthiessen rule is not valid for V_3Ga at different degrees of ordering (the deviation for Nb_3Pt is even stronger than for V_3Ga).

7. Electrical Resistivity in Quenched and Irradiated Samples

Under the assumption that the measured absolute values of $\rho(T)$ for a sample crystallizing in the A15 structure at a given degree of ordering is neither influenced by internal stresses, small amounts of additional phases or other reasons, the following question is of interest: Does the disordering process, i.e. quenching or irradiation, influence the absolute value of the electrical resistivity? The answer can only be given by a direct comparison between quenching and irradiation data at low temperatures.

The variation of $\rho(T)$ after high energy irradiation has been measured in many A15 systems, as V_3Si /217/, Nb_3Sn /165/, Mo_3Ge /138,244/, Mo_3Si /137/, Nb_3Ge /111,251/, Nb_3Al /55/ and others. As an example, the irradiation data on V_3Si /217/ (plotted in Fig. 7.5 for illustration) show

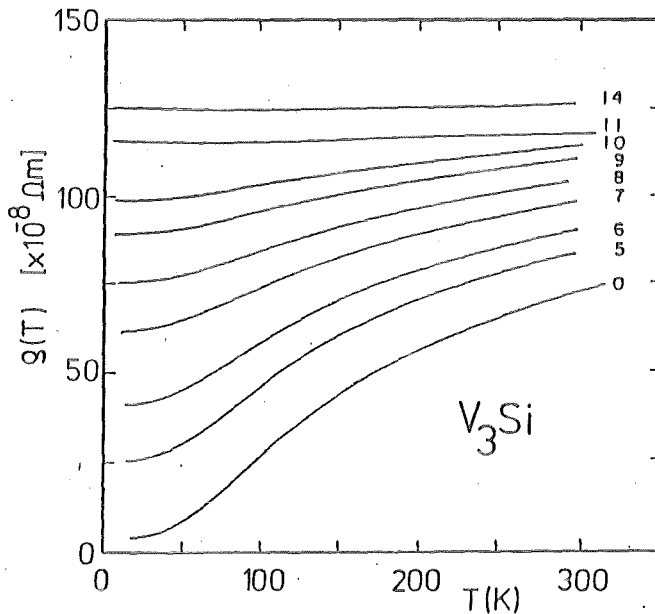


Fig. 7.5 Variation of $\rho(T)$ for a V_3Si single crystal after neutron irradiation ($E > 1$ MeV). The numbers represent increasing fluences (Caton et al. /217/)

that the general shape of $\rho(T)$ changes gradually with disorder, ρ_0 increasing from $3.74 \times 10^{-8} \Omega m$ to $125.2 \times 10^{-8} \Omega m$ for a corresponding change of T_c from 16.90 K to 2.44 K. A similar variation of $\rho(T)$ after irradiation as in V_3Si has been observed for other A15 type compounds, the main difference occurring

at the highest irradiation doses. At these doses, $\rho(T)$ exhibits sometimes a negative slope, reflecting the occurrence of the amorphous phase.

Unfortunately, the system Nb_3Pt is the only one where the variation of $\rho(T)$ has been studied on thermally disordered samples, (see Fig. 7.3), in order that the comparison must be restricted to this compound, where a neutron irradiation study has been performed by Caton and Viswanathan /217/. As mentioned above, the value of $\rho_{300\text{K}}$ in quenched Nb_3Pt is very little affected, varying from $109 \times 10^{-8} \Omega\text{m}$ to $117 \times 10^{-8} \Omega\text{m}$ for a reduction of T_c from 11 K to 7.2 K /142/. This observation suggest that no cracks were introduced by the quenching process. This has also been proved by subsequent ordering heat treatments on the Nb_3Pt sample with the highest ρ_0 value, $87 \times 10^{-8} \Omega\text{m}$, resulting in an almost complete recovery of the original low ρ_0 value for the most ordered sample /142/.

Since the full $\rho(T)$ curves for Nb_3Pt are not reported by Caton and Viswanathan /217/, the comparison will be restricted to the resistivity values at low temperature and at 300 K, both listed in Table 7.1. There is a good agreement between the ρ_0 values of the starting Nb_3Pt samples in both investigations, (Refs. 142 and 217), i.e. $23.3 \times 10^{-8} \Omega\text{m}$ /217/ and $20.1 \times 10^{-8} \Omega\text{m}$ /142/, respectively, the corresponding T_c values being similar, 11 K /142/ and 11.1 K /217/. At room temperature, however, the sample in Ref. 217 shows a smaller resistivity value, $\rho_{300} = 85.9 \times 10^{-8} \Omega\text{m}$, than that reported in Ref. 142, $\rho_{300} = 104.6 \times 10^{-8} \Omega\text{m}$. The origin of this difference is attributed to slight differences in the respective compositions as well as in the composition distribution across the samples. (It should be recalled that the value of T_c may be subject to shielding effects and is inadequate for yielding informations about the sample homogeneity /7/). Nevertheless, the relative changes of ρ_0 and ρ_{300} for both disordering processes can be compared.

It follows that the enhancement of ρ_0 in both argon jet quenched and irradiated Nb_3Pt is comparable for similar changes of T_c (and thus of the order parameter). For disordering corresponding to a decrease of T_c by ~ 4 K, the corresponding variations after thermally disordering are $\Delta\rho_0 = 67.1 \times 10^{-8} \Omega\text{m}$ and $\Delta\rho_{300\text{K}} = 7.1 \times 10^{-8} \Omega\text{m}$ /142/, which is very similar to the change after irradiation, i.e. $\Delta\rho_0 = 10.9 \times 10^{-8} \Omega\text{m}$ and $\Delta\rho_{300} = 63.7 \times 10^{-8} \Omega\text{m}$ /217/.

Treatment	T_c	ρ_0	ρ_{300}	RRR	Ref.
48 hours/1800 ^o C (R) + 7 weeks/750 ^o C	11.0	20.1	110.1	5.48	142
30 min./1800 ^o C (Q) + 16 hours/1000 ^o C	10.15	41.0	107.7	2.63	38
24 hours/1750 ^o C (R)	9.3	51.4	109.9	2.14	38
15 min./1800 ^o C (Q) + 48 hours/1250 ^o C (R)	9.0	65.3	112.2	1.71	142
24 hours/1200 ^o C (R)	9.1	67.5	120.1	1.78	38
30 min./1800 ^o C (Q)	8.1	86.4	116.7	1.35	142
12 hours/1800 ^o C (R) + 3 weeks/900 ^o C	11.1	23.3	85.9	3.69	217
7.5 x 10 ¹⁸ n/cm ²	6.45	87.0	96.1	1.11	217
15 x 10 ¹⁸ n/cm ²	4.31	102.7	107.2	1.04	217
202 x 10 ¹⁸ n/cm ²	3.03	110.6	112.0	1.01	217

Table 7.1. The quantities T_c , ρ_0 , ρ_{300K} , RRR and S for Nb₃Pt samples after disordering by argon jet quenching/142/ and by neutron irradiation/217/.

The present comparison with data obtained on quench disordered Nb₃Pt samples furnishes the first evidence that the changes of the electrical resistivity in irradiated A15 type compounds, extensively reported in the literature, really correspond to changes of the order parameter. It follows that radiation induced effects (e.g. vacancies, depleted zones or the lattice expansion) have a minor importance only on $\rho(T)$. This holds for order parameter values between $S = 0.98$ and 0.88 , thus corresponding to low radiation doses. For heavy radiation doses, enhanced radiation induced effects on $\rho(T)$ have to be expected.

7.4. The Electrical Resistivity at Low Temperatures

7.4.1. Description of $\rho(T)$ below 50 K

In a recent investigation, Caton and Viswanathan /217/ have shown that the model fitting best with the measured data over the entire temperature range for the three compounds V_3Si , Nb_3Pt and Nb_3Al with physically reasonable parameters is the shunting model mentioned above combined with Wilson's expression for s-d scattering in transition metals. At lower temperatures, Wilson's expression for $\rho_1(T)$ yields

$$\rho_1(T) = \rho_{sd} = \kappa_{sd} \left(\frac{T^3}{\rho_{sd}} \right) \int_0^{\theta_{sd}/T} \frac{x^3 dx}{(e^x - 1)(1 - e^{-x})} \quad (7.4)$$

where θ_{sd} is a cut-off temperature similar to the Debye temperature ($\theta_{sd} \approx 400$ K for V_3Si /217/) and κ_{sd} is a constant.

Another possibility to fit $\rho(T)$ over the entire temperature range has been proposed by Milewits et al. /246/:

$$\rho(T) = \rho_0 + b \cdot T^n + c \cdot e^{-T_0/T} \quad (7.5)$$

where ρ_0 , b , c and T_0 are constants. The first two terms are dominant at low temperature ($T < 50$ K), while the exponential term was introduced for taking into account of the saturation at high temperatures ($T \gg 300$ K). This formula differs from the original fit of Woodard and Cody /230/ only by the exponent n in the second term. Rather than interpreting the second term as high temperature limit of the Wilson model of s-d scattering, Milewits et al. /246/ assume that this term expresses a separate contribution to the resistivity and allow n to vary.

The exponent n in Eq. 7.5) will be discussed below, while the quantity T_0 is correlated to the inflection point ($T_i \approx T_0/2$) and represents according to Milewits et al. /246/ the phonon energy necessary to scatter electrons between bands of different pockets of the Fermi surface. Nevertheless, it is reasonable to consider this quantity as a characteristic temperature between

two different temperature regimes of $\rho(T)$. An example illustrating how little this effect is understood is the compound Nb_3Pt . Although this compound has neither extreme values of T_C nor of the electronic density of states, it exhibits the lowest inflection temperature, among all A15 type compounds, $T_i = 39$ K (see Fig. 7.3). It would be interesting to know whether this behavior of $\rho(T)$ in Nb_3Pt reflects some peculiarities in the phonon spectrum. After fast quenching T_i increases up to ~ 60 K.

In addition to the interest in understanding the saturation of ρ at higher T , there have also been attempts to explain the resistivity behavior at low T , i.e. from T_C to 50 K or less. Marchenko et al. /235/ for V_3Si and Webb et al. /241/ for Nb_3Sn and Nb_3Al reported a T^2 dependence of the resistivity. For high T_C A15 type compounds, these authors proposed the formula

$$\rho(T) = \rho_0 + b T^2, \quad (7.6.)$$

to be applied in the temperature range $T_C \leq T \leq 50$ K (in this formula, b is a constant). For other compounds, e.g. Nb_3Sb /241/, the exponential n is not longer 2, but 3.6, while for the low T_C compounds Mo_3Ge and Mo_3Si Gurvitch et al. /244/ found $n = 5$, i.e. an ideal Bloch-Grüneisen behavior. It is thus more convenient to generalize the formula (7.6) to

$$\rho(T) = \rho_0 + b_n T^n, \quad (7.7)$$

and to describe the differences between various A15 type compounds by listing the exponent, n . It may be recalled that Eq. (7.7) is nothing else than the low temperature term in Eq. (7.5).

7.4.2. The Exponent n in $\rho(T)$ at Low Temperatures

As mentioned above, a T^2 behavior of $\rho(T)$ was observed in various high T_C A15 type compounds. This behavior is represented in Fig. 7.6 for various A15 type compounds. From this figure, it can be seen that the validity of the exponential $n = 2$ is restricted to temperatures well below 50 K. In spite of the uncertainties about the real origin of the T^2 dependence, it is interesting to note that the range of validity for $\rho \sim T^2$ is depending on the degree of ordering. As reported by Gurvitch /244,254/ and Lehmann /239/, the upper limit

of the T^2 dependence in Nb_3Sn is shifted from 45 K to 88 K after irradiation causing increase of ρ_0 from 30 to $140 \times 10^{-8} \Omega m$. The same behavior was observed for various other irradiated A15 type compounds, as follows from Table 7.2, where all known resistivity data on A15 type compounds are listed.

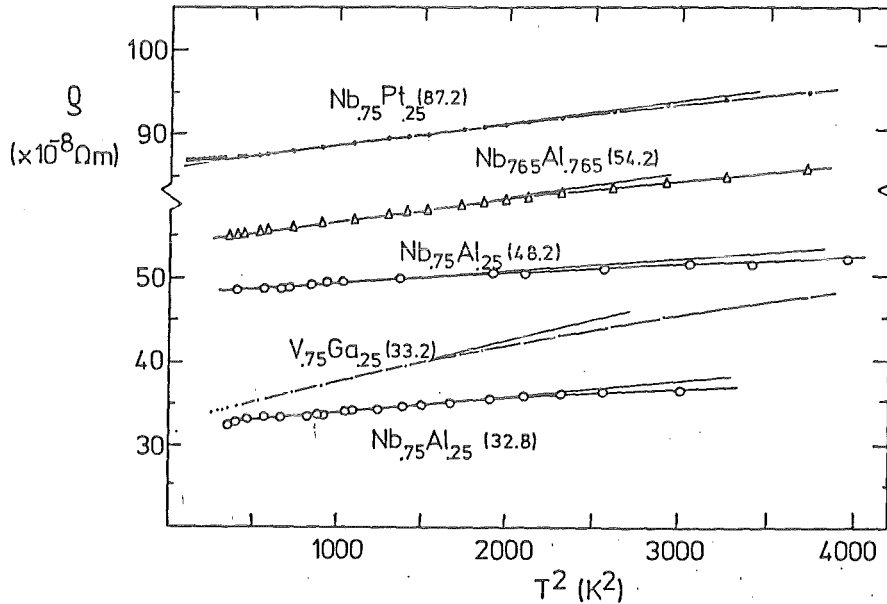


Fig. 7.6. Electrical resistivity vs. T^2 for various A15 type compounds. The numbers in parenthesis are the ρ_0 values (Flükiger /38,142/).

A T^2 behavior of the electrical resistivity at low temperature is not only encountered in high T_C A15 materials, but also in other disordered and amorphous compounds, and several attempts have been made to explain this exponent. As discussed by Allen /247/, theories by Gubanov /268/, Ohkawa /269/ and Cote and Meisel /270/ invoking different mechanisms are, however, not able to explain the particular behavior of $\rho(T)$ in A15 type compounds. Gurvitch et al. /244/ mentioned unpublished calculations correlating the T^2 behavior of $\rho(T)$ with narrow bands at the vicinity of the Fermi level.

It is interesting that at low temperatures, the calculation of $\rho(T)$ assuming phonon-assisted s-d interband scattering and using the phonon spectrum for V_3Si of Schweiss et al. /237/ (or using the model density of states calculated by Testardi /272/ from acoustic data) results in a T^3 dependence ($n = 3$), rather than the T^2 dependence as observed in high T_C A15 type compounds /235,241,254/.

In general, the low temperature behavior in A15 type compounds is described by an exponential, n ranging from 2 to 5. The only exceptions to this behavior are Nb_3Pt , Nb_3Au and the pseudobinary $\text{Nb}_{.75}\text{Au}_{.125}\text{Pt}_{.125}$, where the low temperature behavior is rather complex /38/. The behavior of $\rho(T) - \rho_0$ for Nb_3Pt reveals a deviation from a T^2 dependence below ~ 21 K.

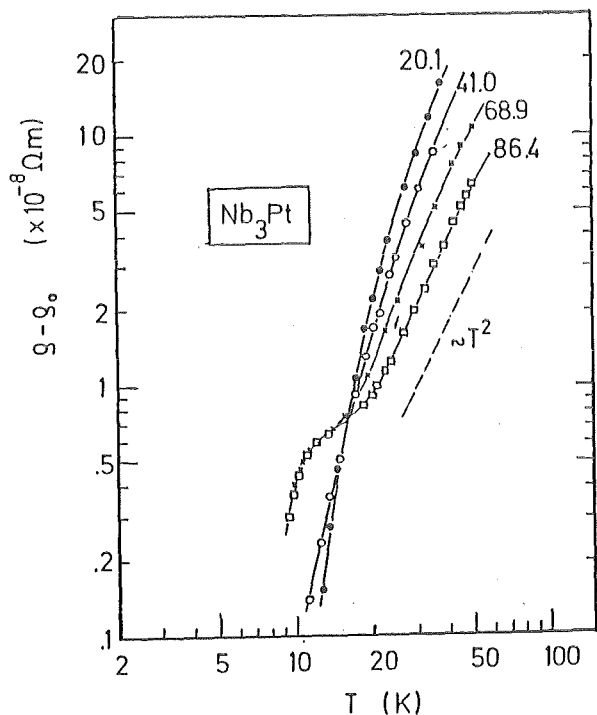


Fig. 7.7. Log - log representation of $\rho(T) - \rho_0$ vs. T for Nb_3Pt after various heat treatments giving rise to different ρ_0 values. The heat treatments are specified in Table 7.1 /38,142/. The numbers are the corresponding ρ_0 values ($\times 10^{-8} \Omega\text{m}$).

The deviation increases for higher ρ_0 values, corresponding to lower degree of ordering, induced by different heat treatments. Another way to represent this deviation consists in establishing a log - log plot (Fig. 7.7.), from which the exponent n can directly be determined. As shown in Fig. 7.7., there is a gradual change of the anomalous low temperature behavior of $\rho(T)$ in Nb_3Pt . For the most ordered sample ($\rho_0 = 20.1 \times 10^{-8} \Omega\text{m}$), a T^5 behavior is observed, while a second slope appears for the quenched states with $\rho_0 = 68.9$ and $86.4 \times 10^{-8} \Omega\text{m}$. All measurements in Fig. 7.7. were determined on the same sample. Reannealing of the sample with $\rho_0 = 86.4 \times 10^{-8} \Omega\text{m}$ (argon jet quenched from 1800°C) leads to the original $\rho(T)$ behavior with only one slope, in order that this is a real effect. It has to be noted that the second slope is present in Nb_3Au and $\text{Nb}_{.75}\text{Au}_{.125}\text{Pt}_{.125}$ even without argon jet quenching.

As indicated in Table 7.2., the presence of two slopes in $\rho(T)$ of Nb_3Pt has also been observed by Caton and Viswanathan /217/, who reported exponents between 3 and 5 at temperatures below 27 K. It is remarkable that the complex behavior of $\rho(T)$ at low temperature does not occur in the analogous V based compounds V_3Pt /206/ and $\text{V}_{.76}\text{Au}_{.24}$ /38/ (see Fig. 7.8.). It is very tempting to advance the hypothesis that the two slopes in the Nb based A15 type compounds (Figs. 7.7. and 7.8.) reflect the mixed nature of these compounds, arising from the fact that Pt has a completely filled d shell while its neighbour, Au, has one s electron. The electrical resistivity measurements would indicate that the compounds Nb_3Pt and Nb_3Au (and the pseudobinary $\text{Nb}_{.75}\text{Au}_{.25}\text{Pt}_{.125}$) behave in some context like pure transition metals ($n \geq 3$), but that they also exhibit some features of the high T_c A15 type compounds containing pure non transition B elements ($n = 2$). This hypothesis is supported by the fact that $\rho(T)$ in V_3Pt exhibits the exponent $n = 3$, observed in A15 type compounds based on transition metals only: in contrast to Nb_3Pt , where T_c (11.1 K) is about the half of that encountered in Nb_3Ge or Nb_3Sn , V_3Pt only exhibits $T_c = 3.7$ K, which is only about 20 % of the value of V_3Si or V_3Ga .

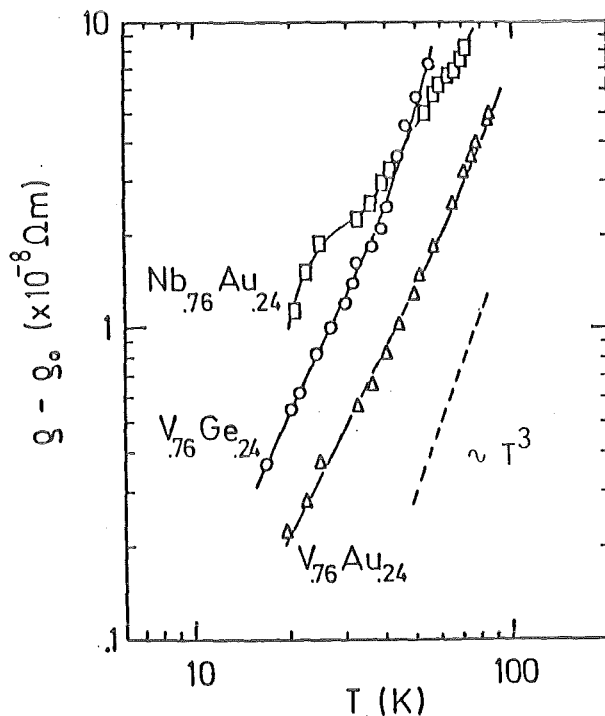


Fig. 7.8. Log - log representation of $\rho(T) - \rho_0$ vs. T for $\text{V}_{.76}\text{Au}_{.24}$, $\text{V}_{.76}\text{Ge}_{.24}$ and $\text{Nb}_{.76}\text{Au}_{.24}$ after various heat treatments /38/.

System	Heat Treatment [°C/h]	T _c [K]	ρ ₀ [x 10 ⁻⁸ Ωm]	n	Temperature Range [K]	Reference
V ₃ Si	Mono	16.9	4.22	2	17 - 25	Caton et al. /217/
	Poly	17.1	6.3	2	17 - 28	Marchenko /235/
	Mono	16.8	5.2	1.5	24 - 38	Taub et al. /253/
	Mono, 1680/48	16.94	2.17	3	22.5-40 ^{a)}	Flükiger /38/
	Poly			3	20 - 40	Gurvitch /271/
	Poly			2	17 - 28	Gurvitch /254/
Nb ₃ Sn	Poly			2		Morton et al. /240/
	Mono	18.2	6.8	2	20 - 28	Hebb et al. /241/
	Film	17.6	27.4	2	< 76.5	Lehmann /239/
	Film	18	11.4	2	18.4 - 30	Gurvitch /254/
	Film, Irrad.		75.7	2	< 88	Gurvitch /254/
	Film, Irrad.		95.7	2	< 88	Gurvitch /254/
V ₃ Ga	Poly, 1200+Q	13.8	32.7	2	19 - 38.5	Flükiger /38,142/
	Poly, 610/336	14.8	24.2	2	20 - 36	Flükiger /38,142/
Nb ₃ Ge	Film	20.5	45	2		Lutz et al. /251/
	Film	19.4	51	2		Lutz et al. /251/
	Film		49.9	2.3	< 36	Gurvitch /254/
Nb ₃ Al	Poly	18.5	55.8	2	20 - 43	Hebb et al. /241/
	Poly, Irrad.	18.5	65	2		Caton et al. /217/
	Poly, Irrad.	12.9	99.7	2		Caton et al. /217/
	Poly, Irrad.	8.4		3		Caton et al. /217/
	Poly		55	2	18.6 - 40	Gurvitch /240/
	Poly, 1960+Q	17.2	48.2	2	19 - 43	Flükiger /38,220/
	Poly, 750/1176	18.8	32.8	2	19 - 43	Flükiger /38,220/
	Film	16.4	64	2	< 45	Lehmann /239/
Nb ₃ Al _{0.735} Al _{0.235}	Poly, 1900/3.5	17.5	54.2	2	19 - 42	Flükiger /38/
	Nb ₃ Al _{0.78} Al _{0.22}	Poly, 1850/24	16.4	105	3	20 - 60
Nb ₃ Au	Poly	11		2	< 35	Gurvitch /339/
	Poly, 750/168	10.9	90.6	1.8	20 - 80	Flükiger (Fig. 7.8)
Nb ₃ Pt	Poly, 900/168	11.1	23.3	5	12 - 47	Caton et al. /217/
	"	"	"	2	27 - 43	
	Poly, Irrad.	6.45	87	3	22 - 36	Caton et al. /217/
	"	"	"	2	36 - 43	
	Poly, 1800/48+Q	8.1	86.4	5	12 - 20	Flükiger (Fig.7.7)
	"	"	"	2	20 - 44	
	Poly, 750/1136	11.0	20.1	>4	< 25	Flükiger (Fig.7.7)
	"	"	"	2	25 - 40	
Poly	11.1		3	12 - 27	Gurvitch /339/	
"	"		2	27 - 43		
Nb ₃ Ir	Poly, 1800/48	1.7	14	3	20 - 45	Flükiger /38/
Nb ₃ Os	Poly, 1800/48	0.95	15.1	3	20 - 44	Flükiger /38/
Nb ₃ Sb	Mono	0.8	~2	3.6		Fisk et al. /338/
V ₃ Ge	Poly, 1600/48	6.0	5.43	2.86	18 - 65	Flükiger (Fig.7.8)
						Morton et al. /240/
V ₃ Pt _{0.76} Au _{0.24}	Poly ^{b)}	2.2	86 ^{b)}	2.4	< 28	Flükiger (Fig.7.8)
V ₃ Pt	Poly, 900/168	3.0	32.9	3	< 65	Flükiger /38/
V ₃ Sn _{0.80}	Poly, 950/6	4.1	26	1.05	20 - 50	Morton et al. /252/
Cr ₃ Si	Poly	<0.030	7.2	5	< 60	Flükiger /38/
Mo ₃ Os	Poly, 1950/0.5	11.4	35.8	3	< 57	Flükiger /38,142/
	Poly, 1100/336	12.1	28.5	3	< 60	Flükiger /38,142/
Mo ₃ Ir _{0.76}	Poly, 1800/24	8.2	61.29 ^{b)}	3	< 50	Flükiger /38/
Mo ₃ Re _{0.65}	Film	12.7	24	3		Lehmann /239/
Mo ₃ Si	Film	1.48	18	5	< 64.5	Lehmann /239/
Mo ₃ Ge	Film	1.49	58	5	< 64.5	Lehmann /239/
	Film	1.6	19	5	10 - 35	Gurvitch /254/
Ti ₃ Pt	Poly	0.49	71 ^{b)}	3	< 40	Flükiger /38/
Ti ₃ Sb	Poly, 850/336	6.54	11.4	2	< 38	Ramakrishnan et al. /249/
Zr ₄ Sn	Poly, 900/120	0.93	144.5 ^{b)}	1.8	< 40	Flükiger /38/

Table 7.2. Electrical resistivity and n coefficient of ρ(T) for A15 type compounds, as well as the temperature range where n is valid.
a) The V₃Si single crystal transforms at 21.5 K, b) These samples show traces of second phases, which may lead to higher ρ₀ values.

According to Gurvitch /254/, a change of the degree of ordering has also a strong effect on the coefficient b in Eq. (7.6). As illustrated in Fig. 7.9., the change of b with fluence on various A15 type compounds is of the same order of magnitude as the change of ρ_0 , which will be discussed in Section 7.6. For all measured A15 type compounds, the coefficient b has been reported as decreasing. In Nb_3Sn for example, b decreases from $8.5 \times 10^{-11} \Omega\text{K}^{-2}\text{m}$ for a single crystal with $\rho_0 = 8 \times 10^{-8} \Omega\text{m}$ /241/ to $1 \times 10^{-11} \Omega\text{K}^{-2}\text{m}$ in irradiated films with $\rho_0 = 100 \times 10^{-8} \Omega\text{m}$.

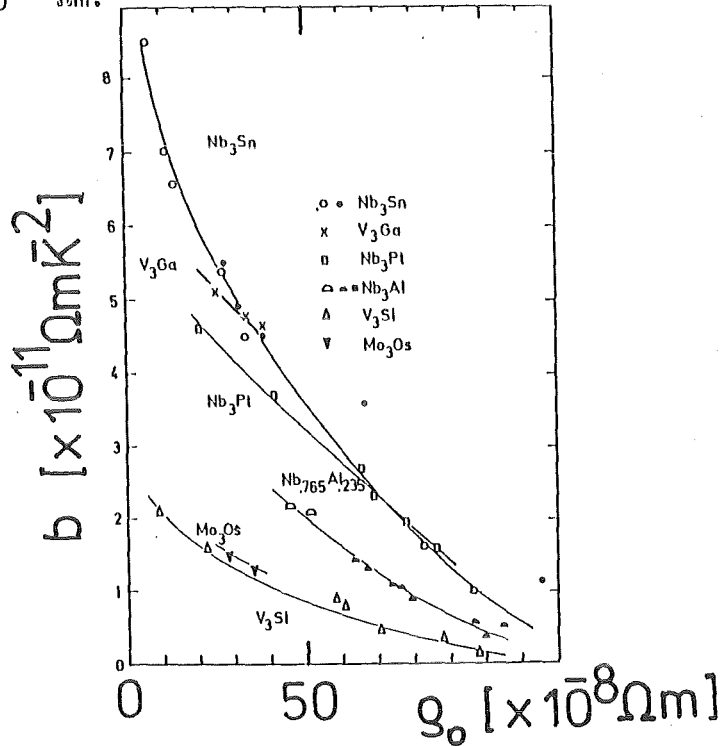


Fig. 7.9. The variation of the coefficient b in Eq. (7.6) for various A15 type compounds at different degrees of ordering, characterized by ρ_0 .
 \circ : Nb_3Sn /241, 254/, \bullet : Nb_3Sn /239/, \square : Nb_3Pt /142/ for the portion of the curve where $n = 2$, \triangle : Nb_3Al /220/, \blacktriangle : Nb_3Al /239/,
 \times : V_3Ga /38//, Δ : V_3Si /239/, ∇ : Mo_3Os /38,142/.

No explicit physical meaning has so far been attributed to the coefficient b , which mainly describes the rate at which $\rho(T)$ increases from ρ_0 to higher temperatures. It is noteworthy that the factors b_3 and b_5 for the compounds where Eq. (7.7) has to be applied rather than Eq. (7.6), having $n = 3$ and $n = 5$, respectively, show a very similar behavior to b with respect to the applied fluence /239/. However, the comparison between the b values for Nb_3Sn and V_3Si in Fig. 7.9. suggests that b does not simply depend on ρ_0 alone.

From the above remarks, it can be concluded that in spite of the data scattering due to different preparation techniques in the various works, but also due to possible traces of additional phases, the following tendencies can be identified (see also Table 7.2):

- a) there is a general agreement toward an exponent $n = 2$ (which could so far not be explained satisfactorily) for high T_c A15 type compounds as Nb_3Sn /239,243/, Nb_3Al /220,239,254/, Nb_3Ge /254,273/, V_3Si /217,254/, V_3Ga /220/, V_3Ge /240/ and Ti_3Sb /249/. The exponent n is not affected by changes of the order parameter. Disordering extends the region of the T^2 behavior towards higher temperatures.
- b) there is a category of A15 type compounds with low T_c values where $n = 5$, i.e. showing the Bloch-Grüneisen behavior: Mo_3Si /239/, Mo_3Ge /239,244/, Cr_3Si /38,250/. On a series of single crystals in the pseudobinary system $(V_{1-x}Cr_x)_3Si$, Berthel et al. /250/ have observed a gradual change from $n = 2$ on the V rich side to $n = 5$ on the Cr rich side,
- c) the third category comprises the "atypical" A15 type compounds with transition B elements, where $n = 3$: Nb_3Ir /220/, Nb_3Os /220/, V_3Pt /220/, Mo_6Re_4 /239/. /239/. A T^3 dependence is in general observed in transition metals and is described by the s-d interband scattering model of Wilson.

There are few A15 type compounds lying between these three main classes, as Nb_3Sn /240,244/, V_3Sn /245/ and the above mentioned Nb_3Pt and Nb_3Au /38,339/. Recently, Gurvitch /271,273/ proposed a correlation between the electron-phonon interaction parameter λ and the exponent n , based on an investigation on intermetallic compounds crystallizing in different crystal structures. In particular, he proposed that compounds with $\lambda > 1$ exhibit n values equal to or close to 2. However, there are strong exceptions to this rule: V_3Si , where n from 2 to 5 have been reported /217,235,253,254/ (see also Table 7.2, containing also unpublished own values on V_3Si close to $n = 3.4$ /38/) and the strong coupled superconductors Pb and $PbBi$ /273/. These important exceptions do not allow to accept the correlation proposed by Gurvitch /273/ in such a simple form, particularly as long as a convincing physical explanation for the occurrence of the exponent $n = 2$ has not been found. Nevertheless, all results mentioned in Table 7.2 together with those of Gurvitch /273/ allow to reformulate the correlation between λ and n after a restriction: for all compounds with $\lambda < 0.8$, there is $3 > n > 5$.

7.5. Compositional Effects on ρ_0

The electrical resistivity in A15 type compounds depends as well on the degree of ordering as on the effective composition. The value of the residual resistivity, ρ_0 , will thus in general be the result of a combination of the two effects. In order to decompose ordering and compositional effects in ρ_0 , the A15 material under study must be either completely ordered ($S = 1$) or perfectly stoichiometric ($\beta = 0.25$). It is convenient to start the discussion with V_3Si and Nb_3Sn , which were proven to be perfectly ordered (see Sect. 5) and exhibit a fairly large homogeneity range. In these both compounds, the changes in ρ_0 in unirradiated samples can directly be attributed to deviations from stoichiometry.

7.5.1. The System V_3Si

The variation of ρ_0 in V_3Si has been studied by Berthel and Pietrass /250/ and by Küpfer and Flükiger /271/ on a series of single crystals and by Flükiger et al. /220/ on a series of polycrystals with grain sizes above 1 mm. The results are shown in Fig. 7.10, where the RRR value ($RRR = \rho_{300K}/\rho_0$) has been plotted as a function of the Si content (the RRR value has been chosen rather than ρ_0 which is not well defined in each case, due to the irregular shape of the crystals). A striking feature of Fig. 7.10 is the sharp variation of the RRR quotient in the region at proximity of the stoichiometric composition.

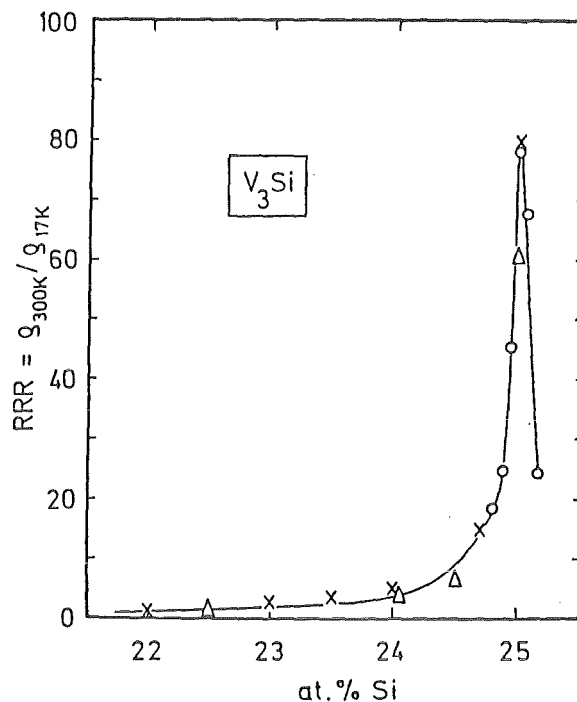


Fig. 7.10. The variation of the RRR ratio in V_3Si as a function of the Si content. o : Berthel and Pietrass /250/, x : Küpfer and Flükiger /271/, Δ : Flükiger et al. /220/.

Between 22 and 14.5 at.% Si, RRR increases from 1 to 6, while the addition of only 0.5 at.% Si from 24.5 to 25 at.% Si causes an increase up to RRR above 80 ! The variation of RRR seems to be symmetrical on both sides of stoichiometry. Fig. 7.10 demonstrates that a very little deviation from stoichiometry, leading to a partial replacement of A or B atoms on the 6c or the 2a sites, respectively, has a considerable effect on the value of ρ_0 . The nearly symmetrical behavior indicates that ρ_0 is mainly dependent on the perturbation due to wrongly occupied atoms, the excess atom being of secondary importance. In Nb_3Ir , another compound with the phase field extending at both sides of $\beta = 0.25$ ($0.22 < \beta < 0.28$), ρ_0 is found to increase faster at the Ir rich side (see later Fig. 7.14).

The behavior of the RRR ratio as a function of composition in the V_3Si system showing a sharp discontinuity at stoichiometry as shown in Fig. 7.10 is certainly the most expressive way to demonstrate that this system is perfectly ordered. The change of ρ_0 with β is strongest when approaching the stoichiometric composition. At the vicinity of $\beta = 0.25$, very small perturbations of the system, e.g. inhomogeneity, small deviations from stoichiometry, impurities, small amounts of ternary additives (see Sect. 8) or deviations from perfect ordering (discussed in 7.6) may cause a considerable increase of ρ_0 . Once the perturbation is important enough, e.g. $\beta \leq 0.245$ in Fig. 7.10, further changes of the state of the system lead to smaller changes in the normal state resistivity. Between $\beta = 0.20$ and 0.245 , RRR varies only from 2 to 5. With a value $\rho(300\text{K}) = 75 \times 10^{-8} \Omega\text{m}$ (see Figs. 7.1 and 7.5) a resistivity ratio $\text{RRR} = 83.7$ corresponds to $\rho_0 = 0.90 \times 10^{-8} \Omega\text{m}$, which is the lowest value reported so far in A15 compounds. This low value is a consequence of the particular way how the V_3Si single crystals were grown. The combination of extremely careful arc melting (with melting losses below 0.1 %) and of excessively long recrystallization times at temperatures close to the solidus (14 days at $1850 \pm 30^\circ\text{C}$) yields very homogeneous polycrystalline samples with large crystallites (grains) up to 5 mm size /220/. The very sharp variation of the RRR ratio close to stoichiometry suggests that the lowest ρ_0 value in V_3Si could even be substantially lower than the value of $0.9 \times 10^{-8} \Omega\text{m}$ mentioned above. At this high quality level, it may even be expected that ρ_0 of V_3Si could be further lowered by using very high quality vanadium (99.99 %) instead of the 99.7 % vanadium used in Ref. 220.

From these considerations, it follows that the lowest reported ρ_0 values for A15 type compounds at stoichiometry or close to this composition must in general be seriously affected by the compositional gradient. Indeed, even small inhomogeneities of say, ± 0.5 at. Si reduce the RRR ratio by a factor of 2 and more! As can be concluded from Fig. 7.10, the effect of the compositional gradient is considerably reduced if the average concentration is more than 0.5 at. % away from stoichiometry.

7.5.2. The System Nb₃Sn

The electrical resistivity in the perfectly ordered A15 type system Nb₃Sn (an order parameter $S = 1.00$ has been reported by Flükiger et al. /9/) has been studied by Devantay et al. /86/ and by Orlando et al. /186/. The former have reported the explicit dependence of ρ_0 on β , which is reproduced in Fig. 7.11.

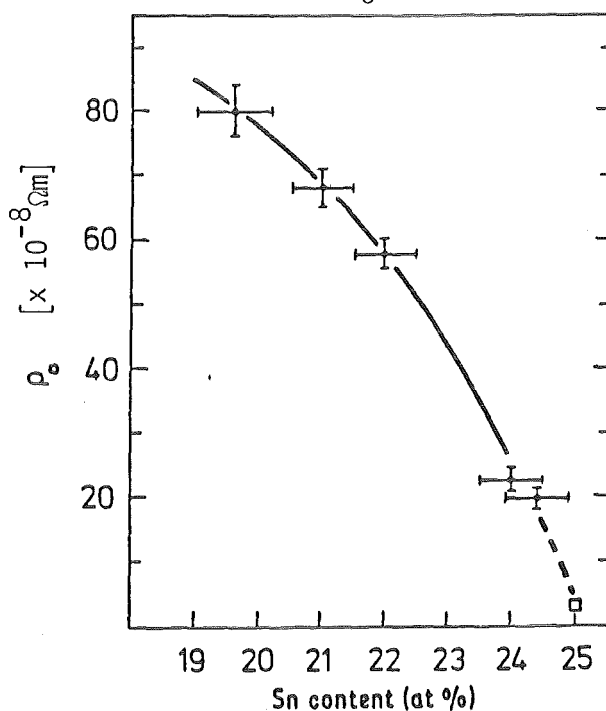


Fig. 7.11. The variation of ρ_0 in the system Nb₃Sn as a function of the Sn content. +: Devantay et al. /86/ (polycrystals, melted and homogenized at 1800 °C), □: Hanak et al. /296/ (single crystal, grown by CVD).

The samples below $\beta = 0.244$ were produced by levitation melting followed by homogenization (12 hours at 1800 °C), both under an argon pressure of 10 kbar. It is not possible to produce stoichiometric Nb₃Sn samples by melting techniques, due to the sluggish slope of the A15/A15 + L phase boundary and to the very low

melting temperature of 930 °C at 25.5 at. % Sn. For illustration, the Nb - Sn phase diagram of Charlesworth et al. /174/ has been reproduced in Fig. 7.12. A better way to prepare stoichiometric samples was found by Hanak et al. /168, 296/ who used the CVD process. It appears that CVD, but also the sintering process yield quite homogeneous Nb₃Sn samples with narrow calorimetric transitions (see Fig. 5.1), while the melted samples /86/ exhibit a noticeable composition gradient. Nevertheless, the data of ρ_0 vs. β in Fig. 7.11 can be considered as representative.

The value of ρ_0 from 19 to 24.4 at. % decreases from 82 to $20 \times 10^{-8} \Omega\text{m}$, corresponding to RRR ratios of ~ 1 and 4, respectively /86/. A further increase of the Sn content by 0.6 at. % lowers ρ_0 to values around $2 \times 10^{-8} \Omega\text{m}$ /185,296/, corresponding to RRR ≈ 40 . The behavior of ρ_0 in Nb₃Sn is very similar to that of V₃Si. The absolute values of ρ_0 at $\beta = 0.25$ are somewhat higher for Nb₃Sn, which is attributed to the metallurgical state of the measured sample, in particular the inhomogeneity.

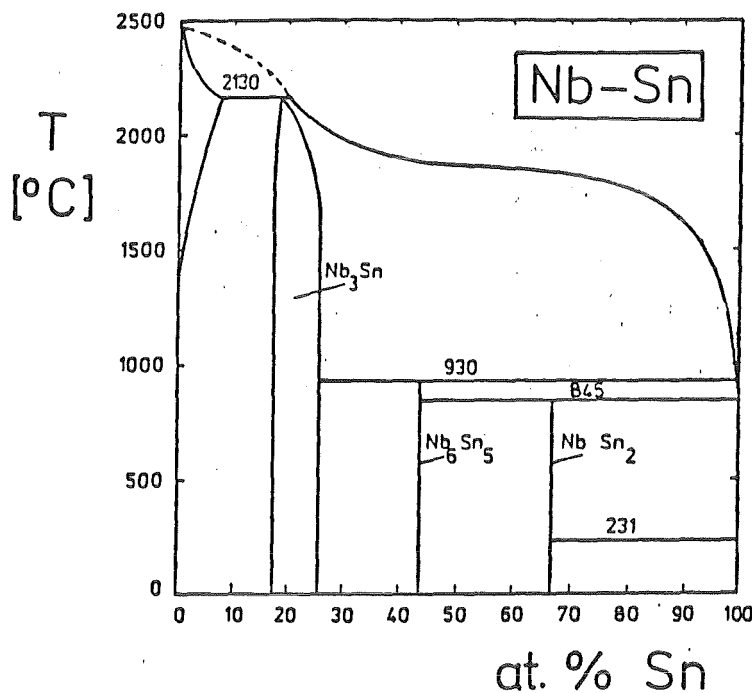


Fig. 7.12. The Nb - Sn phase diagram (After Charlesworth et al. /174/).

7.5.3. The System Nb₃Ge and a Comparison with V₃Si and Nb₃Sn.

In 5.1.1d, it had been mentioned that the system Nb₃Ge is also perfectly ordered, the reported deviation from perfect ordering, $S = 0.92 \pm 0.04$ (Sweedler et al. /68,69/) being rather due to the presence of additional phases (see Fig. 3.7) causing a large measuring error in S. A strong argument in favour of perfect ordering in Nb₃Ge is the variation of ρ_0 vs. β , measured by Kihlström et al. /73/ on a series of coevaporated and well characterized films. These data have been plotted in Fig. 7.13, together with those for Nb-Sn /86/ and V-Si /220/, showing an almost identical ρ_0 vs. β behavior for these three systems. The lowest reported ρ_0 value for Nb₃Ge is $30 \times 10^{-8} \Omega m$, which was confirmed by Schauer et al. /216/. Knowing how strong atomic ordering affects the value of ρ_0 (see paragraph 7.6, but also the system Nb-Al in Fig. 7.13), this behavior can indeed be considered as an important argument indicating that Nb₃Ge is perfectly ordered, but that even the sample with the lowest ρ_0 value exhibits a slight deviation from stoichiometry, the average Ge content being ~ 24 at.%.

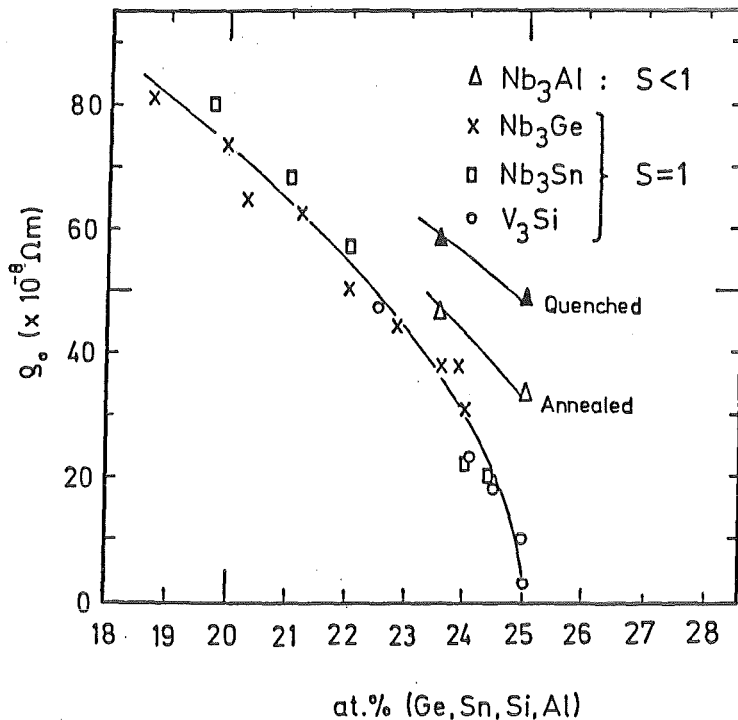


Fig. 7.13. ρ_0 vs. composition in the systems Nb-Sn /86/, V-Si /220/, Nb-Ge /173/ and Nb-Al /191,220/.

Obviously, this does not exclude that small parts of the sample (those with T_C values around 23 K) are even closer to $\beta = 0.25$. This is confirmed by the available specific heat data of Stewart /227/, showing a considerable width of the calorimetric transition at T_C .

7.5.4. The System Nb₃Al.

No systematic variation of ρ_0 vs. β has been undertaken so far in the system Nb-Al. Measurements on two samples with $\beta = 0.235$ and 0.25 recently reported by Flükiger et al. /191,220/ have been added to Fig. 7.13.

The variation of ρ_0 vs. β for Nb₃Al does not fit the common behavior of the three other systems. This is attributed to the fact that Nb₃Al exhibits a deviation from perfect ordering /28/. Both Nb₃Al samples have been prepared by arc melting, followed by a prolonged homogenization heat treatment at 1850 °C. In order to obtain two states with distinctly different degrees of ordering, both samples were first argon jet quenched from 1940 °C (upper points in Fig. 7.13), after which they were annealed 7 weeks at 750 °C (lower points in Fig. 7.13). The corresponding T_C and S values indicate that a change of T_C of 1.8 K corresponds to a difference in the order parameter lying between $\Delta S = 0.01$ and 0.02. this relative variation $\Delta T_C / \Delta S$ agrees with that previously reported by Sweedler and Cox /53/. The compositional inhomogeneity of the stoichiometric Nb₃Al sample is estimated to be smaller than ± 0.5 at. % Al, as deduced from the calorimetric measurements of Junod et al. /248/ on the same sample. As a conclusion, it can be said that the variation of ρ_0 vs. β for Nb₃Al follows the same tendency as for the systems Nb₃Sn, V₃Si and Nb₃Ge, but that the absolute ρ_0 values are enhanced with respect to these three systems due to the lower order parameter value. It can be recognized that for stronger deviations from stoichiometry (e.g. at $\beta = 0.20$) the influence of the degree of ordering on ρ_0 tends to vanish. The effect of atomic ordering on ρ_0 will be treated in the next paragraph.

7.5.5. The System Nb₃Ir.

The variation of ρ_0 with Ir content has been studied by Schneider and Linker /135/ and is represented in Fig. 7.14. The interest in this system arises from

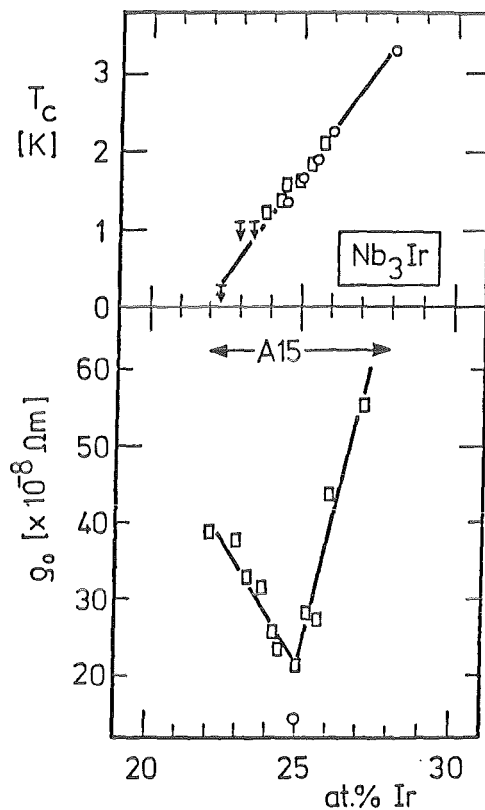


Fig. 7.14: Variation of T_C and ρ_0 as a function of composition in Nb_3Ir .

o: Data on bulk samples (Devantay /206/), \square : Data on thin film samples (Schneider and Linker /135/).

the phase stability at both sides of stoichiometry. Schneider and Linker /135/ found a minimum of ρ_0 at stoichiometry, with an almost symmetrical decrease at both sides. The ρ_0 value of $19.66 \times 10^{-8} \Omega m$ at stoichiometry /135/ agrees well with the value $\rho_0 = 14 \times 10^{-8} \Omega m$ reported by Devantay /206/. On the same figure the variation of T_C with β is represented, showing a continuous increase from < 0.1 K at 22 at. % Ir to 3.3 K at 28 at. % Ir /62/. This shows clearly that the frequently used correlations between T_C and ρ_0 have to be interpreted with care.

7.6. The Effect of Atomic Ordering on ρ_0 .

In the preceding paragraphs it has been shown that ρ_0 in Nb_3Al depends on atomic ordering. A more systematic work has been performed by Flükiger et al. /142/ on Nb_3Pt . This material was chosen because of the unique possibility of varying S within the range $0.88 \leq S \leq 0.98$ by quench and anneal procedures on a single-phased stoichiometric sample. The variation of ρ_0 for different order parameter values is shown in Fig. 7.15.

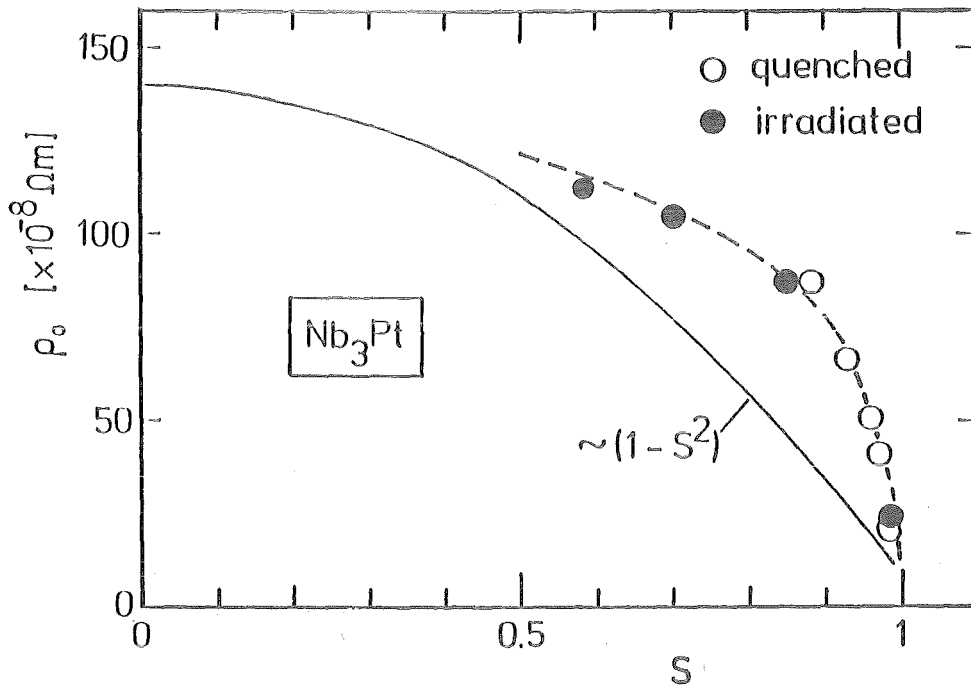


Fig. 7.15. Variation of ρ_0 with S in quenched /142/ and neutron irradiated /217/ Nb_3Pt . The dashed line represents a hypothetical $\rho_0 \sim 1 - S^2$ correlation /257/. (The dashed line is a guide to the eye).

Knowing the good correspondence between T_c and S in quenched and neutron irradiated Nb_3Pt (see Fig. 4.12), it is interesting whether it can be extended to the normal state resistivity ρ_0 . Such a comparison can be made using the ρ_0 values of Caton and Viswanathan /217/ (see Table 7.1), on neutron irradiated Nb_3Pt , estimating the order parameter values from Fig. 4.12. It is seen from Fig. 7.15 that the variation of ρ_0 with order parameter is very similar for quenched and irradiated samples, indicating that the effect of additional radiation induced effects as lattice expansion or static displacements on ρ_0 of Nb_3Pt is negligible when comparing to the effect of A \leftrightarrow B site exchanges.

A comparison between Figs. 7.13 and 7.15 shows that deviations from perfect ordering are at least as effective as compositional changes in increasing the value of ρ_0 . As an example, the occupation of 1% Nb sites by Pt (corresponding to $r_a = 0.99$ or $S = 0.96$) leads to $\rho_0 \approx 40 \times 10^{-8} \Omega m$. The same ρ_0 value in the systems Nb_3Ge , Nb_3Sn and V_3Si would be obtained at a 2% deviation from stoichiometry, thus reflecting the importance of chain integrity for the electrical resistivity.

The most remarkable feature in Fig. 7.15 is the similarity of $\rho_0 = \rho_0(S)$ for both argon jet quenched and neutron irradiated Nb_3Pt (see also Table 7.1). This means that the static displacements and the lattice expansion in the irradiated state do not seriously contribute as additional scattering centers limiting the electronic mean free path. The main contribution arises from the wrongly occupied sites originating by deviations from perfect ordering and/or from perfect stoichiometry. In other words, the enhancement of resistivity in a slightly disordered A15 type compounds is caused by the electronic scattering due the local breakdown of periodicity of the field in the lattice.

It can be easily seen that the curve in Fig. 7.15 does not follow the variation

$$\rho_0(S) = \Delta\rho_0(1-S^2) + \rho_0(S=1) \quad (7.4)$$

proposed by Muto /257/. This is not surprising if one considers that Eq. (7.4) was essentially verified for the system Cu_3Au . In the case of Nb_3Pt the enhancement of ρ_0 with decreasing S is much stronger than described by $\rho_0 \sim (1-S^2)$. At the vicinity of perfect ordering, the variation of $\rho_0(S)$ is strongest, in analogy to the variation $\rho_0(\beta)$ discussed in the preceding paragraph.

After having demonstrated for Nb_3Pt that $\rho_0 = \rho_0(S)$ is almost independent on the way how the disorder was produced, i.e. by quenching or by irradiation procedures, it is now possible to study the variation of ρ_0 with disordering in other A15 type compounds where a deviation from $S = 1$ could only be obtained by irradiation only, quenching procedures being unsuccessful. The available data on systems where S after irradiation was measured (and not only estimated) restricts the choice on two systems, one with a high T_c (Nb_3Sn) and the second one with a low T_c value (Nb_3Ir).

In these both systems, both the values of ρ_0 and S have been measured after irradiation with 20 MeV ^{32}S /136/ and 300 keV He^+ ions /135/, respectively. The data for Nb_3Sn are shown in Fig. 7.16, showing again a strong deviation from a $\sim (1-S^2)$ dependence, as for Nb_3Pt . The presently observed behavior in both systems is closer to $\sim (1-S^4)$, as shown in Fig. 7.16, thus showing that the simple model of Muto /257/ cannot be applied to high T_c A15 type compounds.

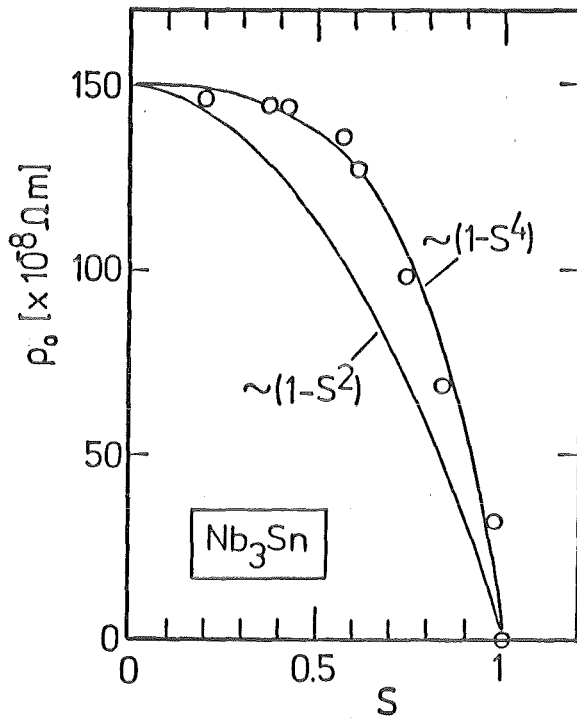


Fig. 7.16. Variation of ρ_0 with S in Nb_3Sn after irradiation with 20 MeV ^{32}S ions (Data extracted from Nölscher et al. /136/. For comparison, calculated dependences with $1-S^2$ and $1-S^4$ are added.

This model could, however, apply to low T_c compounds as Nb_3Ir , where the variation of ρ_0 vs. β close to the stoichiometric composition, reproduced in Fig. 7.14, follows the same scheme as for Cu_3Au /Ref. 257, p. 62/. The variation of ρ_0 vs. S for Nb_3Ir extracted from the data of Schneider and Linker /135/ are shown in Fig. 7.17. In this case, two different samples having composition close to Nb_3Ir have been irradiated by 300 keV H ions or 300 keV He ions, respectively. The value $\rho_0 (S \rightarrow 0)$ in both cases differ by $< 10\%$ only, indicating a little influence of the projectile. The variation of ρ_0 with S , however, shows substantial differences, the dependence $\sim (1-S^2)$ being observed for He ions only. A comparison between Figs. 7.15, 7.16 and 7.17 shows that the initial variation of ρ_0 , for small deviations from perfect ordering is much stronger for the compounds Nb_3Pt and Nb_3Sn than for Nb_3Ir .

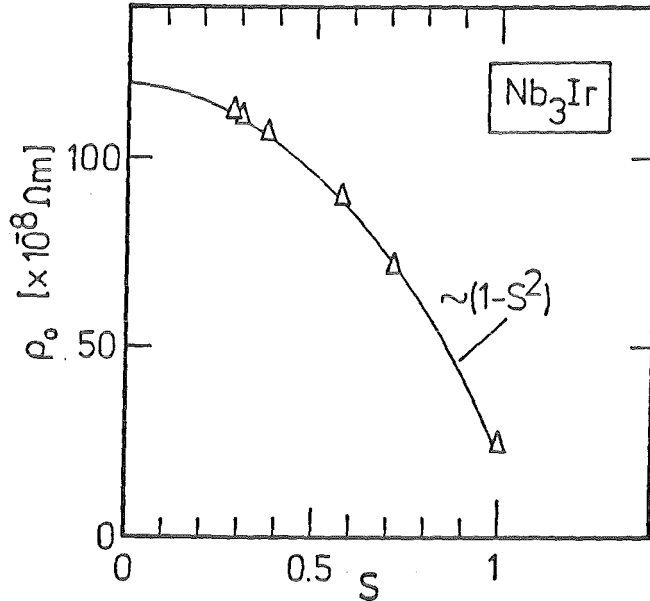


Fig. 7.17. ρ_0 vs. S for Nb_3Ir after irradiation with He ions ($E = 300$ keV), extracted from the data of Schneider and Linker /135/.

The present considerations have been restricted to the few cases where both ρ_0 and S were measured on the same samples. It is possible to extend the comparison to systems where the S values were calculated, i.e. using Appel's theory /304/. The results for the systems Nb_3Ge and V_3Si (not shown here) show a similar behavior to that of Nb_3Sn . At present, no physical model can be proposed for explaining the observed variation of ρ_0 with S in A15 type compounds. Again, the system Nb_3Ir (with a transition B element) shows a different behavior, the variation of ρ_0 with S being slower than for the other compounds with nontransition B elements. This is confirmed by the slow variation of ρ_0 in disordered $Mo_{.3}Os$ (see Fig. 7.3) and $Mo_{.65}Re_{.35}$ /301/.

8. TECHNICAL ASPECTS OF ATOMIC ORDERING MULTIFILAMENTARY WIRES

8.1 General Remarks about Multifilamentary Wires.

In the last years, there has been a growing need for superconducting high field magnets. In the next future, superconducting magnets producing fields above 12 Tesla will still be wound with wires based on A15 type compounds with upper critical fields, $B_{c2}(0)$, exceeding 25 Tesla. Wires based on compounds crystallizing in other phases with high upper critical magnetic fields, e.g. NbN /305/ or $PbMo_6S_8$ /306/, show without any doubt promising current carrying properties, but still need a considerable development before achieving a practical stage. An A15 type material to be used in high field magnets must fulfill the following conditions:

- $T_c \geq 15$ K
- $H_{c2}(4.2$ K) ≥ 25 T
- Grain Size ≤ 200 nm.

In the following, it will be demonstrated that the first two points are influenced by the degree of atomic ordering.

It has already been said in the present work that the first two properties, i.e. T_c and H_{c2} , depend on the degree of atomic ordering. It will be shown in the following that there is an additional condition: the material must be a dirty type II superconductor. This is the point where the degree of ordering plays an important role when optimizing the current carrying capacity of a multifilamentary superconducting wire at high magnetic fields. It has been stated by the author and coworkers /9,191,307,308/ that the knowledge of the order parameter in the investigated A15 type material, e.g. Nb_3Sn , Nb_3Al , V_3Ga , Nb_3Ge ,... is of primary importance for the understanding of the effects leading to an optimization of the critical current density J_c . The effect of ordering on the critical current density J_c of superconducting wires is essentially dominated by the variation of the normal state resistivity ρ_0 , discussed in Sect. 7. For dirty type II superconductors, this quantity is correlated to the value of the upper critical field H_{c2} by the equation

$$H_{c2} \sim T_c \cdot \gamma \cdot \rho_0 \quad (8.1),$$

where T_c is the superconducting transition temperature and γ the electronic specific heat coefficient. It can be easily seen from the variations of ρ_0 with the composition β (Fig. 7.13) and of ρ_0 with the order parameter (Figs. 7.15 and 7.16) that at the vicinity of stoichiometry or perfect ordering $\Delta\rho_0$ largely exceeds the corresponding ΔT_c or $\Delta\gamma$ values. This question will be studied in detail in the following. The attention will be restricted to the three systems Nb_3Sn , Nb_3Al and V_3Ga , which can already be prepared in a multifilamentary configuration.

8.2 Wire Preparation

The numerous methods reported so far for producing multifilamentary wires based on A15 type compounds have all one thing in common: During the mechanical deformation to the final wire diameter, all the constituents have to be ductile, the inherently brittle A15 phase being formed at the end of the deformation process only, by a reaction at temperatures well below $1000^\circ C$. These ductile components are ordinarily combinations between a variety of materials like Nb, V, Cu, Cu-Sn, Cu-Ga, Ta, ..., depending whether Nb_3Sn or V_3Ga is produced /319,320,327/.

Multifilamentary wires have been recently produced at a laboratory scale with another A15 type compound, Nb_3Al /309/ by using the cold powder metallurgical approach /191,310/. Investigations are actually performed in several laboratories for producing Nb_3Al wires at an industrial scale. This constitutes a difficult enterprise, the deformation properties of Nb-Al wires being substantially different from those of the "classical" Nb_3Sn and V_3Ga wires mentioned above.

It is unfortunate that just for the two binary A15 type compounds exhibiting the highest T_c values, Nb_3Ge ($T_c = 23$ K) and Nb_3Ga ($T_c = 20.7$ K), no way is seen so far to obtain the required multifilamentary configuration. This may appear relatively surprising in view of the relative ease with which both compounds can be formed as thin films or tapes, either by sputtering, coevaporation or CVD. This illustrates that the occurrence of a high T_c value in a compound does not necessarily imply its suitability for practical superconducting wires fulfilling the necessary current carrying and stability requirements at high fields.

The main factors deciding in favour of a given material for the use in superconducting high field magnets besides high T_c and $H_{c2}(0)$ values are:

a) its metallurgy (phase stability at compositions close to stoichiometry) and b) its growth kinetics (grain size, pinning behavior at the grain boundaries). Both a) and b) determine the reaction conditions, i.e. reaction time and temperature, which have to be optimized, the criterion being a maximum of J_c , the overall critical current density at the desired field, B_0 .

The search for possible new methods to produce multifilamentary wires based on the A15 type compounds exhibiting the highest T_c and H_{c2} values will in the future mainly be directed towards nonequilibrium methods, the stoichiometric composition being metastable at practical reaction temperatures, i.e. below 1000°C . This can be illustrated by two examples: i) Nb_3Al and ii) $\text{Nb}_3\text{Al}_{.8}\text{Ge}_{.2}$. The latter was recently retained in the amorphous state by fast quenching on a hot substrate. If the amorphous alloy would be ductile enough to permit ulterior plastic deformation, the way would be open to the formation of fine filaments. At present, however, it is too early for estimating the chances of such a procedure.

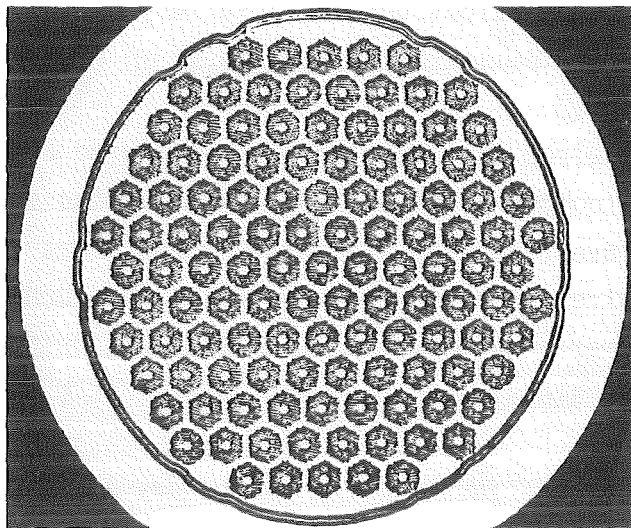


Fig. 8.1. Typical Nb_3Sn multifilamentary superconducting wire. 13.000 Nb_3Sn filaments in a Cu bronze matrix are surrounded by a Ta for protecting the external Cu stabilizer.

8.2.1. The Equilibrium Phase Diagrams of the Systems Nb₃Sn, V₃Ga and Nb₃Al

The A15 phase fields of the systems Nb-Sn /174/ is represented in Fig.7.12, those of V₃Ga /20/ and Nb₃Al /35/ in Fig. 8.2.

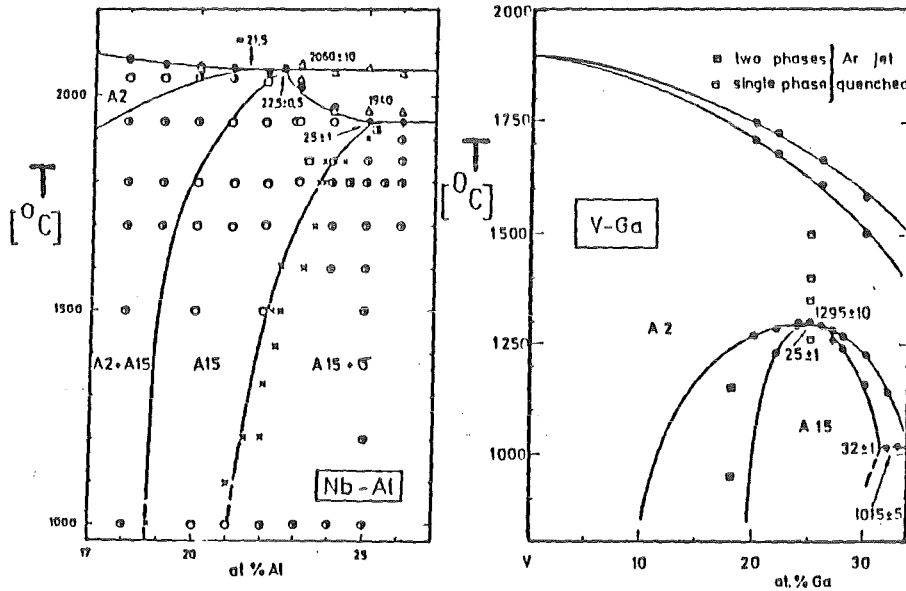


Fig. 8.2. The A15 phase fields in the systems V-Ga /20/ and Nb-Al /35/.

It is seen that the stoichiometric composition in the systems Nb₃Sn and V₃Ga is comprised at all temperatures of the corresponding A15 phase field, while for Nb₃Al, it is stable at 1940°C only, the equilibrium composition at 1000°C being close to 21.5 at.% Al /35/. This difference is of fundamental importance, since practical A15 superconducting wires are always reacted at temperatures below 1000°C: In the case of Nb₃Al, Al contents exceeding 21.5 at.% can only be obtained by nonequilibrium processes. Such processes are necessary, since at 21.5 at.% Al, this compound would only exhibit T_c values around 9 K and H_{c2}(0) values close to 15 T (see Fig. 8.3), i.e. too low for a practical superconducting wire.

8.3. Variation of the Physical Properties with Composition in Various A15 Systems

8.3.1. The Superconducting Transition Temperature

It is interesting to compare the variation of T_c with composition in various A15 type compounds. All high T_c compounds exhibit a maximum at the stoichiometric composition, but the behavior of T_c close to β = 0.25 shows

characteristical differences. An almost linear variation T_C vs. β is observed for V_3Ga , Nb_3Pt and V_3Pt (Fig. 8.3), where the A15 phase extends to both sides of the stoichiometric composition. The same figure also shows that the behavior of γ in these systems is very similar to that of T_C .

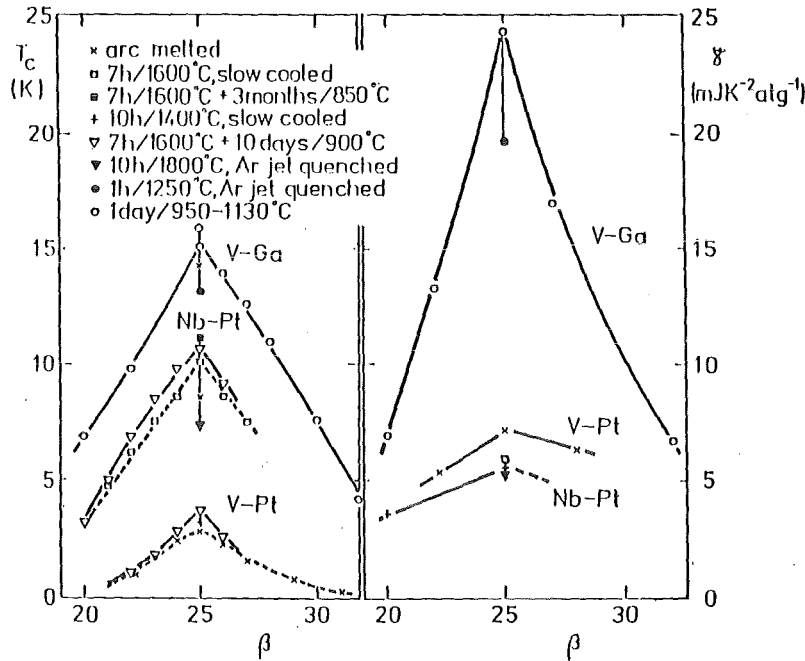


Fig. 8.3. T_C and γ vs. the composition β (in at.%) for the A15 phase in the systems V-Ga, Nb-Pt and V-Pt.

The behavior of T_C in the system V_3Au is plotted in Fig. 8.4. It is particularly interesting due to the strong dependence of T_C on the order parameter, but shows nevertheless a linear dependence. The solubility limit in the A15 phase of V-Au is 24 at. Au, while the highest achievable order parameter is $S_a = 0.94$ (see Table 5.9). An extrapolation of T_C towards $\beta \rightarrow 0.25$ yields $T_C \sim 3.5$ K. Flükiger et al. /18/ have further attempted to estimate T_C for $S \rightarrow 1$ and found $T_C \approx 5$ K.

Although the superconducting transition temperature in Nb_3Ge has been measured on a great number of samples prepared by various methods, the variation of T_C with composition is less known than for other A15 type compounds. At ~ 19.5 at. % Ge, $T_C = 6$ K was reported on arc melted samples /62/. On splat-cooled samples, Matthias et al. /312/ reported $T_C \approx 17$ K. From their lattice parameter value, $a = 0.5150$ nm, the composition can be estimated to 23 at. % Ge. The most difficult question is whether the highest value, $T_C = 23$ K, corresponds to the stoi-

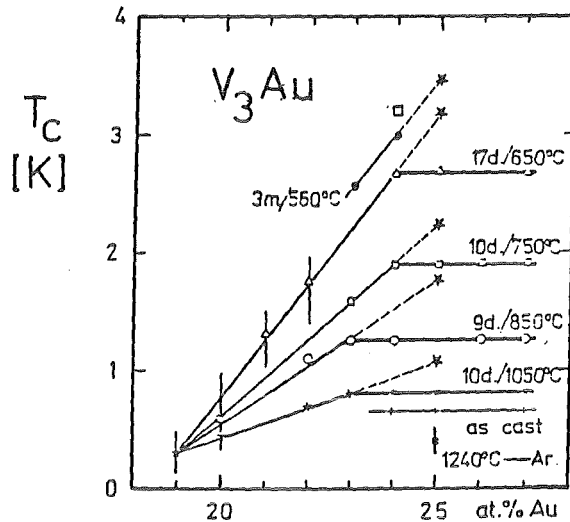


Fig. 8.4. T_C vs. atomic composition for V_3Au , showing the strong dependence on the annealing conditions (i.e. on the order parameter). \square : Van Reuth et al. /3/, $\circ, \Delta, \bullet, +$: Flükiger et al. /18/, \ast : extrapolated to $\beta \rightarrow 0.25$ /18/.

stoichiometric composition. As mentioned earlier in this work several considerations, in particular the variation of ρ_0 with β , lead to the conclusion that Nb_3Ge is perfectly ordered. The lowest ρ_0 value reported so far, $\sim 30 \times 10^{-8} \Omega m$ /73/ suggests an effective composition close to 24.5 at.% Ge. As discussed below, there are arguments suggesting that the correct composition would rather be ~ 24.5 at. % Ge, which is also confirmed by Kihlström et al. /73/.

The variation of T_C in the system Nb_3Ga /7/ and Nb_3Ge /62, 73, 312, 313, 314/ is shown in Fig. 8.5. The system Nb_3Ga has been studied in detail by quench and anneal procedures (Flükiger and Jorda /315/) and shows a slight saturation tendency for T_C .

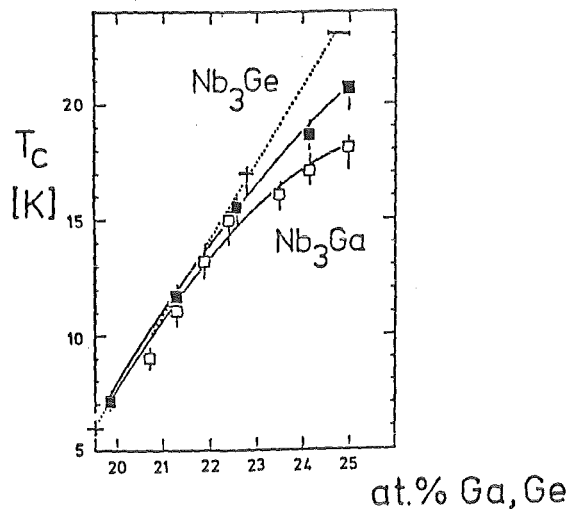


Fig. 8.5. Variation of T_C vs. composition in Nb_3Ga and Nb_3Ge . \square : Nb_3Ga , argon jet quenched /7, 315/, \blacksquare : Nb_3Ga , quenched + 1 month /650°C /7, 315/ \ast : Nb_3Ge , (~ 19 at. % Ge, melted /62/, ~ 23 at. % Ge, splat-cooled /312/, ~ 25 at. % Ge, sputtered /313/ or coevaporated /73, 314/.

This tendency to saturate is also observed in the system Nb_3Al (see Fig. 8.6).

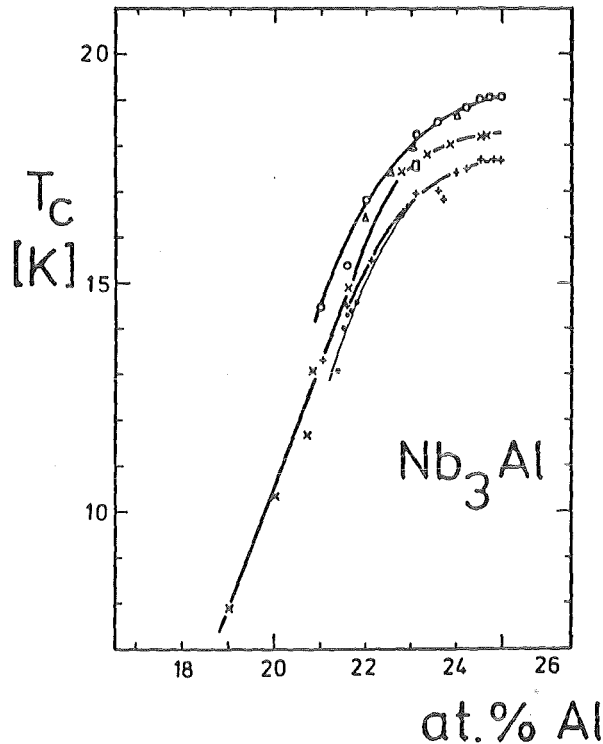


Fig. 8.6. T_C as a function of the Al content in the Nb_3Al phase: + after Ar jet quenching from temperatures ranging from 1100°C up to 1940°C , x: after cooling by radiation (radiation quench) from the same range of temperatures, o: annealed for periods between 30 and 50 days at temperatures ranging from 650 to 750°C , •: prepared by electron beam coevaporation /189/ (From Flükiger et al. /28/).

As stated by Flükiger et al. /28/, the order parameter in the system Nb_3Al decreases from $S_a = 0.97 \pm 0.02$ at 23.1 at. % Al to $S_a = 0.95 \pm 0.02$ at 24.5 at. % Al. Thus, the saturation of T_C could be correlated to the decrease of the order parameter when approaching the stoichiometric composition (see 5.1.1).

An anomalous saturation of T_C close to $\beta = 0.25$ has also been reported in the system Nb_3Sn (see Fig. 8.7). In this case, the cause for the saturation is thought to be different than in Nb_3Al . Indeed, the perfectly ordered state in Nb_3Sn /9/ is thought to create the necessary conditions for the cubic-tetragonal martensitic transformation for Sn contents exceeding 24.5 at. % Sn /86/.

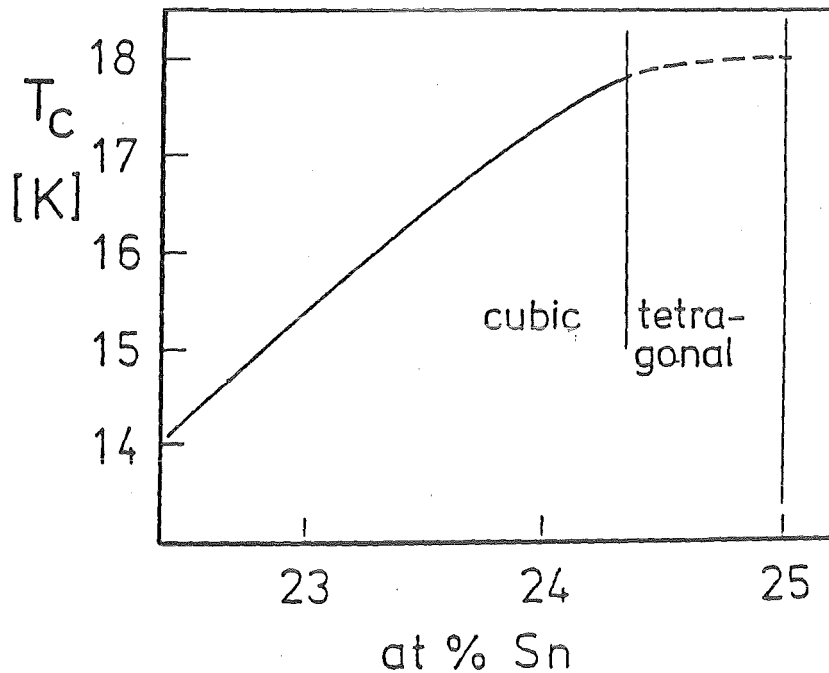


Fig. 8.7. T_C vs. composition in Nb_3Sn (After Devantay et al. /86/)

The extrapolation of T_C to 25 at. % Sn for a hypothetical, cubic and stoichiometric sample would yield $\sim 19K.$, i.e. nearly 1K higher than the reported value for tetragonal stoichiometric Nb_3Sn . This is indirectly confirmed by the slight increase of T_C in alloyed Nb_3Sn occurring simultaneously with the suppression of the martensitic transformation, as shown later in this section.

8.3.2. The Electronic Specific Heat

A further quantity in Eq. (8.1) is the electronic specific heat γ . For obvious reasons, the variation of γ with composition is less known than that of T_C . Nevertheless, the data collected in Tables 6.5 and 6.6 allow a rough picture of this variation. In general, $\gamma = \gamma(\beta)$ in V and Nb based high T_C A15 type compounds varies in a very similar way to $T_C = T_C(\beta)$. This is best illustrated for the systems V-Ga and Nb-Pt in Fig. 8.3. Measurements of γ in the systems Nb_3Sn at $\beta = 0.20, 0.22$ and 0.25 /169, 276/, in the system Nb_3Ge at $\beta = 0.20$ and ~ 0.25 /195, 227/, in the system Nb_3Ga at $\beta = 0.19$ and ~ 0.25 /195, 227/ and V_3Si at $\beta = 0.20, 0.24$ and 0.25 /276/ confirm the general tendency (see Table 6.6).

8.3.3. The Electrical Resistivity

Compositional and ordering effects on ρ_0 of various A15 type compounds have already been described in 7.4 and 7.5. The main conclusion was that a perfectly ordered, stoichiometric A15 type compound should exhibit ρ_0 values well below $10 \times 10^{-8} \Omega\text{m}$ (see Fig. 7.2). The system $V_3\text{Si}$ with particularly favourable metallurgical conditions (precise stoichiometric composition, homogeneity) exhibits the lowest value with $\rho_0 < 1 \times 10^{-8} \Omega\text{m}$, which raises the question whether the latter should be considered as being representative for the true ρ_0 value in A15 type superconductors. This illustrates again the strong influence of small deviation from a perfect A15 crystal on the electrical resistivity ρ_0 , which thus appears as being the most sensitive physical quantity for describing these variations.

For technical superconductors as Nb_3Sn , Nb_3Al and $V_3\text{Ga}$, the ultimate limit of ρ_0 is of little interest only. It is particularly important to recall that between 24.5 and 25 at. % Sn or Si in the systems Nb_3Sn and $V_3\text{Si}$, respectively (and presumably in Nb_3Ge), ρ_0 varies by almost one order of magnitude, which contrasts to the simultaneous change of T_c by 10 % only. In other words, going from $\beta = 0.245$ to 0.25 in these systems corresponds to go from a dirty type II superconductor (with an electronic mean free path $\lambda \leq 3 \text{ nm}$) to a clean type II superconductor with $\lambda > 10 \text{ nm}$. After these remarks, it is now clear why for technical applications only type II superconductors in a dirty state can be envisaged.

8.3.4. The Upper Critical Magnetic Field

In virtue of Eq. (8.1), high values of T_c , γ and ρ_0 lead to a superconductor having a high value of the upper critical magnetic field H_{c2} . Consequently, this quantity is also dependent on atomic ordering and composition. The variation of H_{c2} in various A15 type compounds ($V_3\text{Ga}$, Nb_3Pt , $\text{Nb}_3\text{Au}_{.7}\text{Pt}_{.3}$ and Mo_3Os) is shown in Fig. 8.9. In all these cases, partial disorder was induced by quenching procedures. The corresponding $\rho(T)$ measurements on the same samples have been plotted in Fig. 7.3. In spite of their different behavior with regard to paramagnetic limiting, all investigated systems exhibit large variations of $H_{c2}(T)$ in spite of the small changes in order parameter produced by heat-treatment. For $V_3\text{Ga}$ and Nb_3Pt , increases of the order parameter $\Delta S = 0.03$ and 0.06 cause an increase in $H_{c2}(0)$ of 10 and 16 %, respectively. An even greater increase of

$H_{c2}(0)$ ($\sim 40\%$) is observed for $Nb_3Au_{0.7}Pt_{0.3}$. (The different states of ordering are characterized by the corresponding heat treatments. The order parameter of a ternary system is not defined). For Mo_3Os , however, an increase of $\Delta S = 0.06$

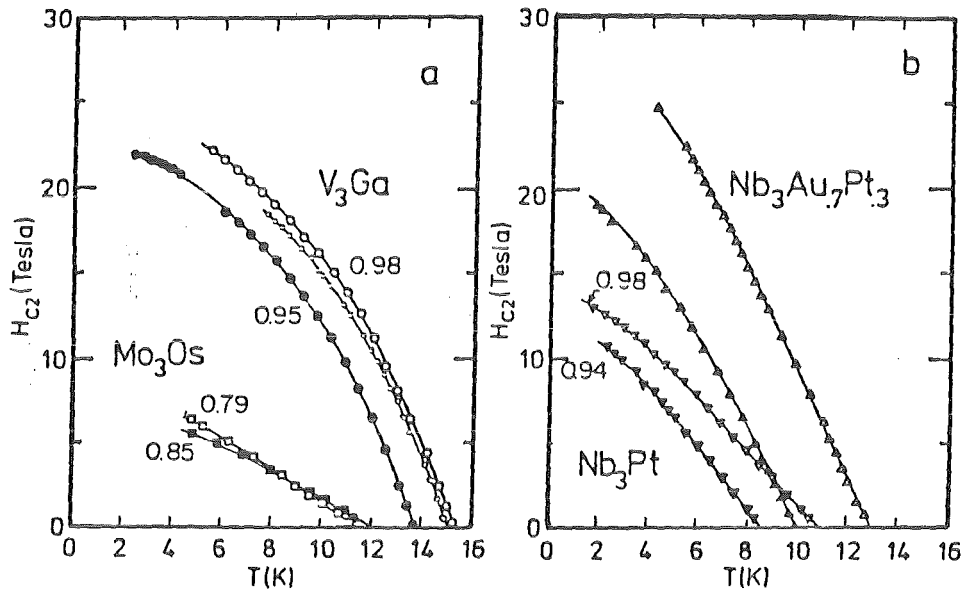


Fig. 8.9. $H_{c2}(T)$ for different ordering parameters, S .

a) V_3Ga ($S = 0.98$ and 0.95); Mo_3Os ($S = 0.85$ and 0.79).

b) Nb_3Pt ($S = 0.98$ and 0.94).

Heat treatment of $Nb_3Au_{0.7}Pt_{0.3}$: 2 weeks at $750^\circ C$ (Δ), and 24 hours at $1250^\circ C$ (∇), followed by quenching (Flükiger et al. /142/).

produced a decrease in $H_{c2}(0)$ from 8.3 to 7.1 Tesla, in good agreement with earlier data. The initial slope, $(dH_{c2}/dT)_{T=T_c}$, is also affected by ordering (see Table 8.1). For Mo_3Os and Nb_3Pt , increasing disorder enhances the value of the initial slope from 0.85 to 1.05 and from 1.6 to 1.95 tesla/K, respectively, in contrast to $Nb_3Au_{0.7}Pt_{0.3}$, for which the initial slope decreased. It should be noted (see Fig. 8.9) that the initial slope is difficult to determine for strongly Pauli paramagnetical limited materials such as V_3Ga . In this case, there is a noticeable variation of this slope very close to T_c and the slope cannot be determined accurately. The errors in this determination make detailed comparisons with S difficult. The upper critical fields of Mo_3Os and $Nb_3Au_{0.7}Pt_{0.3}$ agree with the predictions for a dirty type II superconductor; the value $h(0) = H_{c2}(0)/T_c(dH_{c2}/dT)_{T=T_c}$ for both systems is close to the theoretical value, independent on the degree of order (Table 8.1). It is interesting that $H_{c2}(T)$ for Nb_3Pt falls well above the predictions in agreement with Bongi et al. /317/. In

Compound	Ordering treatment (time /°C)	T _c (K)	S	γ (mJ/K ² cm ³)	$\frac{dH_{c2}}{dT} \Big _{T_c}$ (T/K) ^c	ρ ₀ (X10 ⁻⁸ Ωm)	H _{c2} (0) ^d (T)	H _{c2} (0) ^e	h(0) ^f
V ₃ Ga	3w./610 ^a	15.3		2.87	4.0	20.3	25	27	0.44
V ₃ Ga	1/2h./1250 ^a	15.1	0.98	(2.72) ^c	4.0	24.2	23.1	30	0.38
V ₃ Ga	1/2h./1250 ^b	13.8	0.95	2.37	3.6	32.7	22	33	0.40
Mo ₃ Os	2w./1100 ^a	12.1	0.85	0.57	0.85	28.5	7	6	0.70
Mo ₃ Os	1/2h./1950 ^b	11.4	0.79	0.56	1.05	35.8	8	7	0.69
Nb ₃ Pt	4w./900 ^a	10.9	0.98	(0.58) ^c	1.6	20.1	15	4	0.80
Nb ₃ Pt	1/2h./1800 ^b	8.6	0.94	0.52	1.95	66.6	13	9	0.74
Nb ₃ Au _{0.7} Pt _{0.3}	2w./750 ^a	12.9		1.02	3.3	60.1	30	24	0.70
Nb ₃ Au _{0.7} Pt _{0.3}	1/2h./1550 ^b	10.0		(0.62) ^c	2.9	82.5	21	16	0.70

Table 8.1. High field parameters, specific heat and electrical resistivity of V₃Ga, Nb₃Pt, Nb₃Au_{0.7}Pt_{0.3} and Mo₃Os at different degrees of atomic ordering. ^aSlowly cooled, ^bArgon jet quenched, ^cInterpolated values, ^dExtrapolated from measured data, ^eCalculated from $H_{c2}(0) = 3.06T_c \gamma \rho_0$, ^fCalculated from $h(0) = H_{c2}(0) \left[T_c \cdot \frac{dH_{c2}}{dT} \Big|_{T_c} \right]^{-1}$ (After Flükiger et al. /142/).

addition, an increase of the order parameter from S = 0.94 to S = 0.98 enhances the value of h(0) from 0.74 to 0.80. It can be suggested that the high value of h(0) for Nb₃Pt may be due to d band overlap at the Fermi level.

Numerous metallurgical effects can influence the evaluation of the resistivity at low temperatures. Generally, these effects increase the value of ρ_0 so that estimates of $H'_{c2}(0)$ in Table 8.1 would be expected to give a value larger than measured. Thus it is difficult except under particularly favorable circumstances to determine $H'_{c2}(0)$ using resistivity data. The estimates of $H'_{c2}(0)$ calculated with ρ_c gives values larger than measured for V_3Ga which is consistent with the observed strong paramagnetic limiting. The results for Mo_3Os are close to the measured values, but the results for Nb_3Pt give a calculated value of $H'_{c2}(0)$ which is quite low. Even the relatively dirty $Nb_3Au_{0.7}Pt_{0.3}$ materials give a low calculated value of $H'_{c2}(0)$.

The low resistivity and large residual resistance for well-ordered Nb_3Pt suggests a long mean free path, λ_{tr} . Estimates of $\lambda_{tr} \sim 10$ nm for sample 1 of Fig. 7.3 and $\xi_0/\lambda_{tr} \approx 0.7$ indicate that this material is a relatively clean superconductor.

It is interesting that by introducing 3% Pt atoms on the Nb sites by quenching from $1800^\circ C$, corresponding to an order parameter $S = 0.88$, λ_{tr} is reduced by almost 10, so that Nb_3Pt then becomes a dirty type II superconductor. In addition, the alternation of the mean free path by thermal methods is reversible. Similar estimates for the Mo_3Os materials in Table 8.1 yield $\lambda_{tr} \sim 2$ nm and $\xi_0/\lambda_{tr} \approx 10$ so that these are dirty. Calculations for the well ordered V_3Ga ($T_c = 15.3$ K) yield $\lambda_{tr} \approx 2$ nm and $\xi_0/\lambda_{tr} \approx 0.3$.

Discussing critical current density values J_c at high magnetic fields, it is mostly neglected how strong the chemical composition may influence the value of H_{c2} . H_{c2} vs. composition for the systems Nb-Ge, Nb-Ga, V-Ga, Nb-Pt and V-Pt is illustrated in Fig. 8.10/142/.. For the high T_c compounds Nb_3Ge and Nb_3Ga , a variation $\Delta H_{c2}/\Delta\beta \approx 5$ Tesla per at.% is found. For the paramagnetically limited system V_3Ga , the influence of composition on H_{c2} is considerably smaller, ~ 2 Tesla/at. % Ga. This value is even smaller than in the system Nb-Pt ($\sim 3T/at.\% Pt$ at $\beta < 0.25$), in spite of the considerably lower T_c value of the latter, which is not paramagnetically limited (similarly to all other Nb based A15 type compounds).

Due to the peculiar behavior of T_c at the vicinity of $\beta = 0.25$ in Nb_3Sn (Fig. 8.7) and Nb_3Al (Fig. 8.6), the variation H_{c2} vs. β in these two systems

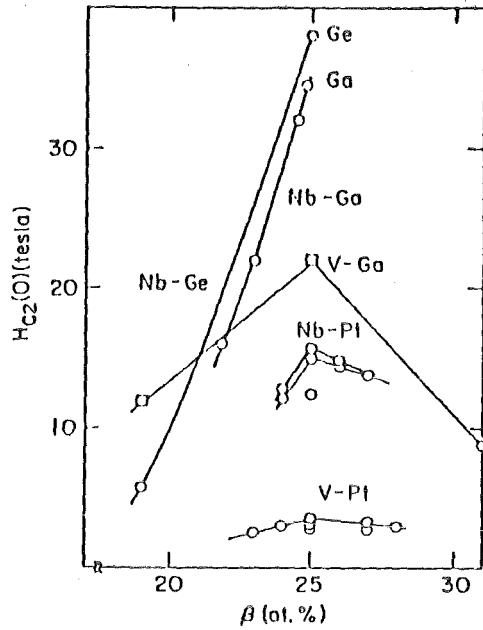


Fig. 8.10. Upper critical field $H_{c2}(0)$ as a function of composition, β , in $A_{1-\beta} B_{\beta}$ compounds for the various A15 compounds. The variation of the points at $\beta = 0.25$ for Nb-Pt and V-Pt show the effects of atomic order (after Flükiger et al. /142/). The slope for Nb-Ge and Nb-Ga is ~ 5 T/at.%.

is expected to be more complex than for Nb_3Ge and Nb_3Ga . For comparison, the variation of both T_c and H_{c2} in the systems Nb_3Sn and Nb_3Al has been plotted in Fig. 8.11.

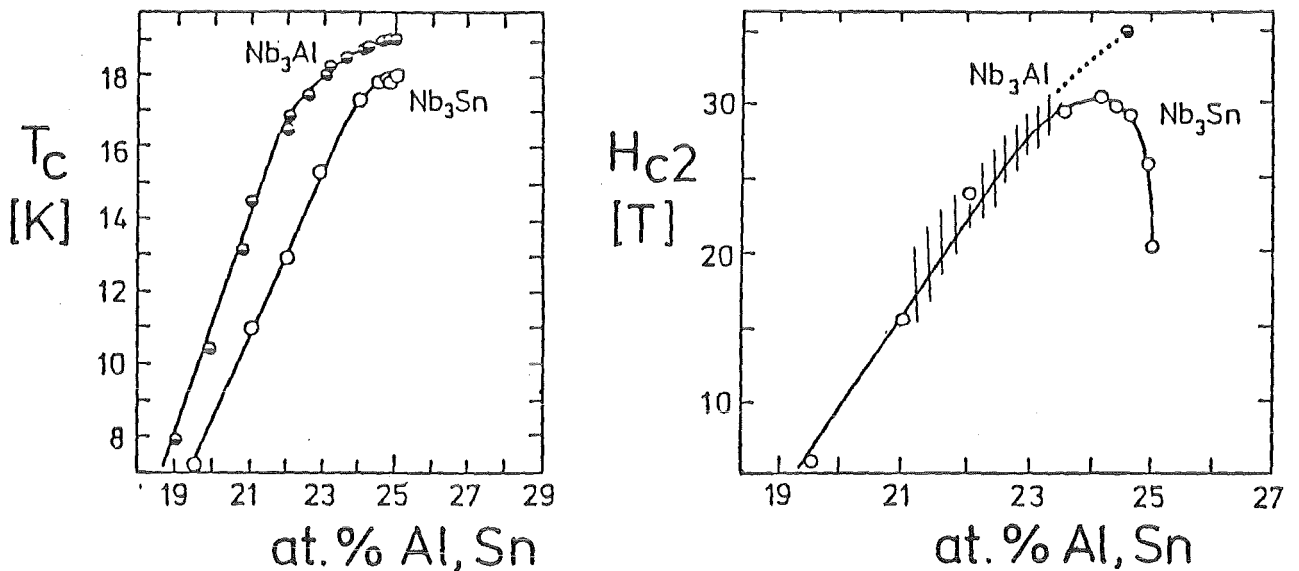


Fig. 8.11. Variation of T_c and $H_{c2}(0)$ as a function of composition in the A15 systems Nb-Sn and Nb-Al (Flükiger /308/). The hatched area for Nb_3Al reflects the uncertainty in determining the atomic compositions from T_c in the work of Kwo et al. /189/.

In contrast to the other two systems, the variation H_{c2} vs. β for Nb_3Sn does not follow the behavior of T_c (86): above ~ 24 at.% Sn, a rapid decrease of $H_{c2}(0)$ is observed /186, 308/, a consequence of the strong variation of the electrical resistivity, ρ_0 , in this composition range /86/. In this compound, the occurrence of both, perfect ordering /9/ and stoichiometry leads to a very low resistivity value, $\rho_0 \approx 2 \mu\Omega\text{cm}$ (185), which is nearly an order of magnitude smaller than the value for 24 at.% Sn, $\rho_0 = 22 \mu\Omega\text{cm}$ /86/. The sharp drop of ρ_0 in this range is caused by the substitution of Sn atoms by B atoms for nonstoichiometric compositions: The relative change of the electronic mean free path is comparatively stronger for small perturbations of the perfectly ordered, perfectly stoichiometric state than for large perturbations (here, the deviation from stoichiometry is understood as a perturbation). Thus, the maximum of $H_{c2}(0)$ in Fig. 8.11 can be explained on the basis of the "dirty limit" equation(8.1) as the result of two opposite effects: i) below 24 at.% Sn, the increase of T_c and γ is dominant over the decrease of ρ_0 , and $H_{c2}(0)$ increases with β , and ii) above 24 at.% Sn, T_c (and probably also γ) shows the above mentioned "saturation", and the strong decrease of ρ_0 dominates, thus leading to the observed decrease of $H_{c2}(0)$ shown in Fig. 8.11.

The variation of $H_{c2}(0)$ for Nb_3Al in Fig. 8.11 combines several data sets, arising from the works of Kwo et al. /189/ on coevaporated thin film samples with T_c values up to 17.8 K (or ~ 23 at.% Al according to Flükiger et al. /28/), and of Foner et. al. /311/ on a bulk sample with $T_c = 18.8$ K (the composition of this sample was estimated from the preparation procedure: after Ref. 28, only Al contents below 24.5 at.% can be retained by arc melting, higher cooling rates being required for retaining compositions closer to stoichiometry).

It can thus be concluded that the variation $H_{c2}(0)$ vs. β in both systems Nb_3Al and Nb_3Sn is almost linear up to ~ 23 at.%, where the slope of ~ 5 T/at.% is almost the same as for the systems Nb_3Ge and Nb_3Ga (Fig. 8.10). Above ~ 23 at.%, different effects correlated with atomic ordering lead to a deviation from linearity:

- a) the decreasing order parameter for $\beta \rightarrow 0.25$ in Nb_3Al leads to a slight curvature,
 - b) the occurrence of perfect ordering in Nb_3Sn leads to excessively low values of ρ_0 at $\beta > 0.245$, thus causing a maximum of H_{c2} between 24 and 24.5 at.% Sn.
- In this system, the maximum of $H_{c2}(0)$ can only be achieved if a small pertur-

bation ($\beta < 0.25$, $S < 1$ due to irradiation or alloying) pushes the system from the "clean" to the "dirty" type II limit.

8.3.5. The Upper Critical Field Slope in Nb₃Sn

It is interesting to analyze the variation with composition of the upper critical field slope at T_c , $(dH_{c2}/dT)_{T_c}$. A comparison between measured and calculated values of the critical field slope in Nb₃Sn has been performed by Devantay et al. /86/ and is plotted in Fig. 8.12. In this work, the slope was calculated for each composition using the expression /186/

$$-\left. \frac{dH_{c2}}{dT} \right|_{T_c} = \left\{ a n^{-4/3} (S/S_F)^{-2} \gamma_V^2 T_c + b \rho_0 \gamma_V \right\} \frac{R(\infty)}{R(\lambda_{tr})} \eta_{H_{c2}}(T_c) \quad (8.2)$$

a and b being numerical coefficients, n the electron density, S/S_F the ratio of the Fermi surface to the free electron Fermi surface and $\gamma_V = \gamma/V_{at}$ the coefficient of the electronic specific heat per unit volume, $\eta_{H_{c2}}(T_c)$ the strong coupling correction factor. Following the work of Orlando et al. /186/, $S/S_F = 0.35$ was adopted (the choice of this value is not critical below about 23 at. % Sn). The strong coupling correction factor $\eta_{H_{c2}}(T_c)$ was assumed to increase linearly from unity to 1.17 within the homogeneity range. The factor $R(\infty)/R(\lambda_{tr})$, related to the coherence length and the mean free path, was taken to be unity over most of the homogeneity range and to be 1.17 for the ideal compound.

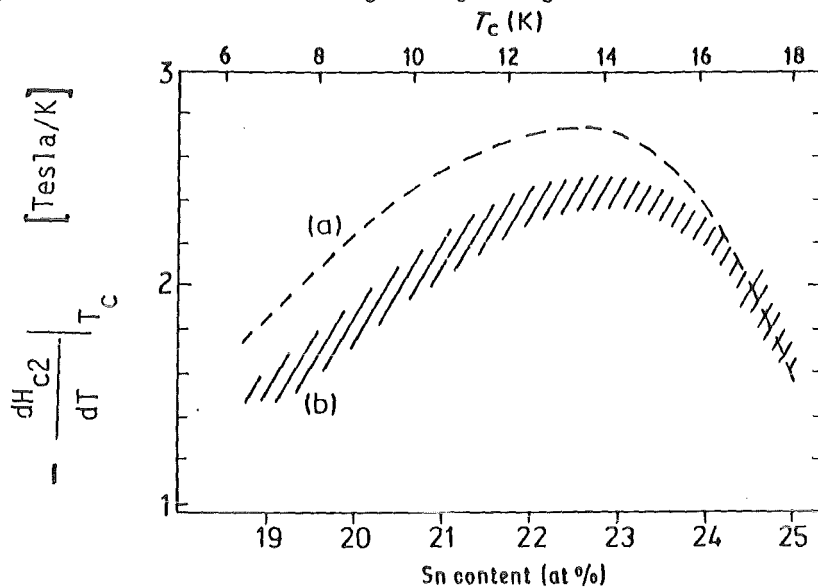


Fig. 8.12. Comparison between calculated (a) and measured (b) upper critical field slope in Nb₃Sn as a function of the Sn content (Devantay et al. /86/).

The calculated values of $(\partial H_{c2}/\partial T)_{T_c}$ are shown in curve a in Fig. 8.12. This curve is based on the resistivity data taken from Fig. 7.11 and a linear variation of the electronic specific heat coefficient between 5 and 13mJ K⁻² per gram atom measured at the Nb-rich boundary and at Nb₃Sn, respectively. Experimentally observed slopes fall within the hatched area b in Fig. 8.12, which is very close to the predicted values.

Obviously, the maximum observed in Fig. 8.12 corresponds to a positive curvature of $H_{c2}(T)$ at the vicinity of $T = T_c$ (Fig. 8.13). The question whether the observed positive curvature of the $H_{c2}(T)$ curve is correlated either to inhomogeneities or to the low temperature martensitic transformation in Nb₃Sn was raised by Devantay et al. /86/. Indeed, one could construct a positively curved $H_{c2}(T)$ plot as the envelope of a family of intersecting straight lines corresponding to a distribution of T_c in the sample. However, an attempt to analyse the measurements using a linear variation of T_c with composition up to $\beta = 0.25$ failed /86/. It may be questioned if the positive curvature is an intrinsic property of Nb₃Sn. Fermi surface and pairing anisotropies could produce such effects, but their occurrence at rather high reduced temperatures, such as observed here, can not easily be understood. Furthermore, Foner and McNiff /315/ have established that the anisotropy of the critical field is small in Nb₃Sn.

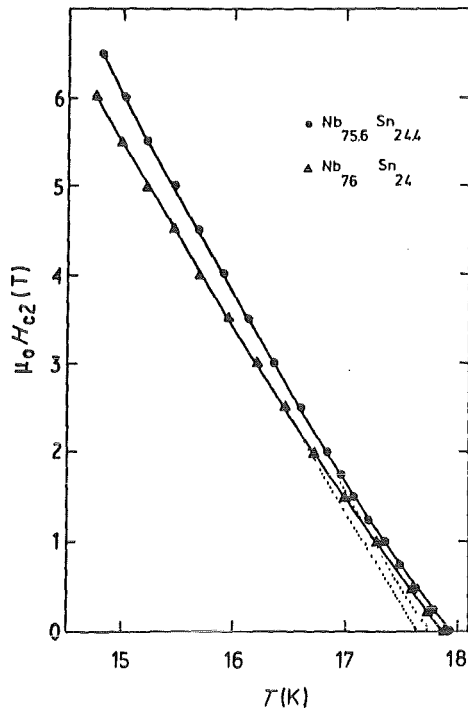


Fig. 8.13. Upper critical fields of near-stoichiometric Nb₃Sn samples vs. T, showing a positive curvature (after Devantay et al. /86/).

The approximate coincidence of the cubic to tetragonal phase boundary near 24.5 at. % Sn and the concentration characterized by the critical field anomaly, suggests that the two facts are related, as proposed by Devantay et al. /86/. These authors found that the required T_c variation for explaining the measured $H_{c2}(T)$ must deviate from linearity, as represented in Fig. 8.7. This behavior has meanwhile been confirmed by other measurements, essentially on alloyed Nb_3Sn samples.

However, the role of the cubic-tetragonal phase transformation on the observed positive curvature is not as decisive as originally supposed in Ref. 86. The real cause for the positive curvature of $H_{c2}(T)$ in Nb_3Sn is the enhanced decrease of ρ_0 approaching $\beta = 0.25$ (see Fig. 7.11), a consequence of the perfectly ordered state in this compound. The martensitic phase transformation has only the effect to lower T_c with respect to linearity at $\beta > 0.245$, reaching $\Delta T_c \approx 1K$ at $\beta = 0.25$. It should be noted here that the occurrence of this transformation is very probably also correlated to perfect atomic ordering.

8.4. The Case of Alloyed Nb_3Sn Wires

The case of alloyed Nb_3Sn multifilamentary wires is another expression of the perfectly ordered state in Nb_3Sn . The critical current density J_c of Nb_3Sn multifilamentary wires at high fields, i.e. above 11 T, has considerably been enhanced in the last years by the addition of third and fourth elements /318,319, 327/. In particular, Ta and Ti additives to multifilamentary Nb_3Sn wires /319, 320/ attained most interest for commercial application. Recently, own studies showed that Ni additions to the core and Zn additions to the bronze (characterized here as Ni+Zn additions) also resulted in an enhancement of J_c with respect to unalloyed Nb_3Sn wires /321/. Based on the GLAG formalism for dirty type II superconductors expressed by Eq. (8.1), it was to expect that the introduction of a small amount of additives to Nb_3Sn may cause an increase in ρ_0 without a drastic depression of T_c and γ , thus leading to an enhancement of the upper critical field H_{c2} . Indeed, for bulk Nb_3Sn and also for samples prepared by coevaporation, there is experimental evidence that for a few atomic percent of additives, the residual resistivity ρ_0 increases sufficiently to give an enhancement in H_{c2} while the specific heat coefficient γ decreases /189,322,323/ and the critical temperature T_c even shows a slight raise /319,321,323/. In the following, the consequences of alloying in Nb_3Sn wires will be briefly described on a representative example, based on a systematical investigation undertaken by the author and coworkers /9,156,191,321,324,325,334/ on the same set of binary and alloyed multifilamentary wires. This complete investigation allows the first direct explanation of the physical properties of alloyed Nb_3Sn wires.

8.4.1. Preparation and Characterization of the Alloyed Nb₃Sn Wires

Nb₃Sn wires with one core and 19 cores without and with additives (Ta, Ti, Ni+Zn, Ga, H) were prepared by standard bronze route. The Ta as well as the Ti additions were added to the Nb core, their respective amounts being 3, 5 and 7.5 wt.% Ta (i.e. 1.6, 2.6 and 4.0 at.% Ta) and 1.6 wt.% Ti (i.e. 3 at.% Ti), the matrix consisting in both cases of Cu-13 wt.% Sn (i.e. Cu-7.5 at.% Sn). For the combination Ni+Zn, Ni was added to the Nb core (0.6 wt.% i.e. 1.0 at.%), while Zn was added to the matrix (Cu-10 wt.% Sn-3 wt.% Zn i.e. Cu-5.6 at.% Sn-3 at.% Zn) /321,324/. The Ga was added to the bronze matrix, its content in Nb₃Sn being later determined to 0.9 at.% /325/. The hydrogen was introduced by performing the reaction heat treatment under H₂ atmosphere. On a selected sample, 0.5 at.% H were determined by chemical and X ray analysis /325/.

The reaction heat treatment was given to wires of 0.6 mm final diameter obtained by standard wire drawing and annealing procedures. At this stage the filaments had about 300 μm diameter for the monofilamentary wires and roughly 60 μm diameter for the 19 core wires. In order to obtain fully reacted Nb₃Sn filaments for the resistivity measurements the 0.6 mm diameter 19 core wires were subsequently deformed to tapes by rolling and intermediate annealings. By this method Nb₃Sn filaments with a thickness of about 10 μm and a width of about 100 μm were obtained, which were then etched out of the Cu-Sn matrix with nitric acid after the appropriate heat treatment.

The configuration of the 19 core wires is represented in Fig. 8.14. It is seen that the cores are uncompletely reacted, the A15 layer varying from 2 to 10 μm thickness, depending on the reaction conditions (temperature and time).

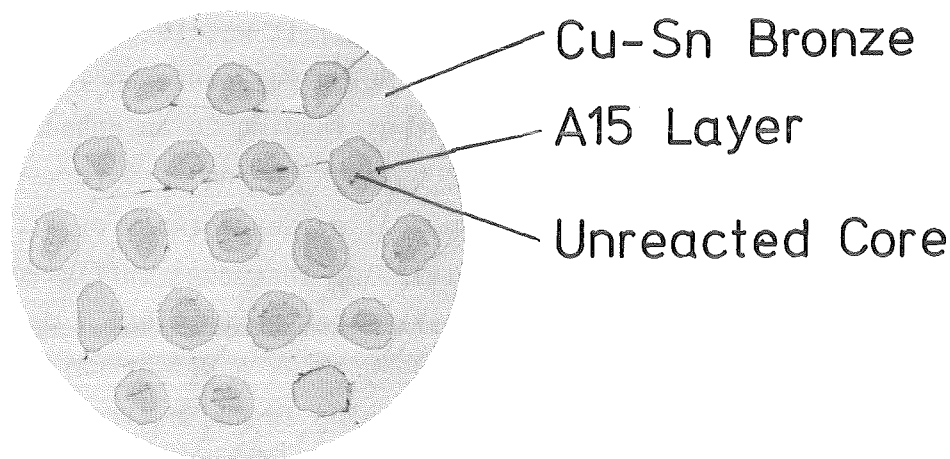


Fig. 8.14. Cross-section of a 19 core bronze processed Nb₃Sn wire after reacting 50 h at 750⁰C (After Drost et al. /321/).

The distribution of the additives in the A15 layer was determined by Auger spectroscopy. A scan through the wire cross section of Ti and Ta alloyed wires is shown in Figs. 8.15 and 8.16.

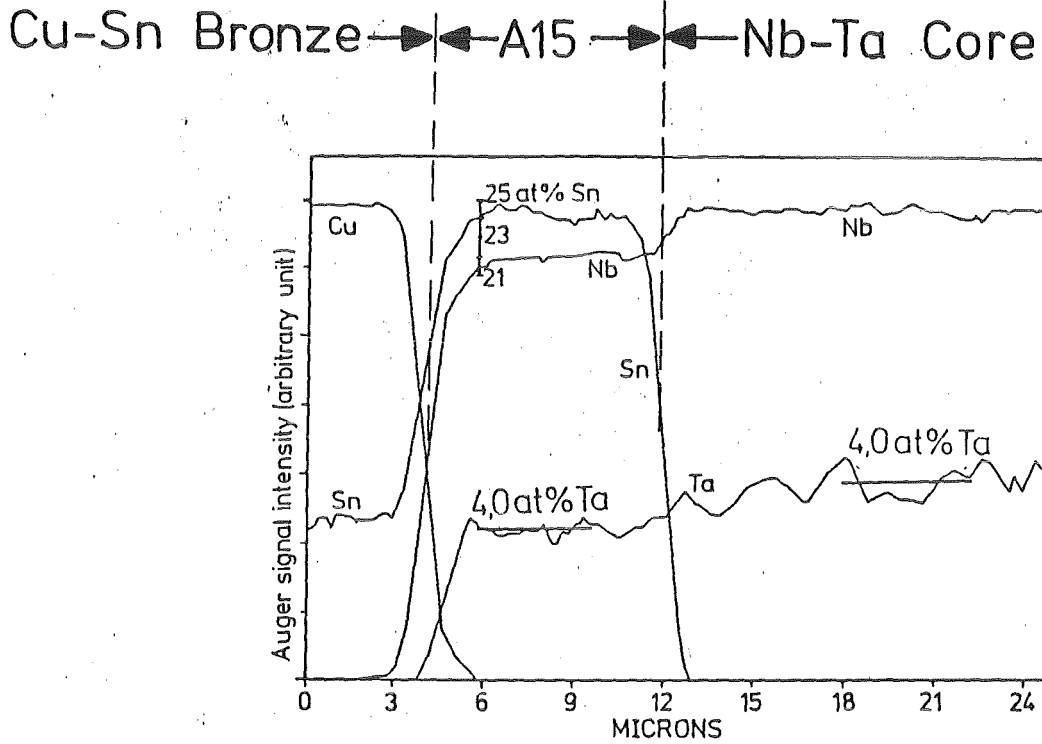


Fig. 8.15. Auger scanning analysis of the cross section of a Nb-4 Ta/Cu-7.5 Sn (at.%) wire after reacting 64 h at 750°C (After Drost et al. /321/).

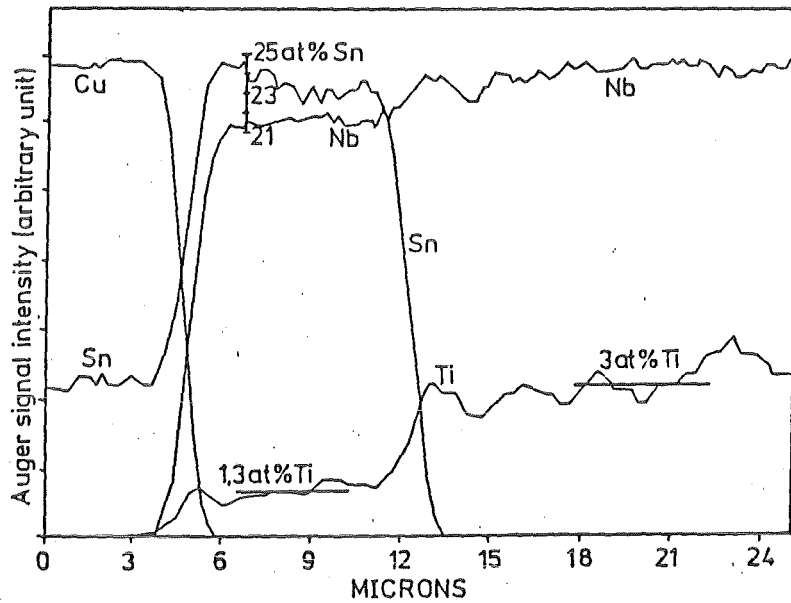


Fig. 8.16. Auger scanning analysis of the cross section of a Nb-3 Ti/Cu-7.5 Sn (at.%) wire after reacting 64 h at 750°C (After Drost et al. /321/).

It is seen that the content of the additive in the A15 layer is approximately constant, i.e. 4 at.% Ta and 1.3 at.% Ti. This constancy is essential for explaining the variations on ρ_0 caused by alloying. In the case of the Ta additive, the Ta content in the A15 layer is the same as originally in the Nb-Ta core. This in contrast to the Ti additive, where the content (1.3 at.%) is lower than in the Nb-Ti core (3 at.%), due to diffusion of Ti into the Cu-Sn matrix. (In Fig. 8.16, the Ti distribution in Cu-Sn is not shown due to overlapping of the corresponding Auger spectra).

An important feature is the distribution of Sn in the A15 layer. In both Figs. 8.15 and 8.16, it is seen that the Sn content is 25 at.% at the Cu-Sn/A15 interface, but lowers to ~ 22 at.% at the A15/Nb-X interface, in agreement to earlier measurements of Smathers et al. /326/. This distribution is of importance for describing the current carrying capacity of optimized Nb₃Sn multifilamentary wires. It should be recalled here that optimized Nb₃Sn wires, i.e. wires with maximum J_c values, have not necessarily fully reacted Nb cores, due to the combined influence of composition profile and grain size. Smaller grain sizes with larger grain boundary interfaces where dislocations, vacancies and other imperfections essentially contribute as "pinning centers" in transporting the superconducting current are indeed more important for optimizing J_c in the field range below 12 T. For the following consideration, only the critical current densities in the high field range ($H > 12$ T) will be of interest, where the value of J_c is dominantly influenced by H_{c2} : This is the field range where atomic ordering influences the current carrying capacity of Nb₃Sn wires.

It must be emphasized that the Sn composition profiles shown in Figs. 8.15 and 8.16 are always observed on A15 filaments which were not completely reacted, i.e. where an unreacted Nb core still subsists. In wires with fully reacted filaments, however, the Sn distribution across the A15 layer is considerably more homogeneous.

8.4.2. Atomic Ordering in Multifilamentary Nb₃Sn Wires

On a binary Nb₃Sn wire with fully reacted filaments and an average composition of ~ 25 at.% Sn (after 64 h/700°C of a multifilamentary wire with 1 μ m filament size), the order parameter was determined after etching away the Cu bronze /9/. Due to the inherent inhomogeneity resulting from the bronze diffusion process, the uncertainty is almost doubled with respect to a bulk sample sintered at 1550°C (see Table 5.1), $\Delta S = \pm 0.03$. Nevertheless, the result on fully reacted A15 filaments is essentially the same, i.e. the Nb₃Sn phase in the filaments

has also to be considered as being perfectly ordered /9/.

The situation in alloyed Nb_3Sn wires can unfortunately not be analyzed by standard diffraction techniques, the sensitivity to small quantities of a third element in the A15 lattice being insufficient. Using the sophisticated ALCHEMI technique, Tafto et al. /328/ were able to determine that both Ta and Ti additives occupy the Nb sites in the Nb_3Sn lattice. It would lead too far to explain in detail the experimental procedure, which is clearly described in Ref. 328. Nevertheless, this result is very important for the understanding of the physical properties of alloyed Nb_3Sn multifilamentary wires. In particular, it shows that the preference for a given atom to occupy the 6c or the 2a lattice site still holds if only small quantities of this element are present in the A15 phase.

8.4.3. The Martensitic Phase Transformation in Alloyed Nb_3Sn Wires

In the binary Nb_3Sn system, the cubic phase is only stable up to 24.5 at.% Sn, higher Sn contents stabilizing the tetragonal low temperature phase/86/. The effect of adding a ternary element to Nb_3Sn is to stabilize the cubic phase at low temperature /329 - 334/. This may be illustrated by the $(Nb_{1-x}Ta_x)_3Sn$ low temperature phase diagram /332/ reproduced in Fig. 8.17 established on samples sintered at 1200°C and on melted samples.

Recently, a detailed low temperature X ray diffraction investigation on

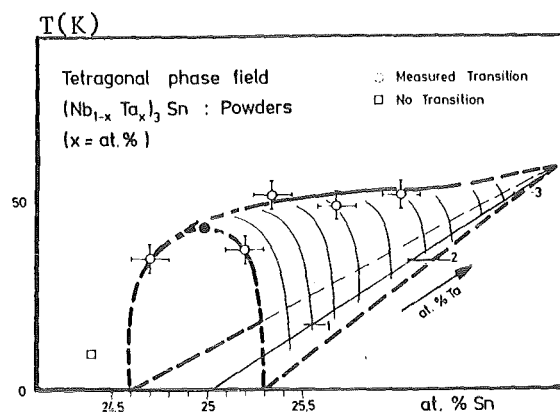


Fig. 8.17. The low temperature $(Nb_{1-x}Ta_x)_3Sn$ phase diagram, established on sintered and melted bulk samples. (Flükiger /332/).

the same binary and alloyed Nb₃Sn wires as used by Drost et al. in Refs. 321, 324 and 325 in the fully reacted state was undertaken by Goldacker and Flükiger /334/. The analyzed wire samples are characterized in Table 8.1. They exhibit somewhat higher lattice parameter values than those previously reported by Drost et al. /321/. The difference is due to the fact that the filaments are now fully reacted, leading to considerably narrower X-ray lines with drastically reduced contributions arising from the low Sn contents. Therefore, the average composition is closer to stoichiometry, which explains the higher lattice parameter values.

The cubic-tetragonal phase transition was suppressed in all Ta and Ti alloyed samples except for that with the lowest investigated Ta content, i.e. 1.7 at.% (number 8). This sample exhibited about 50 % of tetragonal phase and is therefore just located at the cubic/tetragonal phase boundary. The diffraction lines for the tetragonal phase could not be well separated from the cubic line, in order that T_M could not be determined with precision, but lies in the range 20 < T_M < 50 K, thus revealing a broad distribution of (1 - c/a) values over the sample. The diffraction pattern thus confirms the low temperature (Nb_{1-x}Ta_x)₃Sn phase diagram /332/, established on the basis of sintered samples.

No.	Effective Composition (at.%)	Reaction cond. (°C/hours)	a _{300K} (nm)	Volume fraction at 10 K: V _t (1 - c/a); V _c	T _M (K)	t _c (K)
1	Nb ₃ Sn(bulk)	sint. 1500° (100 atm. Ar)	0.52889	0.45(0.0043); 0.55	43	17.8
2	Nb ₃ Sn	800/70	0.52892	0.75(0.0052); 0.25	43	17.9
3	Nb ₃ Sn	750/138	0.52888	≈ 0.5/≈ 0.5	≈ 43	17.9
4	Nb ₃ Sn	700/290	0.52888	0.5(0.0057); 0.5	≈ 43	17.9
5	+ 0.6 H	800/70	0.52934	cubic	-	17.2
6	+ 4.3 Ta	800/70	0.52880	cubic	-	17.9
7	+ 2.8 Ta	800/70	0.52884	cubic	-	18.1
8	+ 1.7 Ta	800/70	0.52888	≈ 0.5(broad); ≈ 0.5	≈ 20 -50	18.2
9	+ 1.3 Ti	800/70	0.52873	cubic	-	18.0
10	+ 1 Ni	800/70	0.52860	cubic	-	18.0
11	+ 0.9 Ga	800/72	0.52876	0.85(0.0043); 0.15	≈ 43	18.3

Table 8.1. Characterization of fully reacted binary and alloyed 19 core Nb₃Sn wires (the same ones as in Refs. 321, 324 and 325) by low temperature X-ray diffractometry (After Goldacker and Flükiger /334/.

Comparing the results in Table I on diffusion reacted samples ($\sim 500^\circ\text{C}$) with those in Fig. 8.17 on sintered or melted samples (1200°C and $>2200^\circ\text{C}$, respectively), it appears that the formation temperatures affects the equilibrium at compositions close to stoichiometry. There is some evidence that with increasing Ta content the composition of the diffusion reacted samples deviates more and more from stoichiometry towards Nb richer contents. This is illustrated by Fig. 8.18. where the lattice parameter variation of the present Ta alloyed Nb_3Sn samples prepared by diffusion reaction is compared to the corresponding data of Kunz and Saur /335/, who investigated the region up to 40 at.% Ta on arc melted samples. The suppression of the phase transition in the system $(\text{Nb}_{1-x}\text{Ta}_x)_3\text{Sn}$ is thus not only due to the increasing Ta content, but also to the increasing deviation from stoichiometry. The shift towards lower Sn contents is in agreement with the results of Tafto et al. /328/.

For Ti alloyed Nb_3Sn no significant lattice parameter shift with increasing Ti content was reported /335/. Therefore the reduction of the lattice parameter of sample 9 is mainly attributed to a deviation from stoichiometry, which itself is sufficient to hinder the phase transformation. The deviation from stoichiometry in Ti alloyed Nb_3Sn samples confirms previous results of Tachikawa et al. /319/.

The occurrence of a lattice instability for the additives Ta and Ti substituting Nb on the 6c sites (as recently shown by Tafto et al. /19/) can be summarized by defining a region in a diagram representing the lattice parameter as a

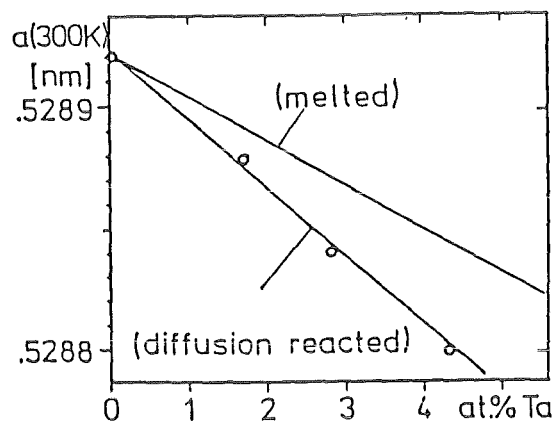


Fig. 8.18. Lattice parameter variation in the system $(\text{Nb}_{1-x}\text{Ta}_x)_3\text{Sn}$ as a function of the Ta content (After Goldacker and Flükiger /334/).

function of the additive content (Fig. 8.19a). It follows that the small contents are sufficient to suppress the phase transformation, which necessarily implies that the transforming region is restricted to very small variations of the lattice parameter with respect to that for binary Nb_3Sn . The situation is, however, quite different for the additives Ga, Al, Sb and Ni substituting Sn atoms on the 2a sites of the A15 lattice. The 0.9 at.% Ga alloyed sample shows a nearly complete cubic/tetragonal phase transformation in spite of a markedly reduced lattice parameter. The same behavior was observed for the additions Al /329/ and Sb / 330, 331/, the latter showing the largest lattice parameter change (the change of sign for $(1 - c/a)$ in $Nb_3Al_{1-x}Sb_x$ for $x > 0.1$ / 331/ is here of secondary importance). These data have been plotted in Fig. 8.19a, which shows a much wider transformation region than for Ta and Ti additions. For the additives in Fig. 8.19b, the lattice parameter change is mainly caused by their substitution, rather than by deviations from the stoichiometric Nb content. It can thus be concluded that the occurrence of the lattice instability in alloyed Nb_3Sn is dominantly influenced by the chemical nature of the additives, which determines their positions in the perfectly ordered /9/ Nb_3Sn lattice. Besides deviations from stoichiometry encountered particularly for Ta and Ti additions, it can be said that the substitution of additives on the 6c sites (Ta, Ti, ...) has a much stronger effect in suppressing the lattice instability of Nb_3Sn than that on the 2a sites (Ga, Al, Sb, Ni). This result can be easily understood in terms of the

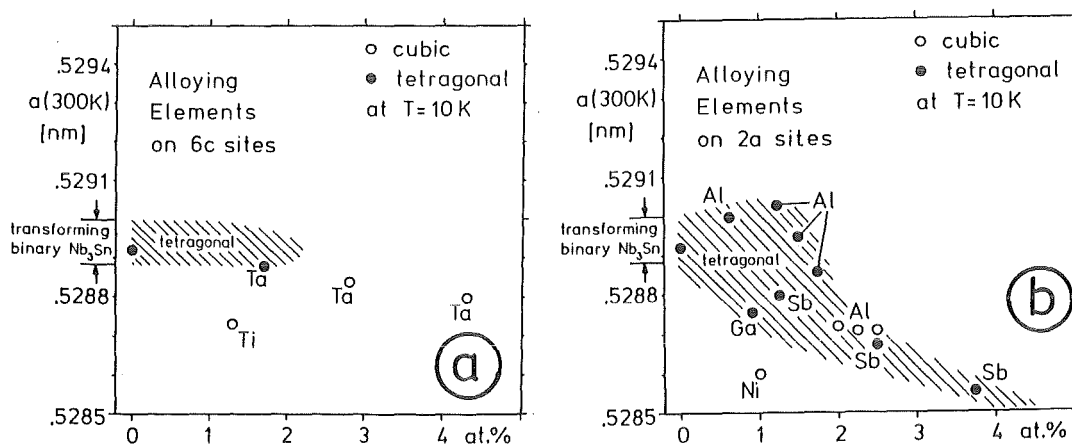


Fig. 8.19. Occurrence of tetragonal phase in Nb_3Sn as a function of different additives. (a) Additives lying on the 6c sites (Ta, Ti). (b) Additives lying on the 2a sites (Ga, Al, Sb, Ni).

stronger interaction between chain atoms.

8.4.4. Superconducting Transition Temperature and Electrical Resistivity in Alloyed Nb₃Sn Wires

The results of the T_c and ρ_0 measurements on the binary and alloyed Nb₃Sn multifilamentary wires characterized in Table 8.1 are represented in Table 8.2/ Fig. 8.20. After a heat treatment of 160 hours at 750°C, the binary probe had a residual resistivity of $16 \times 10^{-8} \Omega m$ and a T_c of 18 K. The extremely long reaction time was necessary to convert the totality of the filament (flattened to a ribbon of $10 \times 100 \mu m^2$ cross section) to A15 phase. By comparing the ρ_0 value of this filament with results obtained for bulk samples /86/, the composition of the A15 phase should lie at about 24 at.% Sn. Actually, from lattice parameter calculation by X ray powder diffractometry for a binary multifilamentary wire reacted at 700°C/107 h, the Sn concentration is found to vary from 22 at.% - 25 at.% centered around 24 at.% /321/.

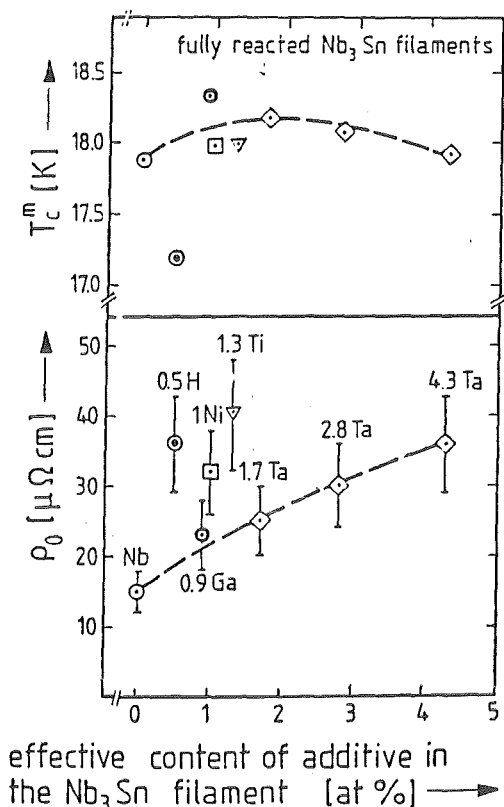


Fig. 8.20. Normal state resistivity ρ_0 and critical temperature T_c for binary and alloyed Nb₃Sn filaments as function of the effective content of the additive (Ta, Ti, Ni + Zn, Ga, H) in the Nb core. The filaments are fully reacted, the reaction conditions are given in Table 8.2. (After Drost et al. /324/).

Composite [at.%]	Reaction [°C/h]	Additive to Nb ₃ Sn [at.%]	T _c [K]	RRR	ρ_0 [x 10 ⁻⁸ Ωm]
Nb/Cu-7.5Sn	750/160	-	17.8	6.5±0.5	15
Nb-0.9Ni/Cu-5.6Sn-3Zn	750/160	1.0 Ni	17.9	3.8±0.3	32
Nb-1.6Ta/Cu-7.5Sn	750/168	1.7 Ta	19.1	4.7±0.3	25
Nb-2.6Ta/Cu-7.5Sn	750/168	2.8 Ta	18.0	4.1±0.3	30
Nb-4.0Ta/Cu-7.5Sn	750/168	4.3 Ta	17.9	3.3±0.3	36
Nb-3.0Ti/Cu-7.5Sn	750/164	1.3 Ti	17.9	2.9±0.3	40
Nb/Cu-5Sn-4Ga	750/164	0.9 Ga	18.25	4.9±0.4	23
Nb/13Sn-II	750/138 + 400/4-II ₂	0.5 II	17.1	3.3±0.3	36

Table 8.2. Characterization of the fully reacted binary and alloyed Nb₃Sn filaments produced by the bronze process. Filament cross section: 10 x 100μm². The abbreviation Nb - 4 Ta/7.5 Sn stays for the composition Nb - 4 at.% Ta/Cu - 7.5 at.% Sn in the unreacted composite. (After Drost and Flükiger / 325/).

For the Ta alloyed samples a nearly linear increase of ρ_0 with increasing amount of Ta is obtained. The values are about 26, 30 and 36 x 10⁻⁸Ωm for 3, 5 and 7.5 wt.% Ta addition (1.6, 2.6, and 4.0 at.%) to the Nb core. As already known, an increase of T_c for small addition of Ta is observed, e.g. 0.3 K for 1.6 at.% Ta. The highest ρ_0 value is achieved for the Ti addition i.e. about 45 x 10⁻⁸Ωm for Nb-1.6 wt.% (3 at.%) Ti alloy core. For Ni + Zn addition the filaments show a value of 30μΩ cm. The T_c values for the filaments with Ti and Ni + Zn addition are also slightly higher than for the unalloyed one. It has already been said that the increase of the residual resistivity for alloyed wires by a factor of about 2 compared to unalloyed ones is only a direct consequence of the high degree of atomic ordering in Nb₃Sn. Indeed, $\Delta\rho_0/\rho_0 \geq 1$ is only possible for perfectly ordered, nearly stoichiometric Nb₃Sn, where ρ_0 is low.

For some samples measurements were also carried out after heat treatment at higher temperature: 800°C for 70 hrs. The corresponding ρ_0 values are only slightly higher than for the 750°C heat treatment, as seen in Fig. 8.20. The respective T_c values are slightly lower and the transition is broader than af-

ter the reaction at 750°C. This could again reflect the dissolution of a small amount of Cu in the A15 phase at the higher reaction temperature, which has still to be demonstrated. Nevertheless, no major changes in the layer composition profile seem to occur in Nb₃Sn wires when increasing the reaction temperature from 750 to 800°C.

From a comparison of the above presented /325/ ρ_0 values on multifilamentary wires with those on alloyed bulk Nb₃Sn by Akihama et al. /322/ and coevaporated Nb₃Sn films alloyed with Ga by Bormann /336/, it can be concluded that independently on the preparation procedure alloying produces a comparable enhancement of ρ_0 . Within the limited range of additive contents where J_c is optimized (see 8.4.5), i.e. a few at.%, ρ_0 increases from 16 to $\sim 40 \times 10^{-8} \Omega m$. The maximum of J_c is achieved for ρ_0 values between 30 and $35 \times 10^{-8} \Omega m$.

8.4.5. Critical Current Density in Alloyed Nb₃Sn Wires

As mentioned above, the opposite requirements of small A15 grain sizes (<150 nm) and a homogeneous Sn distribution in the layer lead to the interesting result that J_c is optimized for incompletely reacted filaments. The corresponding heat treatment conditions (Table 8.3) are substantially different from those in Tables 8.1 and 8.2, where the same set of wires was fully reacted in order to get significant X ray and ρ_0 data.

Fig. 8.21 shows the J_c (in the layer) vs. H curves for unalloyed as well as for Ta, Ti and Ni+Zn alloyed 19 core wires which were prepared under identical conditions. For all these additions an enhancement in the critical current density for fields above 11 T compared to the unalloyed wire was observed. It is remarkable that above 11 T, the J_c vs. B curves for the alloyed wires are almost identical (the average error in calculating J_c of the A15 layer is 5% to 10%), independent on the chemical nature of the additive. For each additive, curves in Fig. 8.21 correspond to the wires with composition and heat treatment yielding the highest current densities in the high field region. The critical current densities for these 19 core wires are in good agreement with the values reported by Springer et al. /320/ and by Tachikawa et al. /319/ for multifilamentary wires with Ta and Ti additives, respectively.

These results suggest that there exists an upper limit for improving the

Number of cores	Composition core/matrix		Reaction condition, °C/h	Layer thickness, μm
	wt%	at%		
19	Nb/13 Sn	Nb/7.5 Sn	700/64	2
1	0.6 Ni/10 Sn-3 Zn	1 Ni/5.6 Sn-3 Zn	800/20	12-16
19	0.6 Ni/10 Sn-3 Zn	1 Ni/5.6 Sn-3 Zn	750/64	14
1	1.6 Ti/13 Sn	3 Ti/7.5 Sn	800/20	26
19	1.6 Ti/13 Sn	3 Ti/7.5 Sn	700/64	8
			750/50	14
19	7 Ta/13 Sn	3.6 Ta/7.5 Sn	725/100	5
			750/50	4
9872	Nb/13 Sn	Nb/7.5 Sn	700/64	~1 (2.5 μm fil. diameter)
3721	7.5 Ta/13 Sn	4 Ta/7.5 Sn	700/64	~1 (4 μm fil. diameter)

Table 8.3. Characterization of the wire samples for J_c measurements. The abbreviation 0.9 Ni/5.6 Sn - 3Zn stays for Nb -0.9 at.% Ni/Cu - 5.6 at.% Sn - 3 at.% Zn in the composite. The A15 layer thicknesses after different heat treatments are also indicated (After Drost et al. /321/).

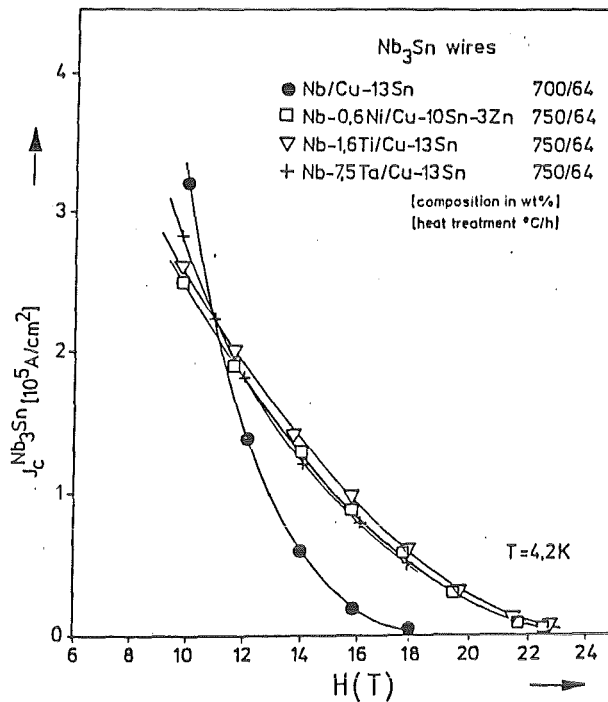


Fig. 8.21. Critical current density in the Nb₃Sn layer vs. H for 19 core wires without and with Ta, Ti and Ni+Zn additives. (After Drost et al. /321/).

high field critical current densities of Nb₃Sn wires by alloying with various additives, whereby optimal composition and heat treatment can differ from one alloying element to another. This limit is achieved when $\rho_0 = 35 \pm 5 \times 10^{-8} \Omega\text{m} / 324$, regardless whether the increase over ρ_0 of the binary Nb₃Sn filament has been achieved by a different content of the additive or by a slight deviation from stoichiometry.

8.4.6. The Upper Critical Fields in Alloyed Nb₃Sn Wires

The usual way to estimate the upper critical field of multifilamentary Nb₃Sn wires consists of establishing a Kramer plot, $J_c^{1/2} H^{1/4}$ vs. H based on J_c measurements and to extrapolate linearly to zero. The intersection occurs at a field called H_{c2}^* which reflects the upper critical field at 4.2 K, the temperature at which J_c was measured. The Kramer plots should not be overinterpreted since they cannot be applied to all superconducting structures. For Nb₃Sn, they give nevertheless an approximate value which is useful in determining relative changes of the upper critical fields after different reaction conditions. It is interesting to compare H_{c2}^* with $H_{c2}(0)$, the upper critical field measured at different temperatures at nearly zero current and extrapolated to $T \rightarrow 0$.

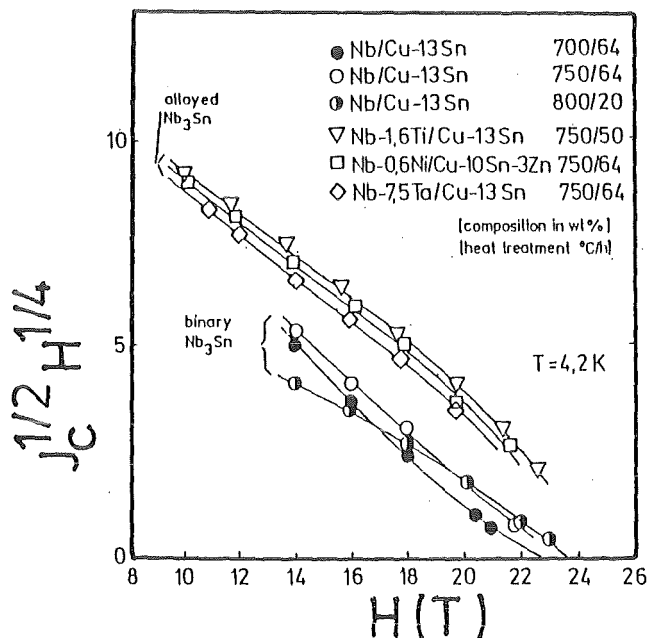


Fig. 8.22. Kramer plots for 19 core Nb₃Sn wires with Ta, Ti, Ni+Zn and without additions, yielding H_{c2}^* values of $\sim 25 \text{ T}$ and $\sim 22 \text{ T}$, respectively (After Drost et al. /321/).

The Kramer plot for the wires characterized in Table 8.3 is shown in Fig. 8.22. It is seen that alloyed Nb_3Sn wires have appreciably higher H_{c2}^* values compared to those of binary (unalloyed) wires. For all alloyed wires, reacted at 750°C , a linear field dependence as predicted by Kramer's theory is only observed up to 18 T. For the higher field region the plots show a downward curvature, in agreement with Suenaga /327.

The behavior for binary Nb_3Sn wires annealed at 700, 750 and 800°C is the following (see Fig. 8.22): a reaction heat treatment at 800°C leads to a downward curvature in the high field region where as the lower temperature of 700°C leads to a slightly upward curvature and a heat treatment at 750°C to a nearly straight line. There is thus a reaction temperature for which the Kramer plots show a linear field dependence. It is suggested that this temperature dependent effect is common to alloyed as well as to unalloyed wires, because Wecker et al./337/ also obtained an upward curvature for Nb_3Sn compounds with Ta additions (prepared by powder metallurgy) at 650°C reaction.

The different curvatures for different reaction temperatures may be connected with the fact that reactions at higher temperatures favour high current densities in the high field region and depress the current densities for lower fields (and vice versa). This effect points out that even the behavior at the highest fields is not only dictated by H_{c2} , but also by pinning. The physical reason for this behavior may be changes in the microstructure, in the distribution of Sn throughout the layer and of Cu at the grain boundaries. The question whether the downward curvature in binary Nb_3Sn wires is caused by small amounts of Cu dissolved into the A15 phase at 800°C is still open.

Due to the peculiar curvatures of the Kramer plots the H_{c2}^* values cannot be calculated accurately. But at least a comparison between binary and alloyed Nb_3Sn can be made: For alloyed wires reacted at 750°C the H_{c2}^* values are 25 to 26 T. For the unalloyed wire the H_{c2}^* values are 23 to 24 T for 750 and 800°C heat treatment and 22 T for 700°C . Thus the drastic increase of ρ_0 for alloyed Nb_3Sn gives a strong evidence for the correlation between ρ_0 and the enhancement of H_{c2}^* for Nb_3Sn with appropriate additives. This confirms earlier measurements of Bormann /323/, obtained on coevaporated Nb_3Sn films with Ga addition.

The upper critical field $H_{c2}(0)$ has been extrapolated from measurements of the initial slope, $dH_{c2}/dT/T_c$ /325/. The measurements were performed on the same

fully reacted binary and alloyed Nb₃Sn wires on which ρ₀ was measured. H_{c2}(0) can be estimated using the GLAG relationships

$$H_{c2}(T=0) = -0.73 \left. \frac{dH_{c2}}{dT} \right|_{T_c} \cdot T_c \quad \text{(Clean limit } \lambda_{tr.} > \xi)$$

and

$$H_{c2}(T=0) = -0.69 \left. \frac{dH_{c2}}{dT} \right|_{T_c} \cdot T_c \quad \text{(Dirty limit } \lambda_{tr.} \leq \xi)$$

The critical fields of the above described wires for temperatures close to T_c are shown in Fig. 8.23. The values H_{c2}^m are indicated at 50% of the magnetic transition. In the chosen temperature range, H_{c2}(T) is linear, in order that H_{c2}(0) can be calculated using Eq. (8.2). The slopes of the different curves in Fig. 8.23 are listed in Table 8.4, as well as the calculated H_{c2}(0) values, and the T_c^m values at 50% of the transition.

From the slope -2.05 T/K and T_c^m = 17.4K (this value is lowered by the pre-stress due to the bronze matrix), one obtains H_{c2}(0) = 26.5 T (clean limit). The alloyed wires all show higher slopes, -2.45, -2.35 and -2.5 T/K for the Ni+Zn, Ta and Ti additive, respectively. In all cases, an enhancement of T_c by 0.2 to

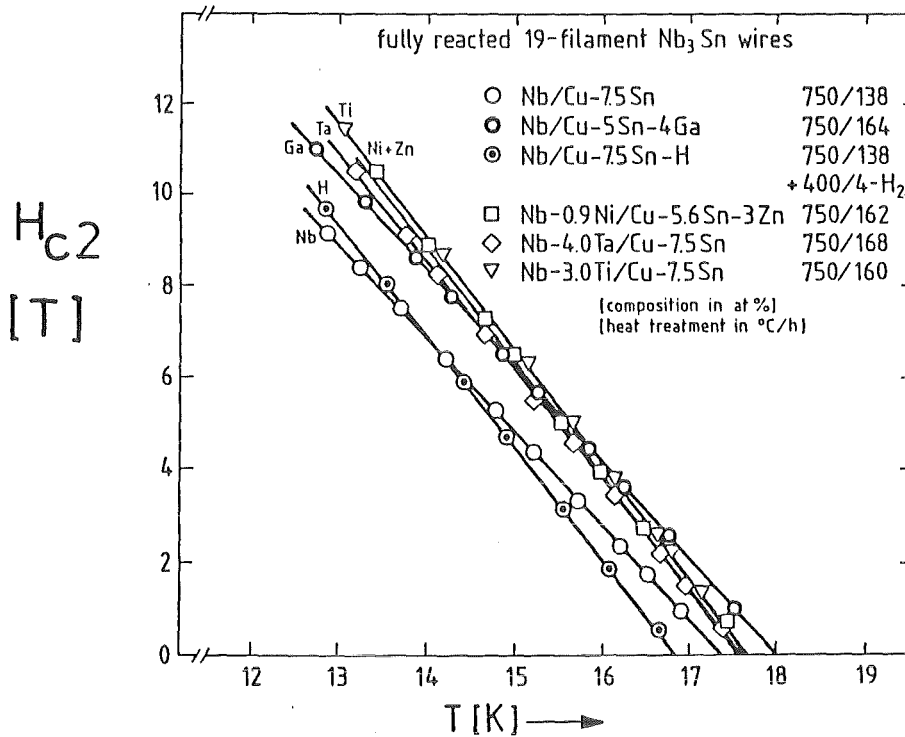


Fig. 8.23. Initial upper critical field slopes for fully reacted binary and alloyed Nb₃Sn wires (After Drost and Flükiger /325/)

0.3K was observed, yielding $H_{c2}(0)$ values of 30, 29 and 31 T for the Ni+Zn, Ta and Ti additive, respectively (dirty limit).

For the Ga alloyed wire, the slope is only 2.1 T/K, but the T_c value (in the bronze) is highest, 18K, yielding $H_{c2}(0) = 28$ T (clean limit since $\rho_0 = 23 \times 10^{-8} \Omega m$). This value is 3 to 4 T lower than that given by Bormann /323/ for Ga alloyed Nb_3Sn films prepared by coevaporation. The difference can be easily explained by the different equilibrium conditions: In the bronze processed wire, the highest Ga solubility is only 0.9 at.%, compared to ~ 2 at.% in the coevaporated film /323/. The H alloyed wire showed an enhanced slope (-2.35 T/K) with respect to binary Nb_3Sn , but a relatively low T_c value (16.9K) yielding $H_{c2}(0) = 28$ T. Possibly, the H content in the sample was too high for getting a higher

Wire Composition Core/Matrix (at.%)	Reaction Treatment ($^{\circ}C$ /hours)	T_c K	$dH_{c2}/dT _{T_c}$ T/K	$H_{c2}(0)$ (Calculated) T
Nb/Cu-7.5 Sn	750/172	17.4	2.05	26.5
Nb-0.9Ni/Cu-6Sn-3Zn	750/162	17.6	2.45	30
Nb-4.0Ta/Cu-7.5Sn	750/168	17.6	2.35	29
Nb-3.0Ti/Cu-7.5Sn	750/160	17.7	2.50	31
Nb/Cu-5Sn-4Ga	750/164	18.0	2.10	28
Nb/Cu-7.5Sn-H	750/172 + 400/4 in H_2	16.9	2.35	28

Table 8.4. $H_{c2}(T)$ data of binary and alloyed Nb_3Sn wires

$H_{c2}(0)$ value. On the other hand, this illustrates the lowering effect of interstitially dissolved hydrogen, in contrast to the metallic substitutes. From the usual $H_{c2}(0)$ behavior at high fields /186/ a decrease of 2T can be estimated from $T \rightarrow 0$ and $T = 4.2K$, yielding $H_{c2}(4.2K)$ lying between 26 and 29 T, which is considerably higher than the values found by the Kramer extrapolation.

The present comparison illustrates the effect of additives on the perfectly ordered Nb_3Sn matrix. It is obvious that a less ordered matrix would not show the observed strong enhancement of $H_{c2}(0)$ with alloying, as can be seen for V_3Ga . In Nb_3Al , the effect of additives is also expected to be much smaller than for Nb_3Sn .

8.4.7. Room Temperature Irradiation of Alloyed and Binary Nb₃Sn Wires

In view of the possible use of superconducting magnets in future fusion reactors, it is interesting whether the expected neutron radiation causes different effects on the current carrying capacity of binary and alloyed Nb₃Sn multifilamentary wires. A series of bronze processed Nb₃Sn wire samples (characterized in Table 8.5) were recently submitted to the 14.8 MeV neutron radiation of the Lawrence Livermore National Laboratory in Livermore by the author and co-workers (Weiss et al. /156/). The wires were irradiated at 300 K up to fluences $\phi t = 3.6 \times 10^{18} \text{ n/cm}^2$, after which measurements of J_c up to 20 T and T_c were performed. The variation of T_c with dosis is represented in Fig. 4.10b.

Wire Sample	Cores	Heat Treatment (hours/°C)	Degree of Reaction	T_c (K)	ΔT_c (K)
A Nb/13Sn	10000	64/700	fully	17.58	2.3
B Nb/13Sn	19	100/700	partially	17.21	2.6
C Nb-1.6Ti/13Sn	19	50/750	partially	17.50	3.1
D Nb-/-6Ni/10Sn-3Zn	19	19	partially	17.87	2.9
E Nb-7Ta/13Sn	61X61	64/700	fully	17.74	3.1

Table 8.5. Binary and Alloyed Nb₃Sn wires submitted to 14.8 MeV neutron irradiation. The wires B,C and D are the same as in Table 8.3, the others are from VAC (Hanau). ΔT_c is the difference between the samples at $\phi t = 0$ and $3.6 \times 10^{18} \text{ n/cm}^2$ (Weiss et al. /156/).

After the maximum dosis, the value of T_c in the wire samples was lowered with respect to that of the unirradiated wire, ΔT_c varying between 2.3 and 2.6 K for the binary wires. For the alloyed wires, slightly larger depressions between $\Delta T_c = 2.8$ and 3.1 K were observed. The decrease of T_c with dosis on all wires is summarized in Fig. 4.10a.

a) Binary Nb₃Sn Wires. The reduced critical current I_c/I_{c0} vs. the applied field for the 10000 core wire (A) is plotted in Fig. 8.24, together with the corresponding change of the critical field H_{c2}^* resulting from the Kramer extrapolation. It is seen that both I_c/I_{c0} and H_{c2}^* follow the same trend, i.e. an initial increase followed by a decrease above the dosis $\phi t = 0.7 \times 10^{18} \text{ n/cm}^2$. This dose at which I_c/I_{c0} reaches a maximum will be called ϕt_m in the following.

On the basis of Eq. (8.1), the plots in Fig. 8.24 can be explained as follows. The enhancement of H_{c2}^* by $\sim 10\%$ in the low dose region is essentially due

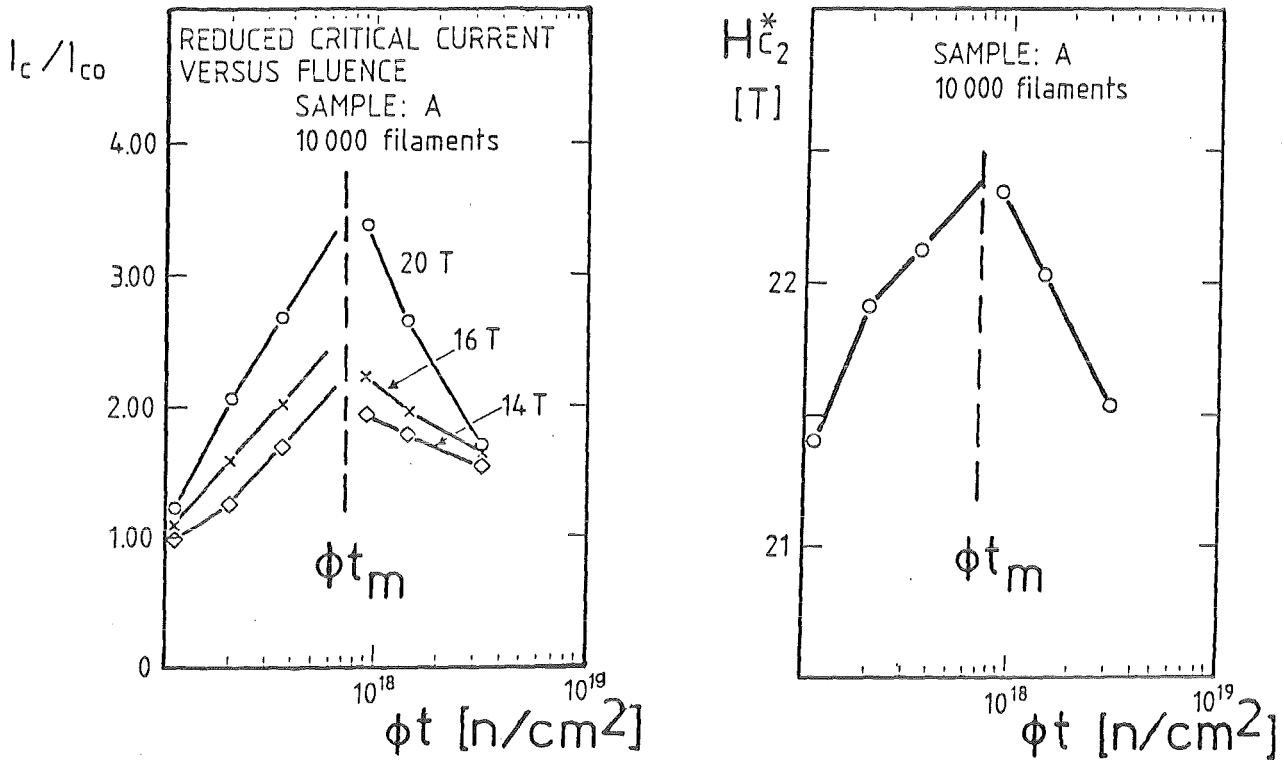


Fig. 8.24. I_c/I_{c0} and H_{c2}^* of a 10000 core bronze processed binary Nb_3Sn wire after low temperature neutron irradiation (After Flükiger et al. /156/).

to the enhancement of the electrical resistivity ρ_0 . Indeed, T_c at ϕt_m is lowered by 0.6 K only, while a similar decrease of γ can be postulated. The enhancement of the upper critical field is reflected by increasing critical currents, particularly at high fields. At 20 T, I_c/I_{c0} lies between 3 and 4, compared to $I_c/I_{c0} = 2$ at 14 T. This confirms that for small deviations from perfect ordering ρ_0 is more sensitive to changes of S than any other physical property, in particular T_c . In addition, the variation of ρ_0 is largest for the first deviation from perfect ordering, as shown by Figs. 7.15, 7.16 and 7.17. The analogy with the variation of ρ_0 at the close proximity of the stoichiometric composition appears when comparing with the ρ_0 vs. β plots for the systems V_3Si , Nb_3Sn and Nb_3Ge in Figs. 7.10, 7.11 and 7.13: The strongest variation of $d\rho_0/d\beta$ or $d\rho_0/dS$ occurs at small deviations from perfect ordering and/or stoichiometry. For deviations exceeding ~ 1 at.% or $\Delta S \approx 0.05$, the rate of increase for ρ_0 is markedly decreased. This is the basis for the understanding why I_c/I_{c0} and H_{c2}^* decrease above the dosis ϕt_m . In this region, $d\rho_0/dS$ is smaller and the decrease of T_c and γ becomes dominant, thus lowering the upper critical fields and the corresponding critical currents at any given value of $h^* = H/H_{c2}^*$.

The binary wire A in Table 8.4 has to be considered as almost fully reacted after the indicated heat treatment of 64 hours at 700 °C (the filament diameter is of the order of 4 μm), thus exhibiting a relatively small gradient in the Sn composition. A similar behavior, but with stronger variations is observed on another binary wire (B) with 19 cores of 300 μm diameter and an Al5 layer of ~ 8 μm thickness after 50 hours at 750 °C. As shown in Figs. 8.15 and 8.16, such a wire exhibits a marked inhomogeneity, the Sn content varying from ~22 to 25 at. %. The results for the wire (B) are represented in Fig. 8.25.

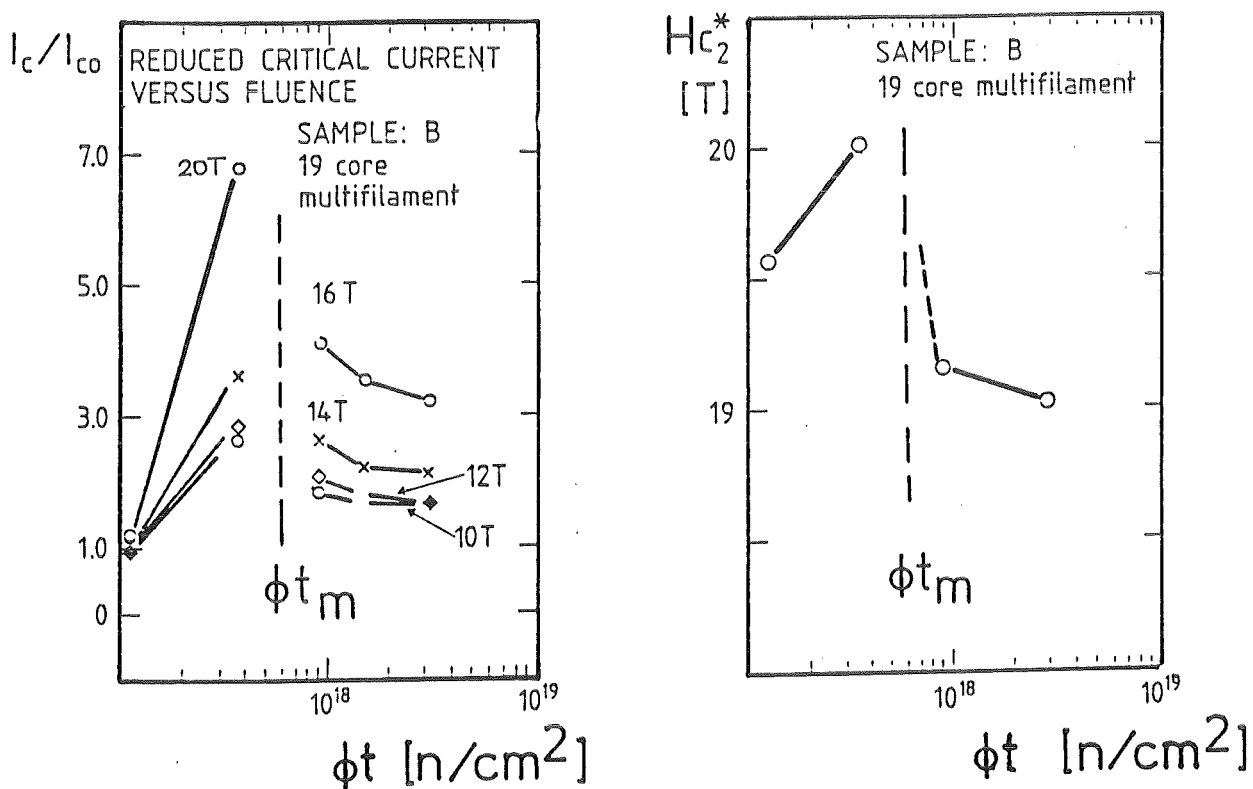


Fig. 8.25. I_c/I_{c0} and H_{c2}^* of a 19 core binary Nb₃Sn wire after low temperature neutron irradiation (After Weiss et al. /156/).

The tendency is similar to that in Fig. 8.24, but ϕt_m appears to be somewhat smaller (0.6 instead of 0.7 x 10¹⁸ n/cm²). As expected for an incompletely reacted wire, the average Sn content is considerably lower than for wire (A), giving rise to a smaller value of H_{c2}^* : 19.6 T instead of 21.4 T. This fits well with the observation of Goldacker and Flükiger /334/ in 8.4.3 that the lattice parameter a in this case is smaller than in fully reacted filaments. The enhancement of I_c/I_{c0} with dose for both wires (A) and (B) can be compared at the same values of the reduced field $\tilde{h}^* = H/H_{c2}^*$. This corresponds roughly to compare the I_c/I_{c0} curve for wire (A) at 16 T with that of wire (B) at 14 T. Nevertheless, the enhancement of I_c/I_{c0} in wire (B) is still more important. It can actually not be said whether this

difference arises from the different prestress conditions in both wires or if it is due to other reasons.

b) Alloyed Nb₃Sn Wires. As seen from Table 8.5, ΔT_c in binary Nb₃Sn wires is of the order of 2.3 to 2.6 K, i.e. considerably smaller than for alloyed wires, where ΔT_c varies from 2.8 to 3.2 K. This trend towards stronger degradation for low temperature neutron irradiated alloyed wires is even accentuated when comparing the behavior of I_c/I_{c0} and H_{c2}^* with dose. The results for the Ti alloyed wire (C) are represented on Fig. 8.26. They are also characteristic for the Ta and Ni+Zn additives

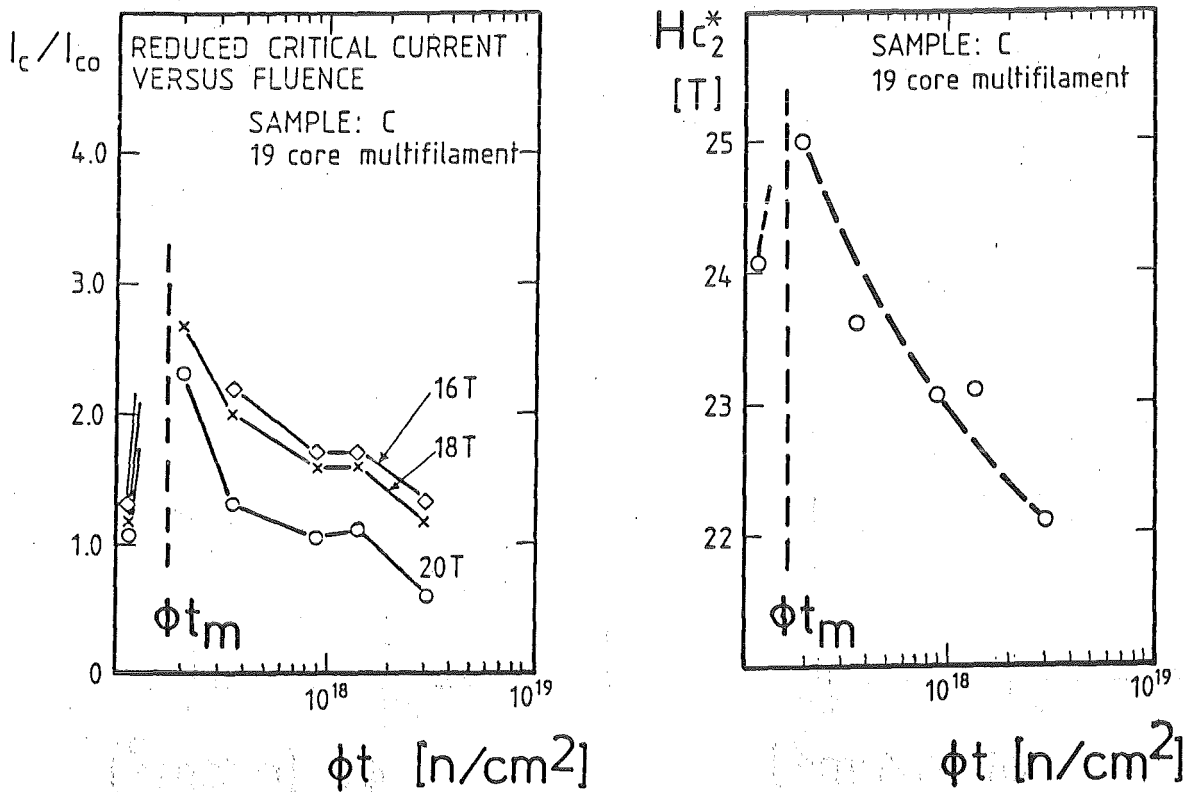


Fig. 8.26. I_c/I_{c0} and H_{c2}^* of a 19 core Ti alloyed Nb₃Sn wire after low temperature neutron irradiation (After Weiss et al. /156/).

The most evident differences between the irradiated binary wires in Figs. 8.24 and 8.25 and the Ti (but also the Ta and Ni+Zn) alloyed wires in Fig. 8.26 are:

- a) The dose ϕt_m for the Ti alloyed wire lies at 0.18×10^{18} n/cm², i.e. it is four times smaller than for binary Nb₃Sn wires. The same value of ϕt_m is also observed for Ta and Ni+Zn additives and seems thus to be a general property of alloyed Nb₃Sn wires.
- b) The enhancement of I_c/I_{c0} at comparable h values is smaller than for the binary wire. At $h^* \approx 0.7$, I_c/I_{c0} for the Ti and Ta alloyed wires is ≈ 3 and 1.2 , respectively, compared with ≈ 4.5 for the binary 19 core wire and ≈ 2.2 for the binary 1000 core wire (see Figs. 8.24 and 8.25).

c) At $\phi t = 3 \times 10^{18}$ n/cm², I_c/I_{c0} for the binary wire at all magnetic fields is higher than before the irradiation, in contrast to the alloyed wires where at this dose level the ratio I_c/I_{c0} is always smaller.

These three points a, b and c have a common origin, the enhancement of ρ_0 after irradiation is smaller for the alloyed wire than for the binary one, due to the higher initial value of the latter. A very simple model can be formulated for explaining these effects, based on the nonlinearity of ρ_0 with doses, found by Lehmann /301/ on ³²S irradiated Nb₃Sn (no ρ_0 data are available for Nb₃Sn after neutron irradiation). After irradiation at the same (small) dose, binary Nb₃Sn beneficiates from the strong initial increase of ρ_0 without degrading T_c and γ too seriously. Alloyed Nb₃Sn wires encounter a slower increase of ρ_0 , thus showing a maximum of H_{c2} at lower fluences. This model explains qualitatively the observed effects and illustrates once more the importance of ordering effects.

The presently discussed ordering effect is without any doubt the most important one for applications. Tokamak fusion magnets producing fields of ~ 12 T will be wound with binary Nb₃Sn multifilamentary wires; even if alloyed Nb₃Sn wires may exhibit slightly higher initial critical current densities at this field /156/.

10. CONCLUSIONS

A15 type compounds have an unique feature: Their superconducting properties depend on the degree of long-range atomic ordering. The aim of the present work was to contribute to the general understanding of the ordering phenomena in this crystal structure. The subject reaches from the variation of physical properties at the superconducting as well as in the normal state to the mechanism leading to the site exchange in annealed or quenched samples and finally, to the consequences of perfect ordering on the current carrying capacity of multifilamentary Nb_3Sn wires.

The effects of atomic ordering can conveniently be studied on samples with a wide range of order parameters. Since quenching from high temperatures results in a restricted variation, $\Delta S \leq 0.10$, it is necessary to include data on irradiated samples, too. It has been shown in Sect. 4 that there are common features between the mechanism of disordering in A15 type compounds submitted to high temperatures and to high energy particle irradiation. Indeed, it was found that both processes produce the same kind of lattice vacancy, a split-vacancy, giving rise to the occupation of a nonequilibrium site, called here "virtual" site (see Fig. 4.1). Due to the complexity of the A15 structure, the simple one-step vacancy diffusion process occurring for example in bcc metals is not longer possible. Site exchanges require now two steps, the first one being the dynamical occupation of the nonequilibrium virtual site. The occupation of the latter is due to the fact that the state of lowest energy after the creation of a 6c vacancy is that corresponding to the shift of one of both neighbours by $a/4$: the virtual site is situated at the center between two 6c sites. It can thus be said that both processes produce the same type of vacancy by different mechanisms, i.e. anharmonic vibrations at high temperature and collision events following the irradiation with high energy particles. One of the main results of this work is that for an A15 compounds with a certain order parameter S , the physical properties will essentially be the same, regardless how this degree of ordering was obtained, i.e. by thermal or irradiation processes. This means that for low fluences, the effect of S is dominant over the secondary radiation induced effects, e.g. static displacements and the corresponding lattice expansion. This has been shown in the case of Nb_3Pt for the variation of T_c (see Fig. 4.12) and of ρ_0 (see Fig. 7.15). After heavy irradiation, the secondary radiation induced effects (the same as above, but now in addition to disordered depleted zones and possibly to radiation induced transformations) will dominate, in order that the observed properties, for example the saturation of T_c are not longer ordering effects.

A particular attention was given to the variation of the order parameter and its consequences on T_c , γ , θ_D , ρ_0 and H_{c2} after fast quenching from high temperatures. The starting point for a deeper understanding of such thermally induced disorder is the knowledge of the reordering kinetics during the cooling process from T_F^0 , the A15 phase formation temperature, down to the temperature of diffusion limit, T_D . It has been found (see Table 4.1) that reordering in A15 type compounds occurs only above T_D , which is correlated to the solidus by the relation $T_D \geq 0.42 \cdot T_F^0$. The reordering kinetics, however, is very different from compound to compound, thus causing individual differences in the highest attainable order parameter in each compound. Although this point could not be proved definitively in the present work, it is thought that the variation of $S(T)/S_{\max}$ vs. T/T_F^0 , $S(T)$ vs. T/T_F^0 is reproduced in Fig. 4.5) should be very similar for all A15 type compounds, but that the rate of reordering during the cooling process is dramatically different from compound to compound. As an example, it has not been possible to induce any deviation from perfect ordering in V_3Si , even after the fastest cooling rates obtained by argon jet quenching, i.e. 10^4 K/s. On the other hand, other compounds like V_3Au , V_3Ga , Nb_3Pt , Nb_3Al and others all exhibit observable changes of S (and of T_c) for quenching rates well below 10^2 K/s, as illustrated by Fig. 10.1.

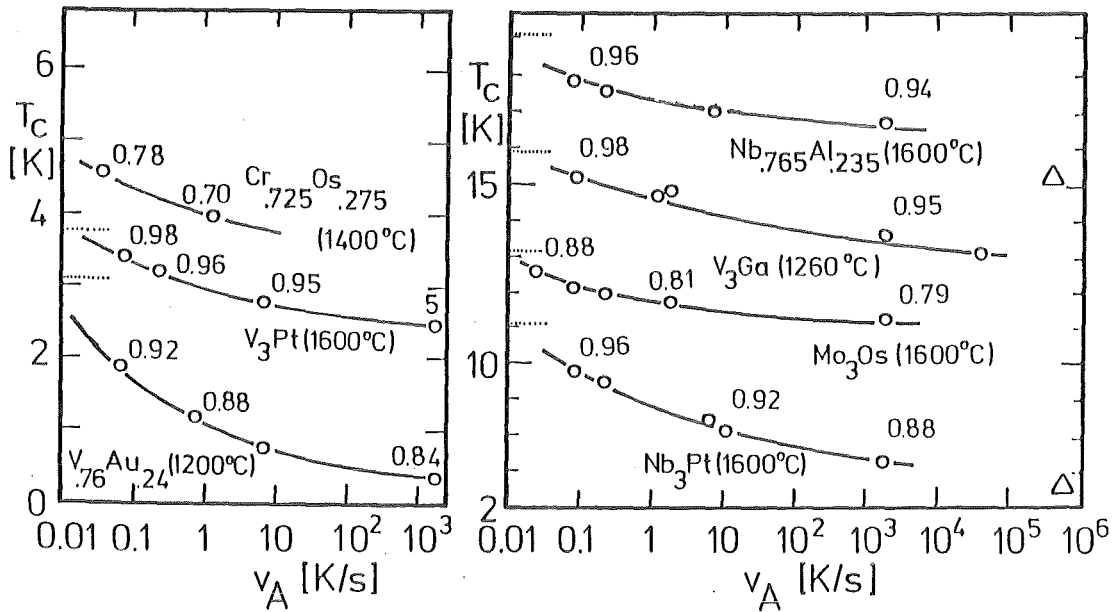


Fig. 10.1. T_c as a function of the cooling rate, v_A , from a fixed temperature for $V_{.76}Au_{.24}$, V_3Pt , V_3Ga , Nb_3Pt and $Nb_{.765}Al_{.235}$. The dotted lines indicate the highest known T_c values, obtained after prolonged annealing at temperatures close to T_D . The numbers indicate the values of S or S_a . The triangles stay for T_c after splat cooling, illustrating the reordering effects during cooldown.

Another way of illustrating the reordering effects during cooldown is the representation of T_C vs. T_A , the annealing temperature. In Fig. 10.2, T_C vs. T_A is represented for V_3Ga which was cooled at two different rates, 5×10^3 K/s (Flükiger and Jorda /26/) and 5×10^4 K/s (Van Winkel et al. /340/). It is seen

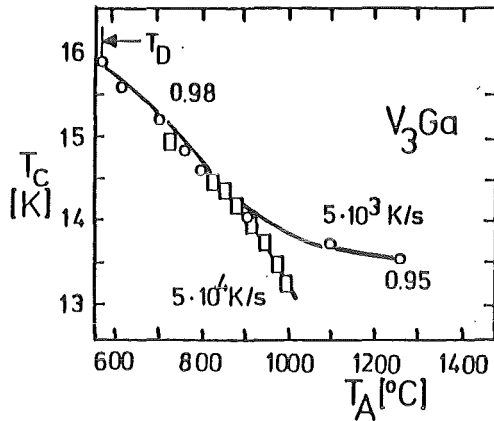


Fig. 10.2. T_C of V_3Ga as a function of T_A , the annealing temperature, for two different cooling rates, 5×10^3 K/s (Flükiger and Jorda /26/) and 5×10^4 K/s (Van Winkel et al. /340/). In this case, $T_D = 560$ °C and $T_C(\text{max}) = 15.9$ K /26/. The numbers represent the order parameter.

that at $T > 850$ °C (or $T/T_F^0 > 0.74$), T_C and thus S start to differ for the two cooling rates. This curve shows clearly the difficulties of inducing higher partial disorder in A15 type compounds by quench procedures: higher cooling rates require smaller sample dimensions, i.e. < 1 mm for 3×10^3 K/s and $15 \mu\text{m}$ for 3×10^4 K/s. Such small particles will sinter together when heated above 1000 °C, which fixes a natural upper temperature limit and thus a lower limit for the order parameter s which can be quenched in by thermal procedures. As a comparison, V_3Si requires cooling rates $v_A > 10^5$ K/s before an effect on T_C can be observed, as reported by Pannetier et al. /120/ after laser quenching experiments. Searching for reasons between the strong difference in the reordering kinetics between V_3Si and V_3Ga , the question about the respective phase stability in these two systems arises.

In the present work, an empirical correlation between the highest attainable order parameter in A15 type compounds (see Figs. 5.2, 5.3 and 5.4) and the phase stability was established. Although there is no particular theoretical basis to describe an explicit correlation between these two phenomena, the present analysis furnishes the experimental confirmation for such an interdependence. Fig. 10.3 summarizes the variation of a) r'_a , the relative occupation factor (Eq. (5.6), representing the order parameter, see Fig. 5.3), b) I , the Raynor stability

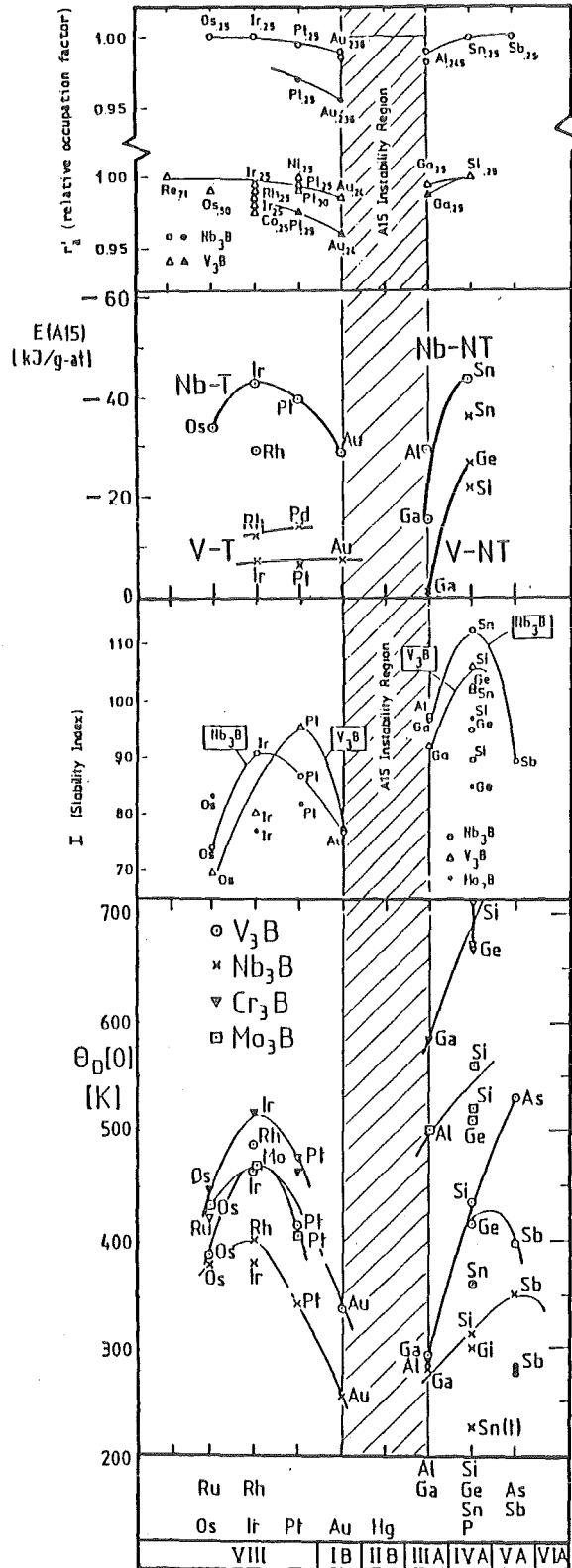


Fig. 10.3. Variation of r'_a , the relative occupation factor (Eq.5.6), I , the Raynor stability index (Eq. 6.8), $E(A15)$, the energy of formation of the A15 phase (see Fig. 6.19) and θ_D , the Debye temperature at 0 K (see Fig. 6.9) as a function of the B electron number of Nb and V based A15 type compounds.

index (Fig. 6.8, see also Fig. 6.17), c) $E(\text{A15})$, the energy of formation of the A15 phase (see Fig. 6.19) and d) θ_D , the Debye temperature (see Figs. 6.2 and 6.9). Although the value of θ_D at 300 K would allow a more direct comparison with the other "high temperature" properties, the values of θ_D at 0 K as determined by calorimetry have been chosen in Fig. 10.3. This choice is due to the fact that these data, listed in Tables 6.5 and 6.6, are by far more complete and reliable than the corresponding values $\theta_X(300\text{K})$ determined in the present work by X ray diffraction on powders (see Fig. 6.2). The effects of phonon softening between 300 and 0 K are considerable (see Fig. 6.4, 6.5 and 6.8), but can be neglected for the present consideration.

In Fig. 10.3, the four quantities r'_a , I , $E(\text{A15})$ and θ_D for Nb and V based compounds have been plotted as a function of the electron number of the B element. The latter has been used throughout the whole work rather than a e/a representation for a better distinction between transition and nontransition B elements. A further purpose was the clear representation of the influence of the chemical nature of the B element: for example, all known A15 type compounds containing Si, e.g. V_3Si , Mo_3Si , Cr_3Si (and probably, but without proof) the metastable Nb_3Si are perfectly ordered. The somewhat surprising fact that the classification is done following the minority B elements is justified by their higher number with respect to A elements.

The representation in Fig. 10.3 shows very clearly that all four considered quantities exhibit a very similar behavior at both sides of the A15 "Instability region". This region is represented by the elements $B = \text{Zn}$, Cd and Hg , for which no stable Nb or V based A15 type compounds exist. The largest variation of the order parameter by thermal processes is observed for $B = \text{Au}$, Al and Ga , i.e. just for the closest compounds to the instability region, as shown in the top figure. For the B elements corresponding to the next columns, i.e. $B = \text{Pt}$ (for transition elements) and $B = \text{Si}$, Ge , Sn (for nontransition elements), r'_a and thus S reaches 1, a certain amount of disorder being only induced for Pt . As mentioned above, it is extremely hard to induce ordering changes for the compounds with $B = \text{Si}$: this is also valid for $B = \text{Ge}$ and Sn , where all quenching attempts were so far unsuccessful. These compounds are the most stable ones, with $r'_a = 1$ and maximum values for I , $E(\text{A15})$ and θ_D . A comparable situation for B transition elements is observed for $B = \text{Ir}$.

Another way to represent the variation of ordering and phase stability in A15 type compounds consists in considering the limits of the A15 phase fields,

as shown in Fig. 10.4. For B = Ru and Os, the compounds are as ordered as possible with $r'_a = 1$, but with a composition exceeding stoichiometry (in the cases of A = Cr and V): $\beta \geq 0.25$. The ideal case is represented by compounds with B = Ir, Si, Ge or Sn, where the stoichiometric composition is stable (except $V_{.80}Sn_{.20}$) and $r'_a = 1$. These ideal A15 type compounds are rather rare: stability is reached either by accomodating the composition towards $\beta > 0.25$ or $\beta < 0.25$ or by the limitation to order parameters $S < 1$.

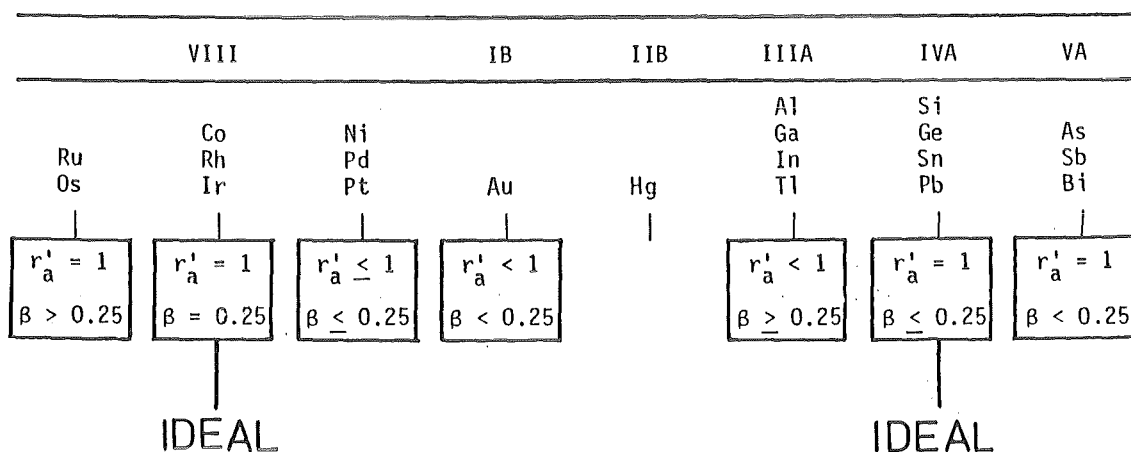


Fig. 10.4. Ordering and stoichiometry in A15 type compounds. The compounds with B elements in the Co, Ni, Ir and Si, Ge, Sn columns are always perfectly ordered. In some ideal cases, e.g. Nb_3Ir , V_3Si and Nb_3Sn , they simultaneously form at perfect stoichiometry.

The observed total variation of S with varying B electron number is of course also reflected by the corresponding variation of T_c . The maximum variation ΔT_c as induced by quench and annealing processes for V and Nb based A15 systems is plotted in Fig. 10.5. The largest variation, $\Delta T_c = 4.2$ K, is obtained for the two pseudobinaries $Nb_{.75}Au_{.175}Pt_{.075}$ and $Nb_{.75}Al_{.20}Ge_{.05}$ at both limits to the instability region. A maximum of ΔT_c would be expected for B = Au, Al and Ga, but in these cases the change in T_c is restricted either by deviations from stoichiometry (for B = Au, while stoichiometry is reached at the highest temperatures only for Nb_3Al and Nb_3Ga) or for perfect ordering (for B = Au, Al and Ga).

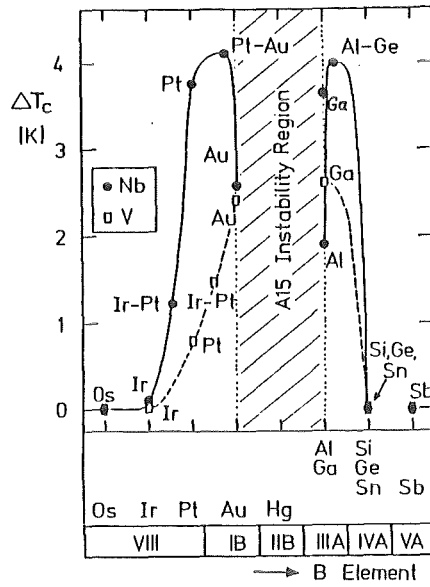


Fig. 10.5. Maximum variation ΔT_c as induced by quench and annealing for various Nb and V based A15 type compounds.

10.2. Variation of the Low Temperature Properties With Atomic Ordering

The variation of T_c for a series of A15 type compounds as a function of the order parameter has been plotted in Fig. 10.6 on the basis of the data listed in Tables of Sect. 5. All order parameter values contained in these tables have been determined by refining diffractometric data and have been critically discussed (and in some cases corrected) in Sect. 5. In order to compare the data between the systems $Cr_{.725}Os_{.275}$, Mo_3Os , Nb_3Ge , Nb_3Al , Nb_3Sn , Nb_3Pt , $Nb_{.736}Au_{.234}$, V_3Ga , V_3Si , V_3Pt and $V_{.76}Au_{.24}$, a normalized representation was chosen: T_c/T_{c0} vs. S/S_0 (or S_a/S_{a0} for the nonstoichiometric systems $Cr_{.725}Os_{.275}$, $Nb_{.736}Au_{.234}$ and $V_{.76}Au_{.24}$). The values for T_{c0} and S_0 are the estimated values for the highest attainable degree of ordering in each compound, the absolute error being inferior to 0.5 K for T_{c0} and 0.02 for S_0 .

The data for Nb_3Ge were also included, although the presence of additional phases and compositional inhomogeneities lead to uncertainties in the absolute value of S of the order of 0.04 to 0.08. It has been stated in Sect. 5 and 7, but also in the discussion of Fig. 10.3 that Nb_3Ge is probably perfectly ordered, and several convincing arguments have been given in these work. The data of Sweedler et al. /68,70,182/ are plotted in Fig. 10.6 assuming $S_0 = 1.00$, and the resulting curve (dotted line) is practically identical to that obtained for the other Nb based systems.

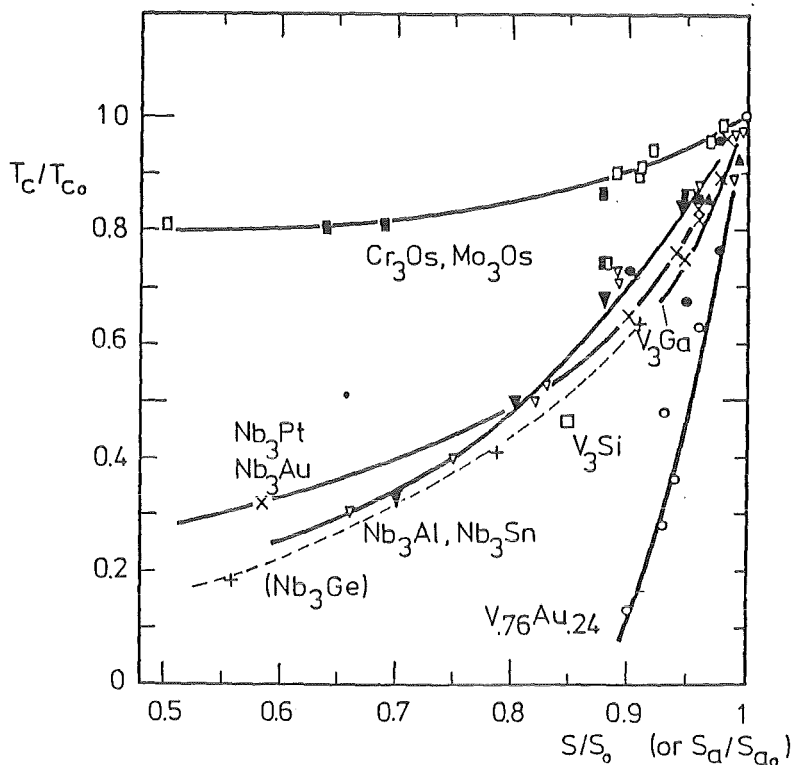


Fig. 10.6. T_c/T_{c0} vs. S/S_0 for the A15 systems Nb_3Sn (∇), Nb_3Al (∇), Nb_3Ge ($+$), Nb_3Pt (\times), $Nb_{.736}Au_{.234}$ (\blacksquare), V_3Si (\square), V_3Ga (\blacktriangle), V_3Pt (\bullet), $V_{.76}Au_{.24}$ (\circ), Mo_3Os (\blacksquare) and $Cr_{.725}Os_{.275}$ (\square), based on the data listed in the tables of Sect. 5. T_{c0} and S_0 are the estimated values for the highest attainable values of T_c and S in each of these compounds.

It follows from Fig. 10.6 that the variation of T_c with the degree of atomic ordering is quite different for each compound. The smallest variation is observed in Mo_3Os and $Cr_{.725}Os_{.275}$, the largest one in $V_{.76}Au_{.24}$. The group of the other V and Nb based compounds occupies an intermediate position in Fig. 10.6, the variation for the former being somewhat stronger (Note the scattering in the data for V_3Pt , being either close to Nb_3Sn /53,220/ or to $V_{.76}Au_{.24}$ /4,193/). It is remarkable that the data for the V and Nb based systems fall within a quite narrow region (except $V_{.76}Au_{.24}$). This behavior is analogous to that of T_c/T_{c0} of irradiated A15 systems (see Fig. 4.10a), where the decrease of T_c of all V and Nb based A15 type compounds nearly fall together. The similarity between the results on thermally treated and irradiated samples has been stated in Sect. 4. The present considerations extend this similarity to the variation of T_c with the order parameter. As a very suggestive way to illustrate the analogy between thermally treated and irradiated samples, both representations, T_c/T_{c0} vs. S/S_0 and T_c/T_{c0} vs. ϕt are compared in Fig. 10.7. This picture shows the significant difference between the Nb and V based systems (which all are situated within a narrow range) and Mo_3Os . Unfortunately, no irradiation data are available for

$V_{.76}Au_{.24}$. There have been attempts to ascribe an universal behavior of T_C/T_{C0} vs. ϕt for high T_C A15 type compounds. It will be discussed below that this behavior is obviously connected to the individual density of states of each compound, which must be sufficiently high. From this point of view, $V_{.76}Au_{.24}$ is an exception, which is possibly correlated to the strongly enhanced spin susceptibility in this compound /97/. There is thus no physical reason which could be advanced for a really "universal" behavior of T_C/T_{C0} vs. ϕt or of T_C/T_{C0} vs. S/S_0 , and

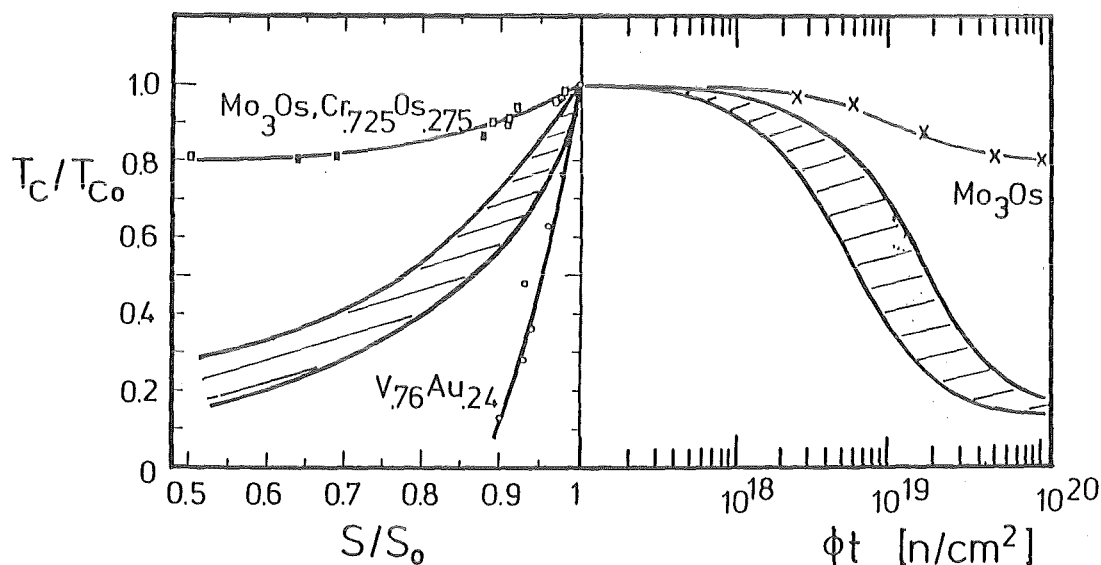


Fig. 10.7 Variation of T_C/T_{C0} as a function of S/S_0 and of ϕt (See Figs. 4.10a and 10.6). The hatched area contains the systems Nb_3Ge , Nb_3Sn , Nb_3Pt , $Nb_{.766}Au_{.234}$, V_3Ga , V_3Si , V_3Pt and Nb_3Al .

it is certainly more correct to say that there is a similarity in the dependence of T_C on the degree of atomic ordering, due to the correlated change in $N(E_F)$, which must only be sufficiently high, in order to dominate over the simultaneous effects of phonon hardening with disordering (see 4.3.6b).

The variation of T_C for low T_C A15 type compounds discussed in Sect. 4 is summarized in Fig. 10.8 which represents the corresponding variations for Mo_3Ge , Mo_3Si and Nb_3Ir . It has been shown in the present work that the enhancement of T_C with irradiation in these compounds is really an ordering effect and is not due to secondary radiation induced effects. In the case of Mo_3Si /158/ (and probably also Mo_3Ge), a decrease of S leads to a decrease of θ_D , thus to a softening of the phonon spectrum. (See Fig.4.32). Since for these low T_C compounds the electronic density of states remains essentially unchanged after irradiation (only a slight increase is reported), the enhancement of T_C must be attributed to the observed phonon softening.

There is thus a contrast between the behavior of high and low T_C A15 type compounds with disordering:

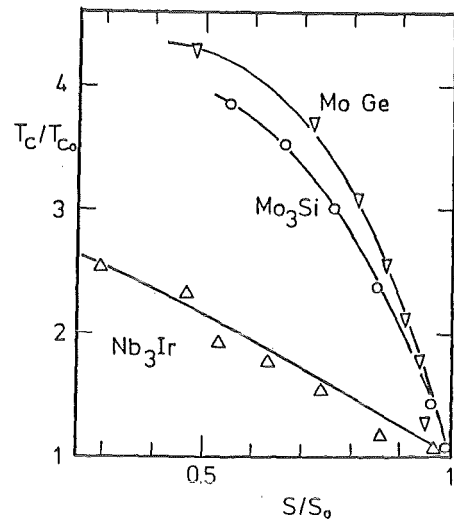


Fig. 10.8. T_C/T_{C_0} vs. S/S_0 for Mo_3Si /137/, Mo_3Ge /138/ and Nb_3Ir /135/.

- a) High T_C materials show a lowering of $N(E_F)$ and an enhancement of θ_D ,
- b) Low T_C materials show a slight enhancement of $N(E_F)$ and a decrease of θ_D .

The origin of the very different behavior in these two classes of materials may be the substantial difference in the pair potentials, essentially in the interaction between the A and B elements, as illustrated for Nb_3Sn and Mo_3Si in Fig. 4.35. This is also the basis for the understanding of the antagonism between the compounds based on Nb and V on one hand and on Cr and Mo on the other. Compounds with a transition B element as $\text{Mo}_{.76}\text{Ir}_{.24}$, Mo_3Os and $\text{Cr}_{.725}\text{Os}_{.275}$ have an intermediate behavior between the above cases a) and b). Indeed, it follows from the data in Table 6.5 that disordering causes here a decrease of both, $N(E_F)$ and θ_D . However, both quantities vary very slightly, thus explaining the small change of T_C .

It is interesting to follow the variation of the electronic density of states with the degree of ordering. The variation of the electronic heat capacity, γ/γ_0 , has been plotted in Fig. 10.9 for the systems $\text{V}_{.76}\text{Au}_{.24}$, V_3Ga , Nb_3Al , Nb_3Pt and V_3Si , based on the data listed in Table 6.5. All these data were determined by calorimetric measurements on thermally treated or irradiated samples. In addition, the variation of γ/γ_0 for Nb_3Sn measured by Lehmann /301/ have also been added to Fig. 10.9, in order to extend the curve to lower S/S_0 values. These data were obtained by measuring the initial slope and ρ_0 on ^{32}S irradiated Nb_3Sn films. The contrast between the variation of γ/γ_0 and of T_C/T_{C_0} is immediately apparent: All specific heat data are practically situated on the same curve, included $\text{V}_{.76}\text{Au}_{.24}$. This demonstrates that the difference between the latter and the other systems in Fig. 10.6 cannot be explained by the variation of $N(E_F)$ alone.

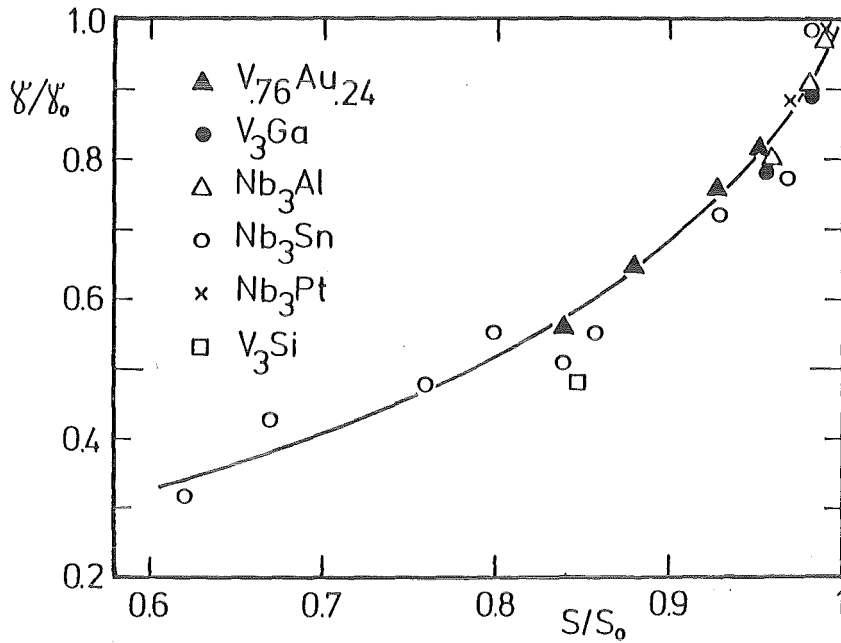


Fig. 10.9. γ/γ_0 vs. S/S_0 for $V_{0.76}Au_{0.24}$, V_3Ga , Nb_3Al , Nb_3Pt and V_3Si (Determined by calorimetry, listed in Table 6.5) and Nb_3Sn (Deduced from the initial field slope and $\rho_0 / 301/$).

From Fig. 10.9 it follows that the initial decrease of γ/γ_0 is strongest for the most ordered state. For example, the decrease of S by 5 % causes a decrease of γ/γ_0 by 20 %, while a further decrease of S by 5% lowers the heat capacity by 10 % only, i.e. half the preceding value. Below $S = 0.7$, saturation effects start to occur. As shown for Mo_3Si /158/, the two modifications a) highly disordered A15 structure and b) amorphous structure exhibit the same electronic density of states.

From the above mentioned specific heat measurements, it is possible to draw some conclusions about the effect of atomic ordering on the variation of λ , the electron-phonon interaction parameter, with the bare electronic density of states, $N_{bs}(E_F)$. The results are represented in Fig. 10.10 and show a strong correlation. The correlation λ vs. $N_{bs}(E_F)$ shows a linear tendency, as predicted by the model of Appel /304/. The slope increases from V_3Au to Nb_3Al , in a very similar way to the variation of T_c vs. γ in Fig. 8.8. It appears that $N_{bs}(E_F)$ undergoes the largest variation with ordering for V based A15 type compounds, while λ is the most changing quantity for the Nb based compounds. A representation of λ vs. $N_{bs}(E_F)$ for A15 compounds with varying compositions yields a similar plot to that in Fig. 10.10. It is interesting that the only compounds for which the slope in a plot like Fig. 10.10 is negative are $Cr_{1-\beta}Ir_{\beta}$ (compositional change), Mo_3Os and $Cr_{0.725}Os_{0.275}$, thus reflecting the antagonism with respect to Nb and V based A15 type compounds.

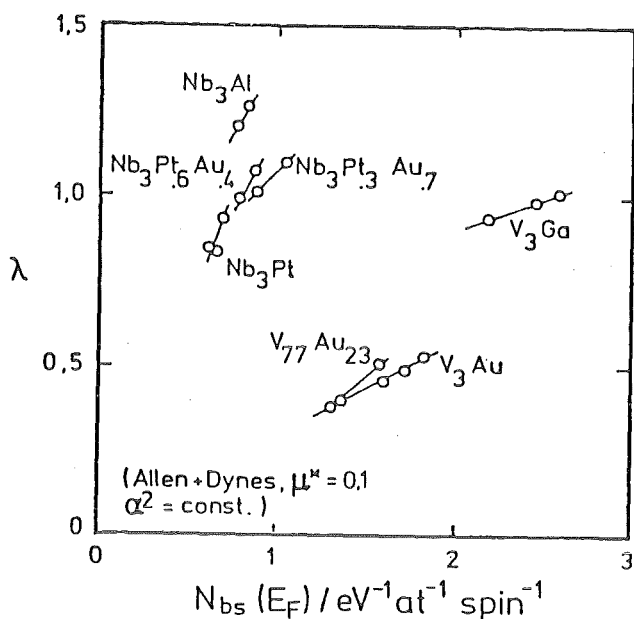


Fig. 10.10. The electron-phonon interaction parameter λ vs. the unrenormalised band structure density of states for various A15 type compounds at different states of ordering (Muller /96/).

The question about a possible further increase of T_C in A15 type compounds above the highest value known so far, $T_C = 23 \text{ K}$ /44/, can now be answered. Among the known systems, only Nb_3Ge could possibly reach slightly higher T_C values if perfect stoichiometry could be reached. The measurements reported in Sect. 8 indeed suggest that Nb_3Ge is perfectly ordered, but that the Ge content would be $\sim 24.5 \text{ at.}\%$ rather than $25 \text{ at.}\%$. In this case, the possible increase in T_C would be restricted to $\Delta T_C \leq 1 \text{ K}$. There have been speculations about very high T_C values in the metastable compound Nb_3Si , which cannot be confirmed by the present work, which would rather suggest that T_C of Nb_3Si would hardly exceed the presently known highest value of 18 K . Indeed, Nb_3Si is produced by explosion techniques (Olinger and Newkirk /130/), starting from the perfectly ordered Ti_3P structure type. Since the transition $\text{Ti}_3\text{P} \rightarrow \text{A15}$ occurs diffusionless /130/, no change of the order parameter during the explosion at $\lesssim 1000 \text{ }^\circ\text{C}$ is expected. The low $H_{c2}(0)$ value of 16 T for Nb_3Si with $T_C = 18 \text{ K}$ would correspond to similar values in very clean Nb_3Sn with the same T_C (Orlando et al. /188/). However, the last proof of this hypothesis would require either measurements of the order parameter or of the electrical resistivity. An attempt on a sample given by G. Stewart (the same one on which the specific heat was measured) failed, the sample containing too much additional phases to allow unambiguous results.

It is interesting to follow how T_C varies when gradually increasing the B electron number. The representation in Fig. 10.11 contains all known A15 systems based on Nb, V, Cr, Mo, Ti and Zr. As mentioned before, the instability region does not exist for Ti and Zr, the corresponding compounds Ti_3Hg and Zr_3Hg being stable (Both are normal down to 0.1 K). For the Nb and V based compounds, it is remarkable that in contrast to the variation of the properties in Fig. 10.3, the systems with B = Au, Al or Ga at the proximity of the instability region do not show any particular change. It can, however, not be anticipated whether the hypothetical compounds with B = Zn, Cd and Hg - would they exist - would exhibit T_C values lying on the dashed line in Fig. 10.11 or below.

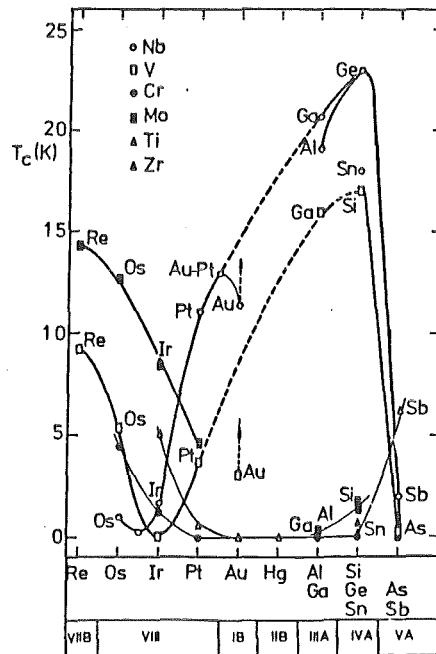


Fig. 10.11. T_C for various A15 type compounds based on V, Nb, Cr, Mo, Ti and Zr. as a function of the electron number of the B element (From Flükiger /7/).

REFERENCES

- / 1/ C.H. Johansson and J.O. Linde, Ann. Physik /4/ 78, 439 (1925)
- / 2/ F.C. Nix and W. Shockley, Rev. Mod. Phys. 10, 1 (1938)
- / 3/ E.C. van Reuth, R.M. Waterstrat, R.D. Blaugher, R.A. Hein and J.E. Cox, Proc. LT 10 (Moscow) Vol. Ib (Moscow: Viniti), 1967, p. 137
- / 4/ E.C. van Reuth and R.M. Waterstrat, Acta Cryst. B24, 186 (1968)
- / 5/ D.O. Welch, G.J. Dienes, O.W. Lazareth and R.D. Hatcher, IEEE Trans. Magn., MAG-19, 889 (1983)
- / 6/ R. Flükiger, Proc. LT 17 (Karlsruhe), Eds. v. Eckern, A. Schmid, W. Weber and H. Wühl, 1984, North-Holland, Vol. I, p. 609
- / 7/ R. Flükiger, in "Superconducting Materials Science - Metallurgy, Fabrication and Application", S. Foner and B.B. Schwartz, Eds., Plenum Press, New York (1981), p. 511
- / 8/ G.W. Cullen, R.L. Novak and J.P. McEvoy, Jr., RCA Rev. 25, 479 (1964)
- / 9/ R. Flükiger, R. Isernhagen, W. Goldacker and W. Specking, Adv. Cryo. Eng., Vol. 30, 364 (1984)
- /10/ J.W. Ekin, IEEE Trans. Magn., MAG-15, 197 (1979)
- /11/ R. Flükiger, W. Schauer, W. Specking, L. Oddi, L. Pintschovius, W. Müller and B. Lachal, Adv. Cryo. Eng., Vol. 28, p. 364 (1982)
- /12/ W. Rehwald, M. Rayl, R.W. Shen and G.C. Cody, Phys. Rev. B6, 363 (1972)
- /13/ J.R. Gavaler, App. Phys. Lett. 23, 480 (1973)
- /14/ B.T. Matthias, E.A. Wood, E. Corenzwit and V.B. Bala, J. Phys. Chem. Sol. 1, 188 (1956)
- /15/ M. Marezio, P.D. Dernier, J.P. Remeika, E. Corenzwit and B.T. Matthias, Mat. Res. Bull. 8, 657 (1973)
- /16/ M.C. Krupka, J. Less Common Metals 19, 113 (1969)
- /17/ E. Röschel, O. Loebich and C.J. Raub, Z. Metallkde, 64, 359 (1973)
- /18/ R. Flükiger, C. Susz, F. Heiniger and J. Muller, J. Less-Common Metals, 40, 103 (1975)
- /19/ B.N. Das, J.E. Cox, R.W. Huber und R.A. Meussner, Metall. Trans. A8, 541 (1977)
- /20/ R. Flükiger, J.L. Staudenmann and P. Fischer, J. Less-Common Metals, 50, 253 (1976)
- /21/ C.E. Lundin and A.S. Yamamoto, Trans. AIME. 236, 863 (1966)

- /22/ G.R. Stewart, L.R. Newkirk and F.A. Valencia, Phys. Rev. 21B, 5055 (1980)
- /23/ S. Basavaiah and S.R. Pollack, Appl. Phys. Lett. 12, 259 (1968)
- /24/ E. Bucher, F. Laves, J. Muller and H.V. Philipsborn, Phys. Lett. 8, 27 (1964)
- /25/ A. Junod, in "Superconductivity in d- and f-Band Metals", Eds. W. Buckel and W. Weber, Academic Press, 1982, p. 89
- /26/ R. Flükiger and J.L. Jorda, Sol. State Comm., 22, 109 (1977)
- /27/ G.W. Webb, IEEE Trans. Magn. MAG-15, 616 (1979)
- /28/ R. Flükiger, J.L. Jorda, A. Junod and P. Fischer, Appl. Phys. Comm. 1, 9 (1981)
- /29/ G.R. Stewart and A.L. Giorgi, Sol. State Comm., 26, 669 (1978)
- /30/ A. Junod, Ph.D., Thèse No 161, 1974, Dépt. Phys. Mat., Condensée Université de Genève, Switzerland
- /31/ The microprobe determination on a series of Nb-Au samples with nominal composition Nb₇₅Au₂₅ was kindly undertaken by R.M. Waterstrat, NBS Gaithersburg, Md., USA
- /32/ G. Seidel and P.H. Keesom, Phys. Rev. 112, 1083 (1958)
- /33/ R.T. Johnson, O.E. Vilches, J.C. Wheatley and S. Gygax, Phys. Rev. Lett., 16, 101 (1966)
- /34/ F. Heiniger, Phys. Kondens. Materie, 5, 243 (1966)
- /35/ J.L. Jorda, R. Flükiger and J. Muller, J. Less-Common Metals, 75, 227 (1980)
- /36/ T. Jarlborg, in "Superconductivity in d- and f-Band Metals", Eds. W. Buckel and W. Weber, Kernforschungszentrum Karlsruhe, 1982, p. 115
- /37/ L.F. Mattheiss, Phys. Rev. 139A, 1893 (1965)
- /38/ R. Flükiger, unpublished results
- /39/ R. Flükiger, A. Paoli and J. Muller, Solid State Commun. 14, 443 (1974)
- /40/ W.L. McMillan, Phys. Rev. 167, 331 (1968)
- /41/ A.K. Ghosh and D.H. Douglass, Ferroelectrics, 16, 269 (1977)
- /42/ W.J. Johnson, C.C. Tsuei, S.I. Raider and R.B. Laibowitz, J. Appl. Phys. 50, 4240 (1979)
- /43/ R. Flükiger and J.L. Jorda, in "Phase Diagrams in Metallurgy and Ceramics" NBS Special Publ. Nr. 196, p. 375 (1978)
- /44/ J.R. Gavaler, M.A. Janocko and C.K. Jones, Proc. LT 13, Vol. 3 (Plenum, New York), 1972, p. 558

- /45/ E. Bucher, F. Heiniger and J. Müller, *Helv. Phys. Acta*, 34, 843 (1961)
- /46/ V.B. Compton, E. Corenzwit, J.P. Maita, B.T. Matthias and F.J. Morin, *Phys. Rev.* 123, 1567 (1961)
- /47/ J.B. Darby, Jr., and S.T. Ziegler, *J. Phys. Chem. Sol.* 23, 1825 (1962)
- /48/ V. Sadagopan, E.R. Pollard, B.C. Giessen and H.C. Gatos, *Appl. Phys. Lett.* 7, 73 (1965)
- /49/ B.T. Matthias, *Phys. Rev.* 97, 74 (1965)
- /50/ R. Flükiger, K. Yvon, C. Susz, R. Roggen, A. Paoli and J. Muller, *J. Less-Common Metals* 32, 207 (1973)
- /51/ B.C. Giessen, U. Jaehniger and N.J. Grant, *J. Less-Common Metals*, 10, 147 (1965)
- /52/ M.M. Collver and R.H. Hammond, *Phys. Rev. Lett.* 30, 92 (1973); S.J. Poon and W.L. Carter, *Solid State Comm.* 35, 249 (1980)
- /53/ A.R. Sweedler and D.E. Cox, *Phys. Rev.* B12, 147 (1975)
- /54/ G. Linker, KfK Report Nr. 3146, Kernforschungszentrum Karlsruhe, March 1981. See also Ref. 55
- /55/ U. Schneider, G. Linker and O. Meyer, *J. Low Temp. Phys.* 47, 439 (1982)
- /56/ G.E. Bacon, *Acta Cryst.* A28, 357 (1972)
- /57/ R.M. Waterstrat and B. Dickens, *J. Appl. Phys.* 45, 3726 (1974)
- /58/ D.T. Cromer and J.B. Mann, *Acta Cryst.* A24, 321 (1968), "Int. Tables for X-Ray Crystallography", Vol. IV, 1974, Table 2.2 A
- /59/ R. Fukamachi, Rep. Inst. Solid State Physics, Univ. Tokyo, Series B, No. 12, May 1971
- /60/ D.T. Cromer and D. Libermann, *J. Chem. Phys.*, 53, 1891
- /61/ F.W. Jones and C. Sykes, *Proc. Roy. Soc.*, A161, 440 (1975)
- /62/ R. Flükiger, Ph.D. Thesis No. 1543, University of Geneva, Switzerland, 1972
- /63/ R. Flükiger, A. Paoli, A. Junod and J. Muller, to be published
- /64/ A. Junod, J.L. Staudenmann, J. Muller and P. Spitzli, *J. Low Temp. Phys.* 5, 25 (1971)
- /65/ J.L. Jorda, R. Flükiger and J. Muller, *J. Less-Common Metals*, 55, 249 (1977)
- /66/ R.G. Mayer, Y. Uzel and H. Kandler, *Z. Naturforschg.*, 21A, 532 (1966)
- /67/ J.L. Jorda, R. Flükiger and J. Muller, *J. Less-Common Metals*, 62, 25 (1978)

- /68/ A.R. Sweedler, C.L. Snead, Jr. and D.E. Cox, in "Metallurgy of Superconducting Materials", Ed. T. Luhman and D. Dew-Hughes, Academic Press, New York 1979, p. 349; A.R. Sweedler, D.E. Cox, S. Moehlecke, R.H. Jones, L.R. Newkirk and F.A. Valencia, J. Low Temp. Physics, 24, 645 (1976)
- /69/ A.R. Sweedler, D.E. Cox and S. Moehlecke, J. Nucl. Mater. 72, 50 (1978)
- /70/ D.E. Cox, A.R. Sweedler, S. Moehlecke, L.R. Newkirk and F.A. Valencia, in "Superconductivity in d- and f-Band Metals", Eds. H. Suhl and M.B. Maple, Academic Press, Inc., 1980, p. 335
- /71/ L.R. Aronin, J. Appl. Phys. 25, 344 (1954)
- /72/ G.H. Kinchin and R.S. Pease, J. Nucl. Energy, 1, 200 (1955)
- /73/ K.E. Kihlstrom, R.H. Hammond, J. Talvacchio, T.H. Geballe, A.K. Green and V. Rehn, J. Appl. Phys. 53, 8907 (1982)
- /74/ H.P. Krämer, W. Schauer, H. Wühl, C. Nölscher, H. Adrian and G. Saemann-Ischenko, IEEE Trans. Magn., MAG-21, 823 (1985)
- /75/ R.D. Blaugher, R.A. Hein, J.E. Cox and R.M. Waterstrat, J. Low Temp. Phys., 1, 539 (1969)
- /76/ S. Moehlecke, D.E. Cox and A.R. Sweedler, J. Less-Common Metals, 62, 111 (1978); Sol. State Commun., 23, 703 (1977)
- /77/ A.R. Sweedler, S. Moehlecke, R.H. Jones, R. Viswanathan and D.C. Johnston, Sol. State Comm., 21, 1007 (1977)
- /78/ D.E. Cox and J.A. Tarvin, Phys. Rev. B18, 22 (1978)
- /79/ A. Taylor, N.Y. Doyle and B.J. Kagle, J. Less-Common Metals, 4, 436 (1962)
- /80/ D.O. Welch, G.J. Dienes, O.W. Lazareth, Jr. and R.D. Hatcher, J. Phys. Chem. Solids, 45, 1225 (1984)
- /81/ R. Flükiger, Adv. Cryo. Eng., Vol. 32, 873 (1986)
- /82/ R. Flükiger, P. Spitzli, F. Heiniger and J. Muller, Phys. Lett. 29A, 407 (1969)
- /83/ P.R. Sahm and T.V. Pruss, Phys. Lett. 28A, 707 (1969)
- /84/ C.C. Koch, J. Phys., Chem. Solids, 34, 1445 (1973)
- /85/ T.H. Courtney, G.W. Pearsall and J. Wulff, Trans. AIME 233, 213 (1965)
- /86/ H. Devantay, J.L. Jorda, M. Decroux, J. Muller and R. Flükiger, J. Mater. Sci., 16, 2145 (1981)
- /87/ A. Guha, M.P. Sarachik, F.W. Smith and L.R. Testardi, Phys., Rev. B18, 541 (1977)
- /88/ W.L. Bragg and E.J. Williams, Proc. Roy. Soc. A145, 699 (1934), A151, 540 (1935)

- / 89/ J.G. Kirkwood, J. Chem. Phys. 6, 70 (1938)
- / 90/ H. Bethe, Proc. Roy. Soc. A150, 552 (1935)
- / 91/ J.L. Staudenmann, Helv. Physica Acta, 47, 39 (1974)
- / 92/ R.M. Waterstrat and R.C. Manuszewski, in "Noble Metal Constitution Diagrams" parts I and II, Natl. Bureau of Standards, Report Nrs. NBS 10571 (1971) and NBS IR 73-415, 1975; Metallurgical Trans., 16A, 1943 (1985)
- / 93/ G.W. Webb and J.J. Engelhardt, IEEE Trans. Magn., MAG-11, 208 (1975)
- / 94/ R. Flükiger, J.L. Staudenmann, A. Treyvaud and P. Fischer, Proc. LT 14, Helsinki 1975, Eds. M. Krusius and M. Vuorio, North-Holland, Vol. 2, p. 1
- / 95/ J.L. Staudenmann, Solid State Comm. 23, 121 (1977); J.L. Staudenmann, P. Coppens and J. Muller, Solid State Comm. 19, 29 (1976)
- / 96/ J. Muller, Reports on Progress in Physics, 43, 641 (1980)
- / 97/ A. Junod, R. Flükiger, A. Treyvaud and J. Muller, Solid State Comm. 19, 265 (1976)
- / 98/ A. Junod, P. Bellon, R. Flükiger, F. Heiniger and J. Muller, Phys. Cond. Materie 15, 133 (1972)
- / 99/ S. Moehlecke, A.R. Sweedler and D.E. Cox, Phys. Rev. B21, 2712 (1980)
- /100/ E.M. Schulson, J. Nucl. Mater., 83, 230 (1979)
- /101/ F. Rullier-Albenque, S. Paidassi and Y. Quéré, J. Physique, 41, 515 (1980)
- /102/ B. Besslein, G. Ischenko, S. Klaumünzer, P. Müller, H. Neumüller, K. Schmelz and H. Adrian, Phys. Lett. 53A, 49 (1975)
- /103/ C.S. Pande, Sol. State Comm., 24, 241 (1977); C.S. Pande and R. Viswanathan, J. Less-Common Metals, 62, 119 (1978)
- /104/ C.S. Pande, J. Nucl. Mater., 72, 83 (1978); C.S. Pande and R. Viswanathan, Journal de Physique, 39, C6-389 (1978)
- /105/ C.S. Pande, Phys. Stat. Sol. (a) 52, 687 (1979)
- /106/ O. Meyer and B. Seeber, Sol. State Comm., 22, 603 (1977)
- /107/ L.R. Testardi, J.M. Poate and H.J. Levinstein, Phys. Rev. B15, 2570 (1977)
- /108/ J. Ruzicka, E.L. Haase and O. Meyer, "Superconductivity in d- and f-Band Metals", Eds. W. Buckel and W. Weber, Kernforschungszentrum Karlsruhe, 1982, p. 107
- /109/ A. Seeger, in Proc. 2^d UN Int. Conf. Peaceful Uses of Atomic Energy (Geneva), Vol. 6, p. 250 (1958); A. Seeger, in "Radiation Damage in Solids" (IAEA, Vienna), Vol. 1, p. 101 (1962)

- /110/ J.A. Brinkman, Amer. J. Phys., 24, 246 (1956)
- /111/ A.K. Ghosh, H. Wiesmann, M. Gurvitch, H. Lutz, O.F. Kammerer, C.L. Snead, A. Goland and M. Strongin, J. Nucl. Mater., 72, 70 (1978)
- /112/ R. Flükiger: Unpublished T_C data on Ar jet quenched Nb₃Pt (Ref. 62) were made available to Dr. D.E. Cox for including in Ref. 99, Fig. 6.
- /113/ C.S. Pande, in "Superconductivity in d- and f-Band Metals", Ed. H. Suhl and M.B. Maple, Academic Press Inc., 1980, p. 349
- /114/ B. Cort, G.R. Stewart, C.L. Snead, Jr., A.R. Sweedler and S. Moehlecke, Phys. Rev. B24, 379 (1981)
- /115/ R. Viswanathan, R. Caton and C.S. Pande, J. Low Temp. Phys., 30, 503 (1978)
- /116/ P. Sigmund, Radiation Effects, 1, 15 (1969)
- /117/ R. Viswanathan, R. Caton and C.S. Pande, Phys. Rev. Lett., 41, 906 (1978); R. Viswanathan and R. Caton, Phys. Rev. B18, 15 (1978)
- /118/ D.O. Welch, C.S. Pande, R. Viswanathan and R. Caton, extracted from an unpublished report
- /119/ R. Meier-Hirmer and H. Küpfer, J. Nucl. Mater., 109, 593 (1982)
- /120/ B. Pannetier, T.H. Geballe, R.H. Hammond and J.F. Gibbons, Physica, 107B, 471 (1981)
- /121/ Y.M. Nikulin, V.Y. Arkhipov, B.N. Goshchitskii, Fiz. Metal. Metalloved., 41, 202 (1976)
- /122/ P. Spitzli, R. Flükiger, F. Heiniger, A. Junod, J. Muller and J.L. Staudenmann, J. Phys. Chem. Solids, 31, 1531 (1970)
- /123/ E.L. Haase and J. Ruzicka, J. Low Temp. Physics, 47, 461 (1962)
- /124/ R.M. Waterstrat, J. Sol. State Chem., 37, 370 (1981)
- /125/ F. Rullier-Albenque, Ph.D. Thesis, 1984, University of Paris/Orsay
- /126/ W.B. Pearson, Philosophical Magazine, 46A, 379 (1982)
- /127/ B.C. Giessen, R. Koch, N.J. Grant, Trans. AIME, 230h, 1268 (1964)
- /128/ R.M. Waterstrat and R.C. Manuszewski, J. Less-Common Metals, 32, 31 (1973)
- /129/ G.J. Dienes and G.H. Vineyard, "Radiation Effects in Solids", New York, Interscience Publ. Inc., 1957
- /130/ B. Olinger and L.R. Newkirk, Sol. State Comm., 37, 613 (1981)
- /131/ W.L. Bond, A.S. Cooper, K. Andres, G.W. Hull, T.H. Geballe, B.T. Matthias, Phys. Rev. Letters, 15, 260 (1965)

- /132/ E.L. Haase and Jiri Ruzicka, J. Low. Temp. Phys., 47, 461 (1982)
- /133/ R.M. Waterstrat, F. Haenssler and J. Muller, J. Appl. Phys., 50, 4763 (1979)
- /134/ T.L. Francavilla, B.N. Das, D.V. Gubser, R.A. Meussner and S.T. Sekula, J. Nucl. Mater., 72, 203 (1978)
- /135/ G. Schneider and G. Linker, to be published
- /136/ C. Nölscher and G. Saemann-Ischenko, Phys. Rev. 32B, 1519 (1985)
- /137/ M. Lehmann and G. Saemann-Ischenko, Phys. Lett., 87A, 369 (1982)
- /138/ M. Lehmann, H. Adrian, J. Bieger, P. Müller, C. Nölscher, G. Saemann-Ischenko and E.L. Haase, Sol. State Comm., 39, 145 (1981)
- /139/ L. Pauling, Acta Cryst., 10, 374 (1957);
L. Pauling, Acta Cryst., 10, 685 (1957)
- /140/ S. Geller, Acta Cryst., 9, 885 (1956);
S. Geller, Acta Cryst., 10, 380 (1957)
- /141/ H.A.C.M. Bruning, Philips Research Reports, 22, 349 (1967)
- /142/ R. Flükiger, S. Foner and E.J. McNiff, Jr., in "Superconductivity in d- and f-Band Metals", Eds. H. Suhl and M.B. Maple, Academic Press Inc., 1980, p. 265
- /143/ P.L. Lam and M.L. Cohen, Phys. Lett., 81A, 457 (1981)
- /144/ R.D. Burbank, R.C. Dynes and J.M. Poate, J. Low Temp. Phys., 36, 573 (1979)
- /145/ L.R. Testardi, R.L. Meek, J.M. Poate, W.A. Royer, A.R. Storm and J.H. Wernick, Phys. Rev. B11, 4304 (1975)
- /146/ J.M. Poate, R.C. Dynes, L.R. Testardi and R.H. Hammond, in "Superconductivity in d- and f-Band Metals", Ed. D.H. Douglass, Plenum Press, New York, 1976, p. 489;
J.M. Poate, L.R. Testardi, A.R. Storm and W.M. Augustyniak, Phys. Rev. Lett., 35, 1290 (1975)
- /147/ M.J. Norgett, M.T. Robinson, I.M. Torrens, Nucl. Eng. Design, 33, 50 (1974)
- /148/ O. Meyer and G. Linker, J. Low Temp. Physics, 38, 747 (1980)
- /149/ J. Pflüger and O. Meyer, Solid State Commun., 32, 1148 (1979)
- /150/ O. Meyer, J. Nucl. Mater., 72, 182 (1978);
O. Meyer, Nucl. Instrum. and Methods, 149, 377 (1978)
- /151/ B.S. Brown, R.C. Birtcher, R.T. Kampwirth and T.H. Blewitt, J. Nucl. Mater., 72, 76 (1978)

- /152/ H. Adrian, G. Ischenko, M. Lehmann, P. Müller, H. Braun and G. Linker, *J. Less-Common Metals*, 62, 99 (1978)
- /153/ A.K. Ghosh and R. Caton, *Sol. State Comm.*, 44, 1083 (1982)
- /154/ A.I. Skvortsov, Y.V. Shemel'ov, V.E. Klepatski and B.M. Levitski, *J. Nucl. Mater.*, 72, 198 (1978)
- /155/ O. Meyer, R. Kaufmann and R. Flükiger, in "Superconductivity in d- and f-Band Metals", Eds. W. Buckel and W. Weber, Kernforschungszentrum Karlsruhe, 1982, p. 11
- /156/ F. Weiss, R. Flükiger, W. Maurer, P.A. Hahn and M.W. Guinan, to be published in *IEEE Trans. Magn.*, MAG - 23 (1987)
- /157/ G. Ischenko, H. Adrian, S. Klaumünzer, M. Lehmann, P. Müller, H. Neumüller and W. Szymczak, *Phys. Rev. Lett.*, 39, 43 (1977)
- /158/ A.V. Mirmelshteyn, A.Y. Karkin, V.Y. Arkhipov and V.I. Voronin, *Phys. Met. Metall.*, 55, 67 (1984)
[*Fiz Metall. Metalloved.*, 55, 79 (1983)]
- /159/ A.E. Karkin, V.E. Arkhipov, B.N. Goshchitskii, E.P. Romanov and S.K. Sidorov, *Phys. Stat. Solidi*, (a) 38, 433 (1976)
- /160/ A.E. Karkin, A.V. Mirmelshteyn, V.B. Arkhipov and B.N. Goshchitskii, *Phys. Stat. Solidi*, (a) 61, K 117 (1980)
- /161/ T.F. Smith, *Phys. Rev. Lett.*, 25, 1483 (1970)
- /162/ R. Flükiger and R. Isernhagen, to be published
- /163/ The author is indebted to Dr. E. Haase from Kernforschungszentrum for consulting of the Mo₃Ge diffraction patterns used in Ref. 138.
- /164/ M. Gurvitch, A.K. Ghosh, B.L. Gyorffy, H. Lutz, O.F. Kammerer, J.S. Rosner and M. Strongin, *Phys. Rev. Lett.*, 41, 1616 (1978)
- /165/ E. Schneider, P. Schweiss and W. Reichardt, in *Proc. Conf. Neutron Scattering, Gatlinburg, Tenn. Vol. 1*, 223 (1976)
- /166/ S.E. Rasmussen and R.G. Hazell, *Acta Cryst.*, B35, 1677 (1979)
- /167/ V.S. Belovol, A.A. Blinkin, S.D. Lovrinenko and V.A. Finke, *Phys. Met. Metallogr.*, 52, 46 (1981)
- /168/ J.J. Hanak and H.S. Berman, "*Crystal Growth*", 1967, Pergamon Press, New York, p. 249
- /169/ L.J. Vieland and A.W. Wicklund, *Phys. Rev.*, 166, 424 (1968)
- /170/ D.W. Woodard and G.D. Cody, *RCA Rev.*, 25, 392 (1964)
- /171/ L.J. Vieland, *Phys. Rev.* 3B, 1804 (1971); *Phys. Rev. Lett.*, 26, 333 (1971)

- /172/ K.R. Keller and J.J. Hanak, Phys. Rev., 154, 628 (1967)
- /173/ R. Mailfert, B.W. Batterman and J.J. Hanak, Phys. Lett., 24A, 315 (1967)
- /174/ J.P. Charlesworth, I. Macphail and P.E. Madsen, J. Mat. Sci., 5, 580 (1970)
- /175/ W.L. Johnson, C.C. Tsuei, S.I. Raider and R.D. Laibowitz, J. Appl. Phys., 50, 4240 (1979)
- /176/ P. Fischer and R. Flükiger, AF-SSP-43,336(1979)
- /177/ K.Y. Liou and P. Wilkes, J. Nucl. Mater., 87, 317 (1979)
- /178/ R. Zee and P. Wilkes, Phil. Mag., 42A, 463 (1980)
- /179/ A. Junod, J. Muller, H. Rietschel and E. Schneider, J. Phys. Chem. Solids, 39, 317 (1978)
- /180/ B.N. Kodess, Phys. Lett., A73, 53 (1979)
- /181/ J.L. Staudenmann, Sol. State Commun., 26, 461 (1978)
- /182/ L.R. Newkirk, F.A. Valencia, A.L. Giorgi, E.G. Sklarz and T.C. Wallace, IEEE Trans. Mag., MAG 11-2, 221 (1975);
L.R. Newkirk and F.A. Valencia "Superconductivity in d- and f-Band Metals", Ed. D.H. Douglass, Plenum Publ. Corp., New York, 1976, p. 461
- /183/ S. Moehlecke, Ph.D. Thesis, 1978, Brookhaven National Laboratory (USA)/ Universidade Estadual de Campinas (Brasil)
- /184/ S. Foner and E.J. McNiff, Jr., Sol. State Comm., 39, 959 (1981)
- /185/ A.J. Arko, D.H. Lowndes, F.A. Müller, L.W. Roeland, J. Wolfrat, A.T. Van Kessel and G.W. Webb, Phys. Rev. Lett., 40, 1590 (1978)
- /186/ T.P. Orlando, E.J. McNiff, Jr., S. Foner and M.R. Beasley, Phys. Rev. B19, 4545 (1979)
- /187/ T.B. Reed, H.C. Gatos, W.J. La Fleur and J.T. Roddy, in "Metallurgy of Advanced Electronic Materials", Ed. G.E. Brock, Interscience Publishers New York, 1963, p. 171
- /188/ A. Müller, Z. Naturforschg., 25a, 1659 (1970)
- /189/ J. Kwo and T.H. Geballe, Phys. Rev. B23, 3230 (1981)
- /190/ E.L. Wolf, J. Zasadzinski, G.B. Arnold, D.F. Moore, J.M. Rowell and M.R. Beasley, Phys. Rev. B22, 1214 (1980)
- /191/ R. Flükiger, W. Goldacker and R. Isernhagen, Adv. Cryo. Eng., Vol. 32, 925 (1986)
- /192/ M.S. Wire, G.W. Webb, D.E. Cox, C.L. Snead, Jr., and A.R. Sweedler, Solid State Commun., 48, 125 (1983)

- /193/ R.A. Hein, J.E. Cox, R.D. Blaugher, R.M. Waterstrat and E.C. van Reuth, *Physica*, 55 (1971), 523
- /194/ J. Muller, R. Flükiger, A. Junod, F. Heiniger and C. Susz, Proc. LT 13, Eds. K.D. Timmerhaus, W.J. O'Sullivan and E.F. Hammel, Plenum Publ. Corp., New York, 1972, p. 446
- /195/ P. Spitzli and R. Flükiger, unpublished
- /196/ E. Röschel, O. Loebich, Jr., and C.J. Raub, *Z. Metallkde.*, 64, 359 (1973)
- /197/ P.J. Becker and P. Coppens, *Acta Cryst. A* 31, 417 (1975)
- /198/ A.R. Sweedler, S. Moehlecke and D.E. Cox, unpublished (referred to in Ref. 78)
- /199/ J.L. Staudenmann, B. de Facio and C. Stassis, *Phys. Rev.* B27, 4186 (1983)
- /200/ A.R. Miedema, *J. Less-Common Metals*, 32, 117 (1973)
- /201/ J.L. Jorda and J. Muller, *J. Less-Common Met.*, 84, 39 (1982)
- /202/ R.M. Waterstrat and E.C. Van Reuth, in "Structural Applications and Physical Metallurgy of Ordered Alloys", Clayton's Publishers, 1970, p. 95
- /203/ C.C. Koch, *J. Phys. Chem. Solids*, 34 (1973), 1445
- /204/ The author is indebted to Dr. R.M. Waterstrat for this information
- /205/ J.E. Cox, A. Hein, Proc. LT 12, Ed. E. Kanda, Academic Press, Japan, 333 (1971)
- /206/ H. Devantay, Ph.D. Thesis (Nr. 1993) Université de Genève, 1981
- /207/ A. Junod, R. Flükiger and J. Muller, *J. Phys. Chem. Sol.*, 37, 27 (1976)
- /208/ P. Spitzli, R. Flükiger, F. Heiniger, A. Junod, J. Muller and J.L. Staudenmann, *J. Phys. Chem. Sol.*, 31, 1531 (1970)
- /209/ A.L. Giorgi, B.T. Matthias and G.R. Stewart, *Sol. State Comm.*, 27, 291 (1978)
- /210/ S.J. Michalek and J.H. Brophy, *Trans. AIME*, 227, 1047 (1963)
- /211/ A. Taylor, N.Y. Doyle and B.J. Kagle, *J. Less-Common Metals*, 4, 436 (1962)
- /212/ K. Girgis and P. Fischer, *AF-SSP-95*, 40 (1976)
- /213/ G.V. Raynor, *J. Less-Common Met.*, 35, 285 (1974); 37, 247 (1974); 38, 91 (1974)
- /214/ G.R. Stewart, L.R. Newkirk and F.A. Valencia, *Sol. State Comm.*, 26, 417 (1978)
- /215/ The author is indebted to Dr. Goldacker for the careful low temperature X ray measurements

- /216/ W. Schauer, W. Goldacker and R. Flükiger, unpublished results
- /217/ R. Caton and R. Viswanathan, Phys. Rev. 25B, 179 (1982)
- /218/ S.J. Williamson and M. Milewits, in "Superconductivity in d- and f-Band Metals", Ed. D.H. Douglass, Plenum Press, New York 1976, p. 551
- /219/ L.R. Testardi, in "Physical Acoustics", Academic Press, Inc., New York, Vol. X, 193-293 (1973)
- /220/ R. Flükiger, H. Küpfer, J.L. Jorda and J. Muller, to be published in IEEE Trans. Magn., MAG - 23 (1987)
- /221/ E. Drost, W. Specking and R. Flükiger, IEEE Trans. Magn., MAG-21, 281 (1985)
- /222/ G.S. Knapp, S.D. Bader and Z. Fisk, Phys. Rev. B13, 3783 (1976)
- /223/ R. Flükiger, F. Heiniger, A. Junod, J. Muller, P. Spitzli and J.L. Staudenmann, J. Phys. Chem. Sol., 32, 459 (1971)
- /224/ V.G. Chudinov, N.V. Moseev, B.N. Goshchitskii and V.I. Protasov, phys. stat. sol., (a) 55, 109 (1979)
- /225/ V.G. Chudinov, N.V. Moseev, B.N. Goshchitskii and V.I. Protasov, phys. stat. sol., (a) 85, 435 (1984)
- /226/ D. Welch and R. Flükiger, Physica 135 B, 353 (1985)
- /227/ G.R. Stewart, Ibid. /36/, 81 (1982)
- /228/ G.R. Stewart, B. Cort and G.W. Webb, Phys. Rev. B24, 3841 (1981)
- /229/ V.I. Surikov, A.K. Shtolz and A.K. Zagriaskii, Dokl. Akad. Nauk, 215, 833 (1974); P.V. Geld, G.I. Kalishevich, V.I. Surikov, A.K. Shtolts and V.L. Zagryaskii, Sov. Phys. Dokl., 19, 230 (1974)
- /230/ D.W. Woodard and G.D. Cody, Phys. Rev. 136, A 166 (1964)
- /231/ Z. Fisk and G.W. Webb, in "Superconductivity in d- and f-Band Metals" - Second Rochester Conference, Ed. D. Douglass, Plenum, New York, 1976, p. 545
- /232/ Z. Fisk and A.C. Lawson, Sol. State Comm., 13, 277 (1973)
- /233/ V.M. Pan, I.E. Bulakh, A.L. Kasatkin and A.D. Shevchenko, J. Less-Common Metals, 62, 157 (1968)
- /234/ J.A. Woollam and S.A. Alterovity, Phys. Rev. B19, 749 (1979)
- /235/ V.A. Marchenko, Sov. Phys. Solid State, 15, 1261 (1973)
- /236/ H. Wiesmann, M. Gurvitch, H. Lutz, A. Ghosh, B. Schwartz, M. Strongin, P.B. Allen and J.W. Halley, Phys. Rev. Lett., 38, 782 (1977)
- /237/ B.P. Schweiss, B. Renker, E. Schneider and W. Reichardt, Ibid. /231/, p. 189

- /238/ R. Isernhagen, unpublished results
- /239/ M. Lehmann, C. Nölscher, H. Adrian, J. Bieger, L. Söldner and G. Saemann-Ischenko, *Ibid* /36/, p. 107
- /240/ N. Morton, B.W. James and G.H. Wostenholm, *Cryogenics*, 18, 131 (1978)
- /241/ G. Webb, Z. Fisk, J.E. Engelhardt and S.D. Bader, *Phys. Rev.* B15, 2624 (1977)
- /242/ A. Herold, Ph.D. Thesis, 1981, Techn. Universität Dresden
- /243/ A. Herold, G. Försterling, K. Kleinstück, *Cryst. Res. Techn.*, 16, 1137 (1981)
- /244/ M. Gurvitch, A.K. Gosh, H. Lutz and M. Strongin, *Phys. Rev.* B22, 128 (1980)
- /245/ A. Oota, K. Yanagida and S. Noguchi, *Jap. J. Appl. Phys.*, 19, 905 (1980)
- /246/ M. Milewits, S.J. Williamson and H. Taub, *Phys. Rev.* B13, 5199 (1976)
- /247/ P.B. Allen in "Superconductivity in d- and f-Band Metals", H. Suhl and M.B. Maple, Eds., Plenum, New York, 1980, p. 291
- /248/ A. Junod, J.L. Jorda, M. Pelizzone and J. Muller, *Phys. Rev.* B29, 1189 (1984)
- /249/ S. Ramakrishnan, A.K. Nigam and G. Chandra, *Sol. State Comm.*, 52, 641 (1984)
- /250/ K.H. Berthel and B. Pietrass, *J. Physique*, 39, C6-383 (1978)
- /251/ H. Lutz, H. Wiesmann, O.F. Kammerer and M. Strongin, *Phys. Rev. Lett.*, 36, 1576 (1976)
- /252/ N. Morton, B.W. James, G.H. Wostenholm and N.A. Howard, *J. Less-Common Metals*, 64, 69 (1979)
- /253/ H. Taub and S.J. Williamson, *Sol. State Comm.*, 15, 181 (1974)
- /254/ M. Gurvitch, in "Superconductivity in d- and f-Band Metals", Eds. H. Suhl and M.B. Maple, Academic Press, New York 1980m p. 317
- /255/ K. Ikeda and T. Nakamichi, *J. Phys. Soc. Japan*, 39, 963 (1975)
- /256/ M. Rosen, H. Klinker and M. Weger, *Phys. Rev.*, 184, 466 (1969)
- /257/ T. Muto in "Order-Disorder Phenomena in Metals", Ed. Lester Guttman, Academic Press, 1956, p. 66
- /258/ J.H. Mooij, *phys. stat. sol. (a)* 17, 521 (1973)
- /259/ J. Labbé and J. Friedel, *J. Physique*, 27, 153 (1966); 27, 303 (1966)
- /260/ L.P. Gorkov, *Sov. Phys., JETP*, 38, 830 (1974)
- /261/ R.N. Bhatt, *Phys. Rev.* B17, 2947 (1978)
- /262/ A.R. Miedema, *J. Phys. F., Met. Phys.*, 3, 1803 (1973); *J. Phys. F., Met. Phys.*, 4, 120 (1974)

- /263/ A.R. Miedema, F.R. de Boer and P.F. de Chatel, J. Phys. F, Met. Phys., 3, 1558 (1973)
- /264/ A. Weinkauff and J. Zittartz, Sol. State Comm., 14, 365 (1974)
- /265/ A. Wenger, G. Burri and S. Steinemann, Sol. State Comm., 9, 1125 (1971)
- /266/ G. Bongi Ø. Fischer and H. Jones, J. Phys. F, Met. Phys., 4, L259 (1974)
- /267/ J.L. Staudenmann, Ph.D. Thesis, Nr. 1735, 1976, Université de Genève
- /268/ A.I. Gubanov, Sov. Phys., JETP, 4, 465 (1957)
- /269/ F.J. Ohkawa, J. Phys. Soc. Japan, 44, 4 (1978)
- /270/ P.I. Cote and B.V. Meisel, Phys. Rev. Lett., 39, 102 (1977)
- /271/ M. Gurvitch, Physica 135B, 276 (1985)
- /272/ L. Testardi, private communication
- /273/ M. Gurvitch, Phys. Rev. Lett., 56, 647 (1986)
- /274/ G. Försterling and E. Hegenbarth, Kristall und Technik, 13, 757 (1978)
- /275/ J. M. Ziman, in "Principles of the Theory of Solids", Cambridge University Press, 1972, p.66
- /276/ A. Junod, T. Jarlborg and J. Muller, Phys. Rev., 27B, 1568 (1983)
- /277/ G.R. Stewart, B. Olinger and L.R. Newkirk, J. Low Temp. Phys., 43, 455 (1981)
- /278/ A. Junod, J.L. Jorda and J. Muller, J. Low Temp. Phys., 62, 301 (1986)
- /279/ G.R. Stewart and A.L. Giorgi, J. Low Temp. Phys., 41, 73 (1980)
- /280/ L.D. Hartsough and R.H. Hammond, Sol. State Comm., 9, 885 (1971)
- /281/ P. Müller, PhD Thesis, 1980, University of Erlangen
- /282/ A. Müller, Naturforschg., 24a, 1136 (1969)
- /283/ H.L. Luo, E. Vielhaber and E. Corenzwit, Z. Physik, 230, 443 (1970)
- /284/ T. Asada, T. Horiuchi, M. Uchida, Jap. J. Appl. Phys., 8, 958 (1969)
- /285/ B.N. Kodess, V.I. Surikov, V.L. Zagryaskii and A.K. Shtolts, Izv. Akad. Nauk, SSSR, Neorg. Mater., 7, 853 (1971)
- /286/ L.F. Mattheiss and D. R. Hamann, Sol. State Commun., 38, 689 (1981).
- /287/ T.F. Smith, T.R. Finlayson and R.N. Shelton, J. Less-Common Metals, 43, 21 (1975)
- /288/ L.R. Testardi and T.B. Bateman, Phys. Rev., 154, 402 (1967)

- /289/ Y.S. Touloukian, R.K. Kirby, R.E. Taylor and P.D. Desai, "Thermophysical Properties of Matter", Vol. 12, Plenum Press, New York, 1975, p. 601
- /290/ J.B. Conway, A.C. Losekamp, Trans. Met., Soc. AIME, 336, 702 (1966)
- /291/ G.W. Hulland, L.R. Newkirk, J. Low Temp. Phys., 29, 297 (1977)
- /292/ M.S. Reddy and S.V. Suryanarayana, J. Mater. Sci. Letters, 2, 171 (1983)
- /293/ B.K. Rao and D.B. Sirdeshmukh, Indian J. Pure Appl. Phys., 18, 56 (1980)
- /294/ A.L. Giorgi, G.R. Stewart, E.G. Szklarz and C.L. Snead, Jr., Sol. State Comm., 40, 233 (1981)
- /295/ E.S. Machlin and S.H. Whang, J. Phys. Chem. Solids, 37, 555 (1976), 39, 607 (1978); E.S. Machlin, Acta Metallurgica, 24, 543 (1976)
- /296/ J.J. Hanak, K. Strater and G.W. Cullen, RCA Rev., 25, 342 (1964)
- /297/ A.N. Christensen, J.E. Jørgensen, L. Pintschovius, F. Gompf, W. Reichardt and N. Lehner, accepted by Phys. Rev.
- /298/ T. Jarlborg, M. Peter and W. Weber, to be published
- /299/ G.S. Cargill, III, R.F. Boehme and W. Weber, Phys. Rev. Lett., 50, 1391 (1983)
- /300/ W. Weber, to be published
- /301/ W. Lehmann, PhD Thesis, 1981, University of Erlangen
- /302/ T. Solleder, V. Essmann and H. Kronmüller, Phys. Lett., 105A, 377 (1984)
- /303/ J.L. Staudenmann, B. de Facio, L.R. Testardi, S.A. Werner, R. Flükiger and J. Muller, Phys. Rev. B24, 6446 (1981)
- /304/ J. Appel, Phys. Rev. B13, 3203 (1976)
- /305/ M. Dietrich, C.H. Dustmann, F. Schmaderer and G. Wahl, IEEE Trans. Magn. MAG-19, 406 (1983)
- /306/ B. Seeber, C. Rossel, Ø. Fischer and W. Glätzle, IEEE Trans. Magn., MAG-19, 402 (1983)
- /307/ R. Flükiger, Journal de Physique 45, C1-365 (1984)
- /308/ F. Flükiger, Annales de Chimie, Science des matériaux, 9, 841 (1984)
- /309/ C.L.H. Thieme, S. Pourrahimi, B.B. Schwartz and S. Foner, Appl. Phys. Lett., 44, 260 (1984)
- /310/ R. Flükiger, IEEE Trans. Magn., MAG-16, 1236 (1980)

- /311/ S Foner, in "High Field Magnetism", Ed. M.Date, North-Holland Publ. Co, 1983, p. 133
- /312/ B.T. Matthias, T.H. Geballe, R.H. Willens, E. Corenzwit and G.W. Hull, Phys. Rev. A139, 1501 (1965).
- /313/ J.R. Gavaler, Appl. Phys. Lett., 23, 480 (1973).
- /314/ B. Krevet, W. Schauer, F. Wüchner and K. Schulze, Appl. Phys. Lett., 36, 704 (1980).
- /315/ S. Foner and E.J. McNiff, Phys. Lett. 58A, 318 (1976)
- /316/ Ø. Fischer, Proc. LT 14, Helsinki, 1975, Eds.M. Krusius and N. Vuorio, Vol. V, p. 172
- /317/ G.H. Bongi, R. Flükiger, A. Treyvaud and Ø. Fischer, J. Low Temp. Phys. 23, 543 (1976)
- /318/ J.D. Livingston, IEEE Trans. Magn. MAG - 14, 611 (1978)
- /319/ K. Tachikawa, T. Asano and T. Takeuchi, Appl. Phys. Lett., 39, 766 (1981)
- /320/ E. Springer, M. Wilhelm, H.J. Weisse and G. Rupp, Adv. Cryo. Eng., Vol. 30, 747 (1984)
- /321/ E. Drost, R. Flükiger and W. Specking, Cryogenics, 24, 622 (1984)
- /322/ R. Akihama, K. Yasukochi and T. Ogasawara, IEEE Trans. Magn., MAG - 13, 803 (1977)
- /323/ R. Bormann, Adv. Cryo. Eng., Vol. 30, 659 (1984)
- /324/ E. Drost, W. Specking and R. Flükiger, IEEE Trans. Magn. MAG - 21, 281 (1985)
- /325/ E. Drost and R. Flükiger to be published
- /326/ D.B. Smathers and D.C. Larbalestier, in "Filamentary A15 Superconductors", Eds. M. Suenaga and A.F. Clark, Plenum Press, 1980, p. 143
- /327/ M. Suenaga, ibid. /7/, p. 201
- /328/ J. Taftø, M. Suenaga and D.O. Welch, J. Appl. Phys 55, 4330 (1984)
- /329/ L.J. Vieland and A.W. Wicklund, Phys. Lett. 34A, 43 (1971)
- /330/ L.J. Vieland, J. Phys. Chem. Sol. 31, 1449 (1970)
- /331/ Y. Fuji, J.B. Hastings, M. Kaplan, G. Shirane, Y. Inada and N. Kitamura, Phys. Rev. B25, 364 (1982)
- /332/ R. Flükiger, Adv. Cryo. Eng. 28, 399 (1982)
- /333/ R. Roberge, H. LeHuy and S. Foner, Phys. Lett. 82A, 259 (1981)
- /334/ W. Goldacker and R. Flükiger, Physica 135B, 359 (1985)
- /335/ W. Kunz and E. Saur, Z. Physik 189, 401 (1966)
- /336/ R.E. Schwall, G.M. Ozeryansky, S. Foner and E.J.McNiff, Jr., J. Appl. Phys., 56, 814 (1984)
- /337/ J. Wecker, R. Bormann and H.C. Freyhardt, J. Appl. Phys., 54, 3318 (1983)
- /338/ Z. Fisk and G.W. Webb, Phys. Rev. Lett., 36, 1084 (1976)
- /339/ M. Gurrvitch, Phys. Rev. Lett., 57, 1962 (1986)
- /340/ A. Van Winkel, A. W. Weber and H. Bakker, J. Phys. F: Met. Phys. F: 14, 2631 (1984)